visit blog:

http://chemlabsoft.blogspot.com/

By

jose07070012

Pass: chester87

+++ebook+++

Chemistry I II III & IV

http://rapidshare.com/users/M43PVR

http://rapidshare.com/users/EOAGQC

http://rapidshare.com/users/N0Z8D9

http://rapidshare.com/users/WL0N86

Fisica

http://rapidshare.com/users/W64NQW

Informatica

http://rapidshare.com/users/NK4WEQ

Matematicas

http://rapidshare.com/users/R6242N

Software Portables

http://rapidshare.com/users/2RY5LP

Music

http://rapidshare.com/users/S2QZPK

Libros Varios

http://rapidshare.com/users/EHBTL0

http://rapidshare.com/users/WEZZXW

Megaupload

http://www.megaupload.com/?f=73GAA8MG

http://www.megaupload.com/?f=A0RQ5JV2

http://www.megaupload.com/?f=85C3HCJW

http://www.megaupload.com/?f=Y0T96I7K

WILEY

Grignard Reagents

New Developments

Edited by
Herman G. Richey, Jr.

Grignard Reagents
New Developments

Edited by

Herman G. Richey, Jr
Department of Chemistry, The Pennsylvania State University, USA

JOHN WILEY AND SONS, LTD
Chichester • New York • Weinheim • Brisbane • Singapore • Toronto

West Sussex PO19 1UD, England

National 01243 779777
International (+44) 1243 779777
e-mail (for orders and customer service enquiries): cs-books@wiley.co.uk
Visit our Home Page on http://www.wiley.co.uk
or http://www.wiley.com

Other Wiley Editorial Offices

John Wiley & Sons, Inc., 605 Third Avenue,
New York, NY 10158-0012, USA

WILEY-VCH Verlag GmbH, Pappelallee 3,
D-69469 Weinheim, Germany

Jacaranda Wiley Ltd, 33 Park Road, Milton,
Queensland 4064, Australia

John Wiley & Sons (Asia) Pte Ltd, Clementi Loop #02-01,
Jin Xing Distripark, Singapore 129809

John Wiley & Sons (Canada) Ltd, 22 Worcester Road,
Rexdale, Ontario M9W 1L1, Canada

British Library Cataloguing in Publication Data

A catalogue record for this book is available from the British Library

ISBN 0 471 99908 3

Typeset in 10/12pt Times by Laser Words, (India) Ltd
Printed and bound in Great Britain by Antony Rowe Ltd, Chippenham, Wiltshire

This book is printed on acid-free paper responsibly manufactured from sustainable forestry, in which at least two trees are planted for each one used for paper production.

Contents

List of Contributors

Preface

1 Mechanistic Features of the Reactions of Organomagnesium Compounds
Torkil Holm and Ingolf Crossland
1.1 Introduction
1.2 Properties of Grignard Reagents
1.2.1 Thermochemistry
1.2.1.1 Heat of Formation of Grignard Reagents
1.2.1.2 C—Mg Bond Dissociation Energies
1.2.2 Oxidation Potentials of Grignard Reagents
1.2.3 Association Equilibria in Grignard Reagents
1.2.3.1 The Schlenk Equilibrium
1.2.3.2 Self Association in Grignard Reagents
1.2.3.3 Association between RMgX and Carbonyl Compounds
1.3 Reactions of Benzophenone(s) with Grignard Reagents
1.3.1 Prediction of a Radical Mechanism and Early Evidence
1.3.2 Reactivity Series and Linear Free Energy Correlations
1.3.3 Radical Probes
1.3.4 A Thermochemical Approach
1.3.5 Kinetic Isotope Effects
1.3.5.1 Isotopic Carbon and Hydrogen in Benzophenone
1.3.5.2 Deuterium Substitution in the Grignard Reagent
1.3.6 CIDNP Observations
1.3.7 A New School in the Study of the Reaction of Benzophenone with Grigna Reagents
1.4 Polar Concerted Reaction Mechanisms
1.4.1 Addition to Aliphatic Ketones
1.4.2 Addition to Acid Derivatives
1.4.3 Concerted Transfer of β-Hydrogen. Reduction
1.5 Reactions with α,β-Unsaturated Carbonyl Compounds

1.6 ET Substrates other than Benzophenone 20
1.6.1 Metal Catalysis 20
1.6.1.1 The Kharasch Reaction 20
1.6.1.2 Reductive Dimerization of Carbonyl Compounds 21
1.6.2 Reactions with Oxygen and with Peroxides 21
1.6.3 Reactions with Azobenzene 22
1.6.4 Reactions with Cinnamic Esters 23
1.7 Solvent Effects 24
1.8 Conclusion 24

2 Nucleophilic Displacements at Carbon by Grignard Reagents 27
E. Alexander Hill
2.1 Introduction 27
2.2 Survey of Coupling Reactions of Grignard Reagents with Organic Halides 29
2.2.1 Reactions with 'Simple' Alkyl Halides 29
2.2.2 Reactions with 'Reactive' Halides 30
2.3 Summary of Cross-coupling Mechanisms 30
2.3.1 S_N2 Displacement Mechanism 31
2.3.2 S_N1 Mechanism 33
2.3.3 Single Electron Transfer (SET) Mechanism 34
2.4 Mechanism of Grignard Cross-coupling Reactions 39
2.4.1 Saturated Alkyl Halides 39
2.4.1.1 Saturated and Aryl Grignard Reagents 39
2.4.1.2 Benzylic and Allylic Grignard Reagents 42
2.4.2 Benzylic and Allylic Halides 43
2.4.3 α-Haloethers and -Thioethers 45
2.5 Other Classes of Substrates 46
2.5.1 Arylmethyl Compounds 46
2.5.2 Polyhalogen Compounds 48
2.5.3 α-Haloketones 49
2.5.4 Other Leaving Groups 50
2.5.4.1 Reaction with Carbocations—No Leaving Group 50
2.5.4.2 Oxy-Anions 51
2.5.4.3 Miscellaneous Leaving Groups 56
2.6 Some Related Topics 57
2.7 Summary and Conclusions 59

3 Hydromagnesiation of Alkenes and Alkynes 65
Fumie Sato and Hirokazu Urabe
3.1 Introduction 65
3.2 Hydromagnesiation of Alkenes 67
3.3 Hydromagnesiation of Conjugated Dienes 79
3.4 Hydromagnesiation of Alkynes 82
3.5 Application of Hydromagnesiation in Selective Synthesis of Natural Products 93
3.6 On the Mechanism of Cp_2TiCl_2-catalyzed Hydromagnesiation of Alkynes with Grignard Reagents 97
3.7 Concluding Remarks 102

4 Stereoselective Addition of Grignard Reagents to Alkenes 107
Amir H. Hoveyda, Nicola M. Heron and Jeffrey A. Adams
4.1 Introduction 107
4.2 Heteroatom-directed Addition of Grignard Reagents to Alkenes 108
4.3 Zr-Catalyzed Diastereoselective Carbomagnesation of Allylic and Homoallylic Alcohols and Ethers 109
4.3.1 Zr-Catalyzed Diastereoselective Ethylmagnesation of Allylic Alcohols and Ethers 109
4.3.2 Zr-Catalyzed Diastereoselective Ethylmagnesation of Homoallylic Alcohols and Ethers 112
4.4 Zirconocene-catalyzed Enantioselective Alkylation Reactions 114
4.4.1 Catalytic Enantioselective Alkylation of Alkenes with Alkylmagnesium Halides 114
4.4.2 Zr-Catalyzed Kinetic Resolution of Unsaturated Heterocycles 119
4.4.3 Zr-Catalyzed Kinetic Resolution of Cyclic Allylic Ethers 123
4.4.4 Related Catalytic Enantioselective Alkylation of Alkenes with Alkylaluminums 125
4.5 Ni-Catalyzed Stereoselective Alkylation of Alkenes with Grignard Reagents 126
4.5.1 Diastereoselective Ni-Catalyzed Addition of Grignard Reagents to Allylic Ethers 128
4.5.1.1 Directed Ni-catalyzed Addition of Grignard Reagents to Allylic Ethers 128
4.5.1.2 Ni-catalyzed Addition of Grignard Reagents to Bicyclic Allylic Ethers 131
4.5.2 Asymmetric Ni-Catalyzed Addition of Grignard Reagents to Allylic Ethers 132
4.5.3 Asymmetric Ni-Catalyzed Addition of Grignard Reagents to Allylic Acetals 134
4.6 Summary and Outlook 135

5 Stereoselective Additions of Chiral Grignard Reagents to Aldehydes: Stereochemical and Mechanistic Principles, with Examples Using α-Amino Grignard Reagents 139
Robert E. Gawley
5.1 Introduction to Stereoselectivity in Grignard Additions 139
5.2 Transition States and Mechanistic Rationales 141
5.3 Topicity and Terminology 143
5.4 Additions of Configurationally Stable Grignards to Aldehydes 145
5.5 Configurational Lability of Benzylic Grignards 146
5.6 Additions of Benzylic Grignards to Aldehydes 148
5.7 Applications to Alkaloid Synthesis 153
5.8 Summary 162

6 Grignard Reagents—Industrial Applications and Strategy 165
Frank R. Busch and David M. De Antonis
6.1 Introduction 165
6.2 Safety and Engineering Considerations Specific to Industrial Applications 166
6.2.1 Typical Equipment Configuration 166
6.2.2 Choice of Solvent 167
6.2.3 Process Hazards Analysis 167
6.2.4 Vent Sizing/DIERS Calculations 168
6.2.5 Grignard Reagent Formation—Process Controls and Interlocks 168
6.2.5.1 Control of Exotherm 168
6.2.5.2 Safety Interlocks 170

9.5 Simple Organomagnesium with Coordination Number 5 and 6 306
9.5.1 Organomagnesium Compounds with Coordination Number 5 307
9.5.2 Organomagnesium Compounds with Coordination Number 6 308
9.6 Difunctional Organomagnesium Compounds 308
9.6.1 Simple Difunctional Organomagnesium Compounds 308
9.6.2 Organomagnesium Compounds Derived from Dienes or Diynes 311
9.6.3 Anthracenemagnesium Derivatives 311
9.7 Organomagnesium Compounds with Polyhapto Carbon Ligands 312
9.7.1 Cyclopentadienyl Derivatives and Related Compounds 312
9.7.2 Carborane Derivatives 314
9.8 Organomagnesium Compounds with Intramolecular and/or Polycoordination 314
9.8.1 Intramolecular Coordination 314
9.8.2 Intramolecular Polycoordination 316
9.8.3 Intermolecular Polycoordination 317
9.9 Heterometallic Organomagnesium Complexes 320
9.9.1 Heterometallic Organomagnesium Complexes with Alkali Metals 320
9.9.2 Heterometallic Organomagnesium Complexes with Aluminum 321
9.9.3 Heterometallic Organomagnesium Complexes with Transition Metals 322
9.10 Conclusions 324

10 X-ray Absorption Spectroscopy and Large Angle X-ray Scattering of Grignard Compounds 329
T.S. Ertel and H. Bertagnolli
10.1 Introduction 329
10.2 EXAFS 330
10.2.1 Theoretical Background 330
10.2.2 Measurement Fundamentals and Techniques 332
10.2.3 Data Analysis 334
10.3 LAXS 335
10.3.1 Theoretical Background 335
10.3.2 Measurement Fundamentals and Techniques 338
10.3.3 Data Analysis 338
10.4 Comparison of EXAFS and LAXS Techniques 339
10.5 Physical Chemistry of Grignard Compounds 340
10.5.1 Introduction 340
10.5.2 Crystallography 341
10.5.3 Molecular Weight Studies 343
10.5.4 Tracer Studies 344
10.5.5 Conductivity Measurements 344
10.5.6 Infrared Spectroscopy 344
10.5.7 NMR Spectroscopy 345
10.5.8 Theoretical Studies 345
10.6 EXAFS and LAXS of Grignard Compounds 347
10.6.1 Introduction 347
10.6.2 EXAFS Studies 348
10.6.3 LAXS Studies 359
10.7 Concluding Remark: Current Structural Picture 363

11 Di- and Polyfunctional Organomagnesium Compounds 367
F. Bickelhaupt
11.1 Introduction 367
11.2 1,1-Di-organomagnesium Reagents 369
11.2.1 Synthesis and Structure 369
11.2.2 Applications 370
11.3 1,2-Di-organomagnesium Reagents 372
11.3.1 Synthesis and Structure 372
11.3.2 Applications 374
11.4 1,3-Di-organomagnesium Reagents 375
11.4.1 Synthesis and Structure 375
11.4.2 Applications 377
11.5 1,4- and Larger α,ω-Di-organomagnesium Reagents 380
11.5.1 Synthesis and Structure 380
11.5.2 Applications 382
11.6 Tri- and Polyorganomagnesium Reagents 385
11.7 Conclusion 389

12 Unusual Organomagnesium Compounds 395
V.V. Smirnov, L.A. Tjurina and I.P. Beletskaya
12.1 Introduction 395
12.2 Cluster Grignard Reagents 395
12.2.1 Metal Vapour Cryosynthesis 395
12.2.2 The Role of Clusters in the Low-Temperature Cryosynthesis of Organomagnesium Compounds 396
12.2.3 Cluster Grignard Reagents—Characterization 397
12.2.4 Cluster Grignard Reagents—Reactions with Organic Halides 399
12.3 Cluster Magnesium Hydrides 401
12.3.1 Theory 401
12.3.2 Magnesium–Hydrocarbon Cryosyntheses 403
12.3.2.1 Alkylbenzenes 403
12.3.2.2 Cyclopentadiene 404
12.3.2.3 Phenylacetylene 405
12.3.2.4 1-Alkenes 406
12.3.2.5 Anthracene 407
12.3.3 Catalytic Properties of Magnesium–Hydrocarbon Adducts 409
12.4 Conclusion 410

Index 411

John F. Garst
Department of Chemistry
The University of Georgia
Athens
Georgia 30602
USA

Robert E. Gawley
Department of Chemistry
University of Miami
PO Box 249118
Coral Gables
Florida 33124-0431
USA

Nicola M. Heron
Department of Chemistry
Merkert Chemistry Center
Boston College
Chestnut Hill
Massachusetts 02467
USA

E. Alexander Hill
Department of Chemistry
University of Wisconsin-Milwaukee
PO Box 413
Milwaukee
Wisconsin 53201-0413
USA

Torkil Holm
Department of Organic Chemistry
The Technical University of Denmark
Building 201
DK-2800 Lyngby
Denmark

Amir H. Hoveyda
Department of Chemistry
Merkert Chemistry Center
Boston College
Chestnut College
Massachusetts 02467
USA

Colin L. Raston
Department of Chemistry
Monash University
Clayton
Victoria 3168
Australia

Fumie Sato
Department of Biomolecular Engineering
Tokyo Institute of Technology
4259 Nagatsuta-cho
Midori-ku
Yokohama
Kanagawa 226-8501
Japan

V.V. Smirnov
Department of Chemistry
Moscow State University
Moscow 119899 Vorobievi Gory
Russia

L.A. Tjurina
Department of Chemistry
Moscow State University
Moscow 119899 Vorobievi Gory
Russia

Ferenc Ungváry
Department of Organic Chemistry
University of Veszprém and
Research Group for Petrochemistry of the
Hungarian Academy of Sciences
8200 Veszprém
Hungary

Hirokazu Urabe
Department of Biomolecular Engineering
Tokyo Insititute of Technology
4259 Nagatsuta-cho
Midori-ku
Yokohama
Kanagawa 226-8501
Japan

Preface

In 1900—the opening year of a new century—a short paper by a lone author reported a simple procedure for preparing solutions of organomagnesium compounds of composition RMgX. The Grignard reagent soon became "...the most important of all organometallic compounds encountered in the chemical laboratory"[1] and the organometallic reagent most chemists first encounter in an introductory organic chemistry course.

Grignard reagents solutions can be prepared with a wide variety of organic groups and are relatively inexpensive. Despite generally being very stable, they readily undergo many useful reactions with a multitude of organic and inorganic substrates. Although much of the vast literature concerning Grignard reagents and related organomagnesium compounds concerns synthetic applications, other features also have interested chemists. Because of the strong propensity of organomagnesium species to form additional bonds–to solvent molecules, to other Rs and Xs, and to substrates–and the usually rapid exchange of groups between magnesiums, establishing their structures has been a challenge. Deciphering the mechanisms of their reactions has been even more challenging. Those struggling with organomagnesium structures and mechanisms at times envy the seeming simplicity of much transition metal organometallic chemistry.

At mid-century, Kharasch and Reinmuth in a lengthy monograph (1400 pages) attempted with remarkable success to comprehensively survey the knowledge about Grignard reagents accumulated by 1950.[2] Even at that time the authors noted that besides omission of reactions with metallic substances some additional selection was inevitable. There have been more recent attempts to prepare a comprehensive survey,[3] but the explosive growth of the chemical literature has year by year made this a more elusive goal. In 1975, it was estimated that the application of Grignard reagents had appeared in 40,000 chemical papers,[4] a number that now is very much larger.

This volume focuses on a dozen areas of organomagnesium chemistry, selected because they have developed significantly or even completely in the last twenty years. Each is treated in more depth than would be possible in a volume that attempted to comprehensively span all of organomagnesium chemistry. The authors are knowledgeable about the area reviewed, have contributed to its development, and are particularly able to provide valuable perspectives. I was fortunate that these distinguished chemists, from eight countries, were willing to devote the time and effort required to write these contributions.

The chapters treat reactions, reaction mechanisms, structures, and new categories of organomagnesium compounds; some cover more than one of these topics. Six chapters focus particularly on reactions of organomagnesium compounds. In the first chapter, Holm and Crossland consider general mechanistic features of reactions of organomagnesium compounds with emphasis on the most important and most studied reaction–addition to carbonyl compounds. Hill reviews another fundamental reaction–nucleophilic displacement at carbon–and considers mechanistic pathways. Two chapters provide accounts of synthetic features and mechanisms of two important newer reactions with alkenes (and alkynes), both involving catalysis by transition metals and producing new organomagnesium compounds: Sato and Urabe describe hydromagnesiation, addition of Mg and a hydrogen atom; Hoveyda, Heron, and Adams

review carbomagnesiation, addition of Mg and an organic group, and stereoselectivity in these additions. Gawley considers stereochemical and mechanistic principles involved in stereoselective additions of Grignard reagents and presents striking examples of synthetically useful additions to aldehydes. Grignard reagents have found a variety of industrial applications; Busch and De Antonis describe procedures and problems specific to performing Grignard reagent chemistry on an industrial scale and provide examples of industrial syntheses.

Two chapters primarily concern Grignard reagent formation. Garst and Ungváry consider in detail mechanisms for the formation of Grignard reagents from organic halides; Raston describes use of the Mg-anthracene complex and related complexes in preparing Grignard reagents, including some inaccessible using classical techniques.

Four chapters concern structural characterization and new structural types of organomagnesium compounds. Bickelhaupt surveys the wealth of structural information about organomagnesium solids that is provided by single crystal X-ray diffraction studies. Ertel and Bertagnolli summarize information from established methods about organomagnesium structures in solution and then describe the application of EXAFS and LAXS techniques; since these newer X-ray methods that provide information about structures in solution are not widely known, the essential theoretical background also is described. Bickelhaupt reviews preparations and reactions of di-organomagnesium compounds and the related cyclic organomagnesium compounds. In the final chapter Smirnov, Tjurina, and Beletskaya describe intriguing studies that suggest the formation of RMg_nX and RMg_nH in which n is greater than one.

At the close of its first century, the Grignard reagent has achieved maturity but exhibits no signs of senescence. These chapters demonstrate that significant developments concerning Grignard reagents and related organomagnesium species are abundant: particularly the portions concerning mechanisms reveal that, in spite of all efforts to date, gaps in our understanding and significant controversies remain. Further reviews of new developments in this century-old but still challenging area of chemistry surely will be needed long past the era of the authors of this book.

REFERENCES

1. Coates, G.E.; Wade, K. *The Main Group Elements*, 3rd ed. (Vol. 1 of Coates, G.E.; Green, M.L.H.; Wade, K. *Organometallic Compounds*); Methuen: London, 1967; Chapter 2.
2. Kharasch, M.S.; Reinmuth, O. *Grignard Reactions of Nonmetallic Substances*; Prentice-Hall: New York, 1954. Although this monograph was published in 1954, coverage was comprehensive only to mid-1950.
3. Notable examples: Ioffe, S.T.; Nesmeyanov, A.N. *The Organic Compounds of Magnesium, Beryllium, Calcium, Strontium, and Barium*; North-Holland: Amsterdam, 1967 [a translation into English of a book published (Nauka Press: Moscow) in Russian in 1963]. Nützel K. *Methoden Org. Chem. (Houben-Weyl), 4th Ed.* **1973**, 13(2a), 47. Silverman, G.S.; Rakita, P.E. *Handbook of Grignard Reagents*; Marcel Dekker: New York, 1996. A survey primarily of synthetic methods: Wakefield, B.J. *Organomagnesium Methods in Organic Synthesis*; Academic: London, 1995.
4. Thayer, J.S. *Adv. Organomet. Chem.* **1975**, 13, 1.

1

Mechanistic Features of the Reactions of Organomagnesium Compounds

Torkil Holm and Ingolf Crossland
Technical University of Denmark

1.1 INTRODUCTION

Almost 100 years have passed since Victor Grignard published his paper [1] on the preparation of ethereal solutions of compounds in which carbon is bonded to magnesium. Since then Grignard reagents have been an obvious choice for organic chemists in many preparations of complex molecules.

Besides being extremely useful, the reagents and the way they react have represented a challenge to chemists and physicists. Both the intimate nature of the reagents in various solvents and the detailed mechanisms of their reactions have been under scrutiny by three or four generations of researchers and the work is continuing. This review will concentrate on advances made in the last two to three decades. Since the authors have been engaged in this type of work throughout this period it is inevitable that the review will focus to a certain extent on their favourite views and topics.

Traditionally, Grignard reagents have been seen as potential anions, capable of nucleophilic additions especially to hetero double bonds as in carbonyl compounds [2]. However, in contrast to usual nucleophiles like amines or sodium alkoxides the reagents do not normally react with alkyl halides without a catalyst. The easy preparation of Grignard reagents actually depends on this fact. The high reactivity toward many carbonyl compounds results from the π bond polarization and the possibility of forming the C–C bond in concert with the formation of the magnesium–oxygen bond. The enthalpy of this reaction is highly negative since the established bonds, oxygen to magnesium and carbon to carbon, are much stronger than the broken bonds, which are the C–Mg bond and the π-CO bond.

In 1929 Blicke and Powers [3] suggested that some carbonyl compounds may react with Grignard reagents by stepwise, homolytic reaction mechanisms, but more than 40 years passed before this theory was generally accepted. The homolytic mechanism and the polar concerted mechanism are shown in Scheme 1.1.

Grignard Reagents: New Developments Edited by Herman G. Richey, Jr © 2000 John Wiley & Sons Ltd.

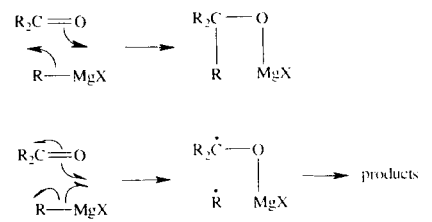

SCHEME 1.1

The two mechanisms may compete and the product(s) from the two processes will often be the same. The distinction between the mechanisms is therefore not simple, but often has to be indirect, based for example on spectroscopy, kinetics or other physical chemical methods.

As seen in Scheme 1.1 the principal difference between the concerted and the stepwise reaction mechanism for addition of a Grignard reagent to a ketone is whether the C–C bond is formed in the rate-determining step or in a separate, radical recombination step. Which mechanism is more effective depends on the properties of both the reagent and the substrate. The concerted mechanism is favoured if the C–Mg bond is strong and the relevant ketyl radical is without efficient stabilization. The stepwise mechanism takes over when the C–Mg bond is weak and the ketyl is effectively stabilized. The strength of the C–Mg bond varies from rather high values in phenyl- and methylmagnesium halides to a very low value in *t*-butylmagnesium halide [4], see Table 1.1.

The driving force for the reaction of Grignard reagents with a carbonyl compound is, as previously mentioned, the formation of the strong bond between magnesium and oxygen. As illustrated in Scheme 1.1, this bond is formed in both the concerted and the stepwise reaction mechanisms.

The reaction of *t*-butylmagnesium chloride with benzophenone is a typical example of the homolytic mechanism suggested:

$$Ph_2CO + t\text{-}BuMgCl \longrightarrow Ph_2\dot{C}OMgCl + t\text{-}\dot{B}u \longrightarrow \text{products} \qquad (1.1)$$

Here the C–Mg bond is weak and the benzophenone ketyl formed is highly stabilized by resonance.

A typical concerted reaction is the one-step addition of methylmagnesium bromide to acetone:

$$(CH_3)_2C{=}O + CH_3MgBr \longrightarrow (CH_3)_3C{-}OMgBr \qquad (1.2)$$

The homolytic mechanism is not possible here because the Me–Mg bond is almost 20 kcal mol^{-1} stronger than the *t*-Bu-Mg bond and the acetone ketyl has little resonance stabilization.

According to the rules for orbital symmetry conservation the four-centre mechanism in Scheme 1 would appear to be forbidden, but very few attempts have been made to describe the orbital transformations in the reactions of Grignard reagents. Much evidence has been presented for the operation of cyclic 6-centre concerted reaction mechanisms (Scheme 1.9), although it has been questioned whether they are in accordance with orbital symmetry rules [5].

This review like earlier reviews [6–14] will deal with the ways and means by which a distinction may be made between the concerted, one-step and the homolytic, multi-step type of reaction mechanism.

In a stepwise reaction, it is sometimes possible to observe an intermediate. The fact that an intermediate is not observed is, however, no proof that the mechanism is truly concerted.

The duality, stepwise or concerted, for the reactions of Grignard reagents is analogous to the duality S_N1–S_N2 for nucleophilic substitution. Formation of an intermediate carbenium ion is possible only when structural features allow conjugative stabilization. In this case reaction is possible even if the favourable bond formation between the electrophilic carbon and the nucleophile has not started. In the absence of such features, the new bond has to be established in concert with the breaking of the old. In the latter case the necessity of a very close approach of the attacking nucleophile to the reaction centre makes steric hindrance the most important factor for the reaction rate of an S_N2 reaction, while the possibility of conjugative or hyperconjugative stabilization of the carbenium ion decides the reaction rate of the S_N1 reaction. Similarly the rate of the concerted addition of a Grignard reagent is highly dependent on steric bulk and/or an optimal conformation in both the reagent and substrate, while the rate of the stepwise reaction depends on the presence of structural features which will favour the formation of radicals.

A reaction mechanism cannot be proved. It can be considered likely if it is impossible to disprove its existence. A mechanism which apparently has been firmly established may at any time undergo revision if new mechanistic tools become available. The mechanisms are elusive but, apparently, the more elusive the more interesting.

It is natural that differences of opinion will arise amongst the chemists who study reaction mechanisms. Organomagnesium compounds are no exception. Disagreements about experimental results and their interpretation should, however, be welcomed since they often serve as a stimulus, to increase the efforts directed towards the subject.

The present review will, because of the complexity of the Grignard reagents, begin with a discussion of some physical and chemical properties of the reagents. Section 1.3 is concerned with the reactions of benzophenone with Grignard reagents. This is because benzophenone has, for many years, been a favourite substrate for researchers in the field and because observations made with benzophenone are valuable for the understanding of other reactions. Section 1.4 deals with concerted reaction mechanisms with carbonyl compounds. Section 1.5 concerns reactions with α,β-unsaturated carbonyl compounds and Section 1.6 concerns non-carbonylic substrates which react by stepwise radical type mechanisms.

1.2 PROPERTIES OF GRIGNARD REAGENTS

1.2.1 Thermochemistry

1.2.1.1 Heat of Formation of Grignard Reagents

The enthalpies of formation of the ethereal solutions were determined for 24 different alkyls by determining the heats of reaction of alkylmagnesium reagents with hydrogen bromide [4,15]:

$$RMgBr + HBr \longrightarrow RH + MgBr_2 \qquad (1.3)$$

The results were checked by measuring the heats of reaction of the formation reaction:

$$RBr + Mg \longrightarrow RMgBr \qquad (1.4)$$

The heats of formation of Grignard reagents in diethyl ether are given in Table 1.1. In comparison with alkyl halides the relative stability of isomeric alkylmagnesium compounds is reversed and follows the sequence primary > secondary > tertiary, for example propyl > isopropyl. In *t*-butylmagnesium bromide the destabilizing effect of the extra α-methyl group is slightly overcompensated by the stabilizing effect of the chain branching, and $-\Delta H_f^\circ$ decreases in the order: isobutyl > butyl > *t*-butyl > sec-butyl.

1.2.1.2 C–Mg Bond Dissociation Energies

The carbon–magnesium bond is rather weak. *t*-Butylmagnesium bromide in diethyl ether undergoes homolytic fission at temperatures between 140° and 200°C according to

$$(CH_3)_3C{-}MgBr \longrightarrow (CH_3)_3\dot{C} + \dot{M}gBr \qquad (1.5)$$

$$\dot{M}gBr + (CH_3)_3\dot{C} \longrightarrow (CH_3)_2C{=}CH_2 + HMgBr \qquad (1.6)$$

Reaction (1.5) showed a positive entropy of activation (12 e.u.) and an activation energy of 40 kcal mol^{-1}. It seems that the rate-determining step for alkene formation is simple homolytic fission of the C–Mg bond and the strength of the C–Mg bond in this reagent is therefore 40 kcal mol^{-1} or slightly greater [4].

Using D(*t*-Bu-MgBr) as an anchor point, the bond strengths in the various alkylmagnesium reagents were obtained from the enthalpies of reaction (1.3). In this reaction the R–Mg bond is broken and the R–H bond formed. By assuming that the differences between the heats of vaporization of RH and RMgBr and between the heats of solution of RH and RMgBr vary very little with R, estimated values for D(R-MgBr) for

Table 1.1. Enthalpies of formation of alkylmagnesium bromides dissolved in diethyl ether and thermochemical bond dissociation energies for the C–Mg bond

R in RMgBr	$-\Delta H_f^\circ$ [RMgBr] (kcal mol^{-1})	D(R-MgBr) (kcal mol^{-1})
Methyl	79.3	60
Ethyl	77.2	49
Propyl	86.2	50
Isopropyl	81.2	44
Butyl	90.4	51
s-Butyl	88.0	44
Isobutyl	93.6	51
t-Butyl	88.6	42
Pentyl	97.2	50
3-Pentyl	93.2	45
Neopentyl	102.8	54
Hexyl	102.2	50
Heptyl	108.1	50
Cyclopropyl	50.5	
Cyclobutyl	54.9	49
Cyclopentyl	80.5	47
Cyclohexyl	90.9	45
Cycloheptyl	90.7	46
Vinyl	63.2*	69
Allyl	63.5	48
Benzyl	60.3	47
Phenylethynyl	16.6	
4-Methylphenyl	58.5	
Phenyl	49.8	69
4-Chlorophenyl	60.1	
Triphenylmethyl	28.8	

*in THF

ethereal Grignard reagents were obtained as shown in Table 1.1.

The Oxygen–Magnesium Bond

The magnesium atom in organomagnesium reagents and in magnesium halides has Lewis acid character and forms coordinative bonds to donor atoms. In a magnesium alkoxide the oxygen forms a polar bond, but also shares its lone pairs with magnesium by back donation [16]. The result is a very strong bond. This is seen, for example, from the strikingly high heats of reaction of Grignard reagents with alcohols. The magnesium in a magnesium alkoxide is no longer electrophilic and does not form coordinative bonds to solvent molecules. In the infrared spectrum, the absorptions of free ether are different from the absorptions of ether coordinated to magnesium. Solutions of magnesium halides and Grignard reagents have magnesium complexed ether, but magnesium alkoxides do not [17].

The reactivity of dialkylmagnesium is in certain respects increased by the addition of potassium alkoxide [18,19]. The reason for this may also be the strong bonding between magnesium and oxygen, which will increase the anionic character of R by the formation of magnesate:

$$R_2Mg + R'OK \longrightarrow R_2MgOR'^-K^+ \qquad (1.7)$$

or to a minor extent even alkylpotassium:

$$R_2Mg + 2R'OK \longrightarrow (R'O)_2Mg + 2RK \qquad (1.8)$$

1.2.2 Oxidation Potentials of Grignard Reagents

Ethereal solutions of Grignard reagents have a certain electrical conductivity. Alkyl radicals are formed at the anode and magnesium at the cathode. It was found by Evans that electrolytic decomposition of the reagents at platinum electrodes takes place at potentials which vary with the alkyl [20], and Evans gave a list of 'decomposition potentials'. By the use of suitable procedures

Table 1.2. Standard oxidation potentials, E_{ox}, at a platinum anode for solutions of alkylmagnesium bromide in diethyl ether relative to SHE (saturated hydrogen electrode). Also shown are the relative decomposition potentials, E_{dec}, by electrolytic decomposition of the reagents between platinum electrodes in diethyl ether

Reagent	E_{ox} (volt)	E_{dec} (volt)
CH_3MgBr	−0.25	1.94
C_2H_5MgBr	−0.66	1.28
C_3H_7MgBr		1.42
i-C_3H_7MgBr	−0.95	1.07
C_4H_9MgBr	−0.53	1.32
i-C_4H_9MgBr	−0.63	
s-C_4H_9MgBr	−0.87	1.24
t-C_4H_9MgBr	−1.07	0.97
C_6H_5MgBr	−0.05*	2.17
$C_6H_5CH_2MgBr$	−0.73	
$CH_2{=}CHCH_2MgBr$	−1.16	0.86
c-C_5H_9MgBr	−0.88	

*estimated

it has been possible to determine standard oxidation potentials relative to SHE (saturated hydrogen electrode) for many types of Grignard reagents [21,9] (Table 1.2).

C–Mg bond dissociation energies correlate fairly well with the oxidation potentials of the Grignard reagents in the sense that a difference in bond dissociation energy of 23 kcal mol^{-1} corresponds roughly to a difference in oxidation potential of 1.00 V [22]. The fact that the slope of the plot is near unity indicates that, although the entropy contribution is unknown, both one-electron oxidation of the Grignard reagents and C–Mg homolysis of the reagents lead to a free radical and an inorganic magnesium species. Very little bonding is indicated between the alkyl radical and the magnesium ion. The one exception is allylmagnesium bromide, which is much more easily oxidized than would be expected from its thermochemical bond dissociation energy. A possible explanation would be that one-electron oxidation of this reagent produces an allyl radical and a magnesium ion which are still in some way bonded.

1.2.3 Association Equilibria in Grignard Reagents

1.2.3.1 The Schlenk Equilibrium

The equation:

$$R_2Mg + MgBr_2 \rightleftharpoons 2RMgBr$$

is an oversimplification for a complex system of fast exchange reactions of ligands (alkyl, halogen, ether molecules) around the magnesium atoms in a solution of a Grignard reagent. The position of the equilibrium is also influenced by the association and aggregation of the individual Schlenk components.

The reaction of $MgBr_2$ with R_2Mg is often exothermic in ether but endothermic in THF (tetrahydrofuran), and the equilibrium may lie far to the right in ether but be near statistical distribution in THF. Values have been found for K_{eq} by thermometric titration, [23] by NMR [24] and by infrared spectroscopy [25].

A value for K_{eq} may be found using kinetic experiments, since dialkylmagnesium and alkylmagnesium halide have widely different reactivities and the Schlenk equilibrium can be manipulated by the addition to a Grignard reagent of extra dialkylmagnesium or magnesium halide [26,27,34].

1.2.3.2 Self Association in Grignard Reagents

Organometallic compounds of Li, Be, and Al form electron deficient bonds. An alkyl group may be shared by a number of metal atoms. For Li and Al the compounds are well defined aggregates of high stability and the existence of the aggregates has a profound influence on the reactivity of alkyllithium and alkylaluminium reagents. Grignard reagents in ether solution form aggregates, presumably via Mg–X–Mg bonding. The degree of aggregation has been studied by osmometric measurements of vapour pressure over the solutions [7,28,29,30]. The presence of monomeric RMgX was denied in 1957 and it was postulated that exchange of R between magnesium atoms was not possible [31]. The work of Ashby as well as that of Vreugdenhil and Blomberg showed that solutions of Grignard reagents are, with the exception of alkylmagnesium chlorides, monomeric at high dilutions [29,30]. Alkyl exchange between the Schlenk components is therefore very fast. Aggregates with an average content of 2–4 molecules are formed at higher concentrations of Grignard reagents, although alkylmagnesium chlorides are dimeric at any concentration. In THF, Grignard reagents are monomeric [29].

In contrast to alkyllithium reagents the association of Grignard reagents has little influence on the reactivity of the reagents. Reactions of Grignard reagents at high dilution are first order with respect to both reagent and substrate. A plot of rate versus [RMgX] often tends to level off at concentrations above 0.1 M, meaning that the apparent reaction order with respect to the Grignard reagent is decreasing and may approach zero. If aggregates of Grignard reagents were of low reactivity, aggregation could be the cause for the rate levelling. It has been found, however, that rate levelling is seen only with substrates which are

Lewis bases, while reactions with substrates of low basicity (benzonitrile [32] or methyl trifluoroacetate [33,34]) show first order dependence on the Grignard reagent even at high concentrations. The limitation of the reactivity at higher concentrations is then correlated to association between reagent and substrate and not to association between reagent molecules [33,35] (see below).

Since alkoxides formed in the reaction of Grignard reagents form complexes with the Schlenk components, the usual way to measure reaction rates has been to use very low concentrations of substrate and obtain pseudo first-order conditions.

Grignard reactions which are higher than first order with respect to the reagent have not been reported. Although reaction mechanisms have been suggested in which two molecules of RMgX are required in the rate determining step [36,37], there has been no reliable kinetic support for termolecular reaction mechanisms.

1.2.3.3 Association between RMgX and Carbonyl Compounds

The reactivity of aliphatic ketones and esters toward Grignard reagents in diethyl ether varies with the concentration of the reagent in a way which is best explained [33,38] by the formation of a 1:1 complex in a very fast equilibrium:

$$R_2C{=}O + RMgX \rightleftharpoons [R_2C{=}O, RMgX] \quad (1.9)$$

$$\frac{[R_2CO,RMgX]}{[R_2C{=}O][RMgX]} = K_{eq} \quad (1.10)$$

K_{eq} has been determined by IR and by UV spectroscopy and increases with the Lewis acidity in the series: $R_2Mg < RMgCl < RMgBr < RMgI$ and with the Lewis basicity in the series: $RCOOR < ArCOAr < ArCOR < RCOR$ [33]. A direct relation between the observed reaction rates and the position of equilibrium (1.9) has been demonstrated for substrates like acetone, methyl acetate [33], alkylisocyanates [35], and 2,4-dimethyl-4′-methylmercaptobenzophenone [39,40] reacting with reagents like butylmagnesium chloride, bromide, and iodide as well as methyl and cyclopentylmagnesium bromides. The rate has been found to increase in proportion to the amount of coordinated substrate. The maximum rate is reached when coordination is close to 100%. The findings have been taken as a confirmation of the theory put forward by Meisenheimer [41] that complex formation is the first step in the addition reaction.

The constant relation between the numerator and the denominator in equation (1.10), however, makes it impossible to decide if the reaction takes place by rearrangement of the complex or by the encounter of a molecule of Grignard reagent and a molecule of uncoordinated substrate. In the case of acetone or methyl acetate reacting with butylmagnesium bromide it was found that an excess of the substrates led to extremely high reaction rates and this may indicate that the complex is a 'blind alley' and not the first step of the addition [9,34]. It is possible that two types of complexes exist, one of which, for stereochemical or other reasons, is inactive but easy to observe in IR or UV spectra. The observable complex has been named a sigma complex. A pi complex, which is not observed by IR spectroscopy, may be reactive and lead to product(s).

Coordination equilibria such as (1.9) are observed by IR spectroscopy in diethyl ether. In strongly coordinating solvents like THF the equilibrium constant is extremely small because the solvent displaces the substrate from magnesium. In accordance with this the kinetics for the reaction of acetone with butylmagnesium bromide in this solvent is first order in reagent and in substrate and the rate is not levelling off with increasing reagent concentration as seen when ether is the solvent [33].

Sigma complexes as above are observed with dialkyl and alkyl-aryl ketones. Diaryl ketones probably form sigma complexes, but the equilibrium cannot be observed by IR spectroscopy. The kinetics for the reaction of 2,4-dimethyl-4′-methylmercaptobenzophenone with methylmagnesium bromide have been interpreted as indicating rearrangement of a complex [40]. If this is correct the equilibrium constant is lower than for dialkyl ketones.

When very dilute solutions of benzophenone in ether (pseudo first-order concentrations) react with solutions of *t*-butyl- and isopropylmagnesium halide of increasing concentrations, a rate-levelling effect is observed at 0.1–0.2 M [26]. The use of benzophenone in excess leads to extremely high reaction rates. These phenomena are of course reminiscent of the complex-type kinetics of acetone [42]. As will be described below, *t*-butyl- and isopropylmagnesium halides react with benzophenone by an ET-radical mechanism (ET is electron transfer) and acetone by a concerted mechanism. It therefore seems strange to have 'complex' effects for both.

A significant difference is seen, however, when the solvent is changed from ether to THF since the reaction of *t*-Bu and *i*-Pr reagents with benzophenone is accelerated about 20 times [43]. THF does not accelerate the reaction of acetone with RMgX or the reaction of benzophenone with methyl- or primary alkylmagnesium halides. The reaction of azobenzene with butylmagnesium bromide by an ET-radical mechanism is faster in THF than in ether [44].

1.3 REACTIONS OF BENZOPHENONE(S) WITH GRIGNARD REAGENTS

1.3.1 Prediction of a Radical Mechanism and Early Evidence

While methyl, ethyl, phenyl, and benzylmagnesium halides produce high yields of the 1,2-addition product in the reaction with benzophenone, it was found in 1929 that propylmagnesium bromide, besides the 1,2-addition product, afforded about 50% of the reduction product benzhydrol [3]. Although it has later been found that this is probably formed in a non-radical process, it nevertheless inspired Blicke and Powers in 1929 to suggest a mechanistic scheme, which at the time of its presentation was speculative, but which is now considered to be a good explanation of most of the experimental facts. What they suggested was an induced homolysis of the Grignard reagent with the production of an alkyl radical and magnesium benzophenone ketyl. Recombination of the radicals would be possible in various ways:

$$RMgX + Ph_2CO \longrightarrow \underset{a}{Ph_2\dot{C}OMgX} + \underset{b}{\dot{R}}$$

$$a + b \longrightarrow \text{1,2-addition product}$$
$$a + b \longrightarrow \text{benzhydrol} + R_{-H}$$
$$b + b \longrightarrow R\text{-}R + R_H + R_{-H}$$
$$a + a \longrightarrow \text{benzopinacol}$$

SCHEME 1.2

The scheme would allow the formation of addition and reduction products as well as benzopinacol and the hydrocarbons R_{-H}, R_H, and R–R.

At the time of this proposal, benzopinacol had not been observed in Grignard reactions with benzophenone and there was the problem that the ketone might be reduced to benzopinacol by particles of magnesium suspended in the reagent [45]. However, it was found that in the reaction of cyclohexylmagnesium chloride with benzophenone, benzopinacol was formed even when using filtered Grignard solutions made from sublimed magnesium [46].

Benzopinacol formed as a by-product was proof that the homolytic mechanism was responsible at least for a part of the reaction. In 1964 two groups found ESR signals from benzophenone ketyl during the reaction of various types of Grignard reagents including phenyl-, butyl-, and benzylmagnesium halides [47,48]. This was an indication that a homolytic mechanism was in operation, but like the finding of 'radical' by-products like benzopinacol it was not possible to tell if the ESR signals were due to a minor side reaction.

The next step in the development was the finding in 1968 [49,50] that in THF using highly purified neopentylmagnesium chloride, the reaction with benzophenone produced a normal 1,2-adduct, but also a 20% yield of benzopinacol and an equivalent amount of neopentane from the neopentyl radical. The result showed that 20% of a primary Grignard reagent had acted by homolysis, but did not reveal if the 80% 1,2-adduct, neopentylbenzhydrol, was formed by radical recombination or by a concerted

mechanism. The authors, however, mentioned the possibility that an unknown fraction of the addition product might have been formed by radical recombination. In the mid-sixties this suggestion stirred the attention of chemists in the field because the Blicke–Powers theory now had a relevant experimental foundation.

Neopentylmagnesium chloride is an unusual reagent because of its extreme bulk and THF has much more solvating power for organometallic species than diethyl ether, which is the commonly used solvent for Grignard reagents. Both factors would promote the operation of a homolytic mechanism as the alternative to a concerted reaction, which would operate with less hindered reagents in less solvating solvents.

Observations were published [51] in 1968 on the course of addition of Grignard reagents to benzophenone using the solvent hexamethylphosphortriamide (HMPT), which has extremely high solvating powers. It was found that, depending on the nature of the alkyl, stable ESR signals for benzophenone ketyl were measured in concentrations up to 0.8% of added benzophenone. The ESR signals increased in the series: Ph < *n*-Bu < *t*-Bu < benzyl, and for solvents in the series: Et_2O < $(Et_3)N$ < THF < DME ≪ HMPT. By the use of fluorenone and benzylmagnesium chloride the yield of stable ketyl signals was 36%!

The results described again showed that homolysis is a realistic mechanistic alternative if provoked by steric bulk and/or strong solvation.

1.3.2 Reactivity Series and Linear Free Energy Correlations

In 1971 a study was made of the kinetics of the reactions of Grignard reagents with benzophenone using diethyl ether as the solvent [52]. Included was an investigation of the products formed in the reaction. For *t*-butylmagnesium chloride it was found that 50% of the product was the 1,4-dihydro-4-*t*-butylbenzophenone. 44% was normal 1,2-addition product and 6% was benzopinacol. 1,6-addition to unsubstituted benzophenone had never been observed before, evidently because the product easily oxidizes in air and decomposes thermally below 100°C.

For a series of substituted benzophenones the product distributions varied between 0 and 55% 1,2-addition, 0–39% 1,4-addition, 0–100% 1,6-addition and 0–21% benzopinacol (Table 1.1 in [52]).

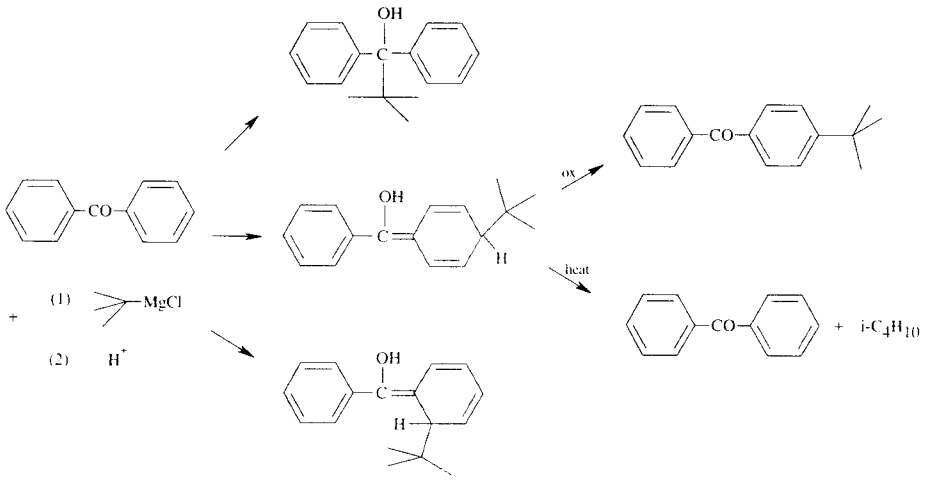

SCHEME 1.3

Although the product distribution was thus extremely sensitive to steric factors, the overall reaction rate was not, since a linear Hammett plot was obtained for log rate versus the sum of the substituent constants. An *ortho* methyl in benzophenone suppressed the ratio of 1,2-addition from 44% to 0%, while a *para* methyl increased it to 55%. With a bulky *t*-butyl or Cl in the *para* position a large fraction of 1,4-addition product was found. The effect of an *ortho* methyl group on the overall rate was the same as the effect of a *para* methyl group. Since a regular Hammett plot, Fig. 1.1, could be made for the overall reaction rate there had to be a common rate-determining step. The initial step was suggested to be ET with production of the ketyl and the *t*-butyl radical. In this case the conclusion concerned both the 'normal' 1,2-addition products and the 'abnormal' free radical type products.

The case for a radical mechanism in the reaction of tertiary Grignard reagents with benzophenone seemed clear. Secondary reagents, like the tertiary, produced 1,2- and 1,6-addition products and again a radical mechanism was indicated. For primary, aromatic, allylic, and benzylic reagents, the mechanism was an open question since the product distribution gave no clues. That electron transfer was possible from the primary neopentylmagnesium chloride had been shown [20], but the steric hindrance and the use of THF might, in this case, have given a normally slow homolytic mechanism a chance.

The question of homolytic or concerted mechanisms for the reactions of primary reagents with benzophenone has not been definitively answered even today and a large number of mechanistic tools have been applied attempting to get to the bottom of this problem.

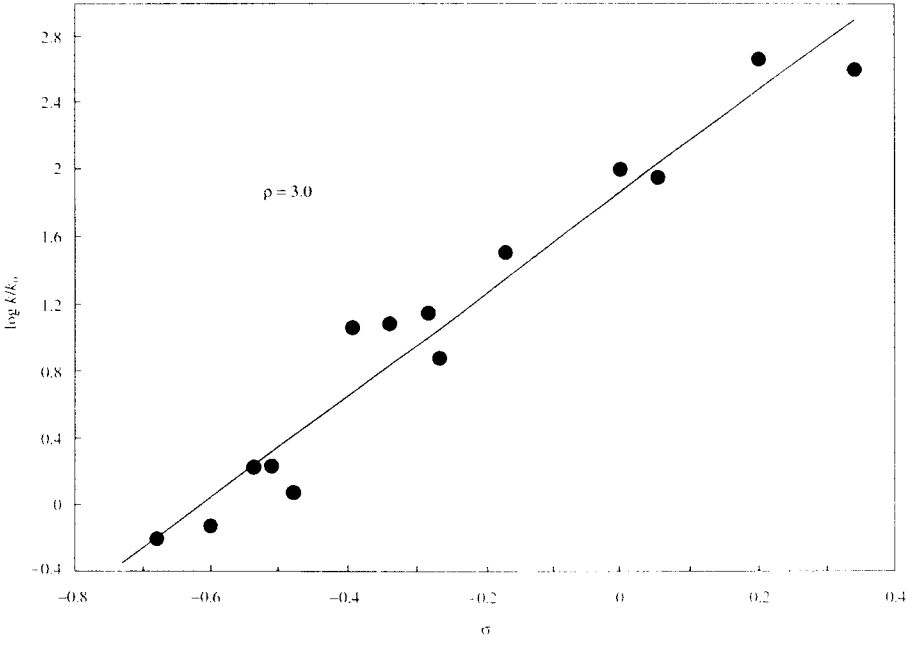

Fig. 1.1. Hammett sigma values against log k_{obs} for the reaction of *t*-butylmagnesium chloride in diethyl ether and substituted benzophenones at 20 C.

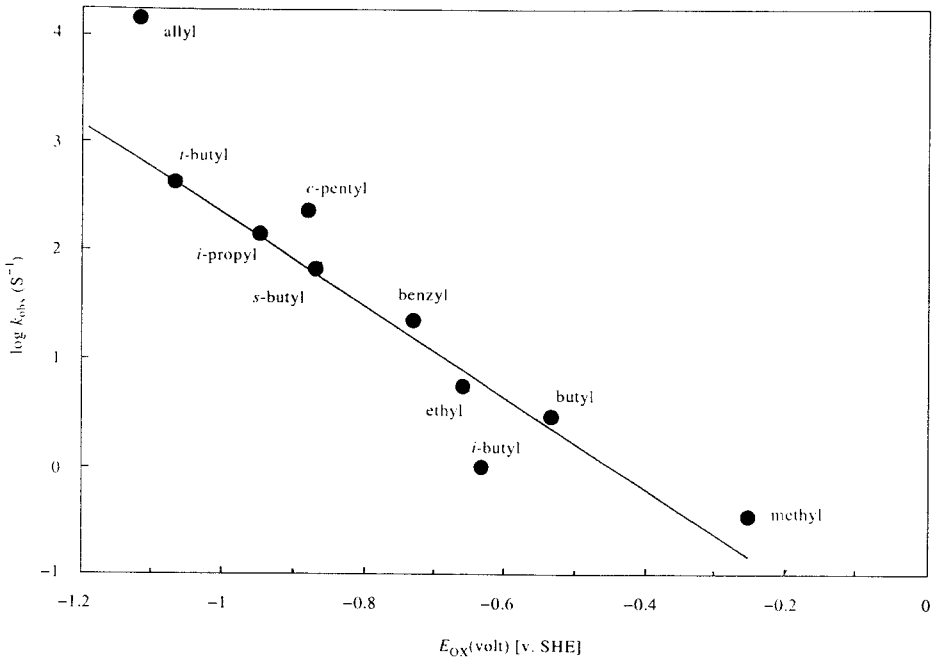

Fig. 1.2. Oxidation potentials of Grignard reagents against pseudo first-order rate constants for the reaction of alkylmagnesium bromides (0.02 M) in diethyl ether with benzophenones (0.25 M at 20°C).

In electron transfer from a Grignard reagent the reagent is oxidized and the substrate is reduced. A plot of the logarithm of the rates of reaction of benzophenone with a series of Grignard reagents versus E_{ox} for the reagent, was linear with certain points falling above or below the plot.

This was interpreted as indicating that the reactions have related mechanisms and that the mechanisms are ET-like. It may be possible, however, that there is a close race between a concerted mechanism and the ET mechanism or that a spectrum of hybrid mechanisms are in operation ranging from clear-cut ET with secondary and tertiary reagents to hybrid radical-concerted mechanisms (see the following section) for primary reagents.

The plot shows that allylmagnesium bromide and cyclopentylmagnesium bromide react faster than the plot of E_{ox}/log rate would indicate, and in both cases concerted six-centre mechanisms are possible alternatives. The mechanisms are shown in Section 1.3, Scheme 1.9, (b) and (a), respectively.

Characteristic for ET reactions with Grignard reagents is that steric requirements are rather low and in principle the relative reactivities of the various types of Grignard reagents might be independent of steric factors. In concerted reactions the steric factor is all-important and, as the reactivity series is useful for distinguishing between S_N1 and S_N2 reactions in nucleophilic substitutions, it should be useful for distinguishing between ET and concerted mechanisms in the reactions of Grignard reagents. The reversal of the reactivity series when going from benzophenone to, for example, benzonitrile was noted by Swain as early as in 1947 [32].

Acetone is a rather unwilling electron acceptor and its reactions with most Grignard reagents must be by polar concerted mechanisms. The reactivity series for the reactions is: allyl > $PhCH_2$ > Ph > Et > Me > Bu > *i*-Pr > *t*-Bu. For benzophenone the series is: allyl > *t*-Bu > *i*-Pr > Et > Pr > Bu > Me > Ph. [9,26]

The two sequences typically represent concerted polar and ET-radical mechanisms. For many substrates the reactivity series are closely related to one or the other. But as will be described later, ET reactions are not totally without steric requirements and concerted reactions are sensitive to both steric and electronic factors. For most Grignard substrates the reactivity series found is therefore unique, but will normally have features in common with either the 'acetone' series or with the 'benzophenone' series. As a rule of thumb it may be said that if phenylmagnesium bromide, which has the strongest C–Mg bond, reacts much faster than *t*-butylmagnesium bromide with the weakest C–Mg bond, the mechanism is concerted, and if on the other hand *t*-butyl is much faster than phenyl, the mechanism is ET.

1.3.3 Radical Probes

Newer developments in the study of the reactions of benzophenone with Grignard reagents have been the use of radical probes. If the alkyl of the reagent has the ability to undergo isomerization as, for example, cyclization or *cis–trans* isomerization, while it exists as a free radical, it is possible to get information about the rate of recombination of alkyl and ketyl in the formation of the various reaction products. 5-Hexenylmagnesium bromide has been used in the study of the free radical type mechanism by its reactions with oxygen [53,54], and the rate of cyclization of the 5-hexenyl radical was known to be 10^5 s^{-1}.

Fig. 1.3.

The probe is useful as a 'radical clock' since it is as mentioned above possible to measure the time spent between the ET and the radical recombination. Cyclization during the reaction is a proof of a radical mechanism (at least for the cyclized part), but that no cyclization has taken place is not a proof against a radical mechanism, but only tells that if a free radical was produced, its lifetime was significantly less than ca. 10^{-6} s.

Although the cyclizable 5-hexenyl probes have been very widely used, other radicals, which in the free state rearrange very fast, have been used either in the alkyl of the Grignard reagent or as the substrate. *cis*-Tetramethylheptenone (*t*-BuCH=CHCO*t*-Bu) for example will rearrange to the *trans* isomer after being converted to the anion radical by accepting an electron [55,56].

In 1977 and 1981 Ashby and Bowers very imaginatively used the 5-hexenyl probe to shed light on the mechanism of reaction of Grignard reagents with benzophenone [57,58]. By the introduction of methyl groups α or β to the magnesium-carrying carbon, tertiary and neopentyl-like reagents were prepared. In the reaction of the simple primary 5-hexenyl reagent the 1,2-addition product obtained was uncyclized. Reaction of the tertiary reagent (1,1-dimethyl-5-hexenylmagnesium bromide) produced an uncyclized 1,2-addition product and a 1,6-addition product, in which cyclization had occurred, Scheme 1.4:

In THF, however, both 1,2- and 1,6-adducts had a cyclized structure. The primary neopentyl-like reagent (2,2-dimethyl-5-hexen-1-ylmagnesium bromide) in diethyl ether surprisingly produced a cyclized 1,2-addition product [58].

In their interpretation the authors assumed that all 1,2-addition in this reaction (cyclized or straight chain) is produced by radical recombination within the solvent cage. Since the lifetime of the cage is 10^{-9} s and the rate of cyclization is 10^5; it is, however, obvious that radicals must escape the cage and diffuse for a period of at least 10^{-6} s. In THF the results with the tertiary reagent are explained simply by diffusion of all the alkyl and ketyl radicals out of the cage and the re-encounter and recombination of the radicals after cyclization

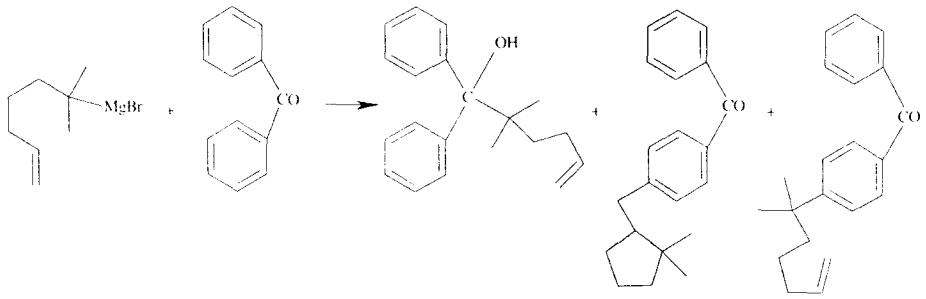

SCHEME 1.4

of the 5-hexenyl chain. The result obtained in diethyl ether is more complicated since the 1,2-addition product is straight chain and the 1,6-product is cyclized. The problem that a reaction produces both a cyclized and a straight chain product is not unique. In the addition of simple primary 5-hexenylmagnesium bromide to benzil the *O*-alkylated product is straight chain and the C-alkylated product is cyclized [59]. In two different addition products to phenyliminophenylindole the ratio of straight chain to cyclized product is 1:1 and 1:3, respectively [60].

An explanation is needed for the large difference in the ratios cyclized/straight chain in products, which all seem to be formed by radical recombination.

In an investigation [61] of the Wittig rearrangement, in which a ketyl and the 5-hexenyl radical were generated by deprotonation of benzhydryl-5-hexenyl ether, the author distinguishes between pairs of radicals which diffuse together randomly (*R*-pairs) and radical pairs which are generated in a well defined position which is favourable for recombination (*S*-pairs).

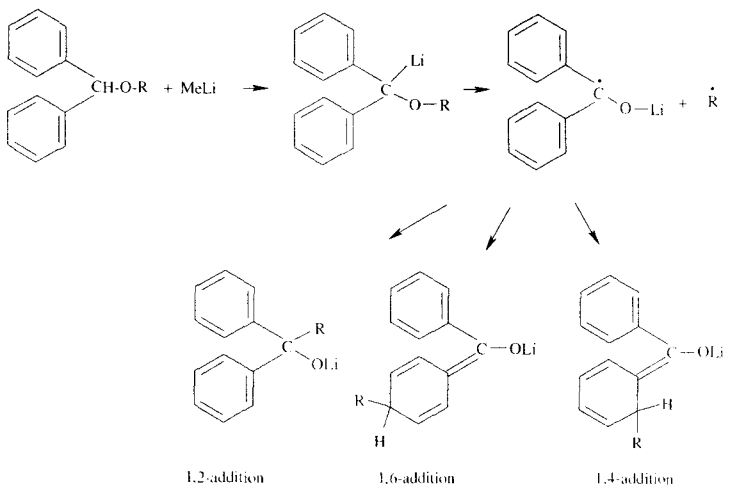

SCHEME 1.5

From the degree of alkyl cyclization found in the products, the rates of radical recombination can be calculated. In the Wittig rearrangement the ketyl and the alkyl radicals are produced as *S*-pairs. The radicals are born close to each other, a situation which invites immediate 1,2-addition within the cage to form an open chain adduct. A fraction of the radicals diffuse and recombine as cyclized 1,4- or 1,6-adducts.

In the analogous Grignard reaction, radical pairs in a favourable position would likewise be obtained if the ET transition state had a more or less defined structure. If ET takes place from the carbon magnesium bond to the carbonyl carbon and requires a certain minimum distance between the two carbons, then some of the radicals formed will be *S*-pairs capable of immediate 1,2-addition.

It would seem to be a reasonable argument that a reaction in which radicals form and recombine without delay is indistinguishable from the concerted reaction mechanism. It is, however, possible to distinguish between them by measuring the relative reactivity of various alkylmagnesium reagents in the two reactions. Garst suggested the word 'radical-concerted' for the mechanism in which immediate recombination of radicals take place [61]. The reactivity series of alkylmagnesium reagents in a radical-concerted reaction will be different from the reactivity series for a truly concerted reaction. It seems possible that the mechanisms of reaction of methyl- and especially of primary alkylmagnesium reagents are radical-concerted in this sense.

The problem of cage products versus escape products in the reactions of benzophenone and Grignard reagents was discussed in a review by Walling [62], who calculated the outcome of reactions of benzophenone ketyl using plausible estimates for the rate constants of the various radical–radical recombinations. He concluded that:

1) In an ET reaction yields of normal addition products can be near quantitative without invoking cage processes. Low ketyl yields are not evidence that only a small fraction of reaction involves ET.
2) Ketyl concentration builds up rapidly and persists after the reaction is complete.
3) High reaction rates give high yields of ketyls and by-products.
4) Under most assumed conditions radicals will have long enough lifetimes to undergo rearrangements which have rate constants of ca. 10^{-5} or greater.
5) Small amounts of traps for R or ketyls may have little effect on the products.

1.3.4 A Thermochemical Approach

An analysis of the Arrhenius activation energy for the reaction of *t*-butylmagnesium chloride with benzophenone showed near identity of the heat of formation of the transition state with the sum of the heats of formation of magnesium benzophenone ketyl and *t*-butyl radical in ether solution [22]. The same was true for secondary reagents, while for primary reagents and for methyl the TS was 4–10 kcal mol^{-1} more stable than the free radicals. The interpretation was that electron transfer is simultaneous with magnesium transfer. Analogously it has been shown that electron transfer and transport of sodium between benzophenone and its sodium ketyl takes place simultaneously [63]. An outer sphere ET preceding magnesium transfer would yield a pair of radical ions of an impossibly high energy since the stabilizing bonding between magnesium and oxygen would be missing.

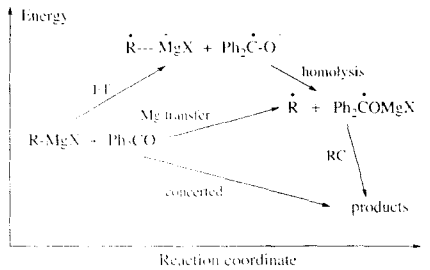

SCHEME 1.6

For tertiary and secondary reagents the radicals are free to diffuse from each other, producing 1,4- and 1,6-addition products, while primary radicals

and methyl, because they have weak bonding to benzopinacol, do not leave the solvent cage and produce only 1,2-addition. Here again we have the problem of being able to distinguish between a truly concerted reaction and a radical-concerted mechanism and as mentioned above the only possibility seems to be to study the reactivity series, which may resemble either the 'acetone-series' or the 'benzophenone-series', respectively.

The results obtained with the tertiary 5-hexenyl probe (see above) indicate that even with tertiary Grignard reagents the alkyl radical has approached the carbonyl in the transition state so that immediate radical recombination in the cage may take place to a certain extent. The bonding, however, must be weak.

1.3.5 Kinetic Isotope Effects

1.3.5.1 Isotopic Carbon and Hydrogen in Benzophenone

Kinetic isotope effects, which are often a useful mechanistic tool, have been measured in several types of reactions of Grignard reagents including reactions with benzophenone. KIEs have been measured for the substitution of ^{13}C and ^{14}C in the carbonyl group in benzophenone and for deuterium substitution in the α and β positions of Grignard reagents. The effect of isotopic carbon in benzophenone has been studied by two groups. The results obtained are not in complete agreement.

^{14}C-KIEs were measured for the reactions of methyl-, phenyl-, benzyl-, allyl-, and *t*-butylmagnesium halide and the values for $^{12}k/^{14}k$ were in the order of 1.055 for phenyl and methyl, smaller for benzyl and close to unity for allyl and *t*-butyl [64]. To obtain an interpretation, the authors looked at the Hammett ρ for the effect of polar substituents in the benzophenone substrate. Methylmagnesium bromide and phenylmagnesium bromide show moderately sized positive values of ρ in their reactions with benzophenones. The *t*-butyl reagent has a very large positive ρ, while allyl has a ρ close to zero. ET to benzophenones was said to be without a significant KIE according to both experiment and theory. Based on the KIEs and the Hammett ρ values determined, it was concluded that among all the possible reaction steps shown in Scheme 1.7, electron transfer (a in Scheme 1.7) was rate determining for allylmagnesium bromide, while C–C bond formation (c in Scheme 1.7) was rate determining for the methyl

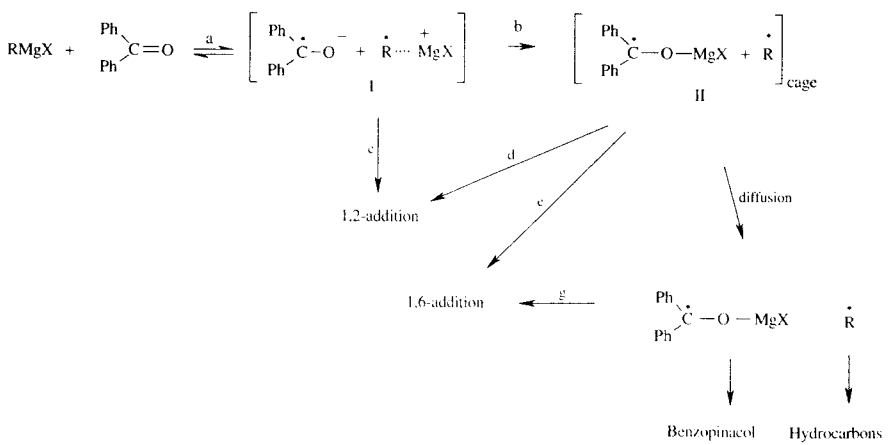

SCHEME 1.7

and the phenyl reagents. For *t*-butyl the rate was determined by an ET pre-equilibrium (a) combined with a rate determining rearrangement of I to II (b in Scheme 1.7).

The above described experiments and interpretations were questioned in an investigation in which ^{13}C KIEs were determined by a different approach [65]. The values for methyl and *t*-butyl Grignard reagents were found to be of the same magnitude. Since ET to benzophenone therefore had a significant kinetic isotope effect it was said to be incorrect to assign a rate-determining ET in the reaction of allylmagnesium bromide on the basis that the KIE was unity. The lack of effect of polar substituents on the rate of a reaction which consists of the transfer of negative charge to benzophenone also seemed strange. The high positive value of ρ which was found for the reaction of *t*-butylmagnesium chloride with benzophenone is and was an indication of a rate determining ET step for this reaction.

The KIE for introduction of 10 deuterium atoms in benzophenone was found to be $k_H/k_D = 1.095$ for the reaction with *t*-butylmagnesium chloride, but 0.986 and 1.000 for methylmagnesium chloride and allylmagnesium bromide. The values for isopropylmagnesium bromide and ethylmagnesium bromide are 1.087 and 1.015. These secondary isotope effects are high when there is a high development of charge in the TS, coinciding with high values of Hammett ρ. Secondary and tertiary Grignard reagents must react by clear-cut ET-homolytic mechanisms. Much less sensitive to polar substituents in benzophenone are the reactions of methyl and primary Grignard reagents, which react by more or less concerted hybrid mechanisms.

Allylmagnesium bromide has an extremely low ρ in the reaction with benzophenone. There is practically no charge development in the TS and the lack of a carbonyl carbon isotope effect shows a balanced formation and breaking of bonds to this carbon. This indicates a cyclic concerted mechanism, Scheme 1.9b, which is even faster than the rate predicted from the oxidation potential of this reagent. The reaction, unlike ET reactions, proceeds without coloration and without pinacol formation and, like concerted reactions, it is slowed by the presence of ortho methyl groups in the benzophenone. In the latter case the ET-homolytic mechanism becomes competitive as seen from the coloration which develops during the reaction of mesityl phenyl ketone.

The KIE for ^{18}O substituted benzophenone was found to be $k_{16}/k_{18} = 1.03$ for *t*-butylmagnesium chloride and 1.00 for methylmagnesium bromide [41]. Tentatively this may mean that the total bonding to oxygen is weaker in the TS for *t*-butyl than in the TS for methyl, in which ketyl formation is not completed.

1.3.5.2 Deuterium Substitution in the Grignard Reagent

1.3.5.2.1 Primary Isotope Effect on the Reduction Process

In their pioneering study in 1956 Dunn and Warkentin [66] showed that only hydrogen from the β-position is transferred from isobutylmagnesium bromide to benzophenone in the reduction process and that k_H/k_D is of the order of 2. A more exact value seems to be 2.3 as measured by the change in the ratio addition/reduction by introduction of a β-D in the isobutyl Grignard reagent [67]. Two β-Ds in butylmagnesium or six β-Ds in isopropylmagnesium bromide changed the addition/reduction ratio by factors of 1.62 and 1.48, respectively [9]. The variation in the KIE indicates variation in the transition state. The truly concerted 6-centre mechanism, Scheme 1.9a, has been suggested to be, for some reagent/substrate combinations, more or less radical-concerted [67]. Scheme 1.8.

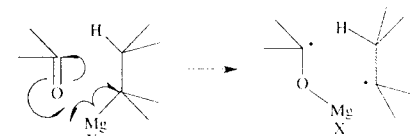

SCHEME 1.8

For a radical-concerted reduction a lower KIE would be expected.

1.3.5.2.2 Secondary Isotope Effects on the Addition Process

The effect of deuterium in the α and β positions of the Grignard reagent was measured in the reaction with aliphatic, aromatic, and α,β-unsaturated ketones [68,69]. All deuterium isotope effects were small. For the reaction of the aliphatic ketone, 2-octanone, inverse KIEs ($k_H/k_D < 1$) were found and the effect was of the order of 1% per D in the α or the β position. C_2D_5MgBr for example reacts with octanone with $k_H/k_D = 0.948$. The same reagent in the reaction with benzophenone showed k_H/k_D very near 1.00. For d_3 methylmagnesium bromide an inverse KIE of 3–4% was found for both octanone and benzophenone. Inverse values of k_H/k_D may be rationalized as due to less steric hindrance in the deuterio reagent [70], typical for a concerted mechanism. Substantial normal KIEs of the order of 5% were found for the addition reaction of d_6 isopropylmagnesium bromide to benzophenone. This result, like a similar rather significant normal KIE for the reaction of β-d_3 ethylmagnesium bromide with benzylideneacetophenone, indicates a homolytic reaction mechanism [68]. In the homolytic reaction the steric factor is of little significance and the effect observed is due to less hyperconjugative stabilization of a free radical by β-D than by β-H. With *t*-butylmagnesium chloride the KIE is much smaller, which was assumed to result from opposing steric and electronic effects.

α,α-Dideuteriopentylmagnesium bromide reacted with benzonitrile and with phenylacetylene with $k_H k_D$ very close to 1.00 [71].

For both isopropylmagnesium and *t*-butylmagnesium bromide the relative yield of 1,6-addition product is increased by using the perdeuterio reagent. The explanation may be that the diffusing *D*-alkyl radicals react more slowly by disproportionation than do the *H*-alkyl radicals.

1.3.6 CIDNP Observations

In the reaction of *t*-butylmagnesium chloride with benzophenone, escaped *t*-butyl radicals react by disproportionation forming isobutane and isobutene. CIDNP signals were observed for the vinylic protons of isobutene [72].

1.3.7 A New School in the Study of the Reaction of Benzophenone with Grignard Reagents

The lack of consensus among chemists engaged in mechanistic work with Grignard reagents and benzophenone was not limited to the interpretation of kinetic isotope effects and Hammett parameters. In 1986 the reaction of Grignard reagents with benzil in THF solution was investigated with the use of ESR [73]. Stable complexes were found. From an interpretation of the EPR spectra the complexes were suggested to contain a dimer of the benzil ketyl ion paired with two cation radicals of the Grignard reagent. A general scheme for the mechanism of the addition reaction to aromatic ketones was suggested, which deviated from earlier schemes by denying that ET is the slow, rate determining step. The slow step in the addition reaction was suggested to be a reaction between the above mentioned radical pair and an extra molecule of Grignard reagent. Rate constants were measured for the disappearance of the coloured complex in the presence of Grignard reagents of various concentrations.

The theory was opposed a year later in a new investigation of the reactions of benzil with Grignard reagents [59]. A very large fraction of *O*-alkylated product was, surprisingly, found to be produced together with normal *C*-alkylated products. The use of 5-hexenylmagnesium bromide gave a straight chain *O*-alkyl product, but a cyclized *C*-alkyl product. More importantly, thermographic rate measurements yielded reaction rates which were six times higher than the published rates for the disappearance of the coloured complex. Instead of being the rate of the addition reaction, the colorimetric rates were suggested to be the rate of reduction of escaped benzil ketyl to benzoin by the excess Grignard reagent. This was likely since benzoin was found among the reaction products. The theory that stable ion radical pairs can exist, which include cation radicals of Grignard reagents and ketyl radicals of benzil or of a benzophenone, had been presented earlier [74], when it was opposed for being an incorrect interpretation of the spectra [75], and for being unconvincing, since the lifetime of a cation radical of a Grignard reagent was suggested to be shorter than a millisecond [59] rather than being hours or years as suggested in Ref. [73].

The reaction scheme, which was proposed for the reactions of benzil in the 1986 investigation, was also proposed with small modifications for the reactions of benzophenone [76]. Blue and pink colours during the reaction in THF of butylmagnesium bromide with benzophenone were interpreted as monomeric and dimeric ketyl.

The rather surprising mechanistic scheme presented in Refs. [73] and [76] was assigned to benzophenone partly on the basis of experiments made with benzil. The present authors have had difficulty in finding a correlation between the experimental results reported and the conclusions made. The authors seem to be suggesting rather than concluding. This is unfortunate since the suggestions have later been referred to as facts. More explanations and more experimental details seem to be needed.

1.4 POLAR CONCERTED REACTION MECHANISMS

1.4.1 Addition to Aliphatic Ketones

In the previous section it was explained that the behaviour of Grignard reagents varies with their structure as well as with the structure of the substrates. As described in Section 1.2.2, Grignard reagents are ordered according to their ease of oxidation at a platinum anode and have characteristic oxidation potentials. *t*-Butylmagnesium bromide is easily oxidized, while methylmagnesium bromide and especially phenylmagnesium bromide resist oxidation. Carbonylic substrates likewise have reduction potentials, which are related to the possibility of resonance stabilization of the ketyl radical formed by ET. In simple aliphatic ketones little stabilization is possible and the reduction potential is very negative. Benzophenone, on the other hand, is easily reduced because the benzophenone ketyl is extremely well stabilized and is even stable in solution. As described in Section 1.3.1–1.3.5, *t*-butylmagnesium chloride transfers an electron to benzophenone in a very fast reaction, but methyl and phenylmagnesium bromides react hundreds of times more slowly.

The reaction of acetone with phenylmagnesium bromide is, however, very fast [26]. In this reaction there is obviously no need for an initial breaking of the carbon magnesium bond. In the reaction the new bonds are formed in concert with the breaking of the old bonds. The concerted reaction, however, requires a close approach of the two molecules.

Reactivity measurements using substrates with widely differing structures have given many clues to the stereochemistry of the transition states for concerted reactions. The magnesium atom is surrounded by coordinated solvent molecules and is bulky. The high reactivity of phenyl Grignard reagent toward acetone could be seen as a result of both molecules being flat and having the ability to align the C–Mg bond very close to the C=O bond, in spite of the aromatic π cloud, in a four-centre TS. Branching at the α-carbon as in isopropyl and *t*-butylmagnesium halide is a hindrance for the approach and *t*-butyl Grignard reagent reacts 420 times more slowly with acetone than does phenyl Grignard [26].

Even if the reaction is concerted, a charge is developed on the α-carbon in the TS. In benzylmagnesium bromide a phenyl group allows delocalization of this charge and the reagent is 1400 times more reactive toward acetone than is *t*-butylmagnesium bromide. The fastest reagent toward acetone is allylmagnesium bromide. The reason is that with this reagent the approach of the carbon atoms, which are to be bonded, are far removed from the bulky magnesium atom in a six-centre transition state, Scheme 1.9(b). The rate has not been measured, but is estimated to be at least 100 000 times faster than the reaction of *t*-butylmagnesium bromide and acetone [43].

Fig. 1.4.

Although the rate of reaction is mainly a question of steric requirements, it is not possible to find a reactivity series for the various Grignard reagents which is valid for many different substrates, simply because each pair of reagents has its own steric requirements. As mentioned, it is useful to compare the reactivities of *t*-butylmagnesium bromide and phenylmagnesium bromide toward a given substrate since the first mentioned has the weakest and the last mentioned the strongest carbon–magnesium bond among the common reagents [4]. At the same time *t*-butyl is extremely bulky and phenyl is fairly unhindered.

1.4.2 Addition to Acid Derivatives

Reactions of Grignard reagents with esters, acid anhydrides, acid chlorides, nitriles, etc. are useful in the preparation of ketones and tertiary alcohols. The reactivity of an unhindered ester is 50–100 times lower than that of a ketone. The low reactivity reflects the low polarization of the ester carbonyl group. The reaction rate for addition is highly dependent on the steric bulk of both the ester alkyl and the alkyl of the Grignard reagent. The first addition to an ester produces a hemiketal salt, which eliminates magnesium alkoxide and forms the ketone, which adds the second molecule of Grignard reagent. That the ketone is a true intermediate is proved by a detailed kinetic study of the rates of formation the various products and by-products [77].

1.4.3 Concerted Transfer of β-Hydrogen. Reduction

In a 1,2-addition the bond formation of carbon to carbon and oxygen to magnesium is concerted with the breaking of C–Mg and π C=O. This requires a four-centre transition state. If the reagent has hydrogen in a β-position, reduction of the carbonyl group by hydrogen transfer is an alternative to the addition process. In this process, shown in Scheme 1.9 (a), a C–H, a π C–C, and a Mg–O bond are formed in concert with the breaking of a C–Mg, a C–H, and a π C=O bond in a six-centre transition state [78].

Since the six-centre transition state is sterically less demanding than a four-centre transition state, reduction will tend to be important with bulky reagents. A syn-periplanar conformation is necessary for the six-centre reduction mechanism. For example, reduction takes place with the exo hydrogen in bornylmagnesium chloride and not with the endo hydrogen [79]. The reduction of benzophenone is 50 times faster with cyclopentylmagnesium bromide than with cyclohexylmagnesium bromide [80], which can be explained by the possibility of having a *cis* periplanar conformation, which is impossible with the cyclohexyl reagent. Reduction of achiral ketones with chiral Grignard reagents may induce chirality in the products [81]. The chirality of the reagent may reside in the alkyl or it may be introduced by using a coordinating chiral solvent.

The second alternative to the Grignard addition is enolization, which requires a hydrogen α to the carbonyl group. The mechanism has a six-centre cyclic transition state and like the reduction process has fewer steric requirements than does addition. [82,83], Scheme 1.9 (c). Branching at the carbons α to carbonyl slows the addition reaction and therefore increases the extent of enolization and reduction. Preparative additions to such ketones requires the use of alkyllithium reagents. The enols may be useful for synthetic purposes since they may add to the carbonyl group in added reactants or in the substrate itself.

Six-centre transition states for the reactions of a carbonyl compound with a Grignard reagent are very efficient if they allow the formation of a Mg–O bond in concert with the shifts of two pairs of π or σ electrons. Five examples are shown in Scheme 1.9 (a)–(e). Concerted reduction and enolization are mentioned above. The allylic addition, Scheme 1.9 (b), is efficient because of the absence of steric hindrance. The carbonyl carbon of an aldehyde may attack ortho to the side chain in benzylmagnesium chloride forming a reactive dihydrobenzene compound, which may add a second molecule of aldehyde, Scheme 1.9 (e) [84]. The conjugate addition to α,β-unsaturated carbonyl compounds, Scheme 1.9 (d), is treated in the following section. An objection to the

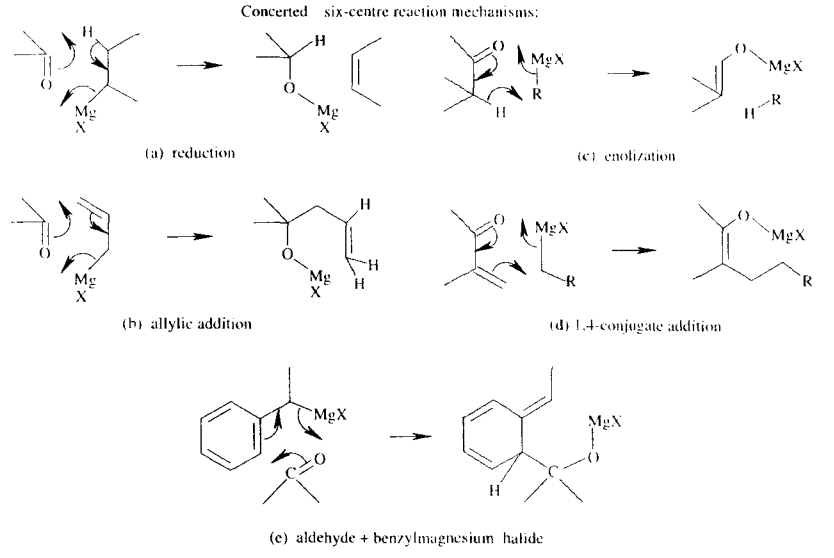

SCHEME 1.9

six-centre mechanisms based on orbital symmetry considerations has been published [5].

1.5 REACTIONS WITH α,β-UNSATURATED CARBONYL COMPOUNDS

α,β-Unsaturated ketones have interesting properties as substrates for Grignard reagents since they are intermediate between the aromatic ketones and the aliphatic ketones. They may accept an electron to form a resonance stabilized ketyl in which the spin is distributed between the carbonyl carbon and the β-carbon. On the other hand, the polarity of the C=O is transmitted through the double bond and the compound will accept a nucleophile at the β-carbon. Conjugate addition products therefore may result from either polar or from ET mechanisms. A truly concerted mechanism for 1,4-addition requires a six-centre TS and this means that C=O and C=C should have a cisoid conformation, Scheme 1.9 (d), as originally suggested by Lutz and Reveley [85].

The necessity of the cisoid conformation was questioned since 2-cyclohexenone, which has a transoid conformation, was able to form 1,4-adducts with various Grignard reagents. Recently it was found, however, that methyl- and phenylmagnesium bromide are unable to add 1,4 to an α,β-unsaturated substrate unless the cisoid conformation is possible [86]. Isopropyl- and *t*-butylmagnesium chloride do, however, react 1,4, but by a homolytic mechanism.

Two alkyls in the β-position are prohibitive for the concerted reaction and mesityl oxide does not add primary Grignard reagents 1,4. This steric hindrance is overcome by the bulky *t*-butylmagnesium chloride. A 25% yield of the overcrowded 4,4,5,5-tetramethyl-2-hexanone is obtained, which obviously is formed, Scheme 1.10, by recombination of magnesium mesityl oxide ketyl and *t*-butyl radical after an initial homolysis [86].

The importance of the cisoid conformation (Scheme 1.9 (d)) is seen from the fact that going from benzalacetone to benzalpinacolone increases the rate of formation of 1,4-adduct from

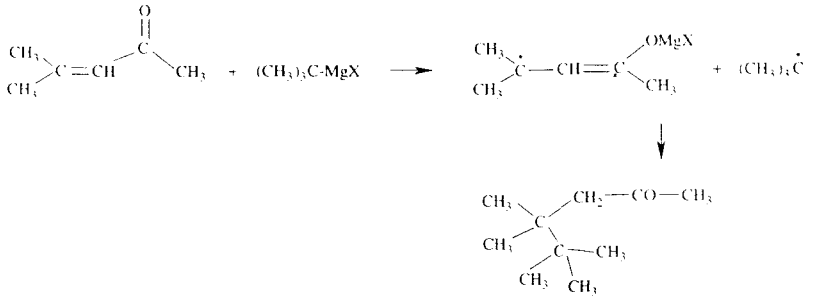

SCHEME 1.10

butylmagnesium chloride by a factor of 10. The reason is that while benzalacetone has a transoid conformation benzalpinacolone is forced to adopt a cisoid conformation because of the interaction between the *t*-butyl group and the distant vinylic hydrogen. The surprising implication is that the introduction of a tertiary butyl group accelerates a sterically demanding reaction [86].

With α,β-unsaturated ketones and esters both homolytic and polar concerted mechanisms may be operating, but combining the study of rate with the exact product distributions makes it possible to find the contribution from either mechanism in almost any reagent/substrate combination.

The use of cuprous salts as a catalyst increases the rate of 1,4-addition and is highly useful for preparative work [87]. Like the metal catalysed reactions described below in Section 6.1, the copper catalysed reactions are not reactions between a substrate and a Grignard reagent. What takes place is fast alkyl exchange between a copper salt and a Grignard reagent followed by a reaction between a complex alkylcopper compound and the substrate. The alkylcopper is regenerated from the addition product by a fast Mg/Cu exchange.

1.6 ET SUBSTRATES OTHER THAN BENZOPHENONE

Although the main subject of this review is reactions of Grignard reagents with carbonylic compounds, five examples of reactions will be mentioned in which the substrates are electron acceptors, but not carbonylic. Since the mechanisms of these reactions have been studied extensively the lessons learned are useful in the study of Grignard reactions in general.

1.6.1 Metal Catalysis

1.6.1.1 The Kharasch Reaction

From the early use of Grignard reagents it was known that certain of their reactions led to products which had to result from free radicals. Most obvious were reactions with alkyl halides, which when small amounts of metal salts were added could produce dimers of the Grignard alkyl along with radical disproportionation products and radical polymerization products of the alkyl of the halide. The reaction type is called the Kharasch reaction because Kharasch and coworkers studied the reaction in detail [88,89]. Pure Grignard reagents do not react with most alkyl halides. But Grignard reagents exchange alkyls very fast with metallic salts with the formation of alkylmetal halides or dialkylmetals:

$$RMgX + MX_2 \longrightarrow RMX + MgX_2 \qquad (1.11)$$

$$2RMgX + MX_2 \longrightarrow R_2M + 2MgX_2 \qquad (1.12)$$

The alkylmetals formed are unstable and dissociate according to either:

$$RMX \longrightarrow R\cdot + \cdot MX \quad \text{or:} \qquad (1.13)$$

$$R_2M \longrightarrow R{-}R + M \qquad (1.14)$$

The monovalent or zerovalent metal species are highly reducing and may react with alkyl or aryl halides:

$$\cdot MX + R'X \longrightarrow MX_2 + \cdot R' \quad \text{or} \qquad (1.15)$$

$$M + R'X \longrightarrow R'MX \qquad (1.16)$$

The reactions shown represent very fast catalytic cycles, which let a Grignard reagent reduce the alkyl halide, being itself oxidized to hydrocarbons via (1.14); alternatively, depending on the nature of R and R', the alkyl halide is reduced to free radicals, which recombine in various ways. The choice of metal may be the deciding factor for the usefulness of the reaction in the preparation of selected hydrocarbons [90].

1.6.1.2 Reductive Dimerization of Carbonyl Compounds

In a metal catalysed reaction of a Grignard reagent the reductive species is either the free metal in a colloid state or a metal salt in a subvalent state like Co^{+1}.

The effect of deuterium in The species, which is reduced in the catalytic cycle described above, need not be an alkyl halide, but may just as well be an easily reduced carbonyl compound like benzophenone. Kharasch showed in 1941 [91] that though methylmagnesium bromide normally adds to benzophenone producing methylbenzhydrol in high yield, the addition of a few per cent of ferric chloride led to the production of benzopinacol instead of the addition product:

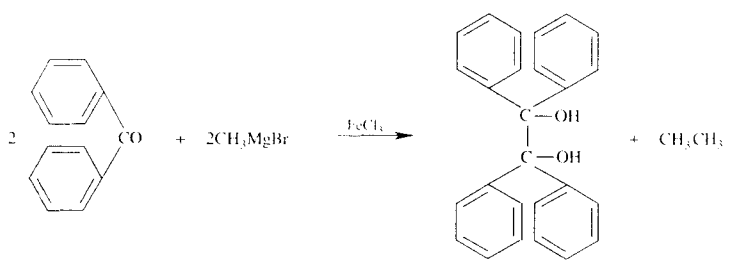

SCHEME 1.11

The catalytic cycle again is the formation of unstable alkylmetals, which decompose according to (1.13) or (1.14). The metal species, by increasing its oxidation state, reduces the substrate but is immediately regenerated by reaction with Grignard molecule(s). As mentioned before, what we observe is only indirectly a reaction of a Grignard reagent, since this only serves as a supplier of reactive metal species. Kharash suggested [2] that monovalent CoCl was the reactive species toward benzophenone since reduction did not take place using pyrophoric cobalt.

Other examples of catalytic reductions using methylmagnesium bromide and $FeCl_3$ are the formation of isomeric diphenyladipic esters from cinnamic esters [92] and tetra-phenylhexandiones from benzylideneacetophenone [93]. Scheme 1.12.

1.6.2 Reactions with Oxygen and with Peroxides

The reaction of Grignard reagents with oxygen has two steps [53,94,95]. The first step is formally an addition of RMgX to O_2. Oxidation of 5-hexenylmagnesium bromide, however, yielded the cyclized cyclopentylmethylperoxide, which proved that the initial step is ET to oxygen with the formation of the free 5-hexenyl radical. The radical diffuses for a sufficiently long time for the cyclization to take place before it adds to oxygen. This is step one of a chain process and step two is exchange of alkyl between the peroxyalkyl radical and a molecule of Grignard reagent.

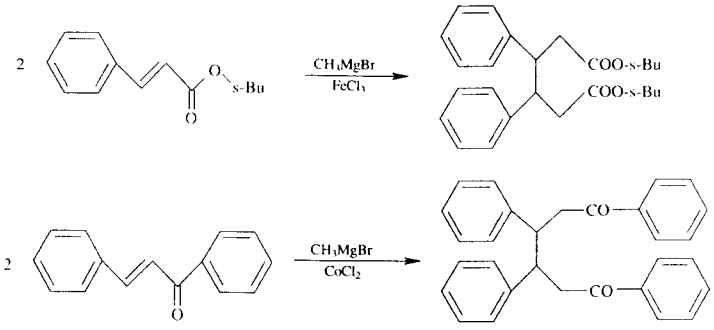

SCHEME 1.12

The reaction of alkylmagnesium reagents with di-*t*-butyl peroxide leads to alkyl *t*-butyl ether, *t*-butyl alcohol, and disproportionation products of the alkyl [96]. Mechanistic studies showed that the initial step is ET. This conclusion was *i.a.* based on a linear correlation of log rate with the oxidation potentials of the Grignard reagents. Reactions of peroxides are extremely sensitive to metal catalysis, but take place even when high-purity magnesium is used.

1.6.3 Reactions with Azobenzene

A fourth example of a radical-type reaction of Grignard reagents is the reaction with azobenzene [97]. It was found that azobenzene in the reaction with methylmagnesium bromide produces hydrazobenzene and ethane [98]. To be able to reduce azobenzene the reagent has to act as an electron donor in an induced homolysis:

SCHEME 1.13

In a mechanistic study [99] the use of a variety of Grignard reagents showed that hydrazobenzene was normally the main product (80% or above) accompanied by 10–15% 1,2-addition product. For allyl-, benzyl-, and *t*-butylmagnesium halide 1,2-addition amounted to 100, 57, and 50%, respectively. Among the by-products were for *t*-butyl Grignard reagent 10% 1,6-adduct and 7% p,p′-di-*t*-butylhydrazobenzene. A small amount of a tetra-*t*-butylazobenzene was isolated. It seems that Mg transfer to azobenzene from the Grignard reagent has produced free alkyl radicals, which after diffusion have attacked *unreacted* azobenzene in a number of consecutive steps. Even a primary reagent like n-butylmagnesium bromide produced 1,6-addition product (2%).

The rates of reaction for the different Grignard reagents were largely linearly correlated to the anodic oxidation potentials of the reagents. 5-Hexenylmagnesium bromide produced 1,2-addition product of which 50% was cyclized.

The conclusion from all observations is that the Grignard reagents transfer magnesium to azobenzene to produce a radical pair in a stepwise mechanism. The transfer, however, takes place in a transition state which is very similar to the concerted six-centre Whitmore–Mosher complex and has rather strict steric requirements. The reaction is radical-concerted. This, for example, explains that in the reaction of *s*-butylmagnesium bromide with azobenzene, 1-butene is formed in a 4:1 ratio relative to 2-butene, while this ratio in reactions with other electron acceptors is below unity. Since the radical pair is formed with a 'conformation' which is ideal for transfer of β-hydrogen this is the main product, but the radicals

may miss this opportunity and either collapse to 1,2-addition product or diffuse out of the cage. The presence of a β-hydrogen facilitates the reaction since reagents which have no β-hydrogen, like methyl or benzyl, or which like *t*-butyl have too much bulk to be able to attain the ideal six-centre conformation, react by ET, but much more slowly than indicated by their oxidation potentials.

1.6.4 Reactions with Cinnamic Esters

Cinnamic acid ethyl ester is a carbonyl compound, which like benzophenone has the ability to accept an electron to form a rather stable anion radical. As an α, β-unsaturated ester it may produce 1,2- and 1,4-addition products in the reaction with alkylmagnesium halides. The use of *t*-butylmagnesium chloride, however, was found to produce up to 50% of a 1,3-addition product [100].

The mechanism of this reaction was studied [101] and was found to involve the production of a *t*-butyl radical and a magnesium ester hemiketal radical, which could recombine to form the normal 1,4-adduct. Diffusion of the radicals out of the cage allowed an attack of the free *t*-butyl radical on the unreacted starting material. This attack took place at the carbon β to the benzene ring with the formation of a stable benzylic radical. This radical exchanges magnesium with the initially formed ester hemiketal. The magnesium compound formed undergoes an internal Grignard addition with the formation of a cyclopropanone hemiketal, which may be isolated after silylation, but which hydrolyses to the 1,3-addition product in weak acid.

The product of addition to cinnamic ester is an obvious 'abnormal' product formed by the reaction of a Grignard reagent. Such products are formed by the reaction of free radicals, which since they are uncharged 'look' for radical stabilization rather than for charge stabilization. The following types of abnormal products are considered as being formed by radical recombination even if the direct proof of the radical mechanism has not been given for all cases.

1) Products resulting from dimerization of the substrate.
2) Unstable dihydro compounds formed by addition to aromatic rings.
3) Additions to a carbon which is not electron deficient.
4) Addition to oxygen, nitrogen, and sulphur.

Examples of 1), 2), and 3) are given above. Addition to nitrogen was described for azobenzene. Addition to carbonyl oxygen may be seen for example in the addition of *t*-butylmagnesium chloride to benzophenone [65]. For α-diketones and ortho quinones, *O*-alkylation may be the main product as described for benzil [59] and quinones [102,103,104]. *S*-alkylation has been seen in the addition to thiobenzophenone [105]. Addition to nitrogen is seen with nitrobenzene [106] and with pyridazinium salts [107]. The products mentioned are produced via a radical mechanism, sometimes in significant amounts but often as unimportant by-products.

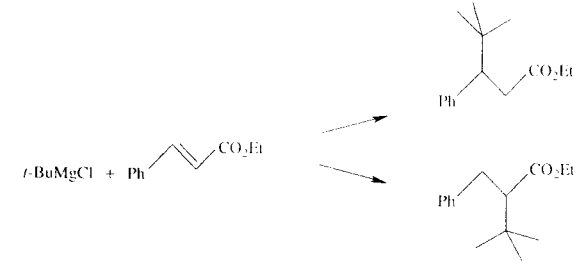

SCHEME 1.14

1.7 SOLVENT EFFECTS

Although alkylmagnesium reagents may be prepared in hydrocarbons like methylcyclohexane or benzene [108], the common solvents used for Grignard reactions are diethyl ether (DEE) and tetrahydrofuran. In special cases use is made of very strongly coordinating solvents like DME, HMPT, or crown ethers [18,72,51].

Several effects are seen when the solvents are interchanged. Going from DEE to THF the Schlenk equilibrium is changed toward a larger content of dialkylmagnesium, R_2Mg, which is much more reactive than RMgX. Comparisons of reactivities in the two solvents therefore only make sense when using halide-free dialkylmagnesium [44]. Dibutylmagnesium is about 100 times less reactive toward acetone, methyl acetate, and *s*-butyl crotonate in THF solution than in ether, but the reactivity toward azobenzene is increased. Toward benzophenone secondary and tertiary reagents are much more reactive in THF than in DEE, while the reactions with primary reagents (butyl- and ethyl) are not accelerated [43].

Reactions which have rate-determining ET have transition states with charge development and should be accelerated in the more polar solvent THF. Since the various coordination equilibria existing in the reaction mixtures are seriously shifted, reactivity changes have to be carefully analysed. Although the ET reaction with azobenzene is accelerated in THF, the ET reaction between *t*-butylmagnesium chloride and di-*t*-butylperoxide is extremely slow in THF [43].

Reactions which take place with polar mechanisms tend to be slow in highly coordinating solvents. This would be a natural consequence if a coordination vacancy on magnesium is needed for engagement with the substrate since vacancies would be extremely rare in a solvent like THF or HMPA.

A Hammett treatment of the reaction of ethylmagnesium bromide with benzophenone in ether [109] showed a linear plot for the ratio addition/reduction with a $\rho = -1$. Changing from DEE to THF led to two linear plots intersecting at $\sigma = -0.15$. The change in ρ must be interpreted as a change in mechanism for the addition. The authors offer very elaborate combinations of mechanisms [109], but the break could be explained by a simple shift from a low ρ concerted mechanism to a high ρ ET mechanism. The reaction merits further study.

Attempts have been made to correlate the viscosity of the solvent with the product distribution and the behaviour of radical probes in the reaction of *t*-butylmagnesium chloride with benzophenone [57].

1.8 CONCLUSION

The fundamental problem in the study of Grignard reactions is to discover whether the mechanism is stepwise or concerted. All Grignard reagents have the potential to react homolytically, but concerted mechanisms may be the most efficient with substrates with low electron affinity. Homolytic mechanisms are recognized by high reactivity of bulky reactants, by abnormal reaction products, and by the possibility of correlation of rate with the oxidation potential of the Grignard reagent. Concerted reactions are found between reagents with a strong C–Mg bond and substrates with low electron affinity. Little steric bulk and favourable conformations are required.

A close race may exist between the two mechanisms and among a series of concerted reactions, exceptions are found in which steric retardation has made the homolytic mechanism competitive. Likewise, series of reactions with homolytic mechanisms show exceptions, in which an especially favourable conformation makes a concerted mechanism competitive.

Between the two types of mechanism a grey zone exists, in which the mechanisms may not be clearly defined. Of these, some appear to react by radical-concerted mechanisms or other types of hybrid mechanisms.

Observations of radical intermediates by ESR or uv-vis spectroscopy like the observation of cyclization of radical probes indicate a homolytic reaction mechanism. A quantitative kinetic analysis is, however, required to reveal the importance of the radical route.

Kinetic isotope effects are of limited usefulness because they are small and because the theoretical prediction of KIEs is not straightforward.

The basic and the most valuable information in the study of reaction mechanisms will always come from kinetic studies. It seems as if reactions of Grignard reagents for which the mechanism is still not obvious should be investigated by traditional kinetic methods using, for example, the Hammett procedure and carefully selected solvents.

REFERENCES

1. V. Grignard, *Ann. Chim.* [7] *24*, 433 **1901**.
2. M.S. Kharasch and O. Reinmuth, *Grignard Reactions of Non-metallic Substances*, Prentice-Hall, New York, **1954**.
3. F.F. Blicke and L.D. Powers, *J. Am. Chem. Soc. 51*, 3378, **1929**.
4. T. Holm, *J. Chem. Soc. Perkin II* **1981**, 464.
5. H. Felkin, Y. Gault and G. Roussi, *Tetrahedron 26*, 3761, **1970**.
6. E.C. Ashby, J. Laemmle and H.M. Neumann, *Acc. Chem. Res. 7*, 272, **1974**.
7. E.C. Ashby, *Pure Appl. Chem. 52*, 545, **1980**.
8. M. Dagonneau, *Bull. Soc. Chim. Fr. II* 269, **1982**.
9. T Holm, *Acta Chem. Scand. B 37*, 567, **1983**.
10. W. Kaim, *Acc. Chem. Res. 18*, 160, **1985**.
11. E.C. Ashby, *Acc. Chem. Res. 21*, 414, **1988**.
12. C. Walling, *J. Am. Chem. Soc. 110*, 6846, **1988**.
13. K. Maruyama and T. Kitagiri *J. Phys. Org. Chem. 2*, 205, **1989**.
14. C. Blomberg, in *Handbook of Grignard Reagents*, Marcel Dekker, inc. **1996**, chapters 11 and 12.
15. T. Holm, *J. Organomet. Chem. 56*, 87, **1973**.
16. T. Holm, *Acta Chem. Scand. B 37*, 797, **1983**.
17. T. Holm, *Acta Chem. Scand. 19*, 1819, **1965**.
18. H.G. Richey and J.P. DeStephano, *J. Org. Chem. 55*, 3281, **1990**.
19. C.G. Screttas and M. Micha-Screttas, *J. Organomet. Chem. 290*, 1, **1985**.
20. W.V. Evans, F.H. Lee, and C.H. Lee, *J. Am. Chem. Soc. 57*, 489, **1935**.
21. T. Holm, *Acta Chem. Scand. B 28*, 809, **1974**.
22. T. Holm, *Acta Chem. Scand. B 42*, 685, **1988**.
23. M.B. Smith and W.E. Becker, *Tetrahedron Lett.* **1965** 3843.
24. G.E. Parris and E.C. Ashby, *J. Am. Chem. Soc. 93*, 1206, **1971**.
25. R.M. Salinger and H.S. Mosher, *J. Am. Chem. Soc. 86*, 1782, **1964**.
26. T. Holm, *Acta Chem. Scand. 23*, 579, **1969**.
27. E.C. Ashby, J. Laemmle and H.M. Neumann, *J. Am. Chem. Soc. 93*, 4601, **1971**.
28. J. Meisenheimer and W. Schlichenmair, *Ber. 61*, 720, **1928**.
29. E.C. Ashby and W.E. Becker, *J. Am Chem. Soc. 85*, 118, **1963**.
30. A.D. Vreugdenhil and C. Blomberg, *Rec. Trav. Chim. Pays-Bas 82*, 461, **1963**.
31. R.E. Dessy, G.S. Handler, J.H. Wotiz, and C.A. Hallingsworth, *J. Am. Chem. Soc. 79*, 3476, **1957**.
32. C.G. Swain, *J. Am. Chem. Soc. 69*, 2306, **1947**.
33. T. Holm, *Acta Chem. Scand. 20*, 2821, **1966**.
34. T. Holm, *Acta Chem. Scand. 21*, 2753, **1967**.
35. A. Holm, T. Holm and E. Huge-Jensen, *Acta Chem. Scand. B 28*, 781, **1974**.
36. C.G. Swain and H.B. Boyles, *J. Am. Chem. Soc. 73*, 870, **1951**.
37. K. Maruyama and T. Katagiri, *J. Am. Chem. Soc. 108*, 6263, **1986**.
38. S.G. Smith and G. Su, *J. Am. Chem. Soc. 86*, 2750 **1964**.
39. S.G. Smith, *Tetrahedron Lett.* **1963**, 409.
40. S.G. Smith and G. Su, *J. Am. Chem. Soc. 88* 3995, **1966**.
41. J. Meisenheimer and J. Casper, *Chem. Ber. 54*, 1655, **1919**.
42. T. Holm, *Acta Chem. Scand. 20*, 1139, **1966**.
43. T. Holm, unpublished results.
44. T. Holm, *Tetrahedron Lett. 28*, 3329, **1966**.
45. M. Gomberg and W.E. Bachmann, *J. Am. Chem. Soc. 49*, 236, **1927**.
46. A.E. Arbuzov and I.A. Arbuzova, *J. Gen. Chem. USSR 2*, 388, **1932**; *CA 27*, 974.
47. G.A. Russell, E.G. Janzen, and E.T. Strom, *J. Am. Chem. Soc. 86*, 1807, **1964**.
48. K. Maruyama, *Bull. Chem. Soc. Jpn. 37*, 2315, **1964**.
49. C. Blomberg and H.S. Mosher, *J. Organomet. Chem. 13*, 519, **1968**.
50. C. Blomberg, R.M. Salinger and H.S. Mosher, *J. Org. Chem. 34*, 2385, **1969**.
51. J.F. Fauvarque and E. Rouget, *C.R. Acad. Sci. Ser. C 267*, 1355, **1968**.
52. T. Holm and I. Crossland, *Acta Chem. Scand. 25*, 59, **1971**.
53. R. C. Lamb, P. W. Ayers, M. K. Toney, and J.F. Garst, *J. Am. Chem. Soc. 88*, 4261, **1966**.
54. J.F. Garst and F.E. Barton, *Tetrahedron Lett.* **1969**, 587.
55. H.O. House and P.D. Weeks, *J. Am. Chem. Soc. 97*, 2770, **1975**.
56. E.C. Ashby and T.L. Wiesemann, *J. Am. Chem. Soc. 100*, 3101, **1978**.
57. E.C. Ashby and J.S. Bowers *J. Am. Chem. Soc. 99*, 8504, **1977**.
58. E.C. Ashby and J.R. Bowers *J. Am. Chem. Soc. 103*, 2242, **1981**.
59. T. Holm, *Acta Chem. Scand. B 41*, 278, **1987**.

60. L. Eberson and L. Greci, *J. Org. Chem. 49*, 2135, **1984**.
61. J.F. Garst and C.D. Smith, *J. Am. Chem. Soc. 98*, 1526, **1976**.
62. C. Walling, *J. Am. Chem. Soc. 110*, 6846, **1988**.
63. N. Hirota and S.I. Weissman, *J. Am. Chem. Soc. 86*, 2537, **1964**.
64. H. Yamataka, T. Matsuyama, and T. Hanafusa, *J. Am. Chem. Soc. 111*, 4912, **1989**.
65. T. Holm, *J. Am. Chem. Soc. 115*, 916, **1993**.
66. G.E. Dunn and J. Warkentin, *Can. J. Chem. 34*, 75, **1956**.
67. T. Holm, *Acta Chem. Scand. 27*, 1552, **1973**.
68. T. Holm and J. Ø. Madsen, *Acta Chem. Scand. B 46*, 985 **1992**.
69. T. Holm, *Acta Chem. Scand. 48*, 362, **1994**.
70. K.C. Williams and T.L. Brown, *J. Am. Chem. Soc. 88*, 4134, **1960**.
71. E.A. Hill and D.C. Link, *Organometallics 1*, 1501, **1982**.
72. V.I. Savin, I.D. Temyachef and F.D. Yambushef, *Zh. Org. Khim. 11*, 1238, **1975**.
73. K. Maruyama and T. Katagiri *J. Am. Chem. Soc. 108*, 6263, **1986**.
74. E.C. Ashby and A.B. Goel, *J. Am. Chem. Soc. 103*, 4983, **1981**.
75. W. Kaim, *Angew Chem. 94*, 150, **1982**.
76. K. Maruyama and T. Katagiri, *Chemistry Lett.* **1987** 735.
77. T. Holm and I. Blankholm, *Acta Chem. Scand. 22*, 708, **1968**.
78. F.C. Whitmore, as quoted by H. S. Mosher and E. La Combe, *J. Am. Chem. Soc. 72*, 3994, **1950**.
79. G. Vavon and B. Angelo, *C. R. Acad. Sci. 224*, 1435, **1947**.
80. T. Holm, *J. Organomet. Chem. 29*, C45 **1971**.
81. H.C. Mosher and E. La Combe, *J. Am. Chem. Soc. 72*, 3994, **1950**.
82. A.G. Pinkus amd A. Sabesan, *J. Chem. Soc., Perkin Trans. 2*, 473, **1981**.
83. A.G. Pinkus and W.C. Servoss, *J. Chem. Soc., Perkin Trans. 2*, **1979**, 1600.
84. R.A. Benkeser and T.E. Johnston, *J. Am. Chem. Soc. 88*, 2220, **1966**.
85. R.E. Lutz and W.G. Reveley, *J. Am. Chem. Soc. 63*, 3180, **1941**.
86. T. Holm, *Acta Chem. Scand. 45*, 925, **1991**.
87. J. Munch-Petersen, *Org. Synth.* Coll. Vol. *5*, 762, **1973**.
88. M.S. Kharasch and W.H. Urry, *J. Org. Chem. 13*, 101, **1948**.
89. M.S. Kharasch, F.L. Lambert and W.H. Urry, *J. Org. Chem. 10*, 298, **1945**.
90. M. Tamura and J. Kochi, *J. Organometallic Chem. 31*, 289, **1971**.
91. M.S. Kharasch and F.L. Lambert, *J. Am. Chem. Soc. 63*, 2315, **1941**.
92. S.R. Jensen, A.-M. Kristiansen and J. Munch-Petersen, *Acta Chem. Scand. 24*, 2641, **1970**.
93. M.S. Kharasch and D.C. Sayles, *J. Am. Chem. Soc. 64*, 2972, **1942**.
94. H. Wuyts, *Compt. rend. 148*, 930, **1909**
95. C. Walling and S.A. Buckler, *J. Am. Chem. Soc. 75*, 4372, **1953**.
96. W.A. Nugent, F. Bertini and J.K. Kochi, *J. Am. Chem. Soc. 96*, 4945, **1974**.
97. H. Gilman and R.M. Pickens, *J. Am. Chem. Soc. 47*, 2406, **1925**.
98. H. Rheinboldt and R. Kirberg, *J. prakt. Chem.* [2], *118* 1, **1928**.
99. T. Holm and I. Crossland, *Acta Chem. Scand. B 33*, 421, **1979**.
100. I. Crossland, *Acta Chem. Scand. B 29*, 468, **1975**.
101. T. Holm, I. Crossland and J.Ø. Madsen, *Acta Chem. Scand. B 32*, 754, **1978**.
102. D. Wege, *Aust. J. Chem. 24*, 1531, **1971**.
103. F. Wessely and J. Kotlan, *Monstsh. 84*, 124, **1953**.
104. B. Miller, *J. Org. Chem. 42*, 1402, **1977**.
105. P. Beak and J.W. Worley, *J. Am. Chem. Soc. 92*, 4142, **1970**.
106. G. Bartoli, E. Marcantoni and M. Petrini, *J. Org. Chem. 57*, 5834, **1992**.
107. I. Crossland and Kelstrup, *Acta Chem. Scand. 22*, 1669, **1968**.
108. D. Bryce-Smith, *Bull. Soc. Chim. France* **1963**, 1418.
109. K. Maruyama and T. Katagiri, *J. Phys. Org. Chem. 4*, 381, **1991**.

2

Nucleophilic Displacements at Carbon by Grignard Reagents

E. Alexander Hill
Department of Chemistry, University of Wisconsin-Milwaukee, Milwaukee, WI 53201

2.1 INTRODUCTION†

By virtue of the polarity of the carbon–magnesium bond, Grignard reagents are an important source of nucleophilic 'anionic' carbon groups. The nucleophilic addition of Grignard reagents to carbonyl and related multiple bonds (including acyl substitutions) is one of the most important C–C bond-forming reactions in organic chemistry (eq. 2.1). In contrast, the cross-coupling reaction—nucleophilic substitution of alkyl halides or other substrates by the 'carbanion' of the Grignard reagent—is more limited in scope (eq. 2.2).

Among the side reactions which limit the utility of cross-coupling is homo-coupling of the alkyl groups of RMgX, R′Y, or both (e.g., eq. (2.3)) [1]. When β-hydrogens are present in either the Grignard reagent or the alkyl halide, disproportionation is possible, leading to alkane, RH and R′H, and alkene, R{−H} and R′{−*H*}. Metal–halogen exchange which, in effect, interchanges the functions of the Grignard reagent and the halide can also occur, although it is less facile for Grignard reagents than for organolithium compounds. The metal–halogen exchange is a potential source of homo-coupling, since both alkyl groups may then appear in both the Grignard reagent and in the substrate.

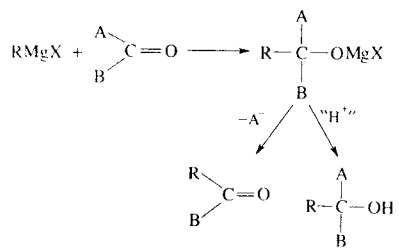

(2.1)

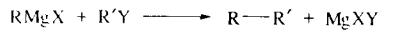

(2.2)

The 'Wurtz coupling' side reaction, which generally accompanies the formation of Grignard reagent from alkyl halide and magnesium, gives products

†The following abbreviations will be used: Me = methyl; Et = ethyl, Pr = propyl; Bu = butyl; Pent = pentyl; Ph = phenyl; Mes = mesityl (2,4,6-trimethylphenyl); OTs = tosylate; THF = tetrahydrofuran; DME = 1,2-dimethoxyethane; DMF = dimethylformamide; DW = dioxane-water; DMSO = dimethylsulfoxide; HMPA = hexamethylphosphoramide. Unless otherwise indicated, the formula RMgX for a Grignard reagent will be taken to represent any of the species of the Schlenk equilibrium.

Grignard Reagents: New Developments Edited by Herman G. Richey, Jr © 2000 John Wiley & Sons Ltd.

equivalent to the homo-coupling of the Grignard reagent (along with disproportionation of the Grignard reagent alkyl). In some cases it is the result of radical intermediates in the formation of the Grignard reagent. For halides which react readily with Grignard reagents, the Wurtz product may be formed instead by coupling between Grignard reagent which has formed and the halide which has not yet reacted.

$$\underset{}{MeMgI} + \underset{}{PhCH_2Cl} \longrightarrow \underset{25\%}{PhCH_2CH_3} + \underset{68\%}{C_2H_6} + \underset{65\%}{PhCH_2CH_2Ph} \quad (2.3)$$

Because of the frequently unsatisfactory success of carbon–carbon bond formation involving the Grignard reagent as nucleophile in substitution reactions, a major branch of research endeavor has grown up around 'catalyzing' this reaction by the addition of a variety of transition metal salts and complexes. In most cases, such catalysis, in fact, involves the intermediacy of organo-transition metal compounds which function as the effective nucleophilic reagent.

In this chapter, we will revisit C–C bond formation by uncatalyzed nucleophilic substitution reactions of Grignard reagents. Two recently published volumes on Grignard reagent chemistry by Wakefield [2] and by Silverman and Rakita [3] include chapters on nucleophilic displacement reactions. The emphasis in these chapters is principally synthetic, and includes both uncatalyzed and catalyzed reactions. A review by Beletskaya, Artamkina, and Reutov [4] in 1976 was concerned with mechanisms of reaction of organometallic derivatives with organic halides, and a 1990 review by Polivin, Karakhanov, and Postnov [5] discussed 'heterolytic cleavage of carbon-element σ-bonds by Grignard reagents.' The classic compendium on Grignard reagent chemistry by Kharasch and Reinmuth [6] includes numerous examples drawn from older literature, and we will frequently cite this volume for a summary of early work.

The emphasis in the present chapter will be on the scope and the mechanisms of reactions in which the 'anionic' alkyl group of the Grignard reagent displaces another group from carbon. As a formal nucleophilic substitution reaction involving a reagent which is a strong nucleophile, the S_N2 mechanism—direct heterolytic displacement by the nucleophile—might be a first choice. However, in many cases, other mechanisms may be more appropriate. Important alternatives include an S_N1 process assisted by the Lewis-acidic magnesium of the Grignard reagent, with a carbocation intermediate, and a single electron transfer (SET) mechanism, with radical intermediates. For future reference, these three mechanisms are illustrated in a generalized and oversimplified form in equations (2.4–2.6).

$$R{-}MgX + R'{-}Y \longrightarrow R{-}R' + MgXY \quad (2.4)$$

$$R{-}MgX + R'Y \longrightarrow \left[RMgXY^{-} + R'^{+}\right] \longrightarrow R{-}R' + MgXY \quad (2.5)$$

$$RMgX + R'Y \longrightarrow \left[RMgX^{\ddagger}, R'Y^{\ddagger}\right] \longrightarrow R{-}R' \longleftarrow \left[R\bullet, R'\bullet, MgXY\right] \quad (2.6)$$

Before discussing the substitution mechanisms more thoroughly, we will survey some examples of Grignard cross-coupling reactions, concentrating on halide displacements with simple alkyl and substituted alkyl groups. After a more detailed examination of the mechanistic possibilities, we will discuss the experimental observations in relation to the mechanisms and look at coupling reactions with other substrates. Because many uncatalyzed coupling reactions with simple alkyl groups are not very successful synthetically, there are relatively few recent examples. Caution should be exercised in drawing mechanistic conclusions based on the older literature, since magnesium contaminated with transition metal impurities might have introduced a catalyzed component into the reaction, and results might have been influenced by the lack of inert atmosphere techniques and modern analytical methods.

2.2 SURVEY OF COUPLING REACTIONS OF GRIGNARD REAGENTS WITH ORGANIC HALIDES

2.2.1 Reactions with 'Simple' Alkyl Halides

As a point of reference, we might note that in typical substitution reactions of saturated alkyl halides occurring by an S_N2 mechanism, methyl halides are most reactive, and reactivity *decreases* with substitution: $1^\circ > 2^\circ > 3^\circ$. Since the rate of competing bimolecular elimination *increases* through the same series, the best yields of substitution products are normally found for methyl and 1° alkyl halides, while 3° halides give elimination almost exclusively. The order of reactivity of the halides as leaving groups is $I > Br \gg Cl \gg F$ [7–9]. Reliable modern examples using simple saturated alkyl halides are not easy to find, and the compilation of Kharasch and Reinmuth cites relatively few reactions of alkyl halides with simple alkyl Grignard reagents. Some pertinent representatives, mostly from the latter, are collected in Table 2.1.

Several of the examples cited in Table 2.1 note the side-products formed. For the most part, reactions are relatively slow in ethyl ether at room temperature or reflux, although iodides react faster.

Table 2.1. Reactions of simple alkyl halides with Grignard reagents[a]

	Halide	RMgX	Products
1	MeI	MeMgI	ethane (>51%)
2	EtBr	EtMgBr	$C_2H_4 + C_2H_6$ (1:1)
3	PrI	EtMgI	alkenes (46% C_2H_4 + 54% C_3H_6) alkanes (66% C_2H_6 + 34% C_3H_8)
4[b]	*i*-PrI	Et_2Mg	C_2H_6 (26%), C_2H_4 (10.5%), C_3H_8 (23.5%), C_3H_6 (8.5%), C_4H_{10} (1.5%), *i*-C_5H_{12} (20%)
5	MeI	*t*-BuMgI	Me_4C
6	*t*-BuCl	MeMgCl	Me_4C (42–50%)
7[c]	$ClCH_2CH_2CMe_2Cl$	BuMgCl	$ClCH_2CH_2CMe_2Bu$ (70%)
8[d]	*t*-BuBr	*t*-BuMgCl	Me_3CCMe_3 (6%), $Me_2C{=}CH_2$ (6%), Me_3CH (39%), 'diisobutylenes'
9	MeI	PhenMgBr[e]	9-methylphenanthrene
10	EtBr	$(Me_5C_6)MgBr$	$(Me_5C_6)Et$ (40%)
11	$PhOC_2H_4Br$	PhMgBr	$PhOCH_2CH_2Ph$ (83%); PhOH
12	*t*-BuI	$PhCH_2MgCl$	$PhCH_2CMe_3$ (30%); $PhCH_2CH_2Ph$
13	RY	Ph_3CMgBr	Ph_3CMe (93-98%); R'Y=MeI Ph_3CEt (73%); R'Y=EtBr
14[f]	$C_7H_{15}Br$	BuMgBr	n-$C_{11}H_{24}$ (THF: 8%; HMPA: 42%)
15[f]	$C_7H_{15}Br$	MeCH=CHMgBr	$C_7H_{15}CH{=}CHMe$ (THF: 71%; HMPA: 43%)
16	EtOTs	$Ph(CH_2)_3MgCl$	$Ph(CH_2)_4CH_3$ (40%)

[a]From ref. [6], unless otherwise indicated. [b]Ref. [10] (yields of C2–C4 products based on 70% yield of gases.) [c]Ref. [11]; in refluxing CH_2Cl_2. [d]Ref. [12]. [e]Phen = 9-phenanthryl. [f]Ref. [13].

More recently, it has been noted that p-$CH_3OC_6H_4$MgBr led to no detectable coupling product with 1-iodohexadecane after 16 h in refluxing THF (97% of iodide recovered) [14]. Grignard reagent **1a** did not react with saturated halides without catalysis [15]. It is not clear if the absence of reaction in these cases reflects the use of less forcing conditions or purer magnesium than in earlier reports. Aryl and benzylic Grignard reagents are more successful in substitution (Table 2.1, entries 9–13).

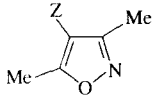

1 a. Z = MgBr
b. Z = Methallyl

Surprisingly, 3° halides led to moderate yields of substitution (Table 2.1, entries 6–8 and 12). With 1-bromoadamantane and some of its homologs, where elimination would violate Bredt's rule, methylmagnesium bromide reacts to give excellent yields of cross-coupling product. Other Grignard reagents gave lower yields, but even *t*-BuMgCl led to 9% of 1-*t*-butyl-adamantane (along with reduction of the halide as the major product) [16]. Use of the somewhat polar but non-basic methylene chloride as solvent was found to be advantageous [11].

Another instance in which synthetically successful substitution is reported is in Table 2.1, entry 11. (Pentyl and benzyl Grignard reagents led mostly to elimination of phenol.) Coordination of magnesium to the oxygen may enhance reactivity to displacement; related compounds (e.g., 2-chloroethyl ether) are reported to react particularly rapidly and selectively with polystyryllithium 'living polymers [17]. One example (entry 16) is included to represent the reactions of sulfate and sulfonate esters. These are discussed in more detail later, but we note that their displacement reactions with alkyl Grignard reagents occur at least as easily as those of the halides, and homo-coupling is less significant.

2.2.2 Reactions with 'Reactive' Halides

In contrast to saturated alkyl halides, some organic halides do react very readily with Grignard reagents. The reactivity of allyl bromide is particularly noteworthy; numerous reports indicate mild reaction conditions, short reaction times, and excellent yields in cross-coupling. Substituted allylic halides also react readily, though with complication by allylic isomer formation. Benzylic halides are reactive toward Grignard reagents, but homo-coupling becomes important or dominant. Some illustrative examples are shown in Table 2.2.

Another group of organic halides which are especially reactive toward displacement by Grignard reagents are those with the halogen alpha to an oxygen or a sulfur. Several examples are summarized in Table 2.3.

2.3 SUMMARY OF CROSS-COUPLING MECHANISMS

Three mechanisms for the cross-coupling of Grignard reagents were introduced in eqs (2.4–2.6). Regardless of mechanism, the process is *formally* a nucleophilic substitution, with the *net* result that a reagent with an available electron pair, **Nu**: (the Grignard alkyl group), replaces another group **L**:, which departs with the electron pair of the **R**—**L** bond (eq. 2.7). A number of charge types are possible, but electron accounting places the constraint that **Nu**: and **L**: each have one more negative unit of formal charge when free than when bonded.

$$\mathbf{Nu}: + \mathbf{R}:\mathbf{L} \longrightarrow \mathbf{R}:\mathbf{Nu} + :\mathbf{L} \qquad (2.7)$$

In Table 2.4, some properties of leaving groups are collected. The order of reactivity of the halides as leaving groups in reactions with Grignard reagents is $I^- > Br^- > Cl^-$. This is the same as that found for either S_N2 or S_N1 mechanisms, and also corresponds to the ease in accepting an electron from a single-electron donor. Hence, the qualitative sequence would be consistent with all three mechanisms. However, sulfonates or sulfates, while good leaving groups, accept an electron only reluctantly. Acyloxy and alkoxy groups are much less reactive.

Table 2.2. Reactions of allylic and benzylic halides with Grignard reagents[a]

	Halide	RMgX	Products
1	allyl-Cl	PrMgBr	$PrCH_2CH{=}CH_2$ (40–50%)
2	allyl-Cl	PhMgBr	$PhCH_2CH{=}CH_2$ (82%)
3	allyl-Br	*t*-BuMgCl	*t*-$BuCH_2CH{=}CH_2$ (85%)
4[b]	allyl-Br	p-$MeOC_6H_4MgBr$	p-$MeOC_6H_4$-$CH_2CH{=}CH_2$, (69%)
5	allyl-I	$PhCH_2MgCl$	$PhCH_2CH_2CH{=}CH_2$ (65%)
6	$CH_3CH{=}CHCH_2Cl$	BuMgBr	$BuCH_2CH{=}CHCH_3$ (60%)
			$BuCH(CH_3)CH{=}CH_2$ (10%)
7[c]	methallyl-Cl	**1a**	**1b** (93%)
8[d]	$PhCH_2Cl$(Br,I)	MeMgI	PhEt (25,22,10%); $(PhCH_2)_2$ (65,70,76%)
			C_2H_6 (68,74,80%)
9	$PhCH_2Cl$	EtMgCl	$PhCH_2CH_2CH_3$ (70%)
10[e]	allyl-Br, $PhCH_2Br$	$(i\text{-PrO})_3SiCH_2MgCl$	$(i\text{-PrO})_3SiCH_2R$ (70%)
11[f]	$PhCH_2Cl$	PhMgBr	$PhCH_2Ph$ (56%), $(PhCH_2)_2$ (6%), Ph_2 (4%), PhH (12%)

[a]From ref. [6], unless otherwise indicated. [b]Ref. [18]. [c]Ref. [15]. [d]Ref. [1] (yields of homo-coupling products reflect two alkyl groups). [e] Ref. [19]. [f]Ref. [20].

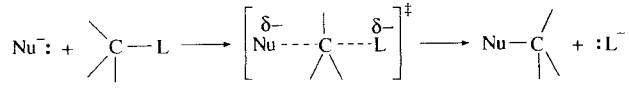

(2.8)

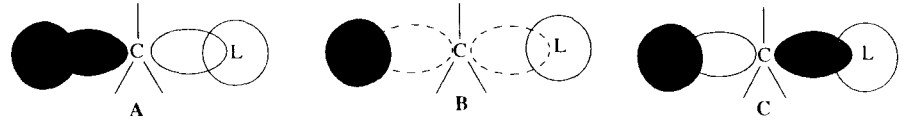

2.3.1 S_N2 Displacement Mechanism

The 'traditional' S_N2 reaction is a concerted process, as illustrated in eq. (2.8). The electron pair of **Nu**: binds to the carbon at which displacement is occurring, simultaneously with the departure of **L**:, along with the electron pair of the **C**—**L** bond. In the transition state for the reaction, two lobes of an orbital of approximately p hybridization on the central carbon overlap with orbitals of **Nu**: and **L**:, respectively. A molecular orbital scheme would assign the two electron pairs noted above to the two lowest molecular orbitals (A and B) of the linear three-center subsystem. From this picture, the observed inversion of configuration follows. Most commonly the nucleophile and the leaving group (after departure) are either neutral molecules or anions (both are depicted as anions in eq. (2.8)). In any event, there must be charged species as reactants, products, or both, and the transition state must be polar.

The S_N2 mechanism of Grignard cross-coupling is the analog of the polar mechanism of addition to carbonyl groups, in that the partially carbanionic carbon of the organometallic functions directly as a nucleophile. As a potential nucleophile for an S_N2 reaction, however, a Grignard reagent has an immediate difficulty. The nucleophile is not simply a carbanion, and the nucleophilic electron pair is not a free unshared pair. Instead, it is either shared in a polar covalent bond between carbon and

Table 2.3. Reaction of α-haloethers and α-halothioethers with Grignard reagents

	Halides	RMgX	Products
1[a]	CH_3OCH_2Cl	BuMgBr	$BuCH_2OCH_3$ (67%)
2[b]		$Ph(CH_2)_2MgBr$	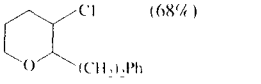 (68%)
3[c]	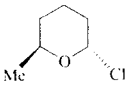	MeMgBr	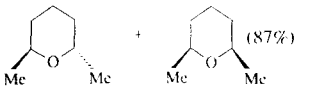 (87%) 3 : 1
4[d]	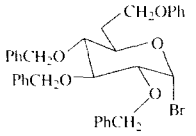	$PhCH_2MgCl$	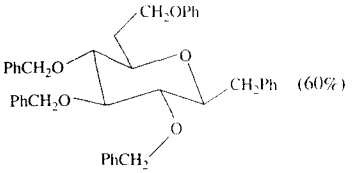 (60%)
5[e]	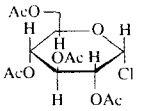	AnMgBr (An = 2–$MeOC_6H_4$)	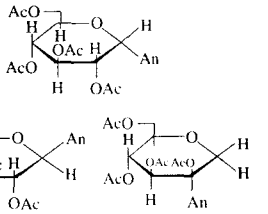
6[f]	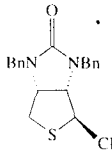 (Bn=benzyl)	MeMgBr	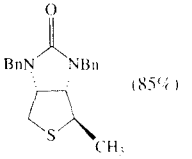 (85%)
7[g]	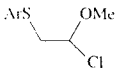	$PhCH_2MgCl$	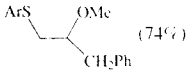 (74%)
8[h]	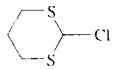	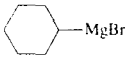	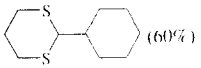 (60%)

[a]Ref. [21]. [b]Ref. [22]. [c]Ref. [23]. [d]Ref. [24]. [e]Ref. [25]. [f]Ref. [26]. [g]Ref. [27] [h]Ref. [28].

Table 2.4. Properties of leaving groups

Leaving group	S_N2[a] k_{rel}	S_N1[a] k_{rel}	$E_{1/2}$[b] $2\text{-}C_8H_{17}X$	χ[c]	BDE[d] CH_3X
I^-	2–5	1.5–7	−1.79	2.36	234
Br^-	(1.0)	(1.0)	−2.34	2.68	293
Cl^-	0.002–0.025	0.004–0.03	−2.69	3.00	349
TsO^-	0.4–6	25–5000	−2.72[e]	3.47	−[f]

[a]Ref. [7], pp 30, 82; Ref. [9], pp 291–292; Ref. [29], pp 374–375; relative reactivities vary with substrate, solvent, and nucleophile. [b]Half-wave potentials (volts, vs. saturated calomel electrode, DMF); ref. [30]. [c]Electronegativities; ref. [31]. [d]Bond dissociation energies (kJ/mol); ref. [29], pp 161–162. [e]Methanesulfonate. [f]$HO-CH_3$, 383; CH_3O-CH_3, 335 kJ/mol.

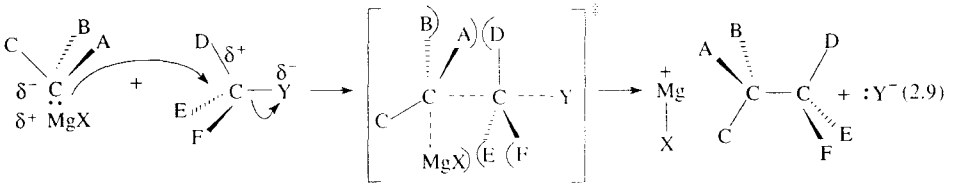

magnesium, or at the least, is the negative charge locus of a very tight contact ion pair. Regardless of the thermodynamics of the displacement, the electron pair is at least partially shielded from an external electrophile by the surrounding organic group and metal. When the electrophile is, itself, the tetrahedral alkyl carbon of an alkyl halide, with only modest fractional positive charge, one might anticipate a substantial barrier to reaction (eq. (2.9)).

A further difficulty for the S_N2 mechanism arises from the polar nature of the substitution process. Grignard reagents are most commonly used in ethers, which are mild 'dipolar aprotic' solvents. As such, they have substantial Lewis basicity for solvation of cationic centers (which contributes to the ether solubility of Grignard reagents), but they offer little in the way of short-range solvation to anions. Hence, an anionic leaving group departs with little assistance from the solvent, and in their initially formed state, the ions of the magnesium salt are separated by the non-polar coupling product (eq. 2.9). It might be noted that these problems are minimized in a polar mechanism of addition of the Grignard reagent to a carbonyl group. Initial coordination of the magnesium to a lone pair of the carbonyl oxygen may position the carbon group of the Grignard reagent to attack the carbonyl carbon, and the magnesium can remain in proximity to the oxygen throughout the course of the addition.

One or more additional molecules of Grignard reagent could help to stabilize the transition state in eq. (2.9) by coordinating with the leaving group, with the nucleophilic Grignard molecule, or with both. If the Grignard reagent is monomeric under reaction conditions, this would lead to higher order kinetics in Grignard, but if the reagent is associated, the kinetics might remain first order. There is obviously further complexity to the kinetics if the various species of the Schlenk equilibrium are considered.

2.3.2 S_N1 Mechanism

Initially, the thought of an S_N1 mechanism with a strong nucleophile, in the relatively non-polar ether solvents used for Grignard reactions, may appear unlikely. However, the magnesiums of the MgX_2, $RMgX$, or R_2Mg species are Lewis acidic in nature (decreasing in the order shown). Coordination with the halide ion (or other leaving group) would

stabilize the transition state for its departure. If the substrate forms a reasonably stable carbocation, assisted ionization of the substrate to an ion pair of the carbocation with the complex magnesium anion becomes feasible (eq. 2.10).

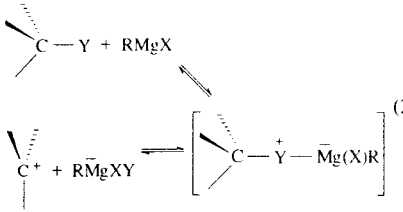

(2.10)

The ion pair in eq. (2.10) could revert to reactants, undergo internal transfer of alkyl or halide from the anion to the carbocation, or react with an external molecule of Grignard reagent. Since the medium is not an hospitable one for ionic species, the lifetime of the ion pair should be short and stereochemistry might be partially preserved, with possible retention of configuration in the internal collapse or inversion in the attack by external reagent.

2.3.3. Single Electron Transfer (SET) Mechanism

Many reactions (including nucleophilic substitutions) which have traditionally been viewed as heterolytic polar reactions can be formulated alternatively as homolytic processes initiated by the transfer of a single electron from one species to another (SET) [32,33]. For an alkyl halide reacting with a nucleophile (with all paired electrons) the alternative polar and SET processes would be formulated as in eq. (2.11). The electron transfer shown is referred to as 'outer-sphere', implying that it occurs as an electron 'jump' between two essentially non-interacting species. An 'inner-sphere' electron transfer involves some bonding interaction between the reacting partners, often with the transfer of an atom or group between them. The importance of electron-transfer mechanisms and their underlying theory have been discussed elsewhere [34,35]. Electron transfer reactions of main group organometallics have also been reviewed [36]. A detailed discussion is beyond the scope of this chapter, but some important points will be summarized qualitatively.

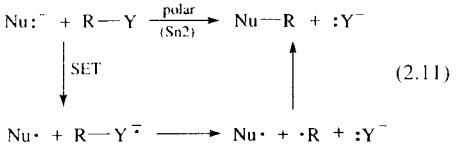

(2.11)

Most commonly, outer-sphere electron transfer reactions, either homogeneous or at an electrode, are discussed in terms of the Marcus theory [37]. Because of its smaller mass, the motion of an electron is much more rapid than nuclear motions (Franck–Condon Principle). For the electron transfer to occur, the arrangement of all the atoms in the system (including solvation) must be identical immediately before and immediately after the transfer. The energies before and after transfer must also be identical, since there is no nuclear motion to provide or accept energy during the transfer (i.e., an adiabatic process). This equality of energies must arise from distortions of both reactants and products to a common geometry, which also has the same energy for either electron 'home'. The transition state for the electron transfer may be represented as a resonance hybrid of the structures before and after the transfer (eq. 2.12).

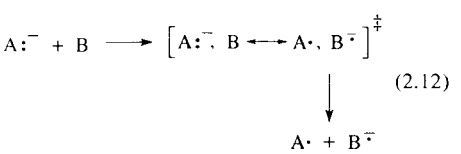

(2.12)

A starting point for discussion is a degenerate 'self-exchange', i.e., $A^{-\cdot} + A \rightleftharpoons A + A^{-\cdot}$. There is no net change in energy, and in the transition state the donor and acceptor partners are identical in energy and geometry. The activation energy for the electron transfer arises from the distortions of A and $A^{-\cdot}$, along with their solvation spheres, in order to achieve their common geometry in the transition state. This energy is referred to as the reorganization energy for the process.

In the non-degenerate electron transfer of eq. (2.12) there is a net energy change in going from reactants to products in their 'relaxed' states. This energy change corresponds to the difference in the standard electrode potentials (E^0) for the oxidation and reduction half-reactions (eq. 2.13). Relative to the self-exchange, exothermicity decreases the activation energy and endothermicity increases it. Thus, the rate depends both upon the thermodynamics of the electron transfer and the energies associated with the structural and solvation changes which must occur to reach the transition state. The Marcus theory additionally provides a framework for quantitative evaluation of these contributions to the rate.

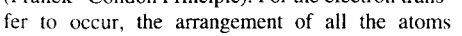

(2.13)

In the reaction of the Grignard molecule with an alkyl halide, the electron transfer step in the SET mechanism takes the form of eq. (2.14). The electrochemical cathodic reduction of organic halides is a well-studied process [38–40], and heterogeneous electron transfer is the probable initial step in the formation of Grignard reagents from alkyl halides and magnesium [41]. A number of homogeneous reactions, including the reaction with aromatic radical anions [40,42], also occur by electron transfer to the alkyl halide.

(2.14)

The alkyl halide radical anion is very unstable and short-lived, decomposing to an alkyl radical and a halide ion. In fact, the electron transfer very likely occurs dissociatively, forming the radical directly with the transfer of the electron (eq. 2.15). This is supported theoretically [43], and is consistent with the fact (see below) that the ease of reduction increases with the stability of the radical formed. Low temperature EPR studies indicate only weak polarization interaction between the radical and the halide ion [44]. Nevertheless, it has been suggested that even this weak interaction might affect the partition of radical species during the lifetime of a radical pair [45]. In contrast, radical ions of aryl halides do have a finite lifetime [46].

(2.15)

If electron transfer to the alkyl halide is dissociative, there should be a large reorganization energy from stretching of the C–X bond close to its breaking point. As a result, the electron transfer step has a relatively high activation energy and slow rate. Because the electron transfer is slow and the fleeting lifetime of the radical anion prevents its reoxidation, the step is 'electrochemically irreversible'. In such a case, the experimental reduction potential is an inaccurate representation of the standard electrode potential for the alkyl halide.

Standard potentials (E^0) have been estimated from thermodynamic properties [34,40,47,48], and also from analysis of the rates of homogeneous electron transfer reductions of alkyl halides on the basis of Marcus theory [49]. In Table 2.5, some experimental reduction potentials and estimates of E^0 are summarized. Despite some puzzling inconsistencies, the experimental and theoretical potentials show general trends toward increasing ease of reduction for Cl < Br < I, and 1° < 2° < 3°. Allyl and benzyl halides are especially easily reduced.

The other half of the electron transfer is the loss of an electron from the Grignard reagent. The nature and stability of the radical cation $RMgX^{+\cdot}$ have been discussed less than those of $R'Y^{-\cdot}$. It is expected to decompose rapidly—possibly within the lifetime of a geminate radical pair—or to be unstable in the same sense as $R'Y^{-\cdot}$ [51]. Other organometallic radical cations are also believed to be very short-lived [52]. However, there is evidence that the radical *t*-BuMg· has a longer lifetime [53]. It might also be noted that long-lived colored species are observed by electronic and EPR spectroscopy in reactions of Grignard reagents with aryl ketones [54]. These are proposed to be ion–radical pair or aggregate complexes, incorporating the ketyl anion ($Ar_2CO^{-\cdot}$) and the radical cation of the Grignard reagent. However, these interpretations

Table 2.5. Reduction potentials of some organic halides[a]

Halide	$E^{0}_{1/2}$ (solvent)	E^{0}_{est} DMF[c]	THF[c]	DMF[d]	DMF[e]
MeBr	−1.72 (DMF) −1.77 (DW)	−1.06	1.32	—	—
EtCl	< −2.1 (DMF)	−1.15	−1.41	—	—
EtBr	−1.89 (DMF) −1.84 (DW)	−0.90	−1.16	—	−1.41
EtI	−1.43 (DW)	−0.92	−1.13	—	—
BuCl	—	−1.05	−1.31	−1.03	—
BuBr	−1.99 (DMF)	−0.90	−1.16	−0.97	−0.88
BuI	—	—	—	−0.83	—
neo-PentBr	−2.13	—	—	—	−1.48
i-PrBr	−2.02 (DMF)	−0.87	−1.13	—	—
sec-BuBr	—	—	—	−0.81	−1.50
t-BuCl	—	−1.07	−1.33	−0.90	—
t-BuBr	−1.95 (DMF) −1.84 (DMSO)	−0.82	−1.08	−0.69	−1.22
t-BuI	−0.98	−0.77	−1.34	−0.59	—
AllylCl	−1.89 (DMSO) −1.67 (DMF)	−0.65	−0.87	—	—
AllylBr	−0.97 (DMSO) −1.05 (DW)	−0.44	−0.70	—	—
AllylI	−0.92 (DMF)	−0.52	−0.73	—	—
$PhCH_2Cl$	−1.70 (DW) −186 (DMF)	−0.65	−0.91	−0.52	—
$PhCH_2Br$	−1.03, −0.98 (BMF)	−0.46	−0.72	−0.40	—
$PhCH_2I$	—	−0.65	−0.86	—	—
PhCl[f]	−2.54 (DMF)				
PhBr[f]	−2.20 (DMF)				

[a]All potentials are listed vs. the normal hydrogen electrode (NHE). [b]Polarographic half-wave potentials at the dropping mercury electrode; refs [38], p 95; [47]; [50], pp 200–204. [c]Thermodynamic estimate; refs [34], p 119; [47]. [d]Thermodynamic estimate; ref. [48]. [e]Kinetic/Marcus treatment estimate; refs [34], p 121; [49]. [f]E^{0} value; ref. [46].

have been questioned because of kinetic considerations and the absence of directly observable EPR spectra of the radical cation [36,51,55].

Decomposition potentials from electrolysis of Grignard reagent solutions were obtained as early as 1935 by Evans, Lee, and Lee [56]. This electrochemical step is completely irreversible. A reinvestigation by Holm [57] led to estimates of E^{0} for a series of Grignard reagents. These were derived from overvoltages measured at a constant electrode current density and adjusted relative to the normal hydrogen electrode. However, there were differences in electrochemical behavior among the Grignard reagents, and problems arising from irreversibility were not rigorously addressed. Despite their shortcomings, these remain the only E^{0} values available for Grignard reagents, and they are the ones quoted in discussions of mechanism [58]. They are listed in Table 2.6 along with a few representative values for other nucleophiles [59]. A clear trend exists for the alkyl Grignard reagents, with tertiary being the strongest reducing agent and methyl the weakest; phenyl is still weaker. Potentials somewhat more negative but parallel in trend have been derived from electrochemical studies of organolithiums [60]. Voltammetric peak oxidation potentials have also been reported for substituted arylmagnesium halides (4-OMe, 4-Me, and 4-Cl), but, because of irreversibility, no attempt was made to derive E^{0} values [61].

Table 2.6. Standard oxidation potentials for Grignard reagents and the other nucleophiles[a]

Nucleophile	Solvents	E^{0}[b]
MeMgBr	Et_2O	−0.25 (−0.5[c,d])
EtMgBr	Et_2O	−0.66
BuMgBr	Et_2O	−0.53 (< −1.2[c,d])
i-BuMgBr	Et_2O	−0.63
i-PrMgBr	Et_2O	−0.95
s-BuMgBr	Et_2O	−0.87
cyclo-PentMgBr	Et_2O	−0.88
t-BuMgBr	Et_2O	−1.07 (−2.0[c,d])
allylMgBr	Et_2O	−1.16 (−1.33[c])
$PhCH_2MgBr$	Et_2O	−0.73 (−1.1[c])
PhMgBr[e]	Et_2O	0.0 (< −0.1[c])
Ph_3C^-	DME	−0.96; −1.06[c] (−0.88[c])
$C_5H_5^-$	THF/HMPA	−0.10
$CH(CO_2Et)_2^-$	DMF	+0.64
PhS^-	THF	+0.1
t-BuO^-	THF	+0.6
SCN^-	THF	+1.4
I^-	THF	+1.1

[a]Summarized in ref. [34], pp 34–37 and ref. [59]. [b]Volts vs. NHE. [c]Oxidation of corresponding RLi in THF/HMPA; ref. [60]. [d]Solvent DME. [e]Extrapolated from a correlation between E^{0} values from ref. [57] and decomposition potentials from ref. [56].

It is clear that Grignard reagents are relatively strong reducing agents among the common nucleophiles, and should, therefore, be good candidates for SET reaction mechanisms. A SET mechanism for addition of Grignard reagents to ketones has been under consideration for some time [62]. A linear correlation between rate constants for addition of Grignard reagents to benzophenone and oxidation potentials of the Grignard reagents supports that mechanism [57]. With the less easily reduced ketone acetone [57] and with carbon dioxide [63], reactivities followed a reversed sequence, in which the steric bulk of the Grignard reagent may be hindering a polar addition. It should be noted that, if the Grignard reagent complexes with the ketone, the electron transfer is better described as inner-sphere.

The Grignard reagent oxidation potentials of Table 2.6 have also proven useful in interpreting

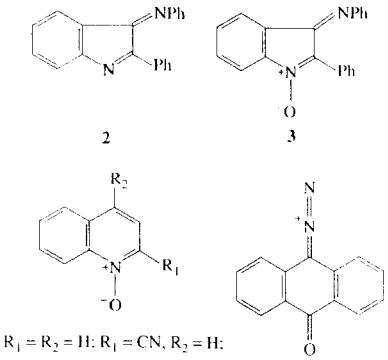

reactions of Grignard reagents with compounds **2** thru **6**. Reaction of **2** ($E^{0} = -0.67$ V)[64] or **3** ($E^{0} = -0.74$ V)[65] with the 5-hexenyl Grignard reagent ($E^{0} \sim -0.52$ V) yields addition products with partial cyclization of the 5-hexenyl to cyclopentylmethyl groups. Although the electron transfer should be endothermic (if Grignard E^{0} values are reliable), quantitative application of Marcus theory predicted rapid electron transfer, and the formation of cyclized products from the 5-hexenyl radical rearrangement 'clock' implies radical intermediates. Reaction of the 5-hexenyl Grignard reagent with several quinoline N-oxides **4**, with E^{0} between −0.97 and −1.69, led only to addition products with the uncyclized 5-hexenyl group [65]. 9-Diazo-10-anthrone **5** ($E^{0} = -0.62$ V) reacted with a variety of Grignard reagents to give radical side-products along with addition products formed by a polar mechanism [66]. The variation in yields was consistent with increased electron transfer reaction with the more easily oxidized Grignard reagents. The indole bisnitrone **6** ($E^{0} = -0.16$ V) oxidized Grignard reagents to radicals, which were trapped by a

stable nitroxyl radical [67]. All Grignard reagents were oxidized, including phenyl ($E^0 = 0.0$ V), and Marcus theory predicted rapid rates for all.

Standard electrode potentials of alkyl halides and nucleophiles have been used to predict the rates of SET alternatives to S_N2 substitution mechanisms [34,49,59,68,69]. A reaction much faster than predicted on the basis of Marcus theory is a likely S_N2 process, while similarity between prediction and rate, favors SET. Despite some disagreement as to the proper treatment of a dissociative electron transfer [48,70], this approach has proven useful in helping to classify reactions as probably S_N2 or SET in mechanism (most successfully with large, delocalized nucleophiles).

The standard electrode potentials listed in Tables 2.5 and 2.6 may be used to assess the energetics of electron transfer from a Grignard reagent to an organic halide. Two additional factors must also be included when considering a SET mechanism for coupling. The first is the reorganization energy, which is high for both the Grignard reagent and alkyl halide. In examples **2–6**, where Grignard reagents react with delocalized, electrochemically well-behaved electron acceptors (with small reorganization energies), it was considered that endothermic transfer is reasonable from the Grignard reagent to an acceptor with E^0 more negative by as much as 0.3 V. Because the electron transfer processes of both Grignard reagent and halide have large reorganization energies, their SET step would have a larger activation energy [58] and more favorable electron transfer thermodynamics might be necessary for the step to be feasible. A second factor is the rate of competing mechanisms. With **2–6**, the competing polar processes are fast, so that a SET mechanism must also be rapid in order to be important. Since many cross-coupling reactions of Grignard reagents are quite slow, even a relatively slow SET mechanism might, by default, be the path followed.

Two kinds of physical evidence may support a SET mechanism. EPR spectroscopy may detect and identify free radicals, often at concentrations present during radical reactions. The concentrations and lifetimes of radical pairs are generally too small for observation, so an EPR spectrum demonstrates only the existence of 'free' radicals. An uncertainty in interpretation is whether the radicals are actual intermediates in the reaction, or the consequence of a minor competing pathway or unrelated side-process.

Chemically Induced Dynamic Nuclear Polarization (CIDNP) is a transient enhancement in the intensity of NMR signals in a molecule which was formed in a reaction involving radical pairs [71]. It is the consequence of a perturbation of nuclear spin level populations resulting from interactions between electron and nuclear spin states in a transient radical pair. The enhancement may be positive, negative, or both (multiplet effect). It depends upon the nature of the precursor radical pair, its mode of formation (geminate formation of the radicals with paired or unpaired spins, or association of 'free' radicals), and whether the product is formed from the radical pair or from free radicals which have escaped from the pair. Despite its usefulness, there is also uncertainty whether the process which produces the nuclear polarization is the same as that by which the major products are formed. EPR and CIDNP observations during reaction between Grignard reagents and alkyl halides will be discussed below.

A more complete summary of the possibilities in a SET mechanism is provided in Scheme 2.1. Dissociative electron addition to the alkyl halide is assumed. The geminate radical pair can combine to form cross-coupling products or escape the 'solvent cage' as 'free' radicals. Either geminate pairs or free radicals can disproportionate in competition with coupling, forming alkane (RH or R′H) and alkene (R{−H} or R′{−H}). The *free* radicals have a variety of other fates: combination to form both cross- and homo-coupling products, abstraction of hydrogen from solvent (to form RH or R′H), diversion by a radical trap, or exchange with alkyl halide or Grignard reagent. If, in fact, the radical cation has a significant lifetime, it could influence product formation. Product-forming steps could then involve reaction of the radical cation with the radical from the alkyl halide. If the radical cation is less reactive than the 'unencumbered'

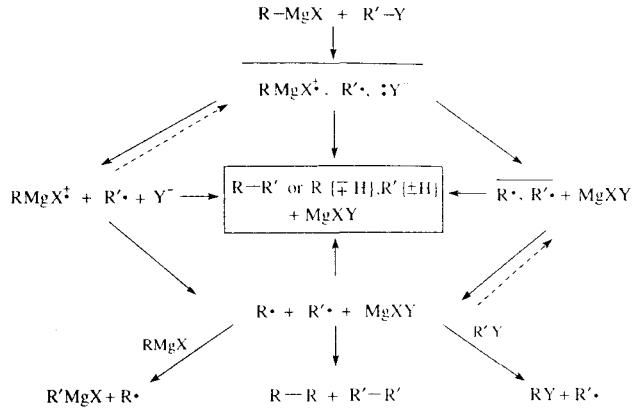

SCHEME 2.1

radical, the probability of escape from the solvent cage would be increased.

Before leaving the discussion of possible mechanisms, it should be pointed out that they may not be as distinctly separated in concept as it may have appeared in their individual descriptions. The distinction between S_N1 and S_N2 in solvolysis reactions is blurred by the probability of varying degrees of nucleophilic solvent participation in the S_N1 transition state [72]. Within S_N2 (eq. 2.8) there can be different extents of bond breaking and bond making in the transition state; at one extreme, a 'loose' transition state with a nearly broken bond to **L**: but little bond making to **Nu**: could be described as 'S_N1-like' [72]. Second-order kinetics may also be expected if **Nu**: reacts with an ion pair formed by rapid, reversible ionization of **RL** [73].

The difference between S_N2 and SET substitution mechanisms also lacks sharpness. It has been noted that a nucleophilic substitution reaction may be described alternatively as the transfer of one electron from the nucleophile to the leaving group, rather than as an electron–pair process: [74]

$$Nu^{\ddagger} + R{\cdot\cdot}L \longrightarrow Nu{\cdot\cdot}R + {}^{\ddagger}L$$

A mechanistic continuum is possible between the extremes of the classical S_N2 and the SET mechanisms. Reactivity has been fruitfully discussed in this context, and it has been proposed, based on a number of criteria, that some substitutions require a merged S_N2 and SET mechanistic description [69,74].

A similar linkage exists between S_N1 and SET. The combination of the carbocation with the nucleophile could occur by a simple polar coordination of the nucleophile's electron pair with the carbocation's vacant orbital, by a stepwise transfer of a single electron followed by radical coupling, or by something in between. In the 'assisted' S_N1 mechanism outlined for Grignard cross-coupling, the charges in the ion pair (eq. 2.10) should facilitate both the electron transfer *from* the magnesium species and *to* the alkyl of the organic halide. A result might be the formation of 'radical' side products in a reaction which is basically ionic in nature.

2.4 MECHANISM OF GRIGNARD CROSS-COUPLING REACTIONS

2.4.1 Saturated Alkyl Halides

2.4.1.1 Saturated and Aryl Grignard Reagents

Reactions of saturated alkyl halides with saturated alkyl Grignard reagents are usually relatively slow.

and frequently produce little cross-coupling product. The electrode potentials listed in Tables 2.5 and 2.6 suggest that the electron transfer from tertiary or secondary Grignard reagents to most of the alkyl halides ranges from slightly exothermic to slightly endothermic. To the extent that these potentials may be relied upon, and provided that the reorganization energies are not too large, they would predict that a SET mechanism is feasible. Electron transfers involving primary and methyl Grignard reagents are less favorable, as are those to methyl halides, but if competing mechanisms are slow enough, the SET process might dominate. Alkyl iodides should be the most susceptible and chlorides the least to SET. The minimal information available on the stereochemistry of the displacement would also be consistent with formation of coupling product from radicals [4,6,75]. Product is largely racemic: residual optical activity could result from orientation in radical pairs or a small amount of S_N2 displacement.

There have been several reports of CIDNP polarization during reactions between saturated alkyl halides and saturated Grignard reagents. The clearest polarizations are seen for the olefinic resonances of disproportionation product; polarization of alkanes from disproportionation and coupling has been reported, but it is more likely to be obscured by other resonances. Studies reported have included the following pairs of reactants: *t*-BuBr with *t*-BuMgCl [12], BuI with BuMgBr [12], BuI with *t*-BuMgCl [12], *t*-BuBr with BuMgBr [12], EtI with Et_2Mg [10], *i*-PrI with Et_2Mg or EtMgBr [10], and *t*-BuBr with *i*-PrMgBr [76]. Reactions were run in THF, and it was necessary to use alkyl iodides or tertiary halides to have a rapid enough reaction to see the CIDNP effect.

Similar and more extensive studies have been made of the RLi + R′Y reaction [77]. For the latter, results support a mechanism analogous to eq. (2.6). A geminate radical pair is formed by transfer of an electron from RLi to R′Y; these radicals couple and disproportionate in competition with diffusion from the 'cage'. Polarized alkyl iodide spectra also result from abstraction of iodine atoms by free alkyl radicals. Metal–halogen exchange did not lead to polarization in the alkyllithium. Although some aspects of the interpretation are not completely straightforward, the CIDNP polarizations observed have been satisfactorily rationalized.

The CIDNP observations with Grignard reagents do not parallel those from the lithium reagents, and more closely resemble those from reactions of the Grignard reagent with alkyl halides *catalyzed by added iron salts* [76,78]. In particular, the 'multiplet effect', in which half of a multiplet is intensified (enhanced absorption) and the other half becomes negative in intensity (enhanced emission), appears with phase reversed from that expected for eq. (2.6). The most straightforward implication of the phase of the multiplet effect is that coupling and disproportionation products result mainly from diffusionally formed rather than geminally formed radical pairs. In the catalyzed reactions, this appears to be because radicals are not generated in pairs, but singly by reaction of reduced transition metal species with the *alkyl halide*. They must then diffuse together in order to disproportionate or couple. The oxidized form of the metal then converts the alkyl group of the *Grignard reagent* to disproportionation or coupling products via a non-radical route. The catalysis is very strong, either by added transition metal salts or by impurities in the magnesium (enhanced by oxidants, including oxygen or halogens) [76]. There is also CIDNP evidence for the occurrence of radical displacements on the alkyl halide (especially iodides) and on the magnesium, which may give exchange or scramble alkyl groups from the two sources (see Scheme 2.1) [79]. In the reaction of *i*-PrI with Et_2Mg [10], polarization of the *i*-PrI was observed, but there was no EtI formed nor polarized EtI resonances in the CIDNP experiment. These results suggest that *i*-Pr• radicals were present during the reaction, but not Et• radicals.

As noted earlier, the observation of CIDNP indicates that the polarized product is formed in a process involving radical pairs, but does not require that all (or even most) of it is formed by that route. It is possible that 'uncatalyzed coupling' with simple alkyl groups does not exist, and that

the reaction is entirely catalyzed by impurities. Alternatively, the uncatalyzed coupling may be a non-radical process (or a radical one producing weaker polarization), in competition with catalyzed side-reactions, so that only polarization from the side-reactions is seen. It is also possible that the radical cation of the Grignard reagent is sufficiently long-lived that it diffuses away before decomposing to a free alkyl radical (Scheme 2.1); then, coupling or disproportionation would then have to occur by diffusive encounters of R• and R•′ radicals.

Another problem with the SET mechanism is the preponderance of disproportionation over coupling products. The ratio k_d/k_c (disproportionation to coupling) is quite small for reaction of two primary radicals (<0.2), but larger for secondary/secondary and *t*-Bu/*t*-Bu encounters (~1 and ~5, respectively) [80,81a]. Thus, cross- or homo-coupling should be the major result in most cases if products are formed by interaction of radicals, whether in a geminate radical pair or from encounter. In view of the CIDNP results noted above, the excess of disproportionation might be from transition metal-catalyzed reaction or a polar E2 elimination. Disproportionation from reaction of the Grignard reagent radical cation, before its cleavage to an alkyl radical, should probably produce alkene with different polarization.

With either tertiary alkyl halides or Grignard reagents, coupling yields are relatively good (entries 5–8, and 12 in Table 2.1). The tertiary halides react more easily without catalysis, and in entry 7 the tertiary halide is displaced in preference to the primary. A tertiary alkyl group from either Grignard reagent or alkyl halide led to CIDNP-polarized alkene under conditions where metal–halogen exchange was absent [12]. Electrode potentials are more favorable to electron transfer for either a tertiary Grignard reagent or halide, so SET becomes a more probable pathway. Coupling yields for reactions involving tertiary Grignard reagents or halides may also be reasonable for radical–radical encounters. Additional evidence favoring a SET mechanism is the isolation of coupling product with rearranged alkyl group in eq. (2.16) [11].

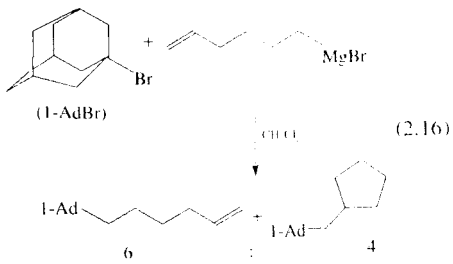

Since the tertiary carbocation is considerably stabilized, the 'assisted' S_N1 pathway (eq. 5) might be considered as a competing possibility. A number of other reactions of tertiary halides have been reported in which unexpectedly good yields of substitution are obtained. These include reactions with $Zn(SCN)_2$ [82], $Zn(SC(O)CH_3)_2$ [83], NaN_3 in the presence of $ZnCl_2$ [84], and metal alkoxides [85]. In the latter case, alkaline earth salts are superior to alkali salts, the reaction gives better yields in non-polar solvents, and crown ethers lower the yield. An intermediate carbocation, in an ion pair or aggregate, seems likely because of the Lewis acidic metal ion and low reducing capability of the nucleophile (Table 2.6). In the reaction of $ArCH{=}CHCH_2Li$ reagents with tertiary halides, a similar competition between SET and a polar 'S_N1-like' process has been proposed in order to explain the regiochemistry and other features, despite the strong reducing ability of the lithium reagent [86]. As noted above, electron transfer to the carbocation within the aggregate is an additional variant.

Aryl Grignard reagents seem less reactive in coupling and may require higher temperatures, but yields are often quite good (Table 2.1, entries 9–11). They are much poorer electron donors than alkyl Grignard reagents (see Table 2.6), so a SET process should be a great deal slower. If the reaction involved aryl radicals, lower coupling yields might also be expected, since those radicals escaping the solvent 'cage' would probably abstract a hydrogen from solvent rather than surviving long enough to couple. Although the sp^2 C–Mg electrons are more tightly held, they may be

sterically more accessible for reaction as a nucleophile in an S_N2 process.

2.4.1.2 Benzylic and Allylic Grignard Reagents

Benzylic and particularly allylic Grignard reagents are quite reactive toward saturated halides and frequently give good yields. Despite the chemical similarity often found between allyl and benzyl groups, the oxidation potentials of the corresponding Grignard reagents are quite different. Allylmagnesium bromide is the strongest electron donor listed in Table 2.6, while benzylmagnesium bromide is toward the middle of the list.

Letsinger and Traynham found that allylmagnesium bromide and benzylmagnesium chloride react with secondary halides with markedly different results [87]. The former coupled with 2-bromooctane in 78% yield and 79–87% inversion of configuration. (The latter is uncertain because of uncertain optical purity of the 2-bromooctane). Benzylmagnesium chloride with 2-bromobutane gave a low yield of coupling product, which was nearly racemic. Alkali metal allylic and benzylic derivatives also couple with secondary halides with high degrees of inversion, in contrast to alkali metal alkyl compounds [75,88]. Those results would support an S_N2 mechanism for the delocalized carbanions, and SET for the saturated alkyllithiums.

The racemization and low yield found with the benzyl Grignard reagent suggest a SET mechanism. On the other hand, despite its large negative E^0, the predominant inversion of configuration with allylmagnesium bromide is more consistent with S_N2. Although some optical activity may be preserved in radical cage reaction products, the high extent of inversion would not be expected [81]. Partial racemization (if it is real) might indicate competing SET or result from racemization of starting material by bromide ion from the Grignard reagent. If both benzyl and allyl Grignard reagents were to react by SET, it would be surprising that the larger benzyl group should diffuse from the radical pair much more efficiently and lead to less cage recombination product. Some substitution reactions by benzylic Grignard reagents appear to be more successful [6], so it is possible that the two mechanisms are closely balanced, and one or the other may be favored by a change in structure or conditions. Because of delocalization, either an allyl or a benzyl group in a Grignard reagent may be less encumbered by the metal, and better able to attack as a nucleophile than an alkyl Grignard reagent. The allyl reagent may be more efficient in this respect because of its ability to react at its γ-position:

$$XMg{-}C^*H_2CH{=}CH_2 + R'{-}Y \longrightarrow XMg^+ + C^*H_2{=}CH{-}CH_2{-}R' + Y^-$$

Two additional delocalized organomagnesium compounds might be noted. First, cp*MgCl (**7**) cross-couples in good yield with cyclopropylmethyl bromide. Rearrangement of the cyclopropylmethyl group, which would have been expected for a radical intermediate, was not observed [89a]. The second is magnesium anthracene, the adduct formed from the interaction of anthracene with magnesium metal, which forms an isolable THF complex **13**. It reacts as a nucleophile with primary and secondary alkyl halides in THF, forming mixtures of dialkyldihydroanthracenes in high yield [89b]. The coupling reactions in these two instances would be consistent with S_N2 substitutions. If the reactions were SET in mechanism, they would require very efficient trapping of the alkyl radical by geminate radical pair combination or scavenging. Benzyl and allylic halides reacted with **8** to produce the corresponding Grignard reagent as the major product; methyl iodide produced methane, ethane, and Me_2Mg in addition to the cross-coupling product; and with PhBr and PhI the major product was benzene. The latter reactions are most easily explained by radical formation via electron transfer to the organic halide.

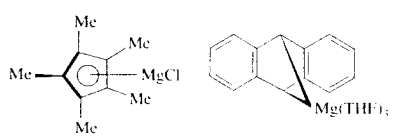

7

8

2.4.2 Benzylic and Allylic Halides

Benzyl and allyl halides are both easily reduced by transfer of an electron (Table 2.5). They are also reactive in both S_N2 reactions (comparable to methyl and 30 to over 100 times faster than 1°) and S_N1 (between 2° and 3° in rate) [7–9]. They might, therefore, be expected to react readily with Grignard reagents by any of the three mechanisms under consideration, and, in fact, they are generally more reactive than alkyl halides.

There is evidence that SET mechanisms are important in reactions of Grignard reagents with allyl and benzyl halides. In one of the rare mechanistic studies of Grignard coupling, Gough and Dixon determined by competition the relative rates of reaction of PhMgBr, BuMgCl, sec-BuMgCl, and *t*-BuMgCl with allyl bromide [90]. The rate increased in the order listed, and the latter three were reported to give a linear Hammett plot with a ρ-value of -1.9. 2,2,3,3-Tetramethylbutane was also observed as a by-product in the *t*-BuMgCl reaction and a weak transient EPR signal was seen. Results were taken to favor a radical pair mechanism, on reasoning that the negative ρ-value implies a lower electron density on the alkyl group in the transition state than in the Grignard reagent. However, it is unclear what substituent constants were used. In our hands, the correlation vs. Taft's σ^*-values of the butyl groups had a remarkably large ρ^*-value of -9! The relative rates are also linearly related to the E^0 values in Table 2.6, with a slope of -2.75. The rate for phenyl is much faster than predicted by either correlation. The interpretation may also be ambiguous, in that the inherent order of polar reactivity of the Grignard reagents, apart from their steric effects, should lie in the same sequence.

Support for a SET mechanism also comes from CIDNP observations in the reactions of *t*-BuMgX with allyl and benzyl bromides [78a]. It is stated (but without details) that the polarization indicates a mechanism involving geminate radical pairs, as expected in eq. (2.6). A study of the reaction of EtMgBr with p-$ClC_6H_4CH_2Br$ led to similar conclusions, though the emphasis was on exchange and disproportionation rather than coupling [91].

Cross-coupling yields from allyl bromide are almost always good, and some benzyl halide reactions are also quite successful (e.g., Table 2.2, entries 9–11). Frequently, however, yields with benzylic and substituted allylic halides are poorer (e.g., Table 2.2, entry 8; allyl bromide and benzyl chloride coupled with **1a** in yields of 75% and 20% [15]). If a SET mechanism leads rapidly to the radical pair [R•,R'•], the same pair would be anticipated from alkyl Grignard and benzyl halide as from benzyl Grignard and alkyl halide. Both of these combinations, in fact, usually lead to poorer cross-coupling yields than the allyl analogs. The contrast has been discussed above (Section 2.4.1) for allyl and benzyl Grignard reagents.

Metal–halogen exchange or alkyl exchanges of the Grignard reagent or alkyl halide (Scheme 2.1) may be responsible for at least some of the homo-coupling side reaction. In our laboratory we found that when benzyl bromide reacts with cyclopentylmagnesium bromide, bibenzyl and benzylmagnesium bromide are seen in the ^{13}C NMR spectrum of the solution after reaction [92]. Exchange of the alkyl halide with the halide ion of the Grignard reagent may also occur more rapidly than coupling, since iodide and bromide are quite reactive nucleophiles. If the tendency to SET increases in the sequence Cl < Br < I, then halide exchange could also increase the probability of SET reaction (with accompanying homo-coupling). It is not clear to what extent these exchanges may contribute generally to homo-coupling.

Another complexity with allylic substrates is the potential for formation of allylic isomers. Reviews by De Wolfe and Young [93], Figidère and Franck [94], and Magid [95] are relevant to this question. Scheme 2.2 illustrates the consequences of S_N1 and SET in the prototype substituted allylic system, crotyl/α-methylallyl. The new bond formation, at either end of the allylic system, could be subject to a 'memory effect' due to restricted reorientation during the lifetime of a radical or ion pair. Alternatively, competition between S_N2 and S_N2' could lead to isomer mixtures (Scheme 2.3). In early work [96], reactions of crotyl and α-methylallyl chlorides with PhMgBr led to mixtures (**9** : **11** ≃ 75 : 25) which

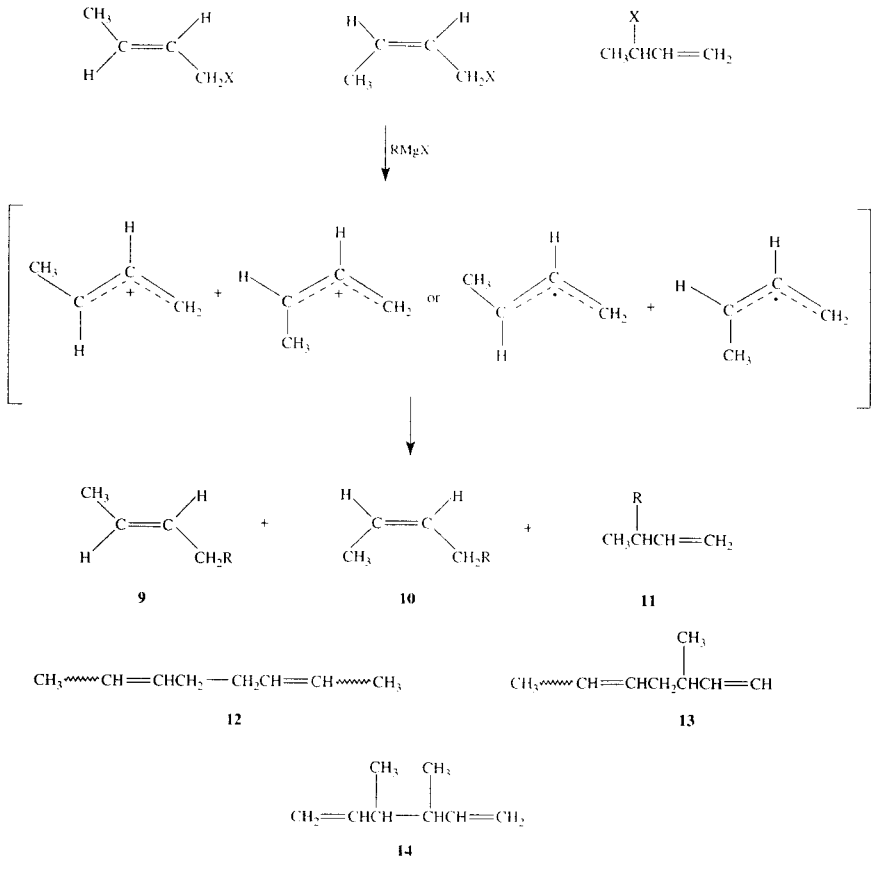

SCHEME 2.2

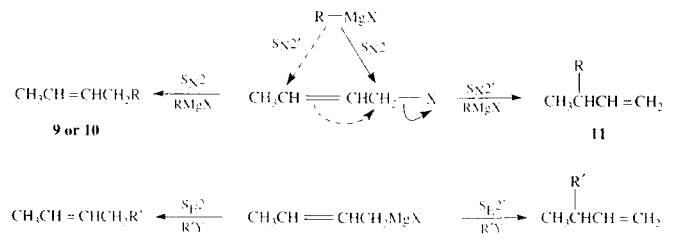

SCHEME 2.3

were indistinguishable within experimental error. More recently, p-$CH_3OC_6H_4MgBr$ gave similar but non-identical mixtures, with compositions sensitive to solvent (Et_2O vs THF) and double bond configuration [97]. Other coupling reactions which have been reported seem to follow a similar pattern [6]. BuMgBr, BuLi and BuNa all gave mostly **9** and **10** with all three chlorides, with double bond configuration largely preserved [98]. However, with *cis*-crotyl chloride and *t*-BuMgCl, **11** was the major product. Results have been explained by versions of the 'assisted S_Ni'' mechanism [97,98], although a case for concerted mechanisms (S_N2 and S_N2') has been made [95].

There is a similar possibility of isomerism in an allylic group coming from the Grignard reagent. Substituted allylic Grignard reagents exist as equilibrium mixtures with the less-substituted allylic isomer predominating [99], but usually react to form the 'S_E2' product' (Scheme 2.3). When dicrotylmagnesium (or crotylmagnesium bromide) reacts with crotyl chloride and its allylic isomer, the major coupling product **13** reflects the preference for formation of the bond at the secondary carbon of the Grignard reagent and the primary carbon of the halide [98]. The regiochemistry could result from concurrent S_N2 and S_N2' processes of the halide and S_E2 and S_E2' processes of the Grignard reagent. More likely, the allylic fragment from the halide is released as a radical or cation en route to product. An assisted S_Ni mechanism, with restricted mobility for carbocation reorientation, and possibly competing S_N2 (particularly at the primary carbon) is probable. It seems less likely that a SET mechanism leads to a product-forming radical pair, since the composition of the mixture of hydrocarbons **12**–**14** differs from that reported for coupling of free crotyl radicals [100].

Some results from our laboratory are also difficult to rationalize in terms of product formation by radical coupling in the reaction of allyl bromide (Scheme 2.4) [92]. A mixture of *exo*- and *endo*-2-norbornylmagnesium bromide reacts with allyl bromide to form the diastereomeric 2-allylnorbornanes in a mixture approximately mirroring the composition of the Grignard reagent. The endo isomer of the Grignard reagent, obtained by preferential destruction of the exo isomer [101], forms only *endo*-2-allylnorbornane. The result would be consistent with 'assisted S_Ni'', in which the allyl cation reacts with retention at the norbornylmagnesium bond, or S_N2, in which the nucleophilic electron pair of the Grignard reagent retains its configuration through the reaction (as it is found to do with carbon dioxide or mercuric chloride [101]). The nearly complete retention of configuration is inconsistent with the norbornyl radical as an intermediate, since radical cage recombinations of radicals do not usually occur with high configurational memory [81], and the norbornyl radical has a modest preference for reaction from the exo side [102]. A SET mechanism is possible only if the radical cation of the Grignard reagent is the product-forming intermediate, and reacts with retention.

A final note might be made of differences which have been reported in the coupling of allyl bromide with phenyl Grignard reagents as conventionally prepared and reagents obtained from cryogenic reaction of the halobenzenes co-condensed with magnesium vapors [103]. The bromo and iodo reagents, formulated as $PhMg_2X$, cross-coupled with low activation energy (3 and 0 kcal/mol, respectively), about an order of magnitude faster than the conventional reagents. Reagents from chloro- and fluorobenzene, formulated as $PhMg_3X$, also reacted rapidly, but mostly exchanged to produce bromobenzene and (after hydrolysis) propene.

2.4.3 α-Haloethers and -Thioethers

An oxygen or sulfur substituted on a carbocationic center greatly stabilizes the species by resonance:

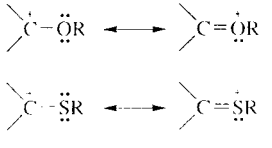

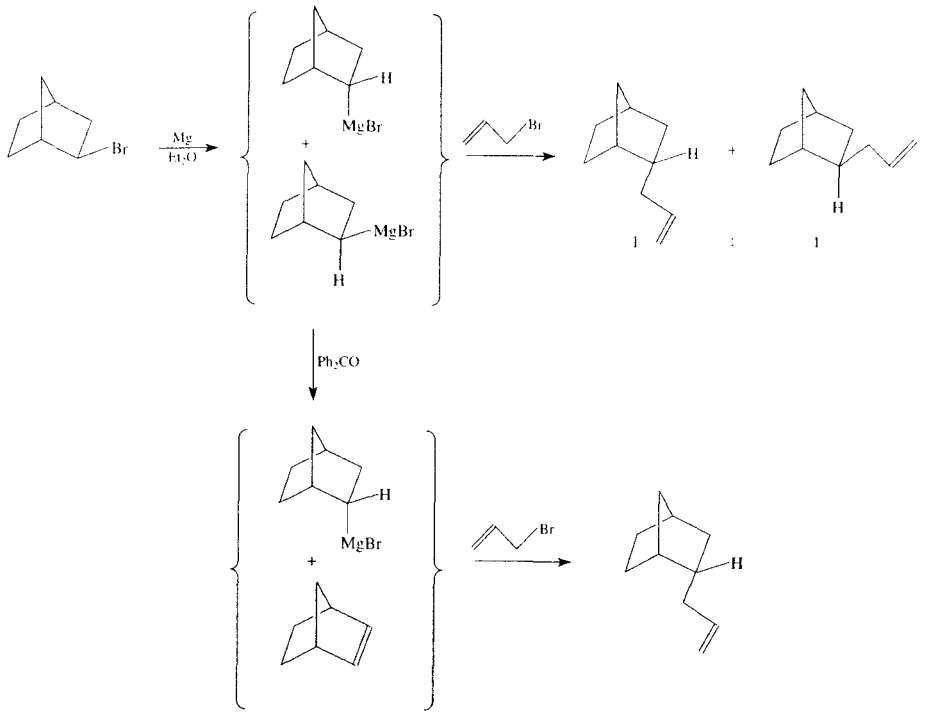

SCHEME 2.4

For this reason, the halogen of α-haloethers or -thioethers is very reactive in S_N1 reactions, and such compounds should also be prime candidates for an S_N1 mechanism in their reaction with Grignard reagents. As noted above (Section 2.2.2), these reactions do occur very readily and often in good yield, and a carbocation is the consensus intermediate [104]. In the reactions collected in Table 2.3, the predominance of retention in entries 3 and 6 and the probable carbocation rearrangement product in entry 5 might be noted.

An oxygen or sulfur also stabilizes an adjacent radical, so a SET mechanism with a radical intermediate might be an alternative. An estimate of the radical stabilization may be made by comparison of the primary C–H bond dissociation energies of propane (100 kcal/mol) and dimethyl ether (93 kcal/mol) [105]. However, the stabilization is only about half that of the allyl radical, and may be insufficient to account for the size of the activating effect on the coupling. (The reaction in entry 2 is complete in less than an hour at −45°C.)

2.5 OTHER CLASSES OF SUBSTRATES

2.5.1 Arylmethyl Compounds

Benzylic Grignard reagents and halides have been discussed previously (Sections 2.4.1.1 and 2.4.2). For either, low yields and homo-coupling are frequently (but not always) encountered, and an SET mechanism (or possibly unintentionally catalyzed side reactions) may be involved.

Triphenylmethylmagnesium bromide (tritylmagnesium bromide) couples in high yield with some halides (MeI, 93–98%; allyl-Br, 88%; $PhCH_2Br$, 90%; Ph_2CHBr, 90%) [6]. When the halide has β-hydrogens, the yield falls, and with *t*-BuBr there is no coupling, but a 75% yield of Ph_3CH is isolated. Trityl halides also couple in good yield with MeMgBr and $PhCH_2MgCl$; lower yields, along with Ph_3CH, are reported for other alkyl Grignard reagents [106]. The trityl radical is frequently mentioned as an intermediate in these reactions [6,20,107–109]. The trityl Grignard reagent should be a good electron donor (Table 2.6) and the trityl halides might accept an electron either directly or after heterolytic cleavage to a trityl cation. The relatively high concentration of stable trityl radicals which builds up in solution should efficiently scavenge the other radical, leading to a prevalence of cross-coupling over homo-coupling [55]. In a SET mechanism, the same radical pair would be generated from combinations with either a trityl Grignard reagent or trityl halide, and similar product mixtures and yields might be expected. Coupling and disproportionation products could also be formed by polar processes—direct S_N2 and/or E2 reaction of Ph_3CMgX with R′Y, and direct reaction of Ph_3C^+ (from Ph_3CY) with $RMgXY^-$.

The reaction of trityl halides with phenyl Grignard reagents has been of interest as a source of the sterically crowded tetraphenylmethane. Yields have been variously reported between 0 and 29%, mostly at the lower end [6]. A major alternative product appears to be **15**, resulting from attachment of the phenyl to a para position of the trityl group. This product has been cited as evidence for a trityl radical intermediate, but it could arise as well from the polar combination of a trityl cation with the Grignard reagent. The trityl radical dimer (**16**) and trityl peroxide are also found as by-products. A more recent report [20] claims a yield of 46% of Ph_4C, but without experimental details or comments on the product. Interestingly, tetraarylmethanes are formed in about 50% yield when the para positions of the trityl group are blocked or an ortho substituent is present [6].

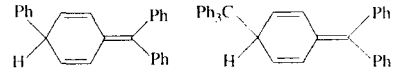

15 **16**

With vinylmagnesium bromide, trityl chloride gave a mixture including cross- and homo-coupling, but the major reaction course produced Ph_3CH and acetylene [107]. An EPR spectrum of $Ph_3C^{\bullet}$ was observed, and products showed CIDNP polarization. A SET mechanism was proposed, in which the radical cation of the Grignard reagent fragments to acetylene and $HMgBr^+$, from which hydrogen is abstracted. Benzhydryl and 9-fluorenyl halides also couple in good yield with Grignard reagents lacking β-hydrogens (PhMgBr [20], MeMgBr, Ph_3CMgBr[6]), but homo-coupling and reduction become more important in other cases. With vinylmagnesium bromide, Ph_2CHCl and $PhCH_2Cl$ gave more homo- than cross-coupling, and no acetylene [107]. CIDNP polarization of the homo-coupling product ($Ph_2\dot{C}HCHPh_2$) was observed and weak EPR was seen.

Trityl derivatives with other leaving groups have been examined as alternatives in coupling with Grignard reagents. They will be included here, although they relate to classes of compounds covered in the following sections. The preformed trityl cation as its perchlorate salt couples in 41% yield with MeMgI, but with PhMgBr only an intractable mixture containing a little Ph_3CH and no cross-coupling could be isolated [108]. Trityl acetate and benzoate likewise reacted with MeMgX to form coupling product; with PhMgBr they gave mostly trityl peroxide and Ph_3CH, and the ESR spectrum of the trityl radical was seen during the reaction [109]. Trityl ethers are also cleaved by Grignard reagents under relatively mild conditions [6]. With alkyl Grignard reagents, Ph_3CH appeared to be the major product; PhMgBr with $PhOCPh_3$ gave up to 20% of Ph_4C at 200°C, but mostly trityl peroxide at low temperature. The Ph_3CH by-product is variously ascribed to abstraction of hydrogen from the ether solvent by $Ph_3C^{\bullet}$, to radical disproportionation, to metal halogen exchange, or to hydrogen transfer from the Grignard reagent. It is not clear whether differences among leaving groups may be attributed to actual

differences in mechanism, to the conditions used, or to the quality of the magnesium available at different times. Assisted ionization to Ph_3C^+ is likely since the leaving groups are poor electron acceptors.

2.5.2 Polyhalogen Compounds

Geminal di- and polyhalides are reactive toward Grignard reagents, but the predominant reaction is usually not substitution. In early work [6], $CHCl_3$ and CCl_4 were reported to react with excess EtMgBr to produce mostly CH_4 and C_2H_4; with $CHBr_3$ and CHI_3, a variety of partial reduction and halogen-exchange products were formed. PhMgBr reacted with $CHCl_3$ to produce a good yield of the apparent substitution product, Ph_3CH, but with $CHBr_3$ and CHI_3, only $Ph_2CH\text{-}CHPh_2$ was formed. CCl_4 gave trityl peroxide, the trityl dimer, and some Ph_3COH. The latter are reminiscent of the reactions of the trityl and benzhydryl halides, and radical intermediates are suggested. A useful example of selective partial reduction is in eq. (2.17); radical abstraction of hydrogen from the solvent is likely [110].

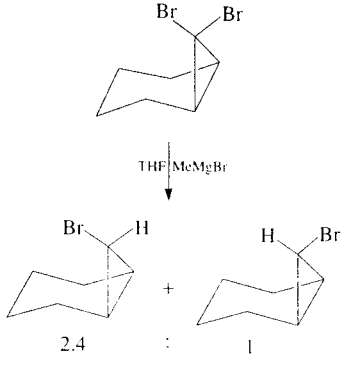

(2.17)

Geminal polyhalides are generally less reactive in nucleophilic substitutions than monohalides [7]. A SET mechanism is likely in their reaction with Grignard reagents, since they accept an electron considerably more readily than monohalides. Some polarographic half-wave reduction potentials ($E_{1/2}$, measured in dioxane-water and adjusted to the NHE) are as follows: CCl_4, −0.54 V; $CHCl_3$, −1.43 V; CH_2Cl_2, −1.99 V; CBr_4, −0.05 V; $CHBr_3$, −0.25 V, CH_2Br_2, −1.24 V [111]. These may be compared with $E_{1/2}$ for mono-halides listed in Table 2.5. (Note that these polarographic potentials are not equivalent to E^0.)

CIDNP has also been observed in the reactions of *t*-BuMgCl with $CHCl_3$ and $PhCHCl_2$ [112]. In both cases, the product was a complex mixture resulting from the various abstraction, coupling, and disproportionation reactions of the radicals produced by electron transfer from the Grignard reagent to the halide. Cross-coupling products were formed in yields of only 9 and 17%, respectively. The polarizations observed implied the formation and reaction of a geminate radical pair, as in eq. (2.6).

Carbenoid intermediates may also be involved. A chain extension product formed when $CHBr_3$ was treated with primary alkyl Grignard reagents is most easily explained by a mechanism involving bromocarbene (eq. 2.18) [113]. When ethyl or phenyl Grignard reagents reacted with $CHCl_3$ or CCl_4 in the presence of cyclohexene, the products included 3,3′-bicyclohexenyl (from coupling of cyclohexenyl radicals), (dichloromethyl)cyclohexane (explained by the addition of $CHCl_2\cdot$ radicals to cyclohexene), and the dihalocarbene adduct of cyclohexene [114].

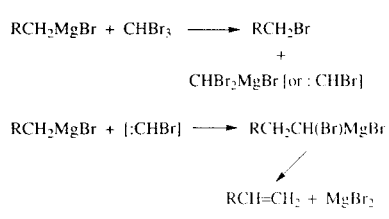

(2.18)

Vicinal dihalides also react readily with Grignard reagents, and again, the usual products are not from substitution at the carbon (eq. 2.19) [115]. The relative ease of accepting an electron makes a SET mechanism appear likely (e.g., $E_{1/2}$ = −0.99 V vs. NHE for $BrCH_2CH_2Br$) [50,111].

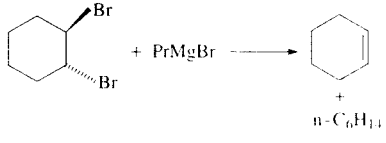

(2.19)

An unexpectedly efficient homo-coupling has been reported to occur when various aryl, vinylic, acetylenic, or alkyl Grignard reagents are treated with 2,3-dichloropropene (eq. 2.20) [116]. Primary Grignard reagents homo-coupled in about 60% yield, but the yield was reduced for secondary and tertiary ones at the expense of cross-coupling. Allene is formed from the 2,3-dichloropropene. Under similar conditions allyl chloride and 2-chloro-3-iodopropene yield mostly cross-coupled product (75 and 90%, respectively) and 2,3-dibromopropene is also reported to give cross-coupling [6]. The proposed mechanism involved initial electron transfer, with eventual generation of two radicals from Grignard reagent per dichloride molecule consumed. Product formation was presumed to occur by coupling of the radicals. Electron transfer to the dichloride is reasonable, in view of the increased ease in reduction of other poly-halides. Questions remain, however. It is surprising that the dichloride should be so unique in its behavior, and also that aryl radicals would survive hydrogen abstraction long enough to couple in high yield.

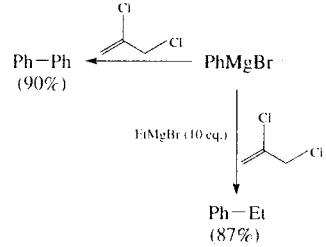

(2.20)

2.5.3 α-Haloketones

A halogen α- to a carbonyl group is often reactive in S_N2 displacements [7]. In fact, 2-chlorocyclohexanone, for example, is converted to 2-phenylcyclohexanone by reaction with PhMgBr in benzene [117]. References [3] and [5] list such reactions without further comment as examples of the displacement of halogens. It might seem surprising that the halogen displacement should be more facile than addition to the carbonyl group. Nevertheless, the displacement via a SET mechanism *might* be favored by the ease of addition of an electron. Cathodic reduction of α-halocycloalkanones occurs readily, yielding reduction, coupling and Favorskii rearrangement products [118]. Peak voltages in cyclic voltammetry of 2-chlorocyclo-hexanone and 2-bromocyclohexanone (−1.62 and −0.56 V) may be compared with $E_{1/2}$ values of simple mono-halides in Table 2.5 (noting again that these are not the same as E^0). However, these are not simple substitution reactions, and in most cases (e.g., eq. 2.21) substitution is the consequence of rearrangement of the magnesium salt of the halohydrin formed by Grignard addition to the carbonyl group [119].

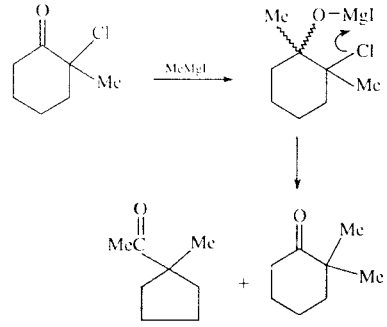

(2.21)

An alternative mechanism involving an epoxide intermediate appears to operate in some cases (eq. 2.22) [120]. When the carbonyl group reactivity is effectively decreased by steric hindrance, a reductive enolization is observed (eq. 2. 23) [121].

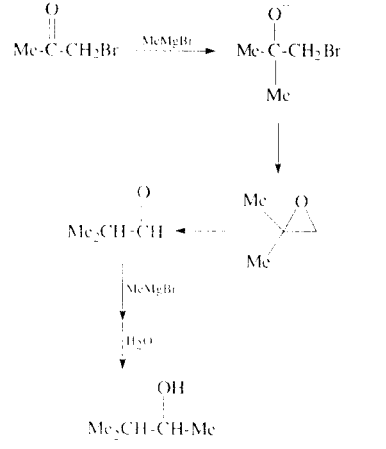

(2.22)

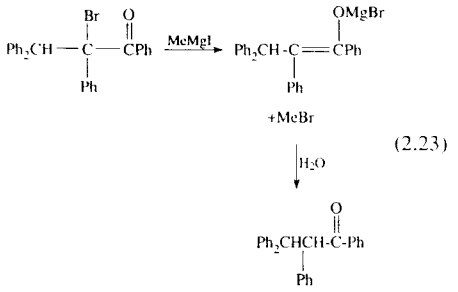

(2.23)

were entirely from addition to a ring carbon. An electron transfer mechanism was preferred, but direct ionic coupling was considered an alternative or competing process.

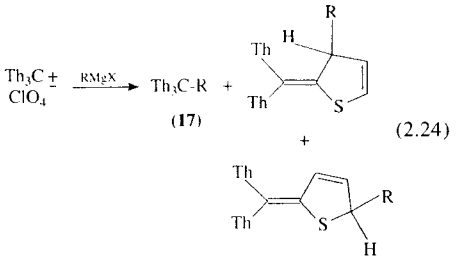

(2.24)

2.5.4 Other Leaving Groups

Groups other than halide may also function as the leaving group in nucleophilic substitution reactions [7,8]. Traditionally important leaving groups include the anions of strong oxy-acids (sulfonates, sulfates, phosphates, p-nitrobenzoates, etc.), neutral oxygen species (water, alcohol, or ether from protonated alcohols and ethers and trialkyloxonium ions, respectively), tertiary amine or dialkyl sulfide molecules (from ammonium or sulfonium ions), and N_2 (from diazonium ions). Leaving group reactivity is roughly related to the stability of the leaving group as a free entity.

2.5.4.1 Reaction with Carbocations—No Leaving Group

One extreme in a displacement reaction would be where the leaving group has already departed, and a preformed stable carbocation reacts with the nucleophile. In this event, the cross-coupling reaction might be either direct polar combination of the carbocation with the Grignard reagent or electron transfer to the carbocation followed by radical recombination.

Reactions of the trityl cation with Grignard reagents have been discussed earlier. The heterocyclic analog, tris-(2-thienyl)methyl perchlorate [108], reacted with a selection of Grignard reagents to yield coupling products in good combined yield (eq. 2.24). The product **17**, from coupling with the central carbon, comprised over half of the product with MeMgI, but decreased to 15% with *t*-BuMgCl, and with aryl Grignard reagents products

Substituted cyclopropenyl cations couple readily with Grignard reagents (eq. 2.25). The ratio of **20** to **19** produced from coupling with **18** was larger for the more easily oxidized Grignard reagents (allyl, benzyl, 3°). This was believed to indicate a mechanistic shift from polar to SET, because the radical corresponding to **18** prefers to dimerize at a phenyl-substituted position [122]. The cycloheptatrienyl (tropylium) ion also couples with Grignard reagents, though in low yields [123]. Oxidation potentials reported for the trityl, tropylium, and triphenylcyclopropenyl cations (−0.13, −0.62, and −1.30 V. vs. SCE, respectively) [124] suggest that the probability of reduction by SET from Grignard reagents should decrease in that sequence. Coupling with Grignard reagents is also reported for **21**–**24**, which are formally carbocations [6].

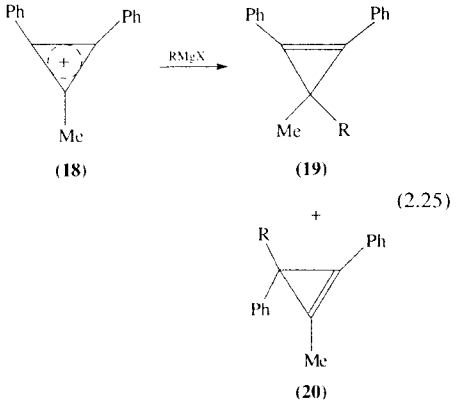

(2.25)

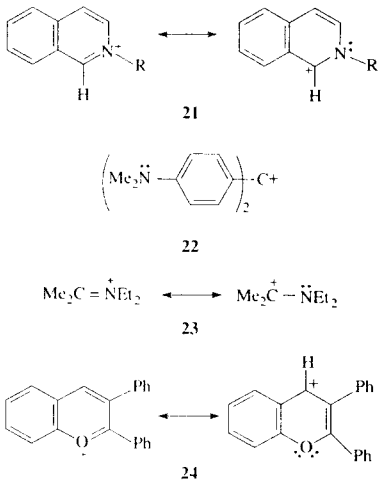

2.5.4.2 Oxy-Anions

Sulfate and Sulfonate Esters.

Sulfates and sulfonates are generally reactive in nucleophilic substitution reactions and couple well with Grignard reagents [6]. Two recent examples are shown in eqs (2.26) [125] and (2.27) [126]. The halide of the Grignard reagent can compete with its 'R' group in the substitution (eq. 2.28), decreasing the yield of coupling or complicating interpretation of the results. A practical approach to increase the cross-coupling yield is to use two moles of the sulfate or sulfonate per mole of Grignard reagent. Alternatively, RMgBr or RMgI might be replaced by R_2Mg (which lacks the halide) or by RMgCl (with a less nucleophilic halide).

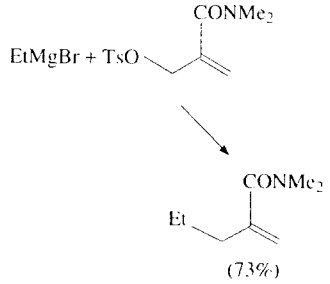

(2.26)

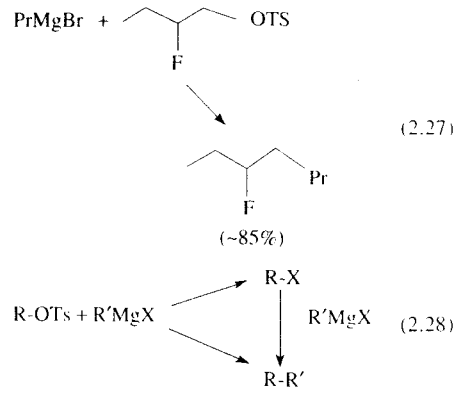

(2.27)

(2.28)

Because of their leaving group reactivity and high negative reduction potential (Table 2.4), sulfates and sulfonates are prime candidates for an S_N2 mechanism (with possible Lewis-acid assistance by the magnesium). There is evidence that the reaction occurs with inversion of configuration [127]. Homocoupling and other side-reactions can occur, at least partly via reaction of the alkyl halide (see eq. 2.28) with Grignard reagent.

Phosphate Esters.

Phosphoric acid is a weaker acid than sulfuric, and so phosphate ions are generally poorer leaving groups. Earlier work indicated a lack of reactivity of Me_3PO_4 or Et_3PO_4 toward Grignard reagents [128]. However, according to more recent reports, if either the Grignard reagent or the phosphate is allylic, coupling occurs quite successfully (although **25** was reported not to react with BuMgCl without catalysis [129]). As in the reactions of allylic Grignard reagents with halides, the group from the Grignard reagent reacts with 'allylic inversion' (92–99%; e.g., eq. 2.29) [130]. A primary allylic 'R'-group from the phosphate undergoes substitution mostly without allylic rearrangement and with preservation of the double bond configuration (eq. 2.30); the internal allylic isomers of the phosphates were not examined [130,131]. This reaction was more selective than those of the corresponding lithium, potassium, and

barium reagents, or with bromide, mesylate, or diethylphosphate as leaving groups [130]. With thiophosphates (e.g., **26**), the regiochemistry at the Grignard reagent allyl group was reversed (98:2) [130], and couplings with copper catalysis led to reversed regioselectivities of allylic groups in both reactants [132]. A double coupling, both of apparent S_N2' regiochemistry, has been used to prepare 2,3-disubstituted 1,3-butadienes (eq. 2.31) [133]. A variety of allylic Grignard reagents react with the chiral phosphate **27** to produce coupling product with ee up to 35% [134]. Cyclic transition states, with bidentate coordination of the phosphate to the magnesium, were suggested to rationalize the observed selectivities [130,134]. The high yield of cross-coupling is also consistent with a polar mechanism, with the departure of the leaving group facilitated by magnesium coordination.

Carboxylate Esters.

Addition to the ester carbonyl group is generally the dominant reaction, but in some cases, displacement of the carboxylate ion is important [6]. Reactions of trityl and benzhydryl esters were noted earlier. A highly stabilized carbocation can also be formed from **28**, which couples with EtMgBr in 67% yield [135].

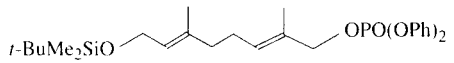

25

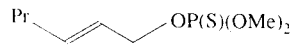

26

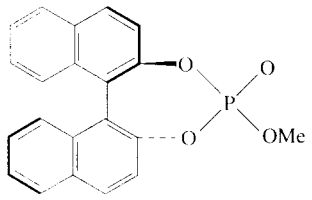

27

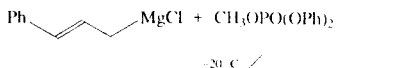

(2.29)

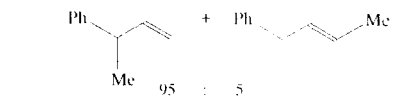

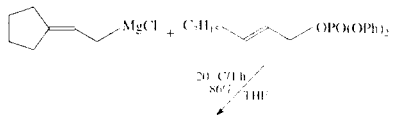

(2.30)

1

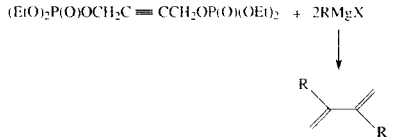

(2.31)

Treatment of methyl, butyl, and benzyl mesitoate esters ($MesCO_2R$) with Grignard reagents under vigorous conditions led to displacements by the halide of the Grignard reagent, rather than simple cross-coupling, but $MesCO_2$-*t*-Bu gave a 24% yield of *t*-Bu-Ph with PhMgBr [136]. As in the case of sulfates and sulfonates, displacement by the halide may complicate mechanistic interpretation, since coupling and other products may be derived from the halide.

Allylic mesitoates react more easily with Grignard reagents to yield cross-coupling products (e.g., eq. 2.32) [137]. In reactions of **29** and **30** with MesMgBr and PhMgBr, respectively, coupling was competitive with carbonyl addition, but *t*-$BuCO_2CH_2CH{=}CH_2$ gave only carbonyl addition with PhMgBr [136]. Substituted allylic groups react mostly at the primary position (eq. 2.32; the *cis* isomer gave a complex mixture, with products arising from probable carbocationic cyclization) [137]. Crotyl mesitoate reacted with

PhMgBr to give entirely crotylbenzene; with its allylic isomer (α-methylallyl mesitoate), crotylbenzene predominated in a 77:23 mixture, similar to that found for the chloride [96,138a]. (Refer to Section 2.4.2 and Schemes 2.2 and 2.3.) α-Methylallyl acetate reacted with MesMgBr to give only the crotyl product [138b].

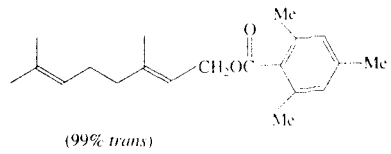

(99% *trans*)

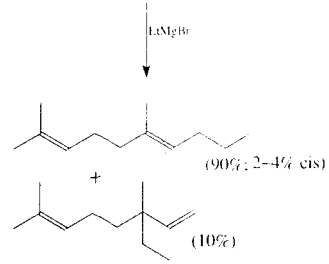

(2.32)

The pivalate ester **31** reacted unexpectedly readily with Grignard reagents [139]. The regio- and stereoselectivity found in the product mixtures was very similar from either *cis* or *trans* reactants, but depended upon the Grignard reagent used. Some homo-coupling product from **31** was also formed.

The formation of allylic rearrangement products from substituted allylic esters suggests the likelihood of an S_N1 mechanism, with S_N2 possibly competing for primary allylic esters. Homo-coupling product in the reaction of **31** may result from

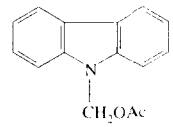

28

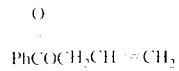

29

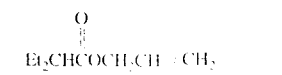

30

electron transfer, either to the ester or to the carbocation in an ion pair. Whether electron transfer leads to cross-coupling or only to side-product is unclear.

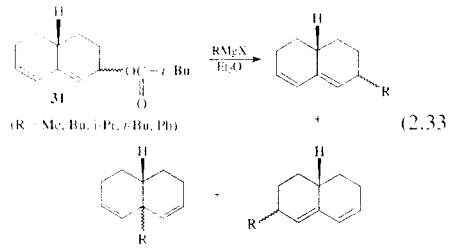

(2.33)

Activated Ethers: Acetals, Orthoesters, Etc.

Alkoxy and hydroxy, by themselves, are extremely difficult to displace, but protonation or coordination to a Lewis acid converts them into much better leaving groups. When attached to a residue which forms a highly stabilized carbocation, alkoxy groups may be readily displaced by a Grignard reagent. This condition is well satisfied for acetals, ketals, and orthoesters, where a cation like **32** is stabilized by resonance with a lone pair on a remaining oxygen. Aminals lose the alkoxy rather than the amino group, generating **33**. A direct nucleophilic displacement of the coordinated alkoxy group is less likely.

Reactions of Grignard reagents with these substrates have become important methods for generation of new C–C bonds. Several illustrative examples are given in eqs (2.34–2.38) [140–144], and numerous others are in references [2, 3, 5, 6]. In unsymmetrical cases there is a preference for displacing the alkoxy group with less α-branching (in the absence of other controlling factors), phenoxy rather than alkoxy, and alkoxy rather than amino or thioalkoxy.

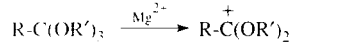

32

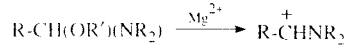

33

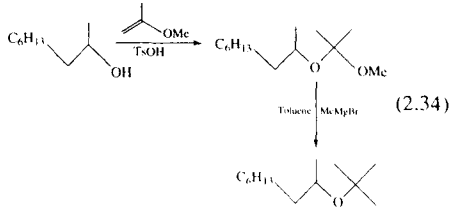

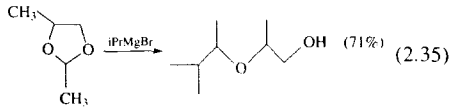

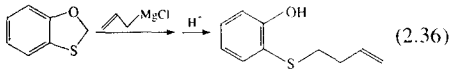

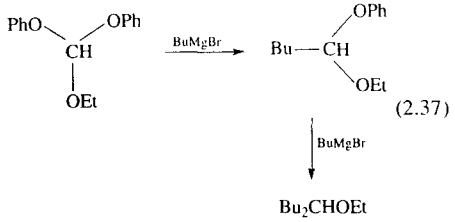

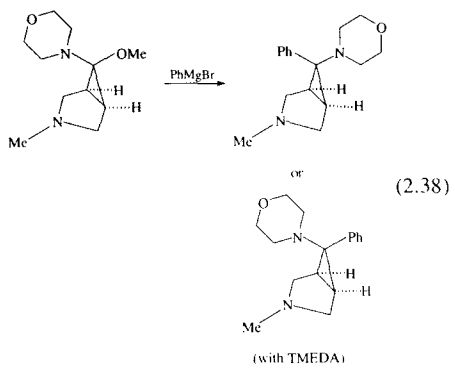

A number of highly selective acetal and ketal cleavages of derivatives of carbohydrates and related compounds have been reported recently [145]. One of these is illustrated in eq. (2.39) [146]. The configuration of the new stereogenic center implies retention in the displacement.

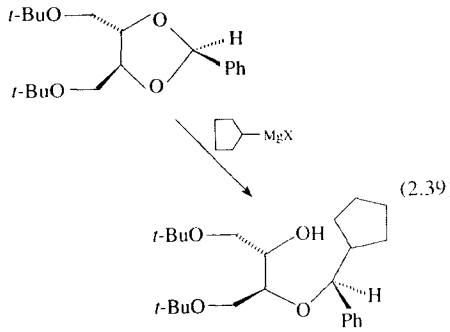

Epoxides (Oxiranes).

The strain of the epoxide ring provides additional driving force which makes displacement of the C–O bond feasible. Ethylene oxide was found very early to react with Grignard reagents (e.g., eq. 2.40) [6]. Often, after the reactants are combined, the temperature is raised by adding benzene and distilling until a vigorous reaction occurs. As in other reactions, the halide and alkyl groups of the Grignard reagent compete for the substrate, and the halohydrin (formed by reaction with the halide ion) may react with the remaining active alkyl groups in the later phase of the reaction.

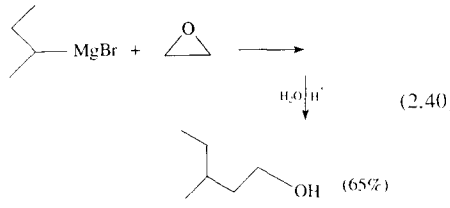

Although the reaction with ethylene oxide is quite successful, substituted epoxides often lead to mixtures. In addition to ring opening by the halide ion, isomerization of the epoxide to an isomeric aldehyde or ketone is catalyzed by the Lewis-acidic species of the Grignard reagent [6,147]. The

rearrangement usually follows the course predicted by opening to form the more stable carbocation, followed by a shift of the better-migrating group on the other carbon (e.g., eqs 2.41–2.43). Grignard reagent then adds to the carbonyl group.

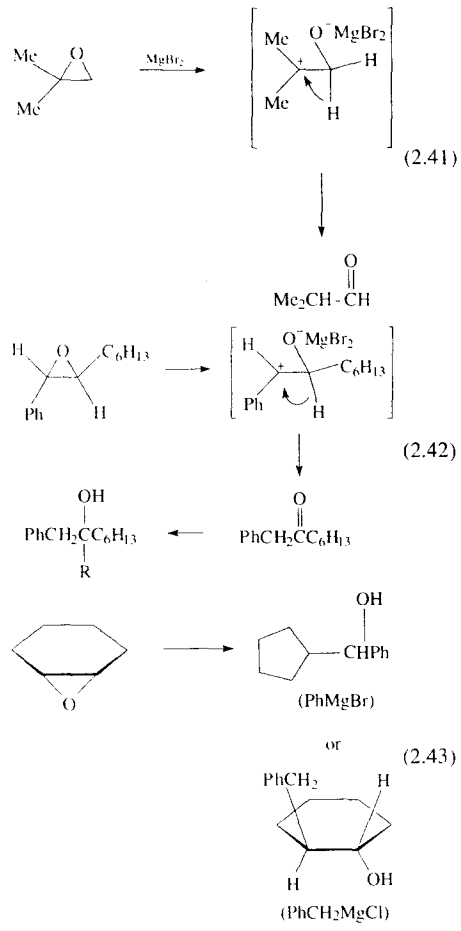

For simple mono-alkyl oxiranes, rearrangement is only a minor competitor to nucleophilic ring opening. Attack occurs mainly at the less-substituted carbon, as expected for an S_N2 mechanism. Trimethylene oxide reacts similarly to ethylene oxide, although somewhat less readily, leading to primary alcohols with a three-carbon chain extension.

Other Ethers.

Certain other ethers which can cleave to especially stable carbocations will react with Grignard reagents under mild conditions. Trityl ethers have been mentioned previously. Several other examples are shown in eqs (2.44–2.46).

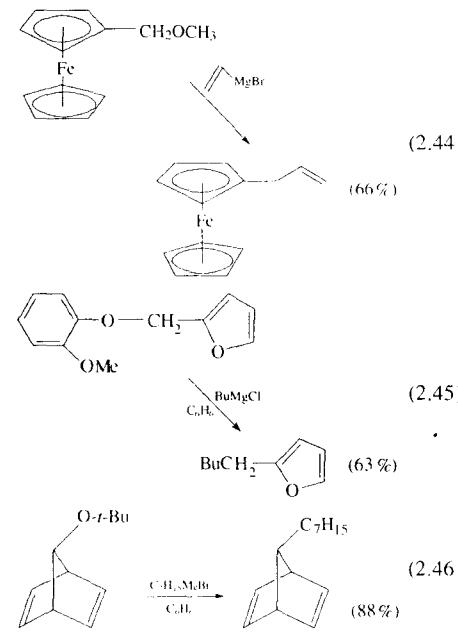

Allylic ethers also cleave relatively easily (usually reflux in benzene). Crotyl o-anisyl ether **34** reacted with PhMgBr to produce a mixture of hydrocarbon isomers [151a] similar to that from reaction of crotyl chloride (see Scheme 2.2). However, contrasting results are illustrated in eq. (2.47), where bond formation at the more substituted carbon occurs [152]. It is possible that an 'S_N1-like' mechanism is favored for allylic compounds with better leaving groups, but that a poorer leaving group has increased tendency to react by S_N2 or S_N2'. Benzyl ethers seem to be

less reactive than the allylic ones [6].

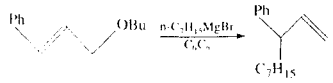

(52%) (2.47)

Even without the advantage of a stable carbocation, other ethers may be cleaved under forcing conditions. Simple alkyl ethers lead to mixtures including elimination but little substitution, and have little synthetic use. However, aryl methyl ethers may be usefully demethylated to the phenol by heating with Grignard reagents (e.g., eq. 2.48) [153].

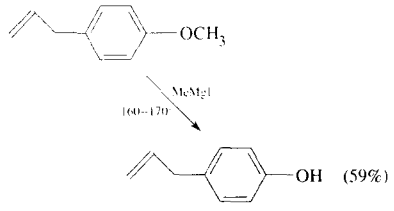

(59%) (2.48)

2.5.4.3 Miscellaneous Leaving Groups

The neutral tertiary amine from a quaternary ammonium ion is a common leaving group in Hoffmann eliminations and nucleophilic substitutions, and it may also be displaced by Grignard reagents under appropriate circumstances. The carbocation corresponding to the displacement in eq. (2.49) is highly stabilized [154]. The displacement in eq. (2.50) occurs under mild conditions, but allyltrimethylammonium ion, with a less stable leaving group, is unaffected under similar conditions [155].

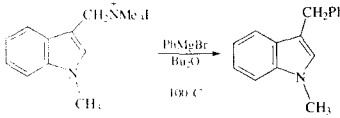

(73%) (2.49)

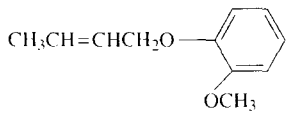

34

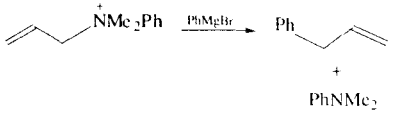

(2.50)

A useful synthetic procedure involves reaction of Grignard reagents with 1-substituted benzotriazoles. The latter substrates have a well developed synthetic chemistry, which adds to the versatility of the method [156] (e.g., eq. 2.51). It is noteworthy that benzotriazole is the leaving group, probably because of its ability to bind to the magnesium, rather than the alkoxy as found generally for aminals.

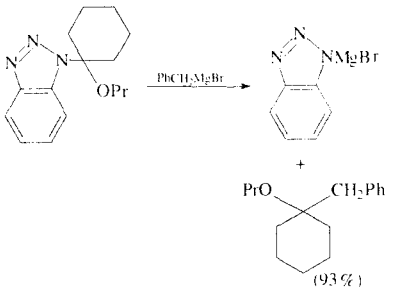

(2.51)

Thioethers are less reactive than ethers, but with sufficient activation they may react (eq. 2.52) [157]. Displacement of benzenesulfinate in eq. (2.53) is facilitated by conjugation of an intermediate carbocation with the ring oxygen. Analogous displacements of benzenesulfinate activated by a nitrogen are also reported [158].

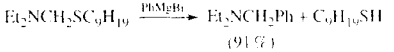

(2.52)

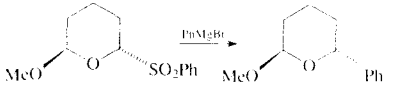

(2.53)

Even carbon anions may be displaced by Grignard reagents. The most commonly encountered case is the displacement of the cyanide ion from α-aminonitriles, where the stability of the nitrogen-conjugated carbocation is dominant (e.g., eq. 2.54) [159]. Other examples involving the cleavage of a C–C bond between stabilized carbocation and

carbanion fragments have been reported (e.g., eq. 2.55) [160].

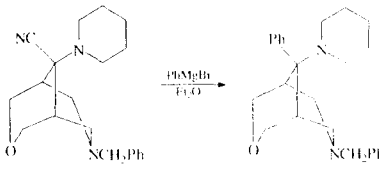

(2.54)

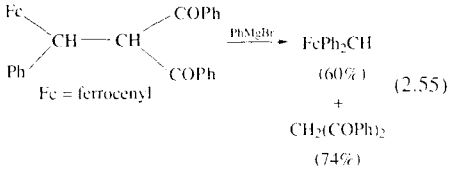

(2.55)

2.6 SOME RELATED TOPICS

In this section, we note several other reactions which are formally nucleophilic substitutions at carbon. Because they fall outside of the mechanistic pattern of the rest of this chapter, their inclusion has been postponed to this point.

Nucleophilic substitution occurs at aromatic carbons only under special circumstances, so one would not normally expect aryl halides to undergo cross-coupling with Grignard reagents. Under reaction conditions similar to those where CIDNP was observed in the reaction of Et_2Mg with *i*-PrI, a slower reaction occurred between Et_2Mg and PhI resulting in metal-halogen exchange [10]. This was followed by a much slower cross-coupling reaction between the Ph_2Mg and EtI produced in the exchange. No CIDNP polarization was noted. There are also older reports of low cross-coupling yields for aryl halides [6]. For these, either a similar metal–halogen exchange preceding coupling or catalysis by transition metal impurities is likely. Electron transfer from ArMgX to Ar′Y is relatively unlikely on the basis of electrode potentials (Tables 2.5 and 2.6); however, reorganization energy should be smaller because of the stability of the aryl halide radical anion, so biaryls might be formed by a SET mechanism under forcing conditions.

Halogens (or other leaving groups) situated ortho- or para- to strongly electron-withdrawing substituents on an aromatic ring may be displaced by addition of the nucleophile to the ring, followed by elimination of the leaving group (S_NAr mechanism). Numerous examples of displacements by Grignard reagents, with hindered ester and ketone, cyano, nitro, and 2-oxazolyl as activating groups, are provided in reference [3]. A more recent illustration is in eq. (2.56) [161]. The electron-poor 2-position of pyridine (and some other heterocycles) is also subject to addition by nucleophiles. The example shown in eq. 2.57 [162] also illustrates the relative ease of displacement of benzenesulfinate from a sulfone. The formation of products with only the uncyclized alkyl group helps to confirm the polar, non-radical nature of the reaction.

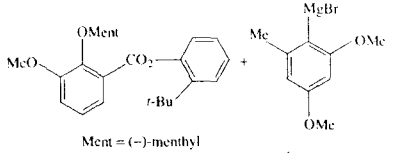

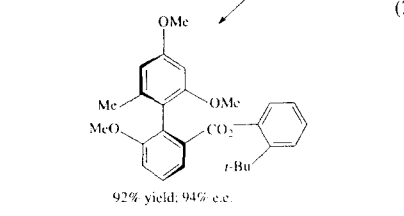

(2.56)

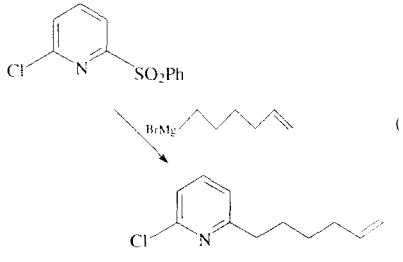

(2.57)

Sulfoxides having at least one electron-poor aryl group also undergo a facile reaction with Grignard reagents, which corresponds to displacement of

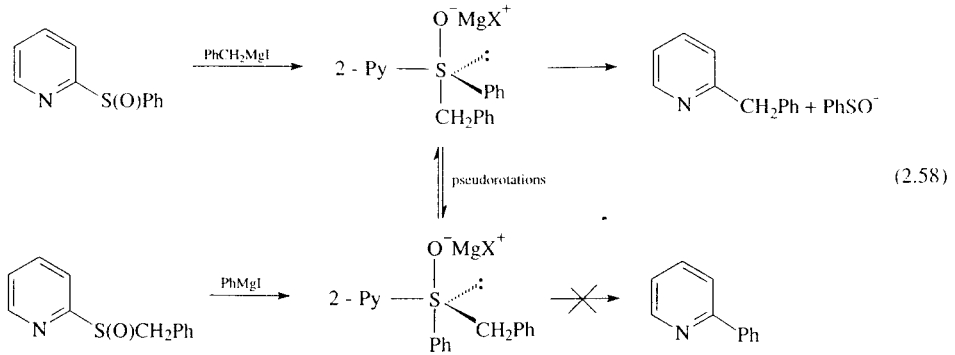

(2.58)

$ArS(O)^-$ or $RS(O)^-$ as the leaving group [163–165]. However, these apparent displacement reactions occur instead by nucleophilic addition to the sulfur, forming a hypervalent sulfurane intermediate. Two of the three organic ligands coordinated to the sulfur may then be extruded as coupling product in a concerted reaction. The groups eliminated are determined by their inherent reactivity, their position in the sulfurane, and the rate of isomerization of the sulfurane by pseudorotation (e.g., eq. 2.58 [164]). The coupling occurs with retention of configuration at sp^2 or sp^3 carbon, and without allylic rearrangement. Competing elimination of Grignard reagent may scramble groups between the sulfoxide and the Grignard reagent, as shown in eq. 2.59 [165]. The contrast with the reaction of sulfones (eq. 2.57) should be noted.

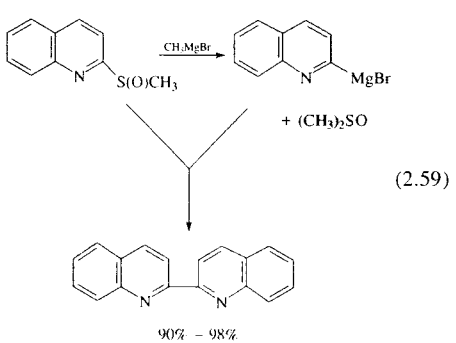

(2.59)

Highly halogenated alkenes undergo displacement by Grignard reagents, probably by an addition–elimination mechanism. An example is shown in eq. (2.60) [166]. The reaction in eq. (2.61) probably has a similar mechanism [167]. An addition–elimination mechanism was also proposed for eq. (2.62) although a sulfurane mechanism similar to eq. (2.58) would be an alternative [168]. Cross-coupling occurs in low yield, accompanied by homo-coupling, in the reaction of β-bromostyrene with pentylmagnesium bromide [13]. Halogen–metal exchange, addition–elimination, or SET mechanisms might be involved.

(2.60)

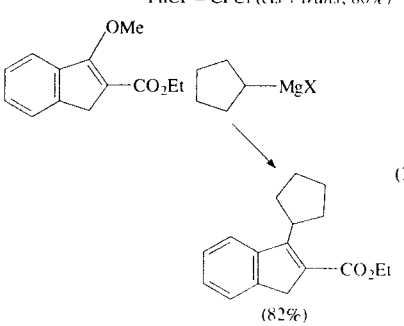

(2.61)

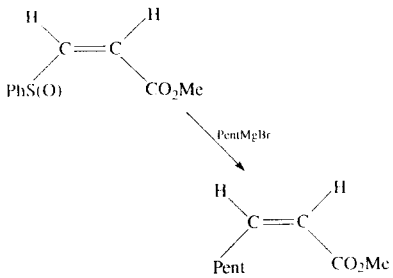

(2.62)

(66%; Z:E = 99:1)

An elimination–addition sequence may be responsible for the reaction in eq. (2.63) [169], although the presumed intermediate resulting from elimination is not detected, and no product corresponding to the alternative orientation of addition is isolated. It is also possible that the mechanism is the same as that for α-haloketones (Section 2.5.3), namely addition to the carbonyl followed by rearrangement with expulsion of the leaving group.

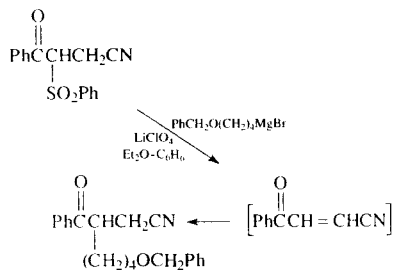

(2.63)

The $S_{RN}1$ radical chain mechanism for nucleophilic substitution [170], as illustrated generally in eqs (2.64a–e), has been absent from our discussions. This mechanism has been shown to occur in many displacement reactions of leaving groups from both aromatic and aliphatic substrates. However, in most of the aliphatic cases the substrates have a nitro or nitrophenyl group (or other effective electron acceptor) in the a-position to the leaving group. The combination of the nucleophile with the radical from the substrate must also form a relatively stable radical-anion in step 2.64b, which is capable of propagating the chain. Some alkyl halides which are unreactive in S_N1 or S_N2, including 1-bromoadamantane [171] and 7-bromonorcarane [172], are found to react with certain nucleophiles (Ph_2P^- and Ph_2As^-) in a photoinitiated $S_{RN}1$ reaction. If the nucleophile is a Grignard reagent, the propagation step 64b would have to take the form shown in (2.64d) or (2.64e). The species $RR'MgX\cdot$ may be involved in the alkyl group exchange which has been found to lead to CIDNP polarization of Grignard reagent resonances [79], but there is no indication that it can rearrange to coupling product.

$$RY \xrightarrow[\text{initiation}]{e} [RY^{\cdot -}] \longrightarrow R\cdot + Y^- \quad (2.64a)$$

$$R\cdot + Nu^- \longrightarrow R - Nu^{\cdot -} \quad (2.64b)$$

$$R - Nu^{\cdot} + RY \longrightarrow R - Nu + [RY^{\cdot -}]$$

$$\downarrow$$

$$R\cdot + Y^- \quad (2.64c)$$

$$R'\cdot + RMgX \longrightarrow [RR'MgX\cdot]$$

$$\downarrow$$

$$RR'^{\cdot -} + MgX^+ \quad (2.64d)$$

$$R'\cdot + RMgX \longrightarrow [RR'MgX\cdot]$$

$$\downarrow$$

$$RR' + MgX\cdot \quad (2.64e)$$

2.7 SUMMARY AND CONCLUSIONS

We have seen in the foregoing sections that there remains considerable uncertainty about the mechanism of cross-coupling of Grignard reagents with organic halides and other substrates. It cannot be said that there is 'a' mechanism by which the alkyl group of the Grignard reagent forms a new C–C bond in displacing a leaving group. Instead, depending upon the particular Grignard reagent and substrate, at least three different mechanisms of reaction may be in accord with experimental evidence or chemical expectations—the S_N2 mechanism of direct nucleophilic substitution, an S_N1 mechanism with ionization to a

carbocationic intermediate, and a SET mechanism originating with electron transfer and involving radical intermediates. In some instances, there is quite clear indication of the mechanism which prevails, while in others there is insufficient basis for a choice.

The SET mechanism is clearly implicated in the reactions of poly-halides, on the basis of their low reduction potentials, the prominence of homo-coupling and reduction among the products, and CIDNP observations which are consistent with product formation via geminally-formed radical pairs. At the other extreme, the a-haloethers ionize to an especially stable carbocation, and very probably react by an S_N1 mechanism. The same may be said of the reactions of ethers of the acetal, orthoester, and aminal type, and certain other ethers, esters, quaternary ammonium ions, etc. which can ionize to highly stabilized carbocations. The leaving groups in these reactions accept an electron reluctantly and are relatively unreactive toward nucleophilic displacements in general, but become much better leaving groups when coordinated to the magnesium. An S_N2 mechanism is very likely in reactions of sulfonates or phosphates (particularly methyl or primary), since the leaving group is relatively reactive without coordination and does not readily accept an electron. Reactions of ethylene oxide and those substituted oxiranes which react without rearrangement should also be S_N2, as should be the cleavages of aryl methyl ethers.

Considerable uncertainty remains for coupling reactions of the saturated alkyl mono-halides, which often occur in low yield, accompanied by homo-coupling. Based on reduction potentials, SET is most likely for reactions of the iodides and tertiary halides; the probability of S_N2 increases for chlorides and methyl halides. Although CIDNP polarization points to radical intermediates, ambiguity in its interpretation raises the possibility that the reactions observed are actually catalyzed by transition metal impurities. Grignard reagent radical cation intermediates of significant lifetime might also influence the observations and the course of the reaction: theoretical or experimental examination of their stability would be useful. When the Grignard reagent is aryl, allylic, or benzylic, S_N2 seems more likely; trityl and other more highly delocalized Grignard reagents may particularly favor S_N2.

Allyl and benzyl halides should be reactive by all three mechanisms. The observation of much homo-coupling in the reaction of benzylic halides with Grignard reagents supports an SET mechanism. High cross-coupling yields for allyl bromide are more consistent with S_N2, and other difficulties with an SET mechanism have been noted (Section 2.4.2). The mixtures of allylic isomers usually obtained from unsymmetrical allylic substrates (e.g., crotyl halides, phosphates, esters, ethers, etc.; see Scheme 2.2) might be accounted for by competing S_N2 and S_N2' mechanisms; however, product formation via allylic radical or carbocation intermediates may be more likely. In the absence of compelling evidence, our current preference is an assisted S_N1 ionization to the carbocation, perhaps accompanied by 'leakage' to radical products by electron transfer in the ion pair and/or competition from S_N2 substitution at the primary position. It seems likely also that evidence for radical intermediates in reactions of trityl carbocations, halides, and other substrates may result from electron transfer to the carbocation, rather than to the covalent substrate itself. It remains a possibility that a similar explanation might apply to tertiary alkyl halides in at least some cases.

REFERENCES

1. R.C. Fuson, *J. Am. Chem. Soc.* **1926**, *48*, 2681.
2. B.J. Wakefield, *Organomagnesium Methods in Organic Synthesis*, Academic, London, **1995**, Chap 8.
3. G.S. Silverman in *Handbook of Grignard Reagents*, G.S. Silverman, P.E. Rakita, Eds., Marcel Dekker, New York, **1996**, Chap 15.
4. I.P. Beletskaya, G.A. Artamkina, O.A. Reutov, *Uspekhi Khim.* **1976**, *45*, 661.
5. Yu.N. Polivin, R.A. Karakhanov, V.N. Postnov, *Uspekhi Khim.* **1990**, *59*, 401.
6. M.S. Kharasch, O. Reinmuth, *Grignard Reactions of Nonmetallic Substances*, Prentice-Hall, New York, **1954**.
7. A. Streitwieser, *Solvolytic Displacement Reactions*, McGraw-Hill, New York, **1962**.
8. J. March, *Advanced Organic Chemistry*, 4th Ed., Wiley, New York, **1992**, Chap 10.

9. F.A. Carey, R.J. Sundberg, *Advanced Organic Chemistry, Part A: Structure and Mechanisms*, 3rd Ed., Plenum, New York, **1990**, Chap 5.
10. L.F. Kasukhin, M.P. Ponomarchuk, Zh.F. Buteiko, *Zh. Org. Khim.* **1972**, *8*, 665.
11. M. Ohno, K. Shimizu, K. Ishizaki, T. Sasaki, S. Eguchi, *J. Org. Chem.* **1988**, *53*, 729.
12. H.R. Ward, R.G. Lawler, T.A. Marzilli, *Tetrahedron Lett.* **1970**, 521.
13. J. Normant, *Bull. Soc. Chim. Fr.* **1963**, 1888.
14. P.L. Castle, D.A. Widdowson, *Tetrahedron Lett.* **1986**, *27*, 6013.
15. A. Alberola, A.M. Gonzalez Nogal, T. Torroba, *Ann. Quim.* **1984**, *80*, 181.
16. E. Osawa, Z. Majerski, P.v.R. Schleyer, *J. Org. Chem.* **1971**, *36*, 205. G. Molle, J. E. Dubois, P. Bauer, *Can. J. Chem.* **1987**, *65*, 2428. A.G. Zhukov, B.G. Rarog, V.A. Topchii, A.G. Yurchenko, *Ukr. Khim. Zh. (Russ. Ed.)* **1990**, *56*, 1119 (*Chem. Abstr.* **1991**, *114*, 163685p).
17. M.-P. Labeau, H. Cramail, A. Deffieux, *Polym. Int.* **1996**, *41*, 453.
18. N.A. Bumagin, A. B. Ponomarev, I. P. Beletskaya, *Zh. Org. Khim., USSR* **1987**, *23*, 1354.
19. D.J. Brondani, R.J.P. Corriu, S.E. Ayoubi, J.J.E. Moreau, M.W.C. Man, *J. Organomet. Chem.* **1993**, *451*, C1.
20. P.R. Singh, S.R. Tayal, A. Nigam, *J. Organomet. Chem.* **1972**, *42*, C9.
21. B. Grédy, *Bull. Soc. Chim. Fr.* [5] **1936**, *3*, 1093.
22. J.C. Chottard, M. Julia, *Bull. Soc. Chim. Fr.* **1968**, 3700.
23. R. Bihovsky, L. Selick, I. Giusti, *J. Org. Chem.* **1988**, *53*, 4026.
24. M.J. Panigot, R.W. Curley, Jr., *J. Carbohydrate Chem.* **1994**, *13*, 293.
25. M. Cai, B. Yeu, S. Wang, A. Mao, D. Qiu, *Gaodeng Xuexiao Huaxue Xuebao* **1987**, *8*, 511 (*Chem. Abstr.* **1988**, *109*, 55092f).
26. H.A. Bates, S. Rosenblum, *J. Org. Chem.* **1986**, *51*, 3447.
27. I.P. Smoliakova, R. Caple, J.W. Brenny, *Synlett* **1995**, 275.
28. C.G. Kruse, A. Wijsman, A. Van der Gen, *J. Org. Chem.* **1979**, *44*, 1847.
29. T.H. Lowry, K.S. Richardson, *Mechanism and Theory in Organic Chemistry*, 3rd Ed., Harper and Row, New York, **1987**.
30. E. Hebert, J.-P. Mazaleyrat, Z. Welvart, L. Nadjo, J.-M. Savéant, *Nouv. J. Chem.* **1985**, *9*, 75.
31. P. Wells, *Prog. Phys. Org. Chem.* **1968**, *6*, 111; N. Inamoto, S. Masuda, *Chem. Lett.* **1982**, 1003; W. Gordy, *Phys. Rev.* **1946**, *69*, 604.
32. G.A. Russell, E.G. Janzen, E.T. Strom, *J. Am. Chem. Soc.* **1964**, *86*, 1807. G.A. Russell, D.W. Lamson, *J. Am. Chem. Soc.* **1969**, *91*, 3967.
33. E.C. Ashby, C.O. Welder, *J. Org. Chem.* **1997**, *62*, 3542 and references therein.
34. L. Eberson, *Electron Transfer Reactions in Organic Chemistry*, Springer-Verlag, Berlin, **1988**, and references therein.
35. Ref 29, pp 229–232.
36. W. Kaim, in *Electron Transfer I, Topics in Current Chemistry*, Vol. 169, J. Mattay, Ed., Springer-Verlag, Berlin, **1944**, pp 231–251; W. Kaim, *Acc. Chem. Res.* **1985**, *18*, 160.
37. R.A. Marcus, *Ann. Rev. Phys. Chem.* **1964**, *15*, 155.
38. A.J. Fry, *Synthetic Organic Electrochemistry*, 2nd Ed., Wiley, New York, **1988**, pp 136–156.
39. D. Kyriacou, *Modern Electroorganic Chemistry*, Springer-Verlag, Berlin, **1994**, pp 122–133.
40. C.P. Andrieux, I. Gallardo, J.-M. Savéant, K.-B. Su, *J. Am. Chem. Soc.* **1986**, *108*, 638.
41. H.R. Rogers, C.L. Hill, Y. Fujiwara, R.J. Rogers, H.L. Mitchell, G.M. Whitesides, *J. Am. Chem. Soc.* **1980**, *102*, 217; J.F. Garst, this volume, Chap. 7.
42. J. F. Garst, *Acc. Chem. Res.* **1971**, *4*, 400.
43. T. Clarke, *Chem. Commun.* **1984**, 93; V.A. Tikhomirov, E.D. German, A.M. Kuznetsov, *Chem. Phys.* **1995**, *191*, 25.
44. M.C.R. Symons, I.G. Smith, *J. Chem. Soc., Faraday Trans. 1*, **1985**, *81*, 1095; M.C.R. Symons, I.G. Smith, *J. Chem. Soc., Perkin Trans. 2* **1981**, 1180.
45. W. F. Bailey, R. P. Gagnier, J. P. Patricia, *J. Org. Chem.* **1984**, *49*, 2098.
46. C.P. Andrieux, C. Blocman, J.-M. Dumas-Bouchiat, F. M'Halla, J.-M. Savéant, *J. Am. Chem. Soc.* **1979**, *101*, 3431.
47. L. Eberson, *Acta Chem. Scand.* **1982**, **B36**, 533.
48. J.M. Savéant, *J. Am. Chem. Soc.* **1992**, *114*, 10595.
49. T. Lund, H. Lund, *Acta Chem. Scand.* **1986**, *B40*, 470.
50. M.R. Rifi, F.H. Lovita, *Introduction to Organic Electrochemistry*, Dekker, New York, **1974**.
51. T. Holm, *Acta Chem. Scand.* **1982**, *B36*, 266.
52. R.J. Klingler, J.K. Kochi, *J. Am. Chem. Soc.* **1980**, *102*, 4790. B. W. Walther, F. Williams, W. Lau, J.K. Kochi, *Organometallics* **1983**, *3*, 688.
53. R. Benn, *Chem. Phys.* **1976**, *15*, 369.
54. K. Maruyama, T. Katagiri, *J. Am. Chem. Soc.* **1986**, *108*, 6263. *J. Phys. Org. Chem.* **1988**, *1*, 21 and **1989**, *2*, 205. E.C. Ashby, A.B. Goel, *J. Am. Chem. Soc.* **1981**, *103*, 4983.
55. C. Walling, *J. Am. Chem. Soc.* **1988**, *110*, 6846.
56. W.V. Evans, F.H. Lee, C.H. Lee, *J. Am. Chem. Soc.* **1935**, *57*, 489.
57. T. Holm, *Acta Chem. Scand.* **1974**, *B28*, 809; **1983**, *B37*, 567.
58. Ref 34, pp 132–136.
59. L. Eberson, *Acta. Chem. Scand.* **1984**, *38*, 439.

60. B. Jaun, J. Schwarz, R. Breslow, *J. Am. Chem. Soc.* **1980**, *102*, 5741; R. Breslow, J.L. Grant, *J. Am. Chem. Soc.* **1977**, *99*, 7745.
61. M. Okubo, T. Tsutsumi, K. Matsuo, *Bull. Chem. Soc. Jpn.* **1987**, *60*, 2085.
62. C. Blomberg, R.M. Salinger, H.S. Mosher, *J. Org. Chem.* **1969**, *34*, 2385; J.F. Fauvarque, E. Rouget, *C.R. Seances Acad. Sci., Ser C* **1968**, *267*, 1355. T. Holm, I. Crossland, *Acta Chem. Scand.* **1971**, *25*, 59. E.C. Ashby, J.B. Bowers, Jr., *J. Am. Chem. Soc.* **1981**, *103*, 2242; T. Holm, this volume, Chap. 1.
63. H. Yamazaki, N. Hayashi, *Chem. Lett.* **1993**, 525.
64. L. Eberson, L. Greci, *J. Org. Chem.* **1984**, *49*, 2135.
65. L. Eberson, L. Cardellini, L. Greci, M. Poloni, *Gazz. Chem. Ital.* **1988**, *118*, 35.
66. P. Bruni, P. Carlone, C. Conti, E. Giorgini, L. Greci, M. Iacussi, P. Stipa, G. Tosi, *Tetrahedron* **1996**, *52*, 6795.
67. P. Carloni, L. Greci, P. Stipa, *J. Org. Chem.* **1991**, *56*, 4733.
68. F.G. Bordwell, C.A. Wilson, *J. Am. Chem. Soc.* **1987**, *109*, 5470; F.G. Bordwell, J.A. Harrelson, Jr., *J. Org. Chem.* **1989**, *54*, 4893.
69. F.G. Bordwell, J.A. Harrelson, Jr., *J. Am Chem. Soc.*, **1987**, *109*, 8112; F.G. Bordwell, J.A. Harrelson, Jr., *J. Am. Chem. Soc.* **1989**, *111*, 1052; K. Daasbjerg, S.U. Pedersen, H. Lund, *Acta Chem. Scand.* **1991**, *45*, 424.
70. J. Grimshaw, J.R. Langan, G.A. Salmon, *J. Chem. Soc., Faraday Trans.* **1994**, *90*, 75.
71. A.R. Lepley, G.L. Closs, Eds., *Chemically Induced Magnetic Polarization*, Wiley, New York, 1973; K.M. Salikhov, Yu.N. Molin, R.Z. Sagdeev, A.L. Buchachenko, *Spin Polarization and Magnetic Effects in Radical Reactions*, Elsevier, Amsterdam, **1984**.
72. Ref 29, pp 335–360.
73. R.A. Sneen, *Acc. Chem. Res.* **1973**, *6*, 46.
74. A. Pross, *Theoretical and Physical Principles of Organic Reactivity*, Wiley, New York, 1995; S.S. Shaik, H.B. Schlegel, S. Wolfe, *Theoretical Aspects of Physical Organic Chemistry, The S_N2 Mechanism*, Wiley, New York, **1992**; Ref 29, pp 349–360.
75. R. D. Guthrie in *Comprehensive Carbanion Chemistry*, E. Buncel, T. Durst, Eds., Elsevier, Amsterdam, **1980**, p 197.
76. R.B. Allen, R.G. Lawler, H.R. Ward, *Tetrahedron Lett.* **1973**, 3303.
77. H.R. Ward, R.G. Lawler, R.A. Cooper, in *Chemically Induced Magnetic Polarization*, A.R. Lepley, G.L. Closs, Eds., Wiley, New York, **1973**, Chap 7.
78. a) R.B. Allen, R.G. Lawler, H.R. Ward, *J. Am. Chem. Soc.* **1973**, *95*, 1692; b) R.G. Lawler, P. Livant, *J. Am. Chem. Soc.* **1976**, *98*, 3710.
79. G.F. Lehr, R.G. Lawler, *J. Am. Chem. Soc.* **1984**, *106*, 4048.
80. J.A. Kerr, in *Free Radicals*, J.K. Kochi, Ed., Wiley, New York, **1973**, pp 9–14. Z.B. Alfassi, in *Chemical Kinetics of Small Organic Radicals*, Z.B. Alfassi, Ed., CRC Press, Boca Raton, FL, **1988**, Vol 1, Chap 6; J.M. Hay, *Reactive Free Radicals*, Academic, London, **1974**, pp 96–102; M. Lazar, V. Klimo, J. Rychly, P. Pelikán, L. Valko, *Free Radicals in Chemistry and Biology*, CRC Press, Boca Raton, FL, 1989, Chap 3.
81. a. T. Koenig, H. Fischer, in *Free Radicals*, J.K. Kochi, Ed., Wiley, New York, 1973, Vol 1, Chap 4; b. L. Kaplan, in *Free Radicals*, J.K. Kochi, Ed., Wiley, New York, 1973, Vol 2, Chap 18.
82. K.N. Gurudutt, S. Rao, P. Srinivas, *Ind. J. Chem.* **1991**, *30B*, 343.
83. K.N. Gurudutt, S. Rao, P. Srinivas, S. Srinivas, *Tetrahedron* **1995**, *51*, 3045.
84. H. Quast, G. Meichsner, B. Seiferling, *Liebigs Ann. Chem.* **1986**, 1981.
85. H. Masada, F. Mikuchi, Y. Doi, A. Hayashi, *Nippon Kagaku Kaishi* **1995**, 114 (*Chem. Abstr.* **1995**, *123*, 32346s); H. Masada, Y. Doi, F. Mikuchi, *Nippon Kagaku Kaishi* **1996**, 175 (*Chem Abstr.* **1996**, *124*, 342186e).
86. J. Tanaka, M. Nojima, S. Kusabayashi, *J. Am. Chem. Soc.* **1987**, *109*, 3391.
87. R.J. Letsinger, J.G. Traynham, *J. Am. Chem. Soc.* **1950**, *72*, 849.
88. D.A. Bright, D.E. Mathisen, H.E. Zieger, *J. Org. Chem.* **1982**, *47*, 3521; H.E. Zieger, D.A. Bright, H. Haubenstock, *J. Org. Chem.* **1986**, *51*, 1180; J. Sauer, W. Braig, *Tetrahedron Lett.* **1969**, 4275.
89. a. R.G. Finke, S.R. Keenan, P.L. Watson, *Organometallics* **1989**, *8*, 263; b. B. Bogdanovic, N. Janke, H.-G. Kinzelmann, *Chem. Ber.* **1990**, *123*, 1507.
90. R.G. Gough, J.A. Dixon, *J. Org. Chem.* **1968**, *33*, 2148.
91. B.J. Schaart, C. Blomberg, O.S. Akkerman, F. Bickelhaupt, *Can. J. Chem.* **1980**, *58*, 932.
92. H.X. Zhou, M.S. Thesis, University of Wisconsin-Milwaukee, **1999**.
93. R.H. DeWolfe, W. G. Young, *Chem. Rev.* **1956**, *56*, 753.
94. B. Figidére, X. Franck, in *Handbook of Grignard Reagents*, G.S. Silverman, P.E. Rakita, Eds., Marcel Dekker, New York, **1996**, Chap 24.
95. R.M. Magid, *Tetrahedron* **1980**, *36*, 1901.
96. K.W. Wilson, J.D. Roberts, W.G. Young, *J. Am. Chem. Soc.* **1949**, *71*, 2019.
97. N.Hj. Lajis, M.N. Khan, *Tetrahedron* **1992**, *44*, 1109.
98. S. Czarnecki, C. Georgoulis, B. Gross, C. Prevost, *Bull. Soc. Chim. Fr.* **1968**, 3713.

99. G.M. Whitesides, J.E. Nordlander, J.D. Roberts, *Disc. Faraday Soc.*, **1962**, *34*, 185; D.A. Hutchison, K.R. Beck, R.A. Benkeser, J.B. Grutzner, *J. Am. Chem. Soc.* **1973**, *95*, 7075.
100. D.J. Pasto, G. L'Hermine, *Tetrahedron* **1993**, *49*, 3259.
101. F.R. Jensen, K.L. Nakamaye, *J. Am. Chem. Soc.* **1966**, *88*, 3437.
102. P.D. Bartlett, B.N. Fickes, F.C. Haupt, R. Helgeson, *Acc. Chem. Res.* **1970**, *3*, 177; G.M. Whitesides, J. San Filippo, Jr., *J. Am. Chem. Soc.* **1970**, *92*, 6611.
103. S.V. Kombarova, L.A. Tyurina, V.V. Smirnov, *Vestn. Mosk. Univ., Ser. 2: Khim.* **1992**, *33*, 151; L.A. Tyurina, S.V. Kombarova, N.A. Bumagin, I.P. Beletskaya, *Metalloorg. Khim.* **1990**, *3*, 48; I.P. Beletskaya, L.A. Tyurina, this volume, Chap. 12.
104. A.J. Kirby, *The Anomeric Effect and Related Stereoelectronic Effects at Oxygen*, Springer-Verlag, Berlin, **1983**, Chap 6.
105. A.J. Colussi, in *Chemical Kinetics of Small Organic Radicals*, Z.B. Alfassi, Ed., Vol 1, CRC Press, Boca Raton, FL, **1988**, pp 25-43.
106. E.V. Uglova, I.S. Popova, O.A. Reutov, *Metalloorg. Khim.* **1992**, *5*, 846.
107. Y.C. Liu, H.-S. Dang, Z.-L. Liu, *Rev. Chem. Intermed.* **1986**, *7*, 111.
108. A. Ishii, J. Nakayama, Y. Endo, M. Hoshino, *Tetrahedron Lett.* **1990**, 31, 2623.
109. M.D. Bell, K.D. Berlin, N.L. Doss, W.J. Leivo, E.D. Mitchell, R.D. Shupe, G.R. Waller, R.D. Grigsby, *J. Chem. Soc., Chem. Commun.* **1968**, 624; K.D. Berlin, R.D. Shupe, R.D. Grigsby, *J. Org. Chem.* **1969**, *34*, 2500.
110. D. Seyferth, B. Prokai, *J. Org., Chem.* **1966**, *31*, 1702.
111. M.v. Stackelberg, W. Stracke, *Z. Electrochem. Angew. Phys. Chem.* **1949**, *53*, 118.
112. V.I. Savin, Yu.P. Kitaev, *Zh. Org. Khim.* **1976**, *12*, 280; V.I. Savin, Yu.P. Kitaev, *Izv. Akad. Nauk SSSR, Ser. Khim.* **1976**, 1281.
113. J. Villieras, *Organomet. Chem. Rev A* **1971**, *7*, 81.
114. M. Davis, L.W. Deady, A.J. Finch, J.F. Smith, *Tetrahedron* **1973**, *29*, 349.
115. M. Mousseron, F. Winternitz, *Bull. Soc. Chim. Fr.* **1946**, 604.
116. J.-W. Cheng, F.-T. Luo, *Tetrahedron Lett.* **1988**, *29*, 1293, Y.-K. Liu, R.-T. Wang, F.-L. Chou, F.-T. Luo, *Bull. Inst. Chem., Acad. Sinica* **1990**, *37*, 43; R.-T. Wang, F.-T. Luo, *Bull. Inst. Chem., Acad. Sinica* **1991**, *38*, 33.
117. M.S. Newman, M.D. Farbman, *J. Am. Chem. Soc.* **1944**, *66*, 1550.
118. I. Carelli, A. Curulli, A. Inesi, E. Zeuli, *J. Chem. Res., Synop.* **1990**, 74.
119. Ref 6, pp 182-189; M. Tiffeneau, *Bull. Soc. Chim. Fr. [5]* **1945**, *12*, 621; T.A. Geissman, R.I. Akawie, *J. Am. Chem. Soc.* **1993**, *151*, 73; M. Hori, T. Kataoka, H. Shimizu, E. Imai, T. Iwamura, K. Maeda, *Chem. Pharm. Bull.* **1986**, *34*, 3599.
120. R.C. Huston, R.I. Jackson, G.B. Spero, *J. Am. Chem. Soc.* **1941**, *43*, 1459.
121. Ref 6, pp 189-196; E.P. Kohler, M. Tishler, *J. Am. Chem. Soc.* **1932**, *54*, 1594.
122. A. Padwa, S.I. Goldstein, R.J. Rosenthal, *J. Org. Chem.* **1987**, *52*, 3278.
123. G. Picotin, A. Faye, P. Miginiac, *Bull. Soc. Chim. Fr.* **1990**, 245.
124. E.M. Arnett, K. Amarnath, N.G. Harvey, J.-P. Chang, *J. Am. Chem. Soc.* **1990**, *112*, 344.
125. C. Najera, B. Mancheno, M. Yus., *Tetrahedron Lett.* **1989**, *30*, 3837.
126. A. Hedhli, A. Baklouti, *J. Soc. Chim. Tunisie* **1995**, *3*, 567.
127. J. Kenyon, H. Phillips, V. Pittman, *J. Chem. Soc.* **1935**, 1072.
128. Ref 6, pp 1339–1345.
129. A. Yanagisawa, N. Nomura, H. Yamamoto, *Synlett* **1991**, 513.
130. A. Yanagisawa, H. Hibino, N. Nomura, H. Yamamoto, *J. Am. Chem. Soc.* **1993**, *115*, 5879.
131. S. Araki, T. Sato, Y. Butsugan, *J. Chem. Soc., Chem. Commun.* **1982**, 285.
132. A. Yanagisawa, N. Nomura, H. Yamamoto, *Synlett* **1993**, 689.
133. S. Araki, M. Ohmura, Y. Butsugan, *Chem. Lett.* **1985**, 963.
134. A. Yanagisawa, N. Nomura, Y. Yamada, H. Hibino, H. Yamamoto, *Synlett* **1995**, 841.
135. K.G. Midzuch, *Zh. Obshch. Khim.* **1946**, 16, 1471.
136. Ref 6, pp 567–572.
137. G.M.C. Higgins, B. Saville, M.B. Evans, *J. Chem. Soc.* **1965**, 702.
138. a. R.T. Arnold, S. Searles, Jr., *J. Am. Chem. Soc.* **1949**, *71*, 2021; b. R. Wehrli, H. Heimgartner, H. Schmid, H.-J. Hansen, *Helv. Chim. Acta* **1977**, *60*, 2034.
139. T.L. Underiner, H.L. Goering, *J. Org. Chem.* **1988**, *53*, 1140.
140. T.M. Wilson, J. Amburgey, S.E. Denmark, *J. Chem. Soc. Perkin Trans. 1* **1991**, 2899.
141. I. A. Mel'nitskii, O.F. Glukhova, T.K. Kiladze, *Dokl. Akad. Nauk SSSR* **1987**, *292*, 1390.
142. S. Cabiddu, E. Margonia, S. Melis, F. Sotgiu, *J. Organomet. Chem.* **1976**, *116*, 275.
143. F. Barbot, P. Miginiac, *J. Organomet. Chem.* **1981**, *222*, 1; L Poncini, *N. Z. J. Sci.* **1983**, *26*, 31; F. Barbot, L. Poncini, B. Randrianoelina, P. Miginiac, *J. Chem. Res. Synop.* **1981**, 343; L. Poncini, *J. Org. Chem.* **1984**, *49*, 2031
144. V. Butz, E. Vilsmaier, *Tetrahedron* **1993**, *49*, 6031.
145. T.-Y Luh, *Pure Appl. Chem.* **1996**, *68*, 635.

146. T.-M. Yuan, S.-M. Yeh, Y.-T. Hsieh, T.-Y. Luh, *J. Org. Chem.* **1994**, *59*, 8192.
147. M. Bartok, K.L. Lang, in *The Chemistry of Heterocyclic Compounds*, A. Hassner, Ed., Wiley, New York, **1985**, Vol 42, Part 3, Chap 1.
148. C.S. Combs, T.S. Wills, and R.D. Giles, *J. Org. Chem.* **1971**, *36*, 2027.
149. H. Normant, *Bull. Soc. Chim. Fr.* [5], **1940**, *7*, 373.
150. A.D. Baxter, F. Binns, T. Javed, S.M. Roberts, P. Sadler, F. Scheinmann, B.J. Wakefield, M. Lynch, R. F. Newton, *J. Chem. Soc., Perkin Trans 1* **1986**, 889.
151. a. R.I. Meltzer, J.A. King, *J. Am. Chem. Soc.* **1953**, *75*, 1355.
152. C.M. Hill, L. Haynes, D.E. Simmons, M.E. Hill, *J. Am. Chem. Soc.* **1953**, *75*, 5408.
153. G. Zemplén, A. Gerecs, *Chem. Ber.* **1937**, *70B*, 1098.
154. H.R. Snyder, E.L. Eliel, R.E. Carnahan, *J. Am. Chem. Soc.* **1951**, *73*, 970.
155. M.S. Kharasch, G.H. Williams, W. Nudenberg, *J. Org. Chem.* **1955**, *20*, 937.
156. A.R. Katritzky, S. Rachwal, G.J. Hitchings, *Tetrahedron* **1991**, *47*, 2683; A.R. Katritzky, S. Rachwal, B. Rachwal, P.J. Steel, *J. Org. Chem.* **1992**, *57*, 4925 and 4932.
157. K.G. Mizuch, R.A. Lapina, *Zh. Obshch. Khim.* **1956**, *26*, 839.
158. D.S. Brown, M. Bruno, R.J. Davenport, S.V. Ley, *Tetrahedron* **1989**, *45*, 4293; D.S. Brown, P. Charreau, T. Hansson, S.V. Ley, *Tetrahedron* **1991**, *47*, 1311.
159. F. Eiden, M. Schmidt, *Arch. Pharm.* **1987**, *320*, 130.
160. A.N. Nesmeyanov, A.N. Pushin, V.A. Sazonova, *Dokl. Akad. Nauk SSSR* **1980**, *255*, 885.
161. T. Hattori, N. Koike, S. Miyano, *J. Chem. Soc., Perkin Trans. 1* **1994**, 2273.
162. N. Furukawa, M. Tsuruoka, H. Fujihara, *Heterocycles* **1986**, *24*, 3337.
163. S. Oae, T. Takeda, J. Uenishi, S. Wakabayashi, *Phosphorous, Sulfur, Silicon*, **1996**, *115*, 179; S. Oae, Y. Inubushi, M. Yoshihara, *Heteroatom Chem.* **1993**, *4*, 185; S. Wakabayashi, Y. Kiyohara, S. Kameda, J. Uenishi, S. Oae, *Heteroatom. Chem.* **1990**, *3*, 225; R.W. Baker, D.C.R. Hockless, G.R. Pocock, M.V. Sargent, B.W. Skelton, A.N. Soblev, E. Twiss, A.H. White, *J. Chem. Soc., Perkin Trans. 1* **1995**, 2615.
164. S. Oae, T. Kawai, N. Furukawa, F. Iwasaki, *J. Chem. Soc, Perkin Trans. 2* **1987**, 405.
165. S. Wakabayashi, Y. Kubo, T. Takeda, J. Uenishi, S. Oae, *Bull. Chem. Soc. Jpn.* **1989**, *62*, 2338.
166. R. Sauvetre, J.-F. Normant, *Bull. Soc. Chim. Fr.* **1972**, 3202.
167. L. Jalander, *Synth. Commun.* **1988**, *18*, 343.
168. C. Cardellicchio, A.R. Cicciomessere, F. Naso, P. Tortorella, *Gazz. Chim. Ital.* **1996**, *126*, 555.
169. R. Giovannini, M. Petrini, *Synlett* **1996**, 1001.
170. Ref 29, pp 409-412, 645-648.
171. R.A. Rossi, S.M. Palacios, A.N. Santiago, *J. Org. Chem.* **1982**, *47*, 4654.
172. R.A. Rossi, A.N. Santiago, S.M. Palacios, *J. Org. Chem.* **1984**, *49*, 3387.

3

Hydromagnesiation of Alkenes and Alkynes

Fumie Sato and Hirokazu Urabe
Department of Biomolecular Engineering, Tokyo Institute of Technology, JAPAN

LIST OF ABBREVIATIONS

Et, ethyl; Pr, *n*-propyl unless otherwise specified; Bu, *n*-butyl unless otherwise specified; C_nH_{2n+1}, *n*-alkyl unless otherwise specified; Bn, $PhCH_2$; Ph, phenyl; Cp, η5-cyclopentadienyl; *n*-, normal; *i*-, iso; *s*-, secondary; *t*-, tertiary; *c*-, cyclo; η^m-, m-hapto; acac, acetylacetonate; AD, asymmetric dihydroxylation; b.p., boiling point; Dibal, diisobutylaluminum hydride; GC, gas chromatography; HMPA, hexamethylphosphoric triamide; NMR, nuclear magnetic resonance; py, pyridine; Red-Al, sodium bis(2-methoxyethoxy)aluminum hydride; rt, room temperature; TBS, *t*-$BuMe_2Si$; THF, tetrahydrofuran; THP, tetrahydropyranyl; TLC, thin layer chromatography.

3.1 INTRODUCTION

Hydrometallation signifies an addition reaction of metal hydrides to carbon–carbon multiple bonds to afford organometallic compounds. In the case where the metal hydride is easily available and the addition reaction proceeds readily, the reaction should become an efficient method for the preparation of organometallic compounds. Moreover, if the resulting organometallic compound shows versatile reactivities, as amply precedented by the hydroboration reactions, the hydrometallation reaction provides useful methodology in organic synthesis. Grignard reagents, which are one of the most versatile organometallic compounds used in a wide variety of synthetic transformations in both academic and industrial research, are mostly prepared by the action of metallic magnesium with organic halides. However, the requisite organic halides are usually prepared by halogenation of alkenes and alkynes, possibly via intermediate alcohols. Thus, in order to circumvent the stepwise process, considerable efforts have been made to develop a direct method, i.e., a hydromagnesiation reaction of these unsaturated compounds, for the preparation of Grignard reagents. Scheme 3.1 illustrates the notion of the hydromagnesiation process, in which the reagents may be (i) magnesium hydrides or (ii) those generated *in situ* from

Grignard Reagents: New Developments Edited by Herman G. Richey, Jr. © 2000 John Wiley & Sons Ltd

Grignard reagents via β-hydride elimination. A specific transition metal catalyst always plays a critical role in making these reactions a high-yield process.

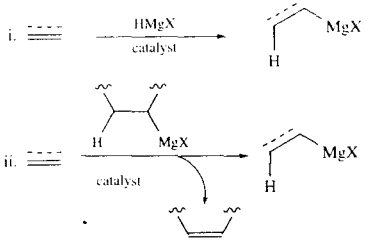

SCHEME 3.1. Hydromagnesiation of olefins and acetylenes.

Magnesium hydride, MgH_2, can be prepared more easily by a few methods than halomagnesium hydrides, HMgX (X = Cl, Br, I). Hydromagnesiation, using this most fundamental magnesium hydride, has been investigated. In fact, in 1958, Podal and Foster reported that MgH_2 underwent addition to ethylene under drastic reaction conditions [1]. However, homologous alkenes are resistant to the addition reaction. Twenty years later, Ashby *et al.* reported that the addition of MgH_2 to such alkenes is accelerated by a catalytic amount of early transition metal compounds such as $TiCl_4$, Cp_2TiCl_2, or ZrX_4 to afford *n*-alkylmagnesium species in good yields and with high regioselectivity [2]. Formation of dialkylmagnesium, R_2Mg, was more intensively investigated by Bogdanovic and coworkers by using active MgH_2 (eq. 3.1) [3,4]. Although these magnesium compounds, strictly speaking, are not Grignard reagents, they can react with a variety of electrophiles like Grignard reagents so that they will be discussed together in the following sections.

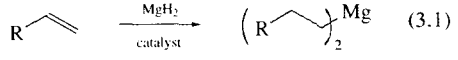

(3.1)

When alkynes are subjected to this hydromagnesiation in place of alkenes, (*cis*-1,2-disubstituted vinyl)magnesium reagents can be prepared in a highly stereoselective manner [2].

In 1962, Cooper and Finkbeiner reported that the addition of a catalytic amount of $TiCl_4$ to an ether solution of 1-alkenes and alkyl Grignard reagents having β-hydrogen(s) brought about a Grignard exchange reaction as shown in eq. (3.2) [5,6]. Some transition metal complexes including Cp_2TiCl_2, $Ti(O\text{-}i\text{-}Pr)_4$, $ZrCl_4$, and VCl_4 are also effective catalysts, but their activities are lower than that of $TiCl_4$. This finding was readily extended to another method of hydromagnesiation starting with easily accessible Grignard reagents as the hydride source. Thus, in Scheme 3.2, a Grignard reagent $R^1CH_2CH_2MgX$ is consumed as a 'HMgX' precursor, while, simultaneously, an olefin, $R^2CH{=}CH_2$, is hydromagnesiated to give a new Grignard reagent. The operational simplicity of this latter process has made this version a practical hydromagnesiation in routine organic synthesis.

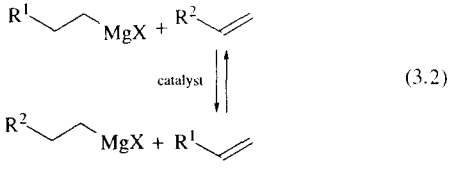

(3.2)

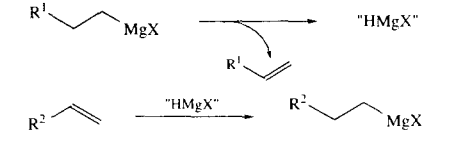

SCHEME 3.2. Transfer of 'HMgX' from a Grignard reagent to an olefin.

Although mono-olefins afforded the corresponding magnesium reagents in good yields by the above method, Cooper and Finkbeiner noted that the $TiCl_4$-catalyzed hydromagnesiation of conjugated dienes resulted in the production of complicated products involving a small amount of the hydromagnesiated product [6]. Sato, *et al.* showed that the conversion of conjugated dienes is best achieved with Cp_2TiCl_2 rather than $TiCl_4$ as the catalyst to afford allylic Grignard reagents in good yields [7]. The reaction proceeds quantitatively with butadiene and with butadienes having a substituent at its 2-position to afford exclusively the allyl Grignard reagents of the depicted structure as shown in eq. (3.3). The reaction, however, does not take place with 4-substituted 1,3-dienes such as 1,3-pentadiene.

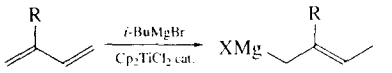

(3.3)

In so far as they had been considered as substrates in the hydromagnesiation reaction, acetylenes had not seemed to be successful candidates. In 1974, Colomer and Corriu reported that Cp_2TiCl_2-catalyzed hydromagnesiation of diphenylacetylene with *i*-PrMgBr afforded a 70% yield of *trans*-stilbene and a 30% yield of a mixture of *cis*-stilbene and 1,2-diphenylethane after hydrolysis, indicating low selectivity associated with this transformation [8]. In 1978, Snider, *et al.* reported that the reaction of a silylacetylene with C_2H_5MgBr in the presence of a nickel catalyst furnished the hydromagnesiation product in 50% yield, but accompanied by 30% yield of the dimer of the acetylene [9]. With the successful result of Cp_2TiCl_2-catalyzed hydromagnesiation of conjugated dienes as described above, Sato and his co-workers reinvestigated Cp_2TiCl_2-catalyzed hydromagnesiation of acetylenes with certain Grignard reagents and found that the reaction proceeds nicely to give stereo-defined alkenyl Grignard reagents (eq 3.4). [10]

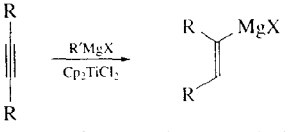

(3.4)

Recently, some important insight into the reaction mechanism was provided by the same group [11]. For instance, taking into account the hydro*titanation* mechanism and regioselectivity shown in eq (3.5), it has been concluded that the hydro*magnesiation* of a 1-(trimethylsilyl)-1-alkyne has the mechanism shown in scheme 3.3. Thus, the hydrotitanation of the silylacetylene with a stoichiometric amount of Cp_2Ti-H, generated from Cp_2TiCl_2 and 2 equiv. of an alkyl Grignard reagent as reductant [12], afforded in a regioselective manner the alkenyltitanium species having the silyl group α to the titanium (eq 3.5). Analogously, Cp_2TiCl_2-*catalyzed* hydromagnesiation of the acetylene is best rationalized by initial hydrotitanation with the titanium hydride species, showing the same regioselection, and then successive titanium/magnesium transmetallation as shown in Scheme 3.3.

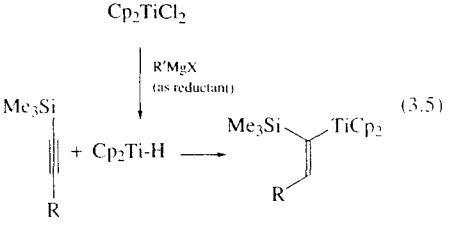

(3.5)

The above series of studies, which has been introduced by earlier review articles [13–22], now ensures the general applicability of the hydromagnesiation method to a variety of unsaturated compounds having alkene, conjugated diene, and alkyne functions, which are discussed in the following sections.

3.2 HYDROMAGNESIATION OF ALKENES

The most fundamental inorganic magnesium hydride, MgH_2, was reported to add ethylene under drastic reaction conditions [1]. However, as alkenes except ethylene are usually resistant to such an addition reaction, this method seems not to be general as such. However, a catalytic amount of Cp_2TiCl_2 dramatically promoted hydrometallation of 1-octene with MgH_2 as evidenced by the fact that quenching the resultant organomagnesium reagent with deuterium oxide or I_2 gave deuterated octane or 1-iodooctane according to equation (3.6) [2]. The magnesium hydride used in this catalyzed reaction was prepared by the reaction of Et_2Mg and $LiAlH_4$ in ether [23] or by metathesis of NaH and $MgCl_2$ in THF [24]. It was isolated by filtration and again suspended in THF to serve the reaction. Among

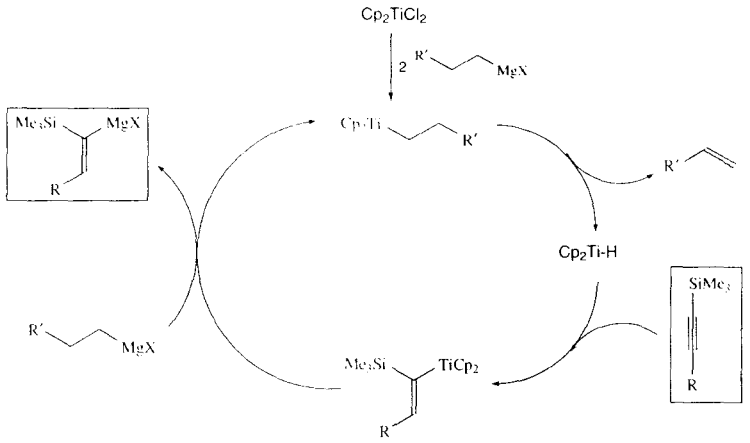

SCHEME 3.3. Proposed mechanism for hydromagnesiation of 1-(trimethylsilyl)-1-alkyne.

a few early transition metal compounds including $TiCl_3$ and $ZrCl_4$, titanocene dichloride was the most effective in combination with the magnesium hydride.

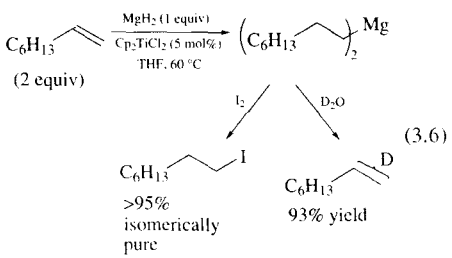

Terminal aliphatic olefins such as 1-hexene and 1-octene enter this reaction to afford (primary-alkyl)magnesium compounds as shown in eq. (3.6). Contrarily as exemplified by styrene, aromatic olefins show a reversal of regioselection to give benzylmagnesium compounds (eq. 3.7). Methylenecyclohexane afforded the magnesium intermediate in moderate yield (eq. 3.8), but other di-substituted olefins shown in Figure 3.1 underwent the hydromagnesiation very sluggishly. The main product is the hydrogenated one which incorporates almost no deuterium atoms upon deuterolysis of the reaction mixture. Tri-substituted olefins such as 1-methylcyclohexene were inert under these reaction conditions.

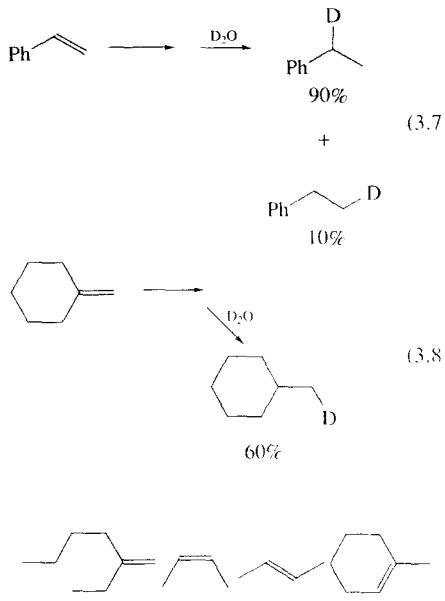

Fig. 3.1.

Hydromagnesiation with inorganic magnesium hydride has been more intensively investigated by the use of active MgH_2 prepared by hydrogenation of Mg with H_2 in the presence of Mg-anthracene and $CrCl_3$ or $TiCl_4$ as the hydrogenation catalyst [3,4,18]. If $MgCl_2$ is further added to the hydrogenation media as a co-catalyst, the reaction period necessary for the generation of active MgH_2 will be shortened (eq. 3.9). It is interesting to note that the above hydrogenation catalyst also shows catalytic activity in the subsequent hydromagnesiation step so that hydrogenation of magnesium metal and the hydromagnesiation of olefins could be carried out in a consecutive manner. In such a case, the titanium catalyst is superior to the chromium one (method A in eq. (3.9)). However, the hydromagnesiation step may be more preferably carried out in the presence of a newly added catalyst consisting of a zirconium halide such as $ZrCl_4$ or ZrI_4 (method B). Hydromagnesiation of ethylene, which is shown in eq. (3.10), illustrates this technique. Ethylene may react violently so that due care must be taken. The catalytic activity of a few transition metal salts in the hydromagnesiation step drops in the following order: $ZrCl_4 > TiCl_4 > HfCl_4$. Noteworthy is the relatively low efficiency observed for Cp_2TiCl_2 in this hydromagnesiation, which is in contrast to the fact that it was the best catalyst in the aforementioned hydromagnesiation with MgH_2 prepared from Et_2Mg and $LiAlH_4$ or by metathesis of NaH and $MgCl_2$ as shown in eq. (3.6). Thus, the activity of the catalyst apparently depends on the quality of MgH_2.

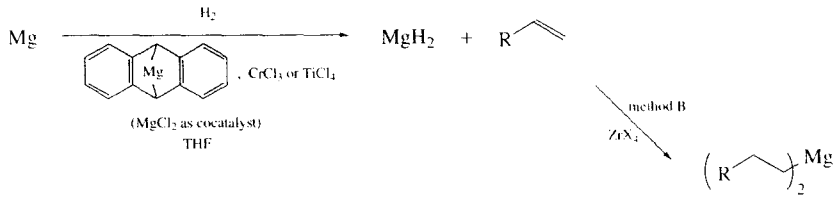

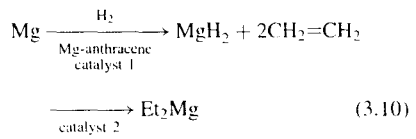

Catalyst 1	Catalyst 2	Method	Yield of Et_2Mg (%)
$CrCl_3$	(catalyst 1)	A	83
$CrCl_3$	$ZrCl_4$	B	97
$TiCl_4/MgCl_2$	(catalyst 1)	A	97

Other 1-alkenes produced the desired R_2Mg in excellent yields as shown in entries 1–6 of Table 3.1, where the catalyst giving the best result is shown. Yields are of the magnesium compound in a reaction mixture determined by acid/base titration and/or gas volumetric analysis. In some representative cases, those of isolated materials are also given. The resulting dialkylmagnesium reagents, which consist of the 1-alkylmagnesium compound with >99.7% regiochemical purity and may be isolated if necessary, were utilized for the synthetic transformations (*vide infra*). Hydromagnesiation of an α-branched terminal olefin such as that in eq. (3.11) proceeded without difficulty to afford the magnesium compounds in good yield and without loss of the enantiopurity [4,29]. The internal olefin moiety was not affected at all. Hydromagnesiation of styrene generated the corresponding benzylic magnesium compounds with approximately 95:5 regioselectivity (determined by

analysis following silylation) (eq. 3.12) [30]. A mixed dialkylmagnesium was obtained in high yield from hydromagnesiation of an equimolar mixture of ethylene and butene (eq. 3.13) [4]. The uniformly high yields of the magnesium compounds shown in eq. (3.10) and entries 1–6 of Table 3.1 should come from the lack of a serious side reaction such as isomerization of the terminal double bond to an inert, internal one, which is not negligible in the Grignard reagent-based hydromagnesiation discussed later.

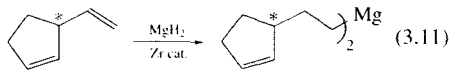

(3.11)

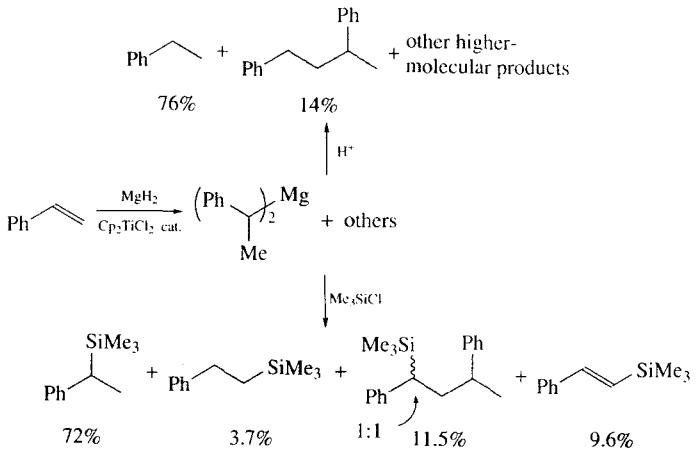

(3.12)

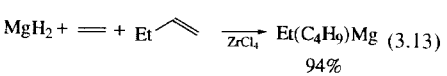

(3.13)

The dialkylmagnesiums obtained herein have wide application as carbon nucleophiles in organic synthesis [4]. In all of the following reactions, only a small excess of R_2Mg to an electrophile was necessary to achieve good to excellent yields. It should also be noted that both of the alkyl groups in R_2Mg were successfully transferred to the product. Scheme 3.4 summarizes representative reactions. Isolation of an intermediate magnesium compound was not necessarily required. Silylation and oxidation of dioctylmagnesium (to give trimethyl(octyl)silane and octanol, respectively) determined the isomeric purity of *n*- vs. *s*-octyl groups in the organomagnesium compound to be 99.7: 0.3, confirming the very high regioselectivity of the hydromagnesiation step.

Dialkylmagnesiums behave like Grignard reagents in alkylation and carbonyl addition, which are among the most important reactions in organic synthesis. Copper-catalyzed alkylation with alkyl bromide was mentioned in an asymmetric synthesis of chaulmoograic acid (eq. 3.14) [4,29]. Reactions with carbonyl compounds are shown in Table 3.2. As expected, aldehydes and ketones afforded secondary and tertiary alcohols in good yields (entries 1–5) [4]. Ethyl propionate reacted with 2 equiv of the R group of R_2Mg to give tertiary alcohol (entries 6 and 7) [4]. The coupling reaction with acyl chlorides was carried out preferably in the catalytic presence of an iron salt to afford ketones (entries 8–13) [4]. Copper-catalyzed conjugate addition to α,β-unsaturated

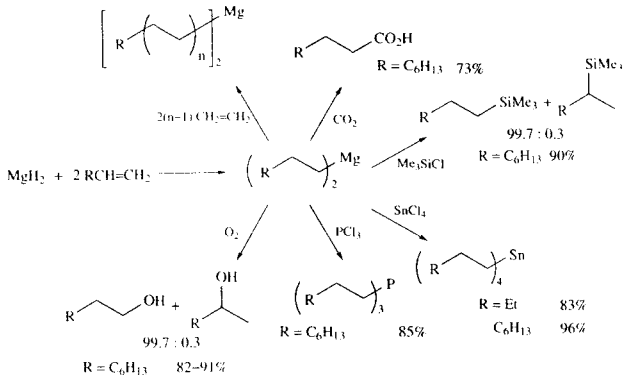

SCHEME 3.4. Transformations based on dialkylmagnesiums.

Table 3.1. Hydromagnesiation of terminal olefins with MgH_2

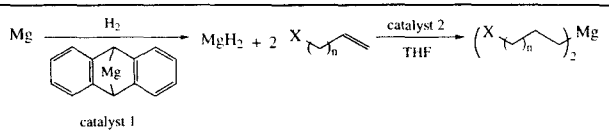

Entry	X	n	Catalyst 1	Catalyst 2	Dialkylmagnesium Yield(%)	Dialkylmagnesium Isolated yield(%)	Ref.
1	H	0	$CrCl_3$	$ZrCl_4$	97	80	4,25,26
2	H	1	$TiCl_4$	catalyst 1	98	—	4
3	H	2	$TiCl_4/MgCl_2$	catalyst 1	86	73	4,26
4	H	6	$CrCl_3/MgCl_2$	catalyst 1	—	69	4,26
5	H	8	(see ref.)	$ZrCl_4$	ca.90	—	4,25
6	H	13	$CrCl_3$	$ZrCl_4$	91	—	4
7	MeO	2	$TiCl_4$ or $CrCl_3$	$ZrCl_4$	—	35	27,28
8	EtO	2	$TiCl_4$ or $CrCl_3$	$ZrCl_4$	—	39	27
9	PrO	2	$TiCl_4$ or $CrCl_3$	$ZrCl_4$	—	60	27
10	BuO	2	$TiCl_4$ or $CrCl_3$	$ZrCl_4$	—	34	27
11	$C_5H_{11}O$	2	$TiCl_4$ or $CrCl_3$	$ZrCl_4$	—	28	27
12	Me_2N	1	$TiCl_4$ or $CrCl_3$	$ZrCl_4$	—	43	27,28
13	Et_2N	1	$TiCl_4$ or $CrCl_3$	$ZrCl_4$	—	47	27
14	Pr_2N	1	$TiCl_4$ or $CrCl_3$	$ZrCl_4$	—	44	27
15	$(i\text{-}Pr)_2N$	1	$TiCl_4$ or $CrCl_3$	$ZrCl_4$	—	11	27
16	Bu_2N	1	$TiCl_4$ or $CrCl_3$	$ZrCl_4$	—	35	27
17	MeEtN	1	$TiCl_4$ or $CrCl_3$	$ZrCl_4$	—	18	27
18	MeBuN	1	$TiCl_4$ or $CrCl_3$	$ZrCl_4$	—	50	27
19	MePhN	1	$TiCl_4$ or $CrCl_3$	$ZrCl_4$	—	30	27
20	Me_2N	2	$TiCl_4$ or $CrCl_3$	$ZrCl_4$	—	52	27,28
21	Et_2N	2	$TiCl_4$ or $CrCl_3$	$ZrCl_4$	—	31	27
22	Pr_2N	2	$TiCl_4$ or $CrCl_3$	$ZrCl_4$	—	18	27
23	MeEtN	2	$TiCl_4$ or $CrCl_3$	$ZrCl_4$	—	40	27
24	MeBuN	2	$TiCl_4$ or $CrCl_3$	$ZrCl_4$	—	37	27

carbonyl compounds is also feasible (entries 14–23) [31].

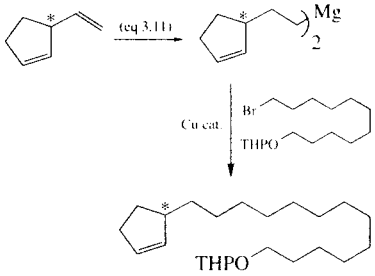

(3.14)

The above method was successfully applied to the preparation of a few kinds of functionalized olefins [27]. The functionalized dialkylmagnesiums obtained herein primarily attract interest in the field of structural chemistry. Nonetheless, these should also be useful carbon nucleophiles in synthetic chemistry. Attempted hydromagnesiation of allyl ethers resulted in the elimination of the alkoxide, not giving the magnesium compounds (eq. 3.15). However, a homo-allyl ether underwent the hydromagnesiation to give the desired product as shown in eq. (3.16). The yield displayed refers to that of the isolated compound so that the actual yield of the organomagnesium compound in a reaction mixture may be somewhat underestimated. X-ray crystallography confirmed the monomeric nature of bis(4-methoxybutyl)magnesium, the structure of which involves intramolecular chelation as shown in Figure 3.2. Analogously, other homo-allyl ethers, allylamines, and homo-allylamines furnished the corresponding di(ω-functionalized alkyl)magnesiums in fair to good yields, which are summarized in entries 7–24, Table 3.1. These bis(alkoxyalkyl)- and bis(aminoalkyl)magnesiums generally show sharp signals in ^{1}H and ^{13}C NMR spectra taken at room temperature. However, at a temperature as low as −80°C, further splitting or coalescence of the peaks was observed dependent upon the individual structure [27].

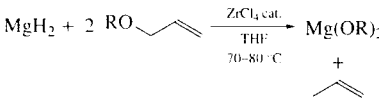

(3.15)

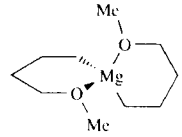

Fig. 3.2.

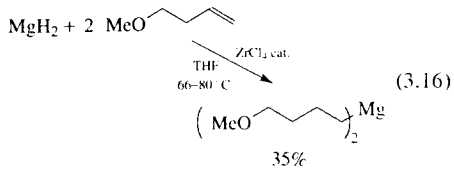

(3.16)

Use of aminomagnesium monohydrides such as Et_2NMgH, as magnesium hydrides has been examined, but their synthetic advantage over MgH_2 is obscure at present (eq. 3.17) [19,32].

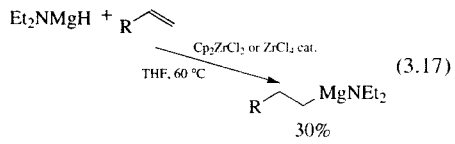

(3.17)

As described in the introductory section, another important method of hydromagnesiation is to use a Grignard reagent as the source of magnesium hydride. In 1962, Cooper and Finkbeiner reported that Grignard reagents having a β-hydrogen are in equilibrium with another olefin to generate a second Grignard reagent in the presence of $TiCl_4$. Through their detailed study [6] which included using several other transition metal catalysts ($TiCl_4$, Ti(O-*i*-Pr)$_4$, Cp_2TiCl_2, $ZrCl_4$, and VCl_4) they showed this reaction to be an efficient method of hydromagnesiation of olefins according to eq. (3.18). Thus, a mixture of an olefin and PrMgBr in ether was heated at reflux in the presence of $TiCl_4$ (this gave the best result among the five preceding transition metal compounds) to afford the new Grignard reagent resulting from the added olefin. The use of a low-molecular- weight Grignard reagent such as Et-, Pr-, *i*-Pr-, or *i*-BuMgX is recommended as the $R^1CH_2CH_2MgX$ in eq. (3.18), since the olefin

Table 3.2. Reaction of R_2Mg with carbonyl compounds

$$\left(MgH_2 + \text{1-alkene} \xrightarrow{\text{Table 3.1, etc.}}\right) R_2Mg + El^+ \xrightarrow{\text{additive}} \text{R-El}$$

Entry	R	El^+	Ratio R_2Mg/El^+	Additive(mol%)	Product(R-El)		Yield(%)[a]	Ref.
1	Et	PhCHO	0.6 : 1	—	PhEtCH(OH)		84	4
2	Et	EtCOEt	0.6 : 1	—	Et_3COH		70	4
3	Et	PhCOEt	0.6 : 1	—	$PhEt_2COH$)		81	4
4	C_8H_{17}	EtCOEt	0.6 : 1	—	$Et_2(C_8H_{17})COH$		63	4
5	C_8H_{17}	PhCOEt	0.6 : 1	—	$PhEt(C_8H_{17})_2COH$		71	4
6	Et	$EtCO_2Et$	1.2 : 1	—	Et_3COH		86	4
7	C_8H_{17}	$EtCO_2Et$	1.2 : 1	—	$Et_2(C_8H_{17})COH$		68	4
8	C_8H_{17}	MeCOCl	0.5 : 1	Fe(acac)$_3$ (7)	$C_8H_{17}COMe$		57	4
9	C_8H_{17}	EtCOCl	0.5 : 1	—	$C_8H_{17}COEt$		71	4
10	C_8H_{17}	EtCOCl	0.5 : 1	Fe(acac)$_3$ (6)	$C_8H_{17}COEt$		58	4
11	C_8H_{17}	PrCOCl	0.5 : 1	Fe(acac)$_3$ (3)	$C_8H_{17}COPr$		60	4
12	C_8H_{17}	PhCOCl	0.5 : 1	—	$C_8H_{17}COPh$		40	4
13	C_8H_{17}	PhCOCl	0.5 : 1	Fe(acac)$_3$ (4)	$C_8H_{17}COPh$		67	4
14	Et	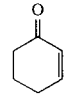	0.52 : 1	CuI•2LiCl(10), Me_3SiCl	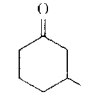	R=Et	92[b]	31
15	C_8H_{17}		0.52 : 1	CuI•2LiCl(10), Me_3SiCl		R=C_8H_{17}	89	31
16	Et	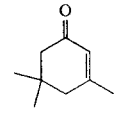	0.52 : 1	CuI•2LiCl(10), Me_3SiCl	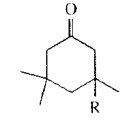	R=Et	95[b]	31
17	C_8H_{17}		0.52 : 1	CuI•2LiCl(10), Me_3SiCl		R=C_8H_{17}	76	31
18	Et	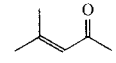	0.52 : 1	CuI•2LiCl(10), Me_3SiCl	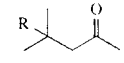	R=Et	37	31
19	C_8H_{17}		0.52 : 1	CuI•2LiCl(10), Me_3SiCl		R=C_8H_{17}	64	31
20	Et	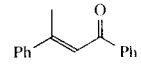	0.52 : 1	CuI•2LiCl(10), Me_3SiCl	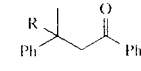	R=Et	20[b]	31
21	C_8H_{17}		0.52 : 1	CuI•2LiCl(10), Me_3SiCl		R=C_8H_{17}	48[b]	31
22	Et	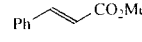	0.52 : 1	CuI•2LiCl(10), Me_3SiCl	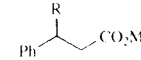	R=Et	73	31
23	C_8H_{17}		0.52 : 1	CuI•2LiCl(10), Me_3SiCl		R=C_8H_{17}	75	31

[a] Based on El^+.
[b] The product was isolated as enol silyl ether.

formed by the Grignard equilibrium ($R^1CH{=}CH_2$: ethylene, propylene, or isobutene, respectively) can be expelled from the reaction mixture to shift the equilibrium to the right. Cp_2TiCl_2 could be used equally well as $TiCl_4$ as the titanium catalyst. The proposed mechanism of this reaction is in Scheme 3.5, in which a titanium hydride, Cl_3TiH, plays an important role in establishing the catalytic cycle [5].

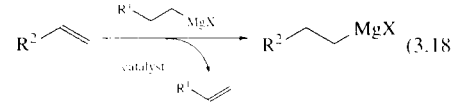

(3.18)

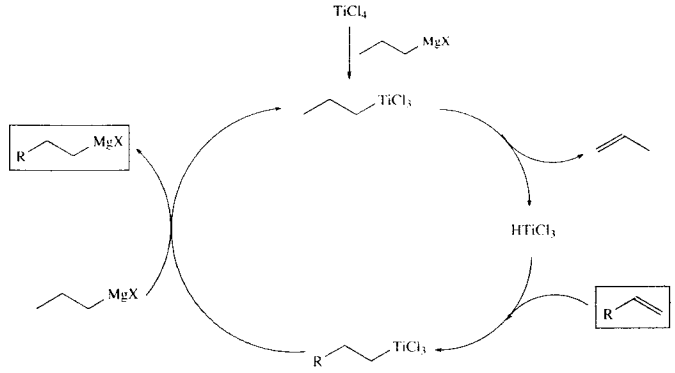

SCHEME 3.5. Proposed reaction course for the titanium-catalyzed Grignard exchange reaction.

Table 3.3 displays a survey of the hydromagnesiation of various olefins with Grignard reagents. Like the aforementioned hydromagnesiation with inorganic MgH_2, terminal olefins are the only acceptable substrates in this reaction, and give 1-alkyl Grignard reagents in a highly regioselective manner. Other types of olefins, cyclohexene, 2-pentene, *trans*-stilbene, α-methylstyrene, β-methylstyrene, and 2-methyl-1-pentene, did not undergo the Grignard exchange reaction at all even under forcing reaction conditions (PrMgBr, $TiCl_4$) [6]. This feature enables a chemoselective hydromagnesiation between different types of olefins, which can be seen in several reactions of Table 3.3. The yields of the Grignard reagents from terminal olefins fall in a fair to good range. One inevitable side reaction obviously lowering the yield is the titanium-catalyzed isomerization of terminal olefins to unreactive internal ones, which is evidenced in the reaction of eq. (3.19) and, in an extreme case, may become a quantitative path [8,33].

In general, terminal alkenes having a hydroxy group in a proximate position show somewhat improved yields as compared to simple 1-alkenes. This likely arises from the stabilization of the intermediate magnesium species by intramolecular coordination with the alkoxide group as depicted in eq. (3.20), preventing the above unfavourable side reaction. Equation (3.20) demonstrates a synthesis of polyisoprenepolyols by hydromagnesiation of an unsaturated alcohol, in which no protection of the hydroxy groups was necessary [34]. Unsaturated alcohols find another synthetic utility for the one-step preparation of lactones via carboxylation of the intermediate as shown in eq. (3.21) [35]. Despite the exhaustive substitution to its allylic position, hydromagnesiation took place with this substrate, affording the desired lactone in a reasonably good yield.

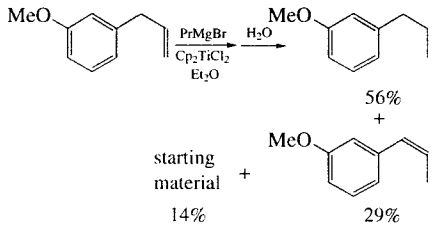

(3.19)

Hydromagnesiation of a terminal olefin followed by the nickel-catalyzed vinylation with excess vinyl bromide provides a one-pot method of two-carbon homologation of the parent olefin as shown in eq. (3.22) [37].

Aromatic olefins afforded benzyl Grignard reagents in good yields, consistent with the aforementioned observation of eqs (3.7) and (3.12). Scheme 3.6 summarizes a comparison of a few

Table 3.3. Hydromagnesiation of 1-alkenes with Grignard reagents

Entry	R	R'MgX	catalyst	El+	El	Yield(%)	Ref.
1	Pr	PrMgBr	$TiCl_4$	HCHO	$CH_2(OH)$–	45	6
2	Bu	PrMgBr	$TiCl_4$			24	6
3	*i*-Pr	PrMgBr	$TiCl_4$	PhCHO	PhCH(OH)–	35	6
4	*i*-Bu	PrMgBr	$TiCl_4$	MeCHO	MeCH(OH)–	37	6
5[a]	$R^1R^2C(OH)CH_2$	*i*-BuMgCl	Cp_2TiCl_2	R^3R^4CO	$R^3R^4C(OH)$–	42-71	34
6	C_6H_{13}	PrMgBr	$TiCl_4$	CO_2	CO_2Me^b	40	6
7	$PhCH_2$	PrMgBr	$TiCl_4$	CO_2	CO_2H	62	6
8	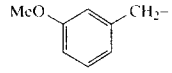	PrMgBr	$TiCl_4$	CO_2	CO_2H	37	33
9	*c*-C_6H_{11}	PrMgBr	$TiCl_4$	CO_2	CO_2H	51	6
10		PrMgBr	$TiCl_4$	CO_2	CO_2H	28	6
11	$Ph_2C(OH)CH_2$	EtMgBr	Cp_2TiCl_2	CO_2	CO_2H	64	35
12		EtMgBr	Cp_2TiCl_2	CO_2	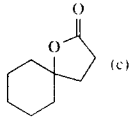 (c)	58	35
13	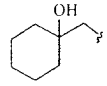	EtMgBr	Cp_2TiCl_2	CO_2	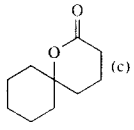 (c)	55	35
14	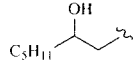	EtMgBr	Cp_2TiCl_2	CO_2	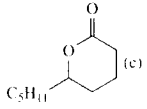 (c)	55	35
15	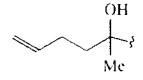	EtMgBr	Cp_2TiCl_2	CO_2	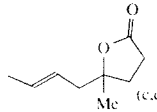 (c,d)	46	35
16	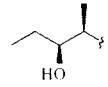	*i*-BuMgCl	Cp_2TiCl_2	CO_2	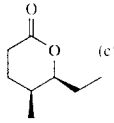 (c)	54	36

(*continued overleaf*)

Table 3.3. (*continued*)

Entry	R	R'MgX	catalyst	El[a]	El	Yield(%)	Ref.
17	C_6H_{13}	PrMgBr	$TiCl_4$	$(EtO)_3CH$	$(EtO)_2CH$-	19	6
18	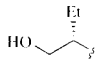	PrMgBr	Cp_2TiCl_2	CH_2=$CHBr$,	CH_3=CH–	72	37
					$(PPh_3)_2NiCl_2$		
19	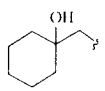	EtMgBr	Cp_2TiCl_2	Me_3SiCl	Me_3Si	59	35
20		PrMgBr	$TiCl_4$	O_2	OH	40	6
21	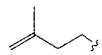	PrMgBr	$TiCl_4$	O_2	OH	45	6

[a] See eq. 3.20 in text.
[b] After esterification.
[c] This structure corresponds to  .
[d] Another terminal olefin isomerized to the internal one.

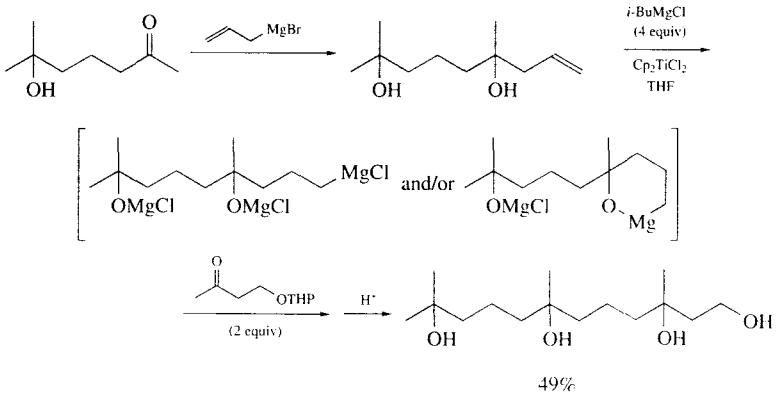

(3.20)

combinations of a Grignard reagent and a titanium compound to effect the hydromagnesiation of styrene: i) *i*-PrMgBr/Cp_2TiCl_2 [8]; ii) *n*-PrMgBr/Cp_2TiCl_2 [7]; and iii) *n*-PrMgBr/$TiCl_4$ [6].

Hydromagnesiation of other styrenes having a substituent on aromatic ring proceeded as expected as shown in eqs (3.23) [6] and (3.24) [38].

(Tribenzylsilyl)ethylene, which has no chance to undergo olefin isomerization, is said to give α-silylalkyl Grignard reagents quantitatively, although the yields of the deuterated and silylated products have not been shown (eq. 3.25) [8].

As shown above, a few functional groups in the olefinic substrate such as ether, hydroxyl (which

exists as alkoxide in reaction media), or internal olefin did not impede the reaction. The newly formed Grignard reagent can be obtained with high regioselectivity and could be trapped regioselectively with a variety of electrophiles such as aldehydes, ketones, carbon dioxide, orthoesters, vinyl bromide, silyl chloride, and oxygen, which broadens the synthetic utility of the hydromagnesiation reaction.

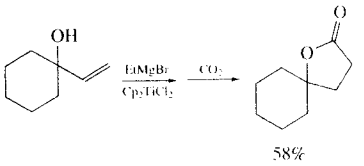

(3.21)

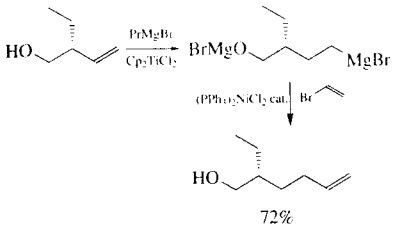

(3.22)

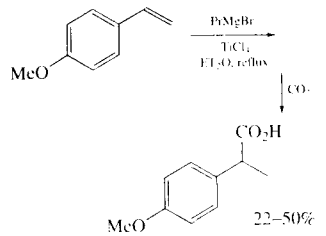

(3.23)

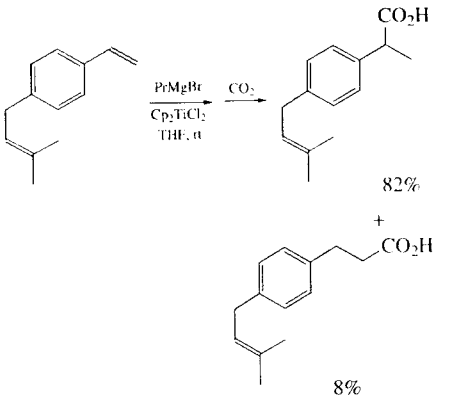

(3.24)

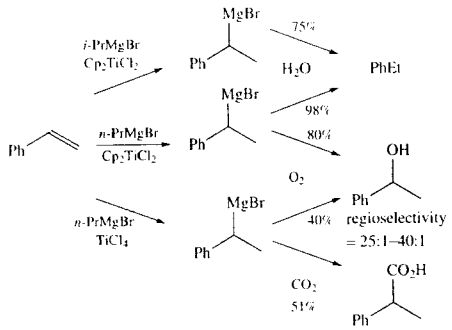

SCHEME 3.6. Hydromagnesiation of styrene with Grignard reagents.

There is another choice of catalyst in hydromagnesiation of alkenes with Grignard

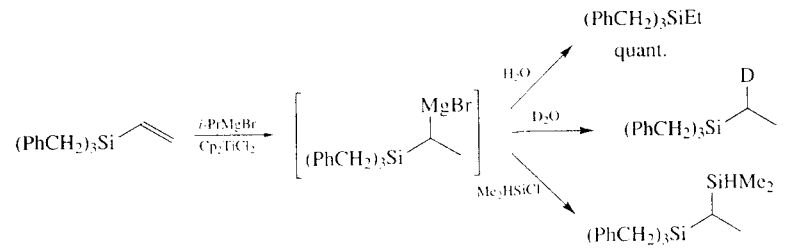

(3.25)

reagents. In 1969, Markó reported that a catalytic amount of a nickel salt also promotes an analogous alkene/Grignard reagent exchange reaction (eq. 3.26) [39–41]. The mechanism of the reaction has been considered to be that shown in Scheme 3.7, in which a Ni–H species, generated by β-hydride elimination from an alkyl-nickel intermediate, catalyzes the key step [14].

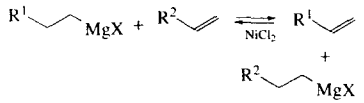

(3.26)

This exchange reaction was readily extended to a hydromagnesiation process. In fact, the hydromagnesiation of an allyl alcohol and a styrene to give a lactone (eq. 3.27) [14] and an

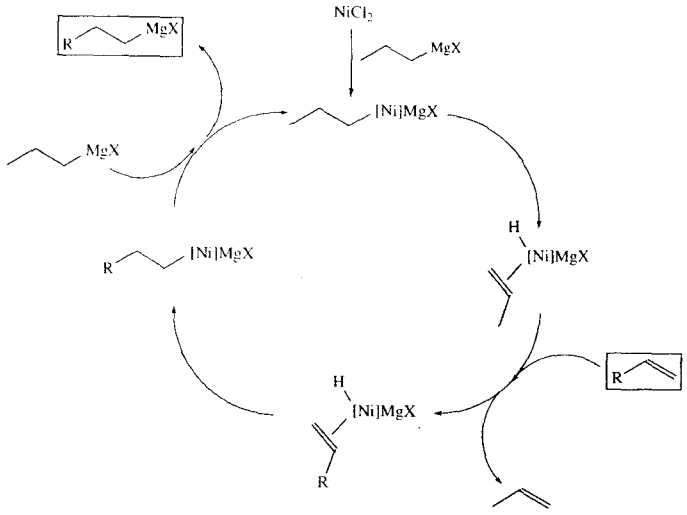

SCHEME 3.7. Proposed reaction course for nickel-catalyzed hydromagnesiation with Grignard reagents.

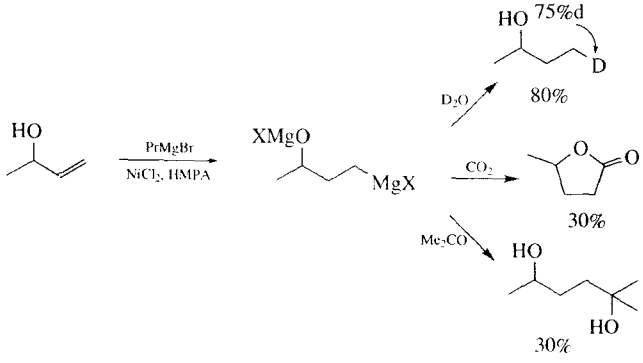

(3.27)

α-arylalkanoic acid (eq. 3.28) [38] were examined. In the transformation of eq. (3.28), extensive optimization of the reaction conditions including the kind of Grignard reagent eventually increased the product yield to as high as 82%. Isolation in only 0.7% yield of the regioisomer, a 3-arylpropanoic acid, showed the high regioselectivity. Thus, terminal alkenes preferably afford 1-alkyl Grignard reagents, whereas styrene derivatives yield the benzyl Grignard reagents as found in the titanium-mediated protocol.

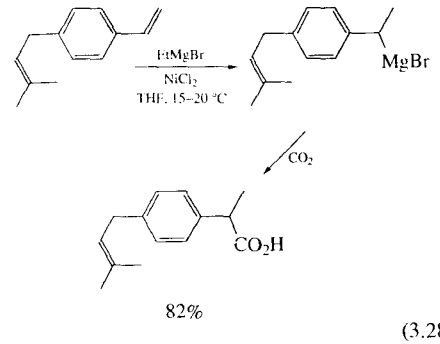

(3.28)

An iron-catalyzed Grignard exchange reaction was reported by Tamura and Kochi in 1971 as shown in eqs (3.29) and (3.30) [15,42,43].

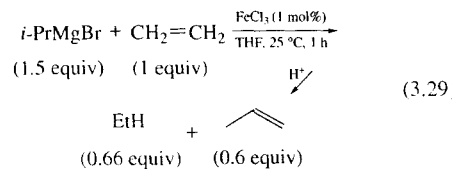

(3.29)

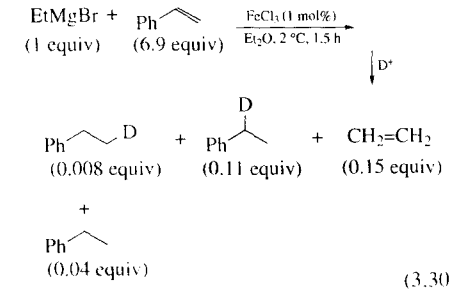

(3.30)

3.3 HYDROMAGNESIATION OF CONJUGATED DIENES

Many examples of the hydromagnesiation of olefins with Grignard reagents under the influence of a titanium catalyst that appeared in the preceding section show the product yields not to be very satisfactory. However, the use of conjugated dienes or acetylenes as the substrate in place of simple alkenes remarkably increases the yield of the organomagnesium compounds as described below. This may result from the following reasons. First, the latter substrates afford structurally and/or electronically more stable intermediates such as allyl- or alkenyl-metal species rather than alkylmetals to make the transformation of eq. (3.2) no longer an equilibrium [7]. The second point is that dienes and alkynes do not undergo the undesired isomerization that is a serious problem in the hydromagnesiation of alkenes to diminish the product yields. Thus, the potential of hydromagnesiation as a versatile synthetic transformation should be more distinctly demonstrated with the following substrates.

The hydromagnesiation reaction with active MgH_2 introduced in eq. (3.9) was attempted on isoprene in the presence of several early transition metal compounds including Cp_2TiCl_2, $TiCl_4$, Cp_2ZrCl_2, and $ZrCl_4$ as the catalyst, but these reactions always afforded a mixture of regioisomers of allylmagnesium intermediates **A** and **B** (eq 3.31, approximately 80:20–30:70 depending on conditions and catalyst), which, upon silylation with Me_3SiCl, afforded regioisomers in addition to stereoisomers [30]. Eq. (3.31) illustrates the reaction catalyzed by Cp_2ZrCl_2, which showed the highest regioselectivity of the hydromagnesiation step. Unfortunately, the formation of regioisomeric allylmagnesium reagents by this method would detract from its value for selective organic synthesis.

However, the synthetic value of this hyromagnesiation procedure has not been tested. They also examined other metal salts including $CoBr_2$, $PdCl_2$, $MnCl_2$, CuCl, $CuCl_2$, and AgBr for this purpose, but the last five salts showed little or no activity.

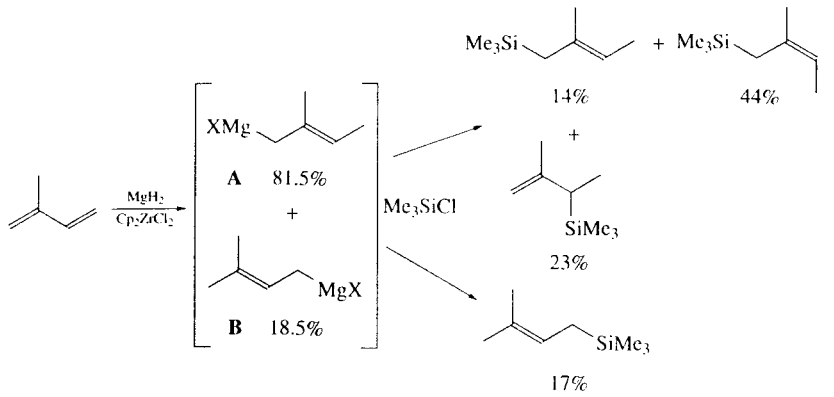

(3.31)

As mentioned in the introductory part, attempted $TiCl_4$-catalyzed olefin hydromagnesiation did not work well on conjugated dienes [6]. However, switching the catalyst from $TiCl_4$ to Cp_2TiCl_2 drastically increased the efficiency of the hydromagnesiation. Thus, under these reaction conditions, 2-alkyl-1,3-butadienes generally afforded allyl Grignard reagents in excellent yields. More surprisingly, a single regioisomer of the allyl Grignard reagent is exclusively formed as shown in eq. (3.32), which was verified by the subsequent reactions with electrophiles [7].

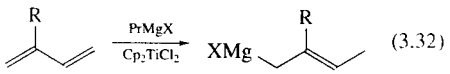

(3.32)

The observed regioselection of hydromagnesiation is identical with that of the hydro*titanation* of the same substrates with a stoichiometric amount of Cp_2Ti-H as shown in eq. (3.33) [12,44]. This fact strongly suggests that the regioselection of eq. (3.32) originates in the hydrotitanation step involved in the catalytic cycle like the one shown in Scheme 3.3 or 3.12 (*vide infra*).

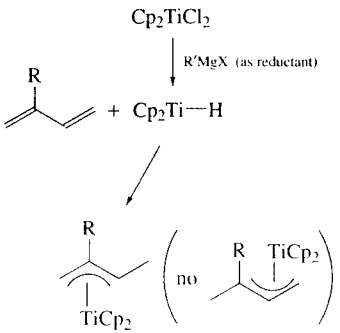

(3.33)

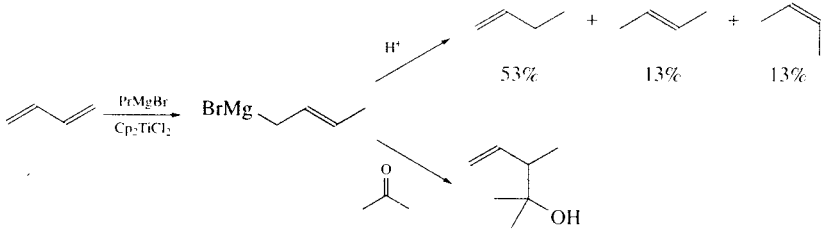

(3.34)

Table 3.4. Hydromagnesiation of conjugated dienes with Grignard reagents

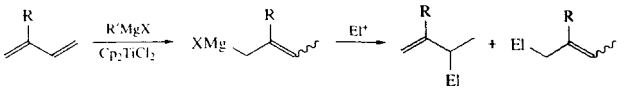

Entry	R	R'MgX	El^+	(A) El	(B) Products(%)	Ref.
1	H	PrMgBr	H_2O	H	**A**(53),*cis*-**B**(15), *trans*-**B** (13)	7
2	Me	PrMgBr	H_2O	H	**A**(76),**B**(21)	7
3	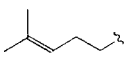	PrMgBr	H_2O	H	**A**(88),**B**(8)	7
4	H	PrMgBr	Me_2CO	$Me_2C(OH)$-	**A**(79)	7
5	Me	PrMgBr	Me_2CO	$Me_2C(OH)$-	**A**(95)	7
6	Me	*i*-BuMgBr	EtCN	EtCO	**A**(78)	46
7	Et	*i*-BuMgBr	EtCN	EtCO	**A**(71)	46
8	Bu	*i*-BuMgBr	EtCN	EtCO	**A**(81)	46
9	Me	*i*-BuMgBr	HCO_2MgBr	CHO	**A**(33)	46
10	Et	*i*-BuMgBr	HCO_2MgBr	CHO	**A**(49)	46
11	Bu	*i*-BuMgBr	HCO_2MgBr	CHO	**A**(66)	46
12	Me_3Si	*i*-BuMgBr	HCO_2MgBr	CHO	**A**(46–55)	47

Although the simple hydrolysis of the allyl Grignard reagents tends to yield a mixture of regio- and stereoisomeric olefins, the reaction with carbon electrophiles such as carbonyl compounds and nitriles usually afforded a single regioisomer (eq. 3.34) [7]. This selective aspect and the versatility of the resultant allylmetal reagents [45] enhance the synthetic utility of this process, even though the substrates are limited to butadiene and 2-substituted butadienes. Additional results are collected in Table 3.4.

Nickel-catalyzed hydromagnesiation of conjugated dienes with Grignard reagents seems less fruitful from the synthetic point of view. Attempted reactions of butadiene and isoprene resulted in a formal hydromagnesiation of the corresponding diene dimer to give a homologous Grignard reagent as shown in eq. (3.35) [48]. Analogously, when isoprene was used as the diene and CO_2 as the quenching reagent, the carboxylic acid shown in eq. (3.36) was formed [49]. If *i*-PrMgCl was replaced by CD_3CD_2MgBr, the deuterated product was obtained, confirming that the hydrogen (deuterium) comes from the Grignard reagent, most likely via β-elimination.

Ordinary hydromagnesiation may be effected by the use of a nickel-pyridine complex like $Ni(py)_4Cl_2$, even though it affords a mixture of regioisomeric allylmagnesium reagents as determined by carboxylation, giving two kinds of carboxylic acids (eq. 3.37) [50]. An alkoxybutadiene underwent the alkylation as well

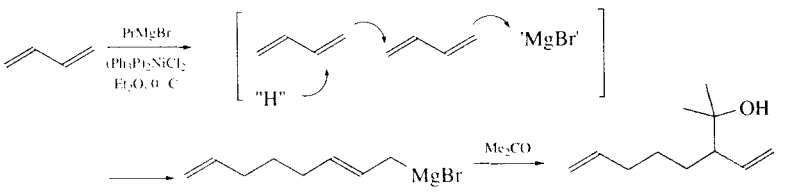

(3.35)

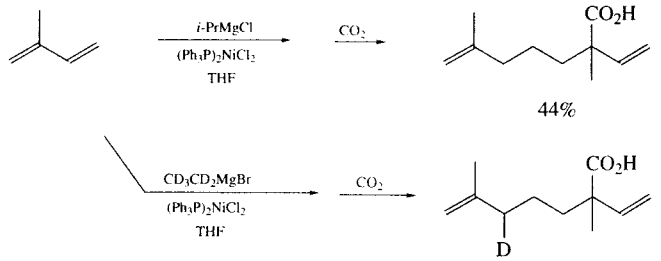

(3.36)

as hydromagnesiation with *i*-PrMgCl in the presence of $(Ph_3P)_2NiCl_2$ to afford the three carbon-elongated carboxylic acid, albeit in a low yield, by quenching with carbon dioxide (eq. 3.38) [51]. In the latter reaction, the use of $Ni(py)_4Cl_2$ again affords regioisomeric carboxylic acids like the preceding equation, showing the importance of the ligand on nickel to control the regioselectivity.

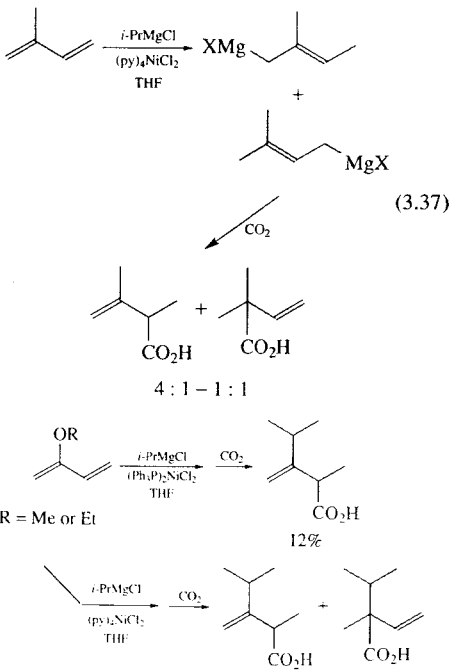

(3.37)

(3.38)

3.4 HYDROMAGNESIATION OF ALKYNES

Hydromagnesiation of alkynes with inorganic hydride, MgH_2 prepared from Et_2Mg and $LiAlH_4$ [23] or from NaH and $MgCl_2$, [24] and a catalytic amount of Cp_2TiCl_2 was carried out in the same manner as described in eq. (3.6) [2]. An internal acetylene underwent this hydromagnesiation to give a deuterated *cis*-olefin in good yield upon exposure to D_2O (eq. 3.39). However, in the case of a terminal acetylene, formation of magnesium acetylide *in situ* hindered a good conversion of the substrate (eq. 3.40). Further study on hydromagnesiation of acetylenes with MgH_2 has not been carried out.

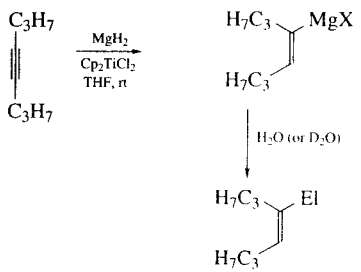

(3.39)

Contrarily, Grignard reagent-mediated hydromagnesiation of acetylenes in the presence of

Cp_2TiCl_2 is much more promising [10] and has found extensive and intensive application in current organic synthesis. The most striking advantages of this method could be condensed as follows. i) The hydride precursor, a Grignard reagent—most typically *i*-BuMgX—is readily obtained and handled with ease. ii) Although terminal acetylenes are not an acceptable substrate as in the above case and as evidenced by the following reaction in eq. (3.41) [8], a wide variety of internal acetylenes undergo this reaction in good to excellent yields. iii) The very high regio- and stereoselectivity was often observed for unsymmetrical acetylenes.

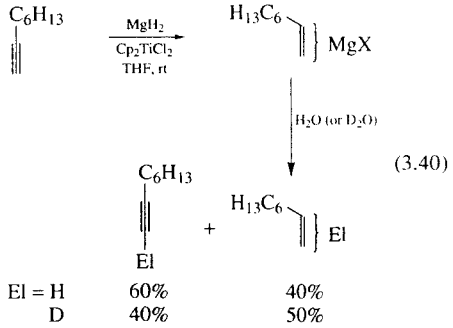

(3.40)

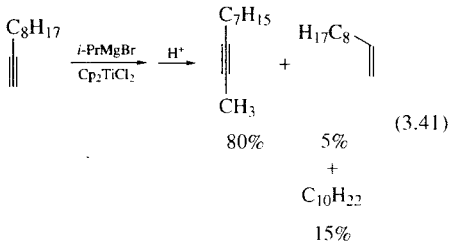

(3.41)

Dialkylacetylenes afford (1,2-*cis*-disubstituted vinyl) Grignard reagents in excellent stereoselectivity (100–95%). A symmetrical acetylene affords virtually a single vinyl Grignard reagent, which was used for the preparation of a dienol (eq. 3.42) [52]. As expected, the hydromagnesiation of unsymmetrical dialkylacetylenes gave two regioisomers in almost equal amounts, but it still finds use as a convenient method for *cis*-hydrogenation of acetylenes via protonation as exemplified in eq. (3.43) [53]. This last example also demonstrates the chemoselectivity—note that the di-substituted olefin survives the reaction conditions. More examples can be seen in Table 3.5.

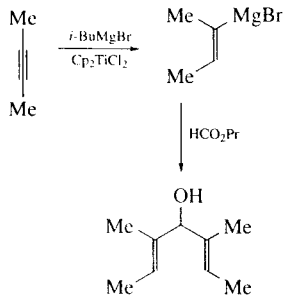

(3.42)

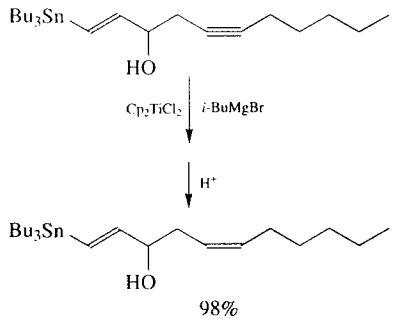

(3.43)

Aromatic acetylenes participated in the reaction without any complication to show as high stereoselectivity as do dialkylacetylenes. Phenyl(methyl)acetylene shows a regioselectivity of synthetically acceptable level (ca 9:1) [10] which is further enhanced to an excellent degree (96:4) by the substitution of a silyl group (eq. 3.44) [10,54]. However, diphenylacetylene no longer afforded the expected *cis*-product cleanly as shown in eq. (3.45) [8].

1-Silyl-1-alkynes show as high regioselectivity (>95:5) as the stereoselectivity (>96:4) exemplified in eq. (3.46) [57]. Table 3.6 surveys the reactions of these substrates. Apparently, the silyl group plays an important role in determining

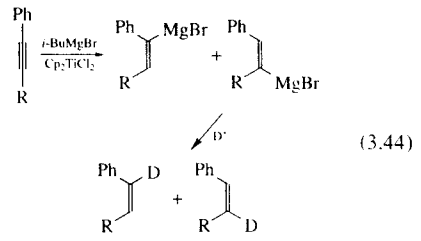

(3.44)

R = Me >99%Z 88:12 85%
Me_3Si >94%Z 96: 4 95%

the regioselectivity as in many other hydrometallation reactions which show the same tendency for this particular substrate [58]. In conjunction with the synthetic utility of the alkenylsilane moiety for further transformations [58], the resultant silylalkenyl Grignard reagents have been utilized in a variety of transformations such as hydrolysis, stannylation, alkylation, and carbonyl addition. Methylation with MeI and allylation with allyl halide proceed as such from the magnesium intermediate, but the alkylation with higher primary-alkyl

Table 3.5. Hydromagnesiation of dialkylacetylenes and aromatic acetylenes with Grignard reagents

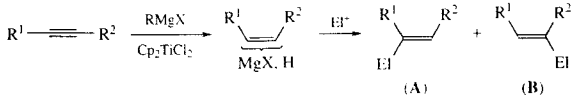

Entry	R^1	R^2	RMgX	El^+	El	Yield(%)	Ref.
1	Me	Me	*i*-BuMgBr	HCO_2Pr	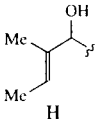	**A** (65) [strictly *E,E*]	52
2	Me	Pr	*i*-BuMgBr	H_2O	H	**A**(92-100) [100% *Z*]	10
3	Me	Pr	*i*-BuMgBr	I_2	I	**A**+ **B**[42:58] (90)	10
4	Et	Et	*i*-BuMgBr	H_2O	H	**A** (92-100) [>99%Z]	10,55
5	Et	Et	*i*-BuMgBr	PhCHO	PhCH(OH)-	**A** (90)	10
6	C_3H_7	C_3H_7	various R_2Mg and RMgX	H^+	H	**A** (—) [95-99%Z]	55
7	C_6H_{13}	$(CH_2)_8OH$	*i*-Bu_2Mg or Pr_2Mg	H^+	H	**A** (100) [>98%]	55
8	C_5H_{11}	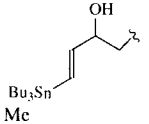	*i*-BuMgBr	H^+	H	**A** (98)	53
9	Ph	Me	*i*-BuMgBr	H_2O	H	**A** (92-100) [>99%Z]	10,56
10	Ph	Me	*i*-BuMgBr	D_2O	D	**A**+**B** (85) [88:12]	10 10
11	Ph	Me	*i*-BuMgBr	MeI	Me	**A**+**B**(80) [90:10]	10
12	Ph	Me_3Si	*i*-BuMgBr	H_2O	H	**A** (95) [>94%Z]	10
13	Ph	Me_3Si	*i*-BuMgBr	D_2O	D	**A**+**B** (—) [96:4]	10
14	Ph	Me_3Si	*i*-PrMgCl	$PhCH_2CHO$	$PhCH_2CH(OH)$	**A** (77) [>95%*E*]	54

iodides needs the assistance of a copper catalyst as illustrated in eq. (3.47) [59].

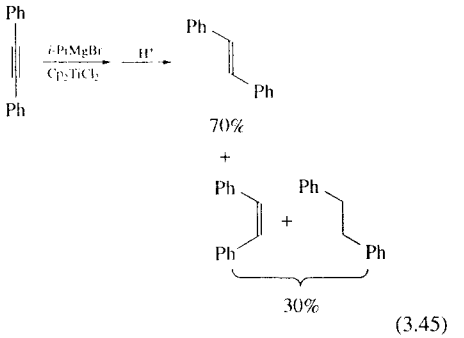

(3.45)

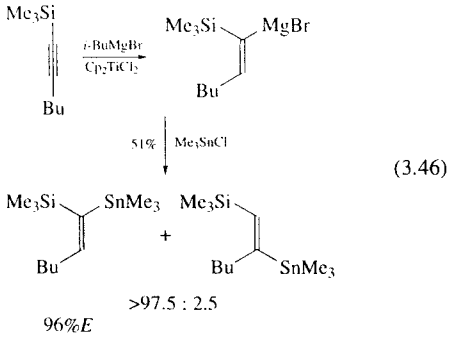

(3.46)

Gratifyingly, propargyl alcohols represent an exceptional type of dialkylacetylene that shows a very high level of both regio- and stereoselectivity. One example is shown in eq. (3.48) [71] and more will be found in Table 3.7. The alcohol moiety was converted to the corresponding magnesium alkoxide *in situ* so that an extra equivalent of Grignard reagent is necessary in addition to that for the hydromagnesiation step. The regio- and stereoselectivities did not decrease even in the case of hydromagnesiation of polyoxygenated substrates (eq. 3.49) [72]. The acetylenic bond in a conjugated enynol behaves like an isolated propargyl alcohol in the hydromagnesiation and subsequent carboxylation to give the expected product as shown in eq. (3.50) [73].

Remarkably, silylpropargyl alcohols demonstrate the first example to violate the rule of formal *cis*-addition of a magnesium hydride species across the carbon-carbon multiple bond in the series of hydromagnesiation reactions. Thus, it should be noted that the products shown in Table 3.8 always have the *trans* configuration with respect to the vinylic hydrogen and electrophile (El), which has not been seen in preceding Tables 3.5–3.7. The origin of this strange behaviour of the substrate was disclosed by analysis of the isomeric composition of the produced allyl alcohols versus the reaction period [76]. The composition determined by the periodical hydrolysis of an aliquot of the reaction mixture is shown in eq. (3.51). Thus, consistent with the rule of *cis* addition, the

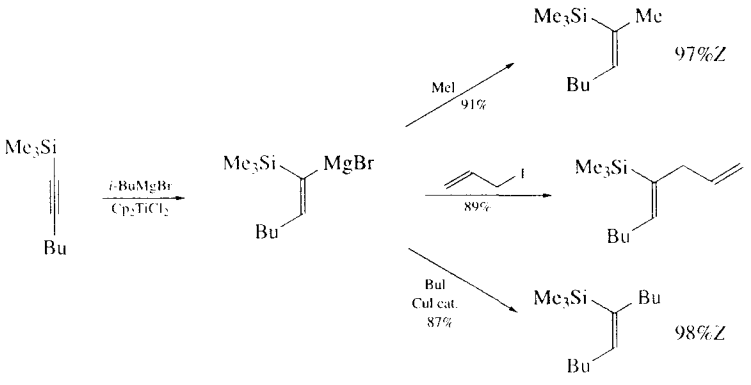

(3.47)

Table 3.6. Hydromagnesiation of (trimethylsilyl)alkynes with Grignard reagents

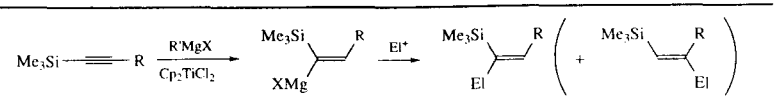

Entry	R	R'MgX	El⁺	El	Yield(%)	Ref.
1	Me	*i*-BuMgBr	 + Me_3SiI	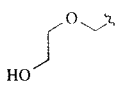	**A** (—)	60
2	Me	*i*-BuMgBr	 + Me_3SiI	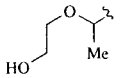	**A**(—)	60
3	Me	*i*-BuMgBr	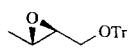 + CuI, Me_2S	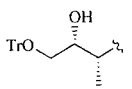	**A** (>53)	36
4	Et	*i*-BuMgBr	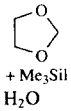 + Me_3SiI	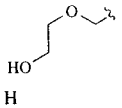	**A** (—)	60
5	Bu	*i*-BuMgBr	H_2O	H	**A** (76) [> 98%*Z*]	10,61
6	Bu	*i*-BuMgBr	D_2O	D	**A**+**B** (—) [95:5]	10
7	Bu	*i*-BuMgBr	Me_3SnCl	Me_3Sn	**A**+**B** (51) [97.5:2.5] [**A**: 96%*E*]	57
8	Bu	*i*-BuMgBr	MeI	Me	**A** (91) [97%*Z*]	59,62
9	Bu	*i*-BuMgBr	allyl-I	allyl	**A** (89)	59
10	Bu	*i*-BuMgBr	BuI/CuI	Bu	**A** (87) [98%*Z*]	59
11	Bu	*i*-BuMgBr	HCHO	$CH_2(OH)$-	**A** (78-87)	63,64
12	Bu	*i*-BuMgBr	MeCHO	MeCH(OH)-	**A** (97)	65
13	Bu	*i*-BuMgBr	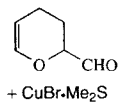 + CuBr·Me_2S	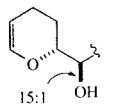 15:1	**A** (66)	66
14	Bu	*i*-BuMgBr	MeCHBrCHO	-CHMeCHO	**A** (*ca.* 50)	47
15	C_5H_{11}	*i*-BuMgBr	HCHO	$Ch_2(OH)$-	**A** (81)	64
16	C_5H_{11}	*i*-BuMgBr	$C_5H_{11}CHO$	$C_5H_{11}CH(OH)$-	**A** (—)	67,68
17	C_5H_{11}	*i*-BuMgBr	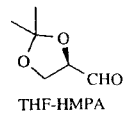 THF-HMPA	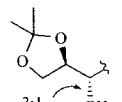 3:1	**A** (>85)	69

Table 3.6. (*continued*)

Entry	R	R'MgX	El⁺	El	Yield(%)	Ref.
18	C_5H_{11}	*i*-BuMgBr	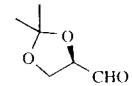 + CuI	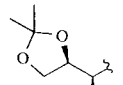 >98:2	**A** (>85)	69
19	C_5H_{11}	*i*-BuMgBr	3-butenyl-I/ CuI	3-butenyl	/**A** (86)	59
20	C_6H_{13}	—	H^+	H	**A** (—)	61
21	$C_{10}H_{21}$	*i*-BuMgBr	HCHO	$CH_2(OH)$–	**A** (78)	63,70
22	$-(CH_2)_6OH$	*i*-BuMgBr	BuI/CuI	Bu	**A** (84)	59

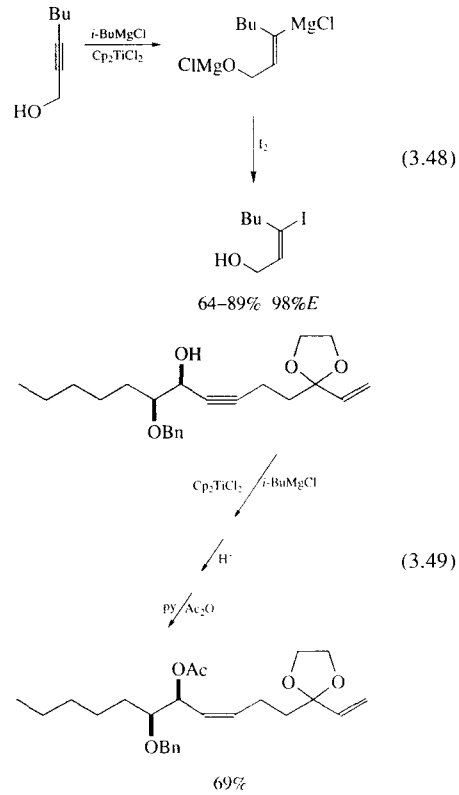

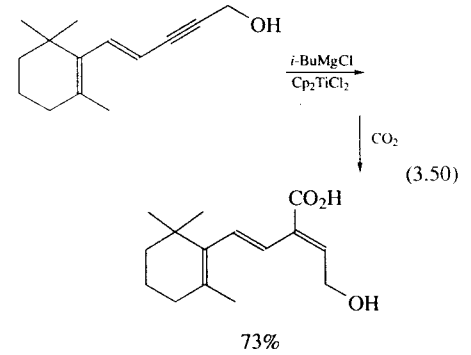

hydromagnesiation of 3-(trimethylsilyl)-2-propyn-1-ol *intrinsically* proceeds in a *cis* fashion, as evidenced by the fact that, in the early stage of the reaction, *cis*-rich allyl alcohol was recovered upon hydrolysis. However, the resulting (*cis*-disubstituted vinyl) Grignard reagent rapidly isomerized to the (more stable) (*trans*-disubstituted vinyl) Grignard reagent during the interval that is required for the completion of the hydromagnesiation step, eventually resulting in the formation of almost 100% pure *trans*-allyl alcohol upon aqueous workup. The driving force of this isomerization apparently comes from its release of the steric strain in the magnesium salt of *cis*-allyl alcohol and, in turn, the formation of thermodynamically favourable, chelation structure

Table 3.7. Hydromagnesiation of propargyl alcohols with Grignard reagents

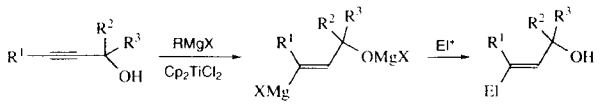

Entry	R^1	R^2R^3COH	RMgX	El^+	El	Yield(%)	Ref.
1	Me	CH_2OH	*i*-BuMgCl	D_2O	D	60–100	71
2	Bu	CH_2OH	*i*-BuMgCl	D_2O	D		71
3	Ph	CH_2OH	*i*-BuMgCl	D_2O	D		71,74
4	Me	CH(Et)OH	*i*-BuMgCl	D_2O	D		71
5	Me	CMe_2OH	*i*-BuMgCl	D_2O	D		71
6	C_5H_{11}		*i*-BuMgCl	H^+	H	46	75
7	*t*-Bu	CH_2OH	*i*-BuMgCl	H^+	H	60 [>93%Z]	76
8	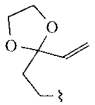	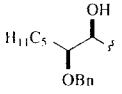	*i*-BuMgCl	H^+	H	>70	72
9	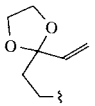	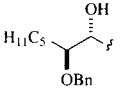	*i*-BuMgCl	H^+	H	>70	72
10	*i*-Bu	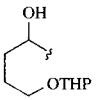	*i*-BuMgBr	H^+	H	—	77
11		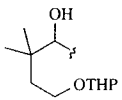	*i*-BuMgBr	H^+	H	68 [>99%Z]	77
12	Bu or Ph	$CH(CF_3)OH$	*i*-BuMgCl	H^+	H	—	78
13	Bu	CH_2OH	*i*-BuMgCl	I_2	I	64-86 [>98%E]	71,79
14	Bu or Ph	$CH(CF_3)OH$	*i*-BuMgCl	I_2	I	—	78
15	Bu	CH_2OH	*i*-BuMgCl	Me_3SiCl +HMPA	Me_3Si	—	80
16	C_6H_{13}	CH_2OH	*i*-BuMgCl	Me_3SiCl +HMPA	Me_3Si	—	80
17	Me	CH_2OH	*i*-BuMgCl	Bu_3SnCl	Bu_3Sn	50	81-83
18	Pr	$CMe(Pr)OH$	*i*-BuMgCl	Bu_3SnCl	Bu_3Sn	79	81,84
19	*i*-Pr	*c*-$C_6H_{11}CHOH$	*i*-BuMgCl	Bu_3SnCl	Bu_3Sn	69	82,83
20	Bu	MeCHOH	*i*-BuMgCl	Bu_3SnCl	Bu_3Sn	32	82,83,85
21	Bu	*c*-$C_6H_{11}CHOH$	*i*-BuMgCl	Bu_3SnCl	Bu_3Sn	75	81-85
22	*t*-Bu	*c*-$C_6H_{11}CHOH$	*i*-BuMgCl	Bu_3SnCl	Bu_3Sn	40	82,83

Table 3.7. (*continued*)

Entry	R^1	R^2R^3COH	RMgX	El^+	El	Yield(%)	Ref.
23	Ph	*c*-$C_6H_{11}CHOH$	*i*-BuMgCl	Bu_3SnCl	Bu_3Sn	72	81,84
24	Bu	CH_2OH	*i*-BuMgCl	MeI	Me	88-92	71
25	Bu or Ph	$CH(CF_3)OH$	*i*-BuMgCl	MeI	Me	—	78
26	Ph	CH_2OH	*i*-BuMgCl	MeI	Me	—	86
27	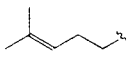	CH_2OH	*i*-BuMgCl	MeI	Me	95	71
28	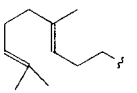	CH_2OH	*i*-BuMgCl	MeI	Me	98	71
29	C_5H_{11}	CH_2OH	*i*-BuMgCl	$C_5H_{11}CHO$	$C_5H_{11}CH(OH)$-	59-62	87
30	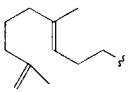	CH_2OH	*i*-BuMgCl	CO_2	CO_2H	65	88
31	"	CH_2OH	*i*-BuMgCl	HCHO	CH_2OH	—	88
32	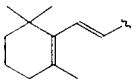	CH_2OH	*i*-BuMgCl	CO_2	CO_2H	73	73
33	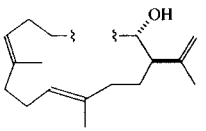		*i*-BuMgBr	CO_2	CO_2H	>61	89

in that of the *trans*-allyl alcohol. To ensure the reproducibility of the high *trans*-selectivity (as well as a complete conversion), the reaction period of the hydromagnesiation should be sufficiently long, preferably with analysis of the progress of reaction by an appropriate analytical method such as TLC, GC, or NMR spectroscopy.

In addition to the high stereoselectivity (>95%) discussed above, the regioselectivity is again exclusively defined as shown in Table 3.8. The resultant Grignard reagents were successfully trapped with a variety of electrophiles. There has been no definite information on the exact structure of the intermediate bis-magnesiated compounds. However, a possible metallacycle structure has been invoked in a metallo-ene reaction to account for the highly stereoselective construction of consecutive stereogenic centres (eq. 3.52) [90]. Optically active propargyl alcohols afforded chiral magnesium intermediates, which, upon reaction with an electrophile, afforded optically active products without loss of the initial enantiopurity [84,91,92]. For example, a preparation of optically active furfuryl alcohol (96% ee) was achieved from an acetylenic diol (97% ee) via the hydromagnesiation method as shown in eq. (3.53) [91].

Other silylpropargyl alcohols such as (phenyldimethylsilyl)propargyl alcohols could be used equally well in this hydromagnesiation reaction, even though steric hindrance of the silyl group is more enhanced than that of the trimethylsilyl group as shown in eq. (3.54) [84]. The recent development in organic synthesis with tin reagents [99] would call for more opportunity of hydromagnesiation of (trialkylstannyl)acetylenes in future as a tool for the preparation of stereo- defined

Table 3.8. Hydromagnesiation of (trimethylsilyl)propargyl alcohols with Grignard reagents

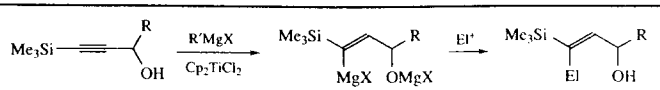

Entry	R	R'MgX	El^+	El	Yield(%)	Ref.
1	H	*i*-BuMgCl	H_2O	H	100	76
2	Me	*i*-BuMgCl	H^+	H	—	93
3	Pr	*i*-BuMgCl	H^+	H	—	93
4	*i*-Pr	*i*-BuMgBr	H^+	H	90	65
5	*t*-Bu	*i*-BuMgBr	H^+	H	85	65
6	C_5H_{11}	*i*-BuMgBr	H^+	H	96	90,94
7	*c*-C_6H_{11}	*i*-BuMgCl	H^+	H	—	93
8	H	*i*-BuMgBr	$PhSSO_2Ph$	Phs	58	95
9	H	*i*-BuMgCl	Bu_3SnCl	Bu_3Sn	—	83
10	Me	*i*-BuMgCl	Bu_3SnCl	Bu_3Sn	73	83,85
11	Pr	*i*-BuMgCl	Bu_3SnCl	Bu_3Sn	58	83,85
12	*i*-Pr	*i*-BuMgCl	Bu_3SnCl	Bu_3Sn	72	81,83,84
13	*c*-C_6H_{11}	*i*-BuMgCl	Bu_3SnCl	Bu_3Sn	67	81,83-85
14	$MeOCH_2$	*i*-BuMgCl	Bu_3SnCl	Bu_3Sn	79	83
15	H	*i*-BuMgCl	MeI	Me	88	76
16	H	*i*-BuMgCl	BuI/CuI	Bu	89 [*E* > 95%]	76
17	H	*i*-BuMgBr	$C_8H_{17}CHO$	$C_8H_{17}CH(OH)$-	84	96
18	H	*i*-BuMgBr	$C_6H_{13}COMe$	$C_6H_{13}CMe(OH)$-	83	96
19	H	*i*-BuMgBr	Pr_2CO	$Pr_2C(OH)$-	80	96
20	H	*i*-BuMgBr	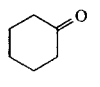		88	96
21	H	*i*-BuMgBr	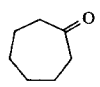		85	96
22	H	*i*-BuMgBr	MeCN	(EtC(=NH)-[a])	28	97
23	H	*i*-BuMgBr	EtCN	(EtC(=NH)-[a])	82	98
24	H	*i*-BuMgBr	*i*-PrCN	(*i*-PrCN(=NH)-[a])	85	98
25	H	*i*-BuMgBr	PhCN	(PhC(=NH)-[a])	88	98
26	Pr	*i*-BuMgBr	MeCN	(MeC(=NH)-[a])	38	98
27	Pr	*i*-BuMgBr	EtCN	(EtC(=NH)-[a])	86	98
28	$C_6H_{13}CH(OH)$-	*i*-BuMgBr	EtCN	(EtC(=NH)-[a])	67	91
29	$C_6H_{13}CH(OH)$-	*i*-BuMgBr	PhCN	(PhC(=NH)-[a])	73	91
30	$C_6H_{13}CH(OTBS)$-	*i*-BuMgBr	PhCN	(PhC(=NH)-[a])	70	91
31	Me	*i*-BuMgBr	CO_2	(CO_2H[b])	74	92
32	C_5H_{11}	*i*-BuMgBr	CO_2	(CO_2H[b])	92	92
33	*C*-C_6H_{11}-	*i*-BuMgBr	CO_2	(CO_2H[b])	86	92
34	$PhCH_2OCH_2$-	*i*-BuMgBr	CO_2	(CO_2H[b])	84	92
35	$C_6H_{13}CH(OH)$-	*i*-BuMgBr	CO_2	(CO_2H[b])	85	91

[a] The products isolated were the corresponding furans. For example, see eq. 3.53 in text.
[b] The products isolated were the corresponding lactones.

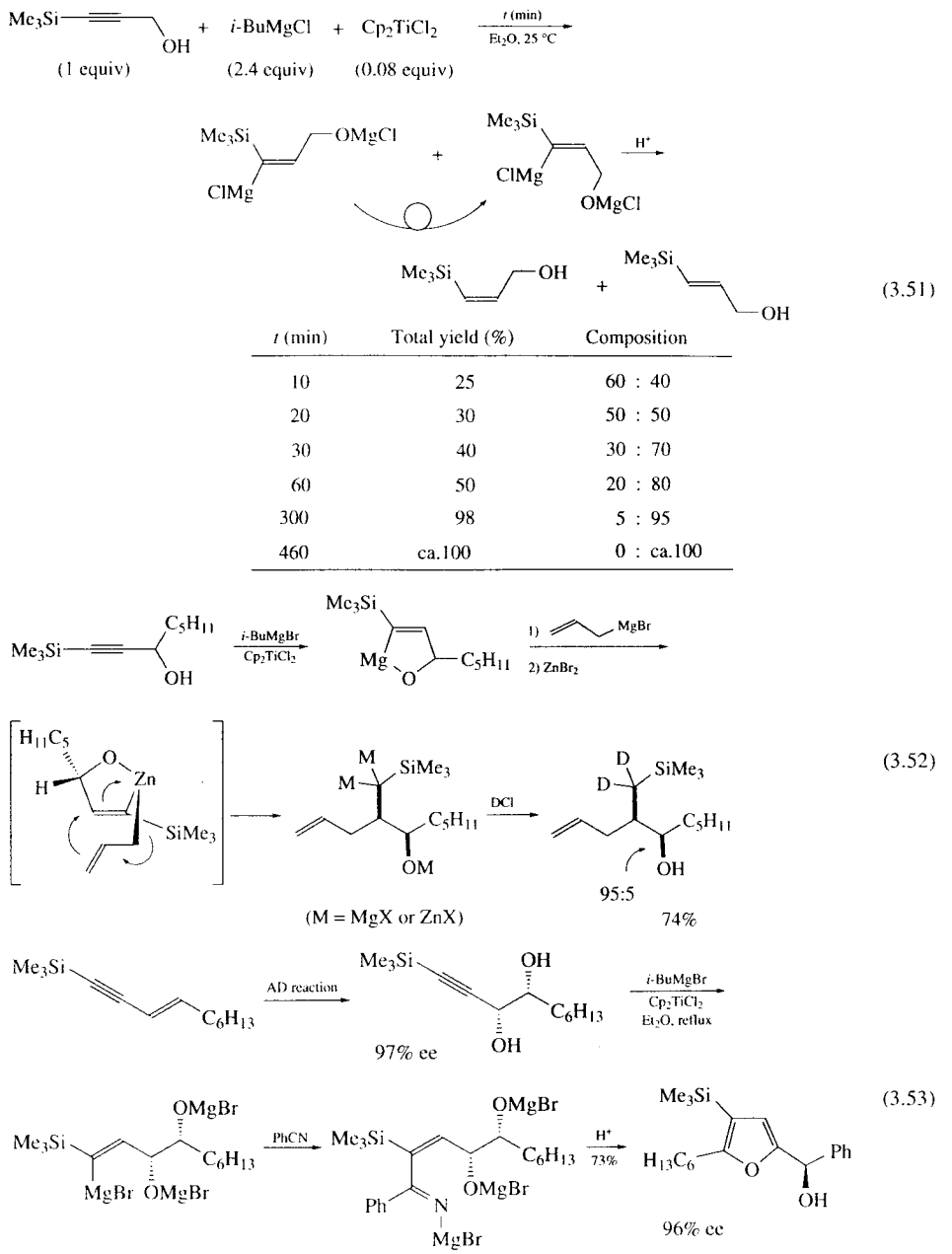

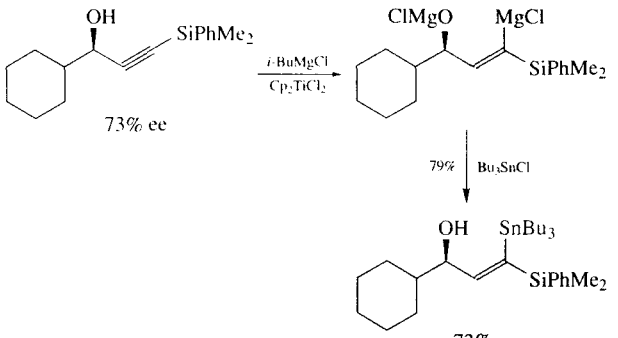

(3.54)

vinylstannanes. In fact, a few recent publications dealing with the hydromagnesiation of substrates of this kind appeared and have disclosed that the reaction proceeds without difficulty, maintaining virtually the same regio- and stereoselectivities as found in the silyl counterparts as shown in eq. (3.55) [82,83]. Table 3.9 shows additional examples related to eqs (3.54) and (3.55).

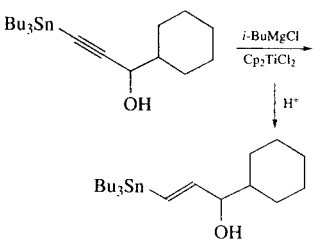

(3.55)

In summary, most types of internal acetylenes experience the *cis* addition of 'H-MgX' to their triple bond to give (*cis*-1,2-disubstituted vinyl) Grignard reagents, while silyl and stannyl propargyl alcohols quite exceptionally give rise to the *trans* addition of the same element across the acetylene bond to furnish (*trans*-1,2-disubstituted vinyl) Grignard reagents. Figure 3.3 illustrates this summary.

Other transition metal-mediated hydromagnesiations involve a nickel-catalyzed reaction [9,100]. However, except for the reaction of eq. (3.56) [9], further synthetic application of this nickel-catalyzed Grignard exchange reaction has not been examined in more detail.

In conclusion, of the aforementioned transition metal-catalyzed hydromagnesiations, the most

Table 3.9. Hydromagnesiation of silyl(other than trimethylsily) and stannylpropargyl alcohols with a Grignard reagent

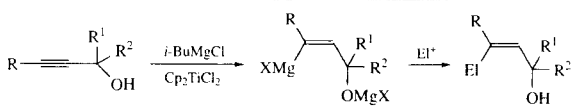

Entry	R	R^1R^2COH	El^+	El	Yield(%)	Ref.
1	Me_2PhSi	*c*-$C_6H_{11}CHOH$	H^+	H	88	83
2	Me_2PhSi	MeCHOH	Bu_3SnCl	Bu_3Sn	51	83,84
3	Me_2PhSi	*c*-$C_6H_{11}CHOH$	Bu_3SnCl	Bu_3Sn	73-79	81,84
4	Me_2PhSi	MeCHOH	MeI	Me	61	83
5	Bu_3Sn	*c*-$C_6H_{11}CHOH$	H^+	H	63	82,83
6	Bu_3Sn	MeCHOH	Bu_3SnCl	Bu_3Sn	53	83
7	Bu_3Sn	*c*-$C_6H_{11}CHOH$	Bu_3SnCl	Bu_3Sn	75	81,84

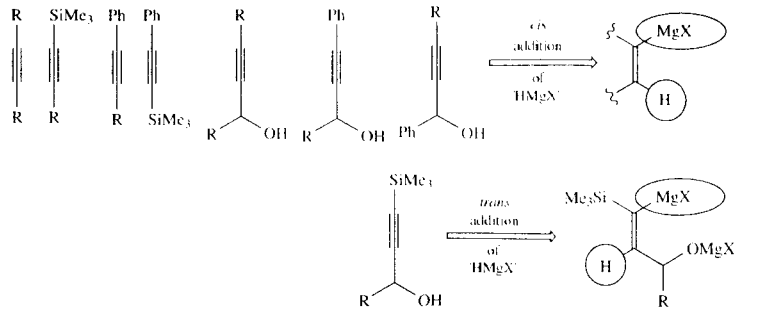

Fig. 3.3.

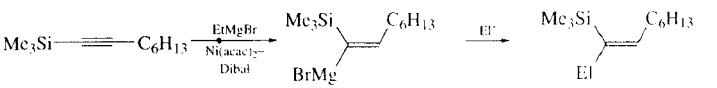

El^+	El	Yield (%)	*Z*/*E*
H_2O	H	50	95:5
D_2O	D	65	95:5
MeCHO	MeCH(OH)-	58	95:5

(3.56)

standard methodology which has the broadest applications in routine organic synthesis is perhaps a titanium-catalyzed hydromagnesiation of olefins and acetylenes with low-molecular Grignard reagents. Some synthetic applications of this method will be illustrated in the next section.

3.5 APPLICATION OF HYDROMAGNESIATION IN SELECTIVE SYNTHESIS OF NATURAL PRODUCTS

The most useful feature of hydromagnesiation is highlighted in the stereoselective construction of di- or tri-substituted olefins starting with acetylenic substrates and an appropriate electrophile. The generation of a (*cis*-1,2-disubstituted vinyl) Grignard reagent and its diastereoselective addition to an aldehyde were ingeniously accommodated to a concise synthesis of boronolide, a medicinally active principle of a certain plant (Scheme 3.8) [66]. Hydromagnesiation of 1-(trimethylsilyl)-1-hexyne was carried out as usual to give the stereodefined Grignard reagent, which was subsequently converted to a copper reagent with $CuBr{\cdot}Me_2S$. Addition of this vinyl-copper reagent to acrolein dimer resulted in the stereoselective formation of *syn*-adduct in a 15:1 ratio. Selective removal of the silyl group yielded the *trans*-allyl alcohol. The *trans* configuration of the double bond was crucial at the final stage to prepare the array of desired polyol centers *via* *cis*-hydroxylation with OsO_4, which completed a synthesis of boronolide.

Hydromagnesiation followed by carbon-chain extension also serves as a stereoselective preparation of the trisubstituted double bonds frequently found in terpenes. The reaction often works in a complementary manner to the existing methods, which is illustrated in the preparation of (*E*,*Z*)- and (*E*,*E*)-farnesols (Scheme 3.9) [71,101]. When the propargyl alcohol was treated with *i*-BuMgCl

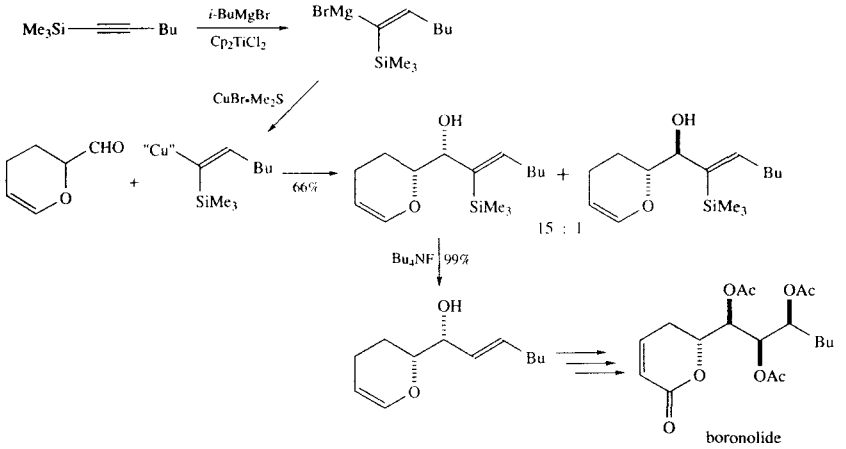

SCHEME 3.8. Synthesis of boronolide.

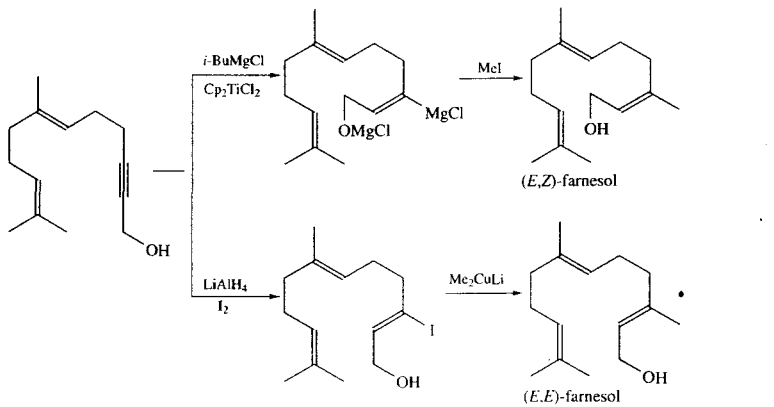

SCHEME 3.9. Synthesis of farnesol.

and Cp_2TiCl_2 in a standard manner, the (*cis*-1,2-disubstituted vinyl) Grignard reagent was formed with high regio- and stereoselectivities. Its methylation directly afforded (*E*,*Z*)-farnesol. In contrast, the same propargyl alcohol was subjected to hydroalumination with $LiAlH_4$ followed by iodinolysis, giving the *Z*-iodo allyl alcohol, which was subsequently methylated with dimethylcopper lithium to form isomeric (*E*,*E*)-farnesol.

In order to introduce substituents to a macrocyclic framework in a stereoselective fashion, a [2,3] Wittig rearrangement of the corresponding macrocyclic allyl propargyl ether is an attractive strategy. Butyllithium in hexane-THF promoted

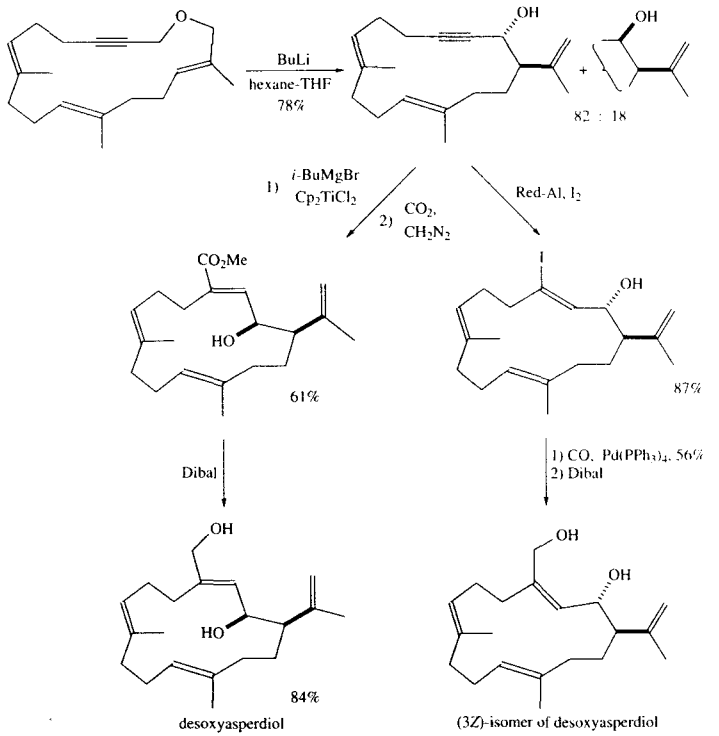

SCHEME 3.10. Synthesis of desoxyasperdiol.

the stereoselective ring contraction of the 17-membered ether in Scheme 3.10 [89] to afford the 14-membered cyclic propargyl alcohol that has the correct relative stereochemistry with respect to isopropenyl and hydroxy groups as well as the configurations of the two tri-substituted olefinic bonds found in desoxyasperdiol, a member of the cembrane diterpenes. Thus, the remaining task is a transformation of the propargyl alcohol moiety in the rearranged product into the E-bis-allyl alcohol moiety in the diterpene. Hydromagnesiation of the acetylenic part followed by trapping with a one-carbon electrophile should be ideal for this purpose and, in fact, worked successfully to complete the final step in the total synthesis of desoxyasperdiol. Herein, the hydroalumination/iodinolysis sequence as shown in Scheme 3.9 again provided a complementary path to prepare the 3*Z*-olefinic isomer of desoxyasperdiol.

In the synthesis of zoapatanol, hydromagnesiation was taken as a viable path to obtain the key intermediate (Scheme 3.11) [88]. Thus, the propargyl alcohol was hydromagnesiated in a standard way and the resulting alkenylmagesium intermediate was quenched with CO_2 to give the stereo-defined carboxylic acid in 65%

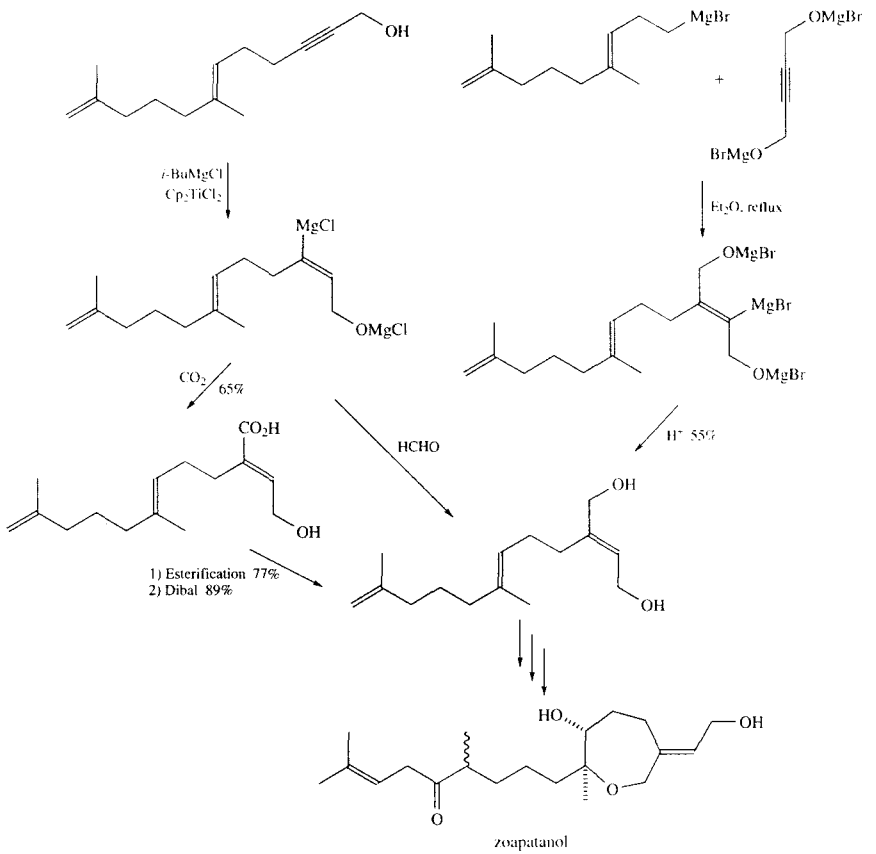

SCHEME 3.11. Synthesis of zoapatanol.

yield. Methyl esterification, efficiently performed with MeI and tetramethylguanidine, and then Dibal reduction, afforded the desired diol in 44% overall yield from the starting propargyl alcohol. In place of the carboxylation, direct coupling with formaldehyde gave the diol in a slightly better yield. A third method taking advantage of *carbo*magnesiation to 1,4-butynediol, requires and, in fact, proceeds in a *trans* mode of addition, to provide the desired diol in one step and in 55% yield.

In addition to the above manipulation of acetylenes, olefins are useful precursors for the generation of terminal Grignard reagents as shown in eq. (3.57). The hydromagnesiation of a terminal olefin followed by carboxylation enabled an asymmetric synthesis of serricornin, a sex pheromone of the cigarette beetle (*Lasioderma serricone* F), from a readily available, optically active olefinic starting material [36].

Other adaptations of the hydromagnesiation reaction in the preparation of key compounds directed

towards synthesis of natural products can be found in the literature [29,33,34,37,53,59,72,73,77,86].

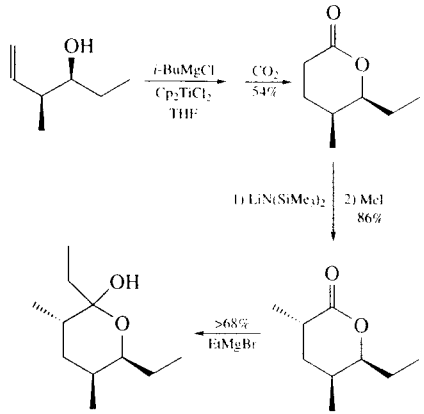

(3.57)

3.6 ON THE MECHANISM OF Cp_2TiCl_2-CATALYZED HYDROMAGNESIATION OF ALKYNES WITH GRIGNARD REAGENTS

The accepted mechanism of the aforementioned hydromagnesiation of acetylenes in the presence of Cp_2TiCl_2 can be drawn as in Scheme 3.12, which resembles that for hydromagnesiation of olefins in the presence of $TiCl_4$ (see Scheme 3.5 where the catalytically active species is Cl_3TiH [5]).

Some discrete observations relevant to the mechanistic hypothesis have been reported. It has been shown that an equilibrium is attained between a starting acetylene and the alkenyl Grignard reagent produced by the hydromagnesiation, provided that the acetylene is a silylated one (eq. 3.58) [102]. Thus, the addition of a different acetylene to the silylalkenyl Grignard reagent, preformed from the

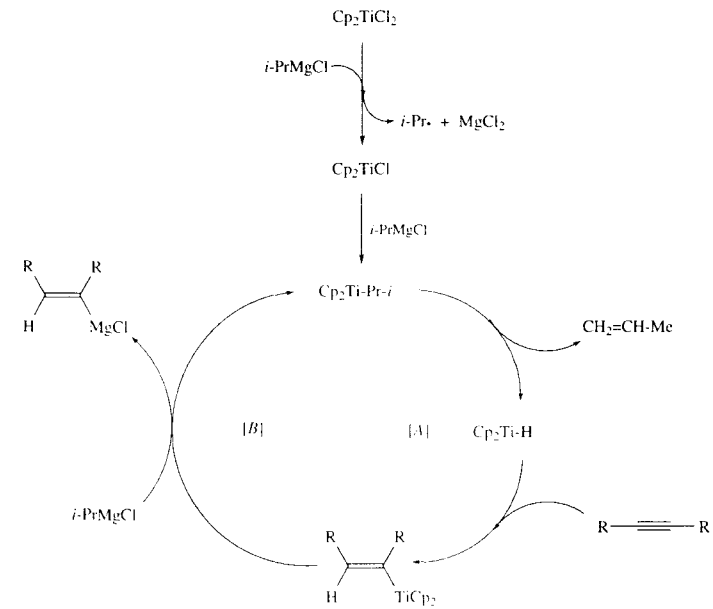

SCHEME 3.12. Proposed mechanism of hydromagnesiation of alkynes with Grignard reagents catalyzed by Cp_2TiCl_2.

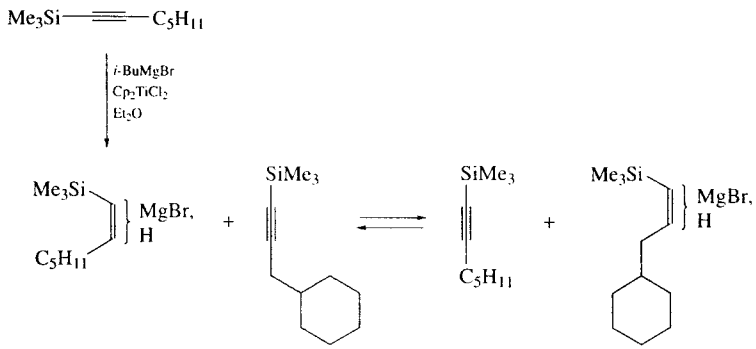

(3.58)

Period (h)	Composition							
0	ca.100	:	100	:	ca. 0	:	0
7.5	82	:	87	:	18	:	13
94.5	48	:	75	:	52	:	25

corresponding silylacetylene and *i*-BuMgBr under Cp_2TiCl_2 catalysis, formed a new alkenyl Grignard reagent and the initial acetylene in the course of a prolonged reaction period.

A separate study showed that the particular electrophile that was used affected the regioselectivity found in the product, possibly due to equilibration between the two regioisomers of the alkenyl Grignard reagent via their parent acetylene during the reaction (eq. 3.59) [102]. However, the relatively low regioselectivity of deuteration (77:23) in this reaction is somewhat puzzling.

A recent study by Gao and Sato showed evidences for the half-cycles [*A*] and [*B*] in Scheme 3.12 to reinforce the probability of the proposed reaction mechanism in Scheme [11]. Generation of Cp_2Ti-H by the reaction of Cp_2TiCl_2 and 2 equiv of *i*-PrMgCl has been established [12]. Hydrotitanation of 6-dodecyne by this titanium hydride generated *in situ* from Cp_2TiCl_2 and *i*-PrMgCl affords the alkenyltitanium species, the presence of which was confirmed by deuterolysis to give *Z*-6-deuterio-6-dodecene in a quantitative yield (eq. 3.60). That the metal in the alkenyltitanium species was titanium (magnesium was an alternative though unlikely possibility) was checked through a reaction with benzaldehyde, which afforded hydrobenzoin in 42% yield as a sole detectable product (eq. 3.60). Hydrobenzoin is a unique product in the reaction of alkenyl*titanium* compounds with benzaldehyde [103], which is in stark contrast to the reaction of alkenyl*magnesium* reagents that affords the normal adduct, (*E*)-1-phenyl-2-pentyl-2-octen-1-ol (compare reactions in eq. (3.61)). Thus, the path proposed in Scheme 3.12 (the half-cycle [A]) to generate the alkenyltitanium species has been confirmed.

The next stage is the examination of the half-cycle [*B*] involving a titanium/magnesium exchange step (Scheme 3.12). Treatment of the alkenyltitanium species, generated as above, with 1 equiv of *i*-PrMgCl followed by the addition of benzaldehyde afforded the normal allyl alcohol in 78% yield, showing the formation this time of the alkenyl*magnesium* species rather than the *titanium* compound (path a in Scheme 3.13). This means that the titanium/magnesium exchange reaction, in fact, has occurred. Interception of another product, Cp_2TiPr-*i*, which spontaneously collapses to Cp_2Ti-H as described above with 4-octyne,

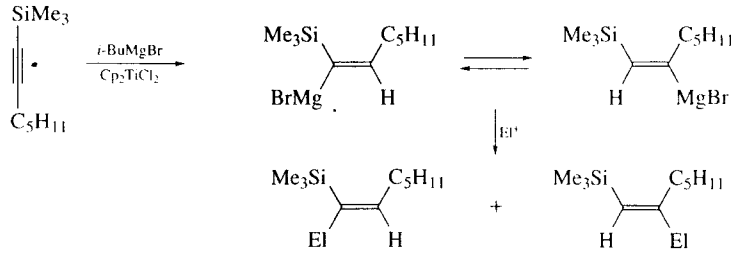

(3.59)

El^+	El	Total yield (%)	Composition
D_2O	D	100	77 : 23
Me_3SiOTf	Me_3Si	80	72 : 28
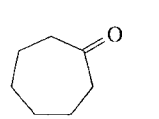	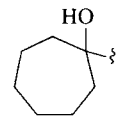	33–44	81–88 : 12-19
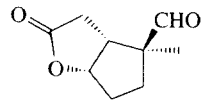	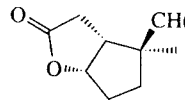	65	94 : 6
CBr_4	Br	82	98 : 2

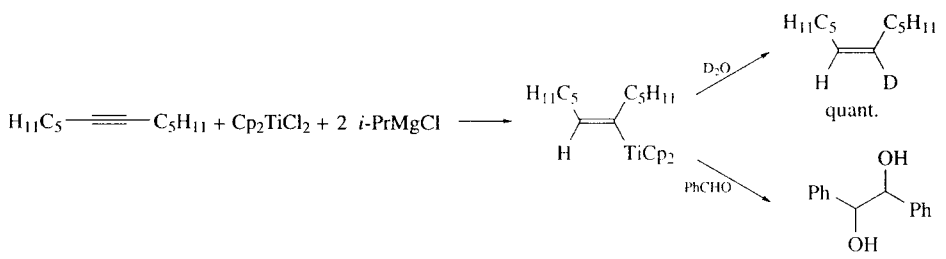

(3.60)

further confirms this process. Thus, when 1 equiv of 4-octyne was added to the reaction mixture, the hydrotitanation of this acetylene proceeded with Cp_2Ti-H generated *in situ*, and, eventually, four alkenylmetal species were formed by successive rapid equilibrations (path b of Scheme 3.13). The alkenylmagnesium species were verified via reaction with benzaldehyde to give the normal addition products in a ratio of 45:55 in 72% combined yield. By affording almost quantitative recovery of deuterated olefins, deuterolysis showed the presence of only alkenylmetal species which therefore include titanium as well as magnesium compounds. These observations are in agreement with the half-cycle [*B*] in Scheme 3.12, and hence the complete cycle proposed in Scheme 3.12 has been confirmed.

Cf.

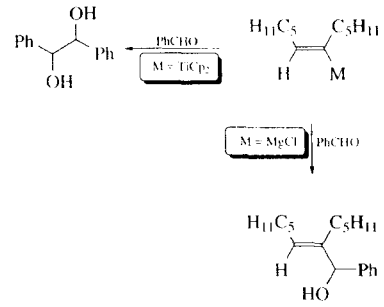

(3.61)

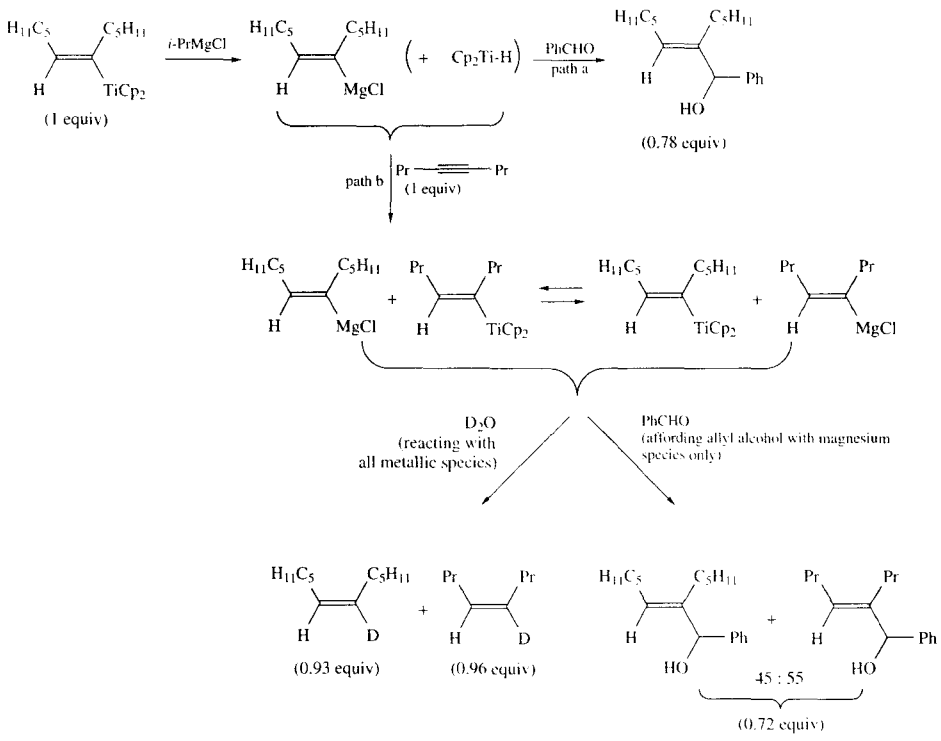

SCHEME 3.13. Confirmation of the half-cycle [*B*].

To clarify how the high regioselectivity is attained in the hydromagnesiation of silylacetylenes, the regioselectivity of the primary hydro*titanation* was examined by deuterolysis [11]. The regioselectivities change with temperature as shown in eq. (3.62). There was actually no change of composition observed at room temperature and at the reflux temperature of ether. Thus under equilibrium conditions, the ratio must have a value around 83:17–85:15.

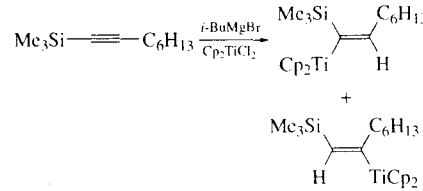

(3.62)

Temp. (°C)	Period (h)	Composition
0	1	60 : 40
rt	1	83 : 17
Et_2O, reflux	2	85 : 15

However, upon addition of *i*-BuMgBr to this 83:17 mixture of regioisomeric alkenyltitanium species followed by quenching with hexanal, the regioselectivity observed in the allyl alcohol was dramatically increased to 95:5 (eq. 3.63). This discrepancy is most likely explained by Scheme 3.14: transmetallation of α-silylalkenyltitanium species is much faster than that of β-silylalkenyltitanium species, leading to formation principally of one alkenylmagnesium reagent, whose reaction with hexanal is responsible for the high regioselectivity.

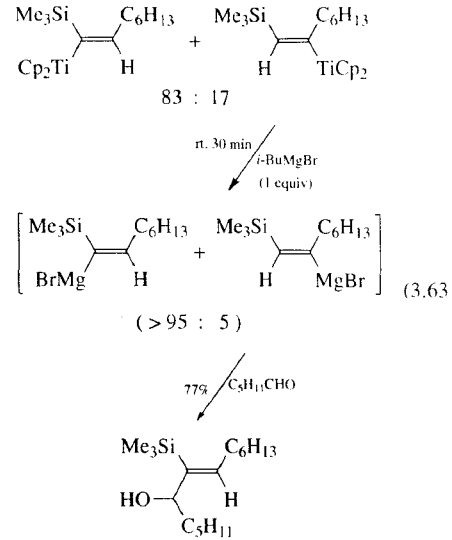

(3.63)

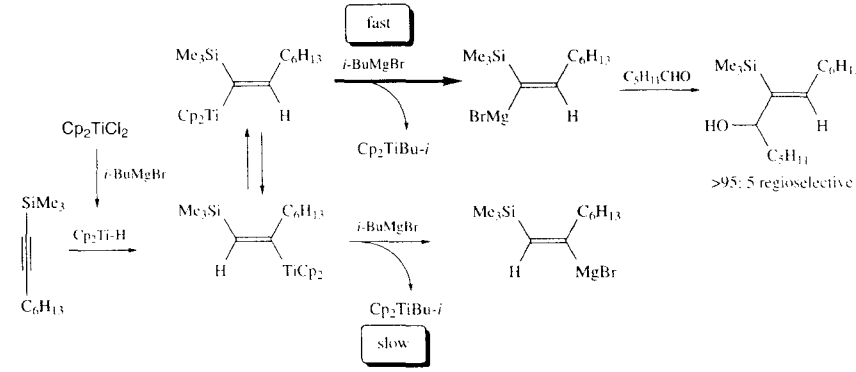

SCHEME 3.14. On the regioselectivity of the hydromagnesiation of 1-(trimethylsilyl)-1-alkyne.

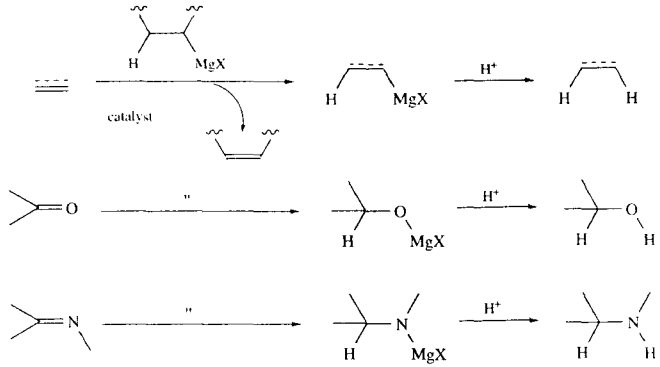

SCHEME 3.15. Hydromagnesiation of various unsaturated bonds.

As can be seen in the above experimental data, the nature of the hydromagnesiation is not necessarily simple and straightforward, because there are many equilibriums between the intermediate species. However, keeping such aspects in mind may be helpful in understanding the nature of the hydromagnesiation reaction, especially with respect to the issue of selectivities.

3.7 CONCLUDING REMARKS

The hydromagnesiation technique to prepare Grignard reagents from olefins and acetylenes not only complements the conventional methods, but also opens up new aspects of chemo-, regio-, and stereoselective formation of Grignard reagents, which is strongly required in modern organic synthesis where selectivity, which is not necessarily attainable by routine methods, is particularly emphasized.

Hydromagnesiation is not limited to carbon–carbon multiple bonds as discussed above, but also occurs with carbon-heteroatom unsaturated bonds as shown in Scheme 3.15. The hydromagnesiation of a carbon-oxygen double bond can be seen in reduction of ketones to secondary alcohols [104], esters to primary alcohols [105], and carboxylic acids to aldehydes [106] with *i*-BuMgBr in the presence of a catalytic amount of Cp_2TiCl_2. The efficient, direct conversion of carboxylic acids to the corresponding aldehydes is noteworthy. Cp_2TiCl_2-catalyzed reduction of imines to amines with BuMgCl represents the hydromagnesiation of carbon–nitrogen double bonds [107].

As far as the role of the transition metal catalysts in the hydromagnesiation is concerned, other hydrometallation reactions such as hydroalumination [108] and the recently reported hydrozincation [109] are catalyzed by the same class of titanium complexes, so all of these reactions can be grouped together. In fact, these reactions show quite similar applicabilities to particular unsaturated compounds and similar regioselectivities with unsymmetrical substrates (eqs. 3.64 and 3.65).

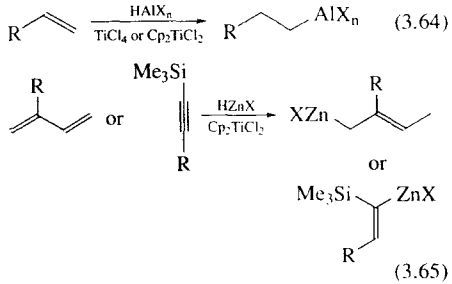

(3.64)

(3.65)

REFERENCES

1. Podal, H.E, Foster, W.E. *J. Org. Chem.* **1958**, *23*, 1848.
2. Ashby, E.C, Smith, T. *J. Chem. Soc., Chem. Commun.* **1978**, 30.
3. Bogdanovic, B, Schwickardi, M, Sikorsky, P. *Angew. Chem. Int. Ed. Engl.* **1982**, *21*, 199.
4. Bogdanovic, B, Bons, P, Konstantinovic, S, Schwickardi, M, Westeppe, U. *Chem. Ber.* **1993**, *126*, 1371.
5. Cooper, G.D, Finkbeiner, H.L. *J. Org. Chem.* **1962**, *27*, 1493.
6. Finkbeiner, H.L, Cooper, G.D. *J. Org. Chem.* **1962**, *27*, 3395.
7. Sato, F, Ishikawa, H, Sato, M. *Tetrahedron Lett.* **1980**, *21*, 365.
8. Colomer, E, Corriu, R. *J. Organomet. Chem.* **1974**, *82*, 367.
9. Snider, B.B, Karras, M, Conn, R.S.E. *J. Am. Chem. Soc.* **1978**, *100*, 4624.
10. Sato, F, Ishikawa, H, Sato, M. *Tetrahedron Lett.* **1981**, *22*, 85.
11. Gao, Y, Sato, F. *J. Chem. Soc., Chem. Commun.* **1995**, 659.
12. Martin, H.A, Jellinek, F. *J. Organomet. Chem.* **1968**, *12*, 149; Martin, H.A, Jellinek, F. *J. Organomet. Chem.* **1967**, *8*, 115.
13. Review: Kharasch, M.S, Reinmuth, O. *Grignard Reactions of Nonmetallic Substances;* Prentice-Hall: New York, **1954**.
14. Review: Felkin, H, Swierczewski, G. *Tetrahedron*, **1975**, *31*, 2735.
15. Review: Kochi, J.K. *Organometallic Mechanisms and Catalysis*, Academic Press: New York, **1978**; Chapter 14.
16. Review: Lindsell, W.E. *in Comprehensive Organometallic Chemistry*; Wilkinson, G, Stone, F.G.A, Abel, E.W, Eds.; Pergamon Press: Oxford, **1982**; Vol. 1, p 155.
17. Review: Sato, F. *J. Organomet. Chem.* **1985**, *285*, 53.
18. Review: Bogdanovic, B. *Angew. Chem. Int. Ed. Engl.* **1985**, *24*, 262.
19. Review: Dzhemilev, U.M, Vostrikova, O.S, Tolstikov, G.A. *J. Organomet. Chem.* **1986**, *304*, 17.
20. Review: Wakefield, B. *Organomagnesium Methods in Organic Synthesis*; Academic Press: London, **1995**; p 54.
21. Review: Sato, F, Urabe, H. *In Handbook of Grignard Reagents*; Silverman, G.S, Rakita, P.E, Eds.; Marcel Dekker: New York, **1996**; p 23.
22. Review: Urabe, H, Sato, F. *In Handbook of Grignard Reagents*; Silverman, G.S, Rakita, P.E, Eds.; Marcel Dekker: New York, **1996**; p 577.
23. Barbaras, G.D, Dillard, C, Finholt, A.E, Wartik, T, Wilzbach, K.E, Schlesinger, H.I. *J. Am. Chem. Soc.* **1951**, 73, 4585.
24. Ashby, E.C, Schwartz, R. *Inorg. Chem.* **1971**, *10*, 355.
25. Knott, W, Klein, K.-D. *Z. Naturforsch.* **1993**, *48b*, 914.
26. Bogdanovic, B, Schwickardi, M, Westeppe, U. *In Organometallic Syntheses*; King, R.B, Eisch, J.J, Eds.; Elsevier: Amsterdam, **1988**; Vol. 4, p 399.
27. Angermund, K, Bogdanovic, B, Koppetsch, G, Krüger, C, Mynott, R, Schwickardi, M, Tsay, Y.-H. *Z. Naturforsch. Teil B* **1986**, *41*, 455.
28. Bogdanovic, B, Koppetsch, G, Schwickardi, M. *In Organometallic Syntheses*; King, R.B, Eisch, J.J., Eds.; Elsevier: Amsterdam, **1988**; Vol. 4, p 404.
29. Wilke, G. *In Organometallics in Organic Syntheses 2*; Werner, H, Erker, G., Eds.; Springer-Verlag: Berlin, **1989**, p 1.
30. Bogdanovic, B, Maruthamuthu, M. *J. Organomet. Chem.* **1984**, *272*, 115.
31. Reetz, M.T, Kindler, A. *J. Chem. Soc., Chem. Commun.* **1994**, 2509.
32. Vostrikova, O.S, Dzhemilev, U.M, Sultanov, R.M. *Izv. Akad. Nauk SSSR, Ser. Khim.* **1983**, 1901.
33. Horeau, A, Ménager, L, Kagan, H. *Bull. Soc. Chim. Fr.* **1971**, 3571.
34. Kobayashi, Y, Sato, F, Miyakoshi, T, Fujita, Y, Shiono, M, Kanehira, K, Suzuki, S. *Synth. Commun.* **1986**, *16*, 597.
35. Eisch, J.J, Galle, J.E. *J. Organomet. Chem.* **1978**, *160*, C8.
36. Kobayashi, Y, Kitano, Y, Takeda, Y, Sato, F. *Tetrahedron* **1986**, *42*, 2937.
37. Xu, Z, Johannes, C.W, Houri, A.F, La, D.S, Cogan, D.A, Hofilene, G.E, Hoveyda, A.H. *J. Am. Chem. Soc.* **1997**, *119*, 10302.
38. Amano, T, Ota, T, Yoshihawa, K, Sano, T, Ohuchi, Y, Sato, F, Shiono, M, Fujita, Y. *Bull. Chem. Soc. Jpn.* **1986**, *59*, 1656.
39. Farády, L, Bencze, L, Markó, L. *J. Organomet. Chem.* **1967**, *10*, 505.
40. Farády, L, Bencze, L, Markó L. *J. Organomet. Chem.* **1969**, *17*, 107.
41. Farády, L, Markó L. *J. Organomet. Chem.* **1971**, *28*, 159.
42. Tamura, M, Kochi, J.K. *J. Organomet. Chem.* **1971**, *31*, 289.
43. Tamura, M, Kochi, J.K. *Bull. Chem. Soc. Jpn.* **1971**, *44*, 3063.
44. Sato, F, Iijima, S, Sato, M. *Tetrahedron Lett.* **1981**, 243; Gao, Y, Iijima, S, Urabe, H, Sato, F. *Inorg. Chim. Acta*, **1994**, *222*, 145; Urabe, H, Yoshikawa, K, Sato, F. *Tetrahedron Lett.* **1995**, *36*, 5595.
45. Review: Yamamoto, Y, Asao, N. *Chem. Rev.* **1993**, *93*, 2207. Roush, W.R. *in Comprehensive Organic*

Synthesis; Trost, B.M, Fleming, I., Eds.; Pergamon Press: Oxford, **1991**; Vol. 2, p 1.
46. Sato, F, Takeda, Y, Uchiyama, H, Kobayashi, Y. *J. Chem. Soc., Chem. Commun.* **1984**, 1132.
47. Sato, F, Kusakabe, M, Kobayashi, Y. *J. Chem. Soc., Chem. Commun.* **1984**, 1130.
48. Felkin, H, Kwart, L.D, Swierczewski, G, Umpleby, J.D, *J. Chem. Soc., Chem. Commun.* **1975**, 242.
49. Viktorov, N.B, Zubritskii, L.M, Petrov, A.A. *Zh. Obshch. Khim.* **1993**, *63*, 1601 [*Chem. Abstr.* **1994**, *120*, 298660w].
50. Viktorov, N.B, Zubritskii, L.M. *Zh. Obshch. Khim.* **1995**, *65*, 311 [*Chem. Abstr.* **1995**, *123*, 313369r].
51. Viktorov, N.B, Zubritskii, L.M. *Zh. Obshch. Khim.* **1996**, *66*, 873 [*Chem. Abstr.* **1996**, *125*, 328826c].
52. Garner, C.M, Prince, M.E. *Tetrahedron Lett.* **1994**, *35*, 2463.
53. Oda, H, Kobayashi, T, Kosugi, M, Migita, T. *Tetrahedron*, **1995**, *51*, 695.
54. Mulzer, J, Melzer, K. *Angew. Chem. Int. Ed. Engl.* **1995**, *34*, 895.
55. Dzhemilev, U.M, Vostrikova, O.S, Sultanov, R.M, Gimaeva, A. *Izv. Akad. Nauk SSSR. Ser. Khim.* **1988**, 2156 [*Chem. Abstr.* **1989**, *110*, 231054b].
56. Hirao, T, Kohno, S, Ohshiro, Y, Agawa, T. *Bull. Chem. Soc. Jpn.* **1983**, *56*, 1569.
57. Rossi, R, Carpita, A, Bellina, F, De Santis, M, Veracini, C.A. *Gazz. Chim. Ital.* **1990**, *120*, 457.
58. Review: Weber, W.P. *Silicon Reagents for Organic Synthesis*; Springer-Verlag: Berlin, **1983**; p 129.
59. Sato, F, Watanabe, H, Tanaka, Y, Yamaji, T, Sato, M. *Tetrahedron Lett.* **1983**, *24*, 1041.
60. Ishikawa, A, Uchiyama, H, Katsuki, T, Yamaguchi, M. *Tetrahedron Lett.* **1990**, *31*, 2415.
61. Hirao, T, Yamada, N, Ohshiro, Y, Agawa, T. *Chem. Lett.* **1982**, 1997.
62. Adam, W, Richter, M. *Chem. Ber.* **1992**, *125*, 243.
63. Kabat, M.M. *Tetrahedron Lett.* **1993**, *34*, 8543.
64. Takeda, Y, Matsumoto, T, Sato, F. *J. Org. Chem.* **1986**, *51*, 4728.
65. Kitano, Y, Matsumoto, T, Sato, F. *Tetrahedron*, **1988**, *44*, 4073.
66. Jefford, C.W, Moulin, M.C. *Helv. Chim. Acta* **1991**, *74*, 336.
67. Yamamoto, K, Kimura, T, Tomo, Y. *Tetrahedron Lett.* **1984**, *25*, 2155.
68. Yamamoto, K, Kimura, T, Tomo, Y. *Tetrahedron Lett.* **1985**, *26*, 4505.
69. Sato, F, Takahashi, O, Kato, T, Kobayashi, Y. *J. Chem. Soc., Chem. Commun.* **1985**, 1638.
70. Kabat, M.M. *Tetrahedron: Asymmetry* **1993**, *4*, 1417.
71. Sato, F, Ishikawa, H, Watanabe, H, Miyake, T, Sato, M. *J. Chem. Soc., Chem. Commun.* **1981**, 718.
72. Tagashi, K, Terakado, M, Miyazaki, M, Yamamoto, K, Takahashi, T. *Tetrahedron Lett.* **1994**, *35*, 3333.
73. Tanaka, K, Kamatani, M, Mori, H, Fujii, S, Ikeda, K, Hisada, M, Itagaki, Y, Katsumura, S. *Tetrahedron Lett.* **1998**, *39*, 1185.
74. Bergens, S.H, Noheda, P, Whelan, J, Bosnich, B. *J. Am. Chem. Soc.* **1992**, *114*, 2128.
75. Trost, B.M, Lautens, M. *J. Am. Chem. Soc.* **1987**, *109*, 1469.
76. Sato, F, Watanabe, H, Tanaka, Y, Sato, M. *J. Chem. Soc., Chem. Commun.* **1982**, 1126.
77. Sarkar, T.K, Ghorai, B.K, Nandy, S.K, Mukherjee, B. *Tetrahedron Lett.* **1994**, *35*, 6903.
78. Koh, M.G, Choi, S.K. *Bull. Korean. Chem. Soc.* **1983**, *4*, 200 [*Chem. Abstr.* **1984**, *100*, 156178h].
79. Nowotny, S, Tucker, C.E, Jubert, C, Knochel, P. *J. Org. Chem.* **1995**, *60*, 2762.
80. Kang, J, Cho, W, Lee, W.K. *J. Org. Chem.* **1984**, *49*, 1838.
81. Lautens, M, Huboux, A.H. *Tetrahedron Lett.* **1990**, *31*, 3105.
82. Lautens, M, Zhang, C.H, Crudden, C.M. *Angew. Chem. Int. Ed. Engl.* **1992**, *31*, 232.
83. Lautens, M, Zhang, C.H, Goh, B.J, Crudden, C.M, Johnson, M.J.A. *J. Org. Chem.* **1994**, *59*, 6208.
84. Lautens, M, Huboux, A.H, Chin, B, Downer, J. *Tetrahedron Lett.* **1990**, *31*, 5829.
85. Lautens, M, Delanghe, P.H.M., *J. Org. Chem.* **1992**, *57*, 798.
86. Oppolzer, W, Spivey, A.C, Bochet, C.G. *J. Am. Chem. Soc.* **1994**, *116*, 3139.
87. Sato, F, Kobayashi, Y. In *Organic Syntheses*; Paquette, L.A., Ed.; Wiley: New York, **1990**; Vol. 69, p 106.
88. Kocienski, P, Love, C, Whitby, R, Roberts, D.A. *Tetrahedron Lett.* **1988**, *29*, 2867.
89. Marshall, J.A, Jenson, T.M, Dehoff, B.S. *J. Org. Chem.* **1987**, *52*, 3860.
90. Marek, I, Lefranmidshiftvicois, J.M., Normant, J.F. *Tetrahedron Lett.* **1991**, *32*, 5969; Normant, J.F, Marek, I, Lefranmidshiftvicois, J.M. *Pure Appl. Chem.* **1992**, *64*, 1857; Marek, I, Lefranmidshiftvicois, J.-M, Normant, J.F. *Bull. Soc. Chim. Fr.* **1994**, *131*, 910.
91. Tani, K, Sato, Y, Okamoto, S, Sato, F. *Tetrahedron Lett.* **1993**, *34*, 4975.
92. Ito, T, Okamoto, S, Sato, F. *Tetrahedron Lett.* **1990**, *31*, 6399.
93. Lautens, M, Delanghe, P.H.M. *J. Org. Chem.* **1995**, *60*, 2474.
94. Kitano, Y, Matsumoto, T, Sato, F. *J. Chem. Soc., Chem. Commun.* **1986**, 1323.
95. Isobe, M, Obeyama, J, Funabashi, Y, Goto, T. *Tetrahedron Lett.* **1988**, 29, 4773.

96. Sato, F, Kanbara, H, Tanaka, Y. *Tetrahedron Lett.* **1984**, *25*, 5063.
97. Barton, T.J, Groh, B.L. *J. Org. Chem.* **1985**, *50*, 158.
98. Sato, F, Katsuno, H. *Tetrahedron Lett.* **1983**, *24*, 1809.
99. Review: Pereyre, M, Quintard, J.-P, Rahm, A. *Tin in Organic Synthesis*; Butterworths: London, **1987**.
100. Duboudin, J.-G, Jousseaume, B. *J. Organomet. Chem.* **1972**, *44*, C1.
101. Corey, E.J, Katzenellenbogen, J.A. Posner, G.H. *J. Am. Chem. Soc.* **1967**, *89*, 4245.
102. Djadchenko, M.A, Pivnitsky, K.K, Spanig, J, Schick, H. *J. Organomet. Chem.* **1991**, *401*, 1.
103. Klei, E, Telgen, J.H, Teuben, J.H. *J. Organomet. Chem.* **1981**, *209*, 297; Klei, E, Teuben, J.H. *J. Organomet. Chem.* **1981**, *222*, 79.
104. Sato, F, Jinbo, T, Sato, M. *Tetrahedron Lett.* **1980**, 2171.
105. Sato, F, Jinbo, T, Sato, M. *Tetrahedron Lett.* **1980**, 2175.
106. Sato, F, Jinbo, T, Sato, M. *Synthesis* **1981**, 871.
107. Amin, S.R, Crowe, W.E. *Tetrahedron Lett.* **1997**, *38*, 7487.
108. Sato, F. *Janssen Chim. Acta* **1990**, *8*, 3.
109. Gao, Y, Urabe, H, Sato, F. *J. Org. Chem.* **1994**, *59*, 5521; Gao, Y, Harada, K, Hata, T, Urabe, H, Sato, F. *J. Org. Chem.* **1995**, *60*, 290.

4

Stereoselective Addition of Grignard Reagents to Alkenes

Amir H. Hoveyda,* Nicola M. Heron and Jeffrey A. Adams
Department of Chemistry, Merkert Chemistry Center, Boston College, Boston, USA

4.1 INTRODUCTION

Alkyl- and arylmagnesium halides represent a useful and important class of reagents to synthetic organic chemists. Perhaps the most significant reason for such prominence is due to the ability of Grignard reagents to react readily, and often stereoselectively, with a wide range of carbonyl functional groups. In contrast, addition of alkyl metals to alkenes is not expected to occur readily under most circumstances. Nonetheless, addition of Grignard reagents to alkenes is a process that bears significant promise in chemical synthesis. This is because such a process would afford a C–C bond, and the development of catalytic C–C bond forming reactions that proceed under mild conditions in a regio-, diastereo- and enantioselective fashion (>95%) remains a critical and challenging task in chemical synthesis [1].

A number of researchers in the sixties and seventies reported that in the presence of appropriate Lewis basic functional groups, a select number of Grignard reagents do add to alkene units; the scope and efficiency of these reactions remained somewhat limited, however. More recently, several investigations have focused on the development of related metal-catalyzed processes, where Grignard reagents react with various olefinic systems. In addition, during the past six years, there have been more reports that indicate that uncatalyzed alkylations can occur on a wider range of substrates, under mild conditions and with appreciable stereochemical control.

This article presents a review of efforts that have been directed on the selective addition of Grignard reagents to alkene-containing substrates. Reactions that involve conjugate addition reactions (processes involving unsaturated carbonyls) are not included [2]. As will be described below, these transformations provide efficient and selective routes to the synthesis of a wide variety of chiral non-racemic organic molecules that can be used in the fabrication of a number of highly functionalized molecules.

Grignard Reagents: New Developments Edited by Herman G. Richey, Jr © 2000 John Wiley & Sons Ltd

4.2 HETEROATOM-DIRECTED ADDITION OF GRIGNARD REAGENTS TO ALKENES

In 1965, Eisch and Husk reported that, in their attempt to prepare allyldiphenyl carbinol by the reaction of benzophenone with allylmagnesium bromide, they also isolated 10–20% of **3**, which is the product of the addition of the Grignard reagent to the desired product **2** [3]. These researchers proposed the intermediacy of **I** (Scheme 4.1), implying the intramolecular delivery of the alkylmetal by the resident hydroxyl unit [4]. Subsequent studies involved the stereoselective addition of allylmagnesium halides to cyclic unsaturated alcohols (**4** → **5**); the observed stereochemical outcome clearly implies the involvement of the alcohol function as a directing unit [5].

Felkin and co-workers reported in 1966 that certain allylic alcohols react with allylmagnesium bromide to afford the corresponding addition products in high yield. The example shown in Scheme 4.2 (**6** → **7**) is illustrative [6]. Felkin's subsequent mechanistic work included kinetic studies, suggesting that the presence of $MgBr_2$, in addition to the alkylmagnesium halide, is required for efficient alkylation [7]. The mechanistic proposal put forth by these workers is depicted in Scheme 4.2. Reactions with other allylic magnesium halides, such as benzyl Grignard reagents, were reported to be significantly more sluggish; incorporation of allylic substituents within the substrate structure was indicated to result in notable diminution in reaction efficiency.

In addition to the work of Eisch and Felkin, another set of key studies was reported by Richey and co-workers, who demonstrated that phenolic hydroxyl units and internal amine groups can direct the addition of Grignard reagents to alkenes [8]. As depicted in Scheme 4.3 (**8** → **9**), reactions with allylic amines, similar to those mentioned above, are regioselective but relatively inefficient and limited to allylmagnesium halides as alkylating agents [9]. As is also depicted in Scheme 4.3, with phenolic substrates (**10** → **11** and **12**), reaction regioselectivity is diminished. These results indicate that the relatively remote and non-Lewis basic heteroatom is still capable of promoting C–C bond formation, as removal or protection of the carbinol unit resulted in significantly slower transformations.

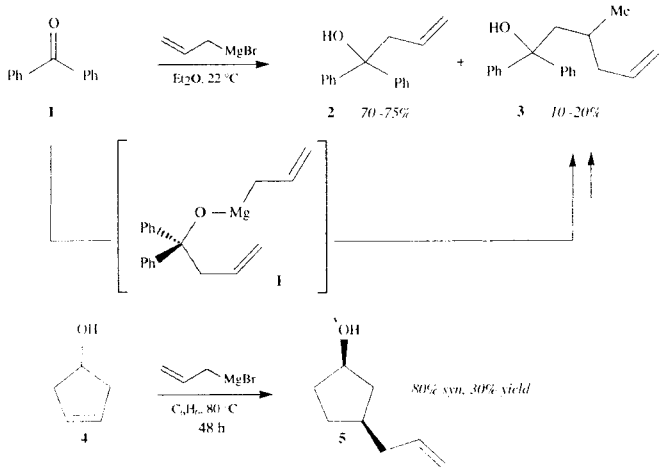

SCHEME 4.1

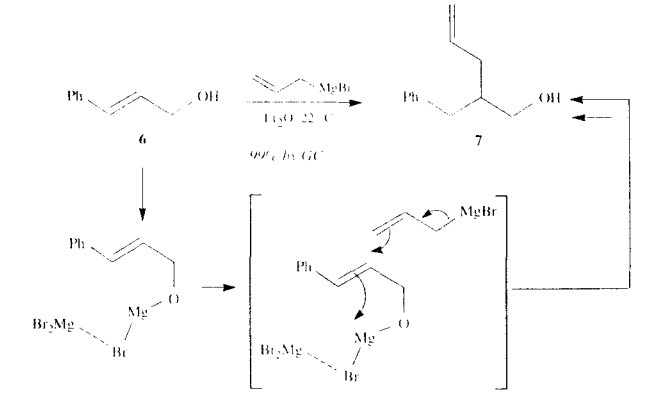

SCHEME 4.2

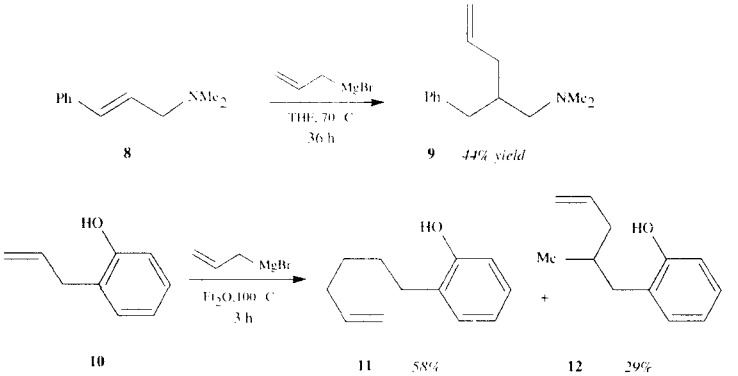

SCHEME 4.3

4.3 Zr-CATALYZED DIASTEREOSELECTIVE CARBOMAGNESATION OF ALLYLIC AND HOMOALLYLIC ALCOHOLS AND ETHERS

4.3.1 Zr-Catalyzed Diastereoselective Ethylmagnesation of Allylic Alcohols and Ethers

In 1991, inspired by pioneering studies of Dzhemilev [10], we investigated the possibility of using a zirconocene catalyst to effect the diastereoselective ethylmagnesation of chiral allylic alcohols and ethers [11]. Thus, as illustrated in Table 4.1, in the presence of 5 mol % Cp_2ZrCl_2 (Et_2O, 22 °C) allylic alcohols readily undergo reaction to afford the corresponding diols diastereoselectively. Although excellent selectivity is attained with the majority of allylic alcohol substrates (such as in reactions of **13** and **15**), the data depicted in Table 4.1 illustrate that with bulkier substituents, selectivity and reaction efficiency suffers (**17** → **18** in Table 4.1).

Table 4.1. Zr-Catalyzed Diastereoselective Ethylmagnesation of Allylic Alcohols.[a]

Entry	Substrate	Product	Selectivity Syn:anti	Yield(%)
1	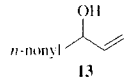 **13**	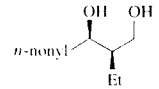 **14**	95:5	70
2	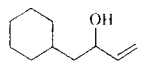 **15**	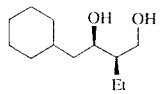 **16**	95:5	72
3	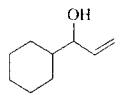 **17**	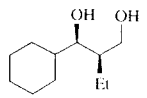 **18**	75:25	47

[a]Reaction condition: 4 equiv. EtMgCl, 5 mol% Cp_2ZrCl_2, 12 h; O_2 at 0°C. All yields are for materials obtained after silica gel chromatography.

Allylic ethers also undergo catalytic ethylmagnesation with excellent selectivity and in good yield (Table 4.2). However, there are several notable differences between the reactions of allylic ethers and alcohols: (1) Zr-catalyzed reactions of allylic ethers afford the anti diastereomers predominantly (vs. the syn isomers observed for alcohols). (2) As the size of the α-alkyl substituent increases, reaction selectivity is also increased, which is also in contrast to the reactions of allylic alcohols. Needless to say, the complementary levels of selectivity observed in reactions of allylic alcohols and ethers represents a useful attribute for applications in organic synthesis. Finally, it is also worth noting that with sterically bulky oxygen substituents, reaction efficiency can suffer significantly: allylic silyl ethers (TBS (*tert*-butyldimethylsilyl)) afford <5% products under identical conditions.

Another notable difference between the Zr-catalyzed ethylmagnesations of allylic ethers and alcohols is the influence of solvent Lewis basicity on reaction selectivity. Thus, as illustrated in Table 4.3, whereas reactions with allylic ethers are entirely insensitive to variations in solvent structure, those of allylic alcohols are strongly influenced. These observations led us to conclude that in the case of allylic alcohols (allylic alkoxides after rapid deprotonation by the Grignard reagent) there is chelation between the Lewis basic heteroatom and a metal center (Zr or Mg); this association, which gives rise to transition state organization and high diastereocontrol, is altered in the presence of Lewis basic THF, thus causing a diminution in selectivity. There is less chelation interruption with the 2,5-dimethylfuran (2,5-DMF) as solvent, because of the less accessible heteroatom. When the least basic solvent, Et_2O, is used, reaction selectivity is at its maximum. Such associations may be absent with the less Lewis basic ethers, thus accounting both for the opposite sense of stereocontrol and the insensitivity to solvent polarity.

Extensive mechanistic studies led us to propose the mechanistic paradigm shown in Scheme 4.4 [12]. Some of the notable features of the proposed pathway include the involvement of two zirconocene units (***i*** → ***ii*** → ***iii***), internal chelation between the resident metal alkoxide and the bound zirconocene (***ii***), and heteroatom-directed cleavage of the intermediate zirconacyclopentane (***iv*** → ***vi*** via ***v***). These mechanistic hypotheses can

Table 4.2. Zr-Catalyzed Diastereoselective Ethylmagnesation of Allylic Ethers.[a]

Entry	Substrate	Product	Selectivity Syn:anti	Yield(%)
1	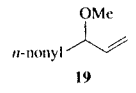 **19**	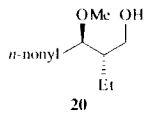 **20**	89:11	80
2	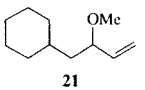 **21**	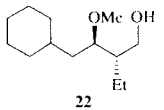 **22**	83:17	90
3	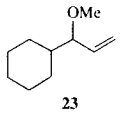 **23**	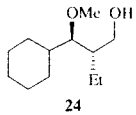 **24**	96:4	90
4	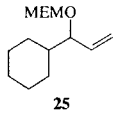 **25**	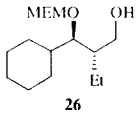 **26**	>99:1	40

[a]Reaction condition: 3 equiv. EtMgCl, 5 mol % Cp_2ZrCl_2, 12 h; O_2 at 0°C. All yields are for materials obtained after silica gel chromatography. MEM (2-methoxyethoxymethyl).

Table 4.3. Influence of Solvent on Diastereoselectivity of Zr-Catalyzed Ethylmagnesation of Allylic Alcohols and Ethers.[a]

Entry	Substrate	Product	Solvent	Selectivity Syn:anti	Yield(%)
1	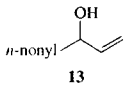 **13**	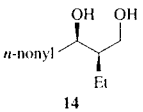 **14**	Et_2O	95:5	70
			2,5-DMTHF	85:15	50
			THF	67:33	85
2	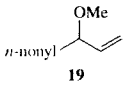 **19**	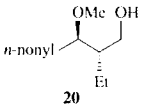 **20**	Et_2O	11:89	80
			THF	11:89	70

[a]See Tables 4.1 and 4.2 for reaction conditions

also account for variations in both the levels and trends of selectivity observed in reactions of allylic alcohols and ethers.

The catalytic and diastereoselective ethylmagnesation reaction was later used in our laboratories to assemble the fragment of the antifungal agent Sch 38516 (Scheme 4.5) [12]. Thus, chiral non-racemic Grignard reagent **28**, obtained from ethylmagnesation of **27**, was treated with 5 mol % $CuBr{\bullet}Me_2S$ and six equivalents of tosylaziridine to afford **29** in 40% isolated yield and 95:5 ratio of diastereomers.

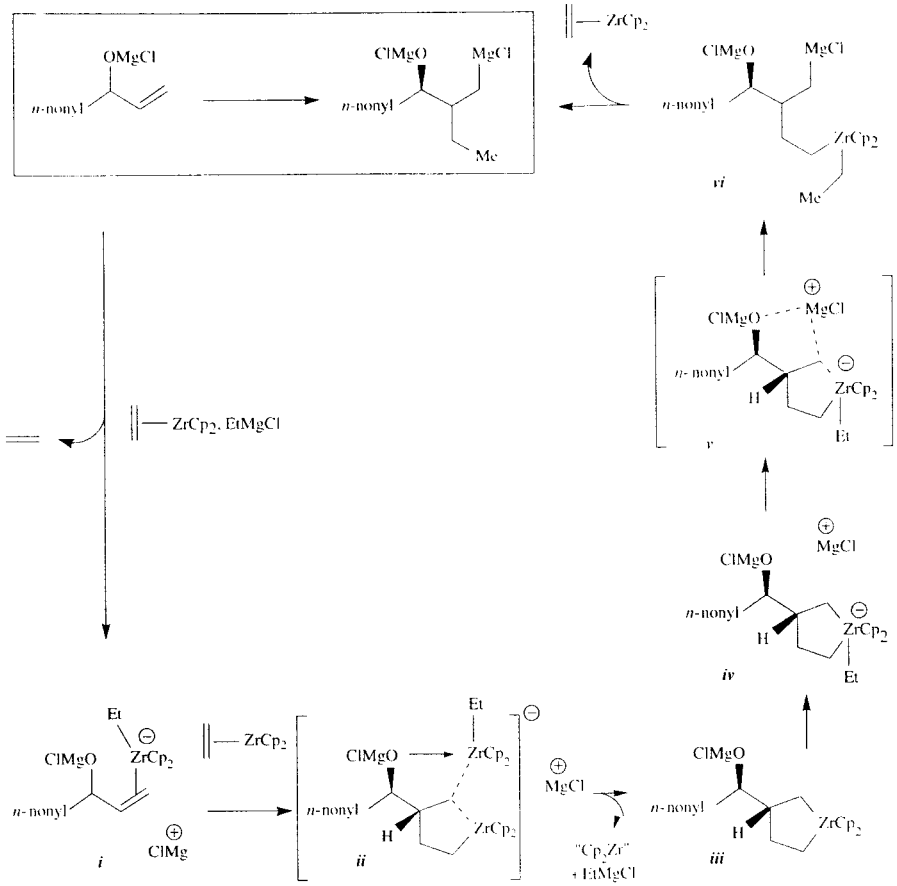

SCHEME 4.4

4.3.2 Zr-Catalyzed Diastereoselective Ethylmagnesation of Homoallylic Alcohols and Ethers

The Zr-catalyzed carbomagnesations of cyclic and acyclic homoallylic substrates were investigated as well. As shown in Table 4.4, anti-homoallylic alcohol **30** is an excellent substrate for ethylmagnesation. In THF or Et_2O, good yields and high levels of diastereoselection are obtained. The less Lewis basic **34** (compared to **30**) affords **35** in 60% yield and 92:8 diastereoselection; in the presence of a competing ligating solvent (THF), little reaction occurs. In contrast to ethylmagnesation of **32**, where the anti-isomer is produced with 85:15 selectivity (55%), carbomagnesation of derived ether, **36**, is non-selective and affords **37** in 35% yield. With **36** as substrate, ≤10% of the product is obtained when the Lewis basic THF is used.

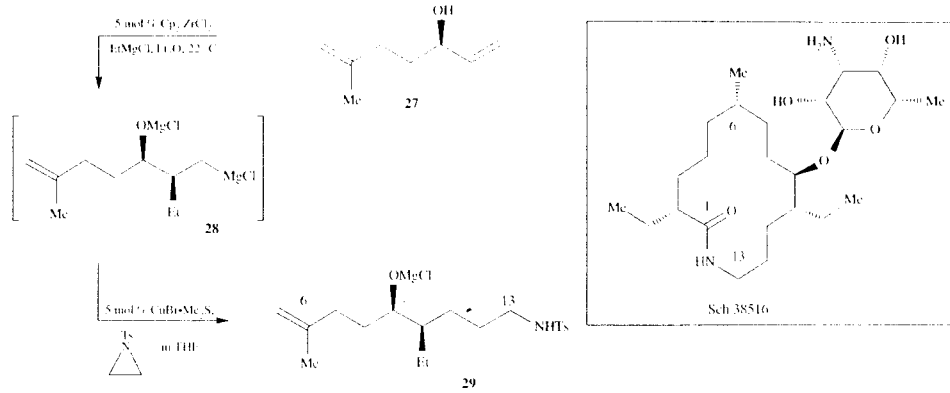

SCHEME 4.5

Table 4.4. Zr-Catalyzed Diastereoselective Ethylmagnesation of Homoallylic Alcohols and Ethers.[a]

Entry	Substrate	Major product	Solvent (% cat)	Ratio[c] (yield)[b]
1	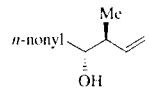 **30**	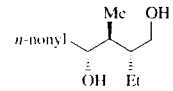 **31**	Et_2O (5) THF (5)	>95:5 (75) >95:5 (75)
2	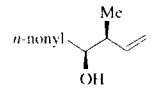 **32**	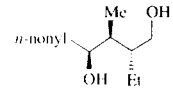 **33**	Et_2O (5) THF (5)	85:15 (55) 85:15 (55)
3	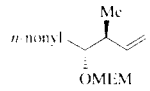 **34**	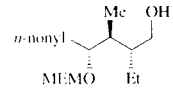 **35**	Et_2O (5) THF (5)	92:8 (60) -(<10)
4	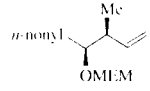 **36**	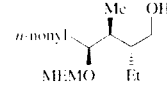 **37**	Et_2O (5) THF (5)	50:50 (35) -(<10)

[a]Conditions: Three equiv. EtMgCl, 5 mol % Cp_2, 25 °, 12 h; $B(OMe)_3$, H_2O_2. [b]Isolated yields of purified products after silica gel chromatography. Mass balance ≥ 90% in all cases. [c]Diastereomeric ratios determined by GLC analysis of the derived lactone.

In contrast to allylic ethers, homoallylic ethers undergo ethylmagnesation with the same sense of stereoselection as the parent metal alkoxide, indicating that heteroatom–metal chelation is perhaps more facile from the homoallylic position than from the allylic site (see below for further discussion). Since the carbon–carbon bond is formed anti to the methyl group, irrespective of the β-oxygen stereochemistry, it can be concluded that the α stereogenic center is primarily responsible for stereochemical differentiation. Consistent with this hypothesis, ethylmagnesation of **39** occurs without diastereoselection (80% yield).

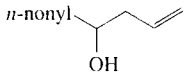

39

The enhancement in reactivity and selectivity induced by an internal Lewis base is such that *n*-PrMgCl and *n*-BuMgCl, normally significantly less reactive than EtMgCl, can be used in the metal-catalyzed process with the more reactive bicyclic homoallylic alcohols and ethers shown in Table 4.5. Whereas reactions of *exo*-5-norbornen-2-ol with *n*-PrMgCl and *n*-BuMgCl yield ≤15% of the two *exo* alkyl isomers non-selectively, *endo*-5-norbornen-2-ol (4 equiv of *n*-alkylMgCl, 10 mol % Cp_2ZrCl_2, 25°C) affords **41a** or **43a** in >99% regioselectivity and >85% yield (Table 4.5). With *n*-BuMgCl two secondary carbon stereogenic centers are formed with excellent stereocontrol (**43**, >95%). When the hydroxyl group is protected as its MEM ether, (2-methoxyethoxymethyl), or with THF as solvent [13], chelation is altered and inferior yields and selectivities are obtained. Similar results are obtained with EtMgCl as the alkylating agent. The data in Table 4.5 are similar to those for reactions of acyclic homoallylic alcohols and ethers (cf. Table 4.4). These findings further support the contention that internal chelation is central to reaction efficiency and selectivity in transition metal-catalyzed carbomagnesation. Mechanistic paradigms discussed above have been used to account for the data in Table 4.5 as well.

4.4 ZIRCONOCENE-CATALYZED ENANTIOSELECTIVE ALKYLATION REACTIONS

4.4.1 Catalytic Enantioselective Alkylation of Alkenes with Alkylmagnesium Halides

As illustrated in Table 4.6, in the presence of 2.5–10 mol % non-racemic $(EBTHI)ZrCl_2$ (**45**) (or (EBTHI)Zr-binol (**46**)) and EtMgCl as the alkylating agent, five-, six-, and seven-membered unsaturated heterocycles undergo facile

Table 4.5. Diastereoselective Zr-Catalyzed Carbomagnesation of Bicyclic Homoallylic Alcohols and Ethers

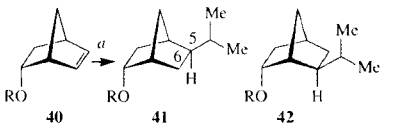

Substrate	R	Solvent	Yield(%)[b]	41:42[c]
40a	H	Et_2O	88	>99:1
		THF	83	97:3
40b	MEM	Et_2O	40	96:4
		THF	40	75:25

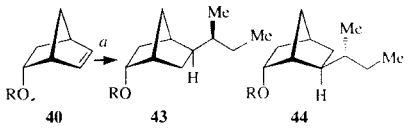

Substrate	R	Solvent	Yield(%)[b]	43:44[c]
40a	H	Et_2O	86	>99:1
		THF	80	98:2
40b	MEM	Et_2O	30	96:4
		THF	27	67:33

[a] 4 equiv. *n*-alkylMgCl, 10 mol % Cp_2ZrCl_2, 40 h; 10 % HCl at 0°C. [b] Isolated yields of purified products. Mass balance > 95 % in all cases. [c] Ratios determined by GLC analysis (of acetates in case of **41a**).

Table 4.6. (EBTHI)Zr-Catalyzed Enantioselective Ethylmagnesation of Unsaturated Heterocycles.[a]

Entry	Substrate	Product	ee (%)	Yield (%)
1		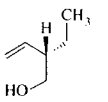	>97	65
2		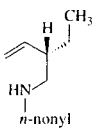	>95	75
3		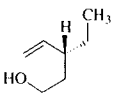	95	73
4	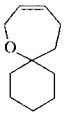	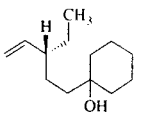	92	75

[a] Reaction condition: 10 mol % (*R*)-**45**, 5.0 equiv. EtMgCl, THF, 22°C for 6-12 hours. Entry 1 with 2.5 mol% (*R*)-**45**

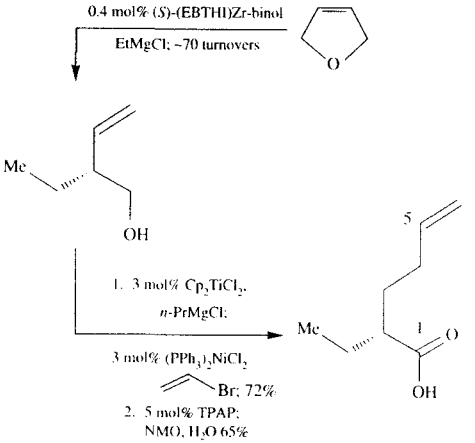

SCHEME 4.6

asymmetric ethylmagnesation (EBTHI: ethylenebistetrahydroindenyl) [14]. The rate of the catalytic alkylation of the product terminal alkenes is sufficiently slower, so that unsaturated alcohols and amines can be isolated in high yield (the second alkylation is not generally diastereoselective). Zr-catalyzed asymmetric alkene alkylation thus affords non-racemic reaction products that bear an alkene and a carbinol unit, functional groups that are readily amenable to a wide range of subsequent derivatization procedures.

We have utilized the stereoselective ethylmagnesation shown in entry 1 of Table 4.6 as a key step in the first enantioselective total synthesis of the antifungal agent Sch 38516 [12a]. As illustrated in Scheme 4.6, further functionalization of the Zr-catalyzed ethylmagnesation product through three subsequent catalytic procedures (Ti-catalyzed hydromagnesation, Ni-catalyzed cross-coupling and Ru-catalyzed oxidation) delivers the requisite carboxylic acid synthon in >99% *ee*. This synthesis route underlines the utility of the Zr-catalyzed carbomagnesation protocol: the reaction product carries an alkene and an alcohol function and can thus be readily functionalized to a variety of other non-racemic intermediates.

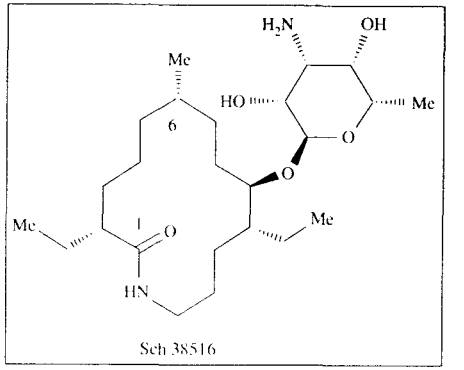

Sch 38516

The catalytic cycle that we have proposed to account for the enantioselective ethylmagnesation is illustrated in Scheme 4.7. Asymmetric carbomagnesation is initiated by the chiral zirconocene-ethylene complex (*R*)-**47**, formed upon reaction of dichloride (*R*)-**45** with EtMgCl [Eq (a); the dichloride salt or the binol complex may be used with equal efficiency] [15]. Coupling of the alkene substrate with (*R*)-**47** leads to the formation of the metallacyclopentane intermediate **i**. In the proposed catalytic cycle, reaction of ***i*** with EtMgCl affords zirconate ***ii***, which undergoes Zr–Mg ligand exchange to yield ***iii***. Subsequent β-hydride abstraction, accompanied by intramolecular magnesium-alkoxide elimination, leads to the release of the carbomagnesation product and regeneration of **47** [16].

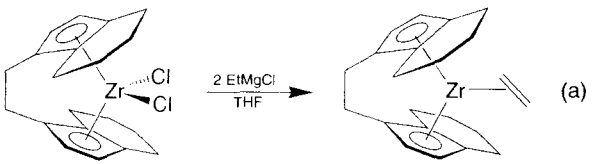

(*R*)-**45** (*R*)-**47**

An important aspect in the carbomagnesation of six-membered and larger heterocycles is the exclusive intermediacy of metallacyclopentanes where a C–Zr bond is formed α to the heterocycle C–X bond. Whether the regioselectivity in the zirconacycle formation is kinetically nonselective and rapidly reversible, where it is only one regioisomer that is active in the catalytic cycle, or whether formation of the metallacycle is kinetically selective (stabilization of electron density upon formation of a C–Zr bond by the adjacent C–X) [17], has not been rigorously determined. However, as will be discussed below, the regioselectivity with which the intermediate zirconacyclopentane is formed is critical in the (EBTHI)Zr-catalyzed kinetic resolution of heterocyclic alkenes.

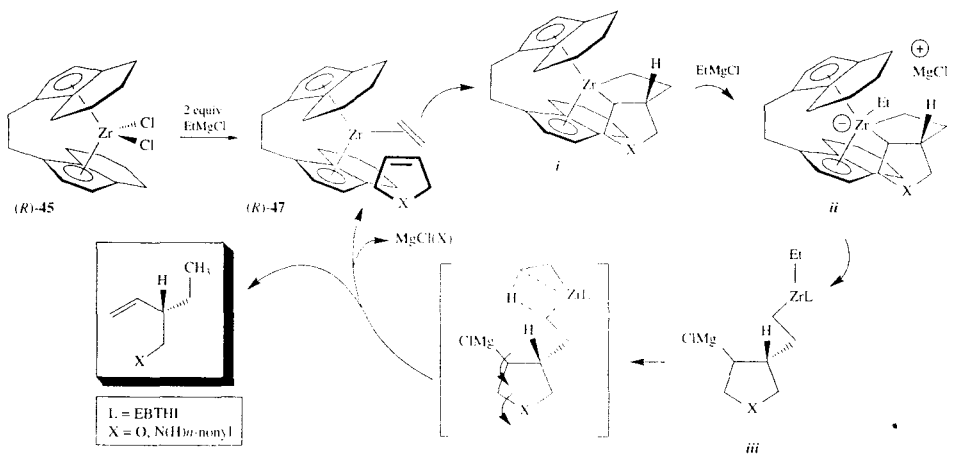

SCHEME 4.7

It is plausible that the (EBTHI)Zr system induces high levels of enantioselectivity as a result of minimization of unfavorable steric and torsional interactions in the complex that is formed between **47** and the heterocycle substrates (Scheme 4.7). The alternative mode of addition, illustrated in Figure 4.1, would lead to costly steric repulsions between the alkene substituents and the cyclohexyl group of the chiral ligand. Thus, reactions of simple terminal alkenes under identical conditions result in little or no enantioselectivity. This is presumably because in the absence of the alkenyl substituent (of the carbon that bonds with Zr in *i*) the aforementioned steric interactions are ameliorated and the alkene substrate reacts indiscriminately through the two modes of substrate-catalyst binding represented in Figure 4.1.

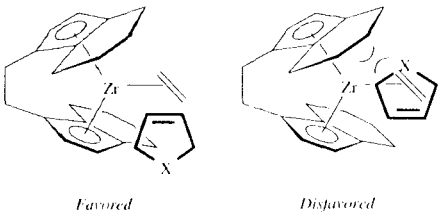

Fig. 4.1. Substrate-catalyst (**47**) interactions favor a specific mode of alkene insertion into the zirconocene–alkene complex.

These alkylation processes become particularly attractive when used in conjunction with the powerful catalytic ring-closing metathesis protocols. The requisite starting materials can be readily prepared in high yield and catalytically [18]. The examples shown in Scheme 4.8 demonstrate that synthesis of the heterocyclic alkene and subsequent alkylation can be carried out in a single vessel to afford unsaturated alcohols and amides in good yield and >99% *ee* (judged by GLC analysis) [19].

Catalytic alkylations where higher alkyls of magnesium are used (Table 4.7) proceed less efficiently (35–40% isolated yield) but with similarly high levels of enantioselection (>90% ee). A number of issues in connection to the data illustrated in Table 4.7 merit comment. (1) With 2,5-dihydrofuran as substrate, at 22°C a mixture of branched (**48** or **50**) and *n*-alkyl products (**49** or **51**) is obtained. When the reaction mixture is heated to 70°C, the branched adducts **48** and **50** become the major product isomers. In contrast, with the six-membered heterocycle, reactions at 22°C are selective (entries 3 and 6, Table 4.2). (2) With *n*-BuMgCl as the alkylating agent, high levels of diastereoselection are observed as well (entry 6).

The aforementioned observations carry significant mechanistic implications. As illustrated in eq. (b)–(d), in the chemistry of zirconocene-alkene

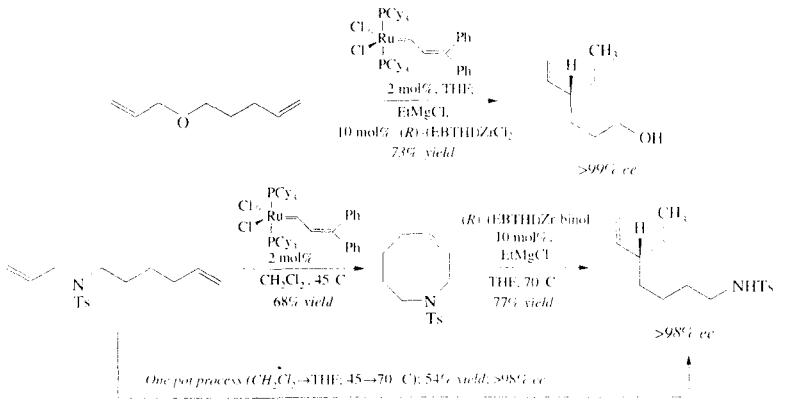

SCHEME 4.8

Table 4.7. (EBTHI) Zr-Catalyzed Enantioselective Carbomagnesation of Unsaturated Heterocycles with Longer Chain Alkylmagnesium Chlorides.[a]

Entry	Substrate	Major product(s)	Temp(°C)	RMgCl	Regioselectivity	ee,%	diastereoselectivity
1		**48**	22	*n*-PrMgCl	2:1	99(**48**), 99(**49**)	—
2		**49**	70	*n*-PrMgCl	20:1	94(**48**)	—
3			22	*n*-PrMgCl	>25:1	98	—
4		**50**	22	*n*-BuMgCl	2:1	>99(**50**),>99(**51**)	15:1
5		**51**	70	*n*-BuMgCl	15:1	90(**50**)	13:1
6			22	*n*-BuMgCl	>25:1	>95	>25:1

[a]Reaction conditions: 5 equiv alkylMgCl, 10 mol % (*R*)-**45**, 16 h; all yields: 35–40% after silica gel chromatography.

complexes that are derived from the longer chain alkylmagnesium halides several additional selectivity issues present themselves: (1) The derived transition metal–alkene complex can exist in two diastereomeric forms, exemplified in eq. (b)–(c) with (*R*)-**52** *anti* and *syn*; reaction through these stereoisomeric complexes can lead to the formation of different product diastereomers (compare eq. (b) and (c), or eq. (c) and (d)). The data in Table 4.7 indicate that the mode of addition shown in eq. (b) is preferred. (2) As illustrated in eq. (c) and (d), the carbomagnesation process can afford either the *n*-alkyl or the branched product. Alkene substrate insertion from the more substituted front of the zirconocene–alkene system affords the branched isomer [eq. (c)], whereas reaction from the less substituted end of the (EBTHI)Zr-alkene system leads to the formation of the straight chain product [eq. (d)]. The results shown in Table 4.7 indicate that, depending on the reaction conditions, products derived from formation of the two isomeric metallacyclopentane formation can be competitive.

Detailed studies from these laboratories shed light on the mechanistic intricacies of asymmetric catalytic carbomagnesations, allowing for an understanding of the above trends in regio- and stereoselectivity [16]. Importantly, our mechanistic studies indicate that there is no preference for the formation of either the *anti* or the *syn* (EBTHI)Zr-alkene isomers (*e.g.*, **52** *anti* vs **52** *syn*); it is only that one metallocene–alkene diastereomer (*syn*) is more reactive. Our mechanistic studies also indicate that zirconacyclopentane intermediates (*i* in Scheme 4.7) do not spontaneously eliminate to the derived zirconocene- alkoxide; Zr–Mg ligand exchange is likely a pre-requisite for the alkoxide elimination and formation of the terminal alkene.

4.4.2 Zr-Catalyzed Kinetic Resolution of Unsaturated Heterocycles

The high levels of enantioselectivity obtained in the asymmetric catalytic carbomagnesation

reactions (Tables 4.6 and 4.7) imply an organized (EBTHI)Zr-alkene complex interaction with the heterocyclic alkene substrates. It therefore follows that if chiral unsaturated pyrans or furans are employed, the resident center of asymmetry may induce differential rates of reaction, such that after ~50% conversion one enantiomer of the chiral alkene can be recovered in high enantiomeric purity. As an example, molecular models indicate that with a 2-substituted pyran, as shown in Figure 4.2, the mode of addition labeled as **I** should be significantly favored over **II** or **III**, where unfavorable steric interactions between the (EBTHI)Zr-complex and the olefinic substrate should lead to significant catalyst-substrate complex destabilization.

As the data in Table 4.8 indicate, in the presence of catalytic amounts of non-racemic (EBTHI)$ZrCl_2$, a variety of unsaturated pyrans can be resolved effectively to deliver these synthetically useful heterocycles in excellent enantiomeric purity [20]. A number of important issues in connection with the catalytic kinetic resolution of pyrans are noteworthy: (1) Reactions performed at elevated temperatures (70°C) afford recovered starting materials with significantly higher levels of enantiomeric purity, compared to processes carried out at 22°C. For example, the 2-substituted pyran shown in entry 1 of Table 4.8, when subjected to the same reaction conditions but at room temperature, is recovered after 60% conversion in 88% ee (vs 96% *ee* at 70°C). (2) Consistent with the models illustrated in Figure 4.2, 6-substituted pyrans

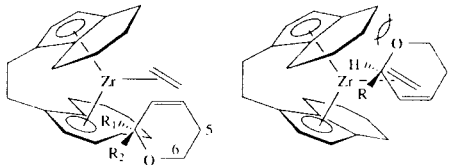

I $R_1 = H, R_2 = alkyl$ **III** $R = alkyl$

II $R_1 = alkyl, R_2 = H$

Fig. 4.2. Preferential association of one pyran enantiomeric with (R)-(EBTHI)Zr-ethylene complex.

Table 4.8. (EBTHI)Zr-Catalyzed Kinetic Resolution of Unsaturated Pyrans.[a]

Entry	Substrate		Conversion (%)	mol% cat.	Unreacted subs. config., ee(%)
1	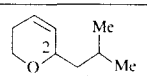		60	10	*R*, 96
2	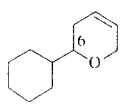		60	10	*S*, 41
3	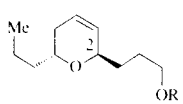	**a** R = MgCl	56	10	*R*, >99
		b R = TBS	60	10	*R*, >99
4	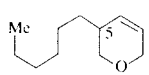		58	20	*R*, 99
5	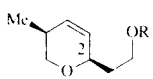	**a** R = MgCl	63	10	*R*, >99
		b R = TBS	61	10	*R*, 94

[a]Reaction conditions: indicated mol% (*R*)-**45**, 5.0 equiv of EtMgCl, 70 C, THF. Mass recovery in all reactions is > 85%.

(Table 4.8, entry 2) are not resolved effectively (C6 substituent should not strongly interact with the catalyst structure; see Figure 4.2); however, with a C2 substituent also present, resolution proceeds with excellent efficiency (entry 3). (3) Pyrans that bear a C5 group are resolved with high selectivity as well (entry 4). In this class of substrates, one enantiomer reacts more slowly, presumably because its association with the zirconocene–alkene complex leads to sterically unfavorable interactions between the C5 alkyl unit and the coordinated ethylene ligand.

The Zr-catalyzed resolution technology may be applied to medium ring heterocycles as well (Table 4.9); in certain instances (*e.g.*, Table 4.9, entries 1–2) the recovered starting material can be obtained with outstanding enantiomeric purity. Comparison of the data shown in entries 1 and 3 of Table 4.9 indicates that the presence of an aromatic substituent can have an adverse influence on the outcome of the catalytic resolution. That the eight-membered ring substrate in Table 4.9 (entry 4) is resolved more efficiently may imply that the origin of the adverse influence is more due to conformational preferences of the heterocycle than the attendant electronic factors (α phenoxy group is a better leaving group than an alkoxy unit).

Availability of oxepins that carry a side chain containing a Lewis basic oxygen atom (entry 2, Table 4.9) has further important implications in enantioselective synthesis: The derived alcohol, benzyl ether or MEM-ethers, where resident Lewis basic heteroatoms are less sterically hindered, undergo diastereoselective uncatalyzed alkylation reactions readily when treated to a variety of Grignard reagents [21]. The examples shown below (Scheme 4.9) serve to demonstrate the excellent synthetic potential of these stereoselective alkylation technologies.

Thus, resolution of the TBS-protected oxepin **54**, conversion to the derived alcohol and diastereoselective alkylation with *n*BuMgBr affords (*S*)-**56** with >96% *ee* in 93% yield. As shown in Scheme 4.9, alkylation of (*S*)-**57** with an alkyne-bearing Grignard agent (⟶ (*S*)-**58**), allows for a subsequent Pauson–Khand cyclization reaction to provide the corresponding bicycle **59** in the optically pure form (NMO: N-methylmorpholine N-oxide). In connection with the facility of these alkene alkylations, it is important to note that the asymmetric Zr-catalyzed alkylations with longer chain alkylmagnesium halides (see Table 4.7) are more sluggish than those involving EtMgCl. Furthermore, when catalytic alkylation does occur,

Table 4.9. Zirconocene-Catalyzed Kinetic Resolution of 2-Substituted Medium-Ring Heterocycles.[a]

Entry	Substrate	Conversion (%)	Time	Unreacted subs. config., ee(%)
1	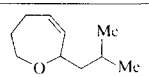	58	30 min	*R*, >99
2	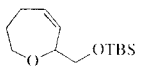	63	100 min	*R*, 96
3	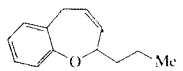	60	8 h	*R*, 60
4	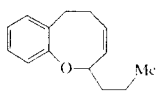	63	11 h	*R*, 79

[a]Reaction conditions: 10 mol % (*R*)-**45**, 5.0 equiv of EtMgCl, 70 C, THF. Mass recovery in all reactions is >85%

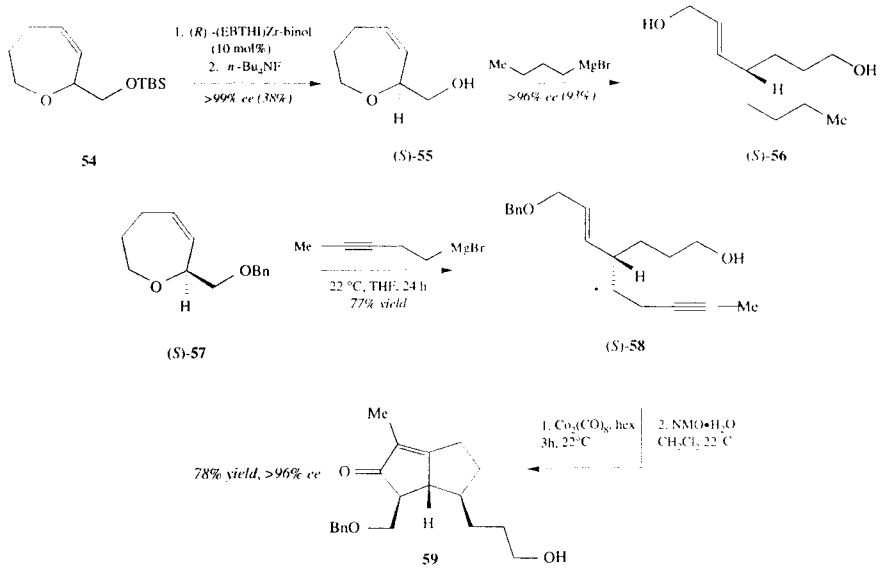

SCHEME 4.9

the corresponding branched products are obtained; that is, with *n*-PrMgCl and *n*-BuMgCl, *iso*-Pr and *sec*-Bu addition products are formed, respectively [16]. The uncatalyzed alkylation reaction described here thus complements the enantioselective Zr-catalyzed protocol.

Zirconocene-catalyzed kinetic resolution of dihydrofurans is also possible, as illustrated in Scheme 4.10 [22]. Unlike their six-membered ring counterparts, both of the heterocycle enantiomers react readily, but through distinctly different reaction pathways, to afford—in high diastereomeric and enantiomeric purity—constitutional isomers that are readily separable. A plausible reason for the difference in the reactivity pattern of pyrans and furans is that, in the latter group of compounds, both olefinic carbons are adjacent to a C–O bond: C–Zr bond formation can take place at either end of the C–C π-system. The furan substrate and the (EBTHI)Zr-alkene complex (*R*)-**47** interact so that unfavorable steric interactions are avoided, leading to the formation of readily separable non-racemic products in the manner illustrated in Scheme 4.10.

Subsequent to our studies, Whitby and co-workers reported that the enantioselective alkylations of the type illustrated in Scheme 4.10 can also be carried out with the non-bridged chiral zirconocene **62** [23]. Enantioselectivities are, however, notably lower when alkylations are carried out in the presence of **62**. As an example, the new chiral metallocene affords **60** and **61** (Scheme 4.10) in 82% and 78% ee, respectively.

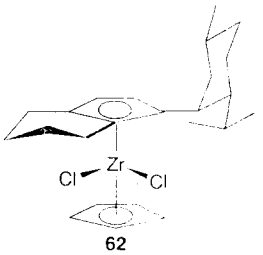

62

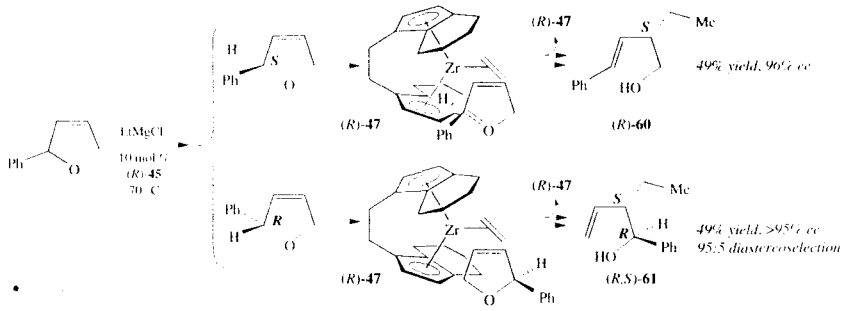

SCHEME 4.10

4.4.3 Zr-Catalyzed Kinetic Resolution of Cyclic Allylic Ethers

As depicted in eq. (e)–(g), kinetic resolution of a variety of cyclic allylic ethers is effected by asymmetric Zr-catalyzed carbomagnesation. Importantly, in addition to six-membered ethers, seven- and eight-membered ring systems can be readily resolved by the Zr-catalyzed protocol. It is worthy of note that the powerful Ti-catalyzed asymmetric epoxidation procedure of Sharpless [24] is often used in the preparation of optically pure acyclic allylic alcohols through the catalytic kinetic resolution of easily accessible racemic mixtures [25]. When the catalytic epoxidation is applied to cyclic allylic substrates, reaction rates are retarded and lower levels of enantioselectivity are observed. Ru-catalyzed asymmetric hydrogenation has been employed by Noyori to effect resolution of five- and six-membered allylic carbinols [26]; in this instance, as with the Ti-catalyzed procedure, the presence of an unprotected hydroxyl function is required.

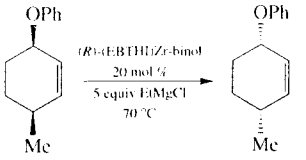

>98% ee @ 55% conversion (e)

(racemic)

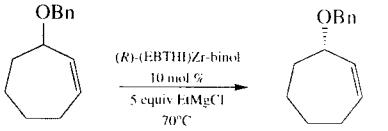

99% ee @ 60% conversion (f)

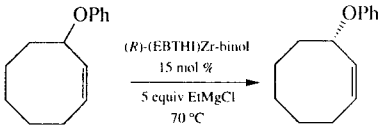

81% ee @ 59% conversion (g)

Modes of addition shown in Figure 4.3 are similar to those shown in Figure 4.2 and are consistent with extant mechanistic work [19]; they accurately predict the identity of the slower reacting enantiomer. It must be noted, however, that variations in the observed *levels* of selectivity as a function of the steric and electronic nature of substituents and the ring size cannot be predicted based on these models alone; more subtle factors are clearly at work. In spite of such mechanistic questions, the metal-catalyzed resolution protocol provides an attractive option in asymmetric synthesis. This is because, although maximum possible yield is ~40%, it requires easily accessible racemic starting materials and conversion levels can be manipulated so that truly pure samples of substrate enantiomers are obtained.

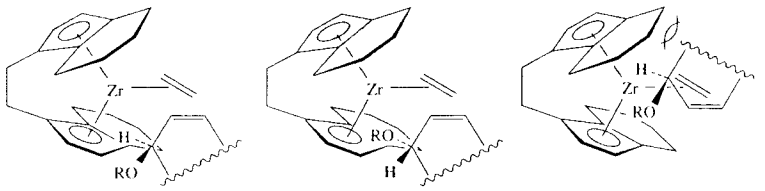

Fig. 4.3. Various modes of addition of cyclic allylic ethers to a (EBTHI)Zr-alkene complex.

The synthetic versatility and significance of the Zr-catalyzed kinetic resolution of cyclic allylic ethers is readily demonstrated in the example provided in Scheme 4.11. Optically pure starting allylic ether, obtained by the above mentioned catalytic kinetic resolution, undergoes a facile Ru-catalyzed rearrangement to afford chromene in >99% *ee* [27]. Unlike unsaturated pyrans discussed above, chiral 2-substituted chromenes are not readily resolved by the Zr-catalyzed protocol. However, optically pure styrenyl ethers, such as that shown in Scheme 4.11, are readily obtained by the Zr-catalyzed kinetic resolution, allowing for the efficient and enantioselective preparation of these important chromene heterocycles by a sequential catalytic protocol.

To examine and challenge the utility of the two-step catalytic resolution-chromene synthesis process in synthesis [28], we undertook a convergent and enantioselective total synthesis of the potent antihypertensive agent (*S,R,R,R*)-nebivolol (**63**) [29]. As illustrated in Scheme 4.12, the two key fragments (*R,R*)-**66** and (*R,S*)-**68**, which were subsequently joined to afford the target molecule, were prepared in the optically pure form by the catalytic resolution technology discussed above. Importantly, efficient and selective methods were established for the modification of the chromene alkenyl side chain. These studies allowed us to enhance the utility of the initial methodological investigations: they demonstrate that, although the carbocyclic system may be used as the framework for the Zr- and the Mo-catalyzed reactions, the resulting 2-substituted chromene can be functionalized in a variety of manners to afford a multitude of chiral non-racemic heterocycles [30]. Another interesting feature of this total synthesis is that, whereas the preparation of (*R,S*)-**66** requires the use of the (*R*)-Zr(EBTHI) catalyst, synthesis of (*R,S*)-**68** is carried out by catalytic kinetic resolution with (*S*)-Zr(EBTHI) complex. Thus, the recently developed procedure of Buchwald [31] is used to resolve *rac*-(EBTHI)Zr to obtain (*R*)-Zr(EBTHI)-binol and (*S*)-Zr(EBTHI)-biphen to accomplish this total synthesis in an efficient manner.

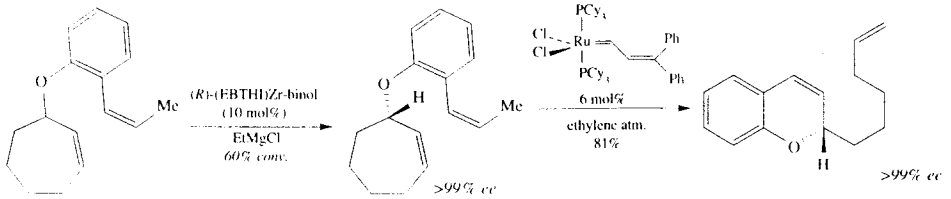

SCHEME 4.11

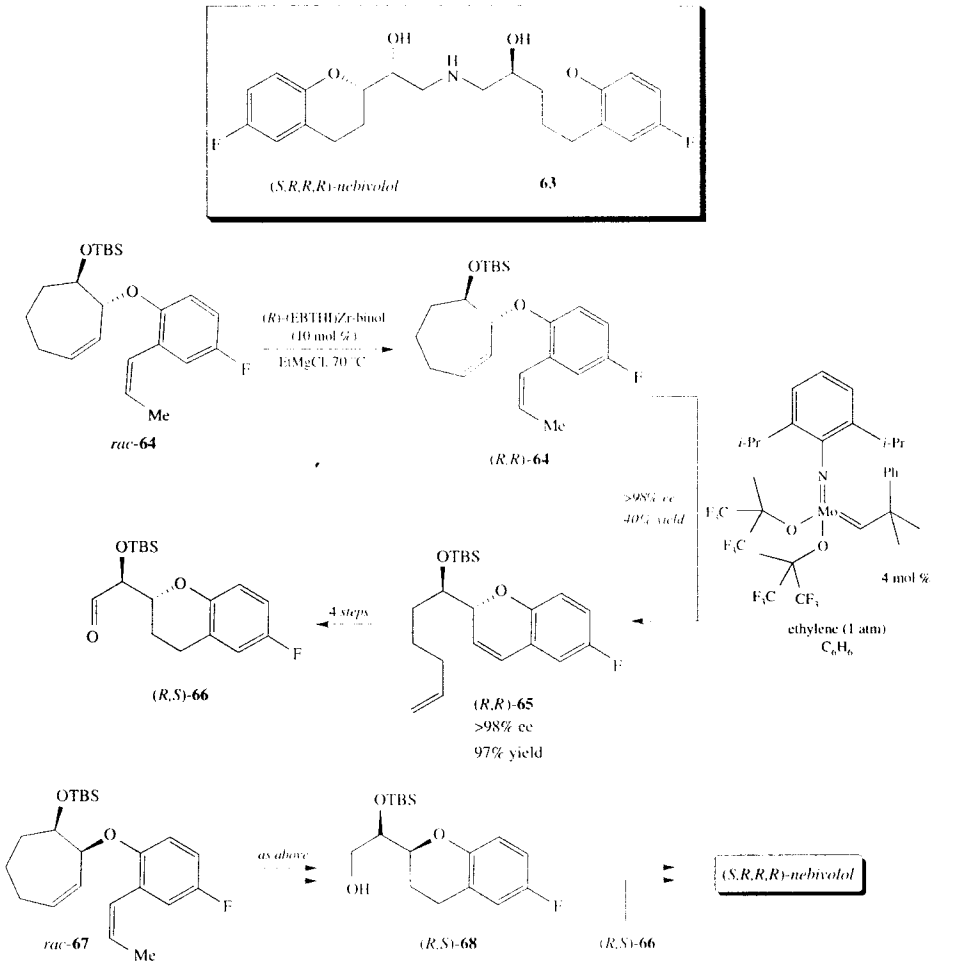

SCHEME 4.12

4.4.4 Related Catalytic Enantioselective Alkylation of Alkenes with Alkylaluminums

The zirconocene-catalyzed enantioselective carbomagnesation accomplishes the addition of an alkylmagnesium halide to an alkene, where the resulting product is suitable for a variety of additional functionalization reactions (see Scheme 4.5). Excellent enantioselectivity is obtained in reactions with Et-, *n*-Pr- and *n*-BuMgCl, and the catalytic resolution processes allow for preparation of a variety of non-racemic heterocycles. Nonetheless, the development of reaction processes where a larger variety

of olefinic substrates and alkylmetals (*e.g.*, Me-, vinyl-, phenylmagnesium halides, etc.) can be added to unfunctionalized alkenes efficiently and enantioselectively, stands as a challenging goal in enantioselective reaction design.

As illustrated below [eq. (h)–(i)], recent reports by Negishi and co-workers, where Erker's nonbridged chiral zirconocene **69** [32] is used as catalyst, constitute an important and impressive step towards this end [33]. An impressive range of alkylaluminum reagents can be added with high efficiency and excellent enantioselectivity (>90% ee). A remarkable aspect of this work is that, through a change in reaction medium (1,1,1-trichloroethane is used as solvent), catalytic alkylations proceed through carbometallation of the alkene (direct addition of cationic alkylzirconium to the alkene, followed by Zr–Al ligand exchange) rather than involving the formation of a metallacyclopentane; under conditions that zirconacyclopentanes serve as intermediates, selectivities are notably lower. Another notable aspect of the Negishi work is that the use of Erkers' system appears to be imperative: with the aforementioned (EBTHI)Zr as catalyst, alkylations are not as efficient or stereoselective.

In 1997, Whitby reported that treatment of 2,5-dihydrofuran with Et_3Al in the presence of 5 mol % **62** leads to the enantioselective formation of **70**, rather than the product obtained from catalytic carbomagnesations (**71**) [34]. This outcome can be rationalized based on Dzhemilev's pioneering report that with Et_3Al, in contrast to EtMgCl (see Scheme 4.7), the intermediate aluminacyclopentane (*i*) is converted to the corresponding aluminaoxacyclopenatane (*ii*). To ensure the predominant formation of **70**, however, catalytic alkylations must be carried out in the absence of any solvent.

4.5 Ni-CATALYZED STEREOSELECTIVE ALKYLATION OF ALKENES WITH GRIGNARD REAGENTS

In the Zr-catalyzed enantioselective alkylation reactions discussed above, we discussed transformations that involve the addition of alkylmagnesium halides and alkylaluminum reagents to olefins. With the exception of studies carried out by Negishi and co-workers, all other processes

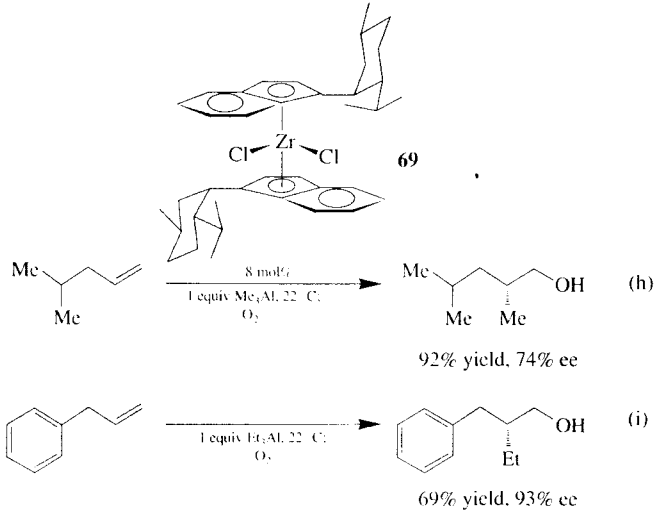

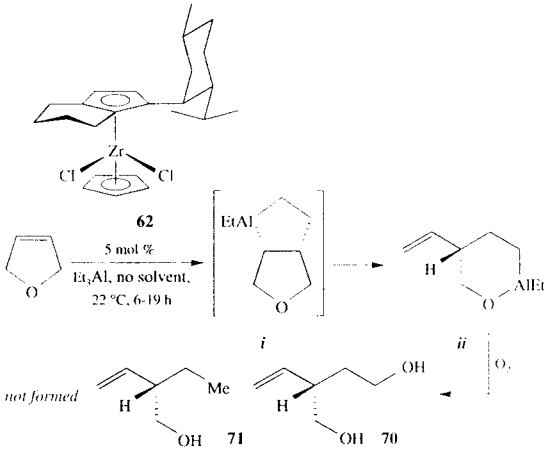

SCHEME 4.13

involve the reaction of a C–C π system that is adjacent to a C–O bond. Also with the exception of the Negishi study (eq. (h) and (i)), where direct alkene carbometallation occurs, all enantioselective alkylations involve the intermediacy of a metallacyclopentane (cf. Scheme 4.7). In this segment of our discussion, we will examine the Ni-catalyzed addition of hard nucleophiles (*e.g.*, alkylmagnesium halides) to alkenes that bear a neighboring C–O unit. These reactions transpire by neither of the above two mechanistic manifolds (metallacyclopentane intermediacy or direct carbometallation). Rather, these processes take place via a Ni-π-allyl complex.

Allylic ethers and alcohols have long been known to react with Grignard reagents in the presence of an appropriate Ni-based complex containing phosphine ligands [35]. These reactions are related to the well-studied Pd-catalyzed allylic substitution reactions that utilize soft nucleophiles [36], and a number of important mechanistic studies on the stereochemical outcome of this class of transformations have been carried out [37].

In general, the catalytic cycle for the transition-metal catalyzed allylic substitution reactions involves initial attack of the metal at the double bond followed by oxidative insertion into the antiperiplanar C–O bond to afford the π-allyl system. At this point, depending on whether soft or hard nucleophiles are used, however, the alkylation reaction proceeds through distinctly different pathways. As shown in Scheme 14, with soft nucleophiles, where Pd is often the metal center of choice, reactions proceed by the backside addition of the nucleophile to the π-allyl system, to afford the new C–C bond with net retention of stereochemistry. However, with hard nucleophiles, where Ni can serve as an effective transition metal template, the reaction usually involves the initial addition of the alkylmetal to the transition metal center, followed by a reductive elimination to lead to the generation of the C–C bond. Such reactions, as a result, take place with net inversion of stereochemistry.

From a catalytic enantioselective reaction design point of view, the latter class of reactions present a more attractive strategy for the transfer of chirality from chiral ligands on the metal to the C–C bond forming event. Indeed, a number of research teams have developed ingenious ligands that overcome the geometric distances that exist in the anti addition of soft nucleophiles to metal-π-allyl systems—a factor that is expected to diminish the asymmetric induction that may be caused by

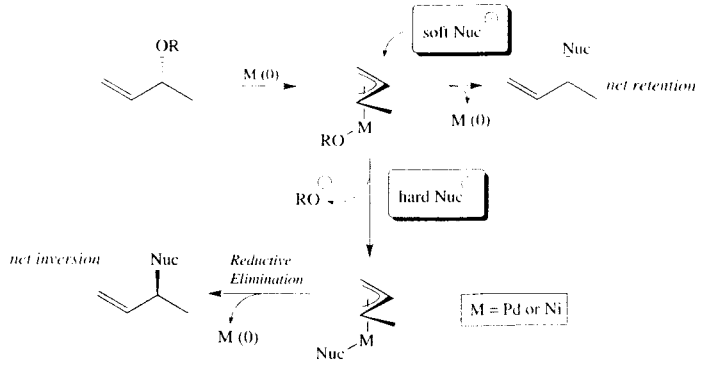

SCHEME 4.14

the metal's chiral ligands [38]. With the reaction of hard nucleophiles, since the alkyl group adds from the same environment inhabited by the metal's chiral ligands, the influence of such ligands in transfering their chirality should be more pronounced.

4.5.1 Diastereoselective Ni-Catalyzed Addition of Grignard Reagents to Allylic Ethers

4.5.1.1 Directed Ni-Catalyzed Addition of Grignard Reagents to Allylic Ethers

In 1995, we began a systematic investigation of directed Ni-catalyzed addition of Grignard reagents to allylic ethers [39]. As illustrated in Table 4.10, when allylic ether **72** is treated with 5 mol % $(PPh_3)_2NiCl_2$ and 5 equiv PhMgBr for 3 hours (THF, 22°C), products **73** and **74** are obtained in only 10% total yield and in equal amounts (3:1 *trans:cis*). In contrast, when phosphine-containing allylic ether **75** is used (entry 2, Table 4.10), **76** is formed regioselectively (**76:77**= 8 : 1) within 3 hours. Whereas ether **72** provides **73** and **74** in 10% yield, allylic substitution products from **75** (**76** and **77**) are obtained in 70–75% isolated yield. When the tether length is increased by one methylene unit (entry 3; **78** as substrate), C–C bond formation is more sluggish (24 hours for **78** vs 3 hours with **75**), but somewhat unexpectedly, regioselectivity is enhanced to >99:1.

The influence of the resident Lewis basic phosphine is especially evident in reactions where MeMgBr is used as the alkylating agent. As depicted in Table 4.11, with substrate **72**, <2% product is detected after 18 hours. In contrast, when **75** is subjected to 5 equiv MeMgBr and 5 mol % $(PPh_3)_2NiCl_2$ (THF, 22°C), **80** is obtained in 74% isolated yield. Moreover, C–C bond formation occurs with complete control of regiochemistry and the product alkene is exclusively *cis* (compare to entry 2 of Table 4.10 for related reaction of PhMgBr).

The data in Tables 4.10 and 4.11 demonstrate that the presence of a Lewis basic group within the substrate structure plays a critical role in determining both the reactivity and selectivity of the catalytic substitution reactions. A telling sign of the purported P-Ni association is that local chirality plays a crucial role in the outcome of this class of reactions. Results of our studies on the Ni-catalyzed reactions of allylic ethers **81**, **82** and **85** are summarized in Table 4.12. Silyl ether **81** is recovered unchanged after treatment with 5 mol % $(PPh_3)_2NiCl_2$ and five equiv PhMgBr (12 h). In contrast, phosphine-containing allylic ether **82** reacts smoothly to afford **83** in 85% isolated yield and with excellent control of regio-, diastereo-, and olefin stereochemistry

Table 4.10. Regioselective Ni-Catalyzed Allylic Substitution of Acyclic Ethers with PhMgBr[a]

Entry	Substrate	Product	Regioselec.[b]	c:t[c]	Yield(%)[d] Time
1	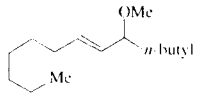 **72**	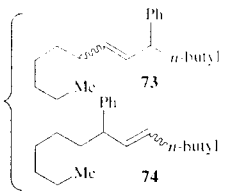 **73** **74**	**73:74** = 1:1	1:3	10, 3 h
2	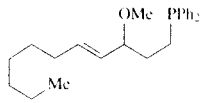 **75**	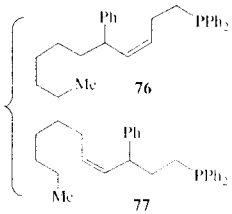 **76** **77**	**76:77** = 8:1	5:1	70 3 h
3	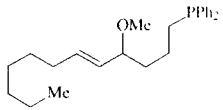 **78**	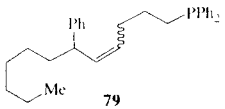 **79**	>99:1	1:1	70 24 h

[a]Conditions: 5 mol % $(Ph_3P)_2NiCl_2$, 5 equiv aryl MgBr, THF, 22°C. [b]Regioselectivity determined by GLC or ^1H NMR analysis, in comparison with authentic materials. [c]Alkene isomer ratios determined through analysis of 300 MHz ^1H NMR spectra. [d]Isolated yield after purification through silica gel chromatography.

Table 4.11. Ni-Catalyzed Allylic Substitution of Acyclic Ethers with MeMgBr[a]

Substrate	Product	Regioselec.[b]	c:t[c]	Yield(%)[d] Time
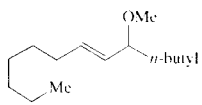 **72**	NO REACTION			— 18 h
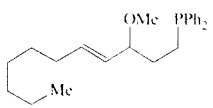 **75**	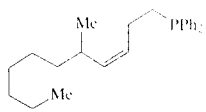 **80**	>99:1	>95:<5	74, 18 h

[a–d]See Table 4.10.

(entry 2). Similarly, catalytic reaction of **82** with MeMgBr proceeds with complete control of selectivity. When allylic ether isomer **85** is treated to Ni-catalyzed reaction conditions with PhMgBr, an equal mixture of regio- and diastereoisomers is obtained in 85% yield after chromatography. As the data in Table 4.12 show, in spite of the low levels of selectivity observed with **85**, this reaction occurs at a rate superior to those of **82**, suggesting that lack of phosphine-Ni association may not be responsible for the diminished levels of regio- and stereochemical control.

It is plausible that directed Ni-catalyzed alkylation reactions described herein proceed through a metal-π-allyl complex, such as **I** or **III** (Scheme 4.15). The stereochemical principles on which this proposal is based, are: (i) anti insertion of the transition metal into the allylic C–O bond; (ii) syn reductive elimination of the resulting π-allyl-Ni-alkyl complex [40].

The stereochemical preferences suggested above are supported by Ni-catalyzed allylic substitution reactions of cyclic ethers **88** and **90** (Scheme 4.16). Whereas reaction of **88** affords **89** in 70% yield in one hour with > 95% diastereo- and regioselectivity (5 mol % $(PPh_3)_2NiCl_2$, 22°C, THF), subjection of **90** to the same conditions results in the complete recovery of the starting material.

Table 4.12. Ni-Catalyzed Reactions of Functionalized Allylic Ethers with Ph- and MeMgBr. Effect of Local Chirality on Selectivity[a]

Entry	Substrate	Grignard reagent	Product	Regioselect.[b]	c : t[c]	ds	Yield(%)[d] time
1	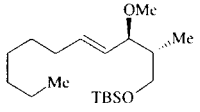 **81**	PhMgBr	NO REACTION				— 12 h
2	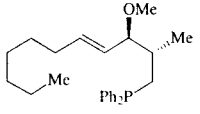 **82**	PhMgBr	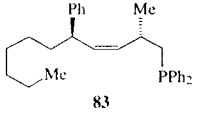 **83**	>99:1	>49:1	10:1	85 6 h
3	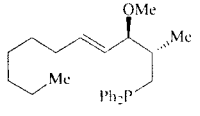 **82**	MeMgBr	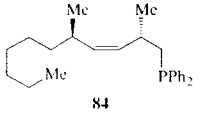 **84**	>99:1	>49:1	>49:1	75 12 h
4	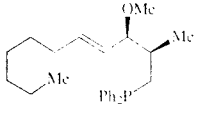 **85**	PhMgBr	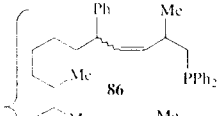 **86** + **87**	1:1		1:1	85 3 h

[a] [d]See Table 4.10

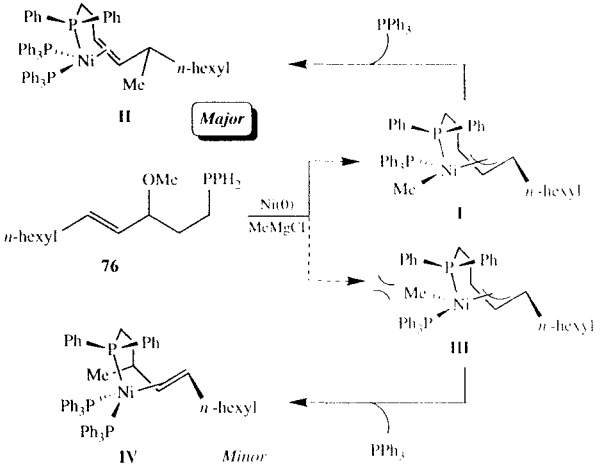

SCHEME 4.15

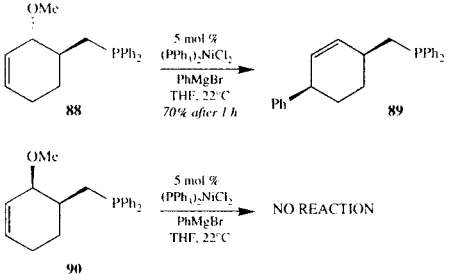

SCHEME 4.16

Intermediates **II** and **IV** in Scheme 4.15 are proposed, since positioning of the internal phosphine in the apical site of the square pyramidal complex, where the PPh_3 is *trans* to an alkyl group, is in accord with the previously suggested mechanistic paradigms [41]. It is tenable that the observed trends in regioselectivity, as suggested by molecular models, are due to unfavorable steric interactions in complex **III** between phenyl groups of the tethered diphenylphosphine and the bound PPh_3 group; such interactions exist to a lesser extent in **I**.

4.5.1.2 Ni-catalyzed Addition of Grignard Reagents to Bicyclic Allylic Ethers

More recently, Lautens and Ma have reported stereoselective Ni-catalyzed addition of Grignard reagents to oxabicyclic substrates [42]. Thus, as depicted in Scheme 4.17, treatment of **91** with MeMgBr in the presence of 2 mol % $Ni(cod)_2$ at (COD: cyclooctadiene) 22°C for nearly a day leads to the formation of **92** as a single stereoisomer in 70% yield after chromatography. These workers illustrate that the choice of Ni precatalyst and solvent is critical to the outcome of these C–C bond forming reactions. As an example, as is also illustrated in Scheme 4.17, when **91** is subjected to MeMgBr but in Et_2O and in the presence of HMPA and 2 mol % (dppp)$NiCl_2$ (dppp: diphenylphosphinopropane), a mixture of **93** and **94** is formed; in contrast, when THF is utilized as solvent, **93** is formed exclusively in 64% isolated yield. These reactions, which likely also involve the intermediacy of Ni π-allyl complexes, represent a potentially useful catalytic procedure, since the resulting products are highly functionalized unsaturated carbocycles that are formed with excellent stereocontrol. Future developments that allow the

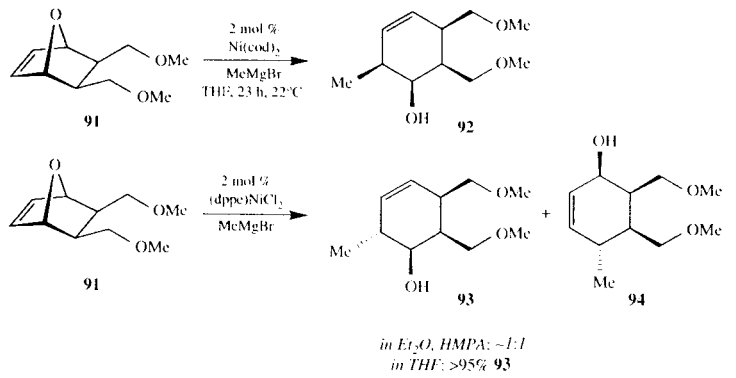

SCHEME 4.17

formation of the alkylation products in the optically pure form, should significantly enhance the utility of this method.

4.5.2 Asymmetric Ni-Catalyzed Addition of Grignard Reagents to Allylic Ethers

As illustrated in Scheme 4.18, Consiglio and coworkers have shown that in the presence of an appropriate chiral Ni catalyst, the addition of EtMgBr to cyclic allylic phenyl ethers occurs with high enantioselection and excellent yield (>84%) [43]. Thus, in the presence of 2 mol % Ni dibromide or dichloride complexes of (+)-(*R,R*)-cyclopentane-1,2-diylbis(diphenylphosphine) (**99**), reaction of cyclopentenyl ether **95** with EtMgBr results in the formation of 3-ethylcyclopentene (*S*)-**96** in 92% yield and with 83% ee. Higher levels of enantiocontrol are observed when (*R*)-6,6'-dimethylbiphenyl-2,2'-diyl)bisdiphenylphosphine (biphemp, **100**) is used as the chiral ligand: (*S*)-**96** is obtained in 93% ee and 90% yield. Variation of catalyst structures demonstrated that the enantioselectivity is dependent on steric rather than electronic factors; in contrast, the nature of the leaving group, solvent, or halide of the Grignard reagent proved not to affect the outcomes of catalytic alkylations.

Catalytic allylic substitutions with cyclohexenyl substrate **97** proceed following similar overall trends but with generally lower levels of enantioselection (Scheme 4.18). Consiglio has suggested that this difference in enantiofacial selectivity may be attributed to the more rigid allyl moiety in the five-membered ring starting material **95**. The present catalytic enantioselective C–C bond forming reaction is only appreciably enantioselective when EtMgBr is used (*e.g.*, 12% ee with MeMgBr and 71% ee with *n*-PrMgBr). Nonetheless this study represents a critical first step towards the development of this class of catalytic asymmetric reactions and does allow ready access to various optically enriched cyclic hydrocarbons.

More recently, RajanBabu has reported that in the presence of appropriate chiral Ni-based catalysts, enantioselective addition of Grignard reagents to acyclic allylic ethers may be effected (Scheme 4.19) [44]. Within this context, a systematic study of the effect of reaction solvent, leaving groups, chiral ligands and nucleophiles was undertaken. As shown in Scheme 4.19, treatment of allylic ether **101** with EtMgBr in the presence of 5 mol % of (*S,S*)-chiraphos-Ni complex (formed upon treatment of $Ni(cod)_2$ with (*S,S*)-chiraphos **102**) results in the formation of (*R*)-**103** in 79% ee and 78% yield.

A significant corollary to the RajanBabu study is that the Ni-catalyzed allylic substitution may be

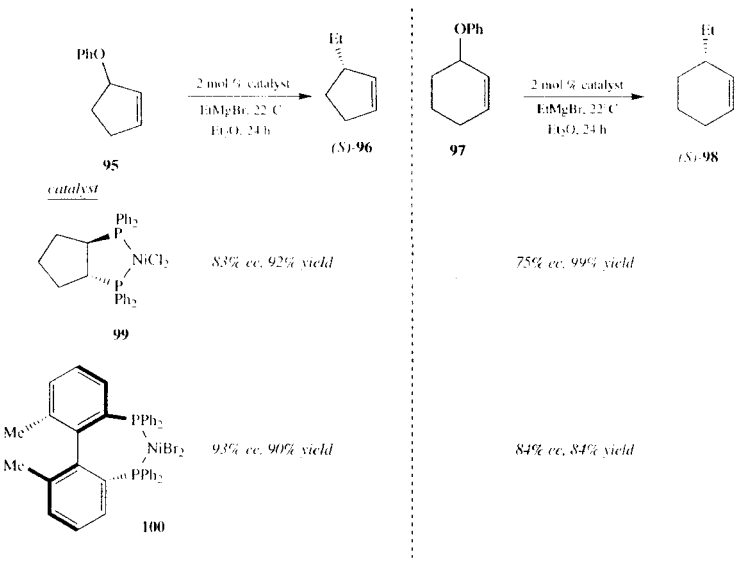

SCHEME 4.18

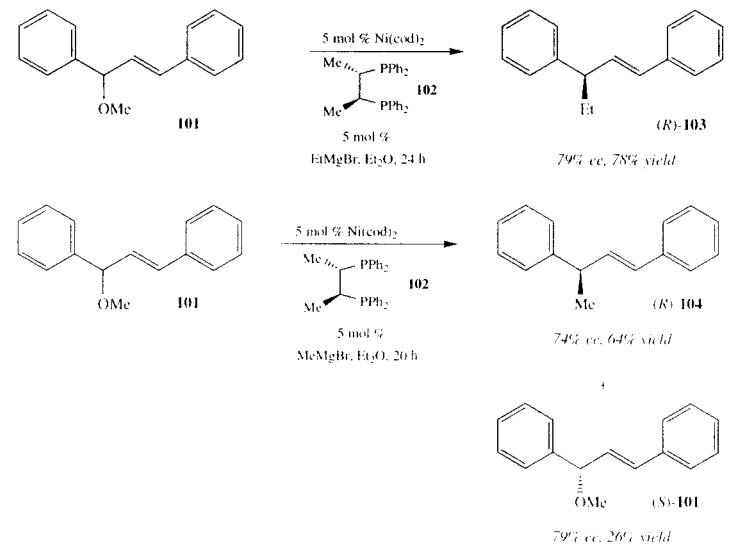

SCHEME 4.19

used in the catalytic kinetic resolution of related chiral allylic ethers. That is, under the same reaction conditions as described above, the allylic ether substrate is recovered in 79% ee (26% yield); furthermore, the alkylation product is isolated in 74% ee and 64% yield. These data in relation to Ni-catalyzed kinetic resolution of acyclic allylic ethers are particularly noteworthy in light of the fact that Consiglio had originally reported that in the catalytic alkylation of racemic 1-phenoxycycloalkenes, there is little or no rate difference between the transformations of the two substrate enantiomers [45]. Since a Ni-π-allyl intermediate is likely to be formed in these reactions, such kinetic resolution data suggest that, at least in certain systems, the ionization step can be enantioselective and could be exploited for control of stereoselectivity.

4.5.3 Asymmetric Ni-Catalyzed Addition of Grignard Reagents to Allylic Acetals

Research in our laboratories has been directed towards the development of Ni-catalyzed and enantioselective addition of Grignard reagents to allylic acetals. In the presence of appropriate Ni complexes (*e.g.*, $(dppe)NiCl_2$), (dppe: diphenylphosphinoethane) these reactions proceed with excellent regioselectivity. As illustrated in Scheme 4.20, we recently established that when cyclopentenyl acetal **105** is treated with EtMgCl in the presence of (*S,S*)-chiraphos$NiCl_2$, (*S*)-**107** is obtained in 53% ee and 85% yield [46]. When the chiral catalyst is prepared in situ, by premixing of $(PPh_3)_2NiCl_2$ and (*S,S*)-chiraphos, enantioselectivity drops to 15%, as there is ~25% background reaction in the presence of $(PPh_3)_2NiCl_2$. When cyclohexenyl acetal **106** is treated with (*S,S*)-chiraphos$NiCl_2$, **108** is obtained in only 11% ee and 80% yield. Remarkably, when the *in situ* method is utilized, (*S*)-**108** is formed in 85% ee (90% yield). Control experiments clearly indicate that it is the excess PPh_3 present in the *in situ* method which is responsible for the dramatic improvement in enantioselection. That there is no diminution of selectivity with the *in situ* method is consistent with the fact that six-membered ring acetals are inert towards alkylmagnesium halides in the presence of $(PPh_3)_2NiCl_2$. The notable enhancement in selectivity is intriguing and unexpected, however.

A better understanding of the above mechanistic dilemma will require future detailed mechanistic studies. Nonetheless, as shown in Scheme 4.21, a variety of Grignard reagents can be used in these Ni-catalyzed enantioselective alkylations to afford a range of non-racemic materials in excellent yield.

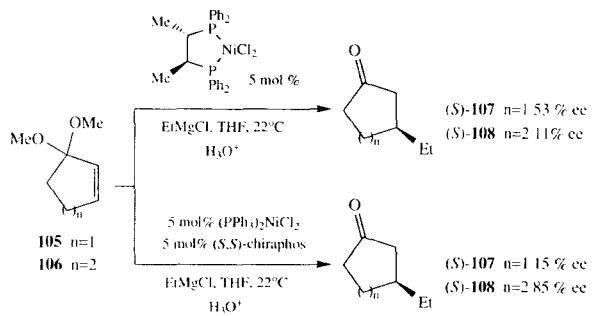

SCHEME 4.20

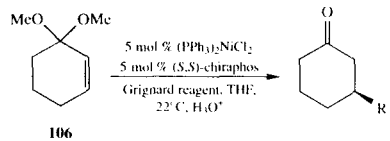

106

Grignard Reagent	*ee, yield (%)*
*n*BuMgCl	85, 85
PhMgBr	83, 67
$PhCH_2CH_2MgBr$	84, 81

SCHEME 4.21

4.6 SUMMARY AND OUTLOOK

The chemistry described in this article demonstrates that chiral metallocene and Ni-phosphine complexes can be used to effect an important reaction that is largely unprecedented in classical organic chemistry: addition of alkylmagnesium halides to unactivated alkenes. Although EBTHI metallocenes have proven to be effective at promoting the above enantioselective transformations, the equipment required to prepare such catalysts (glovebox and high-pressure hydrogenation apparatus), as well as costs associated with the required metallocene resolution (non-racemic binaphthol = \$45/1 g) suggest that more attractive catalyst alternatives may be desired. Promising advances toward more facile syntheses of inexpensive and chiral $(EBTHI)MX_2$ equivalents may eventually provide more practical alternatives to this powerful class of transition metal catalyst. As discussed above, recent advances in the use of nonbridged metallocenes, where a resolution step is obviated, may also provide attractive and effective solutions to this problem.

The chemistry reviewed in this article demonstrates a variety of formerly-inaccessible protocols which are now available that afford C–C bonds in an enantioselective manner. However, we are a long way away from having reached a point where sufficiently diverse protocols are available that will allow us to catalytically and enantioselectively alkylate a considerable range of alkene substrates with almost any alkylmetal system. To reach this goal, metals other than Zr, Ni, Mg and Al may have to be brought into the fold. There is thus little doubt that future exciting discoveries in the area of design and development of useful asymmetric catalytic C–C bond forming transformations are in the making.

ACKNOWLEDGEMENTS

The National Institutes of Health (GM-47480) and the National Science Foundation (CHE-9257580 and CHE-9632278) provide generous support of our programs. Additional support from Pfizer, Johnson & Johnson, Eli Lilly, Zeneca, Glaxo, Monsanto, Sloan and Dreyfus Foundations and the Spanish Ministry of Education are acknowledged. We are most grateful to our co-workers and colleagues Zhongmin Xu, James P. Morken, Ahmad F. Houri, Mary T. Didiuk, Michael S. Visser, Joseph P. A. Harrity, Charles W. Johannes, Daniel C. La, Enrique-Bengoa Gomez, Gabriel A. Weatherhead, Courtney Luchaco, Nina R. Horan, Derek A. Cogan and John D. Gleason for their important contributions to various aspects of the projects described herein.

REFERENCES

1. For general overview of recent advances in this area, see: *Catalytic Asymmetric Synthesis*, Ojima, I. Ed.; VCH Publishers: New York Weinheim, Cambridge **1993**.
2. For a recent review on asymmetric conjugate addition, see: (a) Rossiter, B.E., Swingle, N.M. *Chem. Rev.* **1992**, *92*, 771–806. For catalytic asymmetric conjugate addition of 'soft' nucleophiles, see: Sawamura, M., Hamashima, H., Shinoto, H., Ito, Y. *Tetrahedron Lett.* **1995**, *36*, 6479–6482. (b) Sasai, H., Arai, T., Shibasaki, M.J. *Am. Chem. Soc.* **1994**, *116*, 1571–1572. (c) Conn, R.S.E., Lovell, A.V., Karady, S., Weinstock, L.M. *J. Org. Chem.* **1986**, *51*, 4710–4711. For reactions involving 'hard' nucleophiles, see: (d) Zhou, Q-L., Pfaltz, A. *Tetrahedron Lett.* **1993**, *34*, 7725–7728. (e) Kanai, M., Tomioka, K. *Tetrahedron Lett.* **1995**, *36*, 4275–4278. (f) de Vries, A.H.M., Meetsma, A., Feringa, B.L., *Angew. Chem., Int. Ed. Engl.* **1996**, *35*, 2374–2376. (g) Feringa, B.L., Pineschi, M., Arnold, L.A.,

Imbos, R., de Vries, A.H.M. *Angew. Chem., Int. Ed. Engl.* **1997**, *36*, 2620–2623. (h) Solomon, M., Jamison, W.C.L., McCormick, M., Liotta, D., Cherry, D.A., Mills, J.E., Shah, R.D., Rodgers, J.D., Maryanoff, C.A., *J. Am. Chem. Soc.* **1988**, *110*, 3702–3704. (i) Swiss, K.A., Liotta, D.C., Maryanoff, C.A. *J. Am. Chem. Soc.* **1990**, *112*, 9393–9394. (j) Swiss, K.A., Hinkley, W., Maryanoff, C.A., Liotta, D.C. *Synthesis* **1992**, 127–131.

3. Eisch, J.J., Husk, G.R. *J. Am. Chem. Soc.* **1965**, *87*, 4194–4195.
4. Hoveyda, A.H., Evans, D.A., Fu, G.C. *Chem. Rev.* **1993**, *93*, 1307–1370.
5. (a) Eisch, J.J., J.H.J. Merkley. *Organomet. Chem.* **1969**, 20, 27–31. (b) Eisch, J.J., Merkley, J.H. *J. Am. Chem. Soc.* **1979**, *101*, 1148–1155. (c) Eisch, J.J. *J. Organomet. Chem.* **1980**, *200*, 101–117 and references cited therein.
6. Cherest, M., Felkin, H., Frajerman, C., Lion, C., Roussi, G., Swierczewski, G. *Tetrahedron Lett.* **1966**, 875–879.
7. Felkin, H., Kaeseberg, C. *Tetrahedron Lett.* **1970**, 4587–4590.
8. (a) Richey, H.G., Domalski, M.S., *J. Org. Chem.* **1981**, *46*, 3780–3783. (b) Von Rein, F.W., Richey, H.G. *Tetrahedron Lett.* **1971**, 3777–3780. (c) Richey, H.G., Von Rein, F.W. *J. Organometal. Chem.* **1969**, 32–35.
9. Richey, H.G., Erickson, W.F., Heyn, A.S. *Tetrahedron Lett.* **1971**, *24*, 2183–2186.
10. (a) Dzhemilev, U.M., Vostrikova, O.S., Sultanov, R.M. *Izv. Akad. Nauk SSSR. Ser. Khim.* **1983**, *32*, 218–220. (b) Dzhemilev, U.M., Vostrikova, O.S., Sultanov, R.M., Kukovinets, A.G., Khalilov, A.M. *Izv. Akad. Nauk SSSR. Ser. Khim.* **1983**, *32*, 2053–2060. (c) Dzhemilev, U.M., Vostrikova, O.S. *J. Organomet. Chem.* **1985**, *285*, 43–51, and references cited therein. (d) Dzhemilev, U.M., Ibragimov, A.G., Zolotarev, A.P., Mulukhov, R.R., Tolstikov, G.A., *Izv. Akad. Nauk SSSR. Ser. Khim.* **1989**, *38*, 207–208. (e) Dzhemilev, U.M., Sultanov, R.M., Gaimaldinov, R.G., Tolstikov, G.A., *Izv. Akad. Nauk SSSR. Ser. Khim.* **1991**, *40*, 1388–1393.
11. (a) Hoveyda, A.H., Xu, Z. *J. Am. Chem. Soc.* **1991**, *113*, 5079–5080. (b) A.F. Houri, M.T. Didiuk, Z. Xu, N.R. Horan, A.H. Hoveyda *J. Am. Chem. Soc.* **1993**, 115, 6614–6624.
12. (a) Houri, A.F., Xu, Z., Cogan, D.A., Hoveyda, A.H. *J. Am. Chem. Soc.* **1995**, *117*, 2943–2944. (b) Xu, Z., Johannes, C.W., Houri, A.F., La, D.S., Cogan, D.A., Hofilena, G.E., Hoveyda, A.H., *J. Am. Chem. Soc.* **1997**, *119*, 10302–10316. See also: Schmalz, H-G. *Angew. Chem., Int. Ed. Engl.* **1995**, *34*, 1833–1836.
13. For representative examples where THF alters selectivity, presumably through its deleterious influence on internal chelation, see: (a) (involving Li) Overman, L.E., McCready, R.J. *Tetrahedron Lett.* **1982**, *23*, 2355–2358. (b) (involving Mg) Keck, G.E., Boden, E.P. *Tetrahedron Lett.* **1984**, *25*, 265–268.
14. Morken, J.P., Didiuk, M.T., Hoveyda, A.H. *J. Am. Chem. Soc.* **1993**, *115*, 6997–6998. See also: Schmalz, H-G. *Nachr. Chem. Tech. Lab.* **1994**, *42*, 724–729.
15. Hoveyda, A.H., Morken, J.P., *J. Org. Chem.* **1993**, *58*, 4237–4244.
16. Didiuk, M.T., Johannes, C.W., Morken, J.P., Hoveyda, A.H. *J. Am. Chem. Soc.* **1995**, *117*, 7097–7104.
17. (a) Guram, A.S., Jordan, R.F. *Organometallics* **1990**, *9*, 2190–2192. (b) *ibid.* **1991**, *10*, 3470–3479.
18. (a) Fu, G.C., Grubbs, R.H. *J. Am. Chem. Soc.* **1992**, *114*, 7324–7325. (b) Fu, G.C., Grubbs, R.H. *J. Am. Chem. Soc.* **1993**, *115*, 3800–3801. (c) Grubbs, R.H., Miller, S.J., Fu, G.C., *Acc. Chem. Res.* **1995**, *28*, 446–452 and references cited therein. (d) Schmalz, H-G. *Angew. Chem.* **1995**, *107*, 1981–1984; *Angew. Chem., Int. Ed. Engl.* **1995**, *34*, 1833–1836 and references cited therein. (e) Schrock, R.R., Murdzek, J.S., Bazan, G.C., Robbins, J., DiMare, M., M. O'Regan *J. Am. Chem. Soc.* **1990**, *112*, 3875–3886. (f) Bazan, G.C., Schrock, R.R., Cho, H.-N., Gibson, V.C. *Macromolecules* **1991**, *24*, 4495–4502.
19. Visser, M.S., Heron, N.M., Didiuk, M.T., Sagal, J.F., Hoveyda, A.H., *J. Am. Chem. Soc.* **1996**, *118*, 4291–4298.
20. Morken, J.P., Didiuk, M.T., Visser, M.S., Hoveyda, A.H. *J. Am. Chem. Soc.* **1994**, *116*, 3123–3124.
21. Heron, N.M., Adams, J.A., Hoveyda, A.H., *J. Am. Chem. Soc.* **1997**, *119*, 6205–6206.
22. Visser, M.S., Hoveyda, A.H., *Tetrahedron* **1995**, *51*, 4383–4394.
23. Bell, L., Whitby, R.J., Jones, R.V.H., Standen, M.C.H. *Tetrahedron Lett.* **1996**, *37*, 7139–7142.
24. (a) Martin, V.S., Woodard, S.S., Katsuki, T., Yamada, Y., Ikeda, M., Sharpless, K.B. *J. Am. Chem. Soc.* **1981**, *103*, 6237–6240. (b) Gao, Y., Hanson, R.M., Klunder, J.M., Ko, S.Y., Masamune, H., Sharpless, K.B. *J. Am. Chem. Soc.* **1987**, *109*, 5765–5780.
25. For a review of kinetic resolution, see: (a) Kagan, H.B., Fiaud, J.C. *Top. Stereochem.* **1988**, *18*, 249–330. (b) Finn, M.G., Sharpless, K.B. In *Asymmetric Synthesis*, Morrison, J.D., Ed.; Academic Press: New York, 1985; 247–308.
26. Kitamura, M., Kasahara, I., Manabe, K., Noyori, R., Takaya, H. *J. Org. Chem.* **1988**, *53*, 708–710. For Pd-catalyzed enantioselective synthesis of cyclic allylic esters, see: Trost, B.M., Organ, M.G. *J. Am. Chem. Soc.* **1994**, *116*, 10320–10321.
27. Harrity, J.P.A., Visser, M.S., Gleason, J.D., Hoveyda, A.H. *J. Am. Chem. Soc.* **1997**, *119*, 1488–1489.

28. For the Mn-catalyzed kinetic resolution of 2,2-disubstituted chromenes, see: Vander Velde, S.L., Jacobsen, E.N. *J. Org. Chem.* **1995**, *60*, 5380–5381.
29. G. Van Lommen, De Bruyn, M., Schroven, M. *J. Pharm. Belg.* **1990**, *45*, 355–360 and references cited therein.
30. Johannes, C.W., Visser, M.S., Weatherhead, G.A., Hoveyda, A.H., *J. Am. Chem. Soc.* **1998**, *120*, 8340–8347.
31. Chin, B., Buchwald, S.L. *J. Org. Chem.* **1996**, *61*, 5650–5651.
32. Erker, G., Aulbach, M., Knickmeier, M., Wingbermuhle, D., Kruger, C., Nolte, M., Werner, S. *J. Am. Chem. Soc.* **1993**, *115*, 4590–4601.
33. (a) Kondakov, D.Y., Negishi, E. *J. Am. Chem. Soc.* **1995**, 117, 10771–10772. (b) Kondakov, D.Y., Negishi, E. *J. Am. Chem. Soc.* **1996**, *118*, 1577–1578. See also: Kondakov, D.Y., Wang, S., Negishi, E. *Tetrahedron Lett.* **1996**, *37*, 3803–3806.
34. Dawson, G., Durrant, C.A., Kirk, G.G., Whitby, R.J., Jones, R.V.H. Standen, M.C.H. *Tetrahedron Lett.* **1997**, *38*, 2335–2338.
35. (a) Takahashi, K., Miyake, A., Hata, G. *Bull. Chem. Soc. Jpn* **1972**, *45*, 230–236. (b) Chuit, C., Felkin, H., Frajerman, C., Roussi, G., Swierczewski, G. *Chem. Commun.* **1968**, 1604–1605. (c) Felkin, H., Swierczewski, G.*Tetrahedron* **1975**, *31*,2735–2748. (d) Chuit, C., Felkin, H., Frajerman, C., Roussi, G., Swierczewski, G. *J. Organomet. Chem.* **1977**, *127*, 371–384. (e) Buckwalter, B.L., Burfitt, I.R., Felkin, H., Joly-Goudet, M., Naemura, K., Salomon, M.F., Wenkert, E., Wovkulich, P.M. *J. Am. Chem. Soc.* **1978**, *100*, 6445–6450.
36. For an excellent recent review, see: Trost, B.M., Van Vranken, D.L. *Chem. Rev.* **1996**, *96*, 395–422.
37. Consiglio, G., Waymouth, R.M. *Chem. Rev.* **1989**, *89*, 257–276.
38. For example, see: (a) Hayashi, T., Yamamoto, A., Ito, Y., Nishioka, E., Miura, H., Yanagi, K. *J. Am. Chem. Soc.* **1989**, *111*, 6301–6311. (b) Sawamura, M., Nagata, H., Sakamoto, H., Ito, Y. *J. Am. Chem. Soc.* **1992**, *114*, 2586–2592.
39. Didiuk, M.T., Morken, J.P., Hoveyda, A.H., *J. Am. Chem. Soc.* **1995**, *117*, 7273–7274. (b) Didiuk, M.T., Morken, J.P., Hoveyda, A.H. *Tetrahedron* **1998**, *54*, 1117–1130.
40. Tatsumi, K., Nakamura, A., Komiya, S., Yamamoto, A., Yamamoto, T. *J. Am. Chem. Soc.* **1984**, *106*, 8181–8188.
41. (a) Tatsumi, K., Nakamura, A., Komiya, S., Yamamoto, A. Yamamoto, T. *J. Am. Chem. Soc.* **1984**, *106*, 8181–8188. See also: (b) Hayashi, T., Konishi, M., Kumada, M. *J. Organomet. Chem.* **1980**, *186*, C1-C4. (c) Felkin, H., Joly-Goudket, M., Davies, S.G. *Tetrahedron Lett.* **1981**, 22, 1157–1160. (d) Consiglio, G., Morandini, F., Piccolo, O. *J. Chem. Soc., Chem. Commun.* **1983**, 112–114. (e) Hayashi, T., Konishi, M., Yokota, K-I., Kumada, M. *J. Organomet. Chem.* **1985**, *285*, 359–373. (f) Consiglio, G., Piccolo, O., Roncetti, L. *Tetrahedron* **1986**, *42*, 2043–2053. (g) For an excellent review, see: Consiglio, G., Waymouth, R.M., *Chem. Rev.* **1989**, *89*, 257–276.
42. Lautens, M., Ma, S. *J. Org. Chem.* **1996**, *61*, 7246–7247.
43. (a) Consiglio, G., Indolese, A. *Organometallics* **1991**, *10*, 3425–3427. (b) Indolese, A.F., Consiglio, G. *Organometallics* **1994**, *13*, 2230–2234.
44. Nomura, N., RajanBabu, T.V., *Tetrahedron Lett.* **1997**, *38*, 1713–1716.
45. (a) Consiglio, G., Piccolo, O., Roncetti, L., Morandini, F. *Tetrahedron* **1986**, *42*, 2043. (b) Consiglio, G., Morandini, F., Piccolo, O. *Helv. Chim. Acta* **1980**, *63*, 987–989. (c) Consiglio, G., Morandini, F., Piccolo, O. *J. Chem. Soc. Chem. Commun.* **1983**, 112–114.
46. Gomez-Bengoa, E., Heron, N.M., Didiuk, M.T., Luchaco, C.A., Hoveyda, A.H. *J. Am. Chem. Soc.* **1998**, *120*, 7649–7650.

5

Stereoselective Additions of Chiral Grignard Reagents to Aldehydes: Stereochemical and Mechanistic Principles, with Examples Using α-Amino Grignard Reagents

Robert E. Gawley
Department of Chemistry, University of Miami, USA

5.1 INTRODUCTION TO STEREOSELECTIVITY IN GRIGNARD ADDITIONS[1]

In general, the steric course of addition of a nucleophile to a carbonyl can fall into one of several categories.[2] From the stereochemical standpoint, the most simple is the addition of an achiral nucleophile to a carbonyl whose faces are homotopic, in which case the product is achiral. The addition of phenylmagnesium bromide to acetone (Scheme 5.1a) falls into this category. If the two carbonyl faces are enantiotopic, addition to the *Re* or *Si* faces affords transition states that are chiral and enantiomeric. The addition of phenylmagnesium bromide to acetaldehyde (Scheme 5.1b) is an example of this type of reaction. In an achiral solvent, the two transition states will be isoenergetic (*i.e.* $\Delta\Delta G^{\ddagger} = 0$), and the two enantiomers of the product will be formed in equal amounts.[3] In order for the product ratio to be $\neq 1$, the energies of activation must be different. To render the transition states diastereomeric ($\Delta\Delta G^{\ddagger} \neq 0$), there must be an additional element of chirality. This additional element could be in either of the reactants

[1] Another review on stereoselective additions of chiral α-aminoorganometallics, which includes a literature review of α-aminoorganolithium additions, along with mechanistic rationales and synthetic applications, will appear separately [1].

[2] For detailed glossaries of stereochemical terminology, see pp. 15–40 of ref. [2] and pp.1191–1210 of ref. [3].

[3] In some cases, there may be only one product. For example, the addition of methyllithium to acetaldehyde affords the same product by addition to either (heterotopic) carbonyl face. The transition states are nevertheless enantiomeric due to differing bond lengths between the carbonyl carbon and the two methyls.

Grignard Reagents: New Developments Edited by Herman G. Richey, Jr © 2000 John Wiley & Sons Ltd.

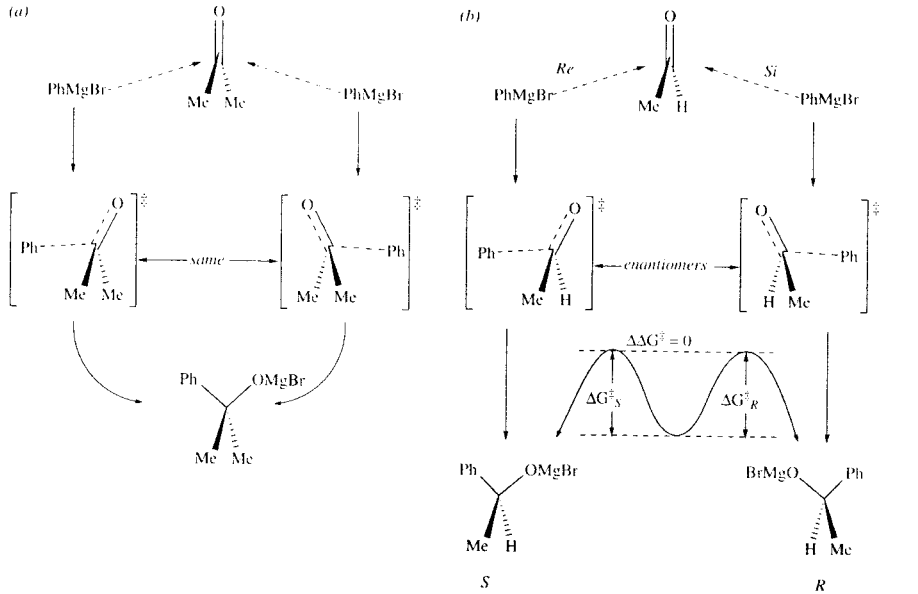

SCHEME 5.1. (a) Addition of phenylmagnesium bromide to either of the homotopic faces of acetone affords identical transition states. (b) Addition of phenylmagnesium bromide to the enantiotopic faces of acetaldehyde affords enantiomeric transition states.

(organometallic or carbonyl), the solvent, or a catalyst, as illustrated by the following examples.

In the early 1950s, several groups began to analyze the factors affecting the stereoselective addition of a nucleophile to faces of carbonyl compounds that are diastereotopic by virtue of a proximate stereocenter. Principal among these were the efforts of Curtin [4], Cram [5] and Prelog [6]. These types of additions may be generalized as shown in Scheme 5.2. If the addition is irreversible (*i.e.*, under kinetic control), the difference in free energy of activation, $\Delta\Delta G^{\ddagger}$, determines the product ratio. Often, the factors that influence the *Re/Si* face-selectivity are complex. For example, in the case of Cram's rule [5], it has taken 40 years to derive a mechanistically sound rationale for the steric course of the addition.[4]

[4] For a history of the evolution of Cram's rule, from 1952 to 1993, see pp. 121–130 of ref. [2].

Another way to render the carbonyl faces diastereotopic is by complexation of a chiral Lewis acid to the carbonyl oxygen. This is the approach taken in, for example, the asymmetric diethylzinc reaction, as shown in Scheme 5.3 [7]. For reviews of such processes, see ref. [8–12], Chapter 5 in ref. [13] and pp 137–141 of ref. [2].

Yet another way to render the transition states diastereomeric is to employ a chiral nucleophile (Scheme 5.4). One such class is organolithium and organomagnesium (Grignard) reagents in which the carbon bearing the metal is sp^3 hybridized and stereogenic. Although many secondary organolithium and Grignard reagents are chiral (*e.g. sec*-BuLi), much of the progress in stereoselective reactions of chiral organometallics has occurred in species containing a heteroatom in the position alpha to the metal. The heteroatom may be a first-row element such as nitrogen or oxygen, or main group elements such as phosphorus, sulfur,

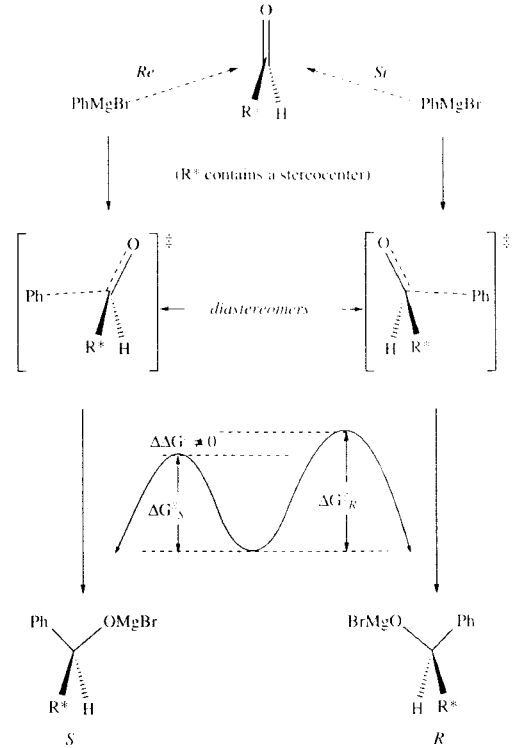

SCHEME 5.2. Addition of phenylmagnesium bromide to a chiral aldehyde affords diastereomeric transition states.

selenium, or tellurium.[5] In this review, I will focus on nitrogen as the heteroatom.

5.2 TRANSITION STATES AND MECHANISTIC RATIONALES

It is of interest to analyze the possible transition state assemblies of additions of chiral Grignard reagents having a stereogenic metal-bearing carbon, with the aim of rationalizing the steric course of the addition. In considering the mechanistic details of such additions, one must ask the following questions:

1. Is the Grignard configurationally stable at the metal-bearing carbon? If so, what is the absolute configuration?
2. Does the addition occur by a polar pathway or a single electron transfer (SET) redox reaction, followed by a radical coupling?
3. If polar, does the addition to a carbonyl occur with retention or inversion at the carbanionic carbon?
4. Is there a preferred topicity for the addition? (*i.e.*, Does the *R* organometallic add to the *Re* face or *Si* face of the aldehyde?)

[5] For numerous reviews of heteroatom-stabilized carbanions, see volumes 1 and 3 of ref. [14].

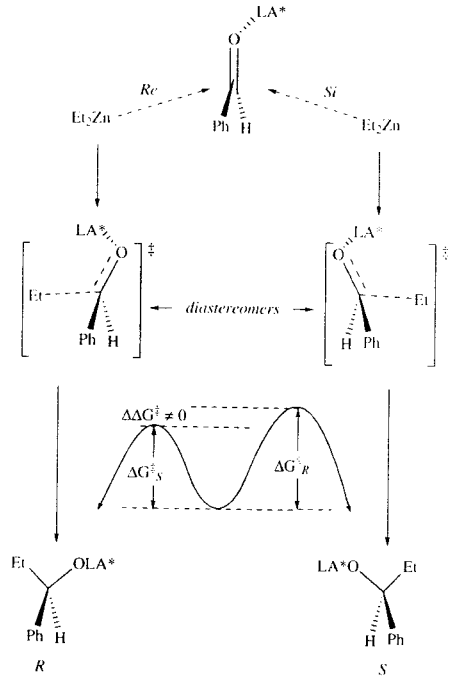

SCHEME 5.3. Addition of diethylzinc to benzaldehyde, catalyzed by chiral Lewis acids [7].

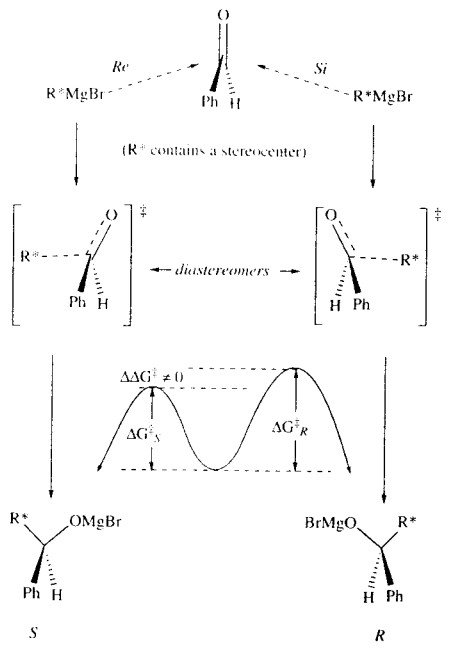

SCHEME 5.4. Addition of a chiral Grignard reagent to benzaldehyde affords diastereomeric transition states.

These considerations are illustrated in Scheme 5.5 for α-aminoorganometallics in general. Depending on the method of metalation, the configuration of the α-aminoorganometallic (boxed) may not be known, and its configurational stability may not be immediately obvious. Nevertheless, in reacting with an electrophile, there are two major pathways that can be followed: a polar addition and a radical mechanism involving oxidation of the carbanion by the electrophile (SET). Scheme 5.5 illustrates an aldehyde as an electrophile because analysis of the ratio of the four possible diastereomeric products may provide an opportunity to determine the mechanistic pathway(s) being followed. For example, if the organometallic is configurationally stable, a polar pathway proceeding with retention of configuration at the carbanionic carbon would give a mixture of the *R,R* and *R,S* addition products. If the configuration of the organometallic is known, then one can deduce the steric course at the carbanionic carbon. Conversely, a configurationally labile carbanion that adds with a given topicity, might give a predominance of the *R,R*/*S,S* pair over the *R,S*/*S,R* pair (or vice versa), but the steric course (inversion *vs.* retention) may not be discernible.

For a radical pathway, two assumptions can be made: (1) pyramidal inversion (and translational motion in the solvent cage) of a free radical is faster than coupling to the aldehyde ketyl, and (2) radical coupling will show poor selectivity in adding to heterotopic carbonyl faces.[6] Under these conditions, an SET path would give an equimolar mixture of all four products.

[6] Stereoselective radical couplings are currently being developed. For reviews, see ref. [15–17].

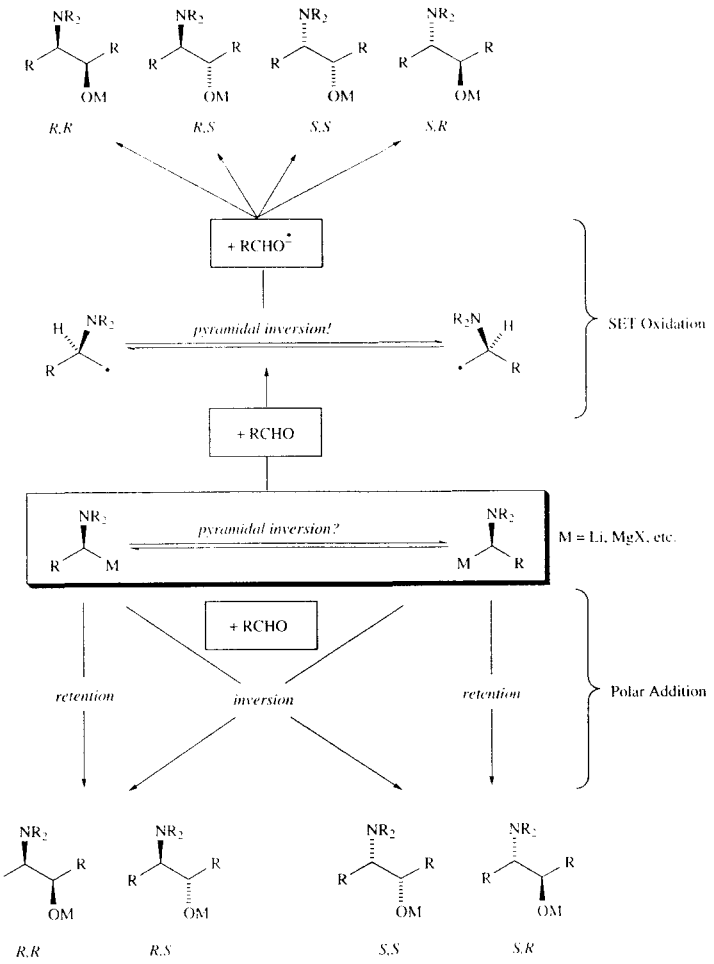

SCHEME 5.5. Mechanistic possibilities for the polar addition of a chiral α-aminoorganometallic to an aldehyde.

Two final points should be made clear. First, the analysis outlined above is only complete if the organometallic is not racemic; otherwise, using the steric course of the reaction to elucidate mechanism is limited. Second, this analysis assumes a monomeric species; Schlenk equilibria and other aggregation phenomena may complicate matters.

5.3 TOPICITY AND TERMINOLOGY

Before proceeding further, it is necessary to define the terminology that will be used to describe relative configuration and topicity in these reactions. In 1982, Prelog and Helmchen proposed the

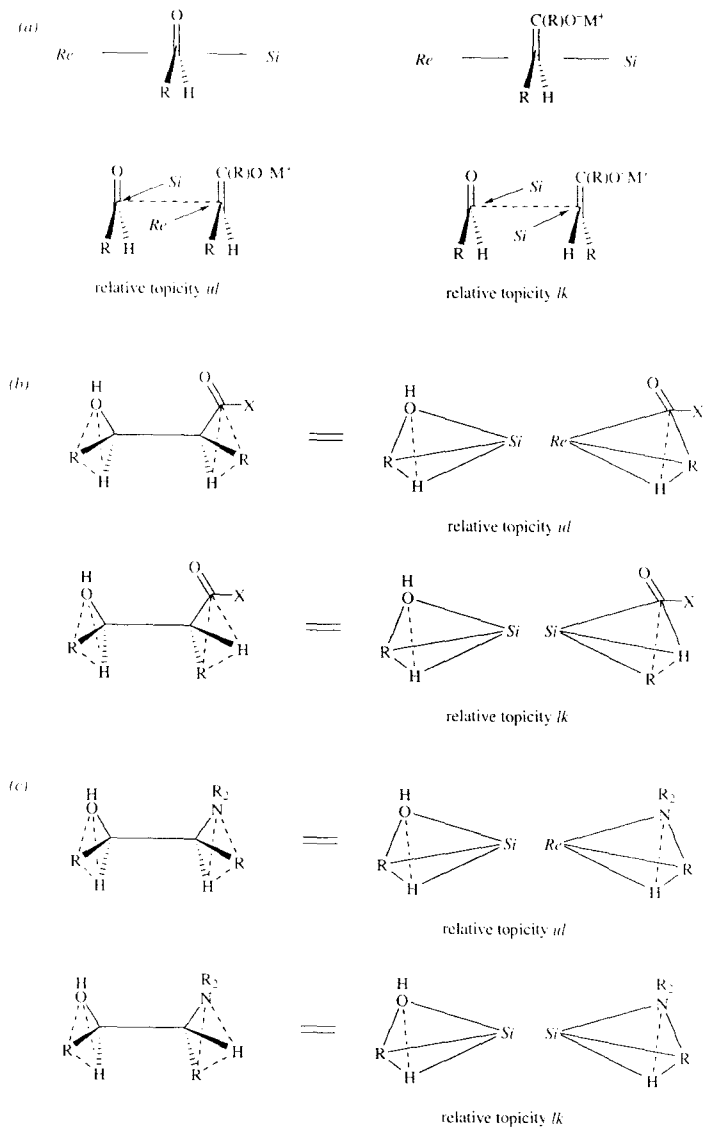

Fig. 5.1. (a) Seebach–Prelog definition of relative topicity, illustrated by addition of an enolate to an aldehyde (note that topicity is independent of enolate geometry); (b) A second way to view the Seebach–Prelog concept; (c) Definition of relative topicity for β-amino alcohols based on relative configuration.

descriptors *l* and *u* (for *like* and *unlike*) to describe relative configuration [18], and this terminology will be used here. Thus, *R,R* and *S,S* pairs of stereocenters have the *l* relative configuration and *R,S* and *S,R* pairs are *u*. Following this precedent, Seebach and Prelog proposed that the steric course of reactions between two trigonal atoms could be classified topologically as *lk* (*like*) for reactions in which the *Re,Re* or *Si,Si* heterotopic faces are joined, and as *ul* (*unlike*) for reactions in which *Re,Si* or *Si,Re* faces were joined, as illustrated in Figure 5.1a [19]. These protocols are based on the CIP sequence rules [18,20] and are unambiguous in all respects when trigonal atoms are involved, because even in the transition state the reacting atoms are still only tetravalent. However, the same rules are not directly applicable to the reaction of a chiral, stereogenic nucleophile such as a Grignard, since the carbanionic carbon is tetrahedral in the ground state and pentavalent in the transition state and (with reference to Scheme 5.5) the reaction may occur with either retention or inversion of configuration (see also Figure 5.2 and the accompanying discussion, below). Nevertheless, examination of the products of the reaction of two trigonal atoms (Figure 5.1b) illustrates how the topicity may be defined based on the relative configuration of the products.[7] Thus, for an aldol addition, the three ligands of each of the former trigonal atoms form the bases of two tetrahedra, with the fourth vertex being the nucleophilic or electrophilic carbon of the other reactant. It can be easily seen that this fourth vertex is sitting on either a *Re* or *Si* face of a triangle and that these descriptors match the relative topicity according to the Seebach–Prelog definitions. Extending this concept to the β-amino alcohol product of addition of an α-aminoorganometallic to an aldehyde is straightforward, as shown in Figure 5.1c.

The illustrations in Figure 5.2 demonstrate why it would be impossible to try to define relative topicity for these reactions based on the reactants. The reaction at the metal-bearing carbon is an S_E2 process, which may occur with either retention or inversion of configuration [21a]. In reactions of

[7] This is not unlike the rationale for the *pref/part* system of assigning relative configuration [21].

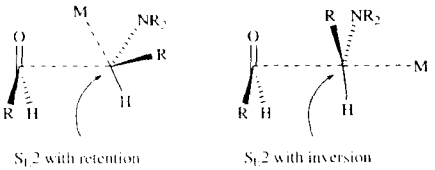

Fig. 5.2. Transition structures of S_E2 reaction with retention and inversion at the metal-bearing carbon.

chiral organolithiums with carbonyl compounds, both pathways are known [21a,22,23]. Thus, the steric course of a reaction such as this must be specified with respect to both topicity *and* retention/inversion at the metal-bearing carbon. Note that the two structures in Figure 5.2 have the same topicity as defined in Figure 5.1c.

5.4 ADDITIONS OF CONFIGURATIONALLY STABLE GRIGNARDS TO ALDEHYDES

All of the examples which follow are metallated nitrogen heterocycles, in which the nitrogen is part of either an amide or amidine group. These species have been called 'dipole stabilized' [24], because of the partial positive charge on the amide or amidine nitrogen. In a saturated heterocycle, such Grignard species are probably configurationally stable for stereoelectronic reasons [25–28], although no definitive experiments have been done. Table 5.1 lists two examples of additions of dipole-stabilized Grignards to benzaldehyde. Example 5.1 is a test of Grignard selectivity reported by Seebach in 1984 [29], although the formamidine auxiliary was developed by the Meyers group to facilitate lithiations [30]. The second example is from our own work [31], and illustrates the power of stereochemistry to probe mechanistic detail in this field. Recall from Scheme 5.5 that a mixture of four diastereomers would be expected if SET is an important mechanistic pathway. In this case, only three are formed, indicating competing mechanisms.

Originally [31], we suggested that this mixture was due to competing polar and radical pathways.

Table 5.1. Diastereoselectivity in the addition of configurationally stable, chiral α-amino Grignard reagents to benzaldehyde

Entry	Organometallic	Conditions	Products: *ul* topicity	Products: *lk* topicity	Reference
1	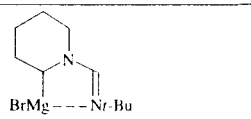	THF −78	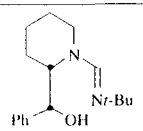 *u*, racemic 66	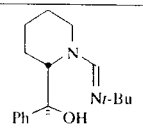 *l*, racemic 34	[29]
2	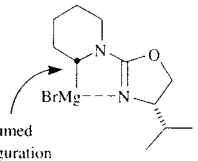 presumed configuration	ether −100 → RT	after auxiliary removal: 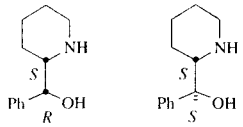 *u*, ≥80% ee ≥90 : 10 er 50	*l*, 50% ee 75 : 25 er 50	[31]

but further analysis leads me to believe that the competing mechanisms are both polar. If SET occurred, coupling of the α-amino radical with the aldehyde ketyl ought to be stereorandom and four diastereomers should be formed in approximately equal amounts; indeed, this was found in the addition of the corresponding lithium reagent to benzaldehyde [31]. The differing amounts of each diastereomer in the Grignard addition, and in particular the near absence[8] of the *R,S* diastereomer suggests that radicals are probably not involved.

5.5 CONFIGURATIONAL LABILITY OF BENZYLIC GRIGNARDS

When the metallated carbon is allylic or benzylic, the barrier to inversion is lowered relative to saturated systems. This was demonstrated by carbon-13 NMR experiments that we reported in 1996 [32]. The system studied was a tetrahydroisoquinolyloxazoline, metallated in the 1-position. The oxazoline ring had a stereocenter, so the two C-1 epimers were diastereomers. Carbon 1 was enriched in carbon-13, and the C-1 region of the spectrum is shown in Figure 5.3. This complex spectrum for a single carbon conforms with earlier findings that pyramidal inversion and Schlenk equilibria complicate the NMR spectra of organomagnesium species [33–38]. Nevertheless, two regions can be discerned: a low-field, temperature-independent region, and a higher field region, near 47 ppm, where a dynamic phenomenon is observed, with two peaks coalescing at −65°.

In 1965, Whitesides and Roberts showed that the ^{1}H NMR spectra (in ether) of dialkylmagnesium species change little below +30° and that Grignard species do not change below temperatures of −70° [35]. Further, the position of the Schlenk equilibrium ($R_2Mg + MgBr_2 \rightleftharpoons 2RMgBr$) is affected by both the concentration of magnesium halide, solvent, and temperature. Relevant to our work is the fact that in THF at low temperatures, the equilibrium is shifted towards the dialkylmagnesium side (relative to its position in ether), and that the Schlenk equilibrium is slow [39]. Control experiments on our system showed that, as

[8] ≤5%, uncertainty due to inaccuracies of polarimetry on the oily addition product.

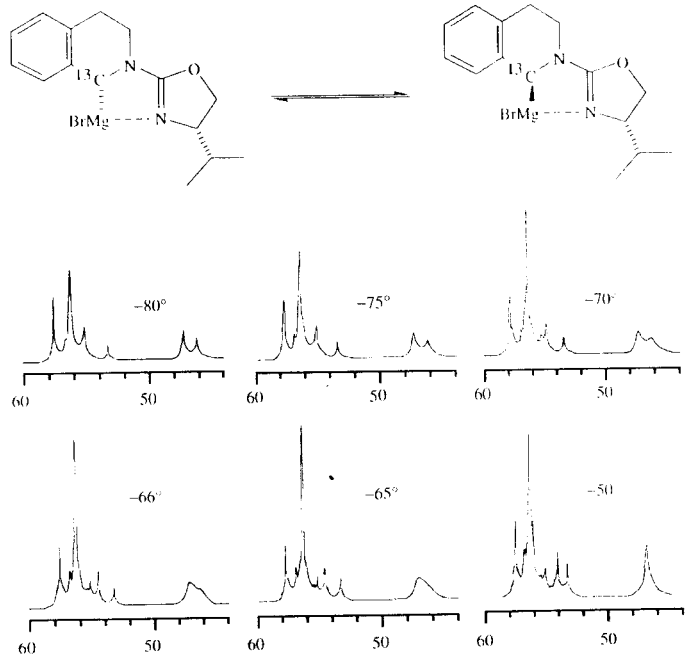

Fig. 5.3. Low-temperature partial C-13 NMR spectrum of the equilibrating Grignard diastereomers shown at top. Only the signals due to C-1 are shown. See text for explanation and assignments.

the magnesium bromide concentration was varied between 0.2 M and 0.5 M (equilibration at 0°), the population of the upfield (temperature dependent) region increased at the expense of the downfield region. We interpret this as a shift of the Schlenk equilibrium toward the Grignard, RMgBr.

Thus, the upfield, temperature-dependent region was assigned to the Grignard monomers, and the two peaks near 47 ppm were assigned to the two diastereomers epimeric at C-1. Interestingly, integration of these two peaks in the −80° spectrum corresponds exactly to the isomer ratio found in the addition to benzaldehyde (*vide infra*).

Whitesides *et al.* found that the (Arrhenius) barrier to inversion of primary Grignard reagents was 11 ± 2 kcal/mole ($A = \exp 9.5 \pm 1.5\ s^{-1}$) [34]. In 1971, Fraenkel concluded that the mechanism of inversion involved a dimeric species and that alkyl bridging is associated with the transition state for inversion [40]. Early attempts at observation of inversion of secondary organomagnesium reagents (4–6 membered saturated rings) showed that the barrier to inversion was quite high [35,41,42], although Maercker showed that 3-cyclohexenyl Grignard undergoes somewhat more rapid inversion, with a lower barrier in THF than in ether [37]. The high barrier is generally attributed to difficulty in bridging of the saturated secondary Grignards, while the lower barrier in the cyclohexenyl system is probably due to assistance by the double bond [39].

The coalescence data from Figure 5.3 correspond to free energies of activation ($\Delta G^{\ddagger}$) in the 9.8–10.1 kcal/mole range at −65°C, with ΔG^0 = 0.3 kcal/mole for the two C-1 epimers [41,42]. This low barrier suggests that chelation, dipole-stabilization, and benzylic activation combine to

lower the inversion barrier, although further experiments on simpler systems will be necessary to establish this conclusively.

The low barrier prevents us from determining the steric course of the reactions of these species with electrophiles, but our working hypothesis is that addition to a carbonyl takes place with retention of configuration at the metal-bearing carbon. Even though there is a low barrier to inversion, benzylic Grignard reagents have been developed that are highly stereoselective in their additions to heteropic carbonyl faces, as outlined below, and useful synthetic methodologies have ensued.

5.6 ADDITIONS OF BENZYLIC GRIGNARDS TO ALDEHYDES

In 1984, Seebach discovered that transmetalation of a lithiated tetrahydroisoquinoline pivalamide to a Grignard reagent increases the simple diastereoselectivity (*ul* relative topicity) to 100%, as shown in Table 5.2 [29,43]. As discussed in a later section, the Zürich group used this high selectivity in efficient syntheses of several (racemic) hydroxybenzyl isoquinoline alkaloids, a strategy that paved the way for a subsequent chiral auxiliary-based approach developed in Miami.

Two approaches have been taken to capitalize on the diastereoselectivity observed in the addition of isoquinoline Grignards to aldehydes found by the Seebach group (Table 5.2). The Seebach group used the chiron approach (chiral tetrahydroisoquinoline pivalamide), and Kelly Rein and Pingsheng Zhang in my group developed oxazoline chiral auxiliaries (Table 5.3). It is important to note that in neither case did the corresponding lithium reagents afford useful diastereoselection.

As shown in entries 1 and 2 of Table 5.3, Seebach found that a relatively simple Grignard reagent was 100% diastereoselective in its addition to benzaldehyde (entry 1), but a more complex system showed relatively modest selectivity (entry 2). The latter example was used in a synthesis of (+)-corlumine (*vide infra*), and stands out as a rare exception to the usually exclusive *ul*

Table 5.2. Simple diastereoselectivity in the addition of configurationally labile, racemic, chiral α-aminoorganometallics to benzaldehyde

Entry	Organometallic	Conditions	Products: *ul* topicity	Products: *lk* topicity	Reference
1	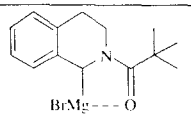	THF −78 → RT	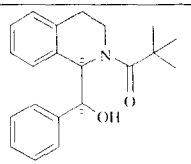 *rac*-*u* 100	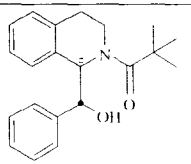 *rac*-*l* 0	[29,43]
2	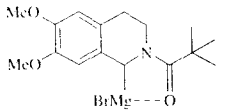	THF −78 → RT	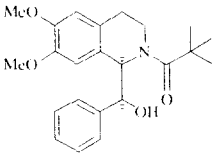 *rac*-*u* 100	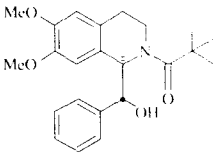 *rac*-*l* 0	[44]

Table 5.3. Diastereoselectivity in the addition of configurationally labile, nonracemic, chiral α-aminoorganometallics to aldehydes. Of the four possible diastereomers, only those found are illustrated

Entry	Organometallic and Aldehyde	Conditions	Products	Reference
1	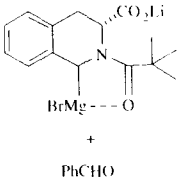 PhCHO	THF −80	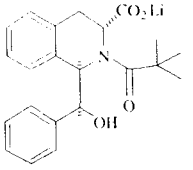 *ul* topicity 100% ds (presumed configuration)	[45]
2	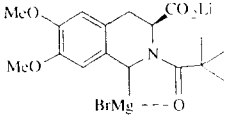 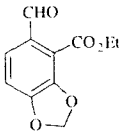	THF −80	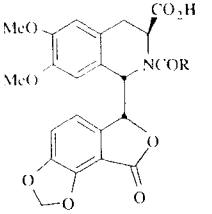 *ul* topicity 60 : 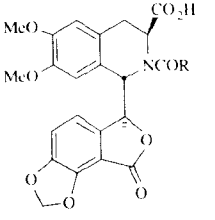 *lk* topicity 40	[45]
3	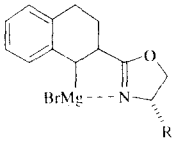 PhCHO R = Me	THF −78	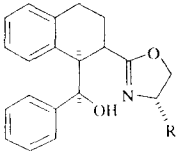 *ul* topicity 50 : 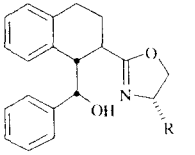 *ul* topicity 50	[32]
4	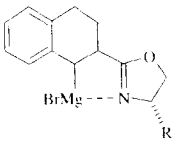 PhCHO R = Et	THF −78	*ul* topicity 62 : *ul* topicity 38	[32]

(continued overleaf)

Table 5.3. (*continued*)

Entry	Organometallic and Aldehyde	Conditions	Products	Reference
5	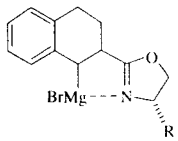 + PhCHO R = *i*-Pr	THF −78°	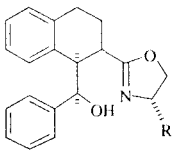 *ul* topicity 66–71 : 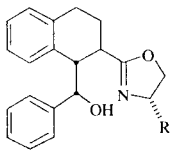 *ul* topicity 34–29	[32,46]
6	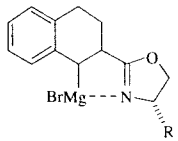 + PhCHO R = *i*-Pr	THF −70°	*ul* topicity 55 : *ul* topicity 45	[32]
7	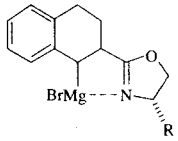 + PhCHO R = *i*-Pr	THF −60°	*ul* topicity 42 : *ul* topicity 58	[32]
8	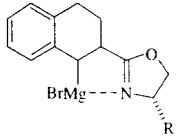 + PhCHO R = *i*-Pr	THF −45°	*ul* topicity 58 : *ul* topicity 42	[32]
9	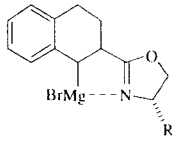 + PhCHO R = Ph	THF −78°	*ul* topicity 71 : *ul* topicity 29	[32]

Table 5.3. (*continued*)

Entry	Organometallic and Aldehyde	Conditions	Products	Reference
10	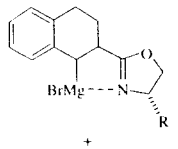 + PhCHO R = Bn	THF −78°	*ul* topicity 70 : *ul* topicity 30	[32]
11	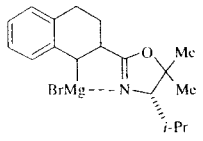 + PhCHO	THF −78°	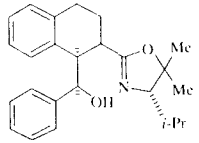 *ul* topicity 80 : 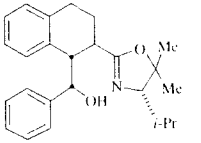 *ul* topicity 20	[32]
12	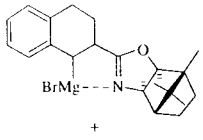 + PhCHO	THF −78°	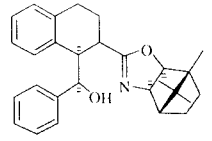 *ul* topicity 33 : 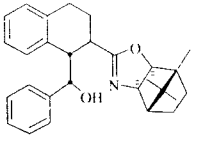 *ul* topicity 67	[32]
13	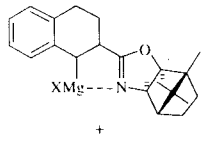 + PhCHO	THF −65°	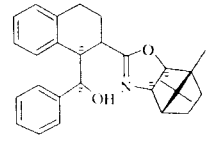 *ul* topicity 20 : 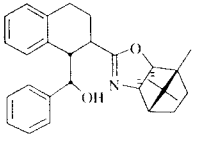 *ul* topicity 80	[32]

topicity exhibited by magnesiotetrahydroisoquinolines in addition reactions [45].

In 1989, Kelly Rein began an investigation into the use of an oxazoline chiral auxiliary to effect diastereoselective additions of Grignard reagents based on the Seebach discovery. The initial effort [46] used an oxazoline auxiliary derived from valine (Table 5.3, entry 5), one that we had used previously in studies of asymmetric alkylations of lithiated tetrahydroisoquinolines [47,48]. Although the selectivity provided by this auxiliary was modest, it was used in the asymmetric synthesis of several hydroxybenzyl isoquinoline alkaloids (*vide infra*), partly motivated by a need to establish the absolute configuration of the addition products. Later, after we became convinced that the approach was worthwhile, Pingsheng Zhang undertook a more systematic investigation of the effect

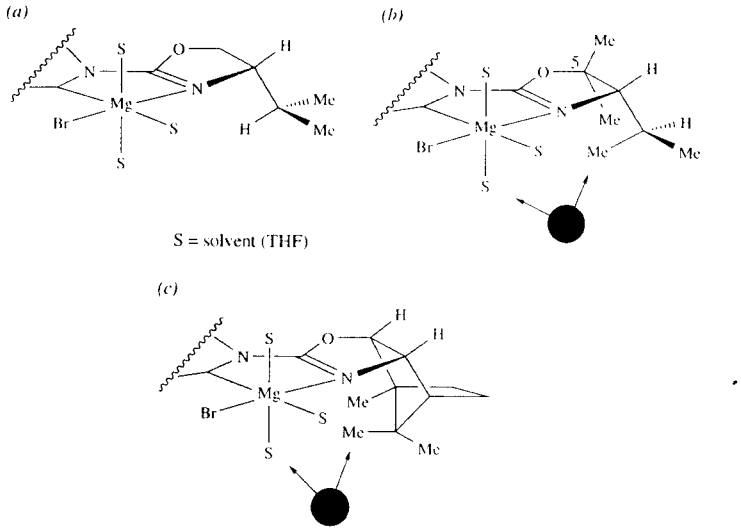

Fig. 5.4. Probable conformation of the magnesiated tetrahydroisoquinolyl oxazoline, based on analogy to the X-ray crystal structure of a magnesiated tetrahyrdoisoquinoline pivalamide [43]. The aldehyde probably coordinates to one of the ligand sites cis to the isoquinolyl carbon prior to reaction. (a) Conformation of isopropyl in 5-unsubstituted auxiliary; (b) Steric crowding produced by rotation of isopropyl in the 5,5-dimethyl derivative; (c) Similar crowding in a camphor-derived auxiliary (enantiomer of that drawn in Table 5.3, entries 12 and 13).

of auxiliary structure and reaction temperature on selectivity [32,49], as summarized in entries 3–13 of Table 5.3.[9]

With oxazolines substituted only in the 4-position, the selectivity peaked at about 70% with either $R = i$-Pr, Ph, or Bn (*c.f.* entries 3–5, 9, and 10) [32]. Note that in all these examples, the aldehyde appears to approach the Grignard from the side opposite R (*i.e.*, β-face as illustrated, assuming chelation of the magnesium by the oxazoline nitrogen).This is in contrast to the chirality sense of the reaction of the lithium analog with alkyl halides, where approach of the electrophile is from the α-face [48]. Although this came as a surprise, we thought we might be able to increase the propensity toward β-approach by making the α-face more crowded. The first approach was to methylate the oxazoline at the 5-position, which forces the isopropyl group to rotate into a conformation that places a methyl group closer to the ligands on the magnesium (Figure 5.4a, b).[10] The modification achieved the desired effect, boosting the diastereoselectivity to 80% (entry 11). The second approach used a different auxiliary, this time one derived from camphor quinone. In this instance (Figure 5.4c), we were also hoping to find a structure that would facilitate separation of the two diastereomeric addition products. The

[9] For the analysis of *u/l* selectivity, NMR is the method of choice, since the two diastereomers are easily distinguished by the coupling pattern of the two methine protons: the coupling constant for the erythro isomer is typically 3–5Hz, whereas the threo pair is typically 7–9 Hz [44,50–53]. To assign absolute configuration, chiral stationary phase HPLC is the method of choice [54].

[10] Chelation of an octahedral magnesium (with the bromine trans to the chelating atom) as shown in this figure is based on analogy to the X-ray crystal structure of a pivalamide Grignard (Table 5.2, entry 1) obtained by the Seebach group [43]. The rationale also assumes that the aldehyde replaces one of the THF ligands (cis to the carbanionic carbon atom on the magnesium) prior to addition.

camphor auxiliary proved useful in that regard (entries 14, 15), since it afforded 80% diastereoselectivity, and one recrystallization of the crude product mixture yielded a single diastereomer [49].

After doing the NMR experiments described above, Pingsheng Zhang noticed a coalescence at −65° [32]. Prompted by this observation, he varied the temperature of the addition, with some unusual results. As outlined in Table 5.3, entries 5–8, the selectivity fell from about 70% to 55% between −78° and −70°; at −60° the chirality sense was reversed, then reversed again at −45°. With the camphor auxiliary, raising the temperature from −78° to −65° increased the selectivity from 67% to 80% (entries 10–11) [32]! This bizarre behavior underscores the point made previously (Scheme 5.5) about seeking mechanistic insight when the carbanion is not configurationally stable.

Nevertheless, the camphor auxiliary provided a single diastereomer in the synthetically useful yield of 50% (isolated, analytically pure, single diastereomer), which compares favorably to the isolated yield of 58% of the single diastereomer obtained using the chiron approach (entry 1). As described in a subsequent section, the auxiliary approach proved useful for several synthetic applications as well.

5.7 APPLICATIONS TO ALKALOID SYNTHESIS

Seebach's 1984 discovery of 100% diastereoselectivity in the addition of tetrahydroisoquinoline Grignards (Table 5.2) to benzaldehyde led to efficient syntheses of several *rac*-hydroxybenzylisoquinoline alkaloids, all via *u* hydroxybenzylisoquinolines (Scheme 5.6). This strategy is similar to that used

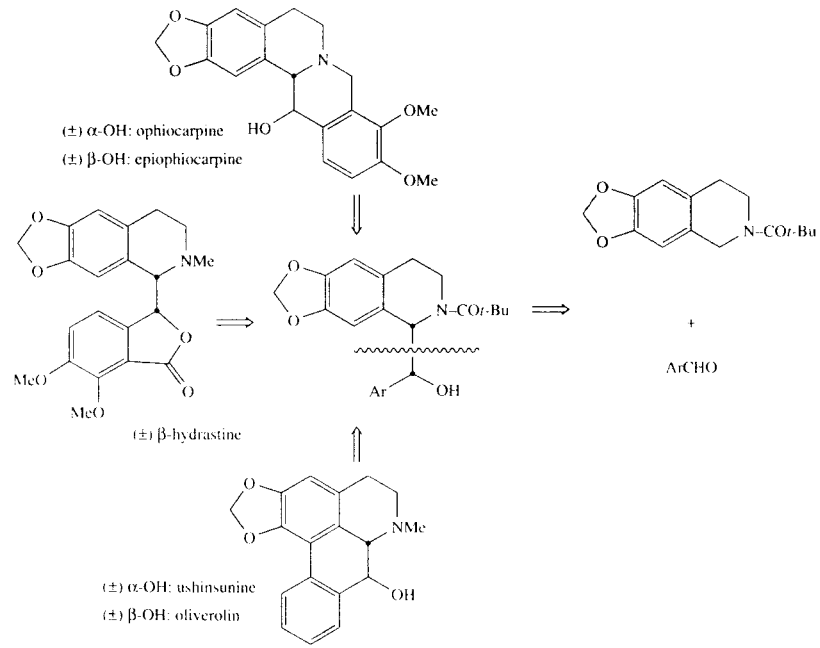

SCHEME 5.6. The Seebach group's retrosynthesis plan for the synthesis of isoquinoline alkaloids by diastereoselective addition of tetrahydroisoquinoline Grignard reagents to aromatic aldehydes [44,59].

(at about the same time) by the Meyers group in the synthesis of a number of isoquinoline alkaloids, where the key step was alkylation of a tetrahydroisoquinoline formamidine with an alkyl halide (1 new stereocenter) (reviews: [55,56]). It is worth mentioning that two of the primary tenets of retrosynthetic analysis [57,58] are to make a bond disconnection that results in the greatest simplification, such as between two stereocenters, and to cleave a bond that divides a target into two halves of approximately equal complexity. In this instance (Scheme 5.6), the addition of the metallated tetrahydroisoquinoline to the aldehyde accomplishes this nicely.

Scheme 5.7 details the execution of this plan as it was applied to the synthesis of β-hydrastine, ophiocarpine, and epiophiocarpine [44]. Lithiation of the methylenedioxytetrahydroisoquinoline pivalamide **1** and transmetalation with magnesium bromide gave the Grignard **2**, which added to a functionalized benzaldehyde with 100% stereoselectivity, giving a hydroxybenzyl derivative that lactonized spontaneously to **3** in 63% overall yield. This key intermediate was then converted into the alkaloids as shown. Saponification of the lactone was accompanied by amide hydrolysis; the resulting amino acid cyclized spontaneously to lactam **4**, which could be reduced to the protoberberine (±)-epiophiocarpine in 81% yield. Alternatively, hydrazinolysis of the crude lactam and acid-catalyzed hydrolysis of the hydrazide gave the depivaloylated amino lactone **5**, which was methylated in 83% yield to give (±)-β-hydrastine. In these two alkaloids, the relative configuration of the two stereocenters is *u* (erythro). To obtain the *l* (threo) relative configuration, pivalamide **6**, obtained by reduction of lactone **3**, could be treated with trifluoroacetic acid/trifluoroacetic anhydride, which effects *N* to *O* acyl migration with inversion of configuration at the carbinol carbon [44,59]. Hydrolysis (86% yield) and ring closure (51%) then gave (±)-ophiocarpine [44].

The obvious extension to the strategy outlined in Scheme 5.6 and Scheme 5.7 was to apply it to the synthesis of enantiopure alkaloids. The Seebach group tried the approach outlined in Scheme 5.8, which began with *S*-dopa as the chiral educt [45]. Methylation of the phenolic hydroxyls and Pictet–Spengler cyclization gave the tetrahydroisoquinoline pivalamide **8**. Dilithiation and transmetalation with one equivalent of magnesium bromide afforded a Grignard species that added to a functionalized aldehyde similar to that used previously (Scheme 5.7). As has already been indicated (Table 5.3, entry 2), this reaction failed to reproduce the high diastereoselectivity found in simpler examples. In fact, this is was a rare example of the failure of this method to afford exclusively *u* (erythro) addition products. The *u/l*-**9** mixture was reductively decarboxylated to give *u/l*-**10**, which could be separated chromatographically. Removal of the pivaloyl group from *u*-**10** and methylation then gave (+)-corlumine.

Since only two of the four possible addition products (**9**) were formed, one may surmise that SET was not responsible for the low selectivity. The minor isomer was the *l* (threo) addition product. The reasons for the loss of selectivity are not known, but undoubtedly involve very subtle differences in Grignard structure, possibly caused by the lithium carboxylate and the two methoxy substituents, although neither of these components on their own caused a loss of selectivity (*cf.* Table 5.2, entry 2 and Table 5.3, entry 1).

In our group, we decided to use a chiral auxiliary in a scheme such as this, with the hope of avoiding some of the problems encountered by the Seebach group. Note that the loss of selectivity encountered in the corlumine synthesis occurred when the tetrahydroisoquinoline carried methoxyl groups in the 6 and 7 positions. Therefore, an issue that had to be addressed was the selectivity of addition of oxygenated isoquinolines. As shown in Scheme 5.9, Pingsheng Zhang found that the bromomagnesium derivatives of tetrahydroisoquinolines **11a** and **11b** were selective in their additions, affording only the two *u* (erythro) diastereomers of **12**. In contrast, the dimethoxy analog **11c** was not erythro selective. *When magnesium bromide was used in the transmetalation, both erythro and threo products were produced with the dimethoxy compound* [32,49]. Transmetalation with magnesium chloride restored the erythro selectivity, and was equally effective with **11a** and **11b** as well.

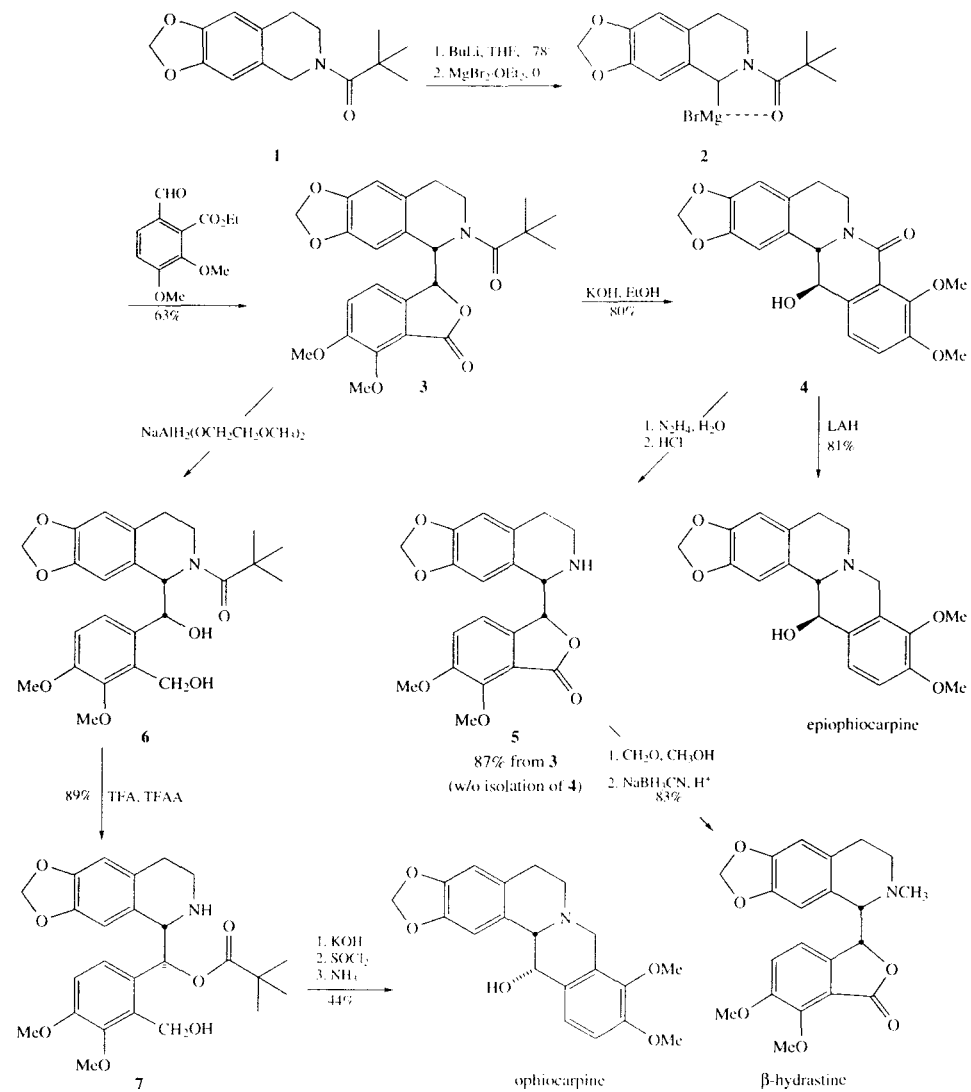

SCHEME 5.7. Seebach's synthesis of (±)-hydroxybenzylisoquinoline alkaloids [44].

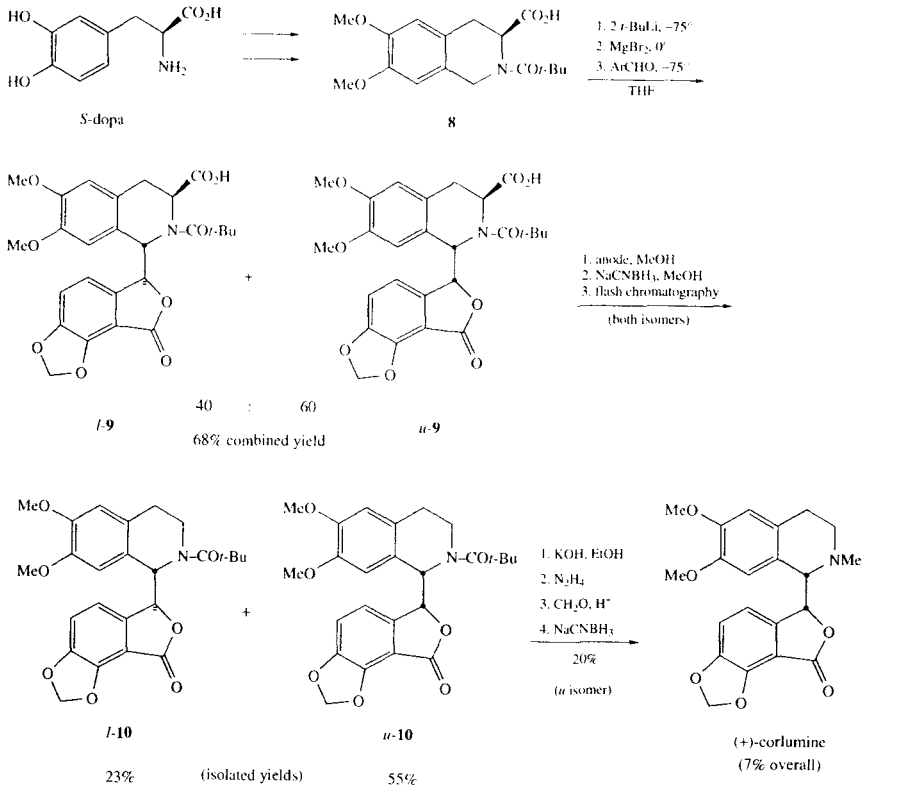

SCHEME 5.8. Seebach's synthesis of (+)-corlumine using a chiral tetrahydroisoquinoline educt [45].

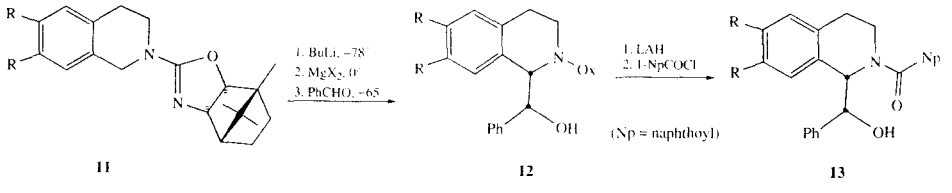

	R	X	%ds	Isolated yield (single isomer)
a	H	Cl or Br	80	50%
b	$-OCH_2O-$	Cl or Br	78	53%
c	MeO	Cl	82	58%

SCHEME 5.9. Generality of the camphor-derived oxazoline chiral auxiliary [32,49] and analysis of the enantiomer ratio by chiral stationary phase HPLC [54].

The reason for these subtle differences is not known, but may involve an interaction between the halogen and the 7-methoxy substituent that causes a slight change in geometry of the magnesium complex, that in turn affects the relative energies of competing transition states [32,49]. Seebach had determined the X-ray crystal structure of an unsubstituted tetrahydroisoquinoline pivalamide Grignard [43]. In it, the bromide is trans to the chelating pivalamide oxygen, as indicated in Figure 5.5a. Assuming that the oxazoline takes the place of the pivalamide as indicated in Figure 5.5b, a methylenedioxy substituent would not affect the structure significantly (Figure 5.5c). However, the most stable conformation of the two methoxy groups has the methyls oriented away from each other, and—in this conformation—the methyl group of the 7-methoxy substituent might encounter the bromine, as shown in Figure 5.5d. Such an interaction could disrupt the geometry of the reagent in the ground state and cause a change of mechanism, or could destabilize the transition state leading to the erythro products. It may be that the smaller van der Waals radius of chlorine (181 pm for *vs.* 195 pm for bromine [60]) simply relieves the crowding sufficiently to allow the stereoselective transition state to prevail. It is worth mentioning that the absolute configurations of both the erythro and threo diastereomers of hydroxybenzylisoquinolines can be determined by HPLC of naphthamide **13** on a Pirkle column, after removal of the oxazoline from **12** and derivatization with naphthoyl chloride [54].

For synthesis targets, we chose the phthalide isoquinoline lactones bicuculline and corlumine [61], and the hemiacetals egenine [62] and corytensine [63,64], shown in Scheme 5.10. These targets were chosen for several reasons. First, the relative and absolute configuration of bicuculline (and its threo diastereomer adlumidine), as well as their diol reduction products are firmly established [65], so that a synthesis of either (or both) would place the configurational assignments for **13a–c** on a firm footing. Second, synthesis of egenine and corytensine would confirm their structures. (There appeared to be some confusion regarding the difference in structure of egenine [62] and corytensine [63]. As a result of an

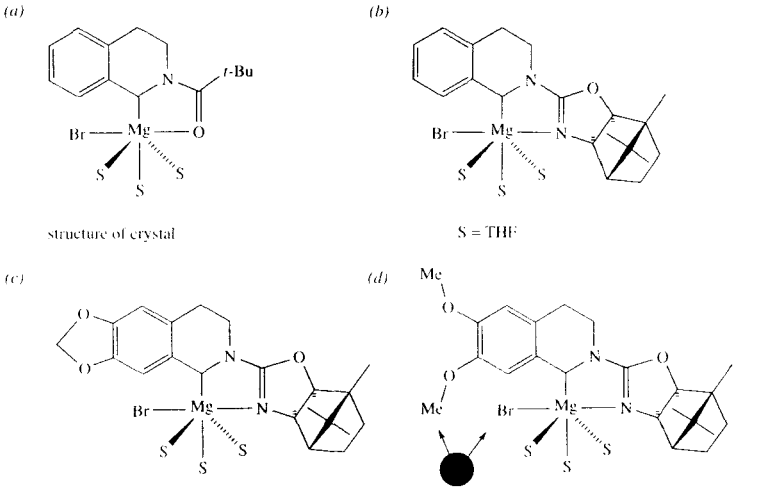

Fig. 5.5. (a) X-ray structure [43]; (b–d) Presumed structure of Grignard monomers, based on analogy to the crystal structure [32,49].

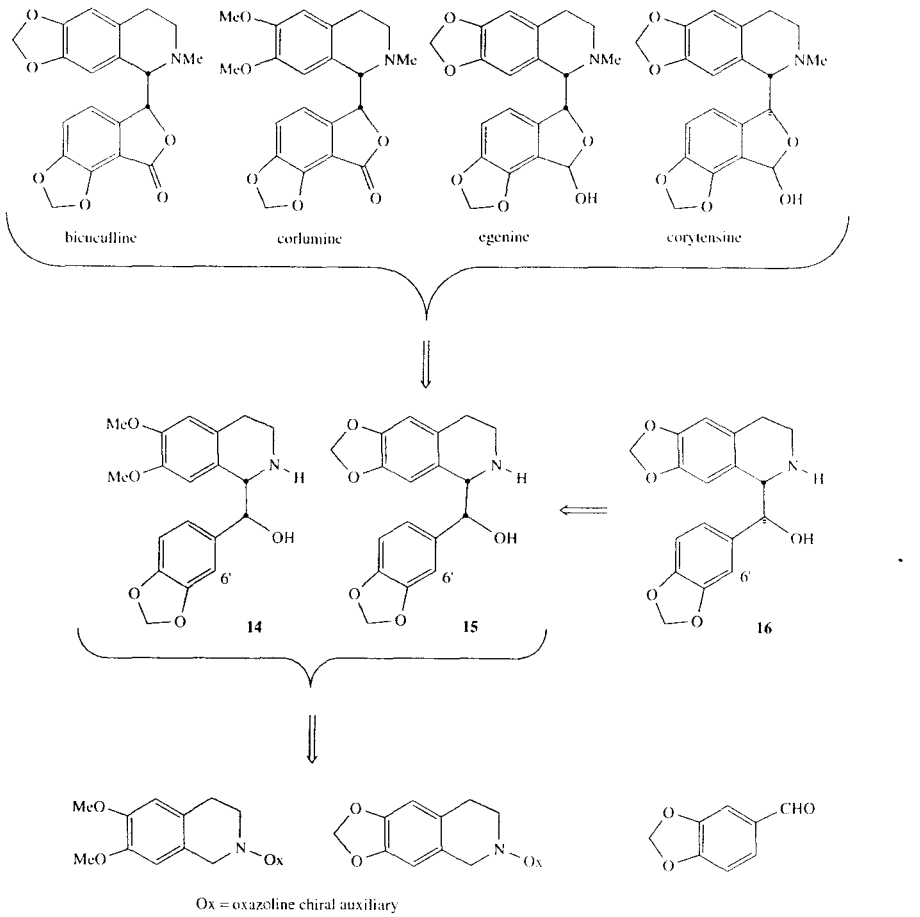

SCHEME 5.10. Synthetic targets and retrosynthetic analysis for phthalide isoquinolines using the camphor-oxazoline chiral auxiliary [32,46,67].

error in transcribing the X-ray crystal structure from ORTEP to a two-dimensional drawing [64], it was originally concluded that the difference between the two was the configuration at the hemiacetal carbon [63]. Since both alkaloids had been isolated by chromatography on silica gel, this struck us as unlikely.) Third, shortly before we began this work, two new alkaloids were reported [66], decumbensine and epi-α-decumbensime (Figure 5.6), and we were interested in confirming their structures as well. Fourth, the synthesis of corlumine could be compared directly to the Seebach effort (Scheme 5.8) [45]. Finally, it was presumed that synthesis of these targets would suffice to demonstrate feasibility of this strategy toward the other alkaloid classes outlined in

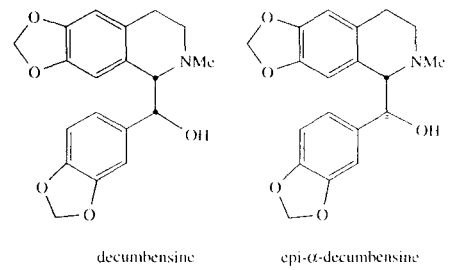

Fig. 5.6. Reported structures for decumbensine and epi-α-decumbensine [66].

Scheme 5.6, since phthalides can be converted to such other classes by known routes (see Scheme 5.7, and refs. [44,55,56], and references cited therein).

Note that the approach outlined in Scheme 5.10 uses piperonal as the aldehyde component and requires functionalization at the 6′-position of **14–16** after the key addition step and auxiliary removal. Kelly Rein tried a more direct approach initially, as shown in Scheme 5.11, but reduction of the aldehyde was the major pathway [68]. No addition product was found, but the isoquinolyloxazoline could be recovered in 30% yield. Grignard reagents may reduce carbonyls by either β-hydride elimination or electron transfer. Since there are no β-hydrogens in this Grignard, SET is the only possible alternative for the production of the observed lactone.

She then developed a successful approach using the valine-derived oxazoline auxiliary (*S*-4-isopropyloxazoline: Table 5.3, entries 5–8) [46,67]. Later, Pingsheng Zhang optimized the process with a better auxiliary as indicated by the examples in Table 5.3 [32,49], and used the auxiliary derived from camphor quinone to synthesize the key hydroxybenzylisoquinoline intermediates **19**, **20**, and **23** shown in Scheme 5.12 [32]. The absolute configuration of the new stereocenters of the addition products from these two auxiliaries (derived from *S*-valine and 1-*R*-camphorquinone oxime) are opposite. In the schemes and accompanying discussion below, the camphor-derived auxiliary is illustrated (Scheme 5.12), but the rest of the synthesis of all the alkaloids except corlumine was actually executed on the enantiomer of that drawn, because it was done with the product of addition using the valine-derived auxiliary. The references in the discussion refer to the relevant papers for each step.

The methylenedioxyisoquinolyloxazoline **17** and the dimethoxyisoquinolyloxazoline **21** were deprotonated with butyllithium, transmetallated with magnesium halide, and added to piperonal with ~80% diastereoselectivity, as shown in Scheme 5.12a and c. The major isomers, **18** and **22**, respectively, were isolated by flash chromatography in the yields indicated. Hydride reduction cleaved the auxiliary and afforded the enantiomerically pure erythro amino alcohols **14** and **15** [32]. Methylation was achieved by cyclization with phosgene and reduction [32,46,67]. To obtain the threo compound **16**, erythro amino alcohol **15** was inverted by acylation and rearrangement, affording enantiopure **16** after reductive cleavage of the pivaloate group (Scheme 5.12b), and methylation to **20** was accomplished as before [67].

The two *N*-methyl (bis)-methylenedioxy compounds (**19** and **20** Scheme 5.12a, b) corresponded to the proposed structures for decumbensine and epi-α-decumbensine (Figure 5.6 [66]), and we had

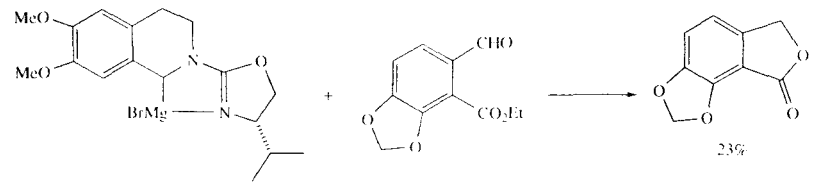

SCHEME 5.11. A convergent synthesis is side-tracked by SET [68].

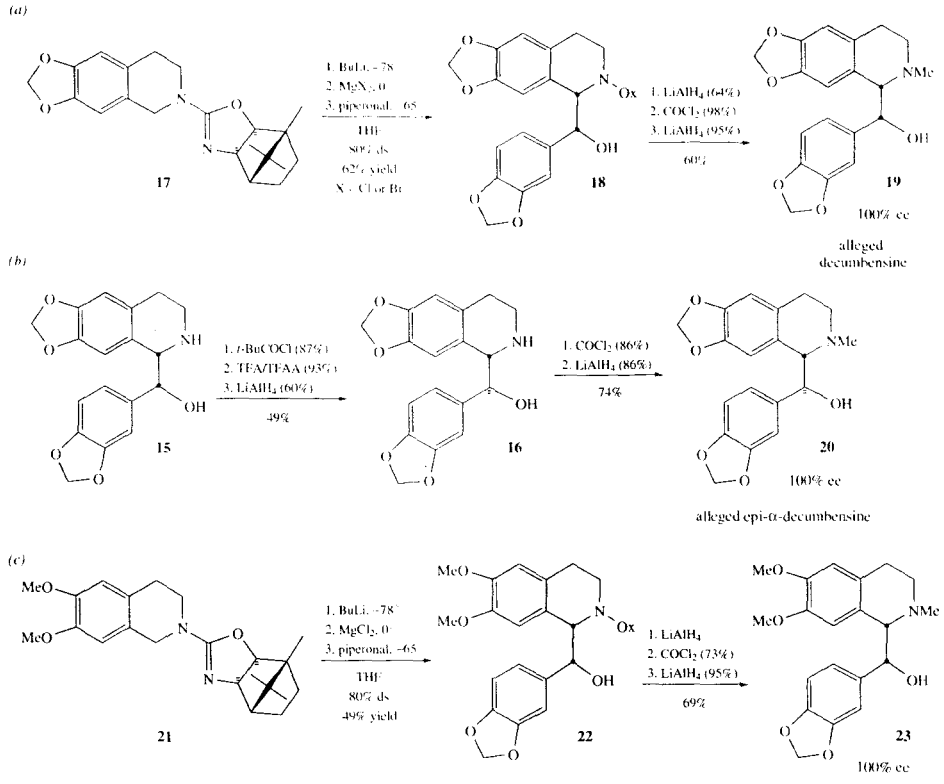

SCHEME 5.12. Synthesis of key intermediates for phthalide isoquinoline alkaloid synthesis [32,46,67].

hoped to confirm the original structural assignments and establish the configuration of our compounds, but their NMR spectra did not match. Rozwadowska had noticed the same thing, and suggested that epi-α-decumbensine might in fact be corytensine [69,70]. We thought that if epi-α-decumbensine and corytensine were the same, then decumbensine and egenine were also probably identical. So, we decided to make them both to settle the matter. But, it was around this time that we noticed the mistake about the structure of corytensine [63,64], along with some misassigned signals in the spectra of both egenine and corytensine (summarized and corrected in ref. [46,67]), and therefore concluded that we would have to choose different targets for comparison to establish configurations. For this, we decided on bicuculline diol and adlumidine diol [65], made by reduction of egenine and corytensine.

Scheme 5.13 shows Kelly Rein's directed metalation strategy for functionalization of the 6′-position. In all three cases, metalation and acylation failed to go to completion. In each case, the product of acylation was accompanied by significant amounts of recovered starting material. Thus the yields are low, but look better if based on unrecovered starting material. Nevertheless, the NMR spectra of the products largely matched literature data (*vide infra*) [67]. Reduction of egenine and corytensine afforded bicuculline diol and adlumidine diol [67], and comparison of rotation and spectral data matched literature values [65]. These correlations confirmed that the chirality sense of the addition was as indicated, and as independently established by chemical correlation (reductive deoxygenation) and chiral stationary phase HPLC [54]. Pingsheng Zhang later tried a number of approaches to improve on this last step, including use of better directing groups on the benzylic oxygen, but nothing seemed to help. Although the goal of improving this metalation was not achieved, Pingsheng did discover a variant of the Snieckus rearrangement [71].

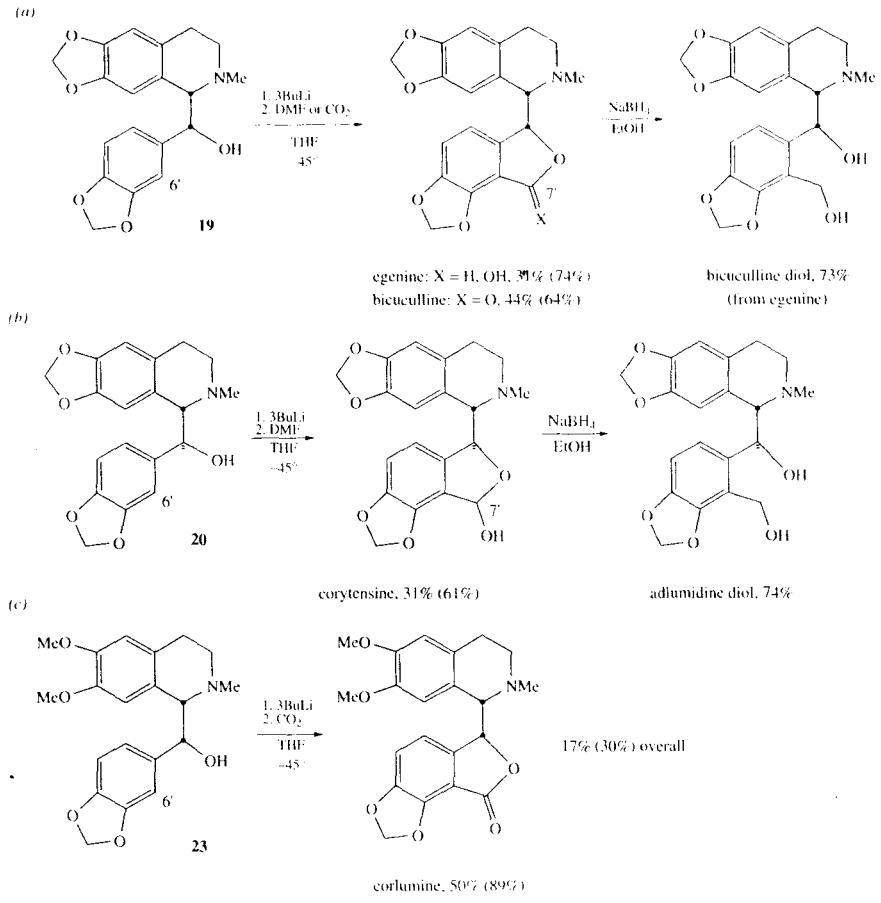

SCHEME 5.13. Directed metalation and acylation of hydroxybenzylisoquinolines for the synthesis of egenine, bicuculline, corytensine, and corlumine [32,46,67]. Yields in parenthesis are based on unrecovered starting material. Reduction of egenine and corytensine yielded bicuculline diol and adlumidine diol, whose rotation and spectral data matched literature values [65].

The identity of egenine with decumbensine, and of corytensine with epi-α-decumbensine deserves some comment. In their report, Zhang *et al.* recorded the proton NMR spectrum of both alkaloids, but the carbon spectrum of only decumbensine, which showed 19 carbons (egenine has 20) [66]. Our synthetic egenine showed 20 lines at 100 MHz, but only 19 at 20 MHz; signals at 123.99 and 124.11 merged at lower field [46,67]. The carbon spectrum recorded by Zhang *et al.* was obtained at 22.63 MHz. Insufficient epi-α-decumbensine was available for a carbon spectrum. In the proton NMR, the hydrogens at C-7′ of egenine and corytensine come at 6.34 and 6.25, respectively, and were mistaken for aromatic peaks by both Shamma [62] and Zhang *et al.* [66]. With our synthetic samples, we used a combination of COSY, HETCOR, off-resonance, and NOE techniques to establish the correct assignments [46]. Under EI conditions, neither egenine nor corytensine showed a molecular ion in the mass spectrum [62,63,72], although both do under DCI conditions [67]. The mass spectra of decumbensine and epi-α-decumbensine were obtained under CI conditions [66], but apparently no molecular ion was observed. So between the absence of a molecular ion in the MS, the low-field methine hydrogen in the proton NMR, and the merger of two signals in the carbon NMR, Zhang *et al.* were honestly misled.

The total synthesis of corlumine by the chiron route beginning with *S*-dopa (Scheme 5.8) and the auxiliary route (Scheme 5.12c and 5.13c) can now be compared directly. Beginning with the tetrahydroisoquinoline species that is metallated and added to the aldehyde, the chiron route proceeds in 7% overall yield, while the auxiliary route is 17% (30% based on unreacted starting material in the last step). The comparison neglects the steps necessary for the conversion of *S*-dopa into the dimethoxytetrahydroisoquinoline pivalamide and for the synthesis and attachment of the chiral auxiliary, but the steps that are compared cover comparable transformations.

5.8 SUMMARY

The addition of stereogenic metal-bearing carbons to prochiral carbonyls is a complex process that may proceed by polar or radical pathways. Determining the steric course of the reaction is only possible with configurationally stable carbanions, but mechanistic understanding is not necessarily a prerequisite to development of useful methods. An auxiliary-based protocol for the synthesis of hydroxybenzylisoquinolines is the most efficient method currently available for the synthesis of enantiopure α-hydroxybenzylisoquinolines such as the phthalideisoquinolines bicuculline, corlumine, egenine, and corytensine, and also of the other alkaloid classes available from them, such as aporphines and protoberberines.

ACKNOWLEDGEMENTS

I am grateful to my colleagues, whose names are mentioned in the references and the text, for their experimental skill and fortitude in a demanding field. Our contributions to this area were supported financially by the National Institutes of Health (GM-37985).

REFERENCES

1. R.E. Gawley in *Advances in Asymmetric Synthesis*, A. Hassner, Ed., JAI: Greenwich, CT, **1998**, Vol. 3, p. 77.
2. R.E. Gawley, J. Aubé, *Principles of Asymmetric Synthesis*, Pergamon (Elsevier Science): Oxford, **1996**, Vol. 14 (Tetrahedron Organic Chemistry Series).
3. E.L. Eliel, S.H. Wilen, L.N. Mander, *Stereochemistry of Organic Compounds*, Wiley-Interscience: New York, **1994**.
4. D.Y. Curtin, E.E. Harris, E.K. Meislich, *J. Am. Chem. Soc.* **1952**, *74*, 2901–2904.
5. D.J. Cram, F.A.A. Elhafez, *J. Am. Chem. Soc.* **1952**, *74*, 5828–5835.
6. V. Prelog, *Helv. Chim. Acta* **1953**, *36*, 308–319.
7. E. Erdik, *Organozinc Reagents in Organic Synthesis*, CRC Press: Boca Raton, FL, **1996**.
8. R. Noyori, M. Kitamura, *Angew. Chem. Int. Ed. Engl.* **1991**, *30*, 49–69.
9. R.O. Duthaler, A. Hafner, *Chem. Rev.* **1992**, *92*, 807–832.
10. K. Soai, S. Niwa, *Chem. Rev.* **1991**, *92*, 833–856.
11. K. Maruoka, H. Yamamoto, in *Catalytic Asymmetric Synthesis*, I. Ojima, Ed., VCH: New York, **1993**, p. 413–440.

12. T. Mukaiyama, *Aldrichimica Acta* **1996**, *29*, 59–76.
13. R. Noyori, *Asymmetric Catalysis in Organic Synthesis*, Wiley-Interscience: New York, **1994**.
14. *Comprehensive Organic Synthesis. Selectivity, Strategy, and Efficiency in Modern Organic Chemistry*, B.M. Trost, I. Fleming, Eds., Pergamon: Oxford, **1991**.
15. G.S. Miracle, S.M. Cannizzarro, N.A. Porter, *Chemtracts-Org. Chem.* **1993**, *6*, 147–171.
16. N.A. Porter, B. Giese, D.P. Curran, *Acc. Chem. Res.* **1992**, *24*, 296–304.
17. D.P. Curran, N.A. Porter, B. Giese, *Stereochemistry of Radical Reactions: Concepts, Guidelines, and Synthetic Applications*, VCH: New York, **1996**.
18. V. Prelog, G. Helmchen, *Angew. Chem. Int. Ed. Engl.* **1982**, *21*, 567–583.
19. D. Seebach, V. Prelog, *Angew. Chem. Int. Ed. Engl.* **1982**, *21*, 654–660.
20. R.S. Cahn, C.K. Ingold, V. Prelog, *Angew. Chem. Int. Ed. Engl.* **1966**, *5*, 385–415, 511.
21. F.A. Carey, M.E. Kuehne, *J. Org. Chem.* **1982**, *47*, 3811–3815.
21a. R.E. Gawley, *Tetrahedron Lett.* **1999**, *40*, 4297–4300.
22. D. Hoppe, A. Carstens, T. Krämer, *Angew. Chem. Int. Ed. Engl.* **1990**, *29*, 1424–1425.
23. A. Carstens, D. Hoppe, *Tetrahedron* **1994**, *50*, 6097–6108.
24. P. Beak, D.B. Reitz, *Chem. Rev.* **1978**, *78*, 275–316.
25. N.G. Rondan, K.N. Houk, P. Beak, W.J. Zajdel, J. Chandrasekhar, P.V.R. Schleyer, *J. Org. Chem.* **1981**, *46*, 4108–4110.
26. R.D. Bach, M.L. Braden, G.J. Wolber, *J. Org. Chem.* **1983**, *48*, 1509–1514.
27. R.E. Gawley, G.C. Hart, L.J. Bartolotti, *J. Org. Chem.* **1989**, *54*, 175–181 and 4726.
28. L.J. Bartolotti, R.E. Gawley, *J. Org. Chem.* **1989**, *54*, 2980–2982.
29. D. Seebach, M.A. Syfrig, *Angew. Chem. Int. Ed. Engl.* **1984**, *23*, 248–249.
30. A.I. Meyers, P.D. Edwards, W.F. Rieker, T.R. Bailey, *J. Am. Chem. Soc.* **1984**, *106*, 3270–3276.
31. K.S. Rein, Z.-H. Chen, P.T. Perumal, L. Echegoyen, R.E. Gawley, *Tetrahedron Lett.* **1991**, *32*, 1941–1944.
32. R.E. Gawley, P. Zhang, *J. Org. Chem.* **1996**, *61*, 8103–8112.
33. G.M. Whitesides, F. Kaplan, J.D. Roberts, *J. Am. Chem. Soc.* **1963**, *85*, 2167–2168.
34. G.M. Whitesides, M. Witanowski, J.D. Roberts, *J. Am. Chem. Soc.* **1965**, *87*, 2854–2862.
35. G.M. Whitesides, J.D. Roberts, *J. Am. Chem. Soc.* **1965**, *87*, 4878–4888.
36. M. Witanowski, J.D. Roberts, *J. Am. Chem. Soc.* **1966**, *88*, 737–741.
37. A. Maercker, R. Geuss, *Angew. Chem. Int. Ed. Engl.* **1971**, *10*, 270–271.
38. D. Liebfritz, B.O. Wagner, J.D. Roberts, *Liebigs Ann. Chem.* **1972**, *763*, 173–183.
39. W.E. Lindsell in *Comprehensive Organometallic Chemistry. The Synthesis, Reactions and Structures of Organometallic Compounds*, G. Wilkinson, F.G.A. Stone, E.W. Abel, Eds., Pergamon: Oxford, **1982**, Vol. 1, p. 155–252.
40. G. Fraenkel, C.E. Cottrell, D.T. Dix, *J. Am. Chem. Soc.* **1971**, *93*, 1704–1708.
41. H. Shanan-Atidi, K.H. Bar-Eli *J. Phys. Chem.* **1970**, *74*, 961–963.
42. J. Sandström in *Dynamic NMR Spectroscopy*, Academic Press: London, **1982**, p. 81–84.
43. D. Seebach, J. Hansen, P. Seiler, J.M. Gromek, *J. Organomet. Chem.* **1985**, *285*, 1–13.
44. D. Seebach, I.M.P. Huber, M.A. Syfrig, *Helv. Chim. Acta* **1987**, *70*, 1357–1379.
45. I.M.P. Huber, D. Seebach, *Helv. Chim. Acta* **1987**, *70*, 1944–1954.
46. K.S. Rein, R.E. Gawley, *Tetrahedron Lett.* **1990**, *31*, 3711–3714.
47. R.E. Gawley, G.A. Smith, *Tetrahedron Lett.* **1988**, *29*, 301–302.
48. K. Rein, M. Goicoechea-Pappas, T.V. Anklekar, G.C. Hart, G.A. Smith, R.E. Gawley, *J.Am. Chem. Soc.* **1989**, *111*, 2211–2217.
49. P. Zhang, R.E. Gawley, *Tetrahedron Lett.* **1992**, *33*, 2945–2948.
50. S. Safe, R.Y. Moir, *Can. J. Chem.* **1964**, *42*, 160–162.
51. T. Kametani, H. Matsumoto, Y. Satoh, M. Nemoto, K. Fukumoto, *J. Chem. Soc., Perkin Trans. 1* **1977**, 376–382.
52. P. Osei-Gyimah, M.T. Piascik, J.W. Fowble, D.R. Feller, D.D. Miller, *J. Med. Chem.* **1978**, *21*, 1173–1178.
53. R.M. McMahon, C.W. Thornber, S. Ruchirawat, *J. Chem. Soc., Perkin Trans. 1* **1982**, 2163–2167.
54. K.S. Rein, R.E. Gawley, *J. Org. Chem.* **1991**, *56*, 839–941.
55. A.I. Meyers, *Tetrahedron* **1992**, *48*, 2589–2612.
56. T.K. Highsmith, A.I. Meyers in *Advances in Heterocyclic Natural Product Synthesis*, W.H. Pearson, Ed., JAI: Greenwich, CT, **1991**, Vol. 1, p. 95–135.
57. E.J. Corey, M. Ohno, R.B. Mitra, P.A. Vatakencherry, *J. Am. Chem. Soc.* **1964**, *86*, 478–485.
58. E.J. Corey, X.-M. Cheng, *The Logic of Chemical Synthesis*, Wiley: New York, 1989.
59. D. Seebach, I.M.P. Huber, *Chimia* **1985**, *39*, 233–234.

60. J. Emsley, *The Elements*, Clarendon: Oxford, 1989.
61. G. Blaskó, D.J. Gula, M. Shamma, *J. Nat. Prod.* **1982**, *45*, 105–122.
62. B. Gözler, T. Gözler, M. Shamma, *Tetrahedron* **1983**, *39*, 577–580.
63. T.-S. Wu, S.-C. Huang, S.-T. Lu, T.-C. Wu, D.R. McPhail, A.T. McPhail, K.-H. Lee, *Heterocycles* **1988**, *27*, 1565–1568.
64. T.-S. Wu, S.-C. Huang, S.-T. Lu, T.-C. Wu, D.R. McPhail, A.T. McPhail, K.-H. Lee, *Heterocycles* **1990**, *31*, 575.
65. G. Nonaka, I. Nishioka, *Chem. Pharm. Bull.* **1975**, *23*, 294–298.
66. J.-S. Zhang, R.-S. Xu, J.C. Quirion, *J. Nat. Prod.* **1988**, *51*, 1241–1242.
67. K.S. Rein, R.E. Gawley, *J. Org. Chem.* **1991**, *56*, 1564–1569.
68. K.S. Rein, unpublished.
69. M.D. Rozwadowska, D. Matecka, D. Brózda, *Tetrahedron Lett.* **1989**, *30*, 6215–6218.
70. M.D. Rozwadowska, D. Matecka, D. Brózda, *Liebigs Ann. Chem.* **1991**, 73–75.
71. P. Zhang, R.E. Gawley, *J. Org. Chem.* **1993**, *58*, 3223–3224.
72. M.D. Rozwadowska, D. Matecka, *Liebigs Ann. Chem.* **1991**, 287–289.

6

Grignard Reagents—Industrial Applications and Strategy

Frank R. Busch and David M. De Antonis
Central Research, Pfizer Inc., Connecticut, USA

6.1 INTRODUCTION

Grignard chemistry is one of the most useful synthetic tools available to the organic chemist to assist in the assembly of complex structures useful in the preparation of pharmaceuticals, food additives, and other industrial chemicals. Yet Grignard chemistry can be difficult on an industrial scale. Grignard reagents and the solvents used are flammable and in some cases may be pyrophoric when exposed to air, thus a number of engineering issues must be considered. With suitable preparation, this powerful bond-forming reaction can be utilized in large-scale operations. This chapter summarizes some of the safe handling and engineering issues with the use of these reagents, and considers equipment set-up, exclusion of moisture, solvents, exothermic reactions, and induction of the reaction, all of which make industrial-scale Grignards challenging.

This chapter is intended to provide an introductory view of industrial applications of Grignard reagents. It is not designed to be a complete guide to conducting large-scale reactions, but instead is aimed at the industrial chemist who wants to consider the issues relating to Grignard chemistry. Neither does it attempt to review the vast variety of reactions of Grignard reagents, which have been reviewed extensively elsewhere [1,2,3,4].

Consideration of process equipment configuration, equipment preparation, process hazards, and reaction safety are introduced first. Operational issues related to industrial scale production, including heat of Grignard reagent formation, and control of the exotherm are discussed next. Initiation of the Grignard reagent formation along with a summary of magnesium forms are then reviewed followed by a summary of methods to initiate the preparation of Grignard reagents. Several examples of industrially useful Grignard reactions are summarized. Finally, waste disposal considerations and a summary of the industrial applications conclude this chapter.

Grignard reagents are known to exist as an equilibrium mixture of the organomagnesium halide ($RMgX$) and the diorganomagnesium (R_2Mg) forms and often exist as dimers or higher oligimers (all of which are further complexed with solvent). For

Grignard Reagents: New Developments Edited by Herman G. Richey, Jr. © 2000 John Wiley & Sons Ltd.

simplicity, throughout this chapter the Grignard reagent is written as RMgX.

6.2 SAFETY AND ENGINEERING CONSIDERATIONS SPECIFIC TO INDUSTRIAL APPLICATIONS

6.2.1 Typical Equipment Configuration

Industrial Grignard reagents are typically manufactured using the batch method of production. Common features of a batch Grignard plant have been previously reported [5,6,7,8]. A simplified equipment flow diagram depicting a typical batch plant configuration is shown in Figure 6.1. A continuous system for production of Grignard reagents was first patented by Hoffman LaRoche in 1965 [9] and subsequently other continuous systems have been proposed [10]; however, the continuous system is typically not used on an industrial scale.

The material of construction for the Grignard reactors and feed vessels R-1, R-2, T-1, and T-2 is typically stainless steel, carbon steel or glass-lined carbon steel. (For convenience the charge tanks and the reactors are numbered in Figure 6.1, so that T-1 refers to Tank 1 and R-1 refers to Reactor 1.) The use of carbon steel must be considered carefully, however, due to the potential introduction of iron which can be a problem in some reactions. The material of construction for R-3 and T-3, the quench equipment, can be glass-lined steel or an acid resistant metal alloy such as Hastelloy C.

Following preparation of the equipment, and establishing an inert atmosphere (typically nitrogen or argon) to exclude oxygen and atmospheric moisture, the first step in the manufacturing process involves the preparation of the organic halide substrate/solvent mixture in feed tank T-1, the organic substrate/solvent mixture in feed tank T-2, the acid/water quench mixture in feed tank T-3, and finally the magnesium/solvent mixture in reactor R-1. It is critical that all Grignard processing equipment be thoroughly dried to less

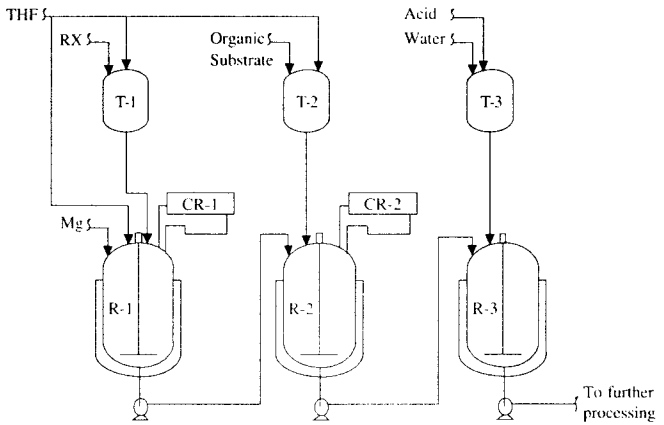

Fig. 6.1. Typical Batch Grignard Plant Equipment Flow Diagram.

than 0.02 w/w% water [11] prior to commencing processing (see Section 6.3.1).

After all of the ingredients have been charged, the magnesium/solvent mixture in R-1 is heated to the desired reaction temperature and an initial charge (5–10% of the total organic halide mixture) is made from T-1 to R-1. After the initial charge, the mixture in R-1 is held until initiation of reaction to the Grignard reagent is observed. This is the most critical part of the Grignard process, for it is absolutely necessary that initiation occur prior to feeding additional substrate (see Section 6.3.4). Failure to do so could lead to a high concentration of unreacted organic halide in R-1, which could result in a runaway reaction. Therefore, the equipment must contain the necessary instrumentation (1) to accurately measure the amount of organic halide delivered, and (2) to assist in the detection of initiation. After reaction initiation is observed, the remainder of the organic halide/solvent mixture is added to R-1 at a controlled flow rate while maintaining R-1 at the desired temperature. The temperature is controlled by applying cooling to the R-1 jacket and/or by controlling the flow rate of the organic halide/solvent mixture.

The Grignard reagent is then reacted with the organic substrate to form the product. Typically, the Grignard reagent is transferred from R-1 to R-2 where addition of the organic substrate/solvent solution from T-2 begins. Reverse addition, i.e., first charging the organic substrate to R-2 followed by the addition of Grignard reagent from R-1, may be desired depending upon the chemistry of the particular Grignard reaction.

Following reaction of the Grignard reagent with the organic substrate, the product is formed as a complex with magnesium. For example, in the case of the addition of a Grignard reagent to a ketone, a complex of the product alcohol with the residual magnesium salts is formed. A quench of the product-magnesium alkoxide complex using aqueous acid is required to liberate the desired product. The product complex is transferred from R-2 to R-3 and the acid/water mixture is then transferred from T-3 to R-3 to quench the product-complex. In contrast to a laboratory procedure in which water may be added to the reaction, the preferred method on a larger scale is to transfer the condensation product from R-2 to R-3. This transfer offers significant enhancements to productivity by maintaining the reaction tank as a dry tank and the quench tank as a wet tank. On industrial scale the time and effort to ensure that a reactor is dry prior to processing (drying, boil-out, and maintaining an inert atmosphere) more than offsets the expense associated with the use of an additional tank. Water alone is sufficient to quench the complex; however, the resulting magnesium salts produce a gelatinous mixture which is difficult to stir. Introduction of an acid converts the gelatinous basic salts to water soluble magnesium salts.

6.2.2 Choice of Solvent

Solvents which are utilized in the preparation and use of Grignard reagents require two main characteristics: first, the solvent must not be a proton donor nor reactive with the magnesium metal prior to the formation of the Grignard reagent, and second, the solvent must be stable in the presence of a strong and nucleophilic base after the reagent has been prepared.

The most common solvents used in the preparation of Grignard reagents are ethers, typically diethyl ether or tetrahydrofuran (THF). Ethereal solvents offer the advantage of stabilizing the Grignard reagent. The stabilization of phenylmagnesium bromide by two diethyl ether molecules was proven by the crystallization of the complex [12]. Due to the low flash point of diethyl ether, THF is frequently the solvent of choice on an industrial scale.

6.2.3 Process Hazards Analysis

Prior to start-up of a production campaign, a process hazards analysis (PHA) should be conducted. A common and generally accepted PHA technique is the HAZOP (**Haz**ard and **Op**erability) method, although alternate techniques can be equally effective [13,14,15]. The purpose of the PHA is to evaluate the manufacturing process to identify and address potential safety issues prior to start-up.

Equipment must be analyzed in conjunction with the process to study the potential for deviation from normal conditions. The probability and consequence of the deviation are considered together to determine the appropriate safeguards to have in place prior to production. Some safety issues that require attention prior to production are given below.

- The reactor vent sizes must be large enough to effectively relieve pressure in an upset condition (see Section 6.2.4).
- The delivery of the organic halide to the Grignard reactor must be accurately measured and controlled to prevent an overcharge (see Section 6.2.5).
- Reactor cooling capacity must be sufficient to control the heat of reaction (see Section 6.2.5).
- Accurate detection of reaction initiation is necessary to prevent a build-up of unreacted organic halide in the Grignard reactor (see Section 6.3.4).
- Use of safety interlocks is necessary to prevent and/or mitigate an upset scenario (see Section 6.2.5).
- Safe handling of magnesium is important to avoid hazardous conditions (see Section 6.2.7).

Note that this list is not meant to be exhaustive but instead serves to highlight some common areas of concern when handling Grignard reagents in a production environment.

6.2.4 Vent Sizing/DIERS Calculations

Prior to running a Grignard reaction on an industrial scale, it is necessary to ensure that the vent area is large enough to effectively relieve pressure in an upset condition. Inadequate pressure relief could lead to severe explosions, extensive equipment damage, and personal injury. The following upset conditions, and the subsequent temperature/pressure rise should be considered.

1. Overcharge or uncontrolled addition of the organic halide, the worst-case scenario being 100% of the organic halide charged prior to inititiation.
2. Ingress of cooling fluids to the Grignard reactor.
3. Loss of cooling.
4. Uncontrolled addition of the organic substrate to the Grignard reagent.

To effectively evaluate the scenarios mentioned above, it is recommended that laboratory calorimetry experiments be conducted to obtain data specific to a given process. Commercial bench scale equipment is available to perform such experiments [16,17]. Typically, the exotherm associated with the formation of the Grignard reagent (~80 kcal/mol Mg) is significantly larger than the exotherm associated with either the subsequent reaction with the organic substrate or the reaction of the Grignard reagent with water. Due to the fact that there is an induction period prior to reaction of the organic halide with magesium, upset scenario 1 is usually chosen as the worst case. Vent-sizing calculations are performed to mitigate and control the associated hazards [18].

The DIERS (AICHE Design Institute of Emergency Relief Systems) method is typically used to estimate the required vent area to adequately relieve pressure for a given scenario. Several papers have been published detailing calculation methods [19–25]. One published calculation method is described in the box below. The equations are given to highlight the variables which must be considered for proper vent size design. The sizing of industrial equipment is conducted by engineers who specialize in reactor design. If existing equipment is going to be used to run Grignard chemistry, then an engineering analysis should be conducted to ensure that adequate venting is available in the event of an upset condition.

6.2.5 Grignard Reagent Formation—Process Controls and Interlocks

6.2.5.1 Control of Exotherm

Following an induction period, the formation of a Grignard reagent is typically fast and exothermic. After the reaction is initiated, the organic halide is usually consumed quickly, allowing the reaction

For a tempered[26] system, assuming homogeneous, two phase venting, vent area based on the DIERS method as developed by Leung[27] can be expressed as:

$$A = \frac{m_o q}{FG\left[\left[\frac{VT}{m_o}\frac{dP}{dT}\right]^{1/2} + (C_p \Delta T)^{1/2}\right]^2}$$

where,

$$q = 0.5 C_p \left[\left(\frac{dT}{dt}\right)_s + \left(\frac{dT}{dt}\right)_m\right]$$

and,

$$G = 0.9\frac{dP}{dT}\left(\frac{T}{C_p}\right)^{1/2}$$

in which the variables are

A = vent area necessary for a desired overpressure (m^2)

ΔT = temperature at the maximum overpressure condition less the temperature at the relief pressure (K)

m_o = mass of the reactor ingredients (kg)

C_p = specific heat of reactor ingredients (J/kg K)

V = volume of the reactor (m^3)

T = temperature of vessel contents at relief set pressure (K)

$\frac{dP}{dT}$ = rate of change of vapor pressure with temperature at relief set pressure (N/m^2K)

F = dimensionless turbulent flow friction factor which accounts for friction losses in the vent piping

G = vent flow capacity per unit area at relief set pressure (kg/m^2s)

q = heat evolution rate per unit mass (W/kg)

$\left(\frac{dT}{dt}\right)_s$ = self heat rate (°C/s) at the relief set pressure

$\left(\frac{dT}{dt}\right)_m$ = self heat rate (°C/s) at the maximum temperature corresponding to the maximum overpressurization

exotherm to be controlled by controlling the rate of addition. Calculations should be made to ensure that the cooling capacity of the reactor and the condenser are properly sized to permit control of the reaction exotherm.

6.2.5.2 Safety Interlocks

Process safety interlocks can be used to prevent and/or mitigate an upset condition. Safety interlocks consist of outputs from process control systems, such as programmable logic controllers or distributed control systems, which trigger an action designed to compensate for an upset condition and thus avoid an accident even in the event of human or computer error. An example of a safety interlock would be the introduction of full cooling if the temperature of a reaction exceeded a safe level.

Safety interlocks are used in Grignard reagent preparation to prevent a build-up of unreacted organic halide. Redundant instrumentation, such as a flow meter in the feed pipe from T-1 to R-1 (refer to Figure 6.1) and weigh cells on T-1 and/or R-1, should be in place to accurately measure the amount of organic halide delivered to the Grignard reactor. The instrumentation should be interlocked to the R-1 inlet valve to stop the flow once the predetermined initial amount of organic halide has been added. A second approach to avoid an overcharge of the organic halide during the pre-induction period (refer to the equipment flow diagram in Figure 6.2) is to employ an additional feed tank, T-4. Instead of charging the halide directly from the organic halide feed tank T-1 to the Grignard reagent reactor R-1, an intermediate holding tank is employed such that the predetermined safe initial charge is made from T-1 to T-4, the quantity of the charge verified in T-4, and then the contents of T-4 are transferred to R-1. This equipment configuration eliminates the chance of operator, software, or instrumentation error resulting in an overcharge of organic halide, which could happen if T-1 is connected directly to R-1. A third, administrative, approach is to require a supervisor to observe the production operation and to initial the batch record to signify that the appropriate charge was made. To mitigate too rapid addition of the organic halide, a flow meter with a high flow interlock set to automatically close the R-1 inlet valve can be employed to minimize the risk of feeding the halide too fast once the reaction has started.

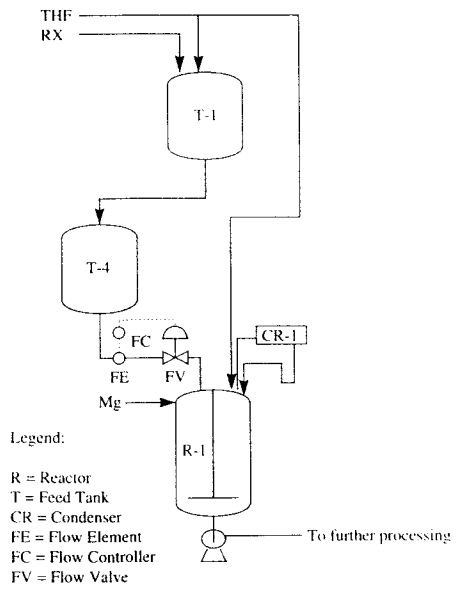

Fig. 6.2. Use of Intermediate Holding Tank to Deliver Organic Halide to the Grignard Reactor.

A higher than expected temperature would be a sign that the cooling capacity is not adequately controlling the exotherm associated with the formation of the Grignard reagent. The use of a high-temperature result in the closure of the R-1 inlet and/or T-1 outlet valve is an example of a safety interlock that should be implemented to guard against insufficient reactor cooling. Similar high-temperature interlocks should be used on R-2 during the reaction of the Grignard reagent and on R-3 during the quench of the Grignard complex. For reactions run under reflux conditions, a high reflux temperature could signal an overload of condensing capacity and could also be interlocked to slow or stop the flow of substrate.

6.2.6 Reactivity of Grignard Reagents—Water, Heating/Cooling Fluids

The introduction of water or heating/cooling fluid in the processing equipment raises additional issues for plant-scale operations. In the laboratory, the introduction of water to a Grignard reagent results in a 'quench' of the reagent. The quench ruins the reaction and generates the hydrocarbon analog of the respective Grignard reagent. Such reactions are typically exothermic [28].

$$RMgX + H_2O \rightarrow RH + Mg(OH)X$$
$$+ \text{heat evolved (20–40 kcal/mol)}$$

The heat generated from an adiabatic quench of a large-scale reaction may be sufficient to boil the solvent (in combination with the generation of hydrogen gas [29]) and over-pressurize the equipment. Therefore, water should be avoided as the cooling medium in the jackets of production equipment. Where it is not practical to eliminate water as the cooling medium, equipment integrity testing must be performed to ensure that water infiltration will not occur. In addition, all water lines to the equipment should be blanked off (a blank is a physical barrier inserted into the line to prevent flow) or preferably, the line physically disconnected. All equipment should be pressure tested to ensure no leaks exist prior to starting any processing. Some other common heating/cooling fluids are shown in Table 6.1.

6.2.7 Safe Handling of Magnesium

The areas in the vicinity of solid magnesium handling need to be kept clean, dry and free of materials which would react with magnesium if a small portion were to spill when being charged to the reactor. Magnesium reacts with water and acids to form hydrogen gas. In addition, magnesium can be easily ignited from an open flame. Burning magnesium chips need to be extinguished using special Met-L-X [32] fire extinguishers. Water should **never** be used on burning magnesium chips.

6.3 REACTION INITIATION

There are many factors that are important to the successful initiation of the Grignard reagent formation. The control of the exotherm typical of this chemistry is dependent upon the reaction initiating smoothly. Following the initial charge of organic halide, the reaction must start prior to the continuation of addition. One of the most important factors, the dryness of the system, is discussed in Section 6.3.1. Other factors, however, should also be considered.

The selection of the organic group and the particular halogen in the organic halide are critical factors in the preparation of the reagent. The industrial chemist, of course, ordinarily is presented with a particular R-group to be used in the Grignard reagent; the selection is frequently decided long before any consideration is given to conducting

Table 6.1. Common Heating/Cooling Fluids and Reactivity with Grignard Reagents

Heating/Cooling Fluid	Reactivity with Grignard Reagents	Comments
Water	yes	Heat of reaction = 20–40 kcal/mol
Dowtherm A*	no	73.5% diphenyloxide [30] 26.5% diphenyl
Dowtherm J*	no	Alkylated aromatics [31]
Syltherm*	no	Dimethylpolysiloxane
Ethylene/Propylene Glycol	yes	Reactive with glycol; additionally, these cooling fluids typically contain 50% water.
Mineral Oil	slight	Liquid hydrocarbons from petroleum.

the reaction on an industrial scale. The selection of the R group has been covered by Silverman from the viewpoint of the structure activity relationship. There is frequently a choice of halogen, although for reasons of cost, availability, and reaction efficiency, the halide is usually limited to chlorine or bromine for industrial processes.

Additionally, many other factors need to be considered in the preparation of Grignard reagents on an industrial scale. Four key factors are summarized below. First, equipment drying is discussed in Section 6.3.1. Second, the magnesium form affects the surface area and ease of reaction initiation and is discussed in Section 6.3.2. Third, initiation of the Grignard reagent formation can be influenced by addition of initiators to the reaction; this topic is discussed in Section 6.3.3. Fourth, the importance of detecting the initiation of the reaction, along with methods to detect the initiation, are summarized in Section 6.3.4.

6.3.1 Equipment Drying

Water appears to be the largest impediment to the initiation of reactions on a production scale. Improper equipment drying can result in a reactor containing a mixture of solvent, magnesium, and unreacted organic halide with which it is difficult or impossible to initiate the reaction [33].

On a laboratory scale, ensuring that the Grignard reaction is conducted in dry glassware does not present a significant challenge. For example, in the laboratory, a flask may be dried under a stream of dry nitrogen gas by heating the apparatus with a Bunsen burner [3c]. However, on commercial scale equipment, drying is much more difficult because the equipment is larger and the piping is more complex. In addition, it is important to keep in mind that the surfaces of equipment, even if they appear to be completely dry, are often covered with a film of water.

The last step in an industrial equipment cleaning procedure typically involves a large volume water flush of the equipment. The objective of the drying process is then to displace any water residues from the cleaning operation that is left behind on the equipment surfaces, including tank and pipe walls, fittings, and valve components. The equipment drying process involves a solvent rinse through all associated piping, reactors, and feed tanks that will be involved in the process. For vessels equipped with a condenser, it is very important to dry the overhead equipment and piping as well. This can be accomplished by heating the solvent to its boiling point and refluxing for a period of time. This operation effectively rinses out the vapor column, condenser, and reflux piping and carries water back to the reactor where it can be removed from the vessel. The solvent is then cooled to ambient temperature and transferred to the next vessel in the equipment train. This sequence is repeated until the level of water in the solvent, after passing through the equipment, is less than the required amount. To dry equipment down to less than 0.02 w/w% water, multiple solvent rinses are usually necessary. Once it is determined to be dry, the equipment is often baked or blown dry with an inert gas for an extra level of protection. Finally, a slight positive pressure of the inert gas can be maintained on processing equipment to further ensure that the equipment, once dry, remains dry.

Prior to performing the above drying operations, it is necessary that the ingoing solvent meets the final water specification. Dry THF can be purchased (water content <0.01%); however, without special precautions, the solvent often picks up moisture to a level of 0.1%, an unacceptable level in most Grignard reactions. To reduce the level back to 0.01%, recycling the solvent through molecular sieves is effective. The heat generated by the adsorbtion of water into the sieves is significant, however, and should be considered when performing this operation.

6.3.2 Different Forms of Magnesium: Advantages and Disadvantages

Magnesium can take a variety of different physical forms: turnings, powder, chips and finely divided metal (such as 'Rieke-magnesium'). Each of these forms offers advantages and disadvantages, as summarized in Table 6.2. This section also considers the issues with mechanical activation of the magnesium metal, while the next section discusses the use of chemical initiators.

Table 6.2. Advantages and Disadvantages of Magnesium Forms

Magnesium Form	Advantages	Disadvantages
Turnings	Ease of Use	Concern about abrasiveness to glassware and glass-lined reaction vessels.
Powdered	More Reactive	Finely divided powder gives faster oxidation of the surface upon exposure to air, can be pyrophoric.
Chips (from sublimation)	Higher purity	Lower surface area results in less reactivity than powdered or turnings.
Rieke-magnesium	More reactive	—Requires extra step in preparation. —Residual magnesium halide present in reaction. Residual potassium may be present. —Difficult preparation on a large scale.

The most commonly used type of magnesium on an industrial scale is magnesium turnings. These are readily available and easy to use. On a laboratory scale, activation of the turnings may be accomplished by the dry stir method [34]. This method is not usually practical in production equipment due to the low stir volume of the magnesium charge; however, the higher shear forces present in a commercial process reactor are helpful in mechanically abrading the surface of the magnesium turnings. Thus, a stir period for the magnesium turnings in the solvent prior to the addition of the reagent permits exposure of fresh magnesium metal on the surface of the turnings. Magnesium powder has higher surface area but is more difficult to handle on an industrial scale. Magnesium chips, which are obtained from sublimation, are more expensive and less available than magnesium turnings.

One of the more interesting methods to activate magnesium is the preparation of Rieke-magnesium [35]. This involves precipitation of highly active magnesium from a magnesium halide solution by reaction with potassium metal. The resulting magnesium precipitate is highly activated and has enormous surface area, both factors leading to enhanced reactivity. In addition to requiring an extra step for the preparation of the magnesium, handling of potassium metal poses sufficient hazards to make this procedure less attractive on a commercial scale. A possible further disadvantage of this method is that potassium ion remains in the product mixture. A recent variation of the Rieke procedure involves preparation of the powdered magnesium by reduction with lithium metal catalyzed with a small amount of naphthalene as an electron carrier [36].

Ultrasound has also been used to activate the reaction with magnesium [37]. The induction time was reported to be very short under ultrasonic irradiation. Luche and Damiano suggest that the activation results from cavitation, although surface effects due to abrasion of the magnesium particles cannot be ruled out.

6.3.3 Initiators—Advantages and Disadvantages

A useful strategy for reaction initiation is the addition of an agent to both dry the reaction medium and to activate the magnesium metal through interaction with the metal surface. There are many methods of initiation of the Grignard reagent formation; these have been summarized previously [38] with emphasis on application to laboratory work. In this section the discussion focuses on the industrial application of several common initiators.

6.3.3.1 Vitride®

Vitride® is a reducing agent that can be used to initiate formation of Grignard reagents. Vitride® is

sodium bis(2-methoxyethoxy)aluminum hydride, 65–70% in toluene. This method is primarily effective due to the removal of water from the system, but also involves surface effects on the magnesium metal. Vitride reacts with all compounds containing active hydrogen and can be used for removing trace levels of moisture [39]. The two step reaction of Vitride® with water is shown below.

$$NaAlH_2(OCH_2CH_2OCH_3)_2 + H_2O \rightarrow$$

$$NaAlO(OCH_2CH_2OCH_3)_2 + 2H_2$$

$$NaAlO(OCH_2CH_2OCH_3)_2 + H_2O \rightarrow$$

$$NaAlO_2 + 2CH_3OCH_2CH_2OH$$

Vitride® also activates the magnesium.

$$NaAlH_2(OCH_2CH_2OCH_3)_2 + Mg \rightarrow$$

$$\text{active } Mg + H_2$$

Vitride® is less toxic than some of the other activating agents. It offers the advantage of both drying the reaction medium and initiating the reaction. Unfortunately, it does leave a residue of aluminum salts in the reaction which must be removed as part of the reaction work-up. The second by-product, 2-methoxyethanol, reacts with the Grignard reagent and results in a slight yield loss. It should be noted that 2-methoxyethanol is classified as a teratogen.

6.3.3.2 Small portion of Grignard Reagent

An excellent method for drying the system is the addition of a small portion of the reagent being prepared, either a lab sample, or more commonly, a small portion of Grignard reagent retained from the previous batch. This method of initiation has the advantage of being indigenous to the process, therefore new chemical impurities are not a concern. A disadvantage of retaining a portion of the previous batch is the potential for one out-of-specification batch to affect multiple lots from a production campaign.

6.3.3.3 Chemical Initiators

Surface Initiators: Another strategy for the activation of magnesium is to etch the surface of the magnesium metal. Such activators added for this purpose include elemental iodine, mercury metal, transition metal salts, methyl iodide and 1,2-dibromethane. The primary mode of action is chemical modification of the magnesium surface. The use of other metal salts, such as zinc chloride, to activate the magnesium have the disadvantage of leaving transition metal ions which may participate in side reactions.

Iodine: Addition of iodine generates pits on the surface of the magnesium metal. Additionally, the initial formation of magnesium(I) iodide serves as a start for the attack on the alkyl halide, which then continues as a chain reaction. Instead of adding iodine, preformed Gilman catalyst (prepared by heating with iodine) can be used.

Mercury: Addition of a small amount of elemental mercury may also form an amalgam, which affects the surface of the metal, and at the least cleans the oxide or water film off of the magnesium surface. Use of mercury is not recommended for either laboratory or industrial scale reactions due to both the toxicity of this metal and the difficulty created for the disposal of the resulting waste streams.

Organic Halides: Addition of methyl iodide or 1,2-dibromoethane is useful in initiation of the Grignard reagent formation [3b,40]. In each case a small portion of the organic halide is added so that the magnesium starts to react with the more reactive alkyl halide, providing reactive sites on the magnesium metal surface where a less reactive organic halide may react. Additionally, the initial formation of a small amount of Grignard reagent may serve to completely dry the reaction medium, giving improved reactivity. The obvious disadvantage with the use of methyl iodide is the generation of a small amount of methyl Grignard which may give a competing reaction when the Grignard reagent is used. This can be a particular problem in the pharmaceutical industry where the purity of the reaction products is critical. This problem is overcome with the use of 1,2-dibromoethane. The initial reagent eliminates to give magnesium bromide and ethylene, which is lost from the reaction as a gas. An additional disadvantage with methyl iodide or 1,2-dibromoethane is that both are suspected carcinogens and must be handled with great care.

6.3.4 Detecting Initiation of Reaction

As previously stated, accurate detection of reaction initiation is of critical importance to ensure a safe, well controlled reaction. As with any exothermic reaction, an increase in temperature, or an increase in cooling required to maintain a constant temperature, is a reliable indicator of reaction initiation. Redundant, calibrated temperature probes are recommended to ensure accurate temperature readings. However, for Grignard reactions run under reflux conditions, the temperature remains relatively constant and therefore cannot be used to determine initiation. In the laboratory, initiation of a reaction run at reflux is often confirmed by observance of increased foaming and/or vigorous bubbles emanating from the magnesium chips in addition to a darkening in color associated with the dissolution of magnesium. These visual observations are often difficult to ascertain in large industrial equipment. An increase in reflux rate will occur upon initiation of reaction; therefore, measurement of the reflux rate can provide a quantitative method of confirming reaction inititiation. However, the lag time between an increase in boil rate and a subsequent increase in reflux return rate must be considered. Recently, real-time online analytical analysis such as FTIR has been shown to provide valuable information regarding the disappearance of the organic halide and the formation of the Grignard reagent [41].

6.4 EXAMPLES OF INDUSTRIAL GRIGNARD CHEMISTRY

Although many examples of Grignard chemistry appear in the literature, processes run on a commercial scale are frequently not reported. Several processes are discussed below as examples of chemistry indicated by the patent literature to be run on an industrial scale.

6.4.1 Tamoxifen

Tamoxifen citrate is a non-steroidal estrogen antagonist [42] used in the treatment of advanced breast cancer. Grignard chemistry plays an important role in the synthesis [42,43]. Key starting materials in the production of tamoxifen (**5**) are bromobenzene and 1-[4-[2-dimethylaminoethoxyphenyl]-2- phenyl-1-butanone (**2**). Following preparation of the Grignard reagent of bromobenzene, **1**, the condensation reaction shown in Scheme 6.1 is key to this synthesis, allowing the two large portions of the tamoxifen molecule to be joined together. Further treatment with acid results in the dehydration of the carbinol (**3**) to the mixed isomers of tamoxifen (**4**). The elimination produces the desired Z-olefin as the major product. This chemistry provides the tetra-substituted olefin in a convergent manner. Further processing of the E/Z mixture [43] (**4**) gives pure tamoxifen (**5**).

6.4.2 Droloxifene

Droloxifene [44], a hydroxy-derivative of tamoxifen, is currently under development by Pfizer and Klinge Pharma for the treatment of osteoporosis. The key starting materials in the production of droloxifene are the THP-ether of 3-bromophenol (**6**) and 1-[4-[2-dimethylaminoethoxy)phenyl]-2-phenyl-1-butanone (**2**). As with tamoxifen, Grignard chemistry plays an important role in the synthesis. This example illustrates the use of a THP protecting group during a Grignard condensation, Scheme 6.2 [45]. THP ethers are particularly effective in protecting groups for Grignard reactions because the group is very base stable, but is cleaved by acid treatment, which is typically included as part of the reaction work-up.

As shown in the tamoxifen example, following condensation, the intermediate tertiary alcohol **8** is acidified leading to elimination and removal of the THP-protecting group. The elimination gives the olefin as a mixture of the E and Z isomers (**9** and **10** respectively), with the desired E-isomer (**9**) as the predominant product. Further processing of the E/Z mixture converts Z isomer (**10**) to the desired products **9**.

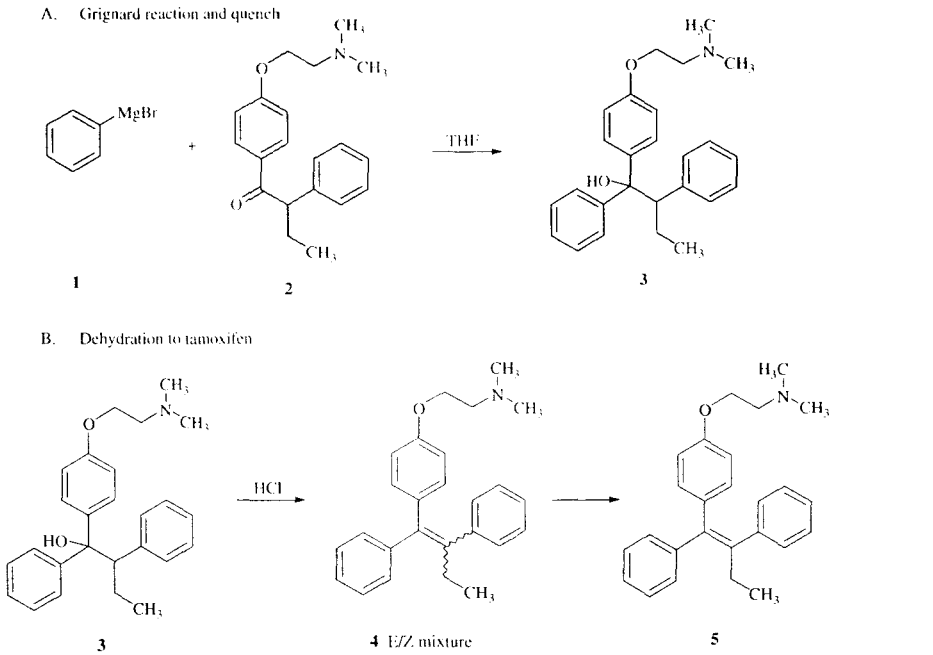

SCHEME 6.1. Preparation of a tetra-substituted olefin–tamoxifen.

6.4.3 Veltol® and Veltol Plus®

Although quite different from the examples above, the use of Grignard chemistry in the synthesis of flavor enhancers is similar to that in the pharmaceutical industry as the food industry must also meet high standards of purity and low residues of synthetic by-products. Veltol® and Veltol Plus® are the Cultor trademark names for maltol and ethyl maltol, respectively. Unlike ethyl maltol, maltol is a naturally occurring substance found in the bark of young larch trees, pine needles, and chicory [46]. Since it is not economically practical to extract large quantities of maltol from naturally occurring substances, both substances are synthetically manufactured. One of the reported industrial syntheses utilizes Grignard chemistry.

Furfuryl aldehyde (**12**) is reacted with the Grignard reagent of an alkyl chloride (**11**, R = Me or Et) to yield the corresponding alcohol (**13**), which is a key intermediate [47] in the production of maltol/ethyl maltol (**14**) [48], shown in Scheme 6.3.

6.4.4 Use of a Grignard Reagent as a Base (Formation of Magnesium Enolates)

One example of the use of Grignard reagents as a base to produce magnesium enolates is the synthesis of the animal health quinolone antibiotic, danofloxacin (**20**), Advocin® [49]. The synthesis of β-ketoesters from acylation of magnesium malonates generated from hydrogen methylmalonate by treatment with magnesium ethoxide or isopropylmagnesium bromide was initially described by Ireland and Marshall [50]. Several refinements

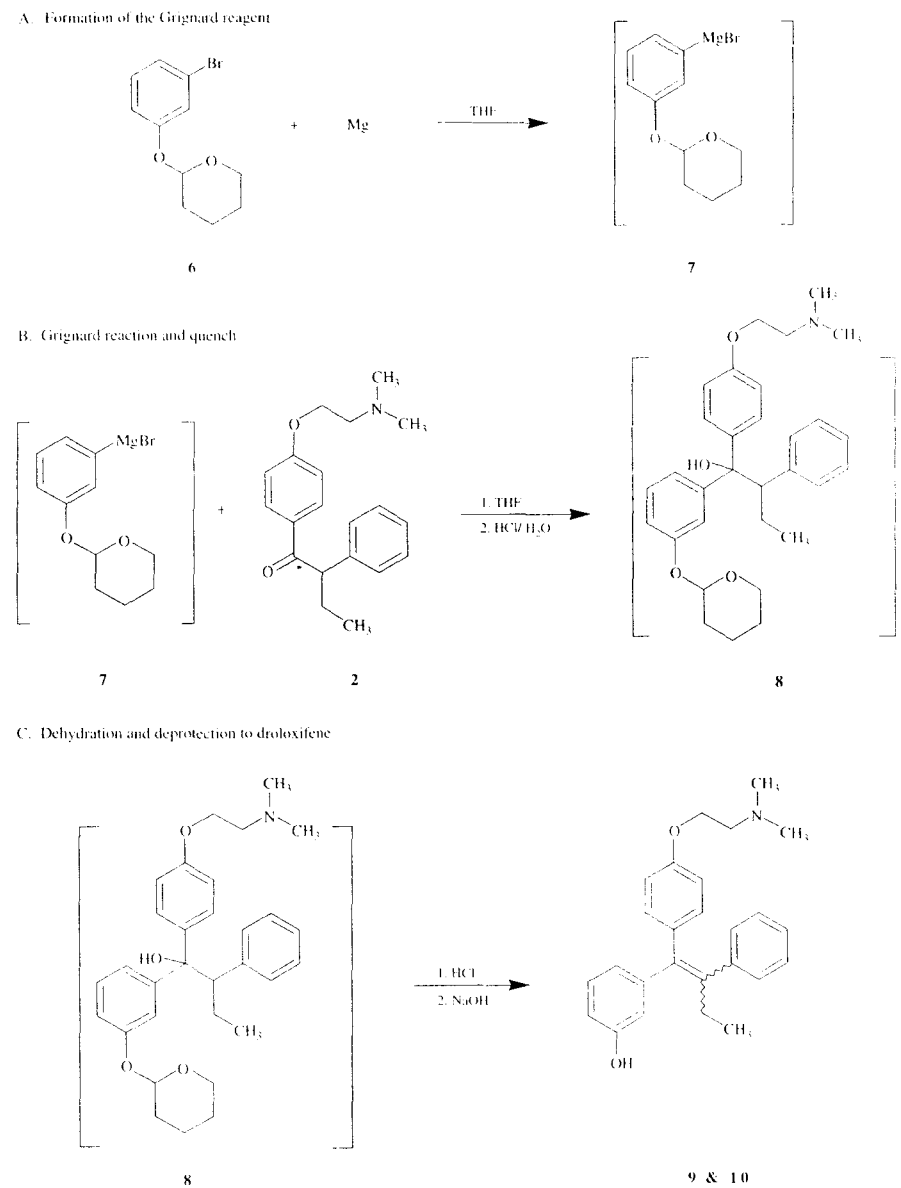

SCHEME 6.2. Preparation of a tetra-substituted olefin–droloxifene.

A. Grignard reaction and quench

12 11 13

B. Preparation of maltol/ethyl maltol

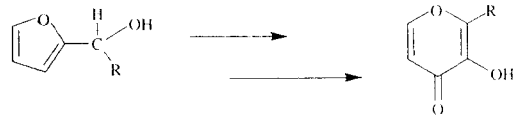

13 14

SCHEME 6.3. Preparation of maltol/ethyl maltol.

have been made to Ireland's method over the years; each has shown that magnesium plays an important role in the stabilization of the malonate-anion while giving selectivity for C-acylation [51]. The literature suggests that good methods to prepare magnesium malonate anions are by addition to the malonic ester of magnesium chloride (along with an added base), magnesium ethoxide, or a Grignard reagent. Experience has shown that use of the Grignard is preferred [49].

The use of methylmagnesium chloride offers several advantages over other methods to prepare β-ketoesters. The magnesium malonate is both more soluble and more stable than the corresponding di-lithium malonate prepared from hydrogen ethyl malonate and two equivalents of *n*-butyllithium [52]. Generation of two equivalents of the dilithio monoethyl malonate dianion requires four equivalents of *n*-butyllithium; thus the magnesium malonate offers considerable advantage for the preparation of β-ketoesters.

The magnesium enolate is prepared from 2.1 equivalents of potassium ethyl malonate (**16**) by treatment with ~2.0 equivalents of alkyl Grignard (usually methyl or ethyl since these are commercially available). The resulting dianion, shown in Scheme 6.4 as **17**, has strong nucleophilicity at the carbon.

Following preparation of an activated acid (acid halide or acyl-imidazole), the two reagents are combined. When the acid chloride is used, two equivalents of **17** are required due to one equivalent of the malonate anion being consumed as a base. The resulting β-ketoester (**19a & b**) exists as a pair of ketol-enol isomers. These are in a pH dependent equilibrium. To complete the synthesis, several steps are required to elaborate the β-ketoester to danofloxacin, **20**.

6.4.5 Naproxen

The final two examples demonstrate the usefulness of Grignard chemistry in the synthesis of analgesics. Naproxen® (**23**) is a product discovered and marketed by Syntex [53]. The compound is a non-steroidal anti-inflammatory (NSAI). Just prior to the expiration of the patent in 1993, Syntex reported annual sales of Naproxen® of $1.05 billion. The synthesis is shown in Scheme 6.5. Several synthetic routes were investigated prior to the development of the commercial route. Following the generation of the Grignard reagent, the magnesium anion is alkylated, giving the desired structure with the entire carbon skeleton in place [54]. Alkylation with the magnesium salt of 2-bromopropionic acid instead of the ethyl ester, used in an earlier synthesis, saves the step to hydrolyze the ester. Resolution is conducted with N-alkyl glucamine which is prepared initially from D-glucose but then is recovered and recycled within the process.

A. Formation of malonate potassium salt

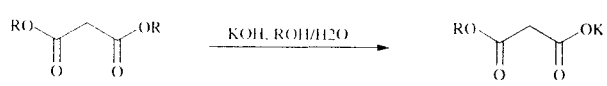

15 16

B. Grignard reagent–magnesium enolate formation

16 17

R' = alkyl X = Cl or Br

C. Formation of beta-ketoester

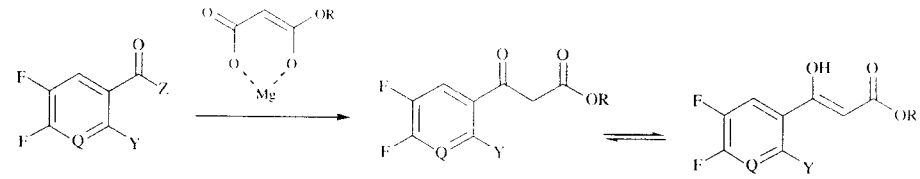

18 19a 19b

Q = N or CH
Y = Cl or F
Z = imidizoyl or Cl

D. Danofloxacin

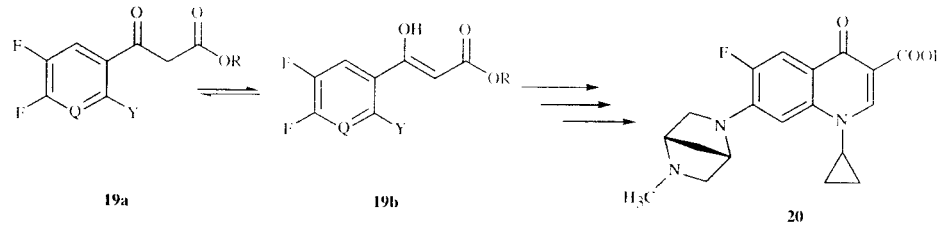

19a 19b 20

SCHEME 6.4. Generation of magnesium malonate for β-ketoester synthesis.

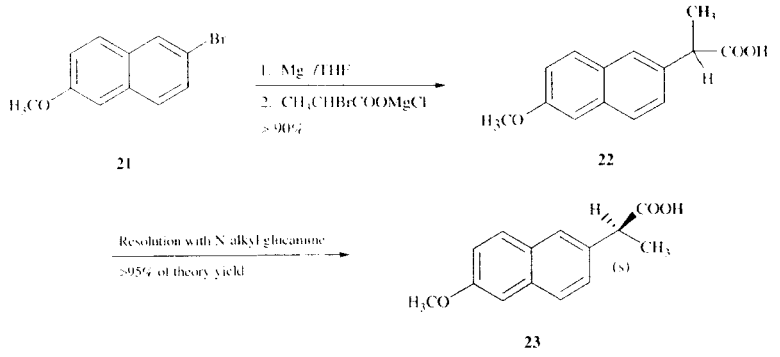

SCHEME 6.5. Naproxen®.

6.4.6 Propoxyphene

Eli Lilly introduced a major medical advance in the treatment of pain in the late 1950's with the introduction of Darvon® (propoxyphene, **26**) [55]. This demonstrates the application of the Grignard reaction to provide a tertiary substituted alcohol.

Following resolution of β-dimethylamino-α-methyl-propiophenone with dibenzoyl-(+)-tartaric acid, the chiral ketone is added to a solution of benzylmagnesium chloride in diethyl ether [56], see Scheme 6.6. Liberation of the alcohol product, **25**, provides the product with the carbon backbone and stereochemistry in place. The tertiary alcohol

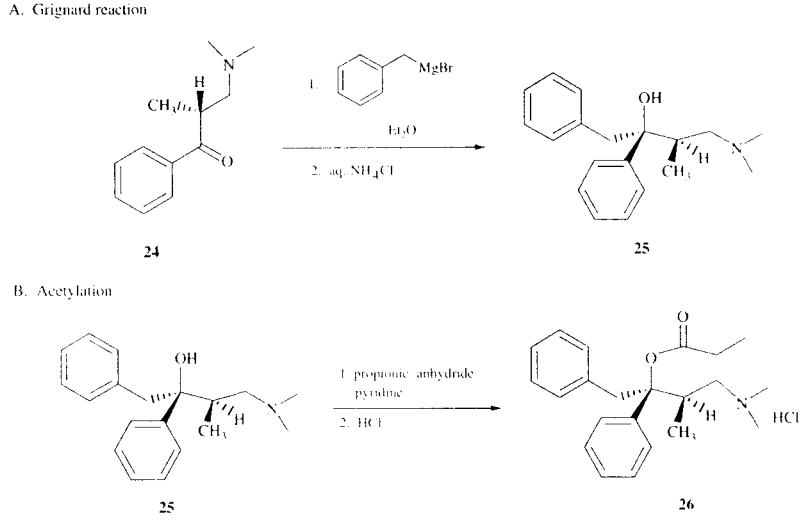

SCHEME 6.6. Propoxyphene.

is then converted to the propionate ester, and the active drug is isolated as the hydrochloride salt.

6.4.7 Additional Examples

There are many other examples of the industrial application of Grignard chemistry. This section is not meant to be exhaustive, but is an overview of the many applications that have been devised for Grignard reagents. The synthesis of β-carotene was described in the early 1950's; this utilized Grignard chemistry [57]. A highly convergent route was developed, based upon the symmetry of β-carotene, in which two equivalents of the acetylenic Grignard reagent are condensed with a diketone, 4-octen-2,7-dione, to provide the entire carbon backbone of β-carotene.

Several examples of the use of Grignard reagents for the synthesis of perfumes are given by Walker [58]. Walker notes that one of the early patents on the industrial application of Grignard reagents was to Victor Grignard, for the development of a process to prepare primary phenyl ethyl alcohol. Grignard's preparation from phenylmagnesium bromide and ethylene oxide gave a purer product than previous methods.

Grignard reagents are also used in the synthesis of organo-silane compounds; treatment of silicon tetrachloride or an alkylsilyl chloride with a Grignard reagent introduces the alkyl group of the Grignard onto the silicon. A review of the preparation of alkylsilyl chlorides (useful in protecting groups), alkylsilanes (useful as reducing agents), and silicones (used as lubricants and for heating/cooling fluids) is beyond the scope of this chapter. The reader is referred to an overview given by Waugh [59].

Although Grignard reagents are frequently reacted with ketones to provide alcohols or elaborated to other products, there is a variation where the Grignard reagents are used to prepare ketones as the product of the reaction. The Grignard reagent is reacted with cadmium chloride to give the organocadmium reagent, which is in turn reacted with an acid chloride or anhydride to produce the desired ketone. For example, the synthesis of methyl 4-keto-7-methyloctanoate is known, starting from isoamyl bromide. Following formation of the Grignard reagent, treatment with cadmium chloride forms diisoamyl cadmium, which in turn is treated with β-carbomethoxypropionyl chloride. This gives the desired product in high yield [60]. The organocadmium adds to the acid chloride but not to the ester or the product ketone. The organocadmium reagents are reported to be superior for the preparation of ketones [61], due to this increased selectivity. However, the use of cadmium reagents has largely gone out of favor due the toxicity of this element and the difficulty of disposal of waste produced by this chemistry.

6.5 WASTE DISPOSAL

All toxic materials should be disposed of in accordance with all local, state, and national environmental (EPA) guidelines. Laboratory waste should be handled and disposed of in accordance with 'Prudent Practices in the Laboratory'; National Academic Press; Washington, DC, 1995 [62]. Waste generated from industrial processing is highly regulated; it is beyond the scope of this chapter to summarize the efforts needed to comply with the many different local regulations. However, one strategy is to minimize the volume and number of waste streams produced. For example, when processing on a large scale, and while the equipment is prepared to handle the off-gasses from the process, it is helpful to rinse drums with the appropriate solvent and to quench any excess reagent present into the reaction mother liquors prior to sending those mother liquors for waste disposal. Following separation of aqueous and organic waste layers, it is often practical to recover the organic solvent by distillation (frequently through a packed column), although consideration must be given to the removal of water and the reintroduction of inhibitors into ether solvents. For example, THF should be stabilized (butylated hydroxy toluene is often used) to prevent the formation of peroxides upon storage.

6.6 SUMMARY

The wide range of uses and the industrial application of Grignard chemistry is a tribute to the

genius of the discovery made by Victor Grignard a century ago. The examples and discussion summarized in this chapter show that the initial discovery has undergone years of refinement to provide a powerful synthetic tool for today's chemist. Each use of the chemistry to solve a synthetic problem or to improve upon an older synthetic route is not just an example, but frequently a refinement, of the techniques and methodology. The examples provided above are just a few of the reactions conducted on a production scale that utilize this chemistry.

The increased availability of tetrahydrofuran (THF) as a solvent in the 1960's greatly increased the production-scale usefulness of Grignard chemistry by avoiding the handling of large quantities of diethyl ether. Although many industrial applications of Grignard chemistry are not published, those discussed in this chapter illustrate the usefulness of this chemistry to the pharmaceutical, food, and chemical manufacturing industries.

Notice: The publisher and authors do not on the basis of this article warrant the use of this chemistry for any specific application. The handling of materials in a chemistry lab or production plant should only be conducted by trained individuals in accordance with safety and environmental regulations. The user accepts complete responsibility for conducting experiments and plant operations in a safe and environmentally acceptable manner.

REFERENCES

1. G.S. Silverman and P.E. Rakita, editors, *Handbook of Grignard Reagents*, Marcel Dekker, Inc., New York, **1996**.
2. B.J. Wakefield, *Organomagnesium Methods in Organic Synthesis*, Academic Press, New York, **1995**.
3. See also: A. J.C. Stowell, *Carbanions in Organic Synthesis*, John Wiley & Sons, New York, 1979; B. Y-H. Lai, Synthesis, **1981**, 585–604; C. L.F. Fieser and M. Fieser, *Reagents for Organic Synthesis*, **1967**, John Wiley & Sons.
4. Several of the other chapters in this book also provide excellent reviews of recent developments in Grignard Chemistry.
5. Kirk-Othmer, *Encyclopedia of Chemical Technology*, 4th edition, 1994, *12*, 768–786.
6. P.E. Rakita, Chapter 5 in reference [1], **1996**.
7. T. Waugh, and R. Waugh, *Adv. Chem. Ser.*, **1959**, *23*, 73–81.
8. P. Colin, and J. Gillin, *Chemical Engineering Progress*, **1969**, *56*, 71–76.
9. Hoffmann-LaRoche, Swiss Patent Appln. No. 71852, **1959**.
10. G. Blackmar, R. Wright, and R. Smith, U.S. Patent #3,911,037, **1975**.
11. The determination of water following drying the equipment, is made by titration of the THF equipment rinse with Karl Fischer reagent. The typical goal is to achieve a result of about 0.02% water content or less in the solvent rinse; although the level of dryness required is dependent upon the Grignard process being performed.
12. a) Early work on the crystallization of the crystal structure can be found in G. Stucky and R.E. Rundle, *J. Am. Chem. Soc.*, **1964**, *86*, 4825–4830. b) Additionally, other chapters in the volume may be of interest. Bickelhaupt (X-ray structures) and Ertel and Bertagnolli (XFAFS and LAXS spectra giving structural information about the species in solution).
13. M. Pitt, *J. Chem. Educ.*, **1987**, *64*, A44–A45.
14. G. Bennett, *J. Hazard. Mater.*, **1996**, *50*, 244–245.
15. L. Goodman, *Chem. Eng. Prog.*, **1996**, *92*, 75–79.
16. H. Fauske, *IChemE Symposium Series No. 102*, **1987**, 133–141.
17. T. Basalik, American Laboratory, **1998**, *30*(4), 33–40.
18. M. Yue, J. Sharkley, J. Leung, *J. Loss Prev. Process Ind.*, **1994**, *7*(5), 413–418.
19. M. Jones, *Plant/Operations/Progess*, **1989**, *8*(4), 200–205.
20. H. Fauske, *IChemE Symposium Series No. 102*, **1987**, 133–141.
21. J. Leung, in *Safety of Chemical Batch Reactors and Storage Tanks*, (Eds A. Benuzzi, and J. Zaldivar), ECS/EEC/EAEC, Brussels/Luxembourg, **1991**, p. 285.
22. J. Singh, *Process Safety Progress*, **1997**, *16*, No. 4, p. 255–261.
23. S. Waldrum, J. Singh, *IChemE Symposium Series* No. 141, **1997**, 367–378.
24. J. Leung, *AIChE Journal*, **1986**, *32*(10), 1622–1634.
25. H. Duxbury, A. Wilday, *IChemE Symposium Series* No. 102, **1987**, 175–185.
26. A tempered system is defined as one in which the reaction heat can be removed by latent heat of vaporization, thus providing some degree of temperature control in a runaway scenario. Conversely, a non-tempered system in which a low vapor pressure solvent is used, exhibits very little latent heat on cooling. Grignard reactions fall into the category of a tempered system since the reaction is conducted in solvents with high vapor pressures such as THF or diethyl ether.

27. For a thorough analysis of reactor vent design, and an understanding of the various reactor venting assumptions and scenarios, the reader is referred to: J. Leung, *AIChE Journal*, **1986**, *32*(10), 1622–1634.
28. M. Yue, J. Sharkley, J. Leung, *J. Loss Prev. Process Ind.*, **1994**, *7*(5), 413–418.
29. Quench of the reagent will generate the corresponding hydrocarbon; however, if the quench occurs prior to the complete formation of the Grignard reagent, or if additional magnesium metal remains in the reactor, then the addition of water may also generate flammable hydrogen gas.
30. *Perry's Chemical Engineering Handbook*, Sixth Edition, **1984**.
31. Kirk-Othmer, *Encyclopedia of Chemical Technology*, 4th edition, **1994**, *12*, 993–1045.
32. Met-L-X powder (sodium chloride) extinguishers are recommended for fires involving combustible metals such as magnesium. The heat of the fire causes the sodium chloride to cake and form an exterior crust which excludes air and smothers the fire.
33. In such a situation, special measures to safely quench the magnesium prior to disposal become important. A plan should be in place to quench and dispose of a reaction which fails to initiate. This planning should address the hazards of such an operation. Quenching of the magnesium will generate hydrogen gas, and proper disposal of the resulting waste streams needs to be evaluated in advance.
34. K.V. Baker, J.M. Brown, N. Hughes, A.J. Skarnulis, and A. Sexton, *J. Org. Chem.*, **1991**, *56*, 698–703.
35. a) R.D. Rieke and P.M. Hudnall, *J. Am. Chem. Soc.*, **1972**, *94*, 7178–7179. b) R.D. Rieke and S.E. Bales, *J. C. S. Chem. Comm.*, **1973**, 879–880. c) R.D. Rieke, S.E. Bales, P.M. Hundall, T.P. Burns, and G.S. Poindexter, *Org. Syn. Col. Vol. VI*, **1988**, 845–852.
36. R.D. Rieke, P.T-Z. Li, T.P. Burns, and S.T. Uhm, *J. Org. Chem.*, **1981**, *46*, 4324–4326.
37. J.-L. Luche and J.-C. Damiano, *J. Am. Chem. Soc.*, **1980**, *102*, 7927-7928.
38. R.D. Rieke and M.S. Sell, Chapter 4 in reference [1].
39. Technical Bulletin, **1995**, Zeeland Chemicals Inc.
40. D.E. Pearson, D. Cowan, J.D. Beckler, *J. Org. Chem.*, **1959**, *24*, 504–509.
41. D. am Ende, D. De Antonis, P. Clifford, C. Santa Maria, 'Safer Scale-up of Grignard Reactions using IR', Applied Systems 4th Users Forum, Annapolis, MD, May 31–June 3, **1998**.
42. M. Harper, D. Richardson, A. Wolpole, British Patent 1013907/1965.
43. R. McCague, *J. Chem. Soc. Perkin Trans. 1*, **1987**, 1011–1015, and references cited therein.
44. H. Schickaneder, R. Loser, and H. Grill, US Patent #5,047,431, assigned to Klinge Pharma GmbH & Co., **1991**.
45. F. Chauez, R. Godinez, *Synthetic Communications*, **1992**, *22*(1), 159–164.
46. *The Merck Index*, Twelfth Edition, **1996**, 974–975.
47. T. Shono, Y. Matsumura, *Tetrahedron Letters*, **1976**, *17*, 1363–4.
48. P. Weeks, T. Brennan, D. Brannegan, D. Kuhla, M. Elliott, H. Watson, B. Wlodecki, R. Breitenbach, *J. Org. Chem.*, **1980**, *45*, 1109–1113.
49. F.R. Busch, R.S. Lehner, and B.T. O'Neill, U.S. Patent #5,380,860, **1995**.
50. R.E. Ireland and J.A. Marshall, *J. Am. Chem. Soc.*, **1959**, *81*, 2907–08.
51. A. M.W. Rathke and P.J. Cowan, *J. Org. Chem.*, **1985**, *50*, 2622–24. B. D.W. Brooks, L.D.L. Lu, and S. Masamune, *Angew. Chem., Int. Ed. Engl.*, **1979**, *18*, 72–73. C. P. Pollet and S. Gelin, *Synthesis*, **1978**, 142.
52. W. Wierenga and H.I. Skulnick, *J. Org. Chem.*, **1979**, *44*, 310–311.
53. I.T. Harrison, B. Lewis, P. Nelson, W. Rooks, A. Roszkowski, A. Tomolonis, and J.H. Fried, J. Med. Chem., **1970**, *13*, 203–205; C. Giordano, G. Castaldi, S. Cavicchioli, and M. Villa, Tetrahedron, **1989**, *45*, 4243–4252; Merck Index, 12th edition, #6504.
54. A. P.G. Holton, U.S. Patent 4,515,811, assigned to Syntex, 5/7/85; B. E. Lodewijk, 'Evolvement of Naproxen Production Over a Twenty Year Time Frame', The Second International Symposium on Technologies for the Production of Enantiomerically Pure Chemicals, March 14–17, **1995**.
55. A. Pohland, U.S. Patent #2,728,779, assigned to Eli Lilly, **1955**.
56. A. Pohland, L.R. Peters, and H.R. Sullivan, *J. Org. Chem.*, **1963**, *28*, 2483–84.
57. v.P. Karrer and C.H. Eugster, *Helvetica Chimica Acta.*, **1950**, *33*, 1172–1174; and for a summary see N. Anand, J.S. Bindra, and S. Ranganathan, *Art In Organic Synthesis*, **1970**, Holden-Day, Inc.
58. G.T. Walker, Perfumery & Essential Oil Record, **1968**, *59*, 887–890.
59. T.D. Waugh, 'Grignard Reaction' in *Encyclopedia of Chemical Technology*, 1st edition, Vol 7, **1966**, 314–324.
60. J. Carson and F.S. Prout, *Org. Synth. Col. Vol. 3*, **1955**, 601–605, John Wiley & Sons.
61. D.A. Shirley, *Org. Reactions*, **1954**, *8*, 28–58.
62. *Prudent Practices in the Laboratory—Handling and Disposal of Chemicals*, National Academy Press; Washington, D.C., **1995**.

7

Mechanisms of Grignard Reagent Formation

John F. Garst[†] and Ferenc Ungváry[‡]
[†]Department of Chemistry, University of Georgia, Athens, GA 30602, USA [‡]Department of Organic Chemistry, University of Veszprém and Research Group for Petrochemistry of the Hungarian Academy of Sciences, 8200 Veszprém, Hungary

7.1 INTRODUCTION

7.1.1 Grignard Reaction

In the common method of preparing a Grignard reagent, a magnesium metal surface Mg_Z (Z denotes the surface) is allowed to react with an organyl halide RX in a suitable aprotic solvent SH [1–3]. Our subjects are the mechanisms of this Grignard reaction.

$$RX + Mg_Z \xrightarrow{SH} RMgX + \text{by-products}$$

typical SH
DEE (diethyl ether)
THF (tetrahydrofuran)

typical by-products

coupling/disproportionation: RR, RH + R(−H) (alkene)
solvent attack: RH + S residues (RS, SS, etc.)

Despite nearly a hundred years of work [4,5], this field remains rich in speculation and short on discriminating fact, a disturbing status for what may be the most-often-used non-trivial reaction [1–3]. This chapter focuses on the most significant results.

7.1.2 Basic Facts [1–3]

Mg_Z is used as turnings, chips, powder, or special preparations (e.g., Rieke Mg). Solvents other than DEE and THF, especially other ethers and aprotic solvents (e.g., tertiary amines), are sometimes used. Lindsell has summarized the influences of various factors [6].

By-products are often dominated by RR, RH, and R(−H) (alkene), which may be formed in yields as high as ~50%. By-products of solvent attack, such as SS and RS, are significant in unusual cases.

Suitable substrates include alkyl, benzyl, allyl, cycloalkyl, vinyl, and aryl iodides, bromides, and

Grignard Reagents: New Developments Edited by Herman G. Richey, Jr © 2000 John Wiley & Sons Ltd.

chlorides (rarely, under special conditions, fluorides). The halogen reactivity order is RI > RBr > RCl > RF. However, because reactions of iodides and bromides occur at or near the diffusion-control limit, they react at similar rates.

'RMgX' represents a mixture of RMgX, R_2Mg, MgX_2 (Schlenk equilibrium) and their aggregates and related ions. These equilibria are not considered here.

Mg_Z is very reactive (standard reduction potentials: Li, −3.045 V; K, −2.924 V; Na, −2.711 V; Mg, −2.375 V). It reacts rapidly with components of the air to develop a surface layer commonly called 'oxide', implying MgO, but now known (Section 7.3.3) to be largely $Mg(OH)_2$. A sufficiently well-developed MgO or $Mg(OH)_2$ adlayer passivates Mg_Z toward further reaction with gaseous O_2 or the atmosphere.

A typical Grignard reaction begins with an induction period during which initiation processes occur. Little appears to happen, and few products are formed, but eventually the induction period ends and the main reaction begins.

If the hydroxide layer is passivating toward the Grignard reaction, then it is responsible, at least partly, for the induction period. Some additives lengthen the induction period (inhibitors) while others shorten it (activators).

Typically, the main reaction, giving Grignard reagent and by-products, is rapid and exothermic. Cooling may be required to maintain control.

Solvent choice can be significant. Initiation can be promoted by a more polar ether. Thus, reactions of some halides (e.g., vinyl or aryl chlorides) initiate in THF (dielectric constant 7.4) but not in DEE (dielectric constant 4.2).

'Reluctant' halides may fail to react—initiation does not occur (e.g., aryl chlorides in DEE). In other instances, reactions occur but by-products dominate (e.g., adamantyl bromide, Section 7.2.17). Both cases can be addressed by activation, one or more special measures taken to promote reactivity, increase the yield of RMgX, or both.

Methods of activation include treating Mg_Z with an acid (e.g., aqueous HNO_3), stirring it dry in an inert atmosphere, preparing it in a special form (e.g., Rieke Mg), and pre-treating it *in situ* with I_2, CH_3I, CH_3CH_2Br, $BrCH_2CH_2Br$, Vitride [$NaAlH_2(OCH_2CH_2OCH_3)_2$], RMgX solution from a previous reaction, an alcohol, etc. The same substances that are used in pre-treatments are sometimes simply included instead in the reaction mixture along with RX. The inclusion of reactive alkyl halides (CH_3I, CH_3CH_2Br, $BrCH_2CH_2Br$) with a reluctant RX is called 'entrainment.' In the unusual case of adamantyl bromide, *not* stirring is a method of activation (Section 7.2.17).

7.1.3 Overview

There have been several recent brief reviews [7–9]. In longer works, the pre-1954 history of mechanistic studies of the Grignard reaction is summarized by Kharasch and Reinmuth in their comprehensive treatise [1] and recent work is covered by Hamdouchi and Walborsky (1996) [10] and van Klink (1998) [11]. On some important points, we differ with interpretations offered by each of these authors.

Mechanisms of Grignard reactions can be divided into two parts, organic and inorganic. The organic mechanism traces R from RX to RMgX and by-products containing residues of R and S.

Organic Mechanism

$$RX \longrightarrow\longrightarrow\longrightarrow RMgX + \text{organic by-products}$$

The inorganic mechanism traces Mg from Mg_Z to RMgX and deals with surface films, inhibition, initiation, and activation. The organic mechanism has received far more study than the inorganic.

Inorganic Mechanism

$$Mg_Z \longrightarrow\longrightarrow\longrightarrow RMgX + MgX_2 + \text{other Mg species (if any)}$$

plus initiation, activation, and other matters concerning the inorganic chemistry of the Mg surface

Pathway ***R***. For at least part of the organic mechanism of many Grignard reactions, overwhelming evidence supports intermediate radicals

Pathway R

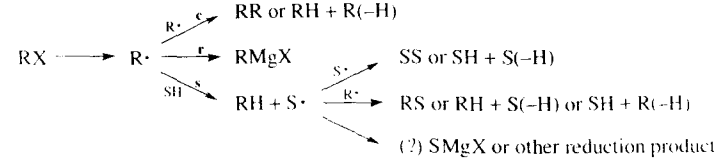

R· ('Grignard radicals') and pathway **R** (Section 7.2.3).

Hereinafter **r**, **c**, and **s** denote radical reduction, coupling/disproportionation, and solvent attack, respectively.

Secondary reactions giving by-products. Although reactions of RMgX with RX to give RR or RH + R(−H) are known, special conditions are required. In typical cases, secondary reactions are not sources of by-products [1,10,12].

Adsorption of R·. In pathway **R**, R· remains adsorbed at Mg_Z until it undergoes **r** [A (adsorption) model] or it doesn't [D (diffusion) model] (Section 7.1.4). Compelling evidence supports the D model and disproves the A model (Sections 7.2.8–7.2.9).

Lifetime of R·. For a typical alkyl halide, the D-model characteristic lifetime of R· in DEE or THF is $\sim 10^{-7}$ s (Section 7.2.8). Since the rate constant k_S (for **s**) for a primary alkyl radical in DEE is $\sim 10^3\ s^{-1}$ [13], **s** is predicted to be insignificant, as is found.

Concentration of R·. For a typical alkyl halide, the D-model concentration of R· near the surface is 10^{-4}–10^{-3} M (Sections 7.2.7–7.2.8). If the rate constant k_C (for **c**) were $3 \times 10^9\ M^{-1}\ s^{-1}$, a typical near-diffusion-control value, the specific rate for **c** (k_C[R·]) would be (3×10^5)–$(3 \times 10^6)\ s^{-1}$, high enough for **c** to be significant, as is found.

Chain Reaction. Under the usual reaction conditions, a chain mechanism is not viable (Section 7.2.19). Trapping intermediate radicals has little, if any, effect on the rate [14–16].

Mg(I) Intermediates. Although they are often proposed [1,10,11], there is no compelling evidence for discrete Mg(I) intermediates such as ·MgX and RMg· (Section 7.3.8). An interesting possibility is that Mg enters the solution as hypovalent clusters Mg_n^{m+} ($m < 2n$) such as Mg_2^{2+}, leading to species such as ZMgMgZ (Z = R or X).

Initial Step. Initial electron transfer has not been distinguished from initial halogen-atom transfer (Section 7.2.21).

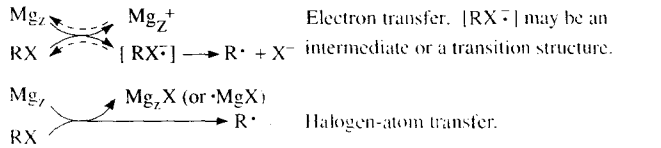

Intermediate RX·−. RX·− may or may not be an intermediate. In reductions of alkyl halides at inert electrodes, there is consistent and persuasive (but not compelling) evidence for dissociative electron transfer (Section 7.2.21). In similar reductions of aryl halides, an intermediate RX·− is well established [17,18].

$$RX \xrightarrow{[e^-]} R\cdot + X^- \text{ (dissociative electron transfer)}$$

$$RX \xrightarrow{[e^-]} RX\cdot^- \longrightarrow R\cdot + X^- \text{ (electron attachment followed by dissociation)}$$

Extent of Pathway ***R***. **R** may be the exclusive pathway for Grignard reactions of typical alkyl

halides. There may be another pathway, **X**, especially for cyclopropyl, vinyl, aryl, and possibly allyl/benzyl halides. Pathway **X** may dominate sometimes. Only scattered results are relevant to the extents to which pathways **R** and **X** compete for various organyl halides (Sections 7.2.8–7.2.12).

Pathway X. The nature of **X** is uncertain (Sections 7.2.9–7.2.11). Possibility **Xa** implies the absence of by-products. In **Xb** any by-products would have to arise from $RX^{\bullet-}$. **Xc** is a portion of a version of **R** in which there is a sub-population of very short-lived radicals R•. **Xc** might be, for example, a geminate reaction (Section 7.2.5) at an active site, that is, a reaction of R• at the active site where it was formed (Section 7.3.11). **Xd** is a solution reaction involving a 'di-Grignard reagent' RMgMgX or related species (Section 7.3.8). If the mechanism involves radical intermediates, then a geminate reaction of a pair such as $[Z_2Mg_2X\ R\bullet]$ could give partial retention. Alternatively, R• would not be an intermediate in **Xd**.

Pathway X (some possibilities)

(a) $RX \xrightarrow[SH]{Mg_Z} RMgX$ (one step)

(b) $RX \xrightarrow[SH]{Mg_Z} RX^{\bullet-} \xrightarrow{Mg_Z} RMgX$ (two steps – no R•)

(c) $RX \xrightarrow[SH]{Mg_Z} R\bullet \xrightarrow{Mg_Z} RMgX$ (timescale $\approx 10^{-10}$ s or less) **X**

$R\bullet \xrightarrow{Mg_Z} RMgX$ (timescale $\approx 10^{-7}$ s) **R**

(d) $RX + XMgMgZ \longrightarrow RMgX + ZMgZ$ (Z = R or X)

$RX + ZMgMgZ \longrightarrow [Z_2Mg_2X\ R\bullet] \longrightarrow RMgX + MgZ_2$ (geminate reaction with partial retention)

$\searrow\ Z_2Mg_2X + R\bullet$ (escape and racemization)

Step r. Metallic corrosion theory suggests electron transfer from Mg_Z (Figure 7.1, Section 7.3.7).

$$Mg_Z^q + R\bullet \longrightarrow Mg_Z^{q+1} + [R^-]$$

$$\xrightarrow{MgX_2} RMgX + X^- \quad (q = \text{charge})$$

This could be concerted or stepwise. In some cases, there is evidence of a carbanion or carbanionoid intermediate (Section 7.2.20). Step **r** is often written instead as the following radical combination [1,10,11]. Electron transfer from Mg_Z

$$R\bullet + \bullet MgX \longrightarrow RMgX$$

has the advantage of including the Grignard reaction in a consistent treatment with other metallic corrosions.

Electrochemical Corrosion. In a classical model of metallic corrosion, reductants are reduced by electron transfer from the metal at cathodic sites while the metal undergoes oxidative dissolution at anodic sites (Figure 7.1).

Combining this with the D model provides a simple description of both the organic and inorganic mechanisms for pathway **R**.

In the Grignard reaction, the medium is poorly conducting. The requirement of effective conduction to prevent the build-up of excessive charge imbalance implies that the cathodic and anodic sites cannot be very far apart.

Corrosion by Reactions of Mg_Z with Species in Solution. It is often proposed that transient species in solution remove Mg atoms as Mg(I) species. As noted earlier, there is no compelling evidence of Mg(I) intermediates (Section 7.3.8).

$$RX \xrightarrow{Mg_Z} R\bullet + \bullet MgX$$

$$R\bullet \xrightarrow{Mg_Z} RMg\bullet$$

Adventitious 'Oxide' Layer. The layer that forms on Mg when it is exposed to the atmosphere under ambient conditions is principally $Mg(OH)_2$ (Section 7.3.3), with small but significant amounts of bicarbonate, HCO_3^-, in the outermost layers. $Mg(OH)_2$ can be converted to MgO by baking.

Induction period. The existence of the induction period shows that there is initial passivation, inhibition, absence of activation, or some combination of these.

Initiation. Initiation may consist of the penetration by RX to Mg_Z, the removal of $Mg(OH)_2$, the consumption of inhibitors, the formation of activators, etc. (Section 7.3.4).

Activation and Inhibition. Activation may (1) remove the passivating $Mg(OH)_2$ layer, (2) promote its penetration, (3) catalyze the reaction of RX at Mg_Z, (4) increase the effective Mg_Z surface area, (5) increase the number of Mg_Z active sites, (6) remove inhibitors, (7) promote initiation or inhibit termination of chain reactions, or (8) involve some combination of these and possibly other effects. Inhibition may be the opposite (Section 7.3.5).

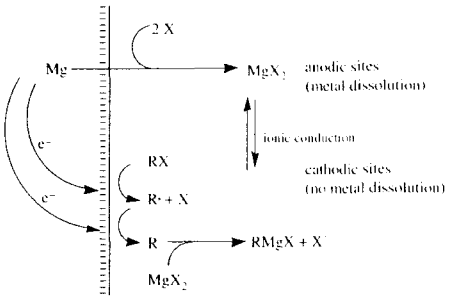

Fig. 7.1. Electrochemical corrosion hypothesis. At anodic sites, atoms are lost from Mg as Mg^{2+}. At cathodic sites, electrons are lost from Mg. Ions are highly aggregated in ether solvents. Their representation here as individuals is schematic, not literal. The low conductivity of the medium requires that anodic and cathodic sites be close to one another, possibly on the atomic scale.

7.1.4 D and A Models

The D and A models are alternative non-chain versions of pathway **R**, differing in whether R• diffuses in solution (D model) or remains adsorbed at Mg_Z (A model) (Figure 7.2). The Walborsky mechanism (Figure 7.3) [7,10], which was generally accepted for about 20 years (beginning in the mid-1960s) included the D model at first ('...the loose radical pair may become solvent separated to give a planar R group which could return to the surface of the magnesium or react with solvent...') [19] but was later changed to an exclusive A model [20].

For the following reasons, the distinction between D and A models is of major importance. Independent of the Grignard reaction, there is a large body of data on reactions of radicals in solution. Solution data on radical reactivities can be used with the D model to make useful quantitative predictions. There is no such body of data for radicals that are adsorbed at a magnesium-solution interface. The possibility of useful quantitative predictions from the A model appears to be remote. Indeed, the A model does not provide

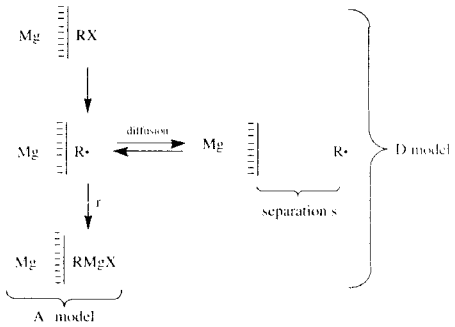

Fig. 7.2. A and D models for pathway **R**. **c** and **s** are not shown. In the D model **c** and **s** occur at all distances from the surface. Different A models invoke different combinations of surface and solution steps for **c** and **s**.

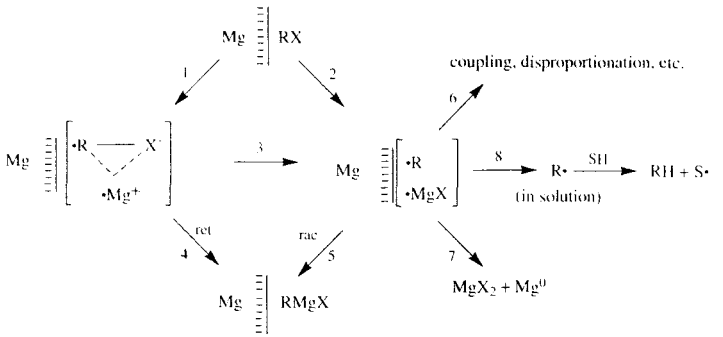

Fig. 7.3. The Walborsky mechanism [7,10]. The bracketed intermediate at left is a 'tight radical anion-radical cation pair,' proposed initially as an intermediate [19] but later supposed to be a transition state [21,22], in which case step 3 vanishes. The bracketed intermediate at right is an adsorbed 'loose radical pair.' In Walborsky's later figures, the Mg of a pair is represented in a way that suggests that it may remain embedded in the surface. Steps 1–4 occur with retention. Step 5 occurs with racemization. All steps occur at the magnesium surface Mg_Y except solvent attack, which is the inevitable fate of a radical that leaves Mg_Y and enters the solution. Desorption (step 8) and subsequent solvent attack are described by Walborsky but not included in his figures.

many definite predictions, qualitative or quantitative. Since prediction is a duty of a scientific theory, the D model is far more promising, *a priori*, than the A model.

Of course, such is not *evidence*. Nature might have dealt a cruel hand and followed the A model. Fortunately, this is not the case (Section 7.2).

Regarding evidence, it is important to realize that evidence *against* the D model is *not* necessarily evidence *for* the A model. Much of what can be cited as evidence against the D model could be a consequence of pathway **X** and therefore cannot be construed as evidence against the D model, which describes pathway **R**.

7.1.5 Occam's Razor

For Grignard reactions, a multitude of hypotheses (often conflicting) have been presented. This is desirable—hypotheses are targets for testing—but such complexity has generated confusion [10,11]. Occam's Razor can be a guide to an efficient and effective research pathway. The simplest viable hypothesis is chosen as the current working hypothesis, which is then modified or rejected only as required by new evidence.

Data are commonly overinterpreted by incorporating unnecessary details into a hypothesis. This happens in at least two ways: (a) compatible alternative hypotheses are included where one would be sufficient to explain the data; (b) other unsupported details are included.

Confusion can arise from compatible alternatives if the data are seen as support for all of them. For example, the Walborsky mechanism provides three possible explanations of partial retention of configuration, (1) pathway **X**, (2) adsorption of R•, and (3) geminate reaction of pairs [R• •MgX] (not proposed by Walborsky, but an obvious possibility). It is a logical error to cite observed retention of configuration in a Grignard reaction as evidence against the D and for the A model. Instead, it is evidence of 1, 2, *or* 3, where 1 and 3 are *compatible* with the D model.

Walborsky's writings are illustrative. In 1964, Walborsky and Young stated, 'The observation that the cyclopropyl Grignard reagent does retain some of its [optical] activity would indicate that the radical intermediate is not entirely free...the radical may be held on the surface of the magnesium' (the figure illustrates •Mg-X with dashes to R•) [19]. Clearly, they viewed the tight radical pair as an adsorbed R• and the loose radical pair as a species 'in which R• is sufficiently separated to permit rotation thereby resulting in racemization.' Nine years later the tight radical pair is 'a radical anion in close association with a univalent magnesium cation' (the figure illustrates R—X•⁻ with dashes to •Mg⁺) and 'the processes pictured...are assumed to take place on the surface of the magnesium' [20]. Thus, the loose radical pair became an adsorbed species in which racemization occurs—the idea that retention is a result of radical adsorption was abandoned. In 1990, it was resurrected: the product from the loose radical pair became 'largely racemic' [7]. In 1993 the tight radical pair ceased to be an intermediate and became a transition state for an elementary reaction, in effect a two-electron transfer [22].

These variations involve unsupported hypothetical details. Occam's Razor requires that such details be omitted where possible, but sometimes they are necessary for the construction of a predictively competent model. In that case, Occam's Razor specifies that the simplest such model should be taken as the working hypothesis. Walborsky's postulate of a 'loose radical pair' violates this principle. Its properties are not described. Is it supposed to be like an ordinary radical pair in solution, with a similar lifetime and with possibilities of geminate reaction or escape? Or is it something else? Why is it included at all? Similar considerations apply to the 'tight radical pair.'

The fundamental aspects of the Walborsky mechanism are an A-model pathway **R** and a competing pathway **X**. The rest is unsupported and superfluous.

In applying Occam's Razor, it seems appropriate to take into account weak evidence favoring a more complex option. Pathway **Xc** may be the simplest viable mechanism that explains partial retention of configuration, since it is in the framework of pathway **R**. However, there are hints that the extent of isomerization correlates inversely with conjugation in RX (Sections 7.2.8–7.2.12). Taking this into account, one might choose another version of **X** as the working hypothesis.

7.2 ORGANIC PART OF THE MECHANISM

7.2.1 Experimental Techniques

These techniques are used in our laboratories. Grignard reactions are conveniently performed on one- to five-mmol scales using custom-made glassware. Because RMgX is prone to oxidation and protonation, dry, oxygen-free conditions must be established and maintained. Glassware is dried in an oven at 120–140°C and the pieces greased and assembled while hot. Silicone grease is suitable. The air in the assembled apparatus is replaced by a dry, oxygen-free inert gas (e.g., argon or nitrogen) by several pumping and filling cycles, using a two-way stopcock. Traces of oxygen and water are removed from the inert gas by passing it through a 30/1200 mm column of active copper (such as BTS catalyst R 3–11) and a 30/400-mm column of drying material (such as Drierite and granulated P_4O_{10}). For a general reference see Shriver and Drezdzon [23].

Dry, oxygen-free ether solvents can be obtained by distilling them from their blue-colored benzophenone ketyl solutions immediately before starting an experiment. A stainless-steel cannula or a TLL-type syringe is a convenient tool for transferring the solvent from one flask to another through silicon-rubber-capped stopcock adapters.

Organic halides are dried over molecular sieves (4A), distilled under inert-gas atmospheres, and protected from light and air before using them in experiments. For the transfer of the dry, oxygen-free organic halides, argon- or nitrogen-purged TLL-type syringes are used.

For reproducible results, magnesium turnings must be either air-dried (r.t.) or oven-baked (120–140 C). Stirring rates should be held constant, since they can, in principle, affect product distributions.

Magnesium bromide etherate, a good reaction medium, can be prepared *in situ* from magnesium turnings and 1,2-dibromoethane, but such solutions contain small magnesium particles and some undissolved $Mg(OH)_2$ and $Mg(HCO_3)_2$ (from the magnesium surface). By filtering under argon or

nitrogen through a porosity-4 sintered-glass frit, a clear solution of anhydrous $MgBr_2$ in ether (ca 2.6 M) can be obtained. On diluting this solution with ether, a second liquid phase is formed in which the magnesium bromide concentration is only about 0.18 M. Saturated solutions of $MgCl_2$ in tetrahydrofuran (ca 0.5 M) can be obtained similarly from Mg turnings and 1,2-dichloroethane. For details see Gmelins Handbuch [24].

The yield of RMgX in a one- to five-mmol-scale experiment is determined by direct titration of the reaction mixture with neat *sec*-butyl alcohol from a microburette (2/0.01 mL) under argon or nitrogen in the presence of ca. 0.1 mg 2,2′-biquinoline or 1,10-phenanthroline as an indicator according to the method of Watson and Eastham [25]. The titration is not affected by metallic magnesium, basic magnesium compounds, or magnesium halides.

In a small-scale experiment using an ethereal solvent, the reaction of an organic halide with magnesium is carried out in a thermostatted reaction vessel fitted with a reflux condenser (0°C) and a silicon-rubber-capped stopcock, using a Teflon-coated magnetic stirring bar. By connecting the reaction vessel through the top of the condenser with a mercury-filled, thermostatted gas burette and an *n*-undecane-filled U-shaped auxiliary manometer, the gas volume change at constant barometric pressure during the reaction and during the accompanying titration with *sec*-butyl alcohol can be followed (Figure 7.4). To ensure accuracy, the reaction vessel and the connecting parts are purged and filled with the gas that will be evolved (e. g., cyclopropane, methane, ethane, propane) instead of argon or nitrogen. Thus, the solution remains saturated in the gas and the composition of the gas phase remains constant throughout the measurements.

After quenching a sample of the product mixture with a minimum amount of brine, or after distilling off all the volatile components into a cold (−79°C) receiver, the composition of the reaction mixture is analyzed by gas chromatography on a fused silica capillary column, using *n*-octane (usually) as an internal standard. Samples to be analyzed are conveniently stored in small vials closed with a Mini-inert valve made of Teflon.

The procedures above are adequate for studies of competitive product formation but not for those of the overall reaction kinetics. In the latter case,

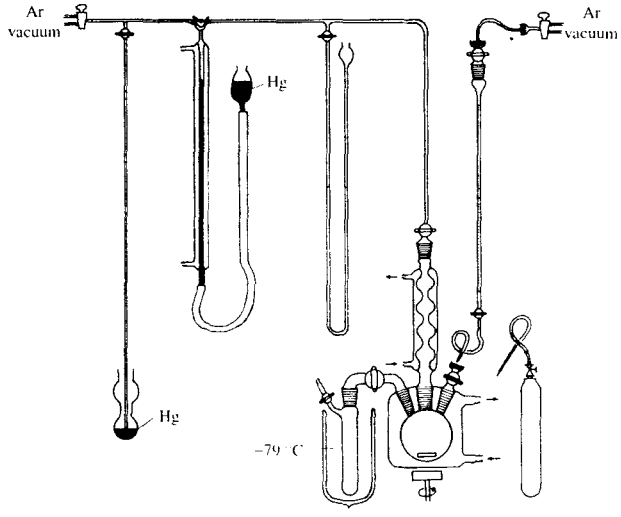

Fig. 7.4. Apparatus for studies of Grignard reactions.

the rate is sensitive to the thickness of the hydrodynamic layer, inside which diffusion controls mass transport and outside which stirring is effective. This thickness is affected by stirring. Moreover, in order to provide a well-defined situation, some appropriate geometry of the Mg_Z must be chosen. Commonly, a partially-immersed disk is rotated at a constant, controlled rate. The hydrodynamics is well-defined and well-known. The thickness of the hydrodynamic layer can be controlled by varying the speed of rotation [26–28].

Whitesides has pointed out that the polarities of ethers containing polar solutes such as RMgX and MgX_2 are much higher than those of pure ethers and, consequently, that these solutes can be expected to affect Grignard reactions [29–31]. In particular, these solutes and the effective polarity of the medium can, both in principle and in specific cases noted later (Sections 7.2.8–7.2.11, 7.2.15, 7.2.17, 7.2.20, 7.2.23, 7.3.1, 7.3.4–7.3.10), affect both the rate of disappearance of RX and the product distribution. If the initial reaction mixture consists only of solvent and RX, the polarity will rise rapidly as the reaction proceeds, due to the formation of RMgX and MgX_2. Initial excesses of one or both of these solutes can maintain a nearly constant polarity of the medium as reaction proceeds.

7.2.2 Rate Law

For a heterogeneous reaction, flux and rate are distinguished. Gross rate refers to the total amount and has units mol s^{-1}. Specific rate (or simply 'rate') is the usual volume-based chemical rate, customary units mol L^{-1} s^{-1}. Flux is area-based, mol cm^{-2} s^{-1}.

Early measurements of Kilpatrick indicated that the rate of loss of RX in the Grignard reaction, after the induction period, is proportional to the area $\mathscr{A}$ of Mg_Z and the concentration [RX] of RX [1,32,33]. This has been verified in careful studies under hydrodynamically controlled conditions, using a rotating assembly of Mg cylinders [29–31] or a rotating Mg disc [26–28]. The global (observable) flux constant κ_G includes a possible influence of diffusion (Equations 7.1–7.3, where v is the flux of reaction and U is the volume of the reaction mixture). Indeed, it appears that most

$$\text{flux} = v = \kappa_G\,[\text{RX}] \quad (\text{mol cm}^{-2}\,\text{s}^{-1}) \tag{7.1}$$

$$\text{gross rate} = \kappa_G \mathscr{A}\,[\text{RX}] \quad (\text{mol s}^{-1}) \tag{7.2}$$

$$\text{rate (specific)} = (\kappa_G \mathscr{A}/U)\,[\text{RX}] \quad (\text{mol L}^{-1}\,\text{s}^{-1}) \tag{7.3}$$

organyl bromides and all iodides react at nearly diffusion-controlled rates [26–28]. The meaning of diffusion control is discussed in the Appendix.

Under hydrodynamically controlled conditions, the yields of RR and RMgX are sensitive functions of $[RX]_0$ [28,34]. Higher $[RX]_0$ give larger rates of formation and therefore steady-state concentrations of R•, favoring **c** relative to **r** because **c** is second order in R• while **r** is first.

When ordinary Mg chips or turnings are used with normal stirring methods, product distributions may be independent of a sufficiently high $[RX]_0$ (typically >0.1 M), suggesting that the reactions are zeroth order in RX [16,34]. A zeroth-order rate law has been confirmed by Whitesides and coworkers for the reaction of cyclopentyl bromide in DEE at 20°C [15]. Possible explanations include: (a) that the growth of the area $\mathscr{A}$ during the reaction compensates for the depletion of [RX]; (b) that changes in the medium adjacent to Mg_Z (e.g., changes in [RMgX] or $[MgX_2]$ or the thickness of a viscous layer) compensate for the depletion of [RX]; and (c) that some event not depending on [RX] (e.g., desorption of a product such as RMgX or MgX_2) governs the rate of RX transport to active sites on Mg_Z. Whatever the reason, it appears that zeroth-order kinetics of typical reactions is an artifact, a consequence of not providing a hydrodynamically defined interface at Mg_Z [15,34,35].

7.2.3 Radical Intermediates—Pathway R

Radical intermediates and pathway **R** are suggested by studies of typical alkyl, cyclopropyl, vinyl, and aryl halides. The intermediacy of R• was suspected in the 1920s, being strongly suggested

by the nature of the by-products, which are consistent with **c** and **s** and which closely resemble the products formed in oxidations of RMgX. Pathway **R** was generally accepted by the 1950s [1]. The 1960s and subsequent years brought a stream of definitive evidence, including occurrences of characteristic radical isomerizations [19,36–45] observations of CIDNP [12,46–51], further delineation of products of coupling/disproportionation and solvent attack [16,26,28,48,50,52], and successful trapping of radicals by TMPO and DCPH [14–16].

Reactions of 1-iodo-1-methyl-2,2-diphenylcyclopropane and 5-hexenyl bromide are among those exhibiting characteristic radical isomerizations. 1-Iodo-1-methyl-2,2-diphenylcyclopropane gives nearly racemic RMgI, which does not itself racemize (Equation 7.4) [20]. Similarly, along with RMgBr, 5-hexenyl bromide gives the cyclized product QMgBr, which is not a product of RMgBr cyclization (Equation 7.5) [38,53–58].

Although trapping by DCPH is inefficient [16], the efficiency of trapping by TMPO·, which is much more reactive, can approach 95% (Equation 7.6) [14,15]. Not only does this support alkyl radical intermediates, but also it indicates that pathway **R** accounts for a very large fraction of the reaction, probably 100%.

CIDNP in RMgX further demonstrates that it is formed from an R· intermediate (Figure 7.5) [12,46–51]. CIDNP results from nuclear-spin selection in reactions of radical pairs [59,60].

Since RMgX does not react with RX under most ordinary conditions [1,10,12], the formation of RR, accompanied by RH and R(−H), points to **c** and pathway **R**. So does the agreement of the yield ratios 2(R[−H])/RR with other radical reactions where **c** occurs. For example, for

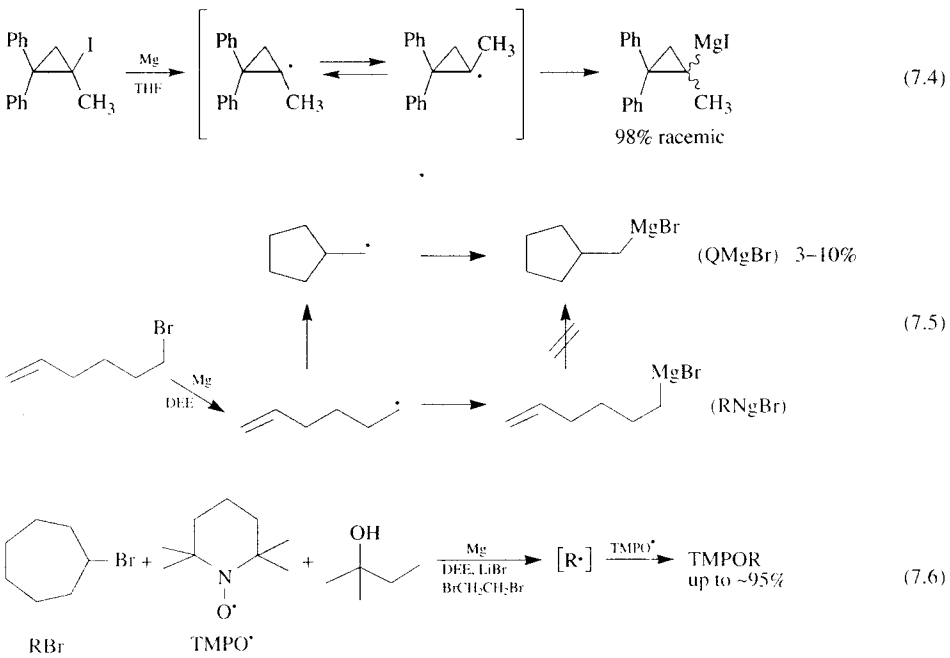

Fig. 7.5. CIDNP in CH_2 protons of CH_3CH_2MgI from the reaction of ethyl iodide with Mg in di-*n*-butyl ether [46]. Top: normal spectrum. Bottom: CIDNP spectrum (*E/A* multiplet effect). This is the expected spectrum for CIDNP in RMgI formed in step **r** from radicals R· that have escaped from pairs [R· R·] formed when independently diffusing radicals meet [47]. There were no indications of net effects, which would have been expected if diffusing radical pairs [R· ·MgI] were significant generators of CIDNP [47]. Reprinted from Bodewitz *et al.* [46]. Copyright 1972, Page No. 283, with permission from Elsevier Science.

the Grignard reaction of cycloheptyl bromide in DEE this ratio is 0.89, agreeing closely with a literature value of 0.95 for cycloheptyl radicals [15]. Similarly, the ratio is 0.13 for the reaction of *n*-hexyl bromide in DEE, a typical value for a primary alkyl radical [52]. Similarly good agreement is found for the reaction of *t*-butyl bromide [35].

Although **s** is negligible in Grignard reactions of typical alkyl halides [52], it is significant in some other cases. Notable among these are reactions of cyclopropyl bromide (in DEE and THF) [52], phenyl bromide (in DEE) [61,63], 1-ethoxy-7-norbornyl bromide (in THF) [64], and adamantyl bromide (in DEE, THF, and di-*n*-butyl ether) [65]. Solvent attack is a definitive indication of radical intermediates, especially when the solvent dimer SS is detected [52,64]. It is hard to imagine how SS could arise in any way other than the coupling of radicals S· generated by **s**.

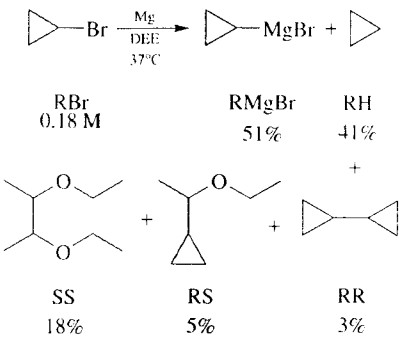

*Adjusted for a small systematic error.
The value in the original publication is 15%.

These and similar facts firmly establish pathway **R** as an important part of mechanisms of Grignard reactions. For typical alkyl halides, especially, **R** may be the only pathway (Section 7.2.8).

7.2.4 Models, Rates, and Rate Constants

If R· is formed and reduced at Mg_Z, there remains the question, "Does R· remain adsorbed at Mg_Z [A (adsorption) model] or not [D (diffusion) model]?" Discussion of this issue requires an understanding the behaviors of surface–molecule pairs ZB, such as [Mg_Z R·], the intermediate in the D model. Much of what follows is based on the work of Brian L. Swift [66].

Superficially, ZB appear to be similar to molecule–molecule pairs AB (e.g., radical pairs [R·

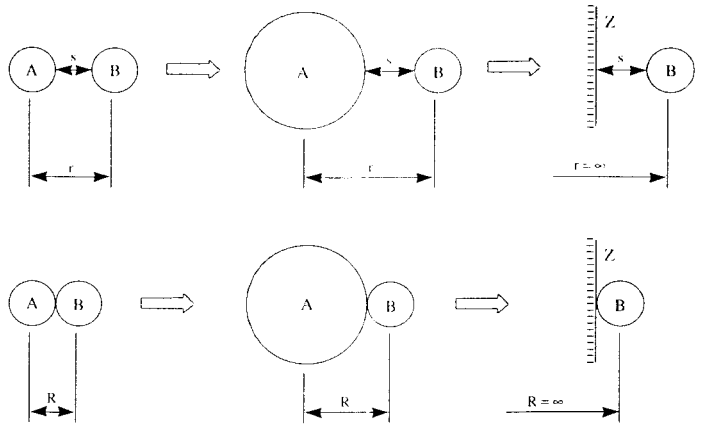

Fig. 7.6. Transformation of an AB into a ZB as the radius of spherical A increases so that $R \rightarrow \infty$ (open arrows). For spherical molecules, the figure also defines the contact radius R, the actual radius r, and the separation s for ZB and AB. $r = R + s$.

R•]), the behaviors of which are well known. Each consists of a molecule B diffusing near its partner. Further, a ZB is the limit approached by an AB as the radius of A increases so that $R \rightarrow \infty$ (Figure 7.6). These similarities encourage the assumption of similar ZB and AB behaviors, but actually there are critically important differences. As examples, we describe behaviors of model pairs of both types. Ignoring or misunderstanding the behavioral differences can lead to fundamental logical errors in interpretations of data [10].

We compare and contrast ZB and AB dynamics through treatments based on those of Smoluchowski–Collins–Kimball (SCK) [67,68] and Noyes [69–72]. Except where otherwise noted, we treat ideal cases. Molecules A and B are modeled as hard, spin-free, isotropically-reactive spheres; surfaces Z are hard, uniform planes; media are structureless, uniform, and isotropic; surfaces and media extend to infinity in all possible directions; and Fick's Laws govern diffusion.

Fick's First Law is the fundamental diffusion equation [72].

$$J = -D(\partial[\mathrm{B}]/\partial x) \quad \text{(Fick's First Law in one dimension)} \quad (7.7)$$

Here D is the relative diffusion coefficient, the sum of the diffusion coefficients of the diffusing particles; x is the coordinate in the direction of diffusion; and J is the net flux of B

$$D = D_{\mathrm{A}} + D_{\mathrm{B}} \quad \text{(for A and B)} \quad (7.8)$$

$$D = D_{\mathrm{B}} \quad \text{(for Z and B)} \quad (7.9)$$

across a plane (at some particular value of x). The negative sign reflects the fact that a positive gradient corresponds to diffusion in the negative direction. The diffusion of A and B relative to one another is identical with the diffusion of B alone, with A held fixed, provided that the relative diffusion coefficient D is assigned to B.

The flux of an elementary heterogeneous reaction of B at a reactive surface Z is described by equation (7.10), where κ is the activation-control flux constant (heterogeneous rate constant) and $[\mathrm{B}]_0$ is the concentration of B in solution at Z ($x = 0$).

$$\text{flux of reaction} = \kappa[\mathrm{B}]_0 \quad (\text{mol cm}^{-2}\,\text{s}^{-1}) \quad (7.10)$$

By Fick's First Law, the flux of reaction is also $D\partial([B]/\partial x)_0$. Equating the two flux expressions gives equation (7.11) and shows how the reactivity

parameter δ arises naturally.

$$\partial([\mathrm{B}]/\partial x)_0 = \delta[\mathrm{B}]_0 \quad (\delta = \kappa/D) \quad (7.11)$$

Equation (7.11) expresses the 'radiation boundary condition' that is applied in solving SCK diffusion–reaction equations. The gross rate and specific rate are given by equations (7.12) and (7.13), where $\mathscr{A}$ is the contact area (area of the locus of the center of B when B is in contact with Z) and U is the volume of the solution.

$$\text{gross rate of reaction} = \kappa[\mathrm{B}]_0\mathscr{A} \quad (\text{mol s}^{-1}) \quad (7.12)$$

$$\text{specific rate of reaction} = \kappa[\mathrm{B}]_0\mathscr{A}/U \quad (\text{mol L}^{-1}\,\text{s}^{-1}) \quad (7.13)$$

For an activation-controlled bimolecular reaction between A and B, $\mathscr{A}$ is $4\pi R^2 N_{\mathrm{A}}$, where $4\pi R^2$ is the contact area of a single molecule A and N_{A} is the number of molecules A. This translates into equation (7.14) for the specific rate,

$$\text{specific rate of reaction} = \kappa(4\pi R^2)L_0[\mathrm{A}][\mathrm{B}] = k_{\mathrm{A}}[\mathrm{A}][\mathrm{B}] \quad (7.14)$$

where L_0 is the Avogadro number and k_{A} is the conventional activation-control rate constant, allowing the identification of k_{A} (equation 7.15).

$$k_{\mathrm{A}} = 4\pi R^2 L_0 \kappa \quad (7.15)$$

For molar concentrations, κ in cm s^{-1}, and R in Å, equation (7.16) relates k_{A} to κ and R.

$$k_{\mathrm{A}} = (7.57 \times 10^5)\kappa R^2 \ (\text{L mol}^{-1}\,\text{s}^{-1}) \quad (7.16)$$

For a diffusion-controlled bimolecular reaction between A and B, the rate constant k_{D} is related to R and D (equation 7.17) [72].

$$k_{\mathrm{D}} = 4\pi R D L_0 \quad (7.17)$$

For molar concentrations, R in Å, and D in cm^2 s^{-1}, equation (7.18) relates k_{D} to R and D.

$$k_{\mathrm{D}} = (7.57 \times 10^{13})RD \quad (\text{L mol}^{-1}\,\text{s}^{-1}) \quad (7.18)$$

The global rate constant k_{G} is observed in most experiments [73–77]. For the ideal case of spherical, isotropically reactive, spin-free molecules, k_{G} is related to k_{A} and k_{D} by equation (7.19). See the Appendix, Equation A7.4, for a corresponding general expression [74–77].

$$k_{\mathrm{G}} = k_{\mathrm{A}}k_{\mathrm{D}}/(k_{\mathrm{A}} + k_{\mathrm{D}}) \quad \text{(ideal case; not general)} \quad (7.19)$$

To facilitate illustration, we select a standard model ZB and a standard model AB. Both are chosen to be initially in contact ($s = 0$). For the standard ZB, we choose parameter values that fit data for the Grignard reactions of primary alkyl bromides in DEE at ~40° C (Section 7.2.8).

$$D = 3.0 \times 10^{-5}\ \text{cm}^2\,\text{s}^{-1}$$

$$\kappa = 30\ \text{cm s}^{-1}$$

$$R = \infty \ \text{(Figure 7.6)}$$

$$\delta = 0.010\ \text{Å}^{-1}$$

For the standard AB, we choose parameter values that might characterize a pair of small alkyl radicals [R• R•]. Such a pair is fully characterized by values of D, κ, and R, which lead to values of k_{A}, k_{D}, and k_{G}.

$$D = 6.0 \times 10^{-5}\ \text{cm}^2\,\text{s}^{-1}$$

$$\kappa = 800\ \text{cm s}^{-1}$$

$$R = 5\ \text{Å}$$

$$\delta = 0.13\ \text{Å}^{-1}$$

$$k_{\mathrm{A}} = 1.5 \times 10^{10}\ \text{L mol}^{-1}\,\text{s}^{-1}$$

$$k_{\mathrm{D}} = 2.3 \times 10^{10}\ \text{L mol}^{-1}\,\text{s}^{-1}$$

$$k_{\mathrm{G}} = 9.1 \times 10^{9}\ \text{L mol}^{-1}\,\text{s}^{-1}$$

The standard value of D is typical for small molecules in a fluid liquid medium. (For cyclopentyl bromide in DEE at 37 C, a value of 9.8×10^{-5} cm^2 s^{-1} has been reported [28].)

Considerations of inert ZB and AB are also instructive, so standard parameter values are chosen for these as well. In each case, they are the same as those for the corresponding standard reactive pair except that $\kappa = 0$ for the inert pair.

7.2.5 Kinetics of ZB and AB

Many of the relevant mathematical results are well known and are not derived here. The present focus is on physical meaning. To enhance this focus, we present figures illustrating quantitative differences between the standard AB and ZB. Some mathematical details and equations that generate these figures are in the Appendix.

The thermal displacement motions of a molecule in solution can be factored into oscillations about mean positions and net displacements. The net displacements constitute diffusion, which can be defined mathematically as the limit of a random walk as the step size approaches zero.

diffusion trajectory a pathway of infinite length that is followed by inert molecules that diffuse in the same way as real (possibly reactive) molecules.

When a diffusing molecule reacts, it stops following its trajectory. However, the trajectory itself continues, describing the way the molecule would have diffused if it had not reacted.

contact trajectory a diffusion trajectory that brings the partners into contact eventually.

non-contact trajectory a diffusion trajectory that never brings the partners into contact.

ZB a surface–molecule pair—a planar surface Z and a molecule B that are in contact or on a contact trajectory.

AB a molecule–molecule pair—molecules A and B that are in contact or on a contact trajectory.

Figure 7.7 illustrates a part of a diffusion trajectory that returns Z and B, but not A and B, to contact. It is not clear whether or not this is a contact trajectory for A and B. As will be seen shortly, a Z and B are always in contact or on a contact trajectory, so they always constitute a ZB, but this is not true of an A and B.

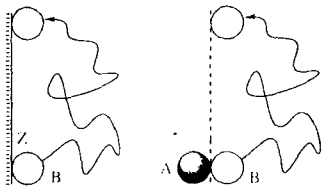

Fig. 7.7. Left: Part of a contact trajectory of a Z and a B. Every trajectory returns them to contact an infinite number of times. Right: The same partial trajectory for an A and B, showing that they do not return to contact at the same time after separation as the Z and B.

geminate pair AB_g an AB whose partners were born simultaneously from the same precursor molecule C [78].

non-geminate pair AB_n an AB arising at the first contact between a non-geminate A and B.

partners members of a ZB or AB.

pair reaction reaction between partners.

geminate reaction geminate pair reaction.

non-geminate reaction non-geminate pair reaction.

Polyá's Recurrence Theorem dictates one of the most important differences between ZB and AB. It states that every random-walk trajectory in one or two dimensions passes through every point in space but that this is not true in three dimensions [79,80]. The Recurrence Theorem is the subject of a famous (among mathematicians) joke.

> A mathematician encounters a drunk staggering randomly in the streets and moaning 'I wanna go home.' The mathematician thinks for a moment, then offers the following helpful advice: 'You're doing fine. Just keep going like you are, but try to stay out of three dimensions.'

For an AB, diffusion in each of three dimensions has consequences, but for a ZB the only diffusion of consequence is in the dimension (x) perpendicular to the plane of the surface. Because effective

ZB diffusion is one-dimensional, the Recurrence Theorem guarantees that every Z and B constitute a ZB, since they always have a contact trajectory. As a consequence of the three-dimensional nature of effective AB diffusion, the same theorem guarantees that some AB will gain non-contact trajectories.

to escape v. to gain a non-contact trajectory.

escape n. the act of escaping.

escaped molecule A or B after escape.

β probability of a contact trajectory when A and B have separation s; β is related to R and r (equation 7.20; Berg gives a simple derivation, pp. 38–39) [81].

$$\beta = R/r = R/(R + s) \tag{7.20}$$

β_Z probability of a contact trajectory when Z and B have separation s.

$$\beta_Z = 1 \text{ (Recurrence Theorem)} \tag{7.21}$$

The timescale of escape is significant. If the escape-limited lifetime of an AB were comparable to or longer than the lifetime of a ZB, then some aspects of the behaviors of AB and ZB might be similar. If the escape-limited lifetime of an AB were much shorter than the lifetime of a ZB, then AB and ZB behaviors would necessarily be very different.

A pair survives if it is in contact or has a contact trajectory. Pairs are destroyed by both pair reaction and escape.

$S(t)$ pair survival probability, a function of time t.

For the standard AB, the escape-limited lifetime is quite short. In Figure 7.8, the survival probabilities $S(t)$ of the standard inert ZB and AB are plotted as a function of time. The AB half-life is 2.5×10^{-11} s and the escape probability is nearly 90% by 10^{-9} s. Once A and B become separated by a few multiples of R, the escape probability (probability that escape has occurred) is high, but escape is not possible for a ZB, no matter how far Z and B are separated.

escape probability (AB) $= 1 - \beta$ (7.22)

escape probability (ZB) $= 1 - \beta_Z = 1 - 1 = 0$ (7.23)

An inert ZB lasts forever. Reactive AB and ZB have shorter lifetimes than their inert counterparts.

Some properties of reactive AB such as geminate radical pairs are commonly probed with traps. In principle, two types of trapping can occur.

pair trapping a non-pair reaction of a member of a surviving pair.

escape trapping a reaction of an escaped molecule.

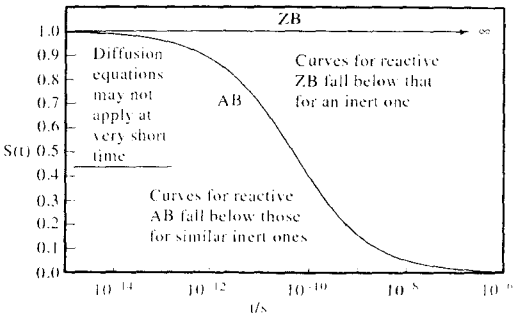

Fig. 7.8. Survival probability $S(t)$ as a function of time t for a standard inert AB and ZB (Equation 7A.22, Appendix).

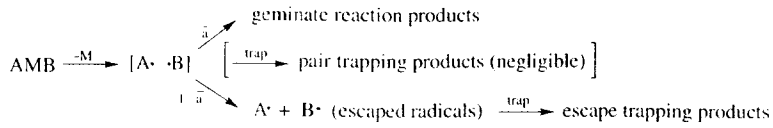

Usually only escape trapping is observed—ordinary radical traps are sufficiently reactive for efficient escape trapping but not for pair trapping [78]. When the escape trapping efficiency approaches 100%, the overall trapping efficiency $1 - \bar{a}$ is independent of the concentration of trap, provided that it is high enough to trap nearly all of the escaped radicals (Figure 7.9).

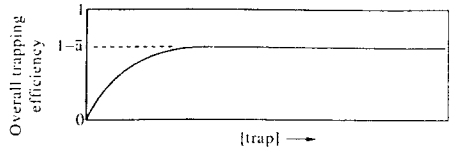

Fig. 7.9. Schematic diagram illustrating typical trapping when radical pairs are generated geminately. At sufficiently high trap concentrations, the overall trapping efficiency $1 - \bar{a}$ is invariant with trap concentration; $\bar{a}$ is the probability of geminate reaction.

A kinetic analysis gives the basis of such trapping experiments. Let a trap for B be present at 1 M and let k_T be its second-order rate constant for reaction with B. Pair trapping must occur within $\sim 10^{-10}$ s; otherwise, AB will have disappeared through either pair reaction or escape. In order for pair trapping to be significant, k_T has to have a value near 10^{10} L mol^{-1} s^{-1}. The reactivities of most ordinary radical traps fall short of this by orders of magnitude. Consequently, pair trapping is rare. Escaped radicals, on the other hand, can have far longer lifetimes, allowing them to be trapped efficiently.

Geminate reaction is often called 'cage' reaction, even though it may include events in which the radicals diffusively separate, return to contact, and react. In some usages, a 'cage' reaction is that of radicals that have remained in adjacent positions in solution (essentially in contact), surrounded by a 'cage' solvent molecules, until they react. In Noyes' nomenclature, this is a primary geminate reaction; other geminate reactions are secondary [78]. Where geminate radical pairs are formed in non-adjacent positions in solution (perhaps with a small molecule M, e.g., CO_2 or N_2, between), all

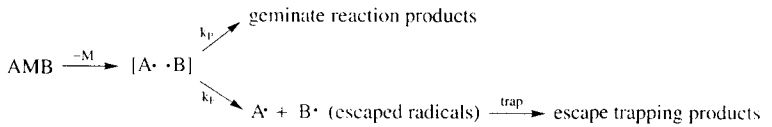

geminate pair reaction is secondary. Primary geminate reaction can occur only when the members of the pair are created in adjacent positions in solution.

In the literature, pair reaction and escape are represented frequently as first-order processes with constant rate coefficients (e.g., k_P for pair reaction, k_E for escape). This is an approximation. If diffusion is important, then k_P and k_E actually vary with time. Unless their time-dependencies are treated, it is better to use probabilities $\bar{a}$ and $1 - \bar{a}$ instead of rate coefficients. Of course, it is immaterial if, as is frequently the case, the only use to which k_P and k_E are put is to express (erroneously) $\bar{a}$ and $1 - \bar{a}$: $\bar{a} = k_P/(k_P + k_E)$, $1 - \bar{a} = k_E/(k_P + k_E)$.

Figure 7.10 illustrates the differences between conventional first-order and SCK diffusion–reaction decay curves, normalized to the same half-life $\tau_{1/2}$. The SCK curve applies to either an AB or a ZB, with the partners in contact at time zero. For an AB, both pair reaction and escape contribute to decay, but only pair reaction contributes for a ZB.

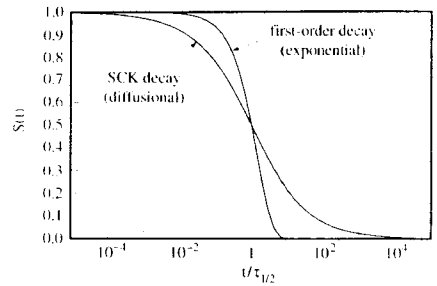

Fig. 7.10. SCK (equation 7A.22, Appendix) and conventional first-order decay curves for the same half-life.

If its disappearance were exponential, an AB would almost certainly disappear before 10 half-lives. For the standard AB, $\tau_{1/2} \approx 10^{-11}$ s, so 10 half-lives is $\sim 10^{-10}$ s. In contrast, a ZB still has a survival probability of a few percent after 1000 half-lives. For the standard ZB, $\tau_{1/2} \approx 10^{-8}$ s, so 1000 half-lives is $\sim 10^{-5}$ s. An SCK pair also disappears more rapidly at the beginning (relative to $\tau_{1/2}$) than one governed by conventional first-order kinetics.

The long disappearance tail for an AB plays an important role in the development of CIDNP. In addition, it can be important in allowing observations of 'second-order' CIDNP, i.e., CIDNP due to spin evolution in daughter radical pairs that result when one (or both) of the original radical members reacts (e.g., by decarboxylation) [50]. The reaction(s) leading to daughter pairs can be relatively slow and still lead to detectable, signature CIDNP because some pairs survive so long. Second-order CIDNP would be seen much less frequently if radical pairs disappeared exponentially. Because CIDNP is so sensitive, only a few percent of the original radical pairs have to give daughter pairs to generate a signature signal. The long decay tail also implies that there can be some pair trapping with ordinary radical traps—in most cases, however, the fraction of the pairs trapped is too small to be noticed.

In the absence of pair trapping, a ZB disappears by pair reaction only. There being no escape, there can be no escape trapping. The conventional AB trapping method that determines the extent of escape and geminate reaction is not applicable to a ZB, for which all trapping is pair trapping. Since a ZB can have a very long lifetime, trapping can occur over a much longer pair lifetime than for an AB.

Figure 7.11 gives the survival probability $S(t)$ for the standard AB and ZB, along with an indication of the timescales of ordinary radical trapping. There can be no significant AB trapping but significant ZB trapping is quite possible.

Solvent attack by a radical is a trapping reaction. If a standard AB diffuses to a radius r of $5R$, that is, $s = 4R = 20$ Å, then the probability that escape has occurred is 0.80 (equations 7.20 and 7.22). In the absence of more reactive traps than the solvent (for typical alkyl radicals, $k_S = 10^3$ s^{-1}), escape trapping by **s** will compete with escape trapping by **c**.

For a standard ZB that reaches the same separation, $s = 20$ Å, the escape probability is zero and the probability ϕ_Z (Equation (7A.25), Appendix) of returning to the surface before reacting with the solvent, as given by equation (7.24), is 0.9988.

$$\phi_Z = e^{-s/\sigma_S} \quad \sigma_S = (D/k_S)^{1/2} \qquad (7.24)$$

For ϕ_Z to be as small as 0.50, s would have to be 12 006 Å. Here σ_S is the **s**-limited characteristic diffusion distance.

In summary, the following are important differences between surface–molecule pairs ZB and molecule–molecule pairs AB. Perhaps the most important lesson here is that the absence of solvent attack in a Grignard reaction is not evidence that

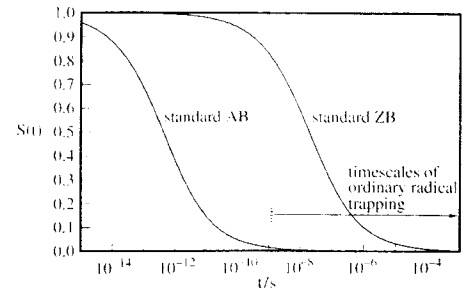

Fig. 7.11. Survival probabilities $S(t)$ for the standard AB and ZB (Equation 7A.22, Appendix).

intermediate radicals R• do not separate from the surface Mg_Z.

Property	AB	ZB	Comment
escape	yes	no	
lifetime	$\sim 10^{-11}$ s	up to ∞	standard AB
trapping	escape only	pair only	ordinary traps
solvent attack	yes	no	alkyl radicals

7.2.6 Infinite-Dilution D Model [82,83]

At infinite dilution, there are no radical–radical reactions. For the case in which the only reactions of R• are **r** and a competing (pseudo-)first-order trapping reaction **q** (which could be **s**) giving product Q and governed by rate constant k_Q, the D-model solution for the yield A of RMgX has a simple form, equation (7.25),

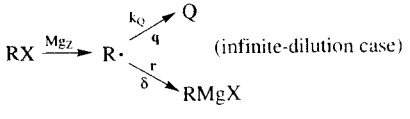

(infinite-dilution case)

$$A = \delta\sigma_Q/(1+\delta\sigma_Q) \quad \text{(infinite dilution)} \qquad (7.25)$$

where $\sigma_Q = (D/k_Q)^{1/2}$, the **q**-limited characteristic diffusion distance. Since the only fates of R• are **r** and **q**, the yield (Q) is $1 - A$ and the ratio of yields (Q)/(RMgX) also has a simple form.

$$\frac{(Q)}{(RMgX)} = \frac{(1\text{-}A)}{A} = \frac{1}{\delta\sigma_Q} = \frac{k_Q^{1/2}}{D^{1/2}\delta} = \frac{(Dk_Q)^{1/2}}{\kappa} \qquad (7.26)$$

These equations can be further simplified by defining **r**- and **q**-limited characteristic lifetimes τ_R and τ_Q of R•. Let τ_Q be $1/k_Q$, the average lifetime of R• as limited by **q**. Let $\tau_R = \tau_Q$ when (Q) = (RMgX). Also, define the **r**-limited characteristic diffusion distance σ_R: $\sigma_R = (D\tau_R)^{1/2}$. Then (from equation 7.26)

$$\tau_R = D/\kappa^2 \qquad (7.27)$$

$$\sigma_R = 1/\delta \qquad (7.28)$$

$$\delta\sigma_Q = (\tau_Q/\tau_R)^{1/2} = 1/(k_Q\tau_R)^{1/2}$$

$$= \sigma_Q/\sigma_R \qquad (7.29)$$

$$A = 1/[1 + (k_Q\tau_R)^{1/2}] \qquad (7.30)$$

and

$$(Q)/(RMgX) = (k_Q\tau_R)^{1/2} = (\tau_R/\tau_Q)^{1/2}$$

$$= \sigma_R/\sigma_Q \qquad (7.31)$$

Thus, the infinite-dilution D model predicts that the ratio (Q)/(RMgX) will be proportional to $k_Q^{1/2}$ provided that τ_R is constant, a condition that is met when D and δ (or κ) are constant. This prediction provided the first test of the D model (Section 7.2.8).

The infinite-dilution D model allows us to address some fundamental questions by comparing and contrasting the standard ZB and AB. The reader should recall that the standard ZB has the D-model properties of the [Mg_Z R•] intermediate in a Grignard reaction of a primary alkyl bromide in DEE and that the standard AB has properties similar to those of a typical pair of small alkyl radicals (e.g., methyl). Thus, the calculations for the standard ZB are really those for the Grignard-reaction intermediate [Mg_Z R•].

(1) How far from Mg_Z do intermediate radicals R• get during the Grignard reaction? Equation (7.32) provides the answer. Here χ is the excursion probability, the probability that the [Mg_Z R•], or any other ZB initially in contact, will reach a separation s, at least, and then suffer pair reaction. For an AB, the corresponding relationship is equation (7.33).

$$\chi = 1/(1+\delta s) = 1/(1 + s/\sigma_R) \qquad (7.32)$$

$$\chi = \beta_s(1 + \beta_s\delta s)^{-1}[1 + (R\delta)^{-1}]^{-1}$$

$$[\beta_s = R/(R+s)\text{(equation 7.20)}] \qquad (7.33)$$

where β_s is the probability that escape has not occurred when $r = R + s$ and $[1 + (\delta R)^{-1}]^{-1}$ is the pair reaction probability a (non-geminate pair) or a (geminate pair), which have the same value in this case [spin-free, isotropically reactive, spherical molecules (equation 7A.8, Appendix)]. Equation (7.33) is general, reducing to equation (7.32) for a ZB ($\beta_s = 1$, $a = 1$).

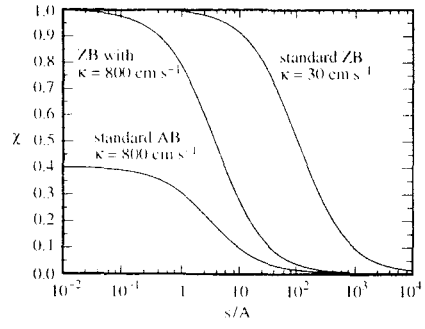

Fig. 7.12. Infinite-dilution D-model excursion probability χ as a function of the separation s for the standard ZB and AB. For comparison with the standard AB, to illustrate the role of escape, a ZB like the standard ZB, except in that it has an activation-control flux constant κ with the same value as the standard AB, is included.

Figure 7.12 shows how χ varies with s for the standard ZB and AB. The differences are dramatic—the values of χ (1000 Å) are 9.1% and 0.12% for the ZB and AB, respectively; χ (100 Å) are 50% and 1.2%; χ (10 Å) are 91% and 9.2%. Of the AB that suffer pair reaction (40% of the total), only 50% reach a separation of 3 Å, but 97% of the ZB do so.

Two factors account for these differences, (a) the standard AB is more reactive ($\kappa = 800\ \text{cm s}^{-1}$) than the standard ZB ($\kappa = 30\ \text{cm s}^{-1}$) and (b) the AB suffers escape but the ZB does not. Figure 7.12 also includes calculations for a ZB that has the κ-value of the standard AB but is otherwise like the standard ZB. A comparison with the standard AB illustrates the influence of escape.

(2) What is the average lifetime of a Grignard radical R•? For typical alkyl bromides in DEE, this is the same as the average lifetime of the standard ZB.

It is tempting to assume that τ_R is the average lifetime of a ZB (as limited by **r**), but this is incorrect—in fact the average lifetime is infinite (see Berg's equation 3.11, p. 43, with $b \to \infty$ [81])! It is infinite for an AB as well.

This rather non-intuitive random-walk property arises as follows. For a small number of trajectories, s becomes extremely large, approaching infinity. Although s will return to zero eventually, the maximum time required has no limit and is, in that sense, infinite. An infinite lifetime along a single trajectory is enough to make the average lifetime infinite.

The half-life (median lifetime) $\tau_{1/2}$ (as limited by **r**) *is* useful as a characteristic lifetime. It is simply related to τ_R (Equation 7.34).

$$\tau_{1/2} = 0.59148/D\delta^2 = 0.59148\tau_R \qquad (7.34)$$

For the standard ZB, $\tau_{1/2} = 2.0 \times 10^{-8}$ s, $\tau_R = 3.3 \times 10^{-8}$ s, and $\sigma_R = 100$ Å.

7.2.7 General D Model [84]

General D models include **r**, **c**, **s**, and **q**. Several cases are distinguished here. In the R case, the most complex, intermediate radicals R• isomerize to Q•, both R• and Q• attack the solvent (forming S• and RH or QH), coupling/disproportionation occurs among all radical intermediates (forming RR, RQ, QQ, RS, QS, and SS), and all radical intermediates are reduced to corresponding Grignard reagents (RMgX, QMgX, and SMgX).

In the most general treatment, the values of the rate constants governing similar reactions of different intermediates would be different, but here we adopt the simplification that they are the same, as illustrated below. This is an excellent approximation when R• and Q• are very similar and S• is negligible. In this approximation, the solutions for the simpler P and T cases are steps in the solution for the R case.

In the P case, groups R and Q are not distinguished. They are lumped into P. This is also the case of a halide PX whose radical P• does not suffer **q**.

In the T case, groups R, Q, and S are lumped into T. This is also the case of a halide TX whose radical T• suffers neither **s** nor **q**.

The T case has a relatively simple steady-state solution [84], equations (7.35–7.37), where F is dimensionless, equation (7.37) defines k_C, v is the flux of formation of R• at Mg_Z, and the yield of each product is the fraction of R groups accounted for by that product. Unless otherwise specified, this

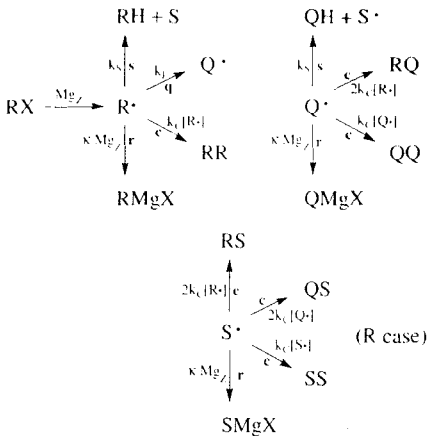

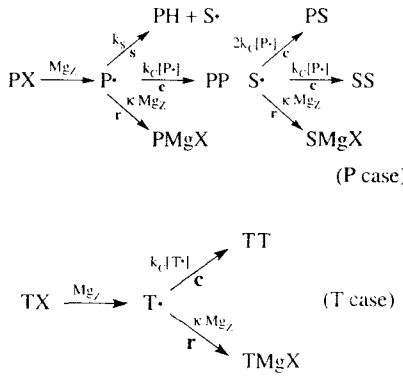

is the yield basis throughout.

$$\frac{(\mathrm{RMgX})^3}{[1-(\mathrm{RMgX})]^2} = \frac{3D^2\delta^3}{4Dk_C v} = F \qquad (7.35)$$

$$(\mathrm{RR}) = 1 - (\mathrm{RMgX}) \qquad (7.36)$$

$$-(\mathrm{d}[\mathrm{R}\cdot]/\mathrm{d}t)_c] = 2k_C[\mathrm{R}\cdot]^2 \qquad (7.37)$$

Figure 7.13 shows the calculated variation in (RMgX) with F. For the parameter values that fit reactions of a primary alkyl bromide RBr in DEE at ~40°C, $F = 22.5$, corresponding to an RMgX yield of 84%. This is for experiments with $[\mathrm{RBr}]_{avg} \approx 1.5$ M [48]. Since higher concentrations are unlikely, the accessible yield region is predicted to be 84–100%, with higher yields resulting for more dilute reaction mixtures, provided that v is proportional to [RBr]. Lower yields could result, in principle, under conditions where the value of κ (or δ) is smaller.

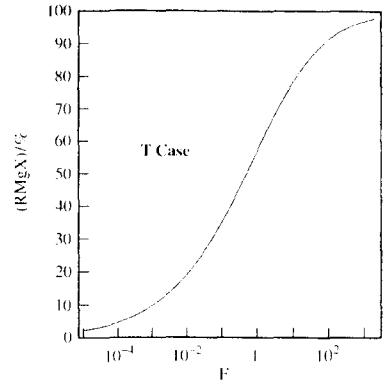

Fig. 7.13. Yield (RMgX) as a function of the dimensionless parameter F (equation 7.35).

The steady-state concentration profile for R· is shown in Figure 7.14, where R is a scaled concentration [R·] and X is a scaled distance x from Mg_Z [84].

$$R = \left(\frac{4k_C}{3k_S}\right)[\mathrm{R}\cdot] \qquad (7.38)$$

$$X = \left(\frac{k_S}{D}\right)^{1/2} s \qquad (7.39)$$

The right and upper axes show unscaled values for reactions of primary alkyl bromides in DEE at ~40°C (standard ZB with $v = 2 \times 10^{-5}$ mol cm^{-2} s^{-1}, $2k_C = 3 \times 10^9$ M^{-1} s^{-1}, and $k_S = 4.4 \times 10^3$ s^{-1}). (The experimental value of k_S is near 10^3 s^{-1}. The exact value is of no consequence here since **s** is not significant.)

There are two striking features. (1) The steady-state values of [R·] are greater than 10^{-4} M at distances up to ~1000 Å from Mg_Z, and even at

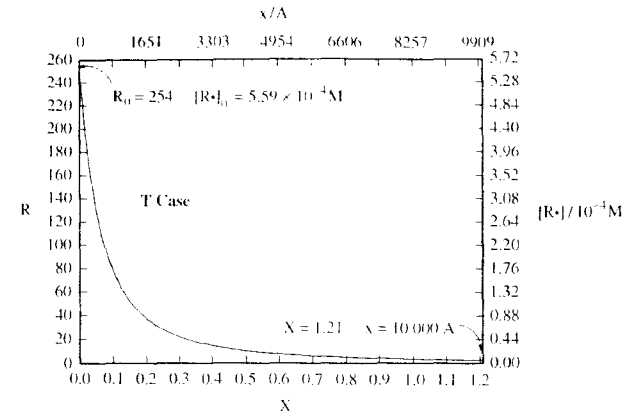

Fig. 7.14. Steady-state concentration profile of R· in the T case (Equations 9 and 10 of Garst, Swift, and Smith) [84]. Parameters that fit data for Grignard reactions of primary alkyl bromides in DEE at ~40°C [83] lead to the unscaled values at the top and right.

10 000 Å they remain significant. (2) The steady-state value of $[\mathrm{R}\cdot]_0$ (concentration of R· at Mg_Z) is nearly 10^{-3} M. 'Intuition' based on radical-pair behavior might not have suggested either such a long tail of significant radical concentrations or such high concentrations near Mg_Z.

Where does most of the **c** occur? This may best be answered by giving some points on a reaction profile: 1% occurs within 3.5 Å of Mg_Z, 10% within 37 Å, 50% within 269 Å, 90% within 1196 Å, and 99% within 3773 Å.

The P and R cases are more complex. Since solvent attack is negligible in reactions of primary alkyl bromide in DEE at ~40°C, the P case reduces to the T case, leaving only the R case to be considered further here.

Although there are six experimental parameters in the R case, the product distribution is completely determined by only three dimensionless ones, V, Δ, and $G^2 - 1$.

$$V = \frac{4k_C v}{3k_S^{3/2}D^{1/2}} \qquad (7.40)$$

$$\Delta = \frac{D^{1/2}\delta}{k_S^{1/2}} \qquad (7.41)$$

$$G^2 - 1 = k_I/k_S \qquad (7.42)$$

The solutions for the concentration profiles are complex (see the Appendix). We illustrate them with the parameter values used above for the T case plus $k_I = 4.4 \times 10^5$ s^{-1}, the value for the cyclization of the 5-hexenyl radical. Thus, the calculations presented here for the R case are D-model predictions for the Grignard reaction of 5-hexenyl bromide in DEE at ~40°C.

Figure 7.15 shows steady-state concentration profiles for the R case (W· = R·, Q·, or S·). Solvent attack and [S·] are insignificant. $[\mathrm{S}\cdot]_0$ is $\sim 2.4 \times 10^{-7}$ M and [S·] reaches its maximum value of $\sim 1.3 \times 10^{-6}$ M at a distance of ~4130 Å. $[\mathrm{R}\cdot]_0$ is high, $\sim 5.4 \times 10^{-4}$ M, but [R·] decreases rapidly with distance from the surface. $[\mathrm{Q}\cdot]_0$ is much lower, $\sim 1.8 \times 10^{-5}$ M, and [Q·] initially increases with distance from the surface, reaching a maximum value of $\sim 6.6 \times 10^{-5}$ M at a distance of ~660 Å. The fraction $[\mathrm{Q}\cdot]/[\mathrm{P}\cdot]$ ($[\mathrm{P}\cdot] = [\mathrm{R}\cdot] + [\mathrm{Q}\cdot]$) increases steadily with distance from the surface, reaching 0.5 when [R·] and [Q·] are both $\sim 6.0 \times 10^{-5}$ M at ~1200 Å from the surface.

Two striking predictions emerge. (1) The fraction I_G of isomerized alkyl groups Q in PMgX (RMgX + QMgX) is calculated to be much lower

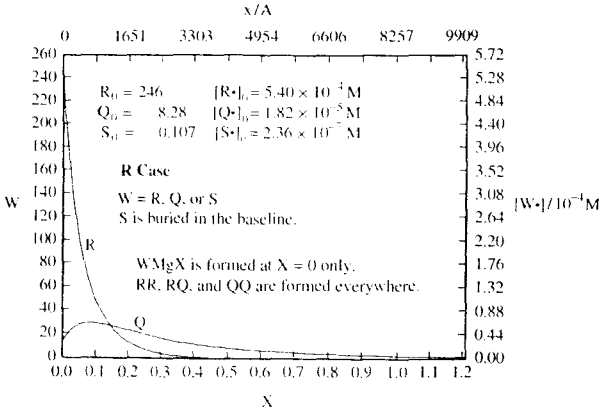

Fig. 7.15. Concentration profiles for the R case, in which R• isomerizes to Q• and both R• and Q• attack the solvent (Equations 9, A33, and A44 of Garst, Swift, and Smith) [84]. W is R or Q. The parameters are those that fit data for Grignard reactions of primary alkyl bromides in DEE at ~40 C (see text).

than that (I_D) in the dimer PP (RR + RQ + QQ): $I_G = 3.3\%$; $I_D = 22\%$. The reason is that Grignard reagent is formed only at Mg_Z but PP is formed everywhere. Since [Q•]/[P•] is minimal at Mg_Z, relatively less Q is incorporated into PMgX than into PP. (2) The calculated value 1.1 of the yield ratio H, equation (7.43), is nearer 1 than 2. For a homogeneous solution, $H = 2$ is expected. The steady-state rates of formation of RR, RQ, and QQ are k_C [R•]^2, $2k_C$ [R•] [Q•], and k_C [Q•]^2, respectively, leading to Equation 7.44 for homogeneous solution (or homogeneous surface reactions.

$$H = \frac{(RQ)}{[(RR)(QQ)]^{1/2}} \qquad (7.43)$$

$$H = \frac{2k_C[R\bullet][Q\bullet]}{(k_C[R\bullet]^2 k_C[Q\bullet]^2)^{1/2}} = 2 \quad \text{(homogeneous)} \qquad (7.44)$$

The fact that dimers are formed at all distances from Mg_Z is again responsible for the unusual result. For the PP formed at any particular distance, $H = 2$ is calculated, but $H = 1.1$ results when the yields are summed over all distances.

7.2.8 Typical Alkyl Halides

Since mechanisms of other reactions vary among classes of organyl halides (alkyl, allyl, benzyl, cyclopropyl, vinyl, aryl, etc.), this can be expected of Grignard reactions as well. Accordingly, we consider the classes individually.

'Typical' alkyl halides are monochloro, bromo, or iodo derivatives of simple alkanes or cycloalkanes. Allylic and benzylic halides, α-haloketones, etc., are excluded, as are cycloalkyl halides with cycloalkyl ring sizes less than five. Cyclopropyl halides, in particular, are treated separately.

There are no data on Grignard reactions that suggest mechanistic differences among typical alkyl chlorides, bromide, and iodides or among typical primary, secondary, and tertiary halides. All react at similar rates, with chlorides being somewhat slower than bromides and iodides, and all give similar distributions of products of **r** and **c**.

An explicit search for solvent-attack products in the Grignard reaction of *n*-hexyl bromide (RBr) in DEE revealed no detectable SS or RS [52]. The yield of RH in excess of R(−H) was no greater than 0.5%, placing the upper limit on

the extent of **s** at 0.5% and confirming many other reports suggesting that solvent attack is negligible in Grignard reactions of typical alkyl halides.

The diversion by TMPO• of up to 95% of the reaction of cycloheptyl bromide suggests that **R** is the dominant, probably exclusive, pathway for Grignard reactions of typical alkyl halides [15]. The dominance of pathway **R** is also supported by the agreement between observed yields and quantitative D-model predictions [83].

In the first test of the D model, the infinite-dilution form was applied to Grignard reactions of primary alkyl bromides **1**–**3** in DEE at ~40°C [82]. The intermediate radicals isomerize, rate constant k_I, forming both RMgBr and QMgBr.

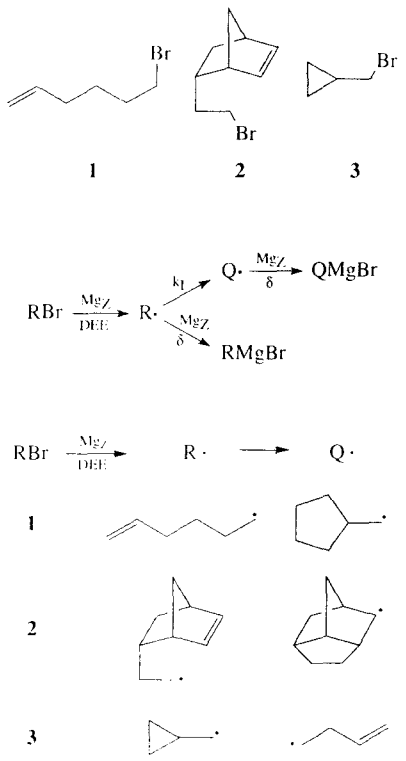

The data conform to the prediction of equation 7.26 (Q = QMgBr, $k_Q = k_I$) that a log–log plot of the yield (QMgBr)/(RMgBr) against k_I will have a slope 1/2 (Figure 7.16). The fit is satisfactory, and the derived value of τ_R is 3.33×10^{-8} s (corresponding to $\delta = 0.010$ Å^{-1}). A better fit for **1** is obtained, with the same value of τ_R, when a general D model is used [83].

When there is little **q** or when its extent far exceeds that of **r**, (Q)/(RMgBr) cannot be determined accurately and plots like that of Figure 7.16 are useless. However, plots of A, equation (7.25), are significant.

Figure 7.17 shows data for nine reactions of typical alkyl halides and five reactions of vinyl, aryl, and cyclopropyl halides. The points for typical alkyl halides fall close to curves for equation (7.25) with τ_R near 10^{-7} s, but those for vinyl, aryl, and cyclopropyl halides fall distinctly off these curves. For the typical alkyl halides, the range of values of k_Q, spanning a factor of 10^{10}, is impressive. So is the variety of reactions **q**: included are solvent

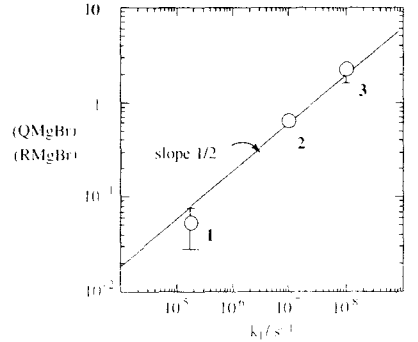

Fig. 7.16. Test of the infinite-dilution D model for Grignard reactions of primary alkyl bromides in DEE at ~40 C. Each bromide RBr provides a radical R• that isomerizes (rate constant k_I) to Q•, which are reduced to RMgBr and QMgBr. The slope of the line is 1/2, as required by equation (7.26). Point **1** is shown here as plotted originally ($k_I = 1.8 \times 10^5$ s^{-1}). A refined estimate of the value of k_I for the 5-hexenyl radical is 4.4×10^5 s^{-1}. Reprinted with permission from Garst, Deutch, and Whitesides [82]. Copyright 1986 American Chemical Society.

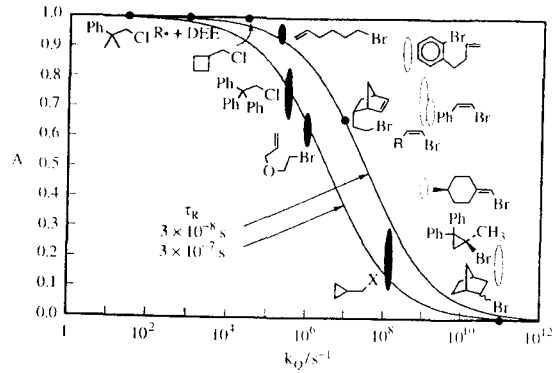

Fig. 7.17. Yield A of RMgX as a function of k_Q. The plotted curves are determined by equation (7.25). Data for all nine reactions of typical alkyl halides (solid ovals) conform to this equation for τ_R near 10^{-7} s, but the data for vinyl, aryl, and cyclopropyl halides (open ovals) do not. This plot is redrawn and augmented from Root, Hill, and Whitesides [85].

attack and inversion at a chiral center as well as several other radical rearrangements.

In judging the quality of fit for typical alkyl halides, several points should be considered. (1) The data are from a number of workers using a variety of reaction conditions and methods. Variations in initial concentrations, identities and concentrations of solvent may all affect A. (2) The effects of **c** on product distributions are ignored. (3) A variation of a factor of 10 in τ_R (curves plotted in Figure 7.17) corresponds to a smaller variation, a factor of $10^{1/2}$, ~3, in the corresponding value of κ or δ.

Reaction **q** can be radical trapping. For Grignard reactions of typical alkyl bromides, trapping by TMPO• and DCPH have been reported [14–16]. The curves in Figure 7.18 are identical with those of Figure 7.17, and the data are plotted in the same manner, A being the yield quotient (RMgBr)/[(RMgBr) + (trapping product)] and k_Q being the pseudo-first-order rate constant for trapping. The data for DCPH and TMPO• are consistent with one another and with the data of Figures 7.16 and 7.17; all imply $\tau_R \approx 10^{-7}$ s.

A potential problem with intermolecular trapping should be noted: the trap concentration can be depleted near Mg_Z, either by the trapping process or by direct reaction of the trap with Mg_Z, leading to less effective trapping than would be observed if the trap were distributed homogeneously. This may be responsible for the trend with [TMPO•] seen in Figure 7.18. Intramolecular trapping, i.e., radical isomerization, is not subject to this effect.

For reactions in DEE using Mg turnings and ordinary stirring, several workers have noted that product distributions are insensitive to the initial concentration of RBr when it is higher than ~0.2 M. On the other hand, when a rotating disk of Mg (345 rpm) partially reacts with *n*-hexyl bromide (RBr) in DEE at 0°C, the yields of RMgBr and products of **c** vary systematically with the average concentration $[RBr]_{avg}$ during the reaction (Figure 7.19) [34,35]. The curves in Figure 7.19 are calculated from equations (7.35) and (7.36) using $v = v_{avg} = \kappa_{RBr}[RBr]_{avg}$ (following the established rate law for hydrodynamically-controlled conditions). Under these assumptions, equation (7.35) becomes equations (7.45)and (7.46). To obtain the plotted curves, C was varied to achieve a best fit: $C = 4.3$ M.

$$\frac{(RMgX)^3}{[1-(RMgX)]^2} = \frac{C}{[RX]} \qquad (7.45)$$

$$C = \frac{3D^2\delta^3}{4k_C\kappa_{RBr}} = \frac{3\kappa^3}{4Dk_C\kappa_{RBr}} \qquad (7.46)$$

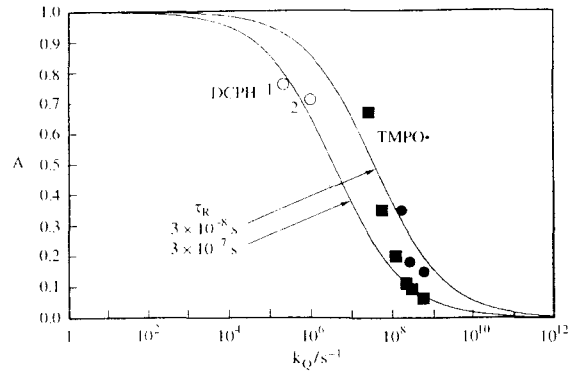

Fig. 7.18. Grignard-radical trapping by DCPH and TMPO•. A = (RMgBr)/[(RMgBr) + (trapping product)]. k_Q is the pseudo-first-order rate constant for radical trapping. Open circles: trap = DCPH. Closed symbols: trap = TMPO•. The curves are identical with those of Figure 7.17. 1: *n*-octyl bromide/DCPH/THF/22°C [16]. 2: 5-hexenyl bromide/DCPH/THF/22 C [16]. Closed squares: cycloheptyl bromide/TMPO•/DEE/*t*-amyl alcohol (5.0 M)/LiBr (0.05 M)/20°C [15]. Closed circles: cyclopentyl bromide/TMPO•/DEE/*t*-butyl alcohol (~0.8 M)/34°C [14].

If $D = 3 \times 10^{-5}$ cm^2 s^{-1}, $k_C = 3 \times 10^9$ M^{-1} s^{-1}, and $\kappa_{RBr} = 1.14 \times 10^{-2}$ cm s^{-1} (as determined directly for the reaction of cyclopentyl bromide under the same conditions) [26], then this value of C corresponds to $\delta = 0.0060$ Å^{-1} and $\tau_R = 9.2 \times 10^{-8}$ s, similar to the values determined from radical isomerization and trapping data and the infinite-dilution D model (Figures 7.16–7.18).

Thus, a hydrodynamically-controlled reaction behaves as expected. The fit to the curve is not strong evidence supporting the D model because other calculations show that the data are not sufficiently precise to discriminate between the curves calculated from equation (7.45) and those for a homogeneous surface model. However, the agreement of the fitted parameter with the value of τ_R determined from radical isomerization data is significant.

A similar variation in yields results from changing the rate of reaction varying the speed of rotation of a reacting disk of Mg. A faster rotation results in a thinner diffusional boundary layer and a faster reaction. For the reaction of cyclopentyl bromide in DEE at 25 C, the yield of RMgBr varies from ~86% for slow rotation to ~36% at 7000 rpm, with products of **c** varying in the opposite way [28].

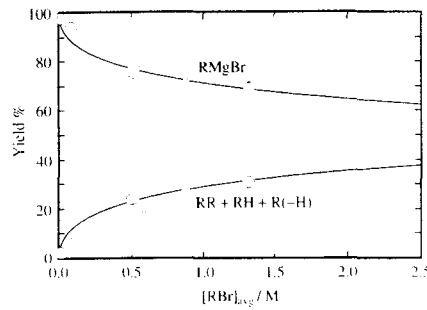

Fig. 7.19. Yields of Grignard reagent (upper) and hydrocarbons (lower) from partial reactions of magnesium (disk rotating at 345 rpm) with *n*-hexyl bromide in DEE at 0 C as functions of the average concentration of *n*-hexyl bromide during the reaction [34,35]. The lowest concentration is 0.017 M. The curves are calculated from equation (7.45) ($C = 4.3$ M) and (7.36).

Bickelhaupt and co-workers have provided extensive data sets for Grignard reactions of 5-hexenyl bromide in DEE at ~40 C, carried out in NMR tubes at high concentrations, $[RBr]_0 \approx 2.1$ M [48]. They determined the yields of RMgBr, QMgBr, RR, RQ, and QQ (Q =

cyclopentylmethyl, which arises through the cyclization of the intermediate 5-hexenyl radical R•). The good precision of their results, over a number of replications, demonstrates that Grignard reactions are reproducible, even when the conditions are not easily controlled. These are invaluable data for testing the D model.

In the general D model, R case, product distributions depend on values of six experimental parameters, v, δ (or κ), D, k_I, k_C, and k_S. For calculations, these values were chosen as follows. The value of v is estimated from data of Rogers *et al.* [29]

$$v = 2 \times 10^{-5} \text{ mol cm}^{-2} \text{ s}^{-1}$$

$$\delta = 0.010 \text{ Å}^{-1}$$

$$D = 3 \times 10^{-5} \text{ cm}^2 \text{ s}^{-1}$$

$$k_I = 4.4 \times 10^5 \text{ s}^{-1}$$

$$2k_C = 3 \times 10^9 \text{ M}^{-1} \text{ s}^{-1}$$

$$k_S = 4.4 \times 10^3 \text{ s}^{-1}$$

and Bodewitz *et al.* [48]. That of δ is extracted from the plot of Figure 7.16. A typical value for a small molecule in a fluid solvent is chosen for D. The value of k_I has been carefully determined [86]. The selected k_C-value is typical of radical-radical reactions of reactive species in fluid solvents [87]. The value of k_S has been determined (for a related primary alkyl radical, octyl) as $\sim 1 \times 10^3$ s^{-1} [13].

Since the exact value of k_S makes no difference in the calculations (solvent attack is negligible), a convenient value of $k_I/100$ was chosen for calculations. Of these values, the most uncertain is v, which was estimated for different conditions from those used in Bickelhaupt's experiments.

When solvent attack is negligible, as here, the value of k_S does not affect the product distribution, leaving five experimental parameters that do. These combine into two dimensionless parameters, V_I and Δ_I, that determine the entire product distribution. For the parameter values listed above, $V_I = 25.0$ and $\Delta_I = 8.26$.

$$V_I = \frac{4k_C v}{3k_I^{3/2} D^{1/2}} \tag{7.47}$$

$$\Delta_I = \frac{D^{1/2}\delta}{k_I^{1/2}} \tag{7.48}$$

The parameter values above predict the product distribution for the Grignard reaction of 5-hexenyl bromide in DEE with startling accuracy (Figure 7.20 left) [83]. The unusual values of I_G, I_D, and H (Section 7.2.7) are noteworthy, as is the fact that the yields (PMgBr) and (PP) are correctly predicted.

Experimentally, 2.8% (I_G) of the Grignard reagent PMgBr is QMgBr while 22% (I_D) of the P groups in PP are Q. Clearly, P groups are not

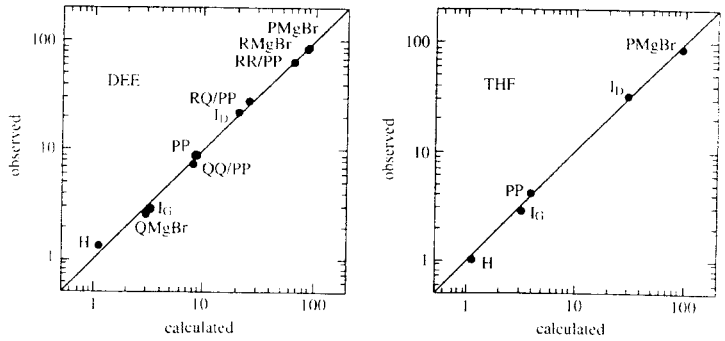

Fig. 7.20. Observed [48] vs calculated [83] yields and yield-based parameters for Grignard reactions of 5-hexenyl bromide (initially ~2.1 M) in DEE (left) and THF (right) at ~40°C. R = 5-hexenyl, Q = cyclopentylmethyl, P = R or Q. I_G = Q in PMgBr, I_D = %Q in PP. $H = (RQ)/[(RR)(QQ)]^{1/2}$.

taken randomly into PMgBr and PP from the same pool of radicals P• (R•, Q•). Otherwise I_G and I_D would have the same value. The experimental result is quantitatively predicted by the D model, in which only radicals at Mg$_Z$ form PMgBr while radicals everywhere form PP, as described previously (Section 7.2.7).

The observed value of H is 1.3, but 2.0 is the value that would be expected if the pseudo-steady-state populations of R• and Q• were spread homogeneously in space or over a surface. The D-model calculation gives $H = 1.1$. Values of H nearer 1.0 than 2.0 result from gradients in the pseudo-steady-state concentration profiles of R• and Q• during the Grignard reaction (Section 7.2.7).

These calculations are for a constant flux v of reaction. If v is proportional to [RX], as it is under hydrodynamically-controlled conditions, then v steadily decreases as a reaction proceeds. The yields of **c** products, in particular, are sensitive to v. A more exact calculation would take into account the variation in v as the reaction proceeds. However, a computational test of this effect showed that the product distribution obtained with decaying values of v is closely approximated by a calculation with a constant, effective value of v [83]. There is also evidence that v does not vary during reactions using Mg turnings and ordinary stirring (Section 7.2.2), further justifying constant-v calculations.

For the more polar and viscous solvent THF, the values of V_I and Δ_I were adjusted and an excellent fit to the experimental data was obtained (Figure 7.20, right) [83]. For the less polar and even more viscous solvents DBE (di-*n*-butyl ether) and DPE (di-*n*-pentyl ether), the quality of the adjusted-parameter fits decreases but is still impressive (Figure 7.21) [83].

For THF, whose viscosity η (0.389 cP) is twice that of DEE (0.194 cP), the fitted values of V_I and Δ_I are 15.0 and 12.7, respectively. Since D and k_C are expected to be affected by η, and since v and κ may be, it is not surprising that the parameter values that give the best fit for THF differ from those for DEE. Correcting D and k_C using Stokes' Law gives $v/v^0 = (V_I/V_I^0)(\eta^0/\eta)^{-1/2}$, $\kappa/\kappa^0 = (\eta^0/\eta)^{1/2}(\Delta_I/\Delta_I^0)$, and $\delta/\delta^0 = (\kappa/\kappa^0)/(\eta^0/\eta)$, where superscript zeroes denote values for DEE and unsuperscripted values are for THF. For THF, $v/v^0 = 0.85$, a plausible value. (The theoretical dependence of v on η is complex—for a rotating disk, v should be proportional to $\eta^{-5/6}$, which would lead to $v/v^0 = 0.56$.)

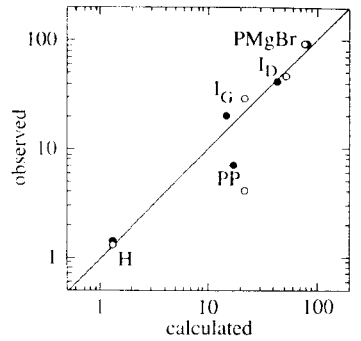

Fig. 7.21. Observed vs calculated yields and yield-derived parameters for Grignard reactions of 5-hexenyl bromide (initially ~2.1 M) in DBE (solid circles) and DPE (open circles) at ~40°C [83].

Table 7.1 contains derived rate parameters for the preceding analyses of data for the Grignard reaction of 5-hexenyl bromide in several solvents [83]. Two shortcomings should be noted. First, the viscosities used in the calculations are for the pure solvents. They are not necessarily identical with or proportional to the viscosities of the product mixtures in which the major parts of the reactions take place. Second, for DBE and DPE, the relatively poor fit introduces considerable uncertainty into V_I values. Those of Δ_I are better determined by the data.

The derived values of v/v^0 are similar for THF and DEE, but distinctly smaller for DBE and DPE. The characteristic radical lifetimes τ_R appear to be much longer in DBE and DPE than in THF and DEE. Both κ- and δ-values decrease while τ_R-values increase along the series THF < DEE < DBE < DPE. This is also the sequence of decreasing solvent polarity, suggesting that effects of polarity may dominate those of viscosity.

Table 7.1. Fitted and Derived Rate Parameters for Grignard Reactions of 5-Hexenyl Bromide in Ethers at ~40°C[a]

SH	V_I	Δ_I	η/cP	ν/ν^0	$10^8\tau_R$/s	κ/cm s^{-1}	$10^2\delta$/Å^{-1}
THF	15.0	12.7	0.389	0.85	1.4	33	2.2
DEE	25.0	8.26	0.194	1.0	3.3	30	1.0
DBE	2.15	2.00	0.506	0.14	57	4.5	0.39
DPE	0.962	1.21	0.80	0.08	160	2.2	0.30

[a] 'Best fit' values of V_I and Δ_I. Other parameters are derived by applying Stokes' Law [83].

Table 7.2. Cyclization in Reactions of 5-Hexenyl Halides in DEE and THF at 37°C

X	SH	$[MgBr_2]_0$	(RMgX)/%	(QMgX)/%	I_G/%[a]	Ref.
Cl	THF	0	93	3.8	3.9	*b*
Br	DEE	0	78	3.8	4.6	*c*
		0.18	73	5.5	7.0	*c*
		2.7	78	4.7	5.7	*c*
	DEE	0	67	1.6	2.3	*b*
	THF	0	90	5.0	5.3	*b*
	DEE		86	2.5	2.9	*d*
	THF		86	2.5	2.9	*d*
I	DEE	0	27	1.1	3.9	*b*

[a] I_G = QMgX)/[(RMgX) + (QMgX)]. For dilute reactions, I_G would be somewhat higher than these values (approaching 10%), which are for initial concentrations of RX in the range 0.4–2.1 M. A relatively large number of cyclized radicals couple/disproportionate. At sufficiently low concentrations, they would form Grignard reagent instead.
[b] Ashby and Oswald [16].
[c] Ungváry [88].
[d] Bodewitz, Blomberg, and Bickelhaupt [48].

For Grignard reactions of 5-hexenyl halides in THF and DEE, I_G is not very sensitive to solvent, halogen, or $[MgBr_2]_0$ (Table 7.2). This contrasts with the behavior of analogous aromatic halides in the same media (Section 7.2.11).

To isolate the effects of polarity, Bickelhaupt investigated the reaction in a series of mixtures of THF and benzene (PhH) [48]. These mixtures have nearly constant viscosities (varying from 0.389 to 0.480 cP), but their polarities decrease with increasing benzene content. It is found that as the benzene content increases, several yields follow the trends expected if κ decreases with polarity: (PMgBr) decreases (from 96 to 63%), (PP) increases (from 4 to 18%), and I_G increases (from 3 to 26%). Strikingly, I_D remains constant, within experimental error, at ~34%.

Figure 7.22 shows how the fitted Δ_I varies with the mole fraction X_{PhH} of PhH under the assumption that V_I varies only with viscosity, using an averaged value of V_I, 8.00, corresponding to the viscosity of pure THF [83]. Straight-line segments connect fitted (Δ_I) or calculated (others) values; plotted circles and squares represent experimental values.

D-model calculations reproduce the observed trends and notable features of the data, as well as the anticipated variation of Δ_I. Δ_I decreases with X_{PhH}, corresponding to an increase in τ_R from 2.3×10^{-8} to 7.9×10^{-7} s as X_{PhH} increases from 0 to 0.87. (PMgBr) decreases with X_{PhH}, (PP) increases, and I_G increases in both the observed data and the calculations. The calculations also reproduce the observed, but perhaps counter-intuitive, insensitivity of I_D to X_{PhH}.

As Lawrence and Whitesides observed [14], Grignard radicals derived from typical alkyl halides have properties that are strikingly similar to those of radicals diffusing in solution. They: (a) are trapped intermolecularly, sometimes with high efficiency; (b) undergo characteristic isomerizations; and (c) generate CIDNP (Section 7.2.3). In addition, product distributions from isomerizing Grignard radicals can be accounted for quantitatively by assuming that they diffuse in solution (D model) and that their isomerization, coupling, and diffusion are all governed by parameters with values appropriate for solution [82,83,85]. In Grignard reactions of 5-hexenyl bromide, the observed incorporation of much larger fractions of cyclopentylmethyl groups (Q) into alkyl dimers PP than into Grignard reagents PMgBr makes it clear that the radicals forming PMgBr and PP are not drawn randomly from the same pool [48]. The D model accounts for all of these observations quantitatively. An A model does not definitely predict any of them and would require special *ad hoc* postulates to accommodate them.

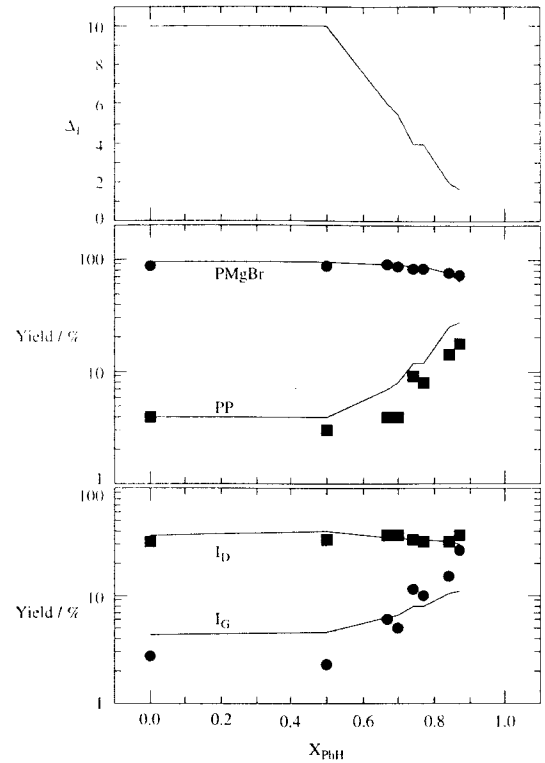

Fig. 7.22. Fitted values of Δ_I (top) and observed (circles and squares) and calculated yield parameters (lines) for Grignard reactions of 5-hexenyl bromide in mixtures of THF and benzene. X_{PhH} is the mole fraction benzene [83]. An averaged value of V_I, corrected for small viscosity variations, was used in the calculations.

7.2.9 Cyclopropyl Halides

Having 60° C–C–C bond angles and a relatively low-lying LUMO [89], cyclopropane is not a typical alkane, nor are cyclopropyl halides and radicals typical alkyl halides and radicals.

Some properties of the cyclopropyl group resemble those of the vinyl group. Like the vinyl group, cyclopropyl is capable of delocalizing interactions (pseudoconjugation) with π centers to which it is bonded [89,90].

Cyclopropyl is a bent σ radical [91–93], not a planar π radical like a typical alkyl radical, and it is about 10^3 times as reactive as a typical alkyl radical in atom-transfer reactions [94]. This suggests that the solvent-attack rate constant k_S will be of the order 10^6 s^{-1} in DEE. Indeed, a measurement for the 2-phenylcyclopropyl radical gave $k_S = 1.6 \times 10^6$ s^{-1} [95].

The partial s character of the singly-occupied orbital also enhances the electron affinity of the cyclopropyl radical [96]. If κ were to reflect the electron affinity of R•, a larger value would be anticipated for cyclopropyl than for a typical alkyl radical. This does not appear to be the case [52,97].

Figures 7.23 and 7.24 give product yields for Grignard reactions of cyclopropyl bromide (CpBr) in DEE [98]. In these experiments, yields of RMgBr were determined by titration, checked in several cases by protonation and determination (volumetric) of the cyclopropane evolved. Other yields were determined by GC, using authentic samples and GC-MS to assign GC peaks.

As noted in Section 7.2.1, the polarities of ethers containing polar solutes such as RMgX and MgX_2 are much higher than those of pure ethers [30]. Such solutes can be expected to affect Grignard reactions. Figures 7.23 and 7.24 show that (CpMgBr) increases at the expense of (CpCp), (CpH), (SS) and (CpS) as concentrations of polar solutes increase. This suggests that polar solutes enhance κ, shift the mechanism toward pathway **X**, or both.

Grignard himself suspected that in the earliest stage of the reaction the products are those of **c** (including MgX_2), with RMgX being formed only after the formation of a critical amount of MgX_2 [1,99]. The present data conform to that scenario, with **s** augmenting **c** as the initially dominant reaction.

Products SS and CpS represent solvent attack unambiguously. In dilute solutions that do not contain $MgBr_2$ initially, **s** is extensive, $\geq$20%. In concentrated solutions, or those containing $MgBr_2$ initially, it is ~2–10%. In every case, the extent of **s** is much higher than in a similar reaction of a typical alkyl bromide (<0.5%) [52].

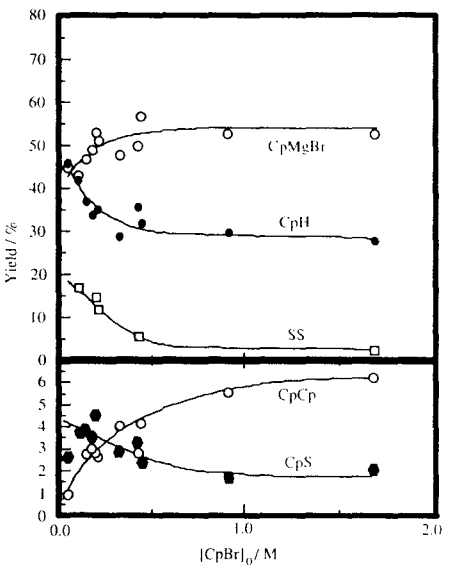

Fig. 7.23. Yields of products of reactions of magnesium with cyclopropyl bromide (CpBr) in diethyl ether (SH) at 37°C as a function of the initial concentration of cyclopropyl bromide ($[CpBr]_0$). Reprinted from Garst *et al.* [98], Copyright 1994, Page No. 370, with permission from Elsevier Science.

Interpretations are complicated by missing data. No disproportionation/coupling ratios are known for 2 Cp•, Cp• + S•, and 2 S•. Further, high reactivities and ignorance of their fates prevent the direct or indirect determination of possible disproportionation products cyclopropene [Cp(−H)] and ethyl vinyl ether [S(−H)]. Perhaps surprisingly, for several experiments the balance of Cp groups is close to 100%, suggesting that cyclopropene, if formed, is accounted for in some form. (Is cyclopropene reduced by Mg/$MgBr_2$ to 1,2-di(bromomagnesio)cyclopropane?) [100,101]. The addition of ethyl vinyl ether to a reaction mixture results in the formation of a gummy deposit on the stirring blade, probably a polymer. In one experiment, ethyl vinyl ether was detected as a product in ~3% yield [88].

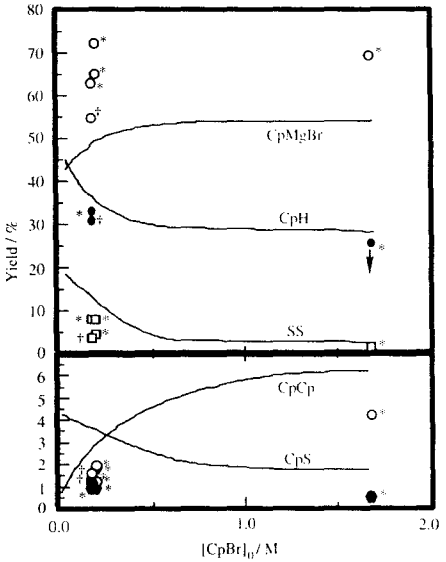

Fig. 7.24. Yields of products of reactions of magnesium with cyclopropyl bromide (CpBr) in diethyl ether (SH) at 37°C as a function of the initial concentrations of magnesium bromide ($[MgBr_2]_0$) and cyclopropyl bromide ($[CpBr]_0$). Symbols: as for Figure 7.23. The curves represent the yields when $[MgBr_2]_0 = 0$ and are taken from Figure 7.23 ·$[MgBr_2]_0 = 0.18$ M. *$[MgBr_2]_0 = 2.6$ M. Reprinted from Garst *et al.* [98], Copyright 1994, Page No. 370, with permission from Elsevier Science.

When no polar solutes are present initially, their concentrations build up quickly. At the high initial concentrations of RX used in synthetic preparations, most of the reaction occurs in the presence of polar solutes. They are further enhanced by the use of $BrCH_2CH_2Br$ (a source of $MgBr_2$) as a promoter. Accordingly, the data in Figures 7.23 and 7.24 that are most representative of synthetic practice are for reactions in media that contain RMgX, MgX_2, or both.

Typical yields under these conditions are (CpMgBr) = 65%, (CpH) = 30%, (CpCp) = 5%, (SS) = 4%, and (CpS) = 2%. When there is no radical isomerization, the D-model product distribution is determined by two composite parameters, V and Δ (equations (7.40) and (7.41)). The observed product distribution is approximated by a D-model calculation (Figure 7.25) with $V = 2.58$ and $\Delta = 2.71$, corresponding to $\delta = 0.0070$ Å^{-1}, $k_S = 2.0 \times 10^6$ s^{-1}, and all other parameters the same as those used in D-model calculations for 5-hexenyl bromide [102]. Taking disproportionation into account will bring the observed and calculated values of (CpH), (CpCp), (SS), and (CpS) even closer. Thus, with plausible parameter values, the D model can describe this product distribution.

It is noteworthy that the value of δ is very close to that for 5-hexenyl and hexyl radicals, despite the more favorable energetics of reduction of cyclopropyl. This suggests that some other factor dominates in determining the value of δ. This could be a property of the medium or interface.

In Walborsky's version of the A model, **s** is the inevitable fate of the few radicals that desorb and enter solution. The CpBr data indicate that more than a few desorb. Indeed, the agreement with

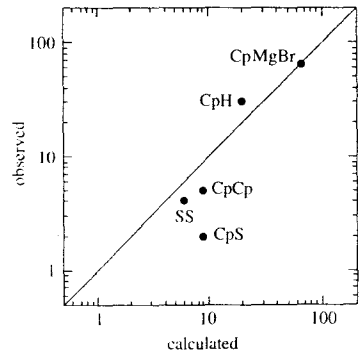

Fig. 7.25. Observed vs calculated yields for Grignard reactions of cyclopropyl bromide in DEE containing polar solutes at 37°C. The calculations use $V = 2.58$ and $\Delta = 2.71$ [102]. Calculated values of (CpCp), (SS), and (CpS) include radical disproportionation products and are consequently too large. The calculated value of (CpH) is for solvent attack only (does not include disproportionation) and is consequently too small.

D-model calculations suggests that none of the intermediate cyclopropyl radicals remain adsorbed.

Desorption and solvent attack are even clearer for reactions of Mg turnings with 2,2,3,3-tetramethylcyclopropyl bromide in DEE, which are interesting for other reasons as well [98]. This bulky substrate does not react when stirred for an hour in DEE alone. However, in 2.6-M $MgBr_2$/DEE a smooth reaction begins immediately. It is distinctly slower than reactions of typical alkyl bromides or of cyclopropyl bromide itself.

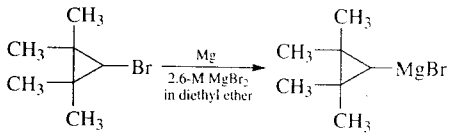

0.16–0.18 M 28%

+

2% + 68%

+

$CH_3CH_2O\,CHCH_3$ (SS)
$CH_3CH_2O\,CHCH_3$

44%

Yields (SS) and (RH) are astonishing, 44% and 68%, respectively. These data are not complicated by disproportionation reactions of R•, which are blocked by the absence of β-hydrogen atoms. Part of the excess of (RH) over (SS) is probably due to disproportionation reactions of R• with S• and part to disproportionation reactions of 2 S•, which give undetectable products S(−H) and SH. The observed yields are approximated by D-model calculations (Figure 7.26) with $V = 0.075$ (~0.03 of the value for CpBr) and $\Delta = 0.413$ (~0.15 of CpBr), consistent with decreases in v, k_C, and δ that could reflect steric effects not operative for CpBr.

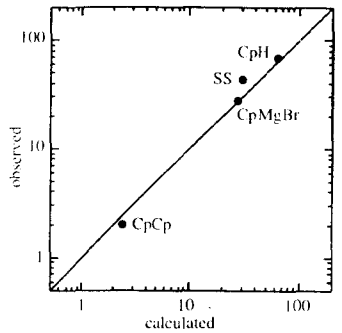

Fig. 7.26. Observed vs calculated yields for Grignard reactions of tetramethylcyclopropyl bromide (initially ~0.17 M) in DEE containing 2.6 M $MgBr_2$ at 37°C [98]. The calculations use $V = 0.075$ and $\Delta = 0.413$.

Systems with extensive solvent attack permit definitive tests of the question, 'Do radicals R• leave Mg_Z and then return and suffer reduction to RMgX?' This is the defining question for the D and A models ('yes' and 'no,' respectively).

More than one A model can be recognized. Possible mechanisms can be distinguished by the roles of adsorption and diffusion for each step, **r**, **c**, and **s**. In an 'A' (adsorption) step, the radicals remain adsorbed Mg_Z until they react. Otherwise, the step is 'D' (diffusion), a reaction of radicals that diffuse in solution. Specifying the nature of the steps in the order **rcs**, three of the possible mechanisms are AAD (Walborsky), ADD, and DDD (D model) [97].

Perdeuterating the solvent will reduce the value of k_S by a factor of ~3–10 (primary kinetic isotope effect), allowing the AAD, ADD, and DDD mechanisms to be distinguished [97]. The AAD mechanism predicts that there will be no effect of deuteration on the product distribution, the ADD mechanism predicts that deuteration will increase **c** at the expense of **s**, and the DDD mechanism predicts that it will increase **r** and **c** at the expense of **s**. Here are the findings of such experiments with CpBr (Table 7.3).

Table 7.3. Solvent Isotope Effects on Products of Reactions of Cyclopropyl Bromide [97]

CpBr (0.40 M) $\xrightarrow[\text{SH(D)}\ 37°C]{\text{Mg}}$ CpMgBr + CpCp + SS + CpS

SH(D)	$[MgX_2]_0$	%			
DEE	0	52	3	7	3
DEE-d_{10}	0	54	14	1.2	3
DEE	2.6 M $MgBr_2$	71	2	5	2
DEE-d_{10}	2.6 M $MgBr_2$	84	4	0.04	0.3
THF	0	58	–	16	10
THF-d_8	0	70	–	0.3	3
THF	0.50 M $MgCl_2$	68	–	4	6
THF-d_8	0.50 M $MgCl_2$	80	–	0.07	6

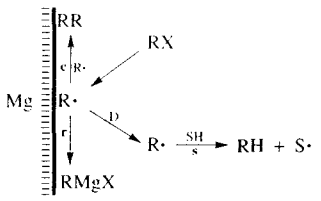

Walborsky Mechanism
AAD

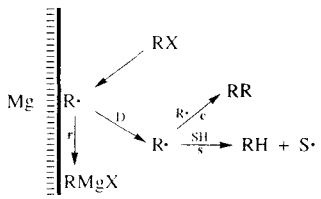

ADD

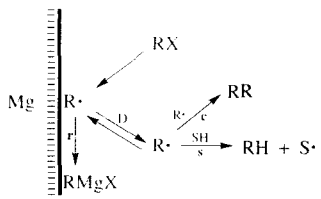

D Model
DDD

In $DEE/MgBr_2$, THF, and $THF/MgCl_2$, solvent deuteration gives a 12–13% increase in (CpMgBr). If **s** is a solution reaction, this disproves the A models (AAD and ADD) definitively.

The D model (DDD) is supported further by agreement between the observed and predicted effects of deuteration on yields. The experimental yield of CpMgBr (71%) in $DEE/MgBr_2$ is matched with $\delta = 0.010$ Å^{-1}, $k_S = 4.4 \times 10^6$ s^{-1}, and the usual values of v, D, and k_C. The observed yield (84%) in DEE-d_{10}/$MgBr_2$ is then matched by decreasing k_S by a factor of 6, that is, assuming that $k_H/k_D = 6$, a plausible value. (A direct measurement of k_H/k_D for this case has not been made. Near matches of calculated with experimental data are obtained with other plausible values of k_H/k_D) [102].

In every case the data contradict predictions of the AAD mechanism. However, in DEE (CpMgBr) is little affected by deuteration, while (CpCp) increases substantially at the expense of (SS), the kind of result expected for the ADD mechanism. Perhaps that mechanism operates here, but it seems unlikely that the mechanism in DEE would be fundamentally different from that in $DEE/MgBr_2$, THF, and $THF/MgCl_2$. One possibility is that the build-up of polar solutes creates a viscous and polar layer adjacent to Mg_Z and that radicals, once they escape this layer, have difficulty reentering it. Alternatively, **c** and **s** dominate the early part

of the reaction, attenuating by dilution the DDD effect of the later part [97].

Optically active 1-halo-1-methyl-2,2-diphenylcyclopropanes in THF and DEE react with magnesium (powder was used in most experiments, though a few with turnings gave similar results) to give Grignard reagents with partial retention of configuration (measured after carbonation, which occurs with retention) (Table 7.4). Control experiments exclude halogen–metal interchange as a source of optical activity in RMgX [20].

The observation of nearly complete racemization for RI militates against an adsorption explanation of retention. Since the rate constants for the inversion and rotation of the cyclopropyl radical are estimated as $\sim 10^{11}$ s−1 [92,93], these data suggest a retention pathway **X** in addition to a radical pathway **R**. Although the D model, with a sufficiently small value of τ_R, could also account for the observed partial retention, the required value of τ_R is not consistent with other data. The smallest value of (Q)/(RMgX) above is 3 (75% racemization, 25% retention). From equation (7.31) with $k_Q = 10^{11}$ s^{-1}, we find $\tau_R = 9 \times 10^{-11}$ s $\approx 10^{-10}$ s. Similarly, for the largest value of (Q)/(RMgX), 49 (98% racemization, 2% retention), we find $\tau_R = 5 \times 10^{-10}$ s. These values are less than those that describe data for typical alkyl halides (Section 7.2.8) by 2–3 orders of magnitude.

Table 7.4. Retention of Configuration in Grignard Reactions of 1-Halo-1-methyl-2,2-diphenylcyclopropanes. [20]

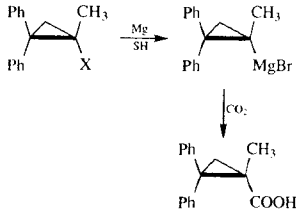

X	SH	T/°C	retention/%ee
Br	DEE	35	14–21
Br	THF	25–28	13
Cl	THF	65	25–26
Br	THF	65	15–19
I	THF	65	2

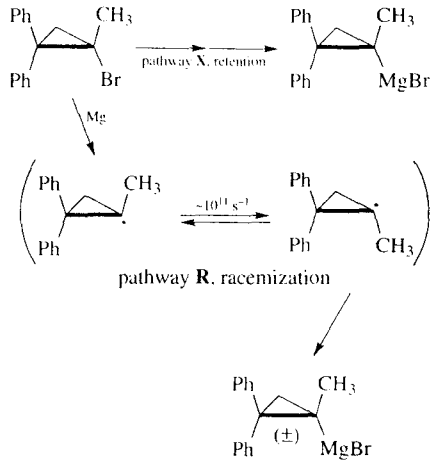

The values of δ and τ_R for D-model descriptions of reactions of cyclopropyl bromide are indistinguishable from those for typical alkyl halides. For $\tau_R = 10^{-7}$ s and $k_Q = 10^{11}$ s^{-1}, ~1% retention of configuration is calculated. Thus, the ideal D model does not account for the observed degrees of retention of configuration in Grignard reactions of 1-halo-1-methyl-2,2-diphenylcyclopropanes. Agreement would require δ-values higher by factors of 10–30.

More complete product analyses, using gravimetric methods and NMR spectroscopy, gave the results below [20]. In evaluating these results, it should be noted that gravimetric methods are prone to losses and that NMR integration is not always very accurate. Mass balances in these experiments are often poor. Products RS and SS, which could have provided checks on the inferred amount of solvent attack, were not determined, nor were possible effects of $MgBr_2$ investigated or taken into account.

Most of the by-products are those expected for **r**, **c**, and **s**. The low yields of RMgBr and relatively high yields of RR, RH, and R(−H) in DEE are striking. For a value of κ that could account for the observed degree of retention in RMgBr (300 cm s^{-1}, 10 times its value for a typical alkyl halide, 30 cm s^{-1}), a very high yield of RMgBr (98%) and a very low yield of **c** products (0.16%) are calculated using the D model [102], disagreeing substantially with the observed yields. The observed by-product yields are consistent instead with κ-, δ- and τ_R-values similar to those for typical alkyl halides and cyclopropyl bromide.

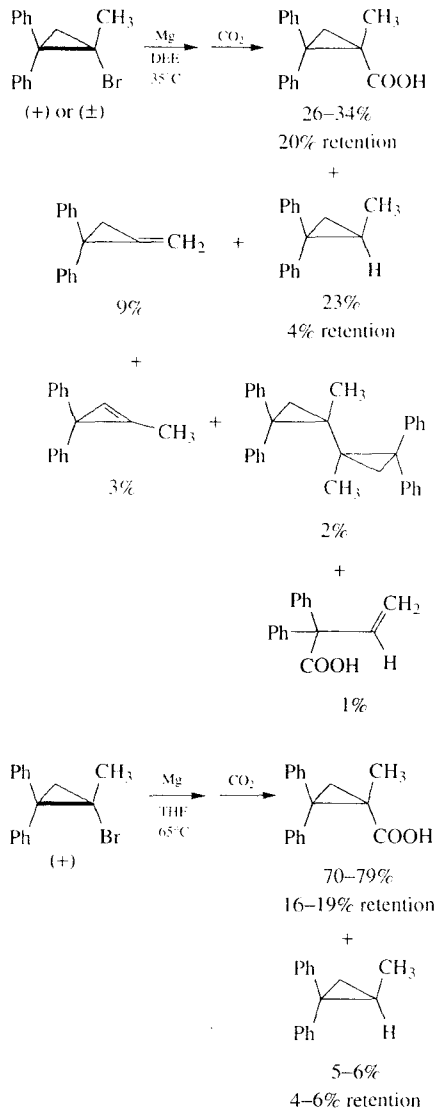

For Grignard reactions of 1-bromo-1-methyl-2,2-diphenylcyclopropanes in DEE-d_{10} and THF-d_8, the reported yields of RD are very low, indicating that there is little solvent attack. Neglecting the possible effects of a kinetic isotope effect on k_S, Walborsky took this to imply that solvent attack is negligible in the proton-containing solvents as well [20].

Data for THF show otherwise [20]. Solvent deuteration increases the yield of RMgBr by 15%, decreases its enantiomeric excess, decreases the yield of RH(D), and increases its enantiomeric excess. These effects reflect a deuterium isotope effect that diverts R· from **s** to **r**. The increase in (RMgBr) indicates that ~15% of RBr gives R· that are diverted in this manner. The discrepancy between this value and the lower (RH), 5–6%, found in THF is probably due to quantitative uncertainties in the analyses.

Walborsky and Aronoff offer the same interpretation without noting that it invokes the D model [20]. If **s** is a solution reaction, as they believed, then these data require that at least ~15% of RBr give radicals R· that leave Mg_Z and suffer subsequent reduction to RMgBr. The actual fraction could be, and probably is, much larger.

As in the CpBr case (above in Section 7.2.9), deuterating DEE has a different result. It has no measurable effect on (RMgBr) or (RH), consistent with the proposition that there is no effect on the product distribution at all [20]. This is probably an illusion. If no products other than RMgBr and RH had been determined for reactions of CpBr, the results would have been similar and the effects of solvent deuteration on yields (RR) and (SS) would have been missed. For 1-bromo-1-methyl-2,2-diphenylcyclopropane, there was no analysis for RR or SS [20]. Thus, it is likely that the

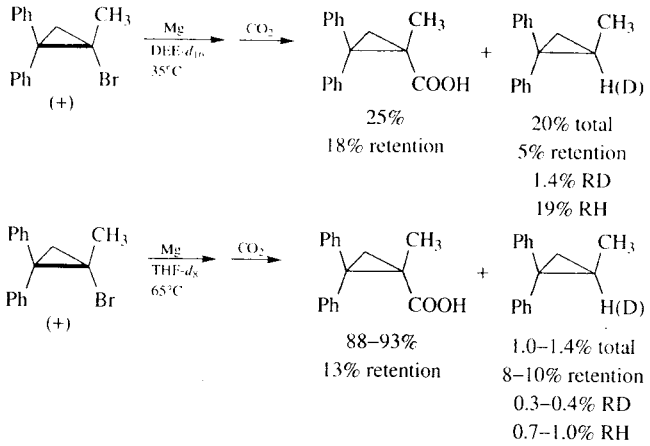

behavior of 1-bromo-1-methyl-2,2-diphenylcyclopropane in DEE and DEE-d_{10} is like that of CpBr [97], which is not consistent with the AAD mechanism of Walborsky.

We are left with inconsistencies. A models are not consistent with the data, but if pathway **R** is the exclusive pathway, then the D model, alone, also fails, since it does not account simultaneously for the observed degrees of retention of configuration and high yields of by-products.

A reconciliation requires another pathway, **X**, either a pathway without an intermediate radical R• or with a subset of intermediate radicals with lifetimes τ_R that are much shorter than those of another subset. One possibility involving two sets of radicals R• (shorter- and longer-lived) is that the initial intermediate pairs could have a much higher reactivity than older pairs. If active sites on Mg_Z were localized on the atomic scale (Section 7.3.11), and if both formation and reduction of R• could occur at the same site or adjacent ones, then geminate reaction and escape (three-dimensional phenomena, Section 7.2.5) could occur on very short time scales (Figure 7.27), the former with partial retention, the latter leading to radical intermediates R• of longer lifetime [103–108].

However, data suggest that extents of non-isomerization (retention being one example) correlate with the conjugation in RX (Sections 2.8–2.11). It is not clear why this should be for geminate reactions at active sites. This suggests that the explanation lies elsewhere.

Initially, Walborsky invoked a retention pathway **X** through an intermediate 'tight radical pair' described as [R•---•MgX] [19], a 'loose radical pair' being [R• •MgX]. Later the 'tight radical pair' became a 'radical anion in close association with a univalent magnesium cation' [19] or a 'tight anion radical-cation radical pair' [7] [$RX^{\bullet-}$---$Mg^{\bullet+}$]. Then electrochemical measurements led him to consider

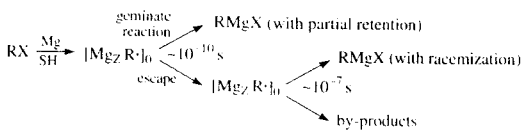

Fig. 7.27. Retention as a consequence of geminate reaction (Section 7.2.5) at an active site (Section 7.3.11).

this to be a transition state instead of an intermediate, at least in some cases, including that of 1-bromo-1-methyl-2,2-diphenylcyclopropane [22]. We do not consider this electrochemical evidence to be compelling and believe that an intermediate anion-radical $RX^{\bullet-}$ best fits all of the data (Section 7.2.21).

The presence of aromatic groups in the 1-halo-1-methyl-2,2-diphenylcyclopropanes suggests the possibility that they could stabilize an intermediate (or transition state) $RX^{\bullet-}$. Walborsky addressed this issue by examining Grignard reactions of an optically active cyclopropyl bromide lacking aromatic rings [21]. There is partial retention of configuration, but distinctly less than in the case of 1-bromo-1-methyl-2,2-diphenylcyclopropane, consistent with the proposition that $RX^{\bullet-}$ is stabilized by the phenyl groups of 1-bromo-1-methyl-2,2-diphenylcyclopropane, the loss of which (in 1-bromo-1-methylspiro[2,5]octane) decreases that stabilization and leads to less retention. It also demonstrates that aromatic rings are not necessary for partial retention, suggesting that the cyclopropyl group itself might stabilize $RX^{\bullet-}$.

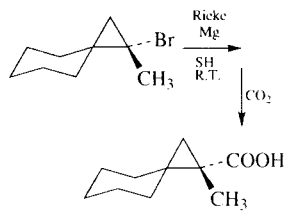

SH = DEE: 25% (10% retention)
SH = THF: 58% (13% retention)

A more complete product analysis was obtained for a reaction of racemic bromide in DEE containing *t*-butyl alcohol-*O*-*d* [21]. The products indicate significant **s**, perhaps 12–23% $\{(0.5-1)\times(47\%-24\%)\}$. In a reaction in DEE-$d_{10}$ (using mechanically-activated Mg turnings, $BrCH_2CH_2Br$ as a promoter, and refluxing for 1 hr), the racemic bromide gave 13% RD, implying 6.5–13% **s**. These uncertainties reflect the fact that RH(D) can be both a direct and indirect product of **s**, arising by disproportionation of R• with S•.

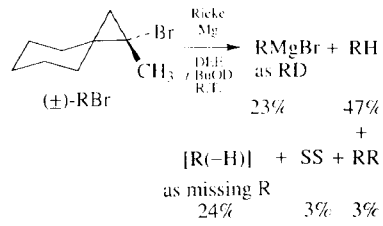

There is much more solvent attack than was claimed for 1-bromo-1-methyl-2,2-diphenylcyclopropane [20]. Instead, the extent of **s** agrees with that for cyclopropyl bromide itself [52,98]. Together with the finding that there is less than 0.5% **s** in a reaction of *n*-hexyl bromide in DEE [52], these finding disprove a set of hypotheses suggested by Walborsky [109]: (a) the only radicals that attack the solvent are those that desorb; (b) their inevitable fate is solvent attack; and (c) fewer cyclopropyl radicals than typical alkyl radicals desorb. These hypotheses predict more solvent attack in reactions of typical alkyl than cyclopropyl halides, opposite from observations [52].

In some reductions of 1-halo-1-methyl-2,2-diphenylcyclopropanes, there appears to be a racemization pathway through an intermediate other than R• [96,110]. Although Walborsky recognized this, he did not propose integrated mechanisms of reductions of these substrates. These matters are discussed further in Sections 7.2.15 and (especially) 7.2.21.

In summary, the data for cyclopropyl halides are consistent with a major, D-model pathway **R**. For reactions of cyclopropyl bromide in DEE/$MgBr_2$, THF, and THF/$MgCl_2$ [97], and of 1-bromo-1-methyl-2,2-diphenylcyclopropane in THF [20], all versions of the A model are disproved by findings that deuterating the solvent increases (RMgBr) by 12–15%. Deuterating the solvent has little effect on (RMgBr) from reactions of cyclopropyl bromide and 1-bromo-1-methyl-2,2-diphenylcyclopropane in DEE [20,97], but for the former

reaction, at least, it increases **c** at the expense of **s** [97], suggesting the ADD model and eliminating the AAD model (Walborsky mechanism). Observations of partial retention of configuration can be accounted for by a pathway **R** with two groups of diffusing intermediate radicals with very different lifetimes ($\sim 10^{-10}$ and $\sim 10^{-7}$ s) (e.g., the freckles model with geminate reaction (Section 7.3.11)) or by a minor retention pathway **X** along which R· is not an intermediate. One possibility for **X** is a pathway through an intermediate $RX^{\cdot -}$ [10,19,20,22] that is stabilized by delocalization over π or pseudo-π systems (cyclopropyl rings have pseudo-π systems) [89,90].

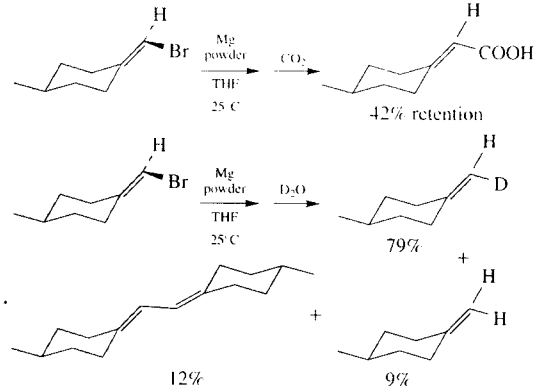

observed large fraction of retention of configuration in RMgBr. Similar results have been reported for reactions of other vinyl halides [10,11].

The products are consistent with mechanisms similar to those that are viable for reactions of cyclopropyl halides (Section 7.2.9). If the D model describes the non-geminate part of pathway **R**, then the values of δ and κ must be similar to those for typical alkyl and cyclopropyl radicals (Sections 7.2.8–7.2.9).

7.2.11 Aryl Halides

Stereochemistry is not an available tool for aryl halides, whose Grignard reactions have received little recent mechanistic attention. Studies of substituent effects on rates of Grignard reactions of aryl bromides in DEE reveal acceleration by electron-withdrawing substituents but do not permit a distinction between electron- and atom-transfer initial steps [31]. From phenyl bromide in DEE, by-products biphenyl, benzene, and 1-phenyl-1-ethoxyethane are formed [61,63], suggesting coupling and attesting to solvent attack by intermediate phenyl radicals.

These results might leave a reader with the impression that pathway **R** dominates. Recent studies suggest otherwise [112].

Aryl and cyclopropyl halides RX are similar in some ways. They lose X to form σ radicals

7.2.10 Vinyl Halides

THF is commonly used for Grignard reactions of vinyl halides because initiation often fails in DEE. Reactions of optically active 4-methylcyclohexylidenebromomethane (RBr) occur with partial retention of configuration and provide evidence of radical coupling (formation of RR, ~12%) and solvent attack (formation of RH, ~9%) [111]. A control experiment showed that racemization did not occur in the unreacted bromide.

The course of this reaction is similar to those of Grignard reactions of cyclopropyl halides, with the large amounts of **c** and **s** again precluding a value of κ (D model) that could account for the

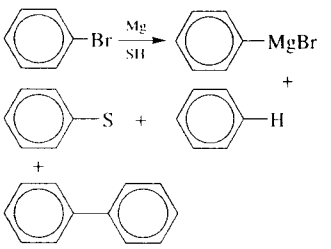

with similar electronegativities and reactivities toward solvents [94]. If Grignard reactions of phenyl halides were similar to those of cyclopropyl halides, then similar D-model calculations would be expected to predict product distributions from phenyl halides.

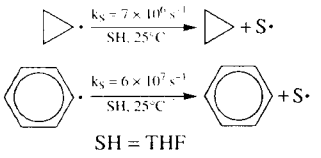

Further, 5-hexenyl and 2-(3-butenyl)phenyl radicals cyclize analogously, the rate constant for the cyclization of the latter being 10^3 that of the former [86,113,114]. If the mechanisms of Grignard reactions of 2-(3-butenyl)phenyl halides were similar to those of 5-hexenyl halides, then similar D-model calculations would be expected to predict product distributions from 2-(3-butenyl)phenyl halides.

In fact, such calculations fail for phenyl and 2-(3-butenyl)phenyl halides [112]. Cyclopropyl and 5-hexenyl halides are not good models for the corresponding aryl halides. Grignard reactions of the aryl halides give far fewer by-products than predicted from their aliphatic models in D-model calculations (equation 2.6.7) using $\tau_R = 3 \times 10^{-8}$ s, a value that describes reactions in DEE and THF of cyclopropyl and 5-hexenyl bromides (Sections 7.2.8–7.2.9).

For phenyl halides, this D model predicts 57% solvent attack. For reactions of phenyl chloride, bromide, and iodide in THF at 37°C and the reaction of phenyl iodide in THF at 67°C, no traces of SS or RS are found, despite the ability to detect SS in yields as low as 0.03% by GC. Reactions in THF give nearly quantitative RMgX (95–106%). The D-model prediction is far from correct [112].

Similarly, for reactions of 2-(3-butenyl)phenyl bromide and iodide, D-model equation (7.31) predicts 78% cyclized Grignard reagent and 22% uncyclized. Much less cyclization is observed.

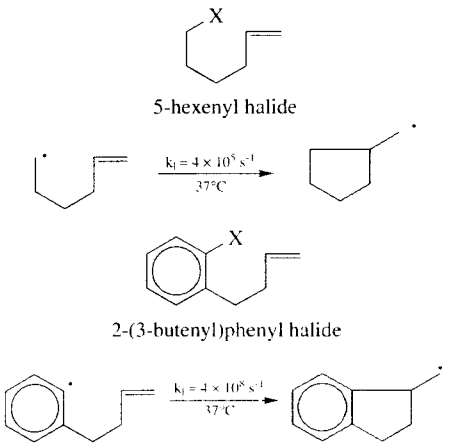

Indeed, for reactions of RBr in THF, cyclic product is hard to detect. Control experiments demonstrate that the Grignard reagents, once formed, do not interconvert. No SS or RS could be detected in any solvent [the rate constant for the cyclization of the 2-(3-butenyl)phenyl radical is seven times that for solvent attack by the phenyl radical] and only traces to small amounts of dimers RR, RQ, and QQ are formed [112].

Even qualitatively, the results for reactions in THF, especially, are striking. In this system, the rate constant for the cyclization of R• is a thousand times that for 5-hexenyl halides, where 3–10% cyclization occurs. Despite this, from 2-(3-butenyl)phenyl bromide and iodide in THF, >98% yields of RMgX are obtained, with ≤1.5% QMgX [112]. This seems inconsistent with a dominant pathway **R** of any kind.

Using equation (7.31) to calculate τ_R from the experimental data for the 2-(3-butenyl)phenyl halides gives values corresponding to a few bond vibrations or less. The corresponding diffusion distances are >1 Å—pseudo-oscillatory motions would dominate diffusion. Equation (7.49), with simple first-order rate laws describing the competition, might be appropriate. Using this equation, the values of τ_R calculated from the data are up to 4×10^{-11} s, still very short lifetimes indeed.

$$(\mathrm{QMgX})/(\mathrm{RMgX}) = k_Q \tau_R \qquad (7.49)$$

Although it may be conceivable that τ_R could be this short, it seems unlikely, especially in view of the evidence from reactions of typical alkyl and cyclopropyl halides that the structure of R• seems to have little effect on τ_R, which may be determined by properties of the medium or the surface. It is more likely that pathway **X** operates [112].

Indeed, **X** appears to dominate. Suppose that τ_R were 3×10^{-8} s (value for 5-hexenyl bromide in DEE) for the pathway **R** (D-model) contribution in reactions of aryl halides and that the only product of pathway **X** were RMgX. Then the implied extent of pathway **X** for the reactions of 2-(3-butenyl)phenyl halides would be >97% [112].

Electrochemical reductions of aryl halides occur through anion-radical intermediates $RX^{\bullet-}$, which fragment to give radicals R• that are then further reduced, either at the electrode or by $RX^{\bullet-}$, in competition with coupling and solvent attack [17,18]. Perhaps this is the substantive difference between Grignard reactions of typical alkyl and aryl halides. In the former case, there is no intermediate $RX^{\bullet-}$, in the latter there is.

Conceivably, R• could be reduced by $RX^{\bullet-}$. In electrolyses, such reductions are believed to be significant only when $RX^{\bullet-}$ has a relatively long lifetime [17,18]. For phenyl bromide, the lifetime is very short, estimated as $\sim 10^{-11}$ s (extrapolated from data of Savéant) [17], making the reduction of R• by $RX^{\bullet-}$ unlikely. Indeed, kinetic analyses of approximate models indicate that steady-state concentrations $[RX^{\bullet-}]$ will not be high enough to allow the reaction of $RX^{\bullet-}$ with R• to compete with the fragmentation of $RX^{\bullet-}$, the coupling of R•, or the reduction of R• by Mg_Z (with $\tau_R = 10^{-7}$ s or less) [102]. Unless there is something special that stabilizes $RX^{\bullet-}$ (e.g., the low polarity of the medium, association with counterions, etc.), this hypothesis can be discarded.

Absent some other reaction of $RX^{\bullet-}$, fragmentation would be its only fate in a Grignard reaction. If so, the resulting mechanism would be kinetically equivalent to pathway **R**. If $RX^{\bullet-}$ invariably fragments to R• and X^-, and is thus not a branching species, its transient intermediacy (or lack thereof) will have no influence on the kinetics of competitive product formation. Based on its successes with typical alkyl and cyclopropyl halides, the D model would be expected to apply.

Since it does not, other possible reactions of $RX^{\bullet-}$ must be considered. In some reductive cleavages of some substituted cyclopropyl halides, an electron transfer to $RX^{\bullet-}$ appears to be required, leading to a dianionic fragmentation transition state (composition RX^{2-}, with associated counterions) [110,115]. Pathway **X** could be such a dianionic pathway. However, no precedent for this pathway for an aryl halide is apparent. According to the literature, aryl intermediates $RX^{\bullet-}$ either fragment or lose an electron, regenerating RX [17,18].

This prompts two questions. (1) Could a dianionic cleavage pathway have escaped detection

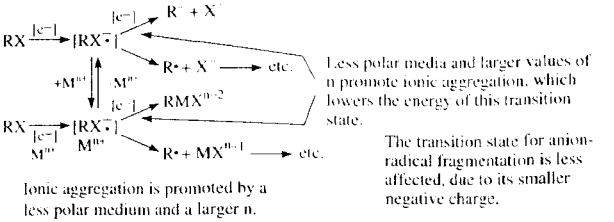

Fig. 7.28. Possible reduction pathways for aryl halides. The dianionic pathway **X** illustrated here could also apply to cyclopropyl and vinyl halides.

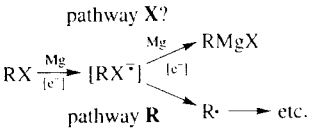

in the electrochemical experiments [17,18]? It appears that the answer could be 'yes.' A dianionic pathway might not have been considered or might not have been distinguished from other pathways. (2) Could a dianionic pathway be absent in the electrochemical reductions but present in the Grignard reaction? 'Yes' is again a possible answer. In Grignard reactions, a dianionic transition state for fragmentation would be stabilized, perhaps greatly, by its association with Mg^{2+} (Figure 7.28). Ionic aggregation is favored by the relatively low polarity of the medium and high charge densities of Mg^{2+} and RX^{2-}. Ionic aggregation can have powerful effects in less polar media [116]. The dianion pathway might not play a role in reductions in the more polar media and with the different countercations used in electrochemical studies. These matters require further study.

7.2.12 Benzylic and Allylic Halides

Benzylic and allylic halides have received little mechanistic attention, probably because their Grignard reactions are complicated by secondary reactions. The reaction of RMgX with RX is faster for benzylic and allylic halides than for others [1]. It is customary to use dilute solutions and large amounts of specially activated Mg to minimize secondary reactions.

$$\mathrm{RMgX} + \mathrm{RX} \longrightarrow \mathrm{RR} + \mathrm{MgX_2}$$

Success has little mechanistic significance because these measures will minimize **c** as well. Although experimental determinations of the separate contributions of **c** and secondary coupling are feasible, they have not been pursued.

The reaction of Mg powder with (+)-(*R*)-1-chloro-1-phenylethane in DEE in the presence of *t*-BuOD gives 88% (+)-(*S*)-1-deuterio-1-phenylethane with net *inversion* (6.2% optical purity) [117]. Although net retention appears to be the more common case, net inversion is also observed in RH formation, presumably by protonation of RMgX, in the Grignard reaction of 1-chloro-1-methyl-2,2-diphenylcyclopropane in THF [20].

It is not clear whether or not the intermediate Grignard reagents are formed with retention in these reactions. They could be, provided that the stereochemistry of protonation were inversion. Conceivably, the stereochemistry of protonation might vary with organic structure, halogen, and medium though effects of aggregation and solvation.

The authors of the work with (+)-(*R*)-1-chloro-1-phenylethane consider their findings to be evidence that 'this reaction proceeds on the magnesium surface within a solvent cage. If it were not so, we would expect only a small amount

of deuterium in [the product RH] because of the disproportionation of the 1-phenylethyl radical and its reaction with solvent.' Since the premise is false (Sections 7.2.6–7.2.9), the conclusion is not justified.

They also conclude that 'racemization of benzylmagnesium halide takes place, through fast structure inversion, just after its formation.' No reason for discounting the possibility that RMgCl was mostly racemic as formed is given [117]—none is evident.

Reasonable conclusions are that RMgCl may be formed (~85%) in 6.2% optical purity, perhaps with net retention, and that **c** (10–15%) competes with RMgCl formation. The ideal D model can describe the bulk of the reaction but perhaps not the reported small optical purity of RMgCl. If the reported optical activity is not an artifact, then it might indicate a pathway **X**.

7.2.13 Area of the Magnesium Surface

If the rate of a Grignard reaction is proportional to the area // of Mg_Z, then increasing // will increase the rates of formation and reduction of R•. Naively, this might be expected to affect the product distribution.

Actually, D-model product distributions are independent of //. If the rate of consumption of RX and formation of R• is proportional to //, then doubling // doubles the gross and specific rates (Section 7.2.2) but does not affect the flux of reaction. In the D model, the flux (not the rate) determines the steady-state concentration profiles in solution that in turn determine the product distribution (Sections 7.2.6–7.2.7).

The situation is similar for an A model in which **r** and **c** occur at Mg_Z. Increasing // will again not affect the flux of reaction. Consequently, it will not affect the steady-state surface densities (mol cm^{-2}) of intermediates. Since these determine the product distribution, a change in // has no effect on that distribution.

For reactions of 5-hexenyl bromide in THF at 22°C with sonication, for example, these predictions have been confirmed. The molar ratio Mg/RBr was varied from 10:1 to 1:1, with $[RBr]_0$ constant, without affecting the product distribution [16].

There are cases where // can affect product distributions. If a secondary reaction of RMgX with RX occurs at a rate that is competitive with that of the overall reaction, then removing RX from solution rapidly, using a high //, will minimize the secondary reaction. This is the rationale for using a high // of reactive Mg_Z in reactions of benzylic or allylic halides [118], where RMgX + RX is faster than usual. Secondary reactions of this type might also be important in reactions of iodides under some conditions (solvent, temperature). For this reason, Kharasch and Reinmuth advise: 'The use of iodides, either as Grignard reagent co-reactants or as starting materials for the preparation of Grignard reagents, in general, is to be avoided' [1].

A second case involves Mg that is so finely divided that the sizes of individual pieces are comparable to those of molecules. In this case, the D-model approximation that Mg_Z is 'infinite' (so large that edge effects are insignificant) fails—R• may escape from the Mg_n cluster at which it is formed. The rate of its subsequent reaction with another Mg_n would be enhanced by higher concentrations of Mg_n, so that surface-area effects would be expected (Section 7.2.18).

7.2.14 Concentration of Halide

In hydrodynamically-controlled reactions, the flux of reaction is proportional to [RX] [26–28]. Consequently, the yields of **c** products increase, at the expense of RMgX, with increasing [RX] (Figure 7.19) [34,35] and with increasing speed of a rotating disk of Mg [28].

In reactions in DEE with Mg turnings and ordinary stirring, the effect of [RX] on the product distribution is small to non-existent over a range down to ~0.2 M, at least (Section 7.2.13), implying that the flux and rate of reaction remain constant as [RX] varies. Explicit zeroth-order in RX has been found for the reaction of cyclopentyl bromide in diethyl ether containing LiBr [15] and for reactions of adamantyl bromide, where a thick deposit (largely biadamantyl) forms on the Mg early in the reaction (Section 7.2.17) [65].

An increase in the effective area // of Mg_Z during the reaction could compensate for the effect of the simultaneous decrease in [RX] [15]. This can

explain the rate observations but not the insensitivity of product distributions to [RX] that is sometimes observed. The latter requires instead a flux of reaction that is independent of [RX], and the flux is independent of // (Section 7.2.13). In the case of adamantyl bromide [65], the variation with time in the thickness of the biadamantyl layer could have an effect on the rate and flux that compensates for the variation in [RBr]. It is not clear how such an explanation could be adapted to cases where there is no deposit (presumably) at Mg_Z. In any event, where there is no evidence of a surface deposit, the apparent insensitivity of rates and fluxes appears to be an artifact of the lack of hydrodynamic control, since it disappears when hydrodynamic control is present (Figure 7.19) [26–30,34,35].

Where secondary reactions of RX with RMgX are important, dilution of RX should enhance RMgX yields. Of course, this is not particularly useful synthetically, where high concentrations are desired. Therefore it is better to address the problem of secondary reactions by using large amounts of reactive Mg and attendant high surface areas // (Section 7.2.13).

7.2.15 Halogen

Optical purities of RCOOH (from the carbonation of RMgX) formed in Grignard reactions of optically active 1-halo-1-methyl-2,2-diphenylcyclopropanes in THF at 65°C vary in the order RCl (25%) > RBr(17%) > RI(2%), the same order as RMgX yields [RCl (85%), RBr (75%) RI (38%)] and opposite the order of RH yields [RI (19%), RBr (6%), RCl (1%)] [20]. There is a straightforward explanation in terms of effects of bond strengths on the pathway to R•. However, aspects of this explanation are puzzling and other possible sources of halogen effects must be considered.

(1) Effects of bond strengths and the ease of bond breaking. In general, rates of carbon–halogen bond-breaking steps vary in the inverse order of bond strengths, C–I > C–Br > C–Cl > C–F. This is order of the extent of racemization (vs retention of configuration) in Grignard reactions of optically active 1-halo-1-methyl-2,2-diphenylcyclopropanes, and it is consistent with a retention pathway **X** in which the C–X bond does not break to form R•, plausibly a pathway through $RX^{\bullet-}$. If pathway **X** were more important for stronger C–X bonds (C–Cl > C–Br > C–I), extents of retention would vary in the order RCl > RBr > RI, as observed [10,20]. The small size of the observed effect, especially between Cl and Br, is surprising, indicating that this explanation should be viewed with caution.

In other reductions of the same substrates, the opposite order of variation of retention with halogen is observed [96,110,115]. In reductions

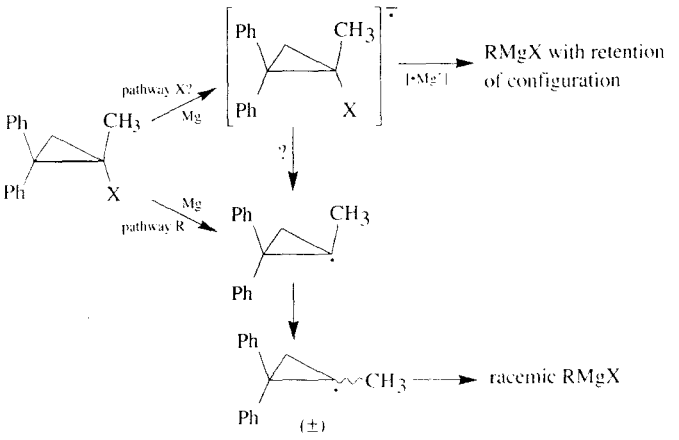

of optically active 1-halo-1-methyl-2,2-diphenylcyclopropanes by alkali naphthalenes (M^+ $Naph^-$) in homogeneous solutions, retention of configuration is an irregular function of solvent, metal ion, concentration, and halogen – K^+: Br > I ≫ Cl; Na^+: Br ≈ I ≫ Cl; Li^+, I > Br ≫ Cl [96,110]. Although it has been argued that the mechanisms of these reactions are different from those of Grignard reactions, an integrated mechanism covering all of these reactions would be more satisfying. In principle, complex competitions involving bond breaking could lead to any order of variation of extents of retention with halogen. This subject is discussed further in Section 7.2.21.

(2) Effects of MgX_2, RMgX, or both. (a) X^- at Mg_Z could affect reactivity there. It affects, for example, the manner of corrosive pitting [119]. (b) Solutes containing X^- could enhance the polarity of the medium and affect reaction steps [98]. (c) There could be specific roles of aggregates containing X^- in some reaction steps. In all of these cases, the effects could vary with *X*.

(3) Effects of diffusion. These originate with high reactivities of RX and inefficient mixing during the period of reaction.

Effects of diffusion are observed for reactions of sodium naphthalene (NaNaph) with 5-hexenyl halides [120,121], which give intermediate 5-hexenyl radicals that cyclize in competition with their further reduction [122–124]. Using ordinary mixing methods, reactions of 5-hexenyl chloride and bromide (RX) with ~0.05-M NaNaph (sodium naphthalene) in DME (1,2-dimethoxyethane) at room temperature give different yield ratios (1-hexene)/(methylcyclopentane) [RCl (8), RBr (4)] [120]. When the same reactions are carried out by evaporating RX and condensing it on the surface of a stirred, ~0.1-M solution of NaNaph, (1-hexene)/(methylcyclopentane) = ~16 for both RCl and RBr (as well as RF and RI) [121].

Figure 7.29 is a schematic diagram illustrating the diffusion–reaction phenomenon that gives rise to the halogen effect that is observed with ordinary

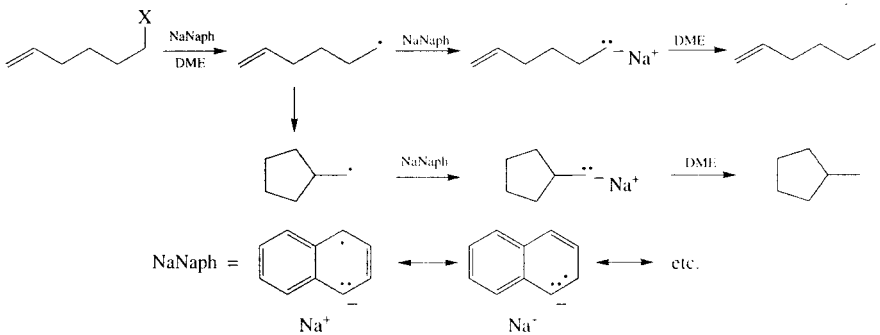

mixing. Initially, reaction occurs at the interface between the solutions of NaNaph (black circles) and RX (open circles) as they come into contact (upper left). This depletes the mixing zone in both reactants (lower left). Initially, R• is formed in the neighborhood of a relatively high concentration of NaNaph, with which it reacts at a diffusion-controlled rate (upper center and right). Therefore it has a relatively short lifetime τ. Later, after concentration gradients have been set up in the mixing zone, R• is formed in the neighborhood of a lower concentration of NaNaph. Therefore its lifetime τ is longer, allowing it more time to cyclize to Q• [120]. Most of the reaction occurs in the depleted mixing zone (lower row). This effect does not operate for a slow reaction, where mixing is faster than reaction.

Since the order of reactivity of RX is RI > RBr > RCl > RF, the lifetimes τ of R• and the

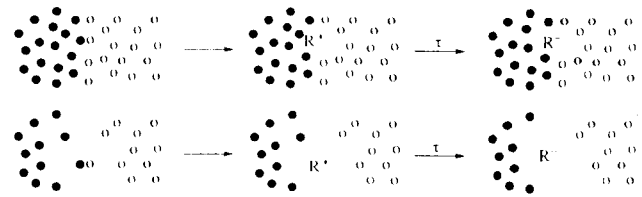

Fig. 7.29. Depletion of reactant concentrations in the mixing zone, leading to a longer lifetime τ of the intermediate radical R• and consequently a higher probability of its cyclization to Q• before being reduced. Upper row: initial events. Lower row: later events.

yield ratio (QH)/(RH) are expected to vary in the same order, as is observed. When diffusion effects are removed (evaporation experiments), the halogen effect disappears, also as observed [121].

Bunnett has detailed the phenomenon for reactions of RX with (Li,Na,K)/NH_3 [125,126]. Rys [127] has discussed related matters and Andrieux and Saveánt have given a quantitative treatment [128,129].

In principle, such effects could operate in Grignard reactions if the reducing species (e.g., solvated electron) were streaming out of the metal. This seems very unlikely, especially for DEE. Similar phenomena might also operate if the sizes of Mg particles were extremely small (Section 7.2.18).

7.2.16 Solvent

In general, more polar ethers promote initiation. Thus THF (dielectric constant 7.4) may succeed where DEE (4.3) does not, especially for vinyl and aryl halides [6,130]. See Section 7.3.4 for possible explanations.

Grignard reactions often fail to initiate in dioxane (DXN). This could be due to its very low dielectric constant (2.2), but there is another possibility. MgX_2 is insoluble in DXN—it is commonly used to prepare R_2Mg by pouring a solution of RMgX into DXN, precipitating MgX_2. If the presence of MgX_2 were required for initiation, then DXN would not support that process.

The dielectric constants of 1,2-dimethoxyethane (DME, glyme) and THF are nearly the same (7.2, 7.4). Nonetheless, solubility problems limit the usefulness of DME for Grignard reactions. Although there is little in the literature at this time, commercial advertisements indicate that derivatives of diglyme ($CH_3OCH_2CH_2OCH_2CH_2OCH_3$) can be useful solvents for Grignard reactions. The solvents permit reactions at higher temperatures than DEE and THF, which can sometimes be advantageous.

7.2.17 Adamantyl Bromide

Reactions of Mg_Z with adamantyl halides are among the most unusual to be considered in the recent literature. 1-Bromoadamantane (adamantyl bromide, AdBr) has received the most attention [65].

Rieke magnesium reacts with 0.25-M AdBr in a stirred DEE solution to give 60% AdH and 30% AdAd but no AdMgBr. A procedure without stirring, using ordinary magnesium chips or turnings, gives up to 60% AdMgBr [65]. The disappearance of AdBr is zeroth-order after the early part of the reaction, during which a precipitate consisting largely of AdAd forms on Mg_Z.

According to one explanation [65], stirring causes the desorption of transient intermediates (Walborsky's [$AdBr^-$ $\cdot Mg^+$], [Ad• $\cdot MgBr$], or both) before they have a chance to form AdMgBr at Mg_Z. Among several serious problems with this is the fact that stirring is unlikely to affect the layer of solvent adjacent to Mg_Z (or any other solid surface), so it cannot sweep away adsorbed transient intermediates. When Mg_Z is shielded by an AdAd deposit, stirring surely has no effect at

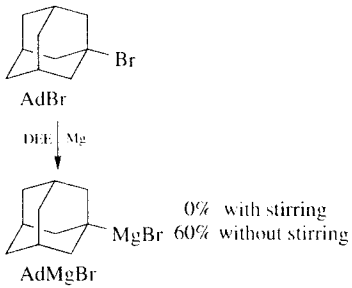

the solid–liquid interface. Thus, this explanation of the effect of stirring, which has been cited as evidence supporting the A model, is not viable.

By adjusting V and Δ, D-model calculations can reproduce the data [66]. For the unstirred reaction of AdBr in DEE, reasonable agreement is obtained with $V = 5.06$ and $\Delta = 2.55$ (compare $V = 2.50 \times 10^{4}$ and $\Delta = 82.6$ for 5-hexenyl bromide). The relatively small values for AdBr could reflect the high viscosity of the AdAd deposit.

For the stirred reaction, the observed yields require $\Delta \leq 0.01$ in D-model calculations [66]. That stirring decreases Δ suggests that it decreases δ and κ and eliminates some condition required for **r**. For example, $MgBr_2$ might be required at Mg_Z. Stirring might leach it out as the AdAd deposit is formed. In the absence of stirring, this refining of the AdAd layer would not occur and the formation of AdMgBr could be possible.

Another possibility is that stirring reduces the thickness of the AdAd layer to the point that radicals invariably escape from it into the bulk solution. They do not return to Mg_Z due to the barrier presented by the high viscosity of AdAd (Section 7.3.10).

In any event, Grignard reactions of AdX offer no support for the A model. They appear to be consistent with the D model.

7.2.18 Slurries of Small Magnesium Clusters

Reactions of small Mg clusters with RX in THF have been reported recently by Négrel and co-workers [131,132]. This method has synthetic promise and its results have a bearing on mechanism as well.

Slurries of finely divided Mg are prepared in THF at −110°C by vaporizing Mg in a rotary metal atom reactor. The resulting pyrophoric Mg clusters are 'clean, alkali halide free, and extremely reactive' [131]. In their Grignard reactions, there is immediate initiation. Reactions tend to be complete in short times (in the case of isopentyl bromide in THF at 20°C, a 'minimum time' for the addition of RBr to the Mg slurry plus <1 min) and they give 100% yields of RH [from isopentyl bromide or *endo*-5-(2′-haloethyl)-2-norbornene], after quenching with 10% aqueous HCl, in reactions at temperatures from −80 to 20°C [131]. In no case have products of **c** (e.g., RR) been found.

Reactions of isopentyl bromide in THF at −80°C are completely inhibited by benzonitrile, *m*-dinitrobenzene, CCl_4, or $CuCl_2$ at molar amounts 10^{-4}–10^{-2} that of RBr. Since 'the important number of active sites excludes the possibility that small quantities of inhibitors might inhibit all the sites' [131], the authors propose that the additives inhibit a chain reaction, the steps of which occur at

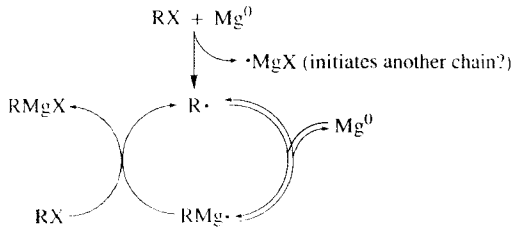

Mg_Z. The reversibility of the reactive capture of R· by Mg^0 provides for the possibility that R· could migrate on Mg_Z or be transferred from cluster to cluster [132].

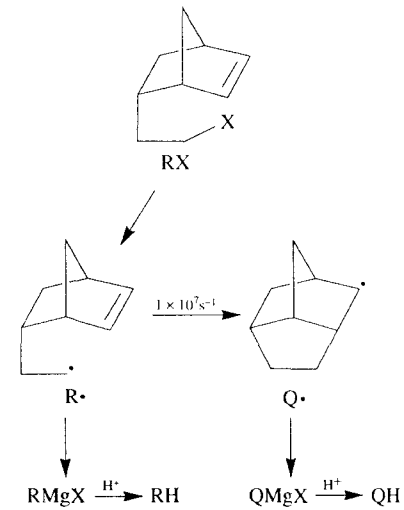

endo-5-(2′-Haloethyl)-2-norbornenes react in THF at room temperature with pronounced effects of halogen and the molar ratio Mg/RX on the extent of cyclization [132]. A solution of 1 mmol RX in 50 mL THF was added dropwise over 30 min to a stirred slurry of 4 mmol Mg in 10 mL THF. The order of the extent of formation of QH is RI > RBr > RCl (Table 7.5).

To investigate the effect of the molar ratio Mg/RX, the required quantity of Mg_n slurry in 10 mL THF was slowly added to a solution of 1 mmol RX in 50 mL THF at room temperature (Table 7.6). Higher proportions of Mg give less QH.

Table 7.5. Yields from Reactions of Small Mg Clusters with *endo*-5-(2′-Haloethyl)-2-Norbornenes in THF at Room Temperature [132]

X	(RH)	(QH)	(QH)/(RH)
Cl	85.4	14.6	0.17
Br	63.7	36.3	0.57
I	43.9	56.1	1.3

This is an unusual protocol for investigating the effect of the ratio Mg/RX. The slow addition of slurries of various Mg_n concentrations would dilute them all in similar ways if reaction were not fast compared with mixing, eliminating the possibility of an effect. The observed effects are a clear indication that the reactions are faster than mixing.

For reactions of bulk magnesium, the evidence eliminates the possibility of a chain mechanism (Section 7.2.19). It is not clear why that should change for reactions of small clusters of Mg atoms. The evidence for a surface chain mechanism should be examined critically.

(a) The number of active sites, or even active particles, might be much smaller than assumed, as van Klink notes [11,131].

(b) van Klink also points out that what Négrel and co-workers report is inhibition of initiation, rather than inhibition of reactions in progress [11,131]. Thus, they tacitly assume that there is no initiation process (no induction periods are observed) or that the chemistry of initiation and the main reaction are identical.

(c) Extremely reactive materials are notorious for adventitious reactions, especially in solution. This could greatly increase the effective amounts of inhibitors over those assumed. For this reason, a determination of the inhibition threshold for water might be especially interesting. Since it is not likely to interfere with a radical chain reaction, a finding of a very small inhibition threshold would invalidate this argument for a chain mechanism.

(d) Perhaps one inhibitor molecule could deactivate a large area of Mg_Z. Indeed, the change

Table 7.6. Effects of Molar Ratio Mg/RX on Reactions of Small Mg Clusters with *endo*-5-(2′-Haloethyl)-2-norbornenes in THF at Room Temperature. [132]

X	Mg/RX	(RH)	(QH)	(QH)/(RH)
Br	0.8	42	58	1.4
Br	4	63.7	36.3	0.57
Br	10	80.1	19.9	0.25
I	0.8	4.8	95.2	20
I	4	43.9	56.1	1.3

brought about by the reaction of a small cluster Mg_n with one inhibitor molecule could, in principle, deactivate the entire cluster. This possible effect is also noted by van Klink [11].

(e) The D model could apply—van Klink noted that intercepting a chain carrier in solution would have as much of an effect as at the surface.

(f) Indeed, plausible explanations of the effects of halogen and Mg/RX in terms of the proposed surface chain mechanism are not obvious. According to this mechanism, the lifetime of R•, and therefore the extent to which it cyclizes, will be halogen-independent, contrary to observation. Also, if the intermediates remain at the surface, the same mechanism predicts that the product distribution will be independent of the area of Mg_Z (Section 7.2.13). The observed effects suggest that intermediates diffuse in solution.

To explore the implications of the D model, we require the physical sizes of the clusters Mg_n. According to one report, $n = 5$ to 30, corresponding to spheres of radius 3.0–5.5 Å if the density is that of bulk Mg [132]. When aggregates are stabilized by PVP [poly(*N*-vinyl-2-pyrrolidone)] and examined by electron microscopy, the average radius is 16 Å, ranging from 8 to 25 Å [133]. Aggregate size could be influenced by PVP and the smallest clusters could be under the detection limit.

In any event, these are molecular sizes. The usual D-model approximation that Mg_Z is 'infinite' (large enough to make edge effects insignificant) fails.

When Mg_n reacts with RX by pathway **R**, the result is a reactive geminate pair [XMg_n R•]. This pair may suffer geminate reaction (probability $\bar{a}$) or escape ($1 - \bar{a}$).

Treating Mg_n as if it were a molecule in solution, we estimate these probabilities. Let D, the relative diffusion coefficient of Mg_n and R•, be 5×10^{11} Å^2 s^{-1}. Let κ for Mg_n be 3×10^9 Å s^{-1}, the value derived from experimental data for reactions of bulk Mg_Z with 5-hexenyl bromide (Section 7.2.8). For spherical reactant molecules, the probability $\bar{a}$ of geminate reaction is related to these parameters by Equation 7.A.8 (Appendix).

If the contact radius R of Mg_n with R• is 10 Å, then $\bar{a} = 0.006$; if R = 20 Å then $\bar{a} = 0.11$; and if R = 30 Å then $\bar{a} = 0.18$. This suggests that the great majority of geminate pairs [XMg_n R•] will escape geminate reaction. The tendency to escape could be even larger if XMg_n (which might be best regarded as $X^- Mg_n^+$) has a lower reactivity toward R• than Mg_n.

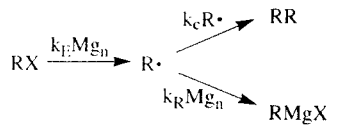

The result is an ordinary solution competition between bimolecular reactions. From the parameter values given above, with R = 20 Å, the following values result for rate constants k_D (diffusion control) and k_A (activation control) for the reaction of Mg_n with R•. The large value of k_D is a consequence of the relatively large values R and D. The actual (global) rate constant k_R is related to k_A as follows (equation 7A.3, Appendix; $k_R = k_G$).

$$k_A = 9 \times 10^9 \text{ M}^{-1}\text{s}^{-1} \text{ (from equation 7.15)}$$

$$k_D = 8 \times 10^{10} \text{ M}^{-1}\text{s}^{-1} \text{ (from equation 7.17)}$$

$$k_R = (1 - \bar{a})k_A$$

Since $\bar{a}$ is small, k_R has nearly the same value as k_A.

Since k_C (3×10^9 M^{-1} s^{-1}) and k_R are nearly equal, the yield ratio (RR)/(RMgX) will be nearly the same as the concentration ratio [R•]/[Mg_n], where [R•] is a steady-state value. From the data given, [Mg_n] is $\sim 10^{-3}$ M. For c to be competitive with RMgX formation, [R•] would have to be comparable with [Mg_n], which is unrealistic. If the rate of addition of RX to the mixture is taken as the homogeneous rate of formation of R•, and the system treated with ordinary steady-state kinetics, then the calculated yield (RR) is negligible, explaining the observed absence of RR [131,132].

This crude calculation ignores possible reaction-mixing phenomena. If small Mg clusters are extremely reactive toward RX, they may be important.

Andrieux and Savéant have given a quantitative treatment for such phenomena for a reaction of an organic halide with a reducing agent E to form a radical R• that is further reduced, perhaps in competition with another reaction [128,129].

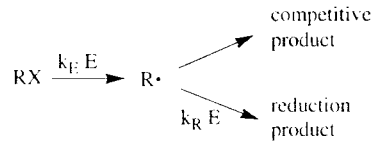

A steady-state is established—a thin reaction zone is embedded in a thicker diffusion zone (Figure 7.30; see Figure 7.29), over which reactant concentrations vary from bulk values at the outer edges to low ones in the reaction zone.

With no stirring, or moderate stirring, the thickness ℓ of the diffusion zone is believed of the order of 10^{-3}–10^{-2} cm when D is of the order 10^{-5} cm^2 s^{-1} [128]. If $\ell = (D\tau_t)^{1/2}$, where τ_t is the characteristic time for traversing the diffusion zone, then $\tau_t = 10^{-1}$–10 s. If the lifetimes of E and RX would be much less than this in the thoroughly mixed solution, then mixing could not be achieved before reaction.

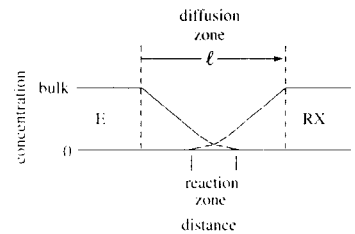

Fig. 7.30. Schematic representation of concentration profiles at the mixing interface between solutions of containing solutes E and RX that are very reactive toward one another [128,129]. E may be a reducing agent such as an alkali naphthalene, a metal supplying solvated electrons, or a solvated-electron solution. Reaction occurs within a reaction zone that is embedded in a diffusion zone.

The characteristic lifetime of RX is $(k_E[E])^{-1}$ and that of E is $(k_E[RX])^{-1}$. If both concentrations are $\sim 10^{-3}$ M, then the homogeneous-reaction-limited lifetimes τ_h are $10^3/k_E$, which is at least one order of magnitude less than τ_t ($\tau_h \leq 10^{-2}$ s) when $k_E \geq 10^5$ M^{-1} s^{-1}. Thus, the minimum value of the rate constant for a reaction that can exhibit reaction-mixing effects is well below the diffusion-control limit. Reactions of Mg_n with RX might well fall into the range for these effects.

If so, then bulk concentrations of reactants help determine the steady-state concentration profiles of reactants and intermediates in the reaction zone. These in turn determine the product distributions. Bulk concentrations are invariant with order of mixing, explaining how effects of the molar ratio Mg/RX could be observed, even with the slow addition of Mg slurries to RX solutions.

To apply the treatment to the present case, we assume: (a) that slurries of molecular-sized Mg clusters act (kinetically) like solutions; (b) that the following mechanism (with R• escaping from its original Mg_n partner) applies; and (c) that Mg_n is deactivated (temporarily) when it reacts with RX. This is Scheme II of Andrieux and Savéant [129], shown at right using their symbols. The yield of RMgX is governed by their competition parameter σ.

$$\sigma = \frac{k_E^{1/3}}{C_E^{2/3}\zeta} \qquad \zeta = \frac{k_1}{k_R}\frac{\ell^{2/3}}{D^{1/3}} \qquad (7.50)$$

where C_E is the bulk concentration of Mg_n. It is assumed here that ζ is constant over the

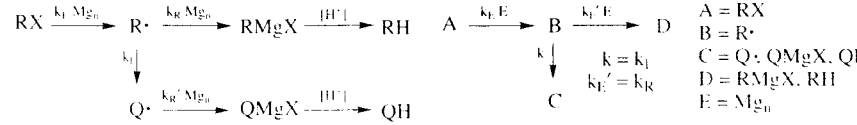

experiments reported by Négrel and co-workers. Thus, equation (7.51) applies, where superscript zeroes denote an arbitrarily chosen reference reaction, selected here as that of RBr with Mg/RX = 4. Andrieux and Savéant give graphs that relate the yields (C) [(QH)] and (D) [(RH)] to σ [128,129].

$$\frac{\sigma}{\sigma^0} = \left(\frac{k_E}{k_E^0}\right)^{1/3} \left(\frac{C_E^0}{C_E}\right)^{2/3} \qquad (7.51)$$

Applying equation (7.51) to the data of Table 7.5, for which $C_E^0/C_E = 1$, gives the relative values of k_E given in Table 7.7. Sensibly, the calculated values of k_E decrease in the order RI > RBr > RCl, one or two orders of magnitude at a time.

Applying equation (7.51) now to the data of Table 7.6, using the previously obtained relative values of k_E (Table 7.7), gives predicted values of σ and (RH), as a function of relative values of C_E, that is, Mg/RX. Calculated and observed yields (RH) are compared in Figure 7.31.

Given the assumptions, these calculations should not be taken too seriously. However, the derived relative values of k_E for RCl, RBr, and RI are plausible and there is excellent [(RBr)] to fair [(RI)] agreement of predicted yields (RH) with variations in Mg/RX, demonstrating that the D model may be able to account for the observations.

This interpretation suffers from at least two specific concerns. First, if k_I, D, and C_E are given measured or plausible values ($k_I = 10^7\ M^{-1}\,s^{-1}$, $D = 5 \times 10^{-5}\ cm^2\,s^{-1}$, $C_E = 10^{-3}$ M) and the upper limit of k_R is taken to be $10^{10}\ M^{-1}\,s^{-1}$, then for the reaction of RBr a value of k_E sufficiently large to justify the treatment is obtained only if $\ell \leq \sim 10^{-4}$ cm, less than estimated by Andrieux and Savéant [128,129]. If ℓ were 10^{-4} cm, k_E would be $5 \times 10^4\ M^{-1}\,s^{-1}$ for RBr, 3×10^2 for RCl, and 1×10^6 for RI. Since Andrieux and Savéant consider that rather large uncertainties affect the *a priori* estimation of ℓ and D, and since the values of C_E are also somewhat uncertain in this case, this may be acceptable [128].

Table 7.7. Relative Values of k_E Derived from Yield Data (Table 7.3) [132] for Reactions of Small Clusters Mg_n (4 mmol Mg in 10 mL THF) with *endo*-5-(2′-Haloethyl)-2-norbornenes in THF at Room Temperature

X	(RH)	σ	σ/σ^0	k_E/k_E^0
Cl	85.4	0.040	0.18	0.0060
Br	63.7	0.22	1.0	1.0
I	43.9	0.63	2.9	23

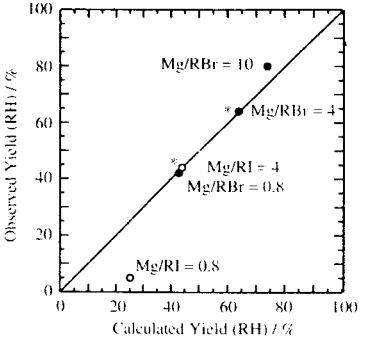

Fig. 7.31. Observed [132] vs calculated yields (RH) from reactions of small clusters Mg_n with *endo*-5-(2′-haloethyl)-2-norbornenes in THF at room temperature, as a function of the concentration of the Mg slurry taken for the reaction. The points marked '*' are fitted.

The second concern is the assumption that Mg_n is deactivated when it reacts with RX. This assumption aligns the D model for Mg_n with the reaction scheme treated by Andrieux and Savéant [128,129], in which the reducing agent E is consumed as it reacts. Otherwise, $[Mg_n]$ would build up continuously in the reaction zone and not reach a steady state.

The deactivation assumption may not be necessary. The mixing-diffusion-reaction phenomenon for Grignard reactions of Mg_n (as E) may not be exactly the same as that treated by Andrieux and Savéant. Gradients similar to those of Figure 7.30 could develop even when E is *not* consumed by the reaction. As E diffuses into the RX solution, a diffusion zone develops over which its concentration decreases in the RX direction, even without reaction. Reinforcing this gradient is a reverse diffusion of the solvent from the RX solution into the E solution. The diffusion zone and gradient will be ever changing position, but if the reaction of RX with E is faster than diffusion, then RX will react with E in the zone of the gradient, with less penetration of more reactive RX toward the region of higher [E] and consequently a lower local [E] at the time R· is formed. This could mimic the case treated by Andrieux and Savéant [128,129].

7.2.19 Chain Mechanisms

Several chain mechanisms have been proposed [131,132,134,135]. For Grignard reactions under ordinary conditions, they are ruled out on several grounds.

(1) The rate law is simple. Under hydrodynamically controlled conditions, the rates of Grignard reactions are proportional to [RX] and the area of Mg_Z (Section 7.2.2). Chain reactions often exhibit more complex kinetics. While this does not exclude all chain mechanisms, it does exclude some and it is consistent with a non-chain mechanism.

(2) Reactions in which significant fractions of the intermediate radicals are trapped by DCPH or TMPO· occur without any large changes in reaction rates (Section 7.2.8, Figure 7.3, Section 7.2.23). Chain reactions would be markedly inhibiting by trapping. This evidence is compelling.

(3) Under ordinary conditions, Grignard reactions of alkyl bromides and iodides give significant yields (up to ~50%) of products of **c** (Section 7.2.8), which would be termination steps of a chain mechanism. For chains of appreciable lengths, only minor fractions of the products are formed in termination steps. This is also compelling evidence.

(4) The D model, a non-chain mechanism, accounts quantitatively for product distributions of reactions of typical alkyl halides (Section 7.2.8).

A chain mechanism for Grignard reactions involving slurries of small magnesium clusters has not been ruled out, but there are plausible alternative interpretations of the evidence (Section 7.2.18).

7.2.20 Carbanion Intermediates

Bickelhaupt and co-workers report evidence pointing to an intermediate with properties of a carbanion R^- in reactions of aryl bromides [136,137]. Although RMgX and R_2Mg are themselves carbanionoid species, the intermediate must be something else.

By-products $R(-H)Mg_2Br_2$ and RH are formed in equal amounts in the Grignard reaction of the following crown ether aryl bromide RBr [136]. Analogous results, with a lower yield of Grignard reagent (16%), are obtained for the homolog of RBr with an additional $-CH_2CH_2O-$ group in the ring. The by-products appear to be formed in a reaction of RMgBr with something present as reaction proceeds. On this basis, the higher yield of RMgBr than that from its homolog is explained by the lower solubility of RMgBr—less is available for by-product formation in solution during the reaction.

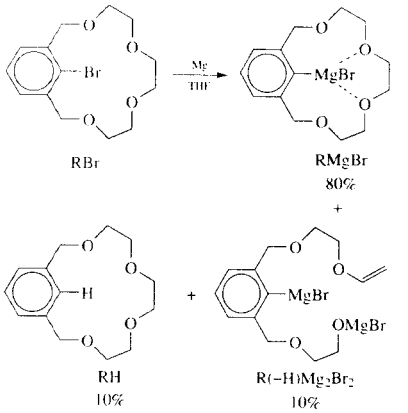

The final reaction mixture is stable, as is a mixture of RMgBr and phenylmagnesium bromide (PhMgBr). When a ten-fold excess of PhBr reacts with Mg in the presence of RH, RH is recovered quantitatively. However, when a similar reaction occurs in the presence of RMgBr, followed by quenching with D_2O and aqueous work-up, no RMgBr survives and a deuterated derivative of $R(-H)Mg_2Br_2$ is formed. These facts suggest the following mechanism, where Ph^- is an intermediate in a reaction of PhBr. In the reaction of RBr, R^- replaces Ph^-.

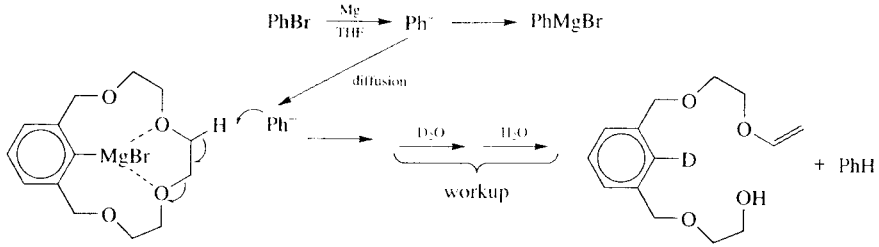

Migrations of $SnMe_3$ in Grignard reactions of 2-bromo(trimethylstannylmethyl)benzene can also be interpreted as reactions of a carbanion intermediate in Grignard reagent formation from an aryl bromide [11,137]. Here the Grignard reagents RMgBr were determined as derivatives $RGeMe_3$ obtained by treating product mixtures with Me_3GeCl.

van Klink investigated this and analogous systems further in an effort to rule out rigorously the possibility that radical, instead of carbanion, intermediates are responsible [11]. Toward this end, to generate genuine aryl radical intermediates, he allowed 2-bromo(trimethylstannylmethyl)benzene to react with SmI_2 in a mixture of THF and HMPA. The deuteration data indicate

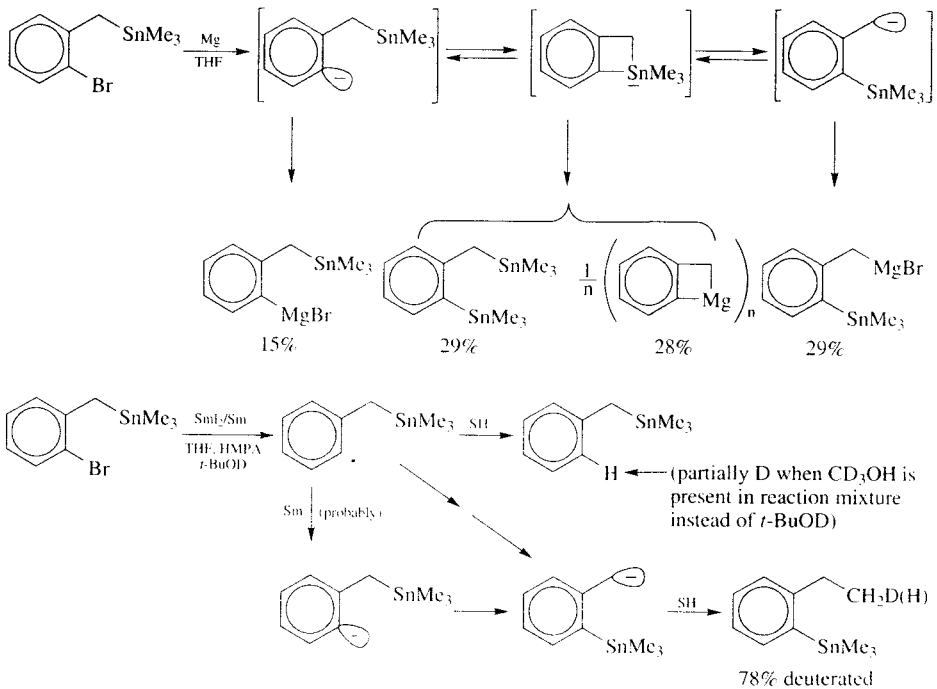

that benzyltrimethylstannane stems from the 2-(trimethylstannyl)phenyl radical and is consistent with the anionic origin indicated for 2-(trimethylstannyl)toluene, although a rearrangement of the radical followed by reduction of the rearranged radical (diagonal arrows) would give the same result.

In some experiments no rearrangement was found. Thus, the radical rearrangement is too slow to compete with solvent attack. The yield of rearranged product varied among experiments, reflecting (it is believed) the amount of Sm adventitiously included in the SmI_2 preparation. This variation is further evidence that it is the carbanion, not the radical, that rearranges, since it appears (surprisingly, perhaps) that SmI_2 alone does not reduce aryl radicals (as it does alkyl radicals) [138,139].

Benzyltrimethylstannane is inert toward SmI_2, but it may react to exchange the trimethylstannyl group with Ph^- when PhBr is included in the reaction mixture and a significant amount of Sm is present. A similar exchange occurs when PhBr reacts with Mg in the presence of benzyltrimethylstannane, which is inert toward PhMgBr. Thus, the behaviors of benzyltrimethylstannane in reactions of PhBr with two different reducing agents, Mg and SmI_2/Sm, are similar [11].

Recent results indicate that R• is not a significant intermediate in a Grignard reaction of phenyl bromide or 2-(3-butenyl)phenyl bromide in THF (Section 7.2.11) [112]. This is additional support for the hypothesis that the cleavages and rearrangements described above, which occur in Grignard reactions of aryl bromides in THF, are not reactions of R•.

Thus far, no evidence has been presented for carbanion intermediates in Grignard reactions of alkyl halides. It is not known whether or not Grignard reactions of alkyl halides have the same effects as those of aryl halides in providing carbanion intermediates for reaction with RMgBr.

The apparent lifetimes and selectivities of the intermediate carbanions require comment. It may be surprising that an R^- not intimately associated with Mg(II) can live long enough to undergo bimolecular reactions selectively. Its association with Mg(II) in the solution might be expected to be very fast and to lead to components of the Schlenk equilibrium ($RMgX$, R_2Mg) that don't undergo or promote the observed rearrangements.

If the carbanion hypothesis is correct, there must be an effective barrier to the association of R^- with Mg(II). Conceivably, this could arise from the tight binding of ligands, including solvent, in the inner sphere of Mg(II) in RMgBr, $MgBr_2$, and R_2Mg. The binding energies of DEE in complexes $ZMgZ'(DEE)_2$ (Z,Z' = Cl, Br, Et, Ph) have been calculated as ~10–14 kcal mol^{-1} [11]. Those for THF may be greater. Perhaps such tight binding could sufficiently slow the S_N1-like conversion of R^- to stable components of the Schlenk equilibrium.

In any event, the carbanion hypothesis is consistent with the view that the reaction of R• at Mg is an electron transfer, similar to a reduction at an inert electrode, and the evidence supporting R^- as an intermediate also supports the electron-transfer mechanism. In turn, this lends some support, however slight, to the hypothesis that the initial step is also an electron transfer, analogous with a reduction of RX at an inert electrode.

It may be that R^- only sometimes an intermediate with a sufficient lifetime to detect through competitive product formation. Especially when high concentrations of MgX_2 are present, its lifetime could be too short to detect in this manner. Indeed, the formation of RMgX under such conditions could be a concerted or nearly concerted reaction among Mg^0, R•, and MgX_2.

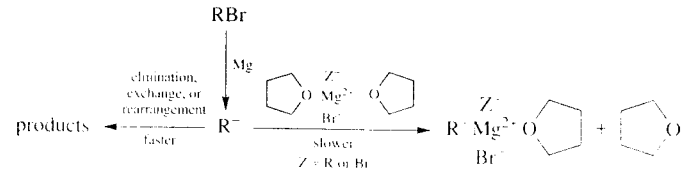

It is conceivable that the nucleophilic intermediate could be something other than R^-, perhaps RMgMgBr or RMgMgR (Section 7.3.8). The dispersal of positive charge over two Mg atoms instead of one could cause these to be more reactive as carbanionoid species than RMgBr and RMgR. Nucleophilic reactions of such dimagnesium Grignard reagents would compete with their reactions as reducing agents for RBr.

7.2.21 Anion-Radical Intermediates in Reductions of Organic Halides

An electron-transfer reduction of RX can be dissociative (no intermediate anion-radical $RX^{\cdot-}$) or non-dissociative (intermediate $RX^{\cdot-}$). Where the non-dissociative pathway is well documented (e.g., aryl halides), only two reactions of the intermediate $RX^{\cdot-}$ are generally posited, dissociation and electron-transfer oxidation [17,18]. However, product evidence suggests that $R\text{-}X^{\cdot-}$ may undergo other reactions, including reduction.

There is strong evidence of intermediates $RX^{\cdot-}$ in electrochemical and chemical reductions of aryl and vinyl halides [17,18]. For Grignard reactions of these substrates, there are indications

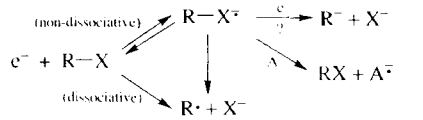

that anion-radical intermediates may be reduced directly (Section 7.2.11). Analogous steps have not been revealed in electrochemical studies.

For a reduction of a typical alkyl halide, it remains unclear whether or not $RX^{\cdot-}$ can be an intermediate. Some theoretical calculations suggest not, but reliability is uncertain and results vary with assumed conditions and methods. Thus, in calculations for electron attachment to CH_3Cl in solution, no intermediate $CH_3Cl^{\cdot-}$ is found for free ions but one is found for ion pairs [140,141].

Suggestive evidence of $RX^{\cdot-}$ is found in product distributions for reactions of 5-hexenyl chloride, bromide, and iodide with disodium tetraphenylethylene $(Na^+)_2$ $:TPE:^{2-}$ in 2-methyltetrahydrofuran [142]. The initial step is electron transfer to give a geminate radical pair, $[R\cdot\ :TPE^{\cdot-}]$ or $[RX^{\cdot-}\ :TPE^{\cdot-}]$. In the former pair, X^- has departed and may not influence subsequent, product-determining

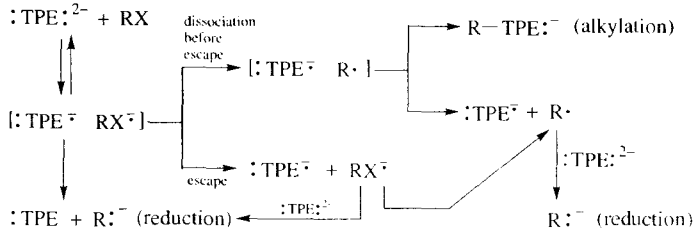

steps. However, a halogen effect on the partitioning between reduction and alkylation products is observed (RI, 66% reduction; RBr, 52%; RCl, 34%). One possible explanation invokes $RX^{\cdot-}$ as an intermediate. If it has a longer lifetime for I than Cl, giving the pair $[RI^{\cdot-}\ :TPE^{\cdot-}]$ more time to escape than the pair $[RCl^{\cdot-}\ :TPE^{\cdot-}]$, then more reduction is expected for RI than RCl, as observed.

It is also possible that $RX^{\cdot-}$ could be reduced directly, either in a geminate reaction with $:TPE^{\cdot-}$ or in a nongeminate reaction with $:TPE:^{2-}$. This evidence of $RX^{\cdot-}$ is not compelling because there is a possibility that the mere presence of X^- in the vicinity of the product-determining reactants could influence partitioning enough to produce the small effects that are seen [142].

ESR spectroscopic studies demonstrate that $RX^{\cdot-}$ can exist, even for typical alkyl halides, under some circumstances. $RX^{\cdot}$ has been detected at low temperatures in special cases (e.g., $CF_3I^{\cdot-}$) [143–145]. Low-temperature ESR also detects species that may be 'complexes' of typical alkyl radicals with halide ions, e.g., $\cdot CH_3 \cdots I^-$ [144,145]. Criteria for distinguishing these 'complexes' from anion-radicals are not clear. An anion-radical $AB^{\cdot-}$ can be described by a three-electron A–B σ bond, $\sigma^2\sigma^{*1}$ and termed a 'σ^*' species [144,145], but delocalized MOs may be more appropriate in some cases, at least. 'Complexes' are thought to have longer, weaker bonds than σ^* species [144,145], but quantum-mechanical descriptions of these species could be similar. Indeed, lengths and strengths of their C–X bonds may lie along a continuum of variation. Therefore we consider both 'complexes' and σ^* species to be anion-radicals $RX^{\cdot-}$.

For electrode reductions, the magnitude of the observed transfer coefficient (symmetry factor) α $(\partial\Delta G^{\ddagger}/\partial\Delta G^0)$ may distinguish dissociative ($\alpha < 0.5$) from non-dissociative ($\alpha > 0.5$) electron transfers [17,18,146]. Under this criterion, a large body of data has been analyzed consistently. However, no treatment such as this, based on energies, can be rigorously definitive (Figure 7.32). In particular, the α criterion could not distinguish a reaction giving a weakly-bonded anion-radical $\cdot R \cdots X^-$ ('complex') from one giving dissociated R· and X^-.

Reductions of optically active 1-halo-1-methyl-2,2-diphenylcyclopropanes are especially interesting (Tables 7.8–7.10). Under various conditions, the extent of retention of configuration in reduction products ranges from 0 to 63%.

A comprehensive interpretation of these data is hampered by uncontrolled variables, missing data, and small magnitudes of some of the effects. Thus, known temperatures range from −78 C (−30 C

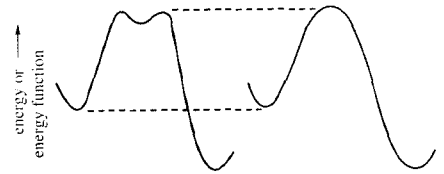

Fig. 7.32. No analysis based on energies can distinguish between reactions with and without intermediates (left and right, respectively).

Table 7.8. Retention of Configuration in Reductions of 1-Halo-1-methyl-2,2-diphenylcycloproanes at 20 C [96,147]

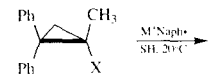

M = Li, Na, K homogeneous solutions

		Retention/%								
		Li			Na			K		
X	SH									
Cl	THF	0.2	<0.1	[100]	0.8	<0.1	[100]	3	<0.1	[100]
Br	THF	32	15	[25]	49	42	[100]	53	42	[25]
I	THF	57	43	[100]	48	42	[100]	41	42	[100]
Br	THF		32			49			53	
Br	DME		17			31			43	
Br	HMPA		3			3			2	
									dicyclohexyl-18-crown-6 added	
Cl	THF							3	0	
Br	THF							53	7	
I	THF							41	18	

Reduction at a glassy carbon electrode, ~ 22 C. $\frac{(Et)_4N^+\ Br^-}{47}$

Br CH_3CN

Bracketed numbers are dilution factors (from 0.9 M).

Table 7.9. Halogen Effects on Retention of Configuration in Reductions of 1-Halo-1-methyl-2,2-diphenylcyclopropanes[a]

Red	Solvent	t/°C	F	Cl	Br	I
Li^0[b]	DEE	24–26		63	45	36
Ca^0 ('bronze')	NH_3	−30		29	11	
Mg^0[d]	THF	65		26	17	2
Li^0	THF	−3	3	10		
KNaph[f]	THF	20		3	53	41
NaNaph[f]	THF	20		0.8	49	48
LiNaph[f]	THF	20		0.2	32	57
KNaph[f]	THF/ crown[g]	20		0	7	18
$Ca(Naph)_2$	THF	−20	0	0		
		−78	0	0		

[a]Tabulated values are optical purities (%) in reduction product.
[b]Walborsky and Aronoff [148,149].
[c]Walborsky and Hamdouchi [150].
[d]Walborsky and Aronoff [20].
[e]Walborsky and Powers [115].
[f]Boche *et al.* [96,110].
[g]Dicyclohexyl-18-crown-6.

Table 7.10. Retention of Configuration in Reductions of 1-Bromo-1-methyl-2,2-diphenylcyclopropane by Metals in Alcohols

Metal	Solvent	ret/%
Mg^0[a]	CH_3OD	23
Li^0[b]	*i*-PrOH	39
Li^0[b]	*t*-BuOH	47
Na^0[b]	CH_3OD	47
Na^0[b]	*i*-PrOH	47
Na^0[b]	*t*-BuOH	46
$K0^0$[c]	*i*-PrOH	44
K^0[b]	*t*-BuOH	44

[a]Walborsky and Rachon [109].
[b]Walborsky *et al.* [151].
[c]Reaction temperatures are not reported in either of these works.

for reactions giving retention) to +65°C, halogen-effect data are not available for Mg^0/DEE and are incomplete for Li^0THF, and for Li^0/DEE the span of the ratio retention/racemization is only a factor of 4 over Cl-Br-I. Therefore we focus primarily on the largest effects, most consistent trends, and most reliable principles.

Homogeneous-solution alkali naphthalenes (MNaph) reductions of 1-halo-1-methyl-2,2-diphenylcyclopropanes in aprotic solvents occur with retention of configuration up to 57% (Table 7.6) [96,110,152]. 1-Bromo- and 1-chloro-1-methyl-2,2-biphenylenecyclopropanes behave similarly [96,110].

In principle, there is a possibility that the product carbanion R^- (or carbanionoid species) could racemize to extents that vary with conditions (solvent, metal, proton source, temperature). However, for lithium, magnesium, and calcium compounds, analogous reactions occur with complete retention under the conditions that have been investigated [10,96,150]. Following Boche and Walborsky, we assume that racemization does not occur once R^- or RM (M = Mg, Ca, Li, Na, *K*) is formed.

In these reactions, reductive trapping is too slow to compete with inversion of R• [110,152]. This rules out a simple mechanism through R•.

Without offering supporting citations, Hamdouchi and Walborsky allege that Garst claims otherwise [10,21]. This allegation is false.

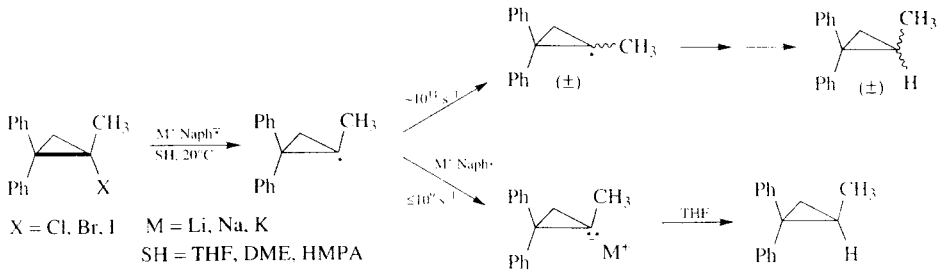

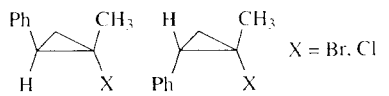

The data provide other evidence against competing radical racemization and reductive trapping. If trapping by MNaph were competing with the racemization of any species, including R•, then the optical purity of the product would decrease with decreasing [MNaph]. For (Br,I)/(Na,K)/THF, this prediction fails—optical purities are independent of [MNaph] [96,110]. Also, retention in KNaph/(Cl,Br,I)/THF reactions are independent of the order of addition of reactant solutions [96,110].

Further, if retention were a consequence of reductive trapping of partially racemized radicals R•, then similar reductions of other substituted cyclopropyl halides, containing fewer aromatic rings, would also be expected to be stereospecific, but they are not [96,110,152]. In cases of fewer aromatic rings, including *cis*- and *trans*-1-bromo- and 1-chloro-1-methyl-2-phenylcyclopropanes, product distributions are independent of halogen and countercation as well as reactant stereochemistry [96,110,152]. In MNaph reductions of substituted cyclopropyl halides, stereospecificity is sometimes accompanied by halogen and counterion effects, while nonstereospecificity is not.

The facts militate against another possible explanation of retention, geminate reactions of MNaph aggregates, which could be significant at the high concentrations used (0.9 M). Consider dimers $(MNaph)_2$, for example. A one-electron electron transfer from one $Naph^-$ of a dimer would leave a geminate pair [R• MNaph]. Since other geminate reactions of initially chiral radical pairs occur with partial retention of configuration [103-108], so could the collapse of [R• MNaph].

Under this explanation, retention in reactions with alkali naphthalenes would be expected for all cyclopropyl halides, but it is found only for those with geminate aryl groups. Evidently retention is a consequence of conjugation.

By excluding reductive trapping of R• as the source of retention in reactions of RX with MNaph, these results show that $RX^{\bullet-}$ is an intermediate and that it suffers fates other than fragmentation and oxidation. There seems to be no other reasonable alternative.

Scheme 7.1 combines elements from Walborsky's mechanism of Grignard reagent formation (pathways 1-2, 1-8-7, and 6-7) [10] and Boche's mechanism (omitting some possible intermediates) for reactions of this substrate with MNaph

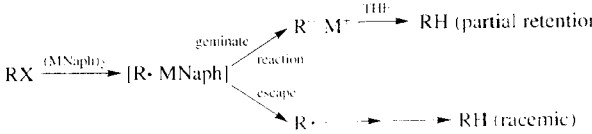

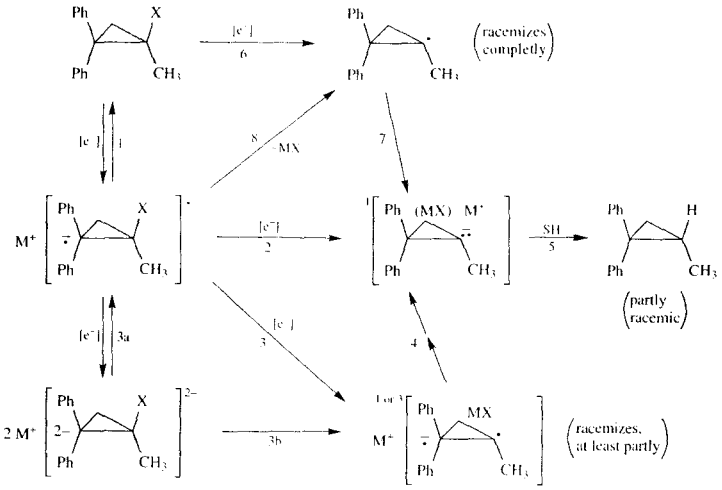

SCHEME 7.1. $[e^-]$ = Naph$^{-\cdot}$, metal$^{\cdot}$, electrode, solvated electron, or RX$^{-\cdot}$.

(pathways 1-2-5 and 1-3-4-5) [96,110,152]. It is generalized with respect to reducing agent and augmented by noting that electron spin factors could be involved in steps 3 and 4. We attempt to understand the data in terms of this mechanism.

A key point in Boche's analysis is that the odd electron in RX$^{-\cdot}$ can occupy an orbital that belongs largely to diphenylcyclopropane, not to C–X, whose antibonding orbital σ^*(C–X) may be the target of electron transfer in the absence of geminate aryl groups [96,110,152]. Walborsky and Powers explain reductions of 1-fluoro-1-methyl-2,2-diphenylcyclopropane, which are unusual in giving large amounts of products of ring opening, similarly [115]. The ring-opened products are believed to proceed from RX$^{-\cdot}$. Parallel reactions of related hydrocarbons have been described [96,105,153,154].

The product of step 3 of Scheme 7.1 must be regarded as an excited state *R$^-$ of R$^-$. *R$^-$ can, in principle, be an electronic singlet or triplet. In either case, it is a kind of diradical, having a substantially localized electron at C-1 with a partner (of either spin) in the aromatic rings.

It is striking how often the extent of retention of configuration (Tables 7.6–7.8) is ~50%, that is, in the range 35–65%. The variation from 35% or 65% to 50% retention is a factor of 1.4 or less in the relative rate constants for retention and racemization, corresponding to a variation in $\Delta\Delta G^{\ddagger}$ of less than 0.21 kcal mol^{-1} at room temperature, a very small quantity. Retention is ~50% for a wide variety of reactions and conditions, including reductions by alkali naphthalenes in THF and DME, at a glassy carbon electrode in CH_3CN, by Li^0 in DEE, and by Li^0, Na^0, and K^0 in alcohols. It is as if ~50% retention were a limiting value governed by factors that are not very sensitive to variations in reducing agent, solvent, metal, homogeneity/heterogeneity, or even temperature.

Most of the competing pathways for racemization and retention in Scheme 7.1 would not be expected to produce such a limit. The pathway that could best account for it may be the singlet version of 1-3-4. Here partial racemization would occur in step 4, where X$^-$ has been lost from the reactant. The rates of racemization and passage from the initial excited state *R$^-$ to the ground state could

be (nearly) insensitive to spectator ions M$^+$ and X$^-$, solvent, temperature, etc.

For step 3, the singlet version would apply if there were an intermediate RX^{2-} (step 3a) in which a delocalized aryl-group orbital contained both added electrons. RX^{2-} would be a singlet and would dissociate to the singlet excited state *R$^-$ (step 3b).

Other options for the ~50%-retention limit pathway have drawbacks. (a) For a triplet or mixed singlet-triplet version of pathway 1-3-4, it is not be clear why spin factors and intersystem crossing would operate in the same way for reductions by metals or electrodes as homogeneous reductions by Naph$^{\cdot}$, yet the presumed limit is found for these types of reactions. (b) Diffusion control of competing steps 2 and 3 could describe reductions by MNaph and solvated electrons but, again, it is not clear how this would apply to reductions by metals and electrodes. If this competition were not diffusion controlled, then a significant step 2 would introduce halogen effects on the limit.

Steps 6 and 8 are not part of the proposed limit pathway. For MNaph reductions that approach the limit, there is additional evidence that they are not significant.

For MNaph/THF reductions with I/(Li$^+$, Na$^+$, K$^+$) and Br/(Na$^+$, K$^+$), halogen, metal-ion, and concentration effects are small to non-existent. If the competition of step 3 with step 8 were significant, there would be a concentration effect. Therefore step 8 does not contribute to racemization, leaving 3 and 6 as possible racemization-determining steps in the limit.

If step 1 were practically reversible, then step 6 would also be eliminated by the absence of a concentration effect. In addition, if step 6 (reversible or not) were a significant factor in determining the extent of retention, halogen effects would be expected, but in fact these are nonexistent to very small in the cases near the proposed retention limit.

Thus, we are left with the singlet pathway 1-3-4 (or 1-3a-3b-4) for the limit of ~50% retention. This applies to Naph$^{-\cdot}$/I/Li$^+$/THF, Naph$^{-\cdot}$/(Br,I)/(Na$^+$, K$^+$)/THF, e$^-$ (glassy C)/Br/Et$_4$N$^+$/CH_3CN, Li^0/(Cl, Br, I)/DEE, and (Li^0, Na^0, K^0)/Br/ROH(D) (Tables 7.6–7.8).

For the remaining Naph$^{-\cdot}$ reactions, Cl/(Li$^+$, Na$^+$,K$^+$)/THF and Br/Li$^+$/THF, not only is there less than 35% retention but also the data exhibit concentration, halogen, and metal-ion effects, implying the incursion of at least one racemization pathway that is excluded in cases of the ~50%-retention limit. Concentration effects suggest step 8. Retention is favored for higher [Naph$^{\cdot}$], as expected for a competition between step 3 (retention, first-order in Naph$^{-\cdot}$) and step 8 (racemization, zeroth-order in Naph$^{-\cdot}$).

The only other possibility in Scheme 7.1 for a concentration effect on the extent of retention is in the competition between steps 6 and 1–3, provided that the reverse of step 1 is significant. If the concentration of naphthalene is low, it may be unlikely that the reverse of step 1 could compete with other reactions of RX$^{-\cdot}$, except as a kinetically insignificant geminate reaction [77]. If step 1 were otherwise practically irreversible, then the competition between steps 6 and 1–3 would not be concentration-dependent.

It is peripherally relevant that in reductions of hexyl fluoride by NaNaph there is clear evidence against a practically reversible electron transfer to hexyl fluoride [155]. Thus, the reactions are cleanly first order in NaNaph and a large excess of naphthalene has no effect on the rate. The possible influence of excess naphthalene on reactions of 1-halo-1-methyl-2,2-diphenylcyclopropanes has not been reported [96,110].

Since step 6 is excluded for some of the reactions of 1-halo-1-methyl-2,2-diphenylcyclopropanes with MNaph and is not necessary to account for data for others, we omit it. Reactions of MNaph can be described by competing pathways 1-3-4 (singlet, ~50% retention) and 1-8-7 (0% retention).

Solvent and metal ion effects in these reactions can be analyzed in terms of established general principles [156–164]. For organoalkali compounds in ethers (and other aprotic solvents) [116], (1) '...solvent effects are expected to be more predictable than cation effects' and (2) 'more polar solvents will...favor, relatively, the anion of

smaller cation affinity' (principle of inversion of solvent effects), where the cation affinity increases as the effective size of the anion decreases or its negative charge increases. The anions being compared are equilibrated and can be species or transition states (equilibrated with reactants and other entities, including transition states, equilibrated with those reactants). Effects of metal ion solvation dominate in less polar, aprotic solvents, where ionic aggregation is important. In more polar, protic solvents, where metal cations are mere spectators, effects of anion solvation dominate. The directions of solvent effects are opposite (inverted) for organoalkali reactions in these classes of solvents [116].

More polar solvents (HMPA > DME > THF; dicyclohexyl-18-crown-6 > THF)[116] favor racemization (Table 7.6). Therefore the anionic transition state for retention has a larger cation affinity than that for racemization. This fits the previous considerations. The transition state for step 8 (racemization) bears a charge -1 while that for step 3 (~50% retention) bears a charge -2, giving the latter the larger cation affinity.

For MNaph/THF, there are irregularities in the metal-ion trends, with retention favored in the order $K^+ > Na^+ > Li^+$ for RCl but $Li^+ > Na^+ > K^+$ for RI at high [NaNaph]. Such inversions are common in organoalkali chemistry [116]. They reflect the competition between gas-phase coulombic interactions and metal-ion solvation, the effects of which have opposite trends (coulombics favors the anion of higher cation affinity; metal-ion solvation, lower). If the transition state for retention has a higher cation affinity than that for racemization, as solvent effects indicate, then the data imply that metal-ion solvation dominates gas-phase coulombics for Cl/(Li^+, Na^+, K^+)/THF but not for I/(Li^+, Na^+, K^+)/THF. This could be a consequence of the relative importance of pathway 1-8-7 for RCl and RI. Coulombics might dominate when the anionic transition state of higher cation affinity is important (RI) and metal-ion solvation otherwise (RCl). Even so, the observed effects may be too small to lend confidence to such a detailed interpretation.

The largest halogen effects in MNaph reactions are between Cl and Br, with retention favored in the order Br ≫ Cl (Table 7.6) for all metal ions. For Li^+ (but not Na^+ or K^+), the order is I > Br ≫ Cl. This implies, in terms of our analysis, that step 3 is favored (relative to step 8) in this order. There is evidence of the same order of halogen effect in reactions of Li^0 with 1-fluoro- and 1-chloro-1-methyl-2,2-diphenylcyclopropanes in THF: F gives only 3% retention while Cl gives 10% (Table 7.7). This could also reflect the competition between steps 3 and 8.

In Grignard reagent formation from 1-halo-1-methyl-2,2-diphenylcyclopropanes, retention is favored in the opposite order, Cl > Br ≫ I [10,20]. This can be accommodated by invoking pathway 6-7 as well as 1-3-4 and 1-8-7, with the halogen effect favoring I (relative to 6) in the order Cl > Br > I. This is not inconsistent with step 3 being favored (relative to 8) in the order I > Br > Cl.

From Mg^0/THF/65°C to Li^0/DEE/(24–26°C), the order of the halogen effect on retention remains the same, but the sensitivity to halogen decreases, as if the order were being tipped from Cl > Br > I toward I > Br > Cl. This effect is also indicated by the data for Li^0/THF/(−3°C), where the order is F > Cl. Unfortunately, data for Mg^0/(Cl,I)/DEE and Li^0/(Br,I)/THF are not available.

Nonetheless, in going from Mg^0/THF/65°C to Li^0/DEE/(24–26°C) to Li^0/THF/(−3°C), the directions of greater reducing power of M^0, higher polarity, and smaller number of available electrons per metal atom, as well as lower temperature, the data suggest a trend in the order of retention from F > Cl > Br > I to I > Br > Cl > F. Since all of these factors may correlate with increasing reducing power, it could be a controlling factor. We leave 'reducing power' vague in the sense that it could refer to either thermodynamic or kinetic factors. By definition, increased reducing power favors steps 1 and 3 over their competitors.

Variations in the temperatures of these experiments could invalidate any conclusions based on comparisons. However, it should be noted that Ca^0(bronze)/NH_3/−30°C gives retention in the order Cl > Br, indicating that temperature alone is not determining, since the reverse order would have been expected, from the data for metal reactions in ethers, if it were.

Thus, data for reductions of 1-halo-1-methyl-2,2-diphenylcyclopropanes appear to conform rationally to a mechanism with competing initial steps 1 and 6 and competing steps 3 and 8 subsequent to 1 (Scheme 7.1). More reducing power favors 1 relative to 6 and 3 relative to 8. When the halogen effect is determined by the 3-8 competition, retention varies in the order I > Br > Cl > F, and when it is determined by the 1-6 competition, it varies oppositely.

The case of Li^0/DEE/(24–26°C) is especially interesting because retention is barely sensitive to the nature of the halogen. This suggests that the reactions are at the ~50%-retention limit, with pathway 1-3-4 dominating. The small variations with halogen that are observed, however, are in the opposite direction from that assigned here to the 3-8 competition. In one possible explanation, the Cl reaction is at the 1-3-4 limit (63% retention observed) while the Br and I reactions involve successively more, but always minor, reaction through 6-7.

Alternatively, pathway 6-7 could always be insignificant. If so, the order of the halogen effect on the 3-8 competition would have to be sensitive to conditions.

It is plausible that it could be. In a reaction in which C–X is cleaved, the nature of the halogen probably plays an important role in determining the cation affinity of the transition state, which in turn influences both gas-phase coulombic and metal-ion solvation energies [116]. It is likely that there can be a strong association between the developing ion X^- and the metal ion M^- or M^{2+}. Thus, there could be a complex set of interactions among the transition state (both developing X^- and residual parts), metal ion, and solvent that could lead to one order of halogen effect on the 3-8 competition under some conditions and another under others. This may be the simplest theory that can accommodate all of the data.

Is it rational that reactions e^-(glassy C)/Br/Et_4N^+/CH_3CN and (Li^0, Na^0, K^0)/Br/ROH(D) be at or near the 1-3-4 limit? Does this not violate the rule that more polar solvents shift the reaction away from the 1-3-4 limit? Possibly not. The principle of inversion of solvent effects, which rationalizes that rule, applies to organometallic compounds in aprotic solvents of low polarity, where ionic aggregation and strong specific solvation of metal ions are both important. Neither the tetraethylammonium/acetonitrile nor the M/ROH combination falls into this category. In these cases, the direct solvation of the anion may dominate. Alcohols, in particular, solvate anions through hydrogen bonding. Then the 'normal,' rather than the 'inverted,' direction of solvent effects would apply: more polar solvents would favor the anion of higher, rather than lower, cation affinity. As we have seen above, for the 3-8 competition the transition state of higher cation affinity is that of step 3. CH_3CN and ROH may be polar enough to drive the competition almost entirely to step 3.

Is it rational that racemic products result from the reaction of $Ca(Naph)_2$ with 1-bromo-1-methyl-2,2-diphenylcyclopropane in THF at −78°C [150]? Perhaps. The change from partial retention (in reactions of alkali-metal naphthalenes) to racemization could be due to temperature (−78°C instead of 20°C) or the change in metal ion. Ca^{2+} might decrease the reducing power of the associated $Naph^{\bullet-}$, allowing step 6 or 8 to dominate (Scheme 7.1).

The reaction of Mg^0 in CH_3OD appears to be close to, but not at, the 1-3-4 limit. This could be a consequence of a lower reducing power of Mg^0 (compared to Li and other alkali metals), allowing some reaction through step 8 (or 6); to a greater tendency toward ionic aggregation for the divalent cation Mg^{2+} (than M^+), which might increase the influence of metal-ion solvation on stereochemistry; or to a specific interaction between Mg^{2+} and the departing Br^-, making it a better leaving group in step 8 (or 6). The first and third of these factors might also operate in ordinary Grignard reactions of 1-halo-1-methyl-2,2-diphenylcyclopropanes in THF and DEE, which are close to the ~50%-retention limit for RCl and RBr and not as close for RI.

The α criterion does not detect an $RBr^{\bullet-}$ intermediate in the reduction of 1-bromo-1-methyl-2,2-diphenylcyclopropane in acetonitrile (0.1-M tetrabutylammonium tetrafluoroborate) at a glassy-carbon electrode ($\alpha = 0.3$) [22]. Walborsky and

Hamdouchi accept the implication of the α criterion and propose that 'a very fast second electron transfer leading to the configurationally stable carbanion occurs at the surface,' accounting for the observed 47% retention found in a similar reduction [147]. In this interpretation, the intermediate R• is reduced so rapidly that 47% retention results. At the same time, these workers adhere to the previous proposal that retention of configuration in the Grignard reaction of the same substrate results from a pathway through a tight radical anion-radical cation pair [$RBr^{\bullet-}$ $\cdot Mg^{+}$]. They conclude that that the tight radical anion-radical cation pair must be a transition state, not an intermediate, because the α criterion rules out $RBr^{\bullet-}$ as an intermediate.

Even though they propose different mechanisms for electrode and Mg^0 reductions, they transfer a conclusion (no $RBr^{\bullet-}$ intermediate) from one case (electrode) to the other (Mg^0), a logical step that cannot be justified if the mechanisms are different. If the mechanism of the electrode reduction were similar to what they propose for the Grignard reaction, then 47% of the electrode reduction would be through a reaction that leads neither to R• nor $RBr^{\bullet-}$, the cases treated by Savéant [17,18], but instead to R^- and X^-, a case that has not been considered. It is not clear what value of α should be expected for the latter case.

It seems likely that similar phenomena (partial retention) in similar reactions (electrochemical and MNaph reductions of 1-bromo-1-methyl-2,2-diphenylcyclopropane) have similar explanations. If so, then $RBr^{\bullet-}$ is an intermediate in both, as discussed earlier, and the α criterion fails.

In their electrochemical studies, Webb *et al.* noted 'that the stereochemistry can be influenced by almost every parameter involved in the reaction, *i.e.*, solvent, electrolyte, electrode, leaving group (Br, I, HgX), extent of reaction, and substituents at the reaction site' [147]. Thus, reductions of 1-bromo-1-methyl-2,2-diphenylcyclopropane in DME/tetra-*n*-butylammonium perchlorate give high yields of racemic RH, while similar reactions in acetonitrile and *N*, *N*-dimethylformamide give ~25% retention. The presence or absence of iodide ion also affects the optical purity of RH.

The direction of solvent effects here is expected to be 'normal,' rather than 'inverted,' since these systems do not contain metal ions. Following the conclusion reached earlier, that the retention transition state has a higher cation affinity than that for racemization, it is predicted that more polar solvents will give more retention. This prediction is realized in the data of Webb *et al.* cited above [147].

Several conclusions can be drawn.

(a) There is no compelling evidence against $RX^{\bullet-}$ as an intermediate in reductions of any organic halide. The tendency to form $RX^{\bullet-}$ increases from typical alkyl halides to vinyl and aryl halides and others containing unsaturated groups. It is well documented for vinyl and aryl halides. If $RX^{\bullet-}$ is an intermediate for a typical alkyl halide, it probably has such a short lifetime (as limited by dissociation) that its only significant processes are dissociation and escape (from a geminate radical pair).

(b) Strong chemical evidence implicates $RX^{\bullet-}$ as an intermediate in some reductions of 1-halo-1-methyl-2,2-diphenylcyclopropanes. It may always be an intermediate. There are indications that the reducing electron can enter an orbital that is delocalized primarily over the aromatic parts of the molecule.

(c) For reductions of 1-halo-1-methyl-2,2-diphenylcyclopropanes, it is also clear that dissociation and oxidation are not the only fates of $RX^{\bullet-}$. For aryl halides, no other reactions of $RX^{\bullet-}$ have been detected, even though electrode reductions have been probed intensely.

(d) Because it is found in homogeneous reductions of 1-halo-1-methyl-2,2-diphenylcyclopropanes, retention of configuration (per se) cannot be regarded as evidence of surface adsorption of an intermediate radical [7,10].

(e) The mechanisms of reductions of 1-halo-1-methyl-2,2-diphenylcyclopropanes are complex and are not understood with confidence. It is dangerous to use Grignard reactions of these halides as models for others or to generalize conclusions drawn from their reactions. Until their reductions are better understood, these halides will

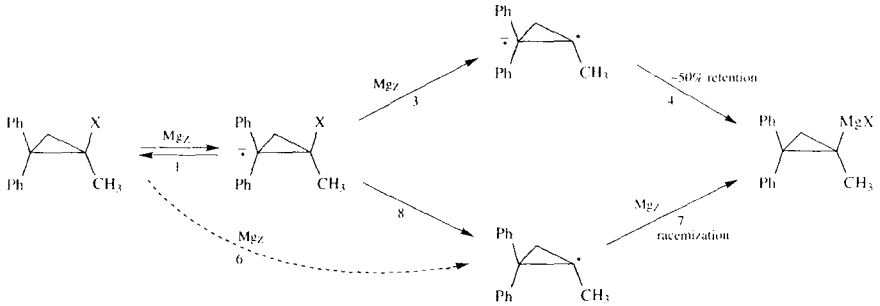

SCHEME 7.2

remain unsuitable as probes of the mechanism of Grignard reactions of other types of halides.

(f) Even so, the known data on extents of retention of configuration in reductions of 1-halo-1-methyl-2,2-diphenylcyclopropanes can be rationalized by a minimal mechanism consisting of pathways 1-3-4 and 1-8-7 of Scheme 7.1. Pathway 1-6-7 may also be significant.

(g) On this basis, a minimal mechanism of Grignard reactions of 1-halo-1-methyl-2,2-diphenylcyclopropanes can be postulated (Scheme 7.2).

Here step 6 (dashed arrow) may not be necessary. This resembles the mechanism of Walborsky, differing from it mainly in introducing an intermediate $*R^-$ (product of step 3) that partially racemizes and allowing R• to diffuse in solution instead of remaining adsorbed at MgZ.

7.2.22 Retention of Configuration, Adsorption of R•, and the D Model

Retention of configuration could result from:

(a) a pathway **X** without an intermediate R• (e.g., **Xa** or **Xb**, Section 7.1.3);
(b) a sufficiently short lifetime of R•, as in a geminate reaction at an active site (pathway **Xc**, Sections 7.1.3 and 7.3.11);
(c) a retention reaction of RX with a product (ruled out in some cases by control experiments; Section 7.2.9);
(d) a retention reaction of RX with an intermediate, such as ZMgMgZ (Z = R or X) (pathway **Xd**, Sections 7.1.3 and 7.3.8);
(e) a viscous or 'frozen' environment adjacent to MgZ, which could slow the rotational relaxation of R• (Section 7.3.10); or
(f) adsorption of R• slowing its rotational relaxation.

None of these has been ruled out rigorously in every case. However, a pathway **Xa** or **Xb** may best satisfy Occam's Razor.

Alternative (f) is among the least likely. This conclusion merits detailed consideration.

In the A model, R• *remains* adsorbed until it suffers **r**. In a D model, *transient* adsorption is possible, although it has not been included thus far in calculations. Provided that the only processes of transiently adsorbed R• are **r** and desorption, product distributions will be independent of whether or not there is adsorption.

Ideal D-model calculations fail to account simultaneously for the extents of retention and by-product formation (Section 7.2.9). The equivalence of equations (7.25) and (7.53) shows that this defect in D-model calculations can be repaired by assigning the initial encounter of R• and MgZ a higher reaction probability than later ones, as in the freckles model with geminate reaction (Section 7.3.11).

Even so, there are strong arguments against a role for surface adsorption of R• in retention of configuration. (1) Retention appears to

correlate with conjugation in the substrate. Adsorption provides no explanation. (2) In the Grignard reaction of 1-iodo-1-methyl-2,2-diphenylcyclopropane in THF (Section 7.2.9) there is almost complete racemization (2% retention). An analogous reaction of 1-fluoro-1-methyl-2,2-diphenylcyclopropane with Li also gives almost complete racemization (3% retention, Table 7.7). Even though the opportunity is presumed to exist for the adsorption of R• to inhibit racemization in these cases, it doesn't. Why should it in others? (3) Retention is observed in homogeneous reductions, where there is no solid surface for R• adsorption (Section 7.2.21).

7.2.23 Arguments Against the D Model

A number of arguments have been raised against the D model [7,10]. None is both valid and compelling.

(1) The ratio **c/s** in Grignard reactions does not match expectations based on studies in which the same radicals are 'in solution.' Therefore Grignard radicals do not enter the solution.

For typical alkyl bromides and iodides, **c** dominates over **s**. Kharasch and Reinmuth assumed that intermediate alkyl radicals R• in solution would not live long enough to undergo much **c** because they would be consumed by **s** [1]. Accordingly, they suggested that they remain adsorbed at Mg_Z, where they are sufficiently mobile for **c**.

This argument is vitiated by its false premise, which is based on data for reactions in which radicals are generated in homogeneous solutions, where **s** is very important. The ratio **c/s** is proportional to [R•]. The argument of Kharasch and Reinmuth does not take into account that [R•] for diffusing Grignard radicals near Mg_Z can be larger than for radicals generated homogeneously by a factor that can approach 10^4 [74,84].

Figure 7.33 shows the relevant reaction scheme and the results of some steady-state calculations. For the homogeneous-solution values shown, the rate ratio **c/s** is about 1. If k_S were larger, due to a higher temperature or a more reactive radical, then **c/s** would be proportionally smaller—for $k_S \geq 10^6$ s^{-1}, appropriate for cyclopropyl or phenyl, **c/s** $\leq 3 \times 10^3$ [R•], smaller than values for typical alkyl radicals by a factor of 10^{-3}. Further, an r-value 10^{-3} M s^{-1} (Figure 7.33) corresponds to a 1-M first-order source with a half-life of ~12 min. If r were smaller, **c/s** would also be smaller because the steady-state [R•] would be smaller. Consequently, for most homogeneous reactions of interest, 1.1 is an approximate upper limit of **c/s**.

In contrast, in Grignard reactions [R•] can approach 10^{-3} M near Mg_Z, making **c/s** tens to thousands of times larger than in homogeneous-solution reactions (Figure 7.33). D-Model calculations predict correctly that **c** will be significant, and **s** not, in Grignard reactions of typical alkyl halides [74,84].

(2) The extents of first-order reactions of R•, such as solvent attack and isomerizations, are much

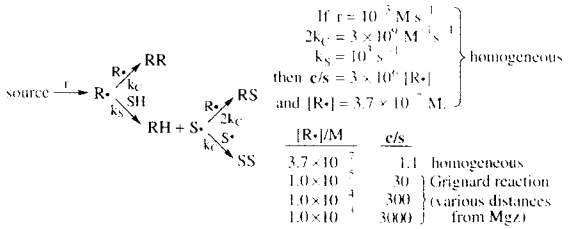

If $r = 10^{-3}$ M s^{-1}
$2k_c = 3 \times 10^9$ M $^{-1}$ s^{-1}
$k_S = 10^3$ s^{-1}
then **c/s** $= 3 \times 10^6$ [R•]
and [R•] $= 3.7 \times 10^{-7}$ M.
} homogeneous

[R•]/M	c/s	
3.7×10^{-7}	1.1	homogeneous
1.0×10^{-6}	30	Grignard reaction
1.0×10^{-4}	300	(various distances
1.0×10^{-3}	3000	from Mg_Z)

Fig. 7.33. Kinetics of radical coupling/disproportionation **c** and solvent attack **s** for radicals generated homogeneously in solution. The computations are for the indicated rate-parameter values; r is the rate of homogeneous formation of R• and **c** and **s** are yields. The table includes values of [R•] (10^{-5}–10^{-3} M) near Mg_Z in a Grignard reaction of a typical alkyl halide, according to the D model.

less in Grignard reactions than for radicals 'in solution.' Therefore Grignard radicals don't enter the solution [7,10].

5-Hexenyl is one example of many. When generated in an ether, the extent of cyclization is near 100% [122]. In Grignard reactions of 5-hexenyl halides, the extent of cyclization is ~3–10% [38,53-58]. Thus, 5-hexenyl Grignard radicals behave differently from those generated homogeneously in solution.

This argument is also based on the false premise that Grignard radicals that leave Mg_Z would behave like those generated homogeneously in solution. If the lifetime of a 5-hexenyl radical generated homogeneously in solution were limited by its reaction with solvent DEE ($k_S = 10^3$ s^{-1}) [13], it would be 10^{-3} s. Since the cyclization rate constant k_1 is 4×10^5 s^{-1} (at ~40°C) [86], almost all radicals would cyclize before attacking the solvent, as is observed [122]. The **r**-limited, D-model lifetimes of Grignard radicals are 10^{-7} s (Section 7.2.8), so little 5-hexenyl cyclization is expected and little occurs. For the same reason, **s** is insignificant.

A successful argument of type 1 or 2 must be quantitative—qualitative arguments can be treacherous. For example, the inefficiency of trapping of intermediate 5-hexenyl radicals by DCPH (efficiency ≤25%) has been cited as evidence for the A model in the belief that DCPH would trap radicals in solution with ~100% efficiency [7,10]. Actually, the data are quantitatively consistent with the D model (Figure 7.18). Similarly, it has been suggested that the product distribution from the Grignard reaction of (2-phenylcyclobutyl)methyl bromide, studied by Hill *et al.* [44], might support the A model [11]. Hill finds 25–45% ring-opening in the Grignard reagent formed in DEE and 60–80% in THF. From these values and Figure 7.16, the implied values of k_1 (rate constant for ring opening in R•) are in the range 10^7–10^8 s^{-1}. This agrees with the value $8 \times 10^7 s^{-1}$ determined by Hill *et al.* at 80°C by an independent method. Thus, Hill's results agree at least semi-quantitatively with D-model predictions. In fact, Hill *et al.* found other evidence of diffusing radicals in their work [44].

For every case of a typical alkyl radical that has been treated quantitatively, the D model accounts well for the observed product distribution. We are not aware of any case where the observed differences in behavior between Grignard radicals and those generated homogeneously cannot be understood in terms of the D model.

Even when a quantitative argument of type 2 is given, a D-model failure can merely indicate that pathway **R** does not described the whole reaction—the D model could still apply to the part through pathway **R**. There is confusion in the literature over this and the Walborsky mechanism. '[The A] model supposes that the intermediate radical interacts with the surface of magnesium to explain why the radicals generated from optically active alkyl halides partially retain their configuration' [131]. Although Walborsky's proposals have varied, in recent versions of his mechanism he does not invoke adsorption of R• to explain the majority of retention [7,10,20]. Instead, he supposes that adsorbed radicals racemize and invokes a pathway **X** to explain most retention.

For cyclopropyl, vinyl, aryl, and other unsaturated systems, ideal D-model calculations fail in one of two ways (Sections 7.2.9–7.2.11). (a) If it is assumed that $\tau_R = 10^{-7}$ s (experimental value for typical alkyl halides), then much more isomerization is calculated than observed. (b) If τ_R is adjusted to fit the data, then unrealistically small values sometimes result. One possible explanation is that a pathway **X** competes with a D-model pathway **R**.

Legitimate arguments against the D model must address the nature of pathway **R**, not the question whether or not it accounts for the entire mechanism. This principle has not always been followed [7,10,20].

Thus, according to one report [165], reactions of *exo*- and *endo*-norbornyl bromides at −70°C give different distributions of Grignard reagents, contradicting the D model, which predicts the same distribution. Even if these findings were correct, they would point to a pathway **X** and not invalidate the D model for the **R** part of the reaction.

In fact, there are serious questions about the findings. For similar reactions at room temperature, experimental error can reasonably include the observed product differences for exo and endo reactants [165]. For the same reaction at 0°C, Root found the same product ratio in reactions of *exo*- and *endo*-RBr, different from the ratios reported by Walborsky [85].

The Walborsky mechanism provides three possible explanations of partial retention, adsorption of R•, pathway **X**, and ultrafast [R• •MgX] collapse. Deciding among them, or partitioning their effects, is a legitimate problem but not one considered by Walborsky, who has opted recently for a retention pathway **X** [7,10,20].

(3) '... strongest support for the A-model comes from using a perdeuterated ether solvent or a radical trap deuterated dicyclohexylphosphine. In all cases, only a small percentage of the radicals leave the surface of magnesium to yield the deuterioalkane' [131].

Reaction of cyclopropyl bromides are especially significant here, since cyclopropyl radicals are much more reactive in H-atom transfer reactions than typical alkyl radicals, so that extensive trapping by DCPH(D) would be expected but is not found [166]. Even so, this evidence is weak for a number of reasons.

First, the extent of solvent attack in cyclopropyl bromide reactions is quantitatively consistent with the D model (Figure 7.25) [52,97].

Second, the notion that there should be solvent attack if R• leaves Mg_Z is fallacious (argument 2). It could be true that 'only a small percentage of the radicals ... yield the deuterioalkane' and false that 'only a small percentage of the radicals leave the surface' [131].

Third, in interpreting their data, Walborsky and co-workers assume that solvent attack is the exclusive and inevitable fate of radicals that leave Mg_Z [166]. This is inherent in the Walborsky mechanism, in which **s** does not compete with **r**, **c**, or any other reaction, implying that the yield of RD in a deuterated solvent will represent the extent of solvent attack in the corresponding undeuterated solvent [7,10,20]. Indeed, the Walborsky mechanism predicts that deuterating the solvent will have no effect at all on the product distribution.

This is contradicted by experimental data [97], including the findings of Walborsky and Aronoff for the reaction of 1-bromo-1-methyl-2,2-diphenylcyclopropane in THF [20]. The apparent support provided by data for the reaction of the same bromide in DEE [20] would probably have disappeared if RR and products containing S had been determined.

In fact, deuterating the solvent reduces the extent of solvent attack in every case that has been examined and increases the yield of RMgX in most cases [97]. Thus, the yield of RD in a deuterated solvent is not a measure of solvent attack in the undeuterated solvent.

In general, Walborsky's interpretations of trapping and solvent attack are based on the 'black-and-white' premise that they are exclusively and inevitably reactions of radicals that leave the surface and are not competitive with any other reactions. This view is refuted by the experimental data. Actually, trapping and solvent attack are competitive with **r** and **c**.

Fourth, for reasonable values of k_D/k_H for solvent attack (~6), D-model calculations correctly predict the magnitudes of solvent isotope effects on product distributions (Section 7.2.9) [97].

Fifth, the experimental method used by Walborsky and co-workers for determining CpD (and CpH) is suspect [166]. The reported yields vary by as much as a factor of two. For the following reasons, they are probably significantly low.

CpD and CpH were determined by PFT ^{1}H NMR after gas-phase transfer and trapping. Such procedures are notorious for losses. Further, 5-s delays between pulses, the method used, are probably inadequate—small, rigid hydrocarbon molecules tend to have unusually long spin-lattice relaxation times. No experiments validating the method were reported [166]. We find increases of a factor of two in the areas of cyclopropane peaks, relative to other components of reaction mixtures, when the pulse delay is increased from 5 to 60 s [88].

These concerns apply to all of the determinations of CpH and CpD reported by Walborsky [166], not only those for CpD from reactions in DEE-d_{10}. Specifically, they apply also to CpH from reactions of CpBr in DEE and THF and to CpD from similar reactions in the presence of DCPD.

Sixth, some of the data for DCPD trapping are internally inconsistent. (a) Walborsky and Zimmermann report the formation of 22% CpH and 4% CpD in reactions of CpBr in DEE containing DCPD [166]. Their interpretation is that only 4% of the reaction is through Cp• that leave Mg_Z. If this were true then DCPD would not have interfered with CpMgBr formation. Yet they find only 6% CpMgBr (compare 18–31% in the absence of DCPD). Something is wrong with the analyses, the assumed chemistry, or both. (b) The reaction of 1-bromo-1-methylspiro[2,5]octane in DEE in the presence of DCPD is reported to give 1-methylspiro [2,5]octane with 6% incorporation of deuterium, while the similar reaction in DEE-d_{10} gives this product with 18% incorporation of deuterium [21]. This implies that DEE-d_{10} is a better radical trap than DCPD, which is not consistent with other experience. These discrepancies are a clear indication of problems with these experiments.

Part of the problem may lie in the chemistry of trapping by DCPH(D). We find that cyclopropylcyclohexylphosphine is a major product when Mg reacts with CpBr in DEE containing DCPH [88]. However it may arise, it is not a product of a simple trapping process. Until inconsistencies and uncertainties are resolved, interpretations of DCPH trapping data for Grignard reactions of cyclopropyl halides must be postponed.

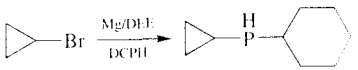

Seventh, for typical alkyl halides, radical trapping data for both DCPH and TMPO• conform to the D model with the value of τ_R near 10^{-7} s (Figure 7.18). The complications that may invalidate DCPH(D)-trapping results for cyclopropyl bromides may not occur with typical alkyl halides.

(4) '[Whitesides and co-workers] merely plotted the yield of product from the reaction of cycloheptylbromide [sic] with magnesium in the presence of TMPO• and *t*-amyl alcohol as a function of time, observed the formation of 95% TMPOc-C_7H_{13}, stated that these results were incompatible with a surface-bound radical and concluded that 95% of the cycloheptyl radicals were free, thereby ignoring processes that compete with trapping by the TEMPO [sic] radical...Mg^0 reduces TMPO• to the anion...oxidation of Grignard reagents in the presence of such agents is also well documented... Consequently, one is left with the question of what species has actually reacted with TMPO• and these experiments do not answer the question of what percentage of radicals leave the surface during Grignard reagent formation' (Hamdouchi and Walborsky, pp 203–204) [10].

This could be misleading. In fact, Whitesides and co-workers considered the complicating processes in great detail [15]. They did many control experiments, and devoted considerable effort to developing reaction conditions under which undesired reactions leading to TMPOR were avoided. Walborsky gives no explanation of how he thinks these measures might have failed. Both the internal consistency of the data and its consistency with the D model and DCPH trapping results (Figure 7.18) support Whitesides' interpretation of the data.

(5) Photolysis of an azo compound RNNR in solution in a slurry of Mg containing gives evidence of the formation of radicals R• but does not yield RMgX, even when $MgBr_2$ is present [167]. This shows that radicals formed in solution which do not diffuse to the Mg surface suffer **r** there.

Such experiments would have been significant if positive results had been obtained. However, negative results are meaningless. There is no assurance that the conditions for RMgX formation, some possibly unknown, are met.

One recognized condition is common to the D and A models: R• must be at Mg_Z in order to be reduced to RMgX. We can estimate the probability that a radical reaches Mg_Z in experiments like those reported.

In four of five experiments reported, Mg powder of unknown particle size was used [167]. In the following calculations, we assume spherical particles of 25 μm radius R, corresponding to a barely visible particle and consistent with commercial Mg powder examined in our laboratory.

For a radical of negligible radius at an initial separation s from the surface of a spherical particle, the probability ϕ that the radical will reach that surface, instead of reacting with the solvent, is given by equation (7.52) (Appendix, Equation A.7.25)

$$\phi = \frac{R}{R+s}\exp[-s(k_S/D)^{1/2}] \qquad (7.52)$$

For $s = 10^5$ Å, $k_S = 10^3$ s^{-1}, and $D = 3 \times 10^{-5}$ cm^2 s^{-1}, $\phi = 0.0022 = 0.22\%$. Thus, at least 99.78% of the radicals that are formed 10^5 Å or more from the surface of the magnesium particle, will never reach it. The slurries consisted of 1.25 mol Mg for 1 L solution. The total volume of solution within 10^5 Å of all of the Mg particles is 30.5 cm^3, about 3% of the total volume of solution. Thus, at least 97% of the radicals are generated at a distance of 10^5 Å or more, and >99.78% of these never reach the surface of a magnesium particle. Continuing this calculation for larger shells leads to the estimate that only 0.8% of the free radicals generated ever reach the magnesium surface [102]. In addition, the data indicate that about half of the radicals undergo geminate reactions and are not available for Grignard reagent formation. Therefore the maximum yield of Grignard reagent that could be formed in these experiments is estimated as ~0.4%. It is not surprising that none was detected.

One experiment (only) used Rieke magnesium, assumed to have an average radius R of 5×10^{-6} cm (0.05 μm) [167]. Calculations for this case indicate that a significant, though not necessarily large, fraction of the radicals could reach a magnesium surface [102]. Rieke Mg was used without additives, specifically, without added $MgBr_2$. Added $MgBr_2$ could be necessary for RMgBr formation in this experiments, or there could be some other unmet requirement.

The question 'Can radicals diffuse to the surface of magnesium and be converted to Grignard reagents?' is answered firmly and affirmatively in the literature. Triphenylmethylmagnesium bromide or iodide in DEE can be prepared in high yield by a reaction of triphenylmethyl with magnesium in the presence of $MgBr_2$ or MgI_2 (Kharasch and Reinmuth, pp 86–87) [1]. Definitive evidence is also provided by solvent isotope effects on RMgX yields (Section 7.2.9) [97]. Additional highly persuasive evidence is provided by the excellent fits of experimental data to D-model computations (Section 7.2.8) [83].

(6) '... early in the reactions of alkyl halides with magnesium, reactive sites are quite small and diffusion of reactants and products is spherical, rather than linear. As the sites grow larger, convection and linear diffusion contribute significantly and mass transport is very complex, so it is remarkable that a model assuming linear diffusion can so accurately predict product ratios' [168].

These comments have been interpreted as a basis for questioning the D model (Hamdouchi and Walborsky, p 109) [10]. Actually, there is nothing 'remarkable' about the ability of equations of 'linear diffusion' to predict product ratios in Grignard reactions. Even though the reactive surface is surely not a uniform plane, this model would be expected to give accurate predictions of product distributions, provided the mechanism were correct, for the following reasons.

In polycrystalline Mg, hemispherical corrosion pits form, grow, overlap, and coalesce, all early in the course of a typical reaction [119,168]. Although the characteristic diffusion distance σ_R of R· in a typical Grignard reaction is only ~100 Å, D-model calculations show that the region of significant c extends a few thousand Å away from the magnesium surface, with a large majority of the products being formed within ~5000 Å of the surface. This suggests that a planar surface approximation for a reactive pit can be expected to be adequate when the diameter is ~50 000 Å or greater, and perhaps for smaller pits. The fraction of the products formed in reactions of such pits of less than 50 000 Å diameter is probably very small.

Indeed, the *smallest* pits observed by Koon *et al.* were 300 000-Å diameter, and their observations were clearly in the initiation phase of reaction. The issue disappears when the magnesium is allowed to react with 1,2-dibromoethane, effecting some chemical polishing, before the reaction is carried out, or as an initiating co-reactant.

The 5-hexenyl-bromide experiments of Bickelhaupt and co-workers [48], which are fit by D model calculations (Figures 7.20 and 7.21). [83] involve very high initial concentrations of RBr (>2 M) and the inclusion of 1,2-dibromoethane. The fraction of products formed in pits smaller than 50 000 Å is probably vanishingly small.

(7) Other arguments against the D model have been based on experiments in alcohol solvents [10,109,151]. The relevant observations for the reaction of Mg with (+)-1-bromo-1-methyl-2,2-diphenylcyclopropane in CH_3OD are retention of configuration (23% optical purity) and absence of products RH and RR of **s** and **c**, respectively.

Even if the reactions are precise analogs of Grignard reactions in ethers, the data do not speak to the issue for reasons given above. They may not be precise analogs—it is reported that the presence of an alcohol in a reaction in an ether can perturb the product distribution [44]. Even so, reactions of Mg with a simple alkyl halide in methanol give both RH and RR, just as observed for a typical Grignard reaction [34]. It is possible that the very high polarity of CH_3OD promotes pathway **X** for cyclopropyl halides but that **X** is not available for a typical alkyl halide.

7.2.24 Arguments Against the A Model

The A model for pathway **R** is unnecessarily complex, has weak predictive power, and is not consistent with experimental facts. The D model for pathway R is simpler, has quantitative predictive power, agrees quantitatively with a large body of data, and is not inconsistent with any experimental facts.

7.3 INORGANIC PART OF THE MECHANISM

7.3.1 Optical and Scanning-Electron Microscopy

Hill, Vander Sande, and Whitesides examined Mg_Z after its reactions with RX, using optical and scanning-electron microscopy [119]. Single crystals, purity 99.999 + %, with selected planes exposed, were used in most experiments. 'The surface of a pure metal is a mosaic of atomic and macro ledges and grain boundaries. Initially, magnesium metal is also covered by a film composed of magnesium oxide and magnesium hydroxide. To remove the oxide film and to decrease the density of defects generated in producing the surface, we polished the surface by using 6% aqueous nitric acid at 0°C. This treatment produced a surface having a low 'pitting factor' (the ratio of the deepest metal penetration to the average metal penetration).'

We now know that the adventitious film is largely $Mg(OH)_2$ and that polishing Mg with aqueous HNO_3 leaves a reconstituted $Mg(OH)_2$ surface (Section 7.3.3). Such polishing smoothes the surface and probably reduces the densities of defects at both the Mg–$Mg(OH)_2$ interface and the $Mg(OH)_2$ external surface.

A typical reaction follows a three-stage course. (1) Corrosion pits form at a number of points. (2) They grow and eventually overlap. (3) Further reaction polishes the surface [119].

When single-crystal spheres of Mg were allowed to react with 0.05 M ethyl bromide in THF at 0°C, clearly defined crystal planes and geometric shapes did not develop. This shows that there is no strong preference for reaction at any particular crystal plane [119].

In reactions at defined crystal planes, RCl (more than RBr) gives pits with planar sides. The basal plane (0001), especially, gives hexagonal pits with planar sides. The difference in pitting selectivity is maintained even when RCl and RBr react at the same rate, but it vanishes when $MgBr_2$ is added to the RCl solution. Thus, benzyl chloride/$MgBr_2$ reacts pit in the same manner as benzyl bromide/$MgCl_2$ reactions. With polycrystalline Mg,

there are no indications of reactivity differences when pits span grain boundaries [119].

The pitting studies admit two conclusions. (1) There is a small preference for loss of Mg along crystal planes. This shows that R• does not bond permanently wherever it happens to collide with Mg_Z. (2) The halide ion in solution influences the course of the loss of Mg. This is consistent with the conventional metallic corrosion mechanism in which metal cations are lost to solution at anodic sites (Sections 7.1.3 and 7.3.7, Figures 7.1 and 7.39) [119].

Activation by I_2, Br_2, or tetraethyl orthosilicate affects the rate of initiation without affecting the initial pit density, indicating that these activators do not introduce new sites for initiation. These and other experiments suggest that initiation occurs at surface defects [119]. It is not clear whether these are defects in the $Mg(OH)_2$ surface or in the underlying Mg surface. Defects in the $Mg(OH)_2$ film could allow the penetration of the solution to Mg_Z.

In related studies with mechanically polished polycrystalline Mg strips, Teerlinck and Bowyer made *in situ* photomicrographic observations in flow systems in which ethyl bromide was allowed to react in THF, apparently at ambient temperatures [169]. In some experiments, they used a chemical indicator for RMgBr that requires the presence of O_2. They also observed pit formation without the indicator.

After 4–8 min of reaction, pits grow but no new ones form. Pit distributions cannot be distinguished from random, suggesting that there is neither inhibition nor autocatalysis of pit formation near one that has already formed [169]. These observations are consistent with those of Whitesides and suggest crystal dislocations or microcrystalline impurities as sites of initiation. Surprisingly, however, scratching the Mg surface with a stainless steel scalpel does not increase pit density, even though pits do form preferentially in the scratches [169].

Chemically polishing with aqueous HNO_3 increases the initiation time and decreases the reactive site density [169]. As noted above, this procedure leaves an $Mg(OH)_2$ surface, not exposed Mg.

I_2 is an especially good activator. When a strip is spot treated with 2% I_2 in THF, it is activated in areas as much as 2 mm from the spot, reflecting the diffusion of some activating species [169]. This might be I_2, as suggested by Teerlinck and Bowyer, but it also might be MgI_2, which is well known for its activating influence (Sections 7.3.5–7.3.6).

7.3.2 Atomic-Force Microscopy (AFM) [170]

Preliminary AFM studies show corrosion along crystal planes (Figure 7.34) [171]. In these μ-scale

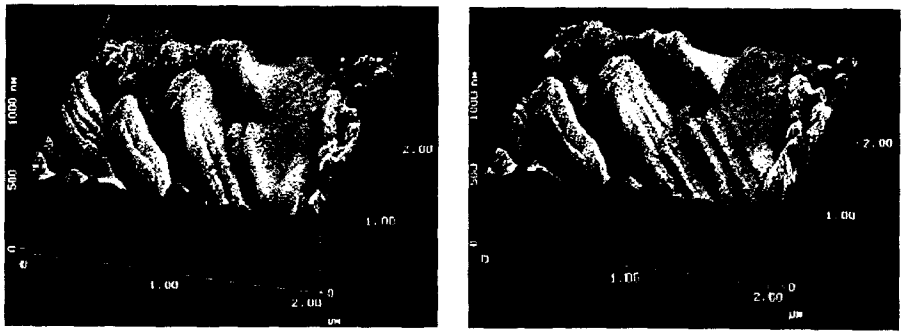

Fig. 7.34. μ-Scale AFM images, four minutes apart, of part of a single-crystal Mg_Z (0001) undergoing reaction with *n*-hexyl bromide in THF at room temperature [171].

images, taken *in situ* as the reaction of *n*-hexyl bromide in THF was proceeding at a mechanically and chemically (aqueous HNO_3) polished basal plane (0001) of a single crystal of Mg, the amorphous 'hills' at the right side and upper left corner of the left image could be $Mg(OH)_2$ that had not been completely removed by the Grignard reaction. Four minutes later, another image (right) shows distinct changes in the middle region, where corrosion is occurring, but little change in the 'hills.' This could be a picture of the boundary of a reactive site, showing exposed Mg (center) and remaining $Mg(OH)_2$ (right and upper left). No independent facts confirming this possible interpretation have been obtained.

7.3.3 Surface Spectroscopy [172]

XPS studies of polycrystalline Mg reveal ^-OH, but no O^{2-}, on a surface that has been chemically polished with 6% aqueous HNO_3 (Figure 7.35). Baking at 450°C generates O^{2-} at the expense of ^-OH, and subsequent exposure to air reverses this change (complete reversal takes ~4 days). Similar results are obtained for mechanically polished Mg and Mg 'out of the bottle.'

Mg turnings give XPS peaks for HCO_3^- but not CO_3^{2-} (Figure 7.36).

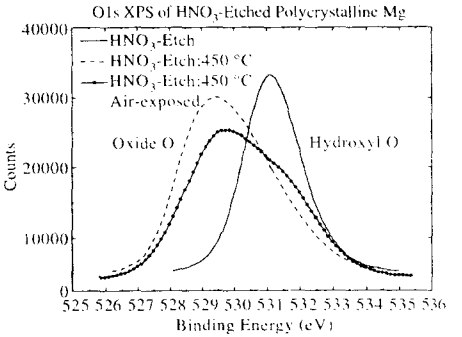

Fig. 7.35. Oxygen-1s XPS spectrum of polycrystalline Mg foil after subsequent treatments: (1) 30-s exposure to 6% aqueous HNO_3; (2) baking at 450°C; and (3) 24-hr exposure to air. From Abreu *et al.* [172]. Reproduced by permission. Copyright 1998 Academic Press, Inc.

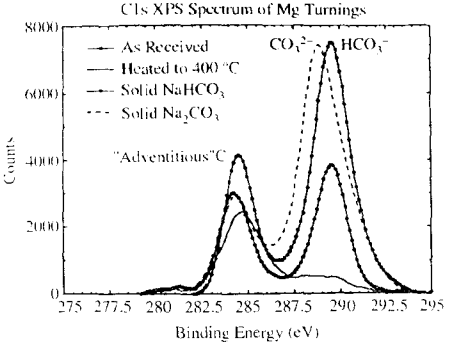

Fig. 7.36. Carbon-1s XPS spectra for $NaHCO_3$, Na_2CO_3, and polycrystalline Mg turnings, as received and after baking at 450°C. 'Adventitious C' may be due to hydrocarbons. From Abreu *et al.* [172]. Reproduced by permission. Copyright 1998 Academic Press, Inc.

Quantitative measurements indicate that the anions of the near-surface layers are no more than 25% HCO_3^-.

7.3.4 Initiation

The induction period is especially annoying when it is erratic, prolonged, or apparently infinite. Plausible hypotheses abound [1,2], but there is no comprehensive, documented understanding of the factors that create the induction period or constitute initiation. The hypotheses in the following list are not all distinct.

(I) Initiation consists of the removal of $Mg(OH)_2$, which is passivating, thereby exposing Mg for reaction.

(A) $Mg(OH)_2$ passivates by acting as a physical barrier preventing RX/SH from reaching Mg_Z.

(B) $Mg(OH)_2$ passivates through electronic effects resulting from its interactions with Mg_Z.

(C) Removal of $Mg(OH)_2$ is by corrosive undercutting. It is not very soluble in ethers, so it flakes off, possibly with some Mg metal attached, as corrosion undercuts the $Mg-Mg(OH)_2$ interface.

(D) Removal of $Mg(OH)_2$ is by dissolution. It is promoted by polar solutes such as MgX_2, $RMgX$, and soluble alkoxides. Dissolution may be very

slow at first, but as the reaction proceeds it accelerates.

(II) Initiation consists of the penetration of the passivating $Mg(OH)_2$ layer, thereby delivering RX to Mg_Z for reaction. It is penetrated at weak points, i.e., channels or other imperfections.

(A) Penetration is enhanced by the increased polarity of the interfacial liquid due to polar solutes such as MgX_2, RMgX, and soluble alkoxides. More polar liquids wet the $Mg(OH)_2$ layer better.

(B) Once penetration has occurred, $Mg(OH)_2$ is removed by corrosive undercutting (Figure 7.37) or dissolution (IA or IB above).

(III) Initiation consists of autocatalytic active site generation. An exposed area of Mg could constitute an active site, as assumed in I, but an active site could also be a more specialized interfacial structure.

(IV) Initiation is an autocatalytic increase in the exposed Mg surface area. Removing $Mg(OH)_2$ increases the exposed surface area, but so could corrosion of a clean spot on Mg_Z to form a more convoluted surface.

(V) Initiation is the autocatalytic formation of MgX_2, RMgX, or both There is evidence in some cases that the earliest stages of reactions may give higher yields of MgX_2 than later stages. MgX_2 and RMgX could be catalytic in several ways.

(A) Their generation converts a less polar liquid at the interface with Mg_Z into a more polar one.

(1) The rate of the reaction of RX with Mg_Z increases in a more polar liquid environment.
   (a) A more polar liquid environment increases the reduction potential of Mg_Z by promoting the dissolution of Mg_2^{+}.
   (b) A more polar liquid stabilizes the transition state for the reaction of RX with Mg_Z.
(2) A more polar interfacial liquid depassivates Mg_Z by dissolving $Mg(OH)_2$.
(3) A more polar interfacial liquid promotes the penetration of $Mg(OH)_2$ and its removal by corrosive undercutting.

(B) There is a specific effect of MgX_2 or RMgX as a catalyst.

(1) The reaction is initiated by •MgX, which is formed from Mg^0 and MgX_2.
(2) The reaction of a complex, e.g., $RXMgX_2$, is faster than that of RX.

(VI) Initiation is the removal of impurities that consume RMgX as it is formed.

(VII) Initiation is the removal of impurities that inhibit the radical chain reaction in which RMgX is formed.

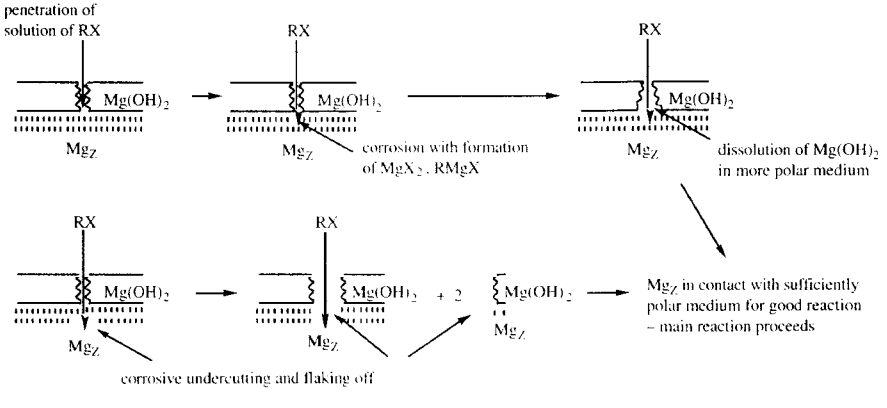

Fig. 7.37. Penetration followed by dissolution or undercutting and flaking of $Mg(OH)_2$ layer. These events could be autocatalytic, increasing the number of reactive sites, their effective areas, and the reactivity of RX at a site.

Reactions with ordinary magnesium ('Grignard' grade) may sometimes initiate better than those of purer forms [1]. Traces of transition-metal impurities such as iron may be responsible. At low levels, such impurities appear not to affect the product distribution adversely, but at higher levels secondary reactions can reduce yields of RMgX [1,16,173,174]. Surface impurities could be sites of initiation.

Tuulmets and co-workers have investigated quantitatively the extension of the induction period by protic additives (water, alcohols) [175,176]. They take as the end of the induction period the disappearance of the color of a trace of added I_2.

For reactions in DEE, the induction period is extended by the same period of time for the same infinitesimally small molar amount of any protic additive. These additives are supposed to react with RMgX as it is formed, adding to the burden of other inhibitors, with similar actions, that are present adventitiously. It is supposed that the rate of the Grignard reaction is constant, or nearly so, during the induction period. RMgX is supposed to act to remove the 'oxide' [actually $Mg(OH)_2$] layer, and as long as RMgX is being destroyed as it is formed, no such action takes place, leaving the active area of Mg_Z constant, and relatively small, during the induction period [175,176].

Although these hypotheses are plausible, the data are also consistent with others. Whatever the mechanism of initiation, RMgX will be formed at the same rate at the end of the induction period, provided that very small amounts of additives do not interfere with or alter the normal initiation processes.

Interesting results are obtained with larger amounts of added protic compounds. [175,176]. Some additives, e.g., water and lower alcohols, increase the induction period non-linearly, with increased amounts having larger effects, per unit. This effect is 'obviously caused by the formation of insoluble products' [Mg(OH)Br, Mg(OR)Br] of the reactions of the additives with RMgX. The insoluble products 'deposit on the surface of the metal' and 'can stop up holes in the oxide film.'

Some additives, e.g., *n*-butyl alcohol, have the opposite effect. Increased amounts effect smaller increases in the induction period. This may indicate that the soluble alkoxide products Mg(OR)Br/-$Mg(OR)_2$ 'can, to some extent, dissolve magnesium oxide [really hydroxide] and thus promote the initiation' (Section 7.3.5) [175].

7.3.5 Activation

The initial rate of a Grignard reaction is expected to be increased by increasing the area of Mg_Z, cleaning it, and introducing reactive sites. These considerations underlie the use of Mg in clean, finely divided forms. Rieke magnesium (μm-scale particles) is formed by reducing MgX_2 in a homogeneous solution [177,178]. Atomic clusters Mg_n (Å-scale particles) are formed by evaporating Mg and condensing it in a suitable solvent [133,179]. The efficacy of finely divided Mg in promoting stubborn reactions and limiting secondary reactions of RMgX with allylic or benzylic RX supports the underlying hypotheses [131,132,177,178].

Mechanical activation of Mg by stirring pieces dry under an inert atmosphere is probably related. Optical and electron microscopy shows that stirring 'causes fragmentation and then further cleavage to form microcrystalline magnesium particles which adhere to the surface. These processes enhance the surface area of oxide-free magnesium when the dry-stir procedure is performed under an inert atmosphere' [118]. Whether or not this interpretation is correct in detail, Mg activated in this way is especially useful for limiting secondary reactions in preparations of allylic or benzylic Grignard reagents [118].

Sonication promotes initiation but does not always influence yields [16,180–183]. It probably involves cavitation at the metal surface, which could have effects on surface-cleansing, local temperature and pressure, and diffusion.

Rieke magnesium contains MgX_2 [178]. Its role in promoting Rieke-magnesium Grignard reactions is not clear, but it could be catalytic.

Among the earliest methods of activation are the addition of I_2 and the preparation of Mg/MgI_2 (Gilman's catalyst) [1,178]. It was proposed that I_2 reacted with Mg to etch it [1], thereby cleaning its

surface. The fact that using a preformed solution of MgI_2 in DEE has essentially the same effect as adding I_2 to the reaction mixture casts doubt on the 'doctrine of etching' [1,184]. The efficacy of Gilman's catalyst may lie in the presence of MgI_2. In DEE $MgBr_2$ can have a similar effect [98], as does $MgCl_2$in THF [88].

The effects of initially added $MgBr_2$ to DEE can be dramatic [98]. Figure 7.38 shows that 0.18 M $MgBr_2$ in DEE eliminates the induction period for the Grignard reaction of cyclopropyl bromide. Other salts, such as $FeCl_3$ [169], can also promote initiation (Section 7.3.4).

Where no reaction occurs in the absence of MgX_2, its presence sometimes allows a useful reaction. Thus, neither pentamethylphenyl bromide nor 2,2,3,3-tetramethylcyclopropyl bromide initiate in DEE, but in 2.6 M $MgBr_2$/DEE they react smoothly [98]. In the early twentieth century, the former substrate was a test case for activation methods, particularly entrainment (Section 7.3.6) [1].

The 'doctrine of etching' is further invalidated by experiments with 2,2,3,3-tetramethylcyclopropyl bromide [98]. (1) Reaction begins immediately when a 2.6-M solution of $MgBr_2$ is prepared *in situ* (from 1,2-dibromoethane and excess Mg) and

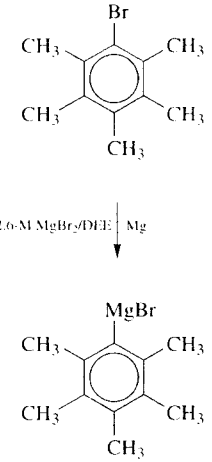

49-80%

RBr is then added. 'Etched' Mg and $MgBr_2$ are both present initially. (2) The reaction fails to initiate when $MgBr_2$ is prepared *in situ*, the $MgBr_2$ solution replaced with pure DEE, and RBr added. 'Etched Mg'is present initially, but $MgBr_2$ is not. (3) The reaction begins immediately when $MgBr_2$

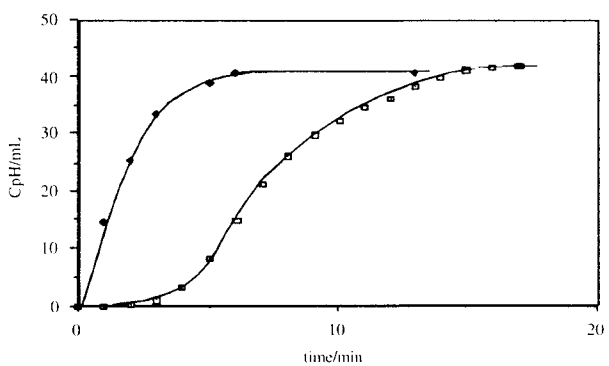

Fig. 7.38. Effect of $MgBr_2$ on the progress, measured by volume of cyclopropane evolved, of the reaction of magnesium turnings with cyclopropyl bromide in DEE, under an atmosphere of cyclopropane at 37 °C. Open squares: $[MgBr_2]_0 = 0$. Closed diamonds: $[MgBr_2]_0 = 0.18$ M. $[CpBr]_0 = 0.18$ M. Reprinted from Garst *et al.* [98]. Copyright 1994, Page No. 368, with permission from Elsevier Science.

is prepared *in situ*, the 'etched' Mg replaced by Mg 'out of the bottle,' and RBr added. 'Etched' Mg is not present initially, but $MgBr_2$ is. (4) Initiation fails when Mg 'out of the bottle' is used with pure DEE. Neither 'etched Mg' nor $MgBr_2$ is present. Thus, the presence or absence of $MgBr_2$ is critical—it is both necessary and sufficient for initiation—but it is immaterial whether or not the Mg has been 'etched.'

When a Grignard reaction initiates, it may be observed that reaction first occurs at one piece of many in the reaction mixture. This may be especially true when one Mg turning is crushed *in situ*, thus providing an effect similar to dry stirring but affecting only one piece. Reaction at other pieces follows shortly. The explanation could lie in the spread of polar solutes (MgX_2, RMgX) generated at the initially reactive piece.

We have observed that the initiation period can be prolonged when only a few Mg turnings are taken for reaction [88]. With a small number, getting one that is prone to initiate is less likely than with a larger number. Also, in stirred mixtures, abrasion of Mg pieces against one another could generate reactive sites.

Blues and Bryce-Smith find that higher alcohols react with Mg faster than RX, forming soluble alkoxides $Mg(OR)_2$, which promote reaction [185]. They report that Grignard reagents form readily, even in a solvent such as toluene or excess RX itself, provided that an alcohol such as isopropyl or an alkoxide such as aluminum isopropoxide is present. These soluble alkoxides may have effects similar to MgX_2 in promoting the dissolution or penetration of the $Mg(OH)_2$ layer or enhancing the rate of reaction of RX at Mg.

Grignard reagents formed in this way may undergo typical reactions, but some have remarkable properties. For example, methylmagnesium iodide prepared in xylene in the presence of $Mg[Al(OiPr)_4]_2$ will dissolve in ethanol to give 'a colourless solution, stable at 20° for an hour or more' [185].

7.3.6 Entrainment

Grignard and others found that Grignard reagents of reluctant halides, mostly aryl, could be prepared by including in the reaction mixture a reactive auxiliary halide, usually CH_3CH_2Br but sometimes another, such as CH_3I [1,186]. Pearson and coworkers improved this 'entrainment' method by using $BrCH_2CH_2Br$ as the auxiliary halide, thus avoiding the formation of an unwanted Grignard reagent along with the target [187].

Mg etching and surface cleaning are possible explanations. However, the efficacy of $MgBr_2$ in promoting reaction in one of the classic test cases, 2,3,4,5,6-pentamethylphenyl bromide in DEE (Section 7.3.5), suggests that entrainment is merely a method of introducing polar solutes (MgX_2, RMgX) [98].

Trapping of intermediate radicals R· (derived from the reluctant halide RX) by the Grignard reagent R′MgX (derived from the auxiliary halide R′X) can sometimes contribute to enhancing yields of RMgX [188]. This is documented for the case of CpBr (cyclopropyl bromide) as RX and *n*-hexyl bromide as R′X. The relative electronegativities of the radicals indicate that the exchange reaction is thermodynamically favored where R· is cyclopropyl, vinyl, or aryl (a π radical) and R′· is alkyl (a σ radical). Indeed, most Grignard-entrainment reactions in the literature are for reactions of aryl halides using auxiliary alkyl halides.

$$R\cdot + R'MgX \longrightarrow RMgX + R'\cdot$$

Even so, it now appears that the major factor in Grignard or Pearson entrainment is the formation of $MgBr_2$. Where pathway **X** is significant, it may be promoted by $MgBr_2$ [98].

7.3.7 Metallic Corrosion

The Grignard reaction may be a classical metallic corrosion reaction, like the rusting of iron in aerated water [189]. If so, then the local cell hypothesis applies—Mg_2^+ enters the solution at anodic sites and electrons leave the metal, being transferred to reductants, at cathodic sites (Figure 7.1, p. 189).

This is consistent with observed effects of polar solutes such as MgX_2 (Sections 7.2.9, 7.3.5, and

7.3.6) A less polar solution layer adjacent to Mg_Z offers less solvation for ions Mg_2^{2+}, X^-, and R^-, and their aggregates. When MgX_2 (or another polar solute) is present, Mg_2^{2+} enters an environment where it is better solvated, so its loss from the metal is more favored thermodynamically.

The formation of R^- could be synchronous, or nearly so, with its association with ^+MgX (or MgX_2) to form RMgX (or $RMgX_2^-$, which becomes RMgX by losing X^-). Bickelhaupt and co-workers have presented evidence that in special cases, at least, R^- may be a distinct intermediate (Section 7.2.20) [136,137].

The complete circuit in local-cell corrosion involves ion conduction in solution between the anodic and cathodic sites (Figure 7.39). When the solvent is very polar, e.g., water, ionic conduction is excellent and the anodic and cathodic sites can be macroscopically separated. The conductivities of solutions of RMgX and MgX_2 in DEE, however, are very low. It is doubtful that the requirement for a complete electrical circuit will allow anodic and cathodic sites to be separated by much more than Å-scale distances, if any, in DEE. In principle, anodic and cathodic sites, if they exist, might be detected by scanning electrochemical devices or STM.

Other hypotheses invoke corrosion in Grignard reactions by direct chemical action [1,10]. No evidence that distinguishes local-cell corrosion from direct chemical action is known to us. However, there is only weak evidence of the discrete Mg(I) intermediates that are required by the hypothesis of direct chemical action (Section 7.3.8). In addition, pitting is a characteristic of local-cell corrosion, which may also be easier to integrate with the D model than direct

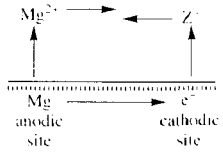

Fig. 7.39. Net ion conduction in the local-cell model of corrosion in the Grignard reaction. Z = R or X.

chemical action. Therefore local-cell corrosion is a suitable working hypothesis.

$$RX + Mg_Z \longrightarrow R\bullet + \bullet MgX + (Mg_Z - Mg)$$

$$R\bullet + Mg_Z \longrightarrow RMg\bullet + (Mg_Z - Mg)$$

7.3.8 Mg(I) Intermediates

The question of distinct Mg(I) intermediates is vexing. They are commonly hypothesized [1,10] but the evidence is slight.

Reaction steps such as the following are easily written. Some have treated •MgX and RMg• as species in solution [51], while others have regarded them as surface or metal-embedded species [10,65].

$$RX + Mg \longrightarrow R\bullet + \bullet MgX$$

$$R\bullet + \bullet MgX \longrightarrow RMgX$$

$$R\bullet + Mg \longrightarrow RMg\bullet \xrightarrow{RX} RMgX + R\bullet$$

$$2\bullet MgX \longrightarrow MgX_2 + Mg$$

Mg^0 found at some distance from Mg_Z, embedded in the precipitated layer of biadamantyl formed in the Grignard reaction of adamantyl bromide, has been interpreted as the result of disproportionation of •MgBr at the surface, giving $MgBr_2$ and Mg^0, which is trapped, protected, and transported as the precipitate forms [65]. However, it could also be the result of mechanical abrasion of stirred Mg or the corrosive undercutting and flaking off of the passivated surface, with pieces of Mg(0) adhering to $Mg(OH)_2$.

There is substantial evidence that R• diffuses in solution (Sections 7.2.8–7.2.9). Consider the following mechanism in which •MgX also diffuses in solution. Here the products are formed in radical–radical reactions. Coupling/disproportionation **c** of R• is diffusion controlled or nearly so. In order for **c** not to dominate the products, the cross-coupling **r** of R• with •MgX would have to be competitive with **c**, that is, also (nearly) diffusion controlled. If all of these radical-radical reactions were diffusion controlled, then the yield of RMgX

would be 50%, less than what is often found. A lower reactivity of •MgX in disproportionation **d** would allow it to build up to higher steady-state concentrations, promoting cross-coupling and diminishing **c** as well as **d**. However, a steady-state analysis shows that the rate ratio **c**/**r** would then be independent of the rate of the initial step, which is not what is observed in rotating-disk experiments, ruling out this mechanism.

$$RX \xrightarrow{Mg_Z} R\bullet + \bullet MgX$$

$$R\bullet + \bullet MgX \xrightarrow{r} RMgX$$

$$2R\bullet \xrightarrow{c} R_2[\text{or } RH + R(-H)]$$

$$2\bullet MgX \xrightarrow{d} Mg^0 + MgX_2$$

The absence of CIDNP resulting from pairs [R• •MgX] speaks against •MgX as an intermediate in solution [51]. The observed CIDNP reflects multiplet effects from [R• R•] pairs only. [R• •MgX] would have a non-zero value of Δg and would give rise to net effects, which are not seen. However, it is conceivable that [R• •MgX] pairs do not generate CIDNP; Δg could be so large that CIDNP is attenuated, or •MgX could remain at the surface where a metallic shielding effect prevents CIDNP, etc.

If •MgX remains adsorbed or embedded in Mg_Z, then it could be present there as an active site for the reaction of RX or R•. This modification of the mechanism above would be a version of the D model in which Mg_Z is 'freckled' with active sites (Section 7.3.11).

If RX were reduced by electron transfer from Mg_Z in a Grignard reaction, then a naïve presumption would be that the metal would be left with an electron deficiency (positive charge), corresponding to the presence of a few $^+Mg(I)$ among many Mg(0), however much metallic delocalization there might be. Actually, the excess charge on Mg might be negative, rather than positive, corresponding to the presence of a few $^-Mg(-I)$ among many Mg(0) (Section 7.3.9).

Kleinberg and co-workers find a cluster of phenomena pointing to Mg(I) in electrolyses at Mg electrodes [190]. (1) Reductants are reduced at the anode as well as the cathode. For example, in the electrolysis of water with Mg electrodes, H_2 is evolved at the anode. (2) The weight lost from the anode is more than is calculated from the current passed on the assumption that Mg(II), only, is lost. The 'mean valence' of the Mg lost from the anode is generally in the range 1.3–1.7. (3) Reduction at the anode continues for a period of time after the current is stopped. (4) There are reductions of species that are physically separated from the anode by a filtering barrier of glass wool. (5) A black powder with reducing properties may form at the anode.

Item 4 suggests a soluble form of Mg(I), but the others are accounted for by the hypothesis that Mg is lost from the anode as either soluble or insoluble Mg(I) as well as Mg(II). The evidence may not be compelling. The weight loss could include that of the original passivating layer of $Mg(OH)_2$. Further, as the anode is cleaned by electrolysis, it could corrode in ongoing reactions with water (or other adventitious reductants) that occur even at a positive Mg electrode. Corrosive undercutting of the passivating layer could lead to the loss of some Mg(0) stuck to the flakes of $Mg(OH)_2$ (black powder with reducing properties), which could be responsible for the reductions seen at and in the vicinity of the anode. Alternatively, those reductions could occur at active sites left by electrolysis. Reduction would eventually cease as impurity reactions led to passivating products. If a little flaked-off $Mg/Mg(OH)_2$ got past the glass wool filter, it could effect the very small amounts of reduction observed in solution near the anode.

The involvement of some unexplained surface process in electrolyses of aqueous salt solutions at Mg electrodes is indicated by the observation, at relatively high current densities, of 'a peculiar cyclic phenomenon: the alternate appearance and dissolution, with gas evolution, of a superficial black deposit on the anode' [191]. Microscopic examination, after washing and drying, of an insoluble black product that forms on the anode showed it to consist of white $Mg(OH)_2$ and an unidentified black substance that 'did not appear to be metallic magnesium' (no further explanation given).

Mixtures of Mg(0) and MgI_2, often used in a slurry with DEE and benzene, can bring about reductions that Mg(0) alone will not [190]. Gomberg and Bachmann proposed that •MgI, formed in these mixtures is the actual reducing agent or the initiator to the reduction process [184].

$$Mg(0) + MgI_2 \rightleftharpoons 2\text{•}MgI$$

However, the enhancement of the reducing powers of Mg(0) by MgI_2 can be explained another way. MgI_2 could provide a polar environment that greatly stabilizes Mg_2^{2+} as it is lost from Mg(0). $MgBr_2$ and $MgCl_2$ sometimes have similar effects on the reducing power of Mg(0).

As far as is known, the Grignard reaction appears to be a typical reduction by Mg. Like others, it is enhanced by the presence of MgI_2, $MgBr_2$, or $MgCl_2$.

Mg_n^{m+}, where $m < 2n$, is worth considering as a possible soluble form of hypovalent Mg. For example, Mg might leave Mg_Z as Mg_2^{2+} instead of Mg^{2+}. Association with Z^- (Z = R or X) would give ZMgMgZ. Calculations indicate that the formation of a 'dimagnesium-Grignard reagent' RMgMgX, under some circumstances, could be energetically more favorable than that of an ordinary Grignard reagent RMgX [11,192]. Once formed, ZMgMgZ could deposit Mg^0 or Mg_2^0 or reduce RX or R• in reactions like the following. It is also conceivable that RMgMgX or RMgMgR could have more nucleophilic reactivity than RMgX or RMgR and could be the 'carbanion' species for which Bickelhaupt and co-workers have given evidence from Grignard reactions of aryl halides in THF (Section 7.2.20) [136,137].

Roles for Mg(I) intermediates in Grignard reactions and other reductions by Mg(0) have not been ruled out but no compelling case in their favor been presented either. They are omitted from our working hypotheses as unnecessary complications.

(Z = R or X)

$$ZMgMgZ \longrightarrow MgZ_2 + Mg^0 \longrightarrow MgZ_2 + Mg^{2+} + 2[e^-] \text{(reduces RX or R•)}$$

$$2\ ZMgMgZ \longrightarrow 2\ MgZ_2 + Mg_2^0 \longrightarrow 2\ MgZ_2 + 2\ Mg^{2+} + 4[e^-]$$

$$ZMgMgZ + RX \longrightarrow Z_2Mg_2X + R\text{•}$$

$$ZMgMgZ + R\text{•} \longrightarrow Z_2Mg_2R$$

$$Z_3Mg_2 + RX \longrightarrow R\text{•} + ZMgX + MgZ_2$$

$$Z_3Mg_2 + R\text{•} \longrightarrow RMgZ + MgZ_2$$

7.3.9 Mg_Z-Solution Interface

Any description of the Mg_Z-solution interface is necessarily speculative. A metal has a natural tendency to lose ions (illustrated as Mg^{2+}) to solution, so that it develops a potential. Ion solvation drives this process, and more polar media

$$Mg_N \rightleftharpoons Mg_{N-1}^{2+}(Mg^{2+})$$

$$\rightleftharpoons Mg_{N-m}^{2m+}(Mg^{2+})_m$$

generate larger reduction potentials. This can explain the effects of salts such as MgX_2 on the reducing power of Mg for solutes in ethers, which are generally not very polar (Sections 7.2.9 and 7.3.5–7.3.8).

It also raises the question of the charge on Mg_Z during a Grignard reaction. If electron loss were to precede that of Mg^{2+}, then Mg_Z would be positively charged during the reaction. However, if the reduction of RX is by electron transfer, then it could be critical that the charge on Mg_Z, and the related potential, be sufficiently negative.

There is another argument for a negative charge on Mg_Z. If losses of Mg^{2+} and electrons from Mg_Z are not very tightly coupled, then each is a candidate for the rate-determining step, as is the diffusion of RX to the surface. The observed

diffusion control for reactions of alkyl iodides and most bromides implies that the loss of Mg^{2+} is not rate-determining and therefore that this step equilibrates at a rate faster than reaction, maintaining a negative charge on Mg_Z [98].

A one-electron transfer from the metal could be accompanied by a simultaneous association of the product X^- with Mg^{2+} already present at the interface.

$$Mg_m^{n-}(Mg^{2+})_p + RX \longrightarrow Mg_m^{(n-1)-}(Mg^{2+})_pX^- + R\text{•}$$

The reaction could be assisted by a coulombic attraction between the developing X^- and Mg^{2+}, perhaps lowering the Mg_Z potential required for the reduction of RX. A similar association of a developing R^- with an Mg^{2+} at the interface could assist the reduction of R•.

Thus, the interface may consist of a negatively charged Mg_Z associated first with Mg^{2+} and then with X^- (Figure 7.40). As reaction proceeds, the loss of Mg^{2+} from the metal compensate for the loss of electrons to RX and R•, maintaining this state. Products RMgX and MgX_2 might temporarily join the polar aggregates at the interface, but they would diffuse into solution as reaction proceeded.

7.3.10 Two Liquid Phases

Grignard reactions of bromides in DEE sometimes give two liquid phases [34,88]. Presumably, these correspond to the phase diagram for $MgBr_2$ in DEE, for which one liquid phase is saturated at ~0.2 M, after which the dissolution of more $MgBr_2$ leads to the separation of a second phase that is ~2.6 M ('$MgBr_2$ etherate') [24]. In Grignard reactions in DEE, phase separation is almost inevitable when relatively large amounts of 1,2-dibromoethane are used to promote reaction [34,88].

This phenomenon could be related to the finding that the intermediate cyclopropyl radicals that attack the solvent in pure DEE are not converted to RMgX when solvent attack is blocked (Section 7.2.9, Table 7.3; the behavior is different in DEE/$MgBr_2$, THF, and THF/$MgCl_2$) [97]. It is possible that the initial part of the reaction in pure DEE leads to enough $MgBr_2$ near the surface to form a layer, possibly thin, of etherate, sandwiched between Mg_Z and the less polar and viscous bulk solution.

Within the etherate layer, radicals would diffuse normally, undergoing their usual reactions. However, if the etherate layer had the right thickness, most of the solvent attack could be by radicals that escaped from it into the bulk solution. When one of these radicals diffused back to the interface between liquid phases, both the viscosity and the polarity of the etherate would act to inhibit its reentering the etherate. If solvent attack were slowed by solvent deuteration, radicals would be diverted to **c**, mostly, rather than **r**, because they would not diffuse to Mg_Z (Figure 7.41).

When the entire medium is etherate, this effect cannot operate, since there is no liquid phase separation. This can explain why radicals diverted from solvent attack in DEE/$MgBr_2$ are converted to RMgX—there is no barrier to their diffusion back to Mg_Z.

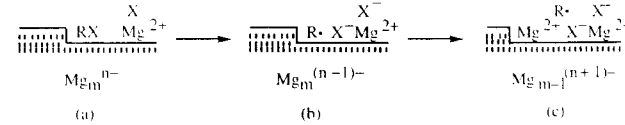

Fig. 7.40. Schematic representation of conjectured interface during a Grignard reaction. Solvent molecules and ion solvation are not shown. (a) Initially, the metal bears a net negative charge n−. RX is in a position to be reduced. (b) Reduction has occurred, leaving the metal with a charge (n − 1)−, and the product X^- is associated with Mg^{2+}. (c) Mg has been lost to the solution as Mg^{2+}, leaving the metal with a charge (n + 1)−. A subsequent reduction of R• restores the original metallic charge. No particular synchrony or asynchrony of steps is implied.

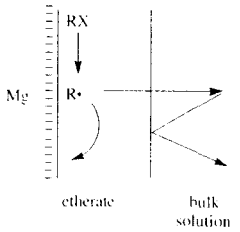

Fig. 7.41. Schematic illustration of a possible effect of a more polar and viscous etherate layer adjacent to Mg_Z. The higher viscosity of the etherate layer and the reduced solubility of R• therein, a consequence of higher polarity, act to block the re-entry of radicals that escape into the bulk solution.

Except for preliminary calculations that indicate that they can operate as described here [102], these proposed effects are not yet supported by additional information. However, there are other possible links to known facts. (1) Perhaps two-phase effects could explain why the fits of D-model calculations are better for solvents DEE and THF than for solvents DBE and DPE (Section 7.2.8). (2) A high viscosity of medium adjacent to Mg_Z, sufficient to slow the rotation of R•, could result in partial retention of configuration (Section 7.2.9), provided that the value of δ were not decreased as well.

7.3.11 Freckled Magnesium

The D model calculations presented here are for an infinite, uniformly reactive, planar Mg_Z (Section 7.2.4) This is not realistic. The success of the calculations is probably due to effects of scale and averaging [83].

Scale is determined by the characteristic diffusion distance σ_R of R• and the thickness of the layer of the medium in which most of the products are formed. For typical alkyl halides in DEE, σ_R is ~100 Å and almost all products are formed within a few thousand Å of Mg_Z (Sections 7.2.6–7.2.8). These are small distances compared with the sizes of Mg turnings, or even powders. Consequently edge-effect errors resulting from the infinite-plane assumption are negligible. An exception might occur with Rieke magnesium—its particle size (perhaps ~1000 Å) may be comparable with the distances at which significant amounts of **c** and **s** occur. Clusters Mg_n with diameters near 30 Å are definitely too small for the infinite-plane approximation (Section 7.2.18).

By similar reasoning, if the surface has patches of uniform reactivity that are at least a few thousand Å across, then the possibility that these are interspersed among unreactive patches will be of no consequence. Effects at patch edges will be negligible.

Averaging occurs when there are small (Å scale), discrete reactive sites ('freckles'). Freckles might consist, for example, of exposed corner atoms on clean portions of Mg_Z undergoing corrosion along crystal planes.

Consider a formulation of the infinite-dilution D model [83] based on Noyes' method of encounters [69,70]. An encounter begins with the first contact of R• with Mg_Z (since the end of the previous encounter, if any) and ends when R• subsequently reaches an arbitrarily chosen separation λ from Mg_Z or suffers **r**, whichever comes first (Figure 7.42). Let α be the probability of **r** during an encounter.

If **q** is a first-order solution reaction that competes with **r**, then the probability A that R•

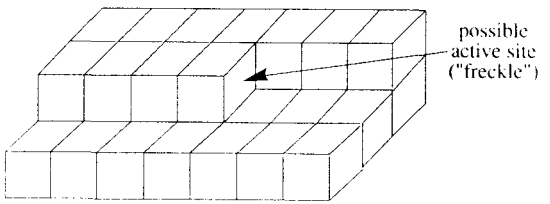

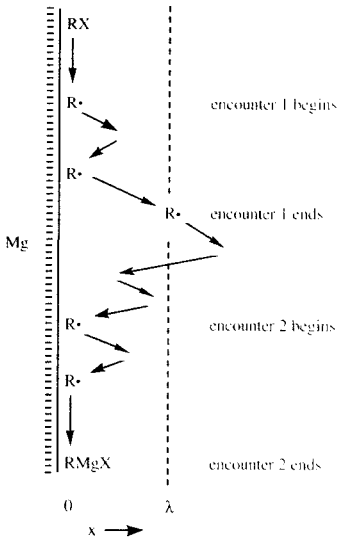

Fig. 7.42. An 'encounter' begins at a first contact of R• with Mg_Z and ends when R• subsequently reaches separation λ from Mg_Z or when **r** occurs before λ is reached.

will suffer **r** (ever) is given by equation (7.53), provided that λ is sufficiently small (σ_Q is defined in Section 7.2.6). Equations (7.25) and (7.53) are

$$A = (\alpha/\lambda)\sigma_Q/[1 + (\alpha/\lambda)\sigma_Q] \qquad (7.53)$$

equivalent – δ is the limit of (α/λ) as λ approaches zero. This gives δ physical meaning: for small values, $\alpha \approx \delta\lambda$. Thus, if $\delta = 0.010$ Å^{-1} and $\lambda =$ 5 Å, then $\alpha \approx 0.05$, meaning that the probability that an R• at Mg_Z will suffer **r** before reaching a separation of 5 Å is 5% [82].

For an Mg_Z of uniform reactivity, α has the same value for each encounter. For a freckled Mg_Z, α varies among encounters, depending on where R• is, relative to freckles, at the beginning of the encounter.

Diffusion can rapidly randomize the distribution of probabilities that encountering radicals arrive at Mg_Z at various distances from freckles, especially if they are dense, at least several per σ_R (100 Å for a typical alkyl halide in DEE) on Mg_Z. Once randomization occurs, the calculated product distribution [using an effective value of α (or δ)] is the same whether Mg_Z is uniform or freckled. Only the interpretation of α differs—for a uniformly reactive Mg_Z the observed value is the same for all encounters—for a freckled Mg_Z it is an average. The assumption of a uniformly reactive Mg_Z is a convenience for D-model calculations, not a necessity. Agreement between calculated and experimental yields does not imply that Mg_Z must be uniformly reactive in actuality.

As noted in Section 7.2.9, if reductions of RX and R• can occur at the same active site, or adjacent ones, then the freckles model can account for partial retention of configuration by including geminate reaction (with partial retention) and escape. In this case, averaging would apply to only part of the reaction. Escape (in three dimensions) from the initial reactive site would leave a surface-radical pair [Mg_Z R•] in which R• diffuses near the freckled Mg_Z without encountering the original

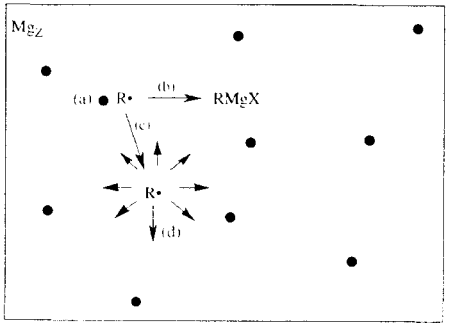

Fig. 7.43. 'Freckles' model and retention of configuration. The heavy dots are active sites (freckles) of very high reactivity toward R•. (a) R• has been formed at an active site. (b) On a very short time scale, ~10^{-10} s, geminate reaction occurs at the original site. Partial retention of configuration results. (c) On the same short time scale, there is three-dimensional escape from the original site. (d) R• is now not at a reactive site. It diffuses in the x direction, normal to Mg_Z, as well as the y and z directions illustrated, randomizing its probability of a future arrival at Mg_Z at a freckle. Only a fraction of its subsequent encounters with the surface is at an active site.

active site again (Figure 7.43). Escaped radicals could randomize, averaging α as above.

The freckles model with retention of configuration (Figures 7.27 and 7.41) corresponds to pathway **Xc** (Section 7.1.3). Although adsorption of R• is not invoked here, a radical cannot diffuse very far before suffering geminate reaction or escape. The characteristic diffusion distance σ_{Xc} is $(D\tau_{Xc})^{1/2}$, where τ_{Xc} is the **Xc**-limited characteristic lifetime. When $\tau_{Xc} = \sim 10^{-10}$ s, $\sigma_{Xc} = 5.5$ Å. σ_{Xc} is smaller for those radicals with even shorter lifetimes. Thus, the freckles D model takes on some of the characteristics of an A model, in that the radicals that suffer geminate reaction remain very close to Mg_Z.

The freckles model for partial retention does not clearly account for the apparent correlation of non-isomerization with conjugation (Sections 7.2.9–7.2.11). This suggests the alternative of a pathway **X** along which R• is not an intermediate (Sections 7.1.3, 7.2.11). Whereas the freckles model invokes successive steps, with branching, a non-R• pathway **X** is a parallel reaction competing with pathway **R**.

7.4 CONCLUSIONS

Radicals R• are intermediates in Grignard reactions of typical alkyl halides RX, but these are not radical chain reactions. Instead, they follow pathway **R**, predominately if not exclusively. In reactions of typical alkyl and cyclopropyl halides, R• in does not remain adsorbed at Mg_Z but instead diffuses in solution (D model).

For halides other than typical alkyl, it is likely that there are pathways **X** along which R• is not an intermediate and there is at least partial retention of configuration. In a pathway **X**, RMgX is probably formed through a dianionic transition state of composition RX^{2-} that is formed from an intermediate $RX^{\bullet-}$.

The α criterion for anion-radical intermediates $RX^{\bullet-}$ ($\alpha < 0.5$) may be useful, but it is not rigorous. There are indications that it may fail for reductions of 1-halo-1-methyl-2,2-diphenylcyclopropanes.

Reductions of 1-halo-1-methyl-2,2-diphenylcyclopropanes, including Grignard reactions, follow complex pathways that are difficult to understand in detail. For this reason, these halides are not good models for others in Grignard reactions.

For Grignard reactions of at least some aryl halides, including halobenzenes, pathway **R** appears to be minor. Apparently, a dianionic pathway **X** dominates. Even though dianionic pathways have not been detected in electrochemical reductions of aryl and other halides, there is clear evidence for them in certain chemical reductions, including those of 1-halo-1-methyl-2,2-diphenylcyclopropanes. Reactions of vinyl halides appear to resemble those of cyclopropyl and aryl halides.

$MgBr_2$ sometimes has a pronounced effect on the initiation of a Grignard reaction. In addition, it sometimes affects product distributions, particularly for cyclopropyl and aryl halides. Differences in effects of MgX_2, X, and THF (vs DEE) on Grignard reactions of typical alkyl halides and others, notably cyclopropyl and aryl halides, may reflect differences in mechanisms, with typical alkyl halides following pathway **R** (insensitive to these factors) and others following **R** and **X** (partitioning sensitive to these factors).

The adventitious layer of salts on Mg_Z does not contain significant O^{2-} unless it is baked. The anions are almost entirely ^-OH with some HCO_3^- in the outer layers. Aqueous nitric acid treatments leave reconstituted $Mg(OH)_2$ layers, perhaps with fewer defects, but it does not leave exposed metallic surfaces.

Retaining well-supported hypotheses, discarding those that are contradicted by experimental data, and applying Occam's Razor to the rest, we set aside Mg(I) intermediates (pending further evidence). In competition with pathway **R**, we invoke a pathway **X** that is unimportant for typical alkyl halides but significant for cyclopropyl and vinyl halides and nearly exclusive for simple aryl halides. We choose pathway **Xb** (Section 7.1.3) as **X**. Even though it is unprecedented for reductions of organyl (including aryl) halides, it may be the simplest possibility that is clearly consistent with an influence of conjugation on the partitioning between pathways **R** and **X**.

For the inorganic part of the mechanism of the main reaction, we posit the electrochemical, local-cell hypothesis of metallic corrosion (Figures 7.1 and 7.39). This makes Grignard reactions mechanistically consistent with other metallic corrosions.

We posit that the $Mg(OH)_2$ layer presents a barrier to penetration of RX to the surface. This and a requirement of a polar medium at the interface can explain the failure of reactions to begin immediately. MgX_2 may promote reaction by helping the reaction mixture penetrate the $Mg(OH)_2$ layer and by providing a polar solution at Mg_Z. We posit corrosive undercutting and flaking off as the major mechanism of Mg_Z cleaning during a Grignard reaction, though we recognize that dissolution could be important (Figure 7.37).

It may be unlikely that all of the choices made here, especially those among poorly supported hypotheses, will survive further tests. Nonetheless, some of these choices are now well established, and taken together with others, they provide an integrated view of Grignard reactions and a satisfactory set of working hypotheses.

ACKNOWLEDGMENTS

We thank the National Science Foundation (grant CHE 9406548) and the Hungarian Academy of Sciences for financial support for the preparation of this chapter and some of the work reported therein. Prof. Friedrich Bickelhaupt provided copies of the thesis of G.P.M. van Klink. Dr. Brian L. Swift laid the foundations for many of the calculations. We thank our colleagues for many discussions and acts of assistance.

APPENDIX

Here we review some relevant aspects of SCK and Noyes theories of diffusion-reaction [71,72]. Consider a bimolecular association in solution (Equation 7A.1).

$$A + B \rightleftharpoons C \qquad (7A.1)$$

Figure 7A.1 shows the fundamental steps of the forward and backward reactions [74–77]

A, B unpaired molecules.
AB_n, AB_g non-geminate and geminate pairs, respectively.

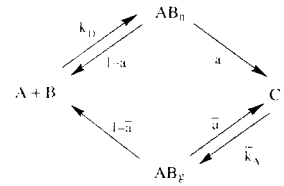

Fig. 7A.1. Steps in the reaction of equation 7A.1 in solution. The one-way arrows arise because pairs AB_n and AB_g are labeled by origin, not state. The principle of microscopic reversibility applies—the states of ABg are among those of AB_n [74–77].

$a, \bar{a}$ probabilities of reaction, instead of escape, of non-geminate and geminate pairs, respectively.

k_D second-order rate constant for non-geminate pair formation. It is also the diffusion-control rate constant for C formation from A and B. When $a \approx 1$, $d[C]/dt = k_D[A][B]$.

$\bar{k}_A$ first-order rate constant for geminate pair formation. It is also the activation-control rate constant for A and B formation from C. When $\bar{a} \approx 0$ or when the system is at equilibrium, $d[A]/dt = d[B]/dt = \bar{k}_A[C]$.

k_A activation-control, second-order rate constant for C formation. $d[C]/dt = k_A[A][B]$ when the system is at equilibrium.

k_G global rate constant for C formation—second-order rate constant for the formation of C in non-geminate reactions (only) of A with B. In most experiments, k_G is the observed rate constant. The diffusion-and activation-control limits of k_G are k_D and k_A, respectively.

k_G global rate constant for A and B formation—first-order rate constant for the formation of A and B from C.

A few algebraic steps lead to general expressions relating rate constants and pair reaction probabilities [74–77] Note that k_D is the limit approached by k_G as $k_A \rightarrow \infty$ with k_D held constant, while k_A is the limit approached by k_G as $k_D \rightarrow \infty$ with k_A held constant.

$$k_G = ak_D \tag{7A.2}$$

$$k_G = (1 - \bar{a})k_A \tag{7A.3}$$

$$k_G = k_D k_A/(k_D + bk_A) \quad b = \bar{a}/a \tag{7A.4}$$

$$k_A/k_D = a/(1 - \bar{a}) \tag{7A.5}$$

In the general case, $\bar{a} \geq a$. This can have important consequences, e.g., pseudo diffusion control. In the ideal case of spin-free, isotropically reactive, spherical molecules, $\bar{a} = a$. Equation (7.19) is often assumed, erroneously, to be general.

$$k_G = (1 - a)k_A \quad \text{(ideal case)} \tag{7A.6}$$

$$k_G = k_D k_A/(k_D + k_A) \quad \text{(ideal case [7.19)}$$

$$k_A/k_D = a/(1 - a) \quad \text{(ideal case)} \tag{7A.7}$$

Equations (7A.7), (7.15), and (7.17) provide an easy identification of the pair reaction probability a in terms of R and δ (κ/D). Dividing (7.15) by (7.17) and setting the resulting expression for k_A/k_D equal to the right side of (7A.7) gives the result.

$$a = \bar{a} = R\delta/(1 + R\delta) = R\kappa/(D + R\kappa) \tag{7A.8}$$

Diffusion control results when $a = 1$, so that $k_G = k_D$. A close approach to diffusion control does *not* require reaction at every contact between A and B, which is often taken to be the diffusion-control limit. All it requires is a nearly 100% probability of reaction instead of escape. Noyes defined an 'encounter' as an event beginning with an initial contact between A and B and continuing as long as they occupy adjacent positions in solution, during which time there may be multiple contacts and rebounds. When an encounter ends (by separation), the probability β_c of a subsequent encounter is not zero (for spherical molecules, $\beta_c = R/r_c$, where r_c is the center-to-center distance between molecules at the end of an encounter).

'Encounter-controlled,' implying reaction at nearly every encounter, is sometimes used in the sense of 'diffusion-controlled,' but actually the rate of encounters (using Noyes' definition) is not the limiting factor in the case of diffusion control. Instead, the limiting rate is that of 'engagements [193]. An engagement begins with the first contact between a particular A and B and ends when they react or escape to permanent separation. It can include several encounters. The rate constant k_D governs engagements. The probability a is that of reaction during an engagement.

For the standard AB (Section 7.2.4), $\delta = 0.13$ Å^{-1} and $a = 0.4$, so the reaction of A and B is slightly slower than the diffusion-control limit ($k_D = 2.3 \times 10^{10}$ M^{-1} s^{-1}; $k_G = 9.1 \times 10^9$ M^{-1} s^{-1}) and is 40% (value of a) diffusion-controlled. From equation (7A.8), for $R = 5$ Å, 50% diffusion control occurs when $\delta = 0.20$ Å^{-1}, 90% when $\delta = 1.8$ Å^{-1}, and 99% when $\delta = 19.8$ Å^{-1}.

This view of diffusion control makes no sense when applied to a surface-molecule reaction. If the diffusion-control rate were the engagement rate, then *all* reactions between Z and B would be diffusion controlled because ZB engagements end only in reaction (there is no escape; Section 7.2.5).

For these reactions, diffusion control is tied instead to hydrodynamic control and the diffusion layer that lies between the surface and the well-stirred main body of solution (Figure 7A.2). A reaction will be influenced by diffusion if there is a low probability ($1 - a_Z$) (Equation 7A.9) that a B that has arrived at Z will leave the diffusion layer.

a_Z probability that a B at Z ($s = 0$) will react there instead of diffusing to the bulk solution ($s = s_D$).

$$a_Z = \delta s_D/(1 + \delta s_D) \tag{7A.9}$$

In an example (B = cyclopentyl bromide in DEE) given by Whitesides, an Mg disc rotating at 250 rpm gives $s_D = 4 \times 10^5$ Å. This reaction will

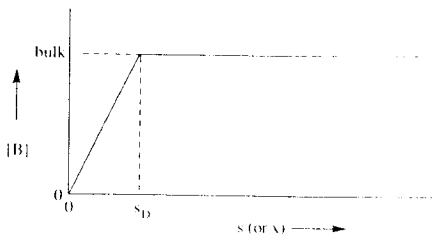

Fig. 7A.2. Approximate concentration profile for a diffusion-controlled reaction of B at a surface Z. The separation (or distance) from Z is s (or x) and s_D is the thickness of the diffusion layer. Outside the diffusion layer, stirring is effective in maintaining the concentration at the bulk value. The approximation here is in the substitution of two straight-line segments for a curve with a continuous slope. For the physically unrealistic case of reaction at every contact (pure diffusion control), $[B]_0$ would be zero. For real cases, it is non-zero, but if it is much less than $[B]_\infty$ then the reaction is nearly diffusion influenced. For pure activation control, $[B]_0 = [B]_\infty$.

be 90% diffusion controlled ($a_Z = 0.9$) when δ is about 2×10^{-5} Å^{-1} and 50% diffusion controlled when δ is 2.5×10^{-6} Å^{-1}. These values are 5–6 orders of magnitude lower than the values of δ that are necessary to produce these levels of diffusion control for an A – B reaction with $R = 5$ Å. They may be plausible estimates of δ for reactions of Mg_Z with RBr, since these appear to lie at the margin of diffusion and activation control.

For $[Mg_Z\ R\bullet]$ δ is much larger, $\sim 10^{-2}$ Å^{-1}. Clearly, this reaction is diffusion controlled, that is, that an R• formed at Mg_Z has only an insignificant chance of leaving the diffusion layer and entering the bulk solution. This justifies the purely reaction-diffusion treatment that we give (Sections 7.2.5–7.2.7).

Noyes defined a function $h(t)$ that is related to $\bar{a}$ and the SCK time-dependent rate constant $k(t)$ [69]. His original definition differs slightly but significantly from that used here.

$h(t)dt$ probability of reaction between partners of a geminate pair AB_g, created at time zero, between times t and $t + dt$.

$$\bar{a} = \int_0^\infty h(t')dt' \tag{7A.10}$$

A discrepancy between SCK and Noyes theories led Naqvi *et al.* to reformulate both [194]. This was not necessary. The discrepancy results from a violation of the Principle of Microscopic Reversibility in Noyes' original treatment [69]. The present definition of $h(t)$ avoids that violation.

Equations 7A.2–7A.7 and 7A.10 are independent of on any particular assumptions about molecular transport. To give form to $h(t)$ and values to a and $\bar{a}$, underlying theories of molecular transport and reactivity must be assumed. Further considerations here are based on the ideal case and SCK theory, which is rooted in Fick's Laws of Diffusion (equations 7.7 and 7A.11).

$$\partial[B]/\partial t = D(\partial^2[B]/\partial x^2) \text{ (Fick's Second Law in one dimension)} \tag{7A.11}$$

Fick's Second Law follows from the First and gives the contribution of diffusion to the variation in [B] (at a particular value of x) with time t. If chemical reactions occur in solution, then appropriate terms (usually mass-action rate terms) must be added to the diffusion term to give the complete equation for $\partial[B]/\partial t$. For diffusion in two or three dimensions, one-dimensional Fick's Laws are generalized to include the other dimensions (diffusion in each orthogonal direction is independent of that in the others).

Fick's Laws may not apply at very short times and diffusion distances. Certainly, at times much less than 10^{-12} s, where a typical characteristic Fickian diffusion distance $(Dt)^{1/2}$ is of the order of 1 Å or less, the extents of oscillatory motions equal or exceed those of net displacements. Also, since molecular clusters tend to persist on this timescale and since motions within and by clusters of real molecules may be subject to 'gear' effects, there may be non-random contributions to relative displacements on very short timescales. These effects are neglected here. Most of the phenomena in which we are interested occur on longer timescales.

In the SCK treatment of A + B → C, an equilibrium distribution of A and B in solution is created at time zero [72]. The rate constant $k(t)$,

defined as rate/[A][B], decreases with time. Its initial (equilibrium) value $k(0)$ is k_A and its 'long-time' value $k(\infty)$ is k_G. According to SCK theory, $k(t)$ is given by equations (7A.12–7A.13) [71,72].

$$k(u) = \frac{4\pi R^2 D L_0 \delta}{1 + R\delta} \times [1 + R\delta \exp(u)\mathrm{erfc}(u^{1/2})] \quad (7A.12)$$

$$u = u(t) = \left(\frac{1 + R\delta}{R}\right)^2 Dt \quad (7A.13)$$

The connection between $k(t)$ and $h(t)$ is [69,70,75]

$$k(t) = k_A \left[1 - \int_0^t h(t')\mathrm{d}t'\right] \quad (7A.14)$$

A comparison of equations (7A.14) and (7A.10) suggests that the time dependence of $k(t)$ is due to the rapid reaction of geminate pairs, though they are not identified as such in the SCK 'sudden creation' approach. That this is correct is clear from an equivalent approach. In a reversible system at equilibrium, let C be made inert at time zero. Geminate pairs are now identifiable, and it is their disappearance that is tracked in the integral of equations (7A.10) and (7A.14). If C is sufficiently dilute, this and the SCK treatments are identical.

From equation (7A.14),

$$h(t) = -\frac{1}{k_A}\frac{\mathrm{d}k(t)}{\mathrm{d}t} \quad (7A.15)$$

Applying equation (7A.15) to the SCK $k(t)$ (equations 7A.12–7A.13) gives the SCK form for $h(t)$ (equation 7A.16). (This can also be derived in other ways [66].)

$$h(t) = \frac{D^{1/2}\delta}{(\pi t)^{1/2}}[1 - \pi^{1/2}u^{1/2}\exp(u)\mathrm{erfc}(u^{1/2})] \quad (\text{AB or ZB}) \quad (7A.16)$$

Although equation (7A.16) was derived for an AB, $h(t)$ remains well defined in the ZB limit ($R \to \infty$). This contrasts with $k(t)$ which becomes infinite in the ZB limit. Thus, equation 7A.16 applies to both AB and ZB. For a ZB specifically, R is not a factor (it disappears in the limit as $R \to \infty$ and equation (7A.17) is the relevant version of equation (7A.16).

$$h(t) = \frac{D^{1/2}\delta}{(\pi t)^{1/2}}[1 - \pi^{1/2}\delta(Dt)^{1/2}\exp(\delta^2 Dt)\,\mathrm{erfc}[\delta(Dt)^{1/2}]] \quad (\text{ZB}) \quad (7A.17)$$

From the definition of $h(t)$, it follows that the probability $R(t)$, that an AB pair reaction has occurred by time t, is given by equation (7A.18). The survival probability is often defined as $1 - R(t)$, which is correct for the survival of the species A and B, whether or not they remain paired. However, $1 - R(t)$ is not the correct expression for the survival probability $S(t)$ of a pair AB because pairs disappear by escape as well as reaction. The total probability that a pair has disappeared by time t, by either pair reaction or escape, is $R(t) + E(t)$, where $E(t)$ is the probability of escape by time t, so $S(t)$ is given by equation 7A.19.

$$R(t) = \int_0^t h(t')\mathrm{d}t' = \frac{R\delta}{1 + R\delta}[1 - \exp(u)\mathrm{erfc}(u^{1/2})] = a[1 - \exp(u)\mathrm{erfc}(u^{1/2})] \quad (7A.18)$$

$$S(t) = 1 - [R(t) + E(t)] \quad (7A.19)$$

The relationship between $E(t)$ and $R(t)$ can be understood as follows. For every contact between A and B, there are three possible outcomes, reaction, escape, and temporary separation, each of which has a certain probability. In the ideal case, these probabilities are constant (time-independent). In the end (infinite time), the only outcomes are reaction and escape—all cases of temporary separation will have been settled in one way or the other (reaction or escape). The ultimate ratio of escape to reaction is $(1 - a)/a$, but since the probabilities of the outcomes of all contacts are the same, $(1 - a)/a$ must be the ratio of the probability of escape to that of reaction for *each* contact and time t.

$$E(t)/R(t) = (1 - a)/a \quad (7A.20)$$

$$S(t) = 1 - [R(t) + (1 - a)R(t)/a] = 1 - R(t)/a \quad (7A.21)$$

$$S(u) = \exp(u)\,\mathrm{erfc}(u^{1/2}) \quad (7A.22)$$

Equation 7A.22 generates the SCK decay plots presented in Figures 7.8, 7.10, and 7.11. That of Figure 7.10 does not depend on particular choices of parameters. Time is represented as multiples of the pair half-life $\tau_{1/2}$, which are the same as multiples of $u_{1/2}$ [value of u for which $S(u) = 1/2$]. From equations (7A.22) and (7A.13)

$$u_{1/2} = 0.59148 \quad (7A.23)$$

$$\tau_{1/2} = 0.59148R^2/D(1 + R\delta)^2 \quad (7A.24)$$

The SCK probability $U(s, k_Q, \kappa, D, R)$ of ultimate reaction between the members of a pair of ideal spherical molecules has been obtained by Naqvi *et al.* for a general case in which the initial separation is s and the molecule B is scavenged in a competing first-order reaction governed by rate constant k_Q,

$$U(s, k_Q, \kappa, D, R) = \beta[1 + \delta^{-1}(R^{-1} + \sigma_Q^{-1})]^{-1} \exp(-s/\sigma_Q) \quad (7A.25)$$

where $\delta = \kappa/D$, $\beta = [1 + (s/R)]^{-1}$ and $\sigma_Q = (D/k_Q)^{1/2}$ [71]. This equation remains valid in the limits, separate or joint, for $s = 0$, $k_Q = 0$, $\delta \to \infty$, and $R \to \infty$, and it reduces in various limits to expressions for probabilities of interest. Thus, for $k_Q = 0$ and $\delta \to \infty$, $U = \beta$ (equation (7.20)). For $R \to \infty$ in addition, $U = \beta_Z = 1$ (equation (7.21)). For $\delta \to \infty$, $U = \phi$ (equation 7.52). For $\delta \to \infty$ and $R \to \infty$, $U = \phi_Z$ (equation (7.24)). For $s = 0$ and $R \to \infty$, $U = A$ (equation (7.25)). For $s = 0$ and $k_Q = 0$, $U = a = \bar{a}$ (equation (7A.8)).

REFERENCES

1. Kharasch, M.S., Reinmuth, O. *Grignard Reactions of Nonmetallic Substances*; Prentice-Hall: New York, **1954**.
2. Silverman, G.S., Rakita, P.E. *Handbook of Grignard Reagents*; Heinemann, H., Ed., Dekker: New York, **1996**.
3. Richey, H.G. *This work*, **1999**.
4. Grignard, V. *C.R. Hebd. Seances Acad. Sci.* **1900**, *130*, 1322.
5. Grignard, V. *Chem. Zentr.* **1900**, *II*, 33.
6. Lindsell, W.E., in *Comprehensive Organometallic Chemistry*; Wilkinson, G., Stone, F.G., and Abel, E.W., Ed., Pergamon: Oxford, **1982**; Vol. 1, pp. 155–163.
7. Walborsky, H.M. *Acc. Chem. Res.* **1990**, *23*, 286–293.
8. Garst, J.F. *Acc. Chem. Res.* **1991**, *24*, 95–97.
9. Walling, C. *Acc. Chem. Res.* **1991**, *24*, 255–256.
10. Hamdouchi, C., Walborsky, H.M., in *Handbook of Grignard Reagents*; Silverman, G.S., and Rakita, P.E., Ed., Dekker: New York, **1996**, pp. 145–218.
11. van Klink, G.P.M. *Formation, Poly-Coordination and Reactivity of Organomagnesium Compounds*; Doctoral thesis, Free University: Amsterdam, **1998**. Promotor: F. Bickelhaupt.
12. Schaart, B.J., Bodewitz, H.W.H.J., Blomberg, C., Bickelhaupt, F. *J. Am. Chem. Soc.* **1976**, *98*, 3712–3713.
13. Newcomb, M., Kaplan, J. *Tetrahedron Lett.* **1988**, *29*, 3449–3450.
14. Lawrence, L.M., Whitesides, G.M. *J. Am. Chem. Soc.* **1980**, *102*, 2493–2494.
15. Root, K.S., Hill, C.L., Lawrence, L.M., Whitesides, G.M. *J. Am. Chem. Soc.* **1989**, *111*, 5405–5412.
16. Ashby, E.C., Oswald, J. *J. Org. Chem.* **1988**, *53*, 6068–6076.
17. Savéant, J.-M. *Adv. Phys. Org. Chem.* **1990**, *26*, 1–130.
18. Savéant, J.-M. *Acc. Chem. Res.* **1993**, *26*, 455–461.
19. Walborsky, H.M., Young, A.E. *J. Am. Chem. Soc.* **1964**, *86*, 3288–3296.
20. Walborsky, H.M., Aronoff, M.S. *J. Organomet. Chem.* **1973**, *51*, 31–53.
21. Hamdouchi, C., Topolski, M., Goedken, V., Walborsky, H.M. *J. Org. Chem.* **1993**, *58*, 3148–3155.
22. Walborsky, H.M., Hamdouchi, C. *J. Am. Chem. Soc.* **1993**, *115*, 6406–6408.
23. Shriver, D.F., Drezdzon, M.A. *The Manipulation of Air-Sensitive Compounds*; 2nd Ed., Wiley-Interscience: New York, 1986.
24. *Gmelins Handbuch der Anorganischen Chemie*; Syst. No. 27, Teil B, p. 168, 1937.
25. Watson, S.C., Eastham, J.F. *J. Organomet. Chem.* **1967**, *9*, 165–168.
26. Root, K.S., Deutch, J., Whitesides, G.M. *J. Am. Chem. Soc.* **1981**, *103*, 5475–5479.
27. Hasler, P., Richarz, W. *Ind. Eng. Chem. Res.* **1989**, *28*, 38–43.
28. Hammerschmidt, W.W., Richarz, W. *Ind. Eng. Chem. Res.* **1991**, *30*, 82–88.
29. Rogers, H.R., Hill, C.L., Fujiwara, Y., Rogers, R.J., Mitchell, H.L., Whitesides, G.M. *J. Am. Chem. Soc.* **1980**, *102*, 217–226.

30. Rogers, H.R., Deutch, J., Whitesides, G.M. *J. Am. Chem. Soc.* **1980**, *102*, 226–231.
31. Rogers, H.R., Rogers, R.J., Mitchell, H.L., Whitesides, G.M. *J. Am. Chem. Soc.* **1980**, *102*, 231–238.
32. Kilpatrick, M., Simons, H.P. *J. Org. Chem.* **1938**, *2*, 459–469.
33. Gzemski, F.C., Kilpatrick, M. *J. Org. Chem.* **1940**, *5*, 264–275.
34. Batlaw, R., Garst, J.F. *Unpublished results.*
35. Batlaw, R., Deutch, J.E., Fujiwara, Y., Garst, J.F., Hill, C.L., Izumi, A., Lawrence, L.M., Shih, Y.-S., Whitesides, G.M. *Unpublished manuscript.*
36. Rüchardt, C., Trautwein, H. *Chem. Ber.* **1962**, *95*, 1197.
37. Patel, D.J., Hamilton, C.L., Roberts, J.D. *J. Am. Chem. Soc.* **1965**, *87*, 5144.
38. Lamb, R.C., Ayers, P.W., Toney, M.K., Garst, J.F. *J. Am. Chem. Soc.* **1966**, *88*, 4261–4262.
39. Maercker, A., Roberts, J.D. *J. Am. Chem. Soc.* **1966**, *88*, 1742.
40. Hill, E.A., Engel, M.R. *J. Org. Chem.* **1971**, *36*, 1356.
41. Richey, H.G., Jr., Veale, H.S. *J. Am. Chem. Soc.* **1974**, *96*, 2541.
42. Hill, E.A. *J. Organomet. Chem.* **1975**, *91*, 123–271.
43. Grovenstein, E., Jr., Cottingham, A.B., Gelbaum, L.T. *J. Org. Chem.* **1978**, *43*, 3332–3334.
44. Hill, E.A., Harder, C.L., Wagner, R., Meh, D. Bowman, R.P. *J. Organomet. Chem.* **1986**, *302*, 5–17.
45. Crandall, J.K., Michaely, W.J., Collonges, F., Nelson, D.J., Ayers, T.A., Gajewski, J.J. *Croat. Chem. Acta.* **1996**, *69*, 1473–1496.
46. Bodewitz, H.W.H.J., Blomberg, C., Bickelhaupt, F. *Tetrahedron Lett.* **1972**, 281–284.
47. Bodewitz, H.W.H.J., Blomberg, C., Bickelhaupt, F., *Tetrahedron* **1973** *29*, 719–726.
48. Bodewitz, H.W.H.J., Blomberg, C., Bickelhaupt, F. *Tetrahedron* **1975** *31*, 1053–1063.
49. Bodewitz, H.W.H.J., Blomberg, C., Bickelhaupt, F. *Tetrahedron Lett.* **1975**, 2003–2006.
50. Bodewitz, H.W.J.J., Schaart, B.J., Van der Niet, J.D. Blomberg, C., Bickelhaupt, F., Den Hollander, J.A. *Tetrahedron* **1978**, *34*, 2523–2527.
51. Schaart, B.J., Blomberg, C., Akkerman, O.S., Bickelhaupt, F. *Can. J. Chem.* **1980**, *58*, 932–937.
52. Garst, J.F., Ungvary, F., Batlaw, R. *J. Am. Chem. Soc.* **1991**, *113*, 5392–5397.
53. Richey, H.G. Jr., Rees, T.C. *Tetrahedron Lett.* **1966**, 4297.
54. Drozd, V.N., Ustynyuk, Y.A., Tsel'eva, M.A., Dmitriev, L.B. *Zh. Obshch. Khim.* **1968**, *38*, 2114.
55. Drozd, V.N., Ustynyuk, Y.A., Tsel'eva, M.A., Dmitriev, L.B. *Zh. Obshch. Khim.* **1969**, *39*, 1991.
56. Hill, E.A., Theissen, R.J., Doughty, A., Miller, R. *J. Org. Chem.* **1969**, *34*, 3681.
57. Walling, C., Cioffari, A. *J. Am. Chem. Soc.* **1970**, *92*, 6609.
58. Kossa, W.G., Jr., Rees, T.C., Richey, H.G., Jr. *Tetrahedron Lett.* **1971**, 3455.
59. Closs, G.L. *J. Am. Chem. Soc.* **1969**, *91*, 4552.
60. Kaptein, R., Oosterhoff, L.J. *Chem. Phys. Lett.* **1969**, *4*, 195.
61. Anteunis, M., Van Shoote, J. *Bull. Soc. Chim. Belg.* **1963**, *72*, 787–796.
62. Zakharkin, L.I., Okhlobystin, O.Y., Bilevitch, K.A. *Tetrahedron* **1965**, *21*, 881–886.
63. Jones, L.A., Kirby, S.L., Kean, D.M., Campbell, G.L. *J. Organomet. Chem.* **1985**, *284*, 159–169.
64. Grootveld, H.H., Blomberg, C., Bickelhaupt, F., *Tetrahedron Lett.* **1971**, 1999–2002.
65. Molle, G., Bauer, P., Dubois, J.E. *J. Org. Chem.* **1982**, *47*, 4120–4128.
66. Swift, B.L., Garst, J.F. *Unpublished work.*
67. Smoluchowski, M. v. *Ann. Physik (Leipzig)* **1915**, *48*, 1103.
68. Collins, F.C., Kimball, G.E. *J. Colloid Sci.* **1949**, *4*, 425.
69. Noyes, R.M. *J. Chem. Phys.* **1954**, *22*, 1349.
70. Noyes, R.M. *Prog. React. Kinet.* **1961**, *1*, 129.
71. Naqvi, K.R., Mork, K.J., Waldenstrom, S. *J. Phys. Chem.* **1980**, *84*, 1315–1319.
72. Rice, S.A. *Diffusion-Limited Reactions*; Elsevier: Amsterdam, 1985.
73. Berg, O.G. *Chem. Phys.* **1978**, *31*, 47.
74. Garst, J.F. *J. Chem. Soc., Chem. Commun.* **1987**, 589–590.
75. Garst, J.F. *J. Chem. Soc., Chem. Commun.* **1987**, 1440–1441.
76. Garst, J.F. *J. Chem. Soc., Faraday Trans. 1* **1989**, *85*, 1245–1255.
77. Garst, J.F. *J. Am. Chem. Soc.* **1992**, *114*, 1168–1173.
78. Noyes, R.M. *J. Am. Chem. Soc.* **1955**, *77*, 2042–2045.
79. Pólya, G. *Mathematische Annalen* **1921**, *84*, 149–160.
80. Doyle, P.G., Snell, J.L. *Random Walks and Electric Networks*; Mathematical Association of America: 1984.
81. Berg, H.C. *Random Walks in Biology*; Princeton University Press: Princeton, N.J.., 1983.
82. Garst, J.F., Deutch, J.E., Whitesides, G.M. *J. Am. Chem. Soc.* **1986**, *108*, 2490–2491.
83. Garst, J.F., Swift, B.L. *J. Am. Chem. Soc.* **1989**, *111*, 241–250.

84. Garst, J.F., Swift, B.L., Smith, D.W. *J. Am. Chem. Soc.* **1989**, *111*, 234–241.
85. Root, K.S., Hill, C.L., Whitesides, G.M. *Unpublished manuscript.*
86. Chatgilialoglu, C., Ingold, K.U., Scaiano, J.C. *J. Am. Chem. Soc.* **1981**, *103*, 7739–7742.
87. Carlsson, D.J., Ingold, K.U. *J. Am. Chem. Soc.* **1968**, *90*, 7047–7055.
88. Ungváry, F., Garst, J.F. *Unpublished results.*
89. Ballard, R.E., in *The Chemistry of the Cyclopropyl Group*; Rappaport, Z., Ed., Wiley: Chichester, 1987, pp. 213–254.
90. Tidwell, T.T., in *The Chemistry of the Cyclopropyl Group*; Rappaport, Z., Ed., Wiley: Chichester, 1987, pp. 565–632.
91. Fessenden, R.W., Schuler, R.H. *J. Chem. Phys.* **1963**, *39*, 2147–2195.
92. Johnston, L.J., Ingold, K.U. *J. Am. Chem. Soc.* **1986**, *108*, 2343–2348.
93. Deycard, S., Hughes, L., Lusztyk, J., Ingold, K.U. *J. Am. Chem. Soc.* **1987**, *109*, 4954–4960.
94. Johnston, L.J., Scaiano, J.C., Ingold, K.U. *J. Am. Chem. Soc.* **1984**, *106*, 4877–4881.
95. Varick, T.R., Newcomb, M. *Unpublished results*, personal communication.
96. Boche, G., Walborsky, H.M., in *The Chemistry of the Cyclopropyl Group*; Rappaport, Z., Ed., Wiley: Chichester, 1987, pp. 701–808.
97. Garst, J.F., Ungvary, F., Baxter, J.T. *J. Am. Chem. Soc.* **1997**, *119*, 253–254.
98. Garst, J.F., Lawrence, K.E., Batlaw, R., Boone, J.R., Ungváry, F. *Inorg. Chim. Acta* **1994**, *222*, 365–375.
99. Grignard, V. *Bull. Soc. Chim. Fr.* **1907**, *1*, 256–262.
100. Wiberg, K.B., Bartley, J.W. *J. Am. Chem. Soc.* **1960**, *82*, 6375.
101. Bickelhaupt, F. *Pure Appl. Chem.* **1986**, *58*, 537–542.
102. Garst, J.F. *Unpublished calculations.*
103. Kopecky, K.R., Gillian, T. *Can. J. Chem.* **1969**, *47*, 2371.
104. Greene, F.D., Berwick, M.A., Stowell, J.C. *J. Am. Chem. Soc.* **1970**, *92*, 867.
105. Walborsky, H.M., Chen, J.-C. *J. Amer. Chem. Soc.* **1971**, *93*, 671–675.
106. Engstrom, J.P., Greene, F.D. *J. Org. Chem.* **1972**, *37*, 968.
107. Garst, J.F. *J. Am. Chem. Soc.* **1975**, *97*, 5062–5065.
108. Garst, J.F. *J. Phys. Chem.* **1980**, *84*, 1995–1997.
109. Walborsky, H.M., Rachon, J. *J. Am. Chem. Soc.* **1989**, *111*, 1896–1897.
110. Boche, G., Schneider, D.R., Wintermayr, H. *J. Am. Chem. Soc.* **1980**, *102*, 5697–5699.
111. Walborsky, H.M., Banks, R.B. *Bull. Soc. Chim. Belg.* **1980**, *89*, 849–868.
112. Garst, J.F., Boone, J.R., Webb, L., Lawrence, K.E., Baxter, J.T., Ungváry, F. *Unpublished manuscript.*
113. Johnston, L.J., Lysztyk, J. Wayner, D.D.M., Abeywickreyma, A.N., Beckwith, A.L.J., Scaiano, J.C., Ingold, K.U. *J. Am. Chem. Soc.* **1985**, *107*, 4594–4596.
114. Abeywickrema, A.N., Beckwith, A.L.J. *J. Chem. Soc. Chem. Commun.* **1986**, 464–465.
115. Walborsky, H.M., Powers, E.J. *Isr. J. Chem.* **1981**, *21*, 210–220.
116. Garst, J.F., in *Solute-Solvent Interactions*; Coetzee, J.F. and Ritchie, C.D., Ed., M. Dekker: New York, 1969, pp. 539–605.
117. Egorov, A.M., Anisimov, A.V. *J. Organomet. Chem.* **1994**, *479*, 197–198.
118. Baker, K.V., Brown, J.M., Hughes, N., Skarnulis, A.J., Sexton, A. *J. Org. Chem.* **1991**, *56*, 698–703.
119. Hill, C.L., Vander Sande, J.B., Whitesides, G.M. *J. Org. Chem.* **1980**, *45*, 1020–1028.
120. Garst, J.F. *Prepr. - Am. Chem. Soc., Div. Petrol. Chem.* **1968**, *13*, D65–D76.
121. Garst, J.F. *J. Am. Chem. Soc.* **1968**, *90*, 7159–7160.
122. Garst, J.F., Ayers, P.W., Lamb, R.C. *J. Am. Chem. Soc.* **1966**, *88*, 4260–4261.
123. Garst, J.F. *Acc. Chem. Res.* **1971**, *4*, 400–406.
124. Garst, J.F., in *Free Radicals*; Kochi, J.K., Ed., Wiley: New York, 1973; Vol. 1, pp. 503–546.
125. Tremelling, M.J., Bunnett, J.F. *J. Am. Chem. Soc.* **1980**, *102*, 7375–7377.
126. Meijs, G.F., Bunnett, J.F., Beckwith, A.L.J. *J. Am. Chem. Soc.* **1986**, *108*, 4899–4904.
127. Rys, P. *Acc. Chem. Res.* **1976**, *9*, 345–351.
128. Andrieux, C.P., Savéant, J.-M. *J. Am. Chem. Soc.* **1993**, *113*, 8044–8049.
129. Andrieux, C.P., Savéant, J.-M. *J. Phys. Chem.* **1993**, *97*, 10879–10888.
130. Normant, H. *C. R. Hebd. Seances Acad. Sci.* **1954**, *239*, 1510.
131. Péralez, E., Négrel, J.-C., Chanon, M. *Tetrahedron Lett.* **1994**, *35*, 5857–5860.
132. Péralez, E., Négrel, J.-C., Chanon, M. *Tetrahedron* **1995**, *51*, 12601–12610.
133. Péralez, E., Négrel, J.-C., Goursot, A., Chanon, M., *Main Group Met. Chem.* **1998**, *21*, 69–76.
134. Hörak, M., Palm, V., Soogenbits, U. *Reakts. Sposobn. Organ. Soedin.* **1975**, 709–719. Cited by Péralez *et al.*
135. Chanon, M. *Bull. Soc. Chim. Fr.* **1982**, *7–8*, 197–238.
136. Markies, P.R., Akkerman, O.S., Bickelhaupt, F., W.Smeets, J.J., Spek, A.L. *J. Am. Chem. Soc.* **1988**, *110*, 4284–4292.

137. De Boer, H.J.R., Akkerman, O.S., Bickelhaupt, F., *Angew. Chem.* **1988**, *100*, 735–737.
138. Inanaga, J., Ishikawa, M., Yamaguchi, M., *Chem. Lett.* **1987**, 1485.
139. Inanaga, J., Ujikawa, O., Yamaguchi, M. *Tetrahedron Lett.* **1991**, *32*, 1737.
140. Clark, T. *J. Chem. Soc., Chem. Commun.* **1984**, 93.
141. Clark, T., Illing, G. *J. Chem. Soc., Chem. Commun.* **1985**, 529–530.
142. Garst, J.F., Roberts, R.D., Pacifici, J.A. *J. Am. Chem. Soc.* **1977**, *99*, 3528–3529.
143. Kerr, C.M., Williams, F. *J. Am. Chem. Soc.* **1971**, *93*, 2805.
144. Symons, M.C.R. *Pure Appl. Chem.* **1981**, *53*, 223–238.
145. Symons, M.C.R. *Acta Chem. Scand.* **1997**, *51*, 127–134.
146. Andrieux, C.P., Gallardo, I., Savéant, J.-M. Su, K.-B. *J. Am. Chem. Soc.* **1986**, *108*, 638–647.
147. Webb, J.L., Mann, C.K., Walborsky, H.M. *J. Am. Chem. Soc.* **1970**, *92*, 2042–2050.
148. Walborsky, H.M., Aronoff, M.S. *J. Organomet. Chem.* **1965**, *4*, 418.
149. Walborsky, H.M., Aronoff, M.S., *J. Organomet. Chem.* **1973**, *51*, 55–75.
150. Walborsky, H.M., Hamdouchi, C. *J. Org. Chem.* **1993**, *58*, 1187–1193.
151. Walborsky, H.M., Ollman, J., Hamdouchi, C., Topolski, M. *Tetrahedron Lett.* **1992**, *33*, 761–764.
152. Boche, G., Schneider, D.R., *Tetrahedron Lett.* **1978**, 2327.
153. Walborsky, H.M., Pierce, J.B., *J. Org. Chem.* **1968**, *33*, 4102–4105.
154. Staley, S.W., Rocchio, J.J. *J. Am. Chem. Soc.* **1969**, *91*, 1565–1566.
155. Garst, J.F., Roberts, R.D., Abels, B.N. *J. Am. Chem. Soc.* **1975**, *97*, 4925–4929.
156. Garst, J.F., Hewitt, C., Walmsley, D., Richards, W., *J. Am. Chem. Soc.* **1961**, *83*, 5034–5035.
157. Garst, J.F., Cole, R.S. *J. Am. Chem. Soc.* **1962**, *84*, 4352–4353.
158. Garst, J.F., Walmsley, D., Hewitt, C., Richards, W.R., Zabolotny, E.R. *J. Am. Chem. Soc.* **1964**, *86*, 412–418.
159. Zabolotny, E.R., Garst, J.F. *J. Am. Chem. Soc.* **1964**, *86*, 1645–1646.
160. Garst, J.F., Zabolotny, E.R., Cole, R.S. *J. Am. Chem. Soc.* **1964**, *86*, 2257–2261.
161. Garst, J.F., Zabolotny, E.R. *J. Am. Chem. Soc.* **1965**, *87*, 495–501.
162. Garst, J.F., Klein, R.A., Walmsley, D., Zabolotny, E.R. *J. Am. Chem. Soc.* **1965**, *87*, 4080–4084.
163. Garst, J.F., Richards, W.R. *J. Am. Chem. Soc.* **1965**, *87*, 4084–4086.
164. Pacifici, J.G., Garst, J.F., Janzen, E.G. *J. Am. Chem. Soc.* **1965**, *87*, 3014.
165. Walborsky, H.M., Topolski, M. *J. Am. Chem. Soc.* **1992**, *114*, 3455–3459.
166. Walborsky, H.M., Zimmermann, C. *J. Am. Chem. Soc.* **1992**, *114*, 4996–5000.
167. Walborsky, H.M., Topolski, M., Hamdouchi, C., Pankowski *J. Org. Chem.* **1992**, *57*, 6188–6191.
168. Koon, S.E., Oyler, C.E., Hill, J.H.M., Bowyer, W.J. *J. Org. Chem.* **1993**, *58*, 3225–3226.
169. Teerlinck, C.E., Bowyer, W.J. *J. Org. Chem.* **1996**, *61*, 1059–1064.
170. Wade, T., Garst, J.F., Stickney, J.L. *Rev. Sci. Instrum.* **1999**. In press.
171. Wade, T., Stickney, J.L., Garst, J.F. *Unpublished results.*
172. Abreu, J.B., Soto, J.E., A. Ashley-Facey, Soriaga, M.P., Garst, J.F., Stickney, J.L. *J. Colloid Interf. Sci.* **1998**, *206*, 247–251.
173. Allen, R.B., Lawler, R.G., Ward, H.R. *Tetrahedron Lett.* **1973**, 3303–3306.
174. Lehr, G.F., Lawler, R.G. *J. Am. Chem. Soc.* **1984**, *106*, 4048–4049.
175. Tuulmets, A., Heinoja, K. *Org. Reactiv. (Tartu)* **1990**, *27*, 27–41.
176. Tuulmets, A., Kirss, M. *Main Group Met. Chem.* **1997**, *20*, 345–349.
177. Ricke, R.D., Hudnall, P.M. *J. Am. Chem. Soc.* **1972**, *94*, 7178.
178. Rieke, R.D., Sell, M.S. *Handbook of Grignard Reagents*; Silverman, G.S., and Rakita, P.E., Ed., Dekker: New York, 1996, pp. 53–77.
179. Négrel, J.-C., Gony, M., Chanon, M., Lai, R. *Inorg. Chim. Acta* **1993**, *207*, 59–63.
180. Renaud, P. *Bull. Soc. Chim. Fr.* **1950**, *17*, 1044.
181. Sprich, J.D., Lewandos, G.S. *Inorg. Chim. Acta* **1983**, *76*, 1241.
182. Pugin, B., Turner, A.T. *Advances in Sonochemistry*; Mason, T.J., Ed., JAI Press: London, 1990; Vol. 1, Chapter 3.
183. Tuulmets, A., Kaubi, K., Heinoja, K. *Ultrasonics Sonochem.* **1995**, *2*, S75–S78.
184. Gomberg, M., Bachmann, W.E. *J. Am. Chem. Soc.* **1927**, *49*, 236.
185. Blues, E.T., Bryce-Smith, D. *Chemistry and Industry* **1960**, December 10, 1533–1534.
186. Grignard, V. *C.R. Hebd. Seances Acad. Sci.* **1934**, *198*, 625.
187. Pearson, D.E., Cowan, D., Beckler, J.D., *J. Org. Chem.* **1958**, *24*, 504–509.
188. Garst, J.F., Ungvary, F., Batlaw, R. *J. Am. Chem. Soc.* **1991**, *113*, 6697–6698.
189. Davis, J.R. *Metals Handbook*; 9th Ed., ASM International: Metals Park, OH, 1987; Vol. 13.

190. Rausch, M.D., McEwen, W.E., Kleinberg, J. *Chem. Rev.* **1957**, *57*, 417–437.
191. Petty, R.L., Davidson, A.W., Kleinberg, J. *J. Am. Chem. Soc.* **1954**, *76*, 363–366.
192. Jasien, P.G., Dykstra, C.E. *J. Am. Chem. Soc.* **1983**, *105*, 2089.
193. Garst, J.F., Barton, F.E., II; Morris, J.I. *J. Am. Chem. Soc.* **1971**, *93*, 4310. Footnote 5.
194. Naqvi, K.R., Waldenstrøm, S., Mork, K.J. *J. Phys. Chem.* **1982**, *86*, 4750–4756.

8

Applications of Magnesium Anthracene in Forming Grignard Reagents

Colin L. Raston
Department of Chemistry, Monash University, Melbourne, Australia

8.1 INTRODUCTION

The magnesium–anthracene complex [Mg(anthracene)$(THF)_3$] [THF = tetrahydrofuran] is a versatile reagent which can react in a variety of ways [1–4]. The complex was originally prepared by Ramsden in 1965 [5] from elemental magnesium and anthracene in THF. It was not until early last decade that full synthetic details and applications of the complex and variations thereof were explored, mainly by Bogdanovic *et al.* [4] and Raston *et al.* [2,6]. This was triggered both by the potential of magnesium–anthracene in the catalytic formation of MgH_2 under mild conditions [4,7] and in forming Grignard reagents of benzylic halides [2,6].

This chapter focuses on the application of Mg(anthracene)$(THF)_3$ and related magnesium–anthracene complexes in forming Grignard reagents, detailing the formation of the complexes in general and their properties, the types of Grignard reagents which can be prepared, competing reactions, the mechanism of formation of the Grignard reagents, hybrid supported magnesium–anthracene complexes and their utility in forming Grignard reagents, and future prospects. These ambivalent complexes can act as diorganomagnesium species (electrophilic attack on the anthracene with heterolytic cleavage of the Mg–C bonds) or as sources of magnesium (homolytic cleavage of Mg–C bonds). For the latter there is a clear distinction between (i) the complexes acting as soluble sources of zero valent magnesium or as single electron donors, and (ii) the complexes forming highly activated magnesium *via* equilibration with anthracene and metal which then reacts with the organic substrate. For (ii) the anthracene can be described as a phase transfer catalyst for generating metallic magnesium, as long as it is not consumed in side reactions. Conjugated olefins also react with elemental magnesium in coordinating solvents such as THF. Their syntheses and applications in organic synthesis are beyond the scope of this chapter and are detailed elsewhere [1–3,8].

Grignard Reagents: New Developments Edited by Herman G. Richey, Jr. © 2000 John Wiley & Sons Ltd.

8.2 FORMATION AND PROPERTIES OF MAGNESIUM ANTHRACENE

Mg(anthracene)$(THF)_3$ is an orange, pyrophoric compound, conveniently prepared in high yield directly from magnesium powder with anthracene in THF, Scheme 8.1. Activation of the metal is effective with 1,2-dibromoethane [9] or bromoethane [10,11]. Typically a two-fold excess of the anthracene is used to ensure all the magnesium is consumed and this takes 48 hours to complete. Collection of the solid gives a green mother liquor containing the anthracene radical anion species and it can be used for the synthesis of a new batch of Mg(anthracene)$(THF)_3$ over the same timescale on addition of one equivalent of anthracene and one equivalent of magnesium, and so on. Mg(anthracene)$(THF)_3$ has also been prepared electrochemically using sacrificial magnesium [12], by the reaction of sodium anthracene and magnesium bromide in THF [13] and by treating Mg(butadiene)$(THF)_n$ with anthracene in THF [14]. Addition of magnesium chloride to a slurry of Mg(anthracene)$(THF)_3$ in THF affords a solution rich in the radical anion species from which a discrete complex has been isolated, $[Mg_2(\mu\text{-}Cl_3)(THF)_6]^+[C_{14}H_{10}]^\bullet$ [15], Scheme 8.1.

The rate of formation of Mg(anthracene)$(THF)_3$ at 60°C is proportional to the anthracene concentration and magnesium surface area, whereas at 25 C it is proportional to the magnesium surface area [10]. Kinetic studies show the complex, anthracene, magnesium and THF are in a temperature dependent, reversible equilibrium with the complex being favoured at low temperature. Decreasing the concentration of the anthracene shifts the equilibrium in favour of the metal and sonication of such mixtures is a convenient method for preparing highly activated magnesium [16–18]. Indeed the resulting magnesium is equivalent in reactivity to that formed by condensation of magnesium in an inert solvent, and also to Rieke's magnesium (magnesium halide reduction by a group I metal) [19]. This comes from a comparative study of intra-molecular magnesium—ene reactions, equation (8.1) [18]. Heating [Mg(anthracene)$(THF)_3$] to 200°C under high vacuum to remove anthracene and THF yields highly activated magnesium, as does heating MgH_2

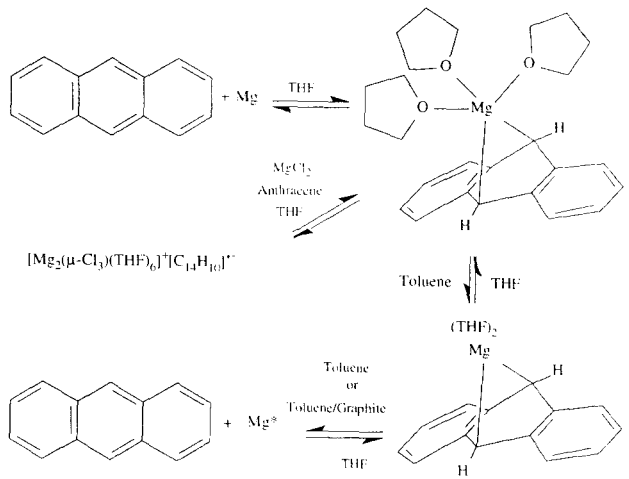

SCHEME 8.1

to greater than 250 C *in vacuo* or greater than 300 C under normal pressure [13,20].

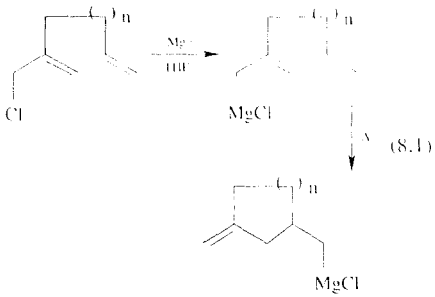

(8.1)

Mg(anthracene)$(THF)_3$ is sparingly soluble in THF, ca. 3 g/l at 23°C [10,11]. It decomposes in non-donor solvents such as toluene, benzene and hexane to anthracene and elemental magnesium, as mirrors or highly activated, finely divided metal. In toluene and benzene this decomposition occurs *via* a yellow intermediate which analyses as the bis-THF adduct, Scheme 8.1 [9,21,22]. Magnesium butadiene (as a bis-THF adduct) similarly decomposes in toluene [21]. On the basis of solid state NMR spectroscopy the bis-THF adduct of magnesium–anthracene has greater covalency in the Mg–C(9,10) interactions than does Mg(anthracene)$(THF)_3$ [22]. The presence of graphite in toluene or diethyl ether accelerates the decomposition of Mg(anthracene)$(THF)_3$ to its constituents, affording finely divided magnesium (particle size *ca.* 6 μm) which is dispersed on the graphite flakes. There is no evidence for the formation of the magnesium/graphite intercalation compound. This form of magnesium is non-pyrophoric yet highly activated, demonstrated, for example, by rapidly affording Mg(anthracene)$(THF)_3$ on the addition of anthracene and THF which is complete in 15 minutes, in contrast to 48 hours using commercially available magnesium [5]. Solution ^{13}C NMR studies on Mg(anthracene)$(THF)_3$ are consistent with magnesium bridging the C(9) and C(10) carbon centres [10].

Magnesium also reacts with a variety of substituted anthracenes in THF, equation (8.2) [9,15, 22–25], usually involving temperature dependent equilibria [4,9]. Anthracene derivatives containing internally coordinating ether and amino groups have similarly been prepared and characterized spectroscopically, and some complex formation rates established [27]. 9,10-Diphenylanthracene behaves differently, reacting with magnesium in THF at 20°C affording deep blue solutions of the radical anion complex, Mg(9,10-diphenylanthracene)$_2$ which crystallizes as the hexakis—THF adduct, presumably containing $Mg(THF)_6^{2+}$ [4]. Heating to 60°C gives the dianion complex and free anthracene. Phenazine is isoelectronic with anthracene and undergoes reduction to the radical anion by magnesium in THF, or to the dianion in the presence of magnesium bromide [28], and to the radical anion by the heavier group 2 elements, Ca, Sr and Ba [29].

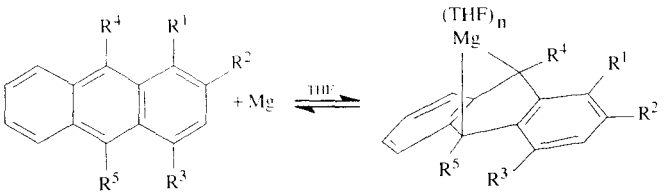

(8.2)

R^2 = Me, $R^{1,3-5}$ = H, n = 3
$R^{1,3}$ = Me, $R^{2,4,5}$ = H, n = 3
R^4 = Me, $R^{1-3,5}$ = H, n = 3
R^4 = Et, $R^{1-3,5}$ = H, n = 3
$R^{4,5}$ = Me, R^{1-3} = H, n = 3

R^4 = Ph, $R^{1-3,5}$ = H, n = 3
$R^{4,5}$ = Ph, R^{1-3} = H, n = 3
$R^{4,5}$ = $SiMe_3$, R^{1-3} = H, n = 2
R^4 = $SiMe_3$, $R^{1-3,5}$ = H, n = 2
R^4 = $SiMe_2CH_2Ph$, $R^{1-3,5}$ = H, n = 2

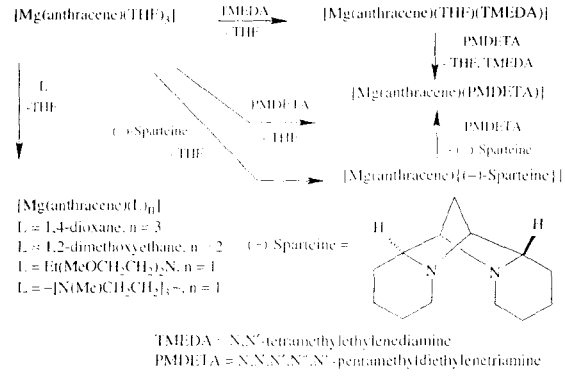

SCHEME 8.2

Mg(anthracene)$(THF)_3$ and magnesium–substituted anthracene/THF donor complexes undergo rapid donor ligand displacement reactions with a variety of *N*- and *O*-donor solvents, and these are summarized in Scheme 8.2 [9,21]. They react in a similar way to the parent compound, Mg(anthracene)$(THF)_3$, for example, affording 9,10-dihydroanthracene on protolysis [21]. Mg(anthracene)(TMEDA)(THF) can also be prepared directly from magnesium, anthracene, THF and TMEDA at room temperature, but the reaction is much slower than the formation of Mg(anthracene)$(THF)_3$, taking ca. 7 days, cf. 48 hours, Scheme 8.1. Also, in contrast to the formation of Mg(anthracene)$(THF)_3$ is that stoichiometric quantities of magnesium and anthracene, and also TMEDA suffice, showing that the TMEDA adduct has greater stability with respect to its constituents (Mg, anthracene, donor ligands) than Mg(anthracene)$(THF)_3$. This is consistent with the indefinite stability of the TMEDA adduct in diethyl ether, toluene and benzene, in contrast to Mg(anthracene)$(THF)_3$ decomposing to its constituents in the same solvents. Mg(anthracene)(PMDETA) can be similarly prepared from its constituents, albeit in the presence of THF. Evidently for these reactions the presence of THF is required to effect the electron transfer processes. Although, (−)-sparteine fails to react with magnesium and anthracene in THF, it slowly forms Mg(anthracene){(−)-sparteine} in toluene. The more bulky bidentate tertiary amine, (−)-sparteine, leads to a four coordinate species rather than a five coordinate species using TMEDA, and the (−)-sparteine adduct is of interest as a potential source of 'optically active' magnesium [9]. The higher stability of the tertiary amine adducts of magnesium–anthracene is noteworthy in studying reactions of magnesium anthracene in solvents other than THF.

Treatment of the bis-THF adduct of magnesium–9-trimethylsilylanthracene with TMEDA gives Mg(9-trimethylsilylanthracene)(TME-DA)(THF), and thus an expansion of the metal coordination from four to five. The bis-THF adduct of magnesium 9,10-bis(trimethylsilyl)anthracene undergoes exchange of the two donor groups by TMEDA, in this case retaining the four-fold coordination, and this exchange is reversible, depending on the concentration of the competing donor ligands [9]. It appears that the steric hindrance associated with only one trimethylsilyl group on the anthracene results in a complex which is at the threshold between four and five coordination.

Metathetical exchange of the anthracene attached to magnesium in Mg(anthracene)$(THF)_3$ by other anthracenes is a useful way of

preparing magnesium–silyl substituted anthracene complexes, equation (8.3), and preparing supported magnesium anthracene complexes [9,25,26,30]. This relates to the ability of silicon to stabilize charge by polarization [31] and that silylated anthracenes are more easily reduced than anthracene. Other exchange reactions have been reported [9].

Related chemistry is the reaction of Mg(anthracene)$(THF)_3$ with cyclooctatetraene (=COT) affording [Mg(COT)$(THF)_{2.5}$], although the same complex is more conveniently prepared by sonication of the reaction mixture of magnesium, COT and a catalytic amount of anthracene. The implied intermediate is Mg(anthracene)$(THF)_3$ which undergoes metathetical exchange with COT.

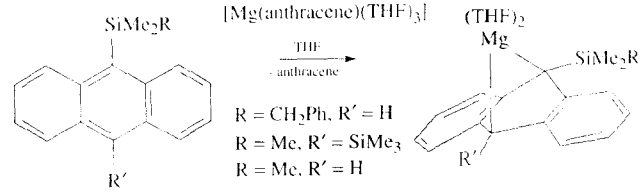

(8.3)

Scheme 8.3 [9]. Mg(anthracene)$(THF)_3$ reacts with fluoranthene to give the radical anion complex $[Mg(THF)_6]^{2+}[fluoranthene]_2^{\bullet-}$, the same compound being formed from fluoranthene and magnesium in THF [2]. Addition of TMEDA to the fluoranthene complex gives an unstable pink solid which deposits elemental magnesium over several hours.

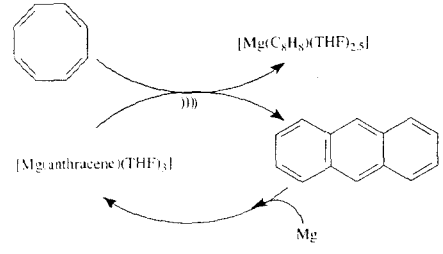

SCHEME 8.3

The five coordinate structure of Mg(anthracene)$(THF)_3$, Figure 8.1, has been authenticated [32] along with that of a related complex bearing methyl groups in the 1,3 positions on the anthracene, $R^{1,3}$ = Me, $R^{2,4,5}$ = H, n = 3 [14] equation (8.2), and two structures of four coordinate complexes where the anthracene is substituted at the C(9,10) positions, $R^{4,5}$ = $SiMe_3$, R^{1-3} = H, n = 2, [9,23] equation (8.2), and the four coordinate TMEDA analogue [9]. All structures show that the metal centres are attached to the reduced arene through the C(9,10) positions and that the anthracene is folded along the C(9,10) vector by 27–43°, the metal centre being in a strained metallacyle ring system. The Mg–C distances, *ca.* 2.22 Å for magnesium-trimethylsilyl substituted anthracene complexes, or *ca.* 2.30 Å for the others, together with the folding and associated loss of aromatic character, and NMR spectroscopy data are consistent with the presence of polarized covalent Mg–C bonds involving sp^2 carbon centres. The steric effect of the trimethylsilyl groups results in a lower coordination number, and slightly greater covalency.

8.3 REACTIONS: GENERAL CONSIDERATIONS

Mg(anthracene)$(THF)_3$ and related complexes are highly reactive, and this relates to the weakness of the Mg–C bonds, and undergo a diverse range of reactions. The nature of the reactions with organic halides is variable with the complexes acting either as sources of metal, as single electron reductants or as nucleophiles. These are dealt with in the following sections. For other organic substrates they react mainly as nucleophiles and the reactions are summarized in Scheme 8.4 (equations 8.4–8.6).

Fig. 1.1. Molecular projection of Mg(anthracene)$(THF)_3$ [32].

Protolysis results in the formation of the corresponding 9,10-dihydroanthracenes [4,10,15,21,24, 33]. Mg(anthracene)$(THF)_3$ and the 9-methylanthracene substituted analogue undergo insertion of a single ethylene at 85°C and 60 bar ethylene, Scheme 8.4 [34]. For the substituted complex the insertion is into the Mg–C_{tert} bond. Further insertion does not occur due to the removal of the ring strain in the original metallacycle. In THF above 60 C Mg(anthracene)$(THF)_3$ results in ring opening of THF and insertion of buteneoxy units into Mg–C bonds [10]. A similar reaction occurs on treating Mg(anthracene)$(THF)_3$ with ethyl acetate or acetone, yielding a ketone or a tertiary alcohol respectively, the substitution being at the C(9) position [4]. In contrast, reaction of the magnesium–9,10-dimethylanthracene complex affords respectively the bicyclic tertiary alcohol and a C(1) substituted 1,2-dihydroanthracene, Scheme 8.4 [24]. Steric hindrance directs attack of the electrophilic acetone through the C(1) position rather than C(9) position of anthracene. Some benzylic

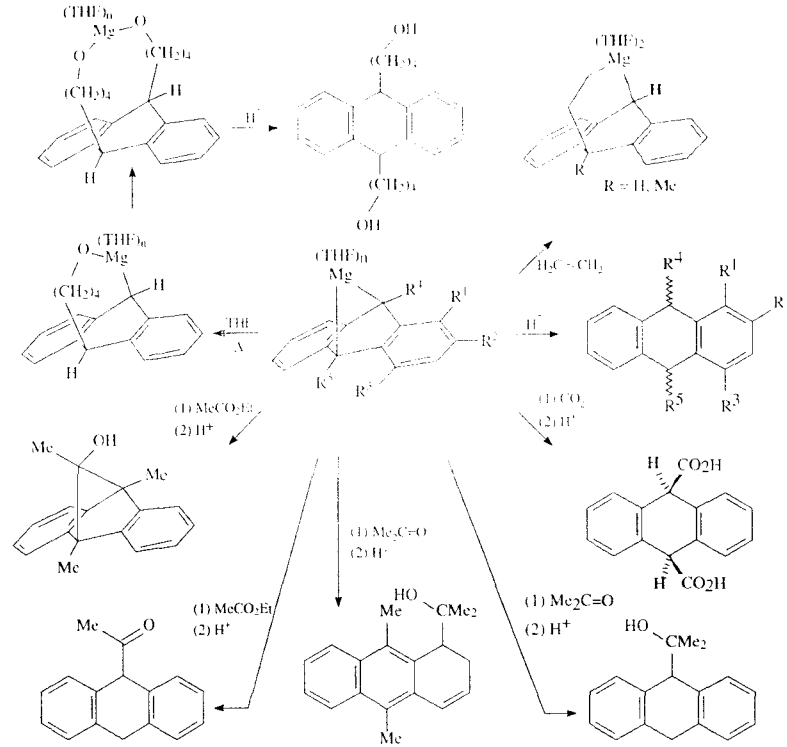

SCHEME 8.4

ethers undergo C–O cleavage with Mg(anthracene)$(THF)_3$ affording benzylic 'Grignard' reagents and this is further discussed in Section 8.4 dealing with the reactions of benzylic halides [35]. Related to this is the ring opening of epoxides by the radical anion complex $Mg(naphthalene)_2$ [36].

Mg(anthracene)$(THF)_3$ is a versatile reagent for preparing other organometallic compounds; it reacts with titanocene and zirconocene dichlorides to give metallocene derivatives of anthracene which are bound through the central ring to the divalent metal centres [37]. Compounds with silicon bridging the C(9,10) positions of anthracene have similarly been prepared from dialkylmetal chlorides [5,38], and reaction of Mg(anthracene)$(THF)_3$ with trimethylsilyl chloride gives mainly 9,10-bis(trimethylsilyl)-9,10-dihydroanthracene. In these cases the Mg(anthracene)$(THF)_3$ acts as a nucleophile (heterolytic cleavage of Mg–C bonds) [4]. In contrast, the reaction with tri-*n*-butylchlorostannane results in homolysis of the Mg–C bonds affording hexa-*n*-butyldistannane and anthracene [4]. Here Mg(anthracene)$(THF)_3$ acts as a reducing agent *via* electron transfer. Similarly a polymer supported di-stannane arises from the reaction of Mg(anthracene)$(THF)_3$ with a polymer bound tin(IV) halide resin [45]. Mixed aluminium and

magnesium complexes are formed on treating Mg(anthracene)(THF)$_3$ with trimethylaluminium, dialkylaluminium hydride and diethylaluminium ethoxide. Similar reactions of magnesium-9,10-bis(trimethylsilyl)anthracene give aluminium metallacyles with the metal bridging the C(9,10) positions of the anthracene [15,40–42]. Finally, complex Mg(anthracene)(THF)$_3$ can act a powerful reducing agent towards transition halides, notably $TiCl_4$ and $CrCl_3$, yielding homogeneous catalysts for the hydrogenation of magnesium to magnesium hydride [4], and in forming low valent group 5 phosphine complexes [43]. The reaction of $TaCl_4(dmpe)_2$ with Mg(anthracene)(THF)$_3$ gives both $TaCl_2(dmpe)_2$ and Ta(η^4-anthracene)$(dmpe)_2$Cl (dmpe = 1,2-bis(dimethylphosphino)ethane) [43].

8.4 FORMATION OF GRIGNARD REAGENTS

The product from the reactions of magnesium anthracene complexes with organic halides depend on the nature of the organic halide, the choice of solvent and temperature. Benzylic halides afford Grignard reagents in high yield, and allylic halides afford Grignard reagents in modest yields. With a few exceptions, other halides result in products from the reduced anthracene in the complexes acting as single electron donors, as discussed later, or as nucleophiles, Scheme 8.5 [4,33,44,45].

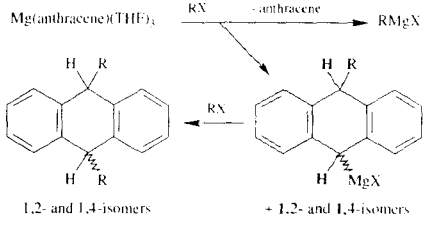

SCHEME 8.5

Benzylic and allylic type Grignard reagents can be difficult to prepare or inaccessible using magnesium powder and turnings as in the classical method of Grignard reagent formation. This is in part due to the stability of the benzylic or allylic centred radical (R· or RX$^{\cdot-}$), allowing departure from the metal surface and thus greater probability of forming Wurtz—coupled products and/or the higher reactivity of the organic halide towards the preformed Grignard reagent. These side reactions can be restricted to some extent by using highly activated magnesium (Section 8.2). Magnesium–anthracene complexes are soluble sources of magnesium and further restrict Wurtz coupling.

Examples of some unusual benzylic Grignard reagents readily prepared using magnesium–anthracene complexes are shown in Figure 8.2. They are either accessible using the classical method but under special conditions (choice of halide, solvent and temperature, activated magnesium), or are inaccessible using the classical method, in most cases even when using highly activated forms of magnesium. A typical experiment in preparing a Grignard reagent using magnesium–anthracene complexes involves the slow addition of a THF solution of the organic halide to a stoichiometric amount of the complex as a slurry in THF usually at 0°C or ca. 20°C and with a target concentration of the Grignard (or poly-Grignard) reagent close to 0.1 M. Immediately after addition of the first few drops of the halide solution, the mixtures turn from orange/yellow to deep green which persists until all the magnesium complex is consumed and the addition of organic halide is complete, whereupon the solution becomes colourless or pale red/brown, with a few exceptions such as the Grignard reagent of triphenylmethyl chloride or bromide. These Grignard reagents are highly coloured and it is difficult to judge the end point of the reactions. Discharge of the green colour is a reliable guide to completion of the Grignard reagent formation and is an attraction of using the method. Moreover, it is a guide as to whether Wurtz coupling prevails since such coupling requires more than the stoichiometric amount of the halide to consume all the magnesium–anthracene complex.

The aforementioned green solutions contain paramagnetic species, which are most likely radical anions of the various anthracenes. Absence of hyperfine coupling in the EPR spectra of

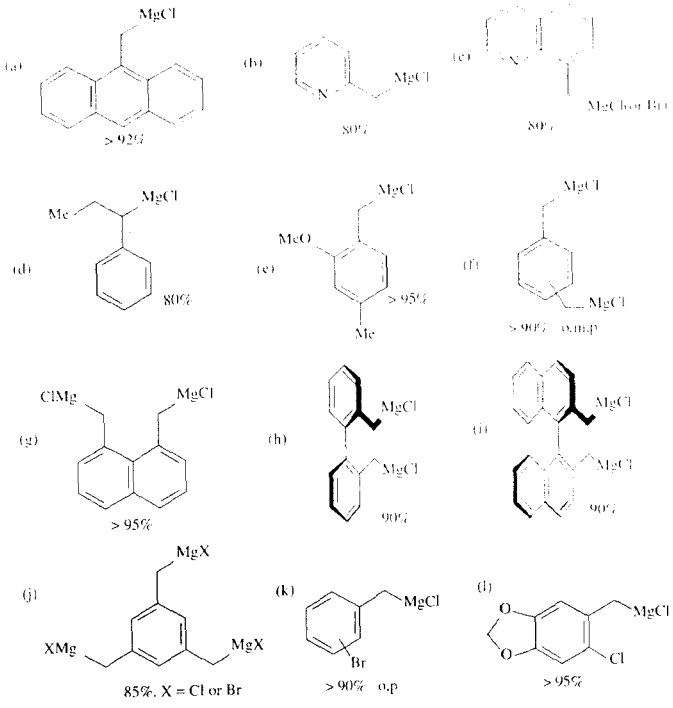

Fig. 8.2. Unusual benzylic Grignard reagents prepared in high yield on treating magnesium–anthracene complexes with organic halides in THF [35,44].

these solutions may be due to rapid electron transfer between radical anions and 'preformed anthracene'. The presence of radicals implies that electron–transfer reactions prevail (Section 8.4.3). The choice of magnesium–anthracene complex has little effect on the overall yield of the target Grignard reagent.

Formation of the Grignard reagents is usually complete in one hour, an exception being the formation of the Grignard reagent of 9-chloromethylanthracene which takes 36 hours for >92% yield [44]. Choice of target concentrations of ca. 0.1 M is a compromise between practicality and a sufficiently high dilution to disfavour Wurtz coupling. The same concentration is used for the synthesis of some benzylic di-Grignard reagents using the classical method, albeit under rather critical conditions [46]. The choice of temperature for the reaction is based on minimizing Wurtz coupling by operating at low temperature, yet not low enough to stop the reaction of the magnesium–anthracene with the halide which can occur below ca. −20°C.

Where the magnesium–anthracene complexes are stable in non-coordinating solvents, they are effective in forming Grignard reagents of benzylic halides in such solvents. The co-ligands on the metal of these complexes most likely stay attached to the metal centre in the generated Grignard reagent. Mg(anthracene)[(−)-sparteine] exchanges

donor ligands in THF. In using toluene as the solvent, it reacts with (±)-α-methylbenzyl chloride to give the Grignard reagent with 7% ee based on the derived carboxylic acid, (equation 8.4) [44]. The asymmetric induction occurs either during the formation of the Grignard reagent or thereafter *via* equilibration of the two diastereoisomers of Mg[(−)-sparteine][CH(Me)Ph].

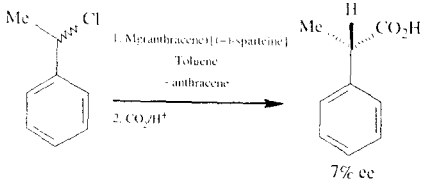

(8.4)

Magnesium-1,3-butadiene complexes exclusively undergo substitution reactions with organic halides, although they can act as a source of metal with other substrates, e.g. I_2, yielding MgI_2 and the butadiene [47,48]. Reaction of $Mg(COT)(THF)_{2.5}$ with benzyl chloride in THF yields the Wurtz—coupled product.

A secondary reaction has been identified in the reaction of magnesium–trimethylsilyl substituted anthracene complexes with benzylic halides, which is the addition of preformed Grignard reagent with the generated anthracene, equation (8.5) [44]. However, this is slow enough not to be a serious problem. The addition is favoured by the electron-withdrawing silyl substituents; otherwise more forcing conditions are required [49].

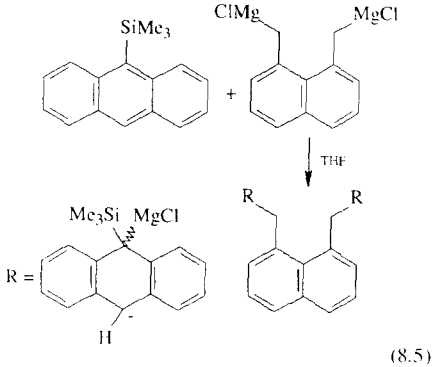

(8.5)

8.4.1 Mono-Grignard Reagents—Special Features

Formation of the Grignard reagent of 9-chloromethylanthracene, Figure 8.2(a), is atypical in the time required for its formation; 36 hours for >92% yield using Mg(anthracene)(THF)$_3$ [44]. Some 9-methylanthracene is formed as a result of H-abstraction from the solvent, a common reaction type for alkali–metal–arene complexes [50]. Use of excess magnesium–anthracene complex has no effect on the rate of formation of the Grignard reagent or on the yield, with all the magnesium–anthracene complex being converted to a metal(anthracene)* species [44]. No Grignard reagent is formed for the bromo-compound. Incorporation of trimethylsilyl groups on the anthracene attached to magnesium slows the reaction even further, as expected by polarizing silyl groups stabilizing charge with the polarization and disfavouring electron transfer [44]. The same Grignard is the implied intermediate in the *in situ* trapping reaction of 9-chloromethylanthracene by $ClSiMe_3$, where the conditions of the reaction are critical since further reaction between the 9-[trimethylsilyl)methyl]anthracene generated and magnesium is possible [51].

Secondary benzylic Grignard reagents are formed in modest yields [44]. 1-(chloro- or bromophenyl)propane for example give 80% and 70% yield respectively of the Grignard reagent, the competing reactions being addition to anthracene, Scheme 8.5, 18% and 3% respectively, and Wurtz—coupling, 25% for the bromide.

The synthesis of Grignard reagents of benzylic halides bearing electron releasing oxygen-centred groups on the aromatic rings, e.g. Figure 8.2(e,l), using magnesium–anthracenes is a significant development in Grignard chemistry [35,52,53]. This, coupled with the ability of oxazolines to activate *o*-methoxy groups towards nucleophilic substitution by Grignard reagents [54], leads to a new synthetic route to preparing naturally occurring anthraquinones in high yield [52,53]. The key reactions involved are the formation of the Grignard reagent and its reaction with *o*-methoxyarydihidrido-oxazoles, en route to the

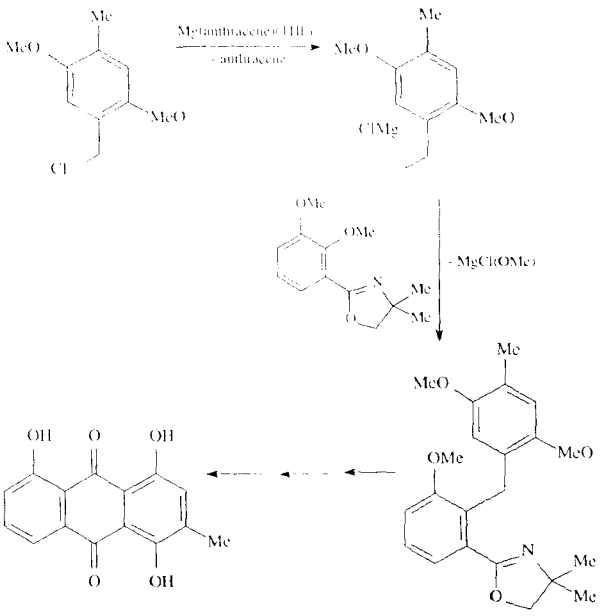

SCHEME 8.6

synthesis of chrysophanol, for example, as shown in Scheme 8.6.

Allyl halides are at the threshold between forming Grignard reagents and anthracene addition products, 50–70% and 30–50% respectively, Scheme 8.5 [44]. The addition is a primary process, as opposed to a secondary reaction of the preformed Grignard reagent with the anthracene, equation (8.5). For these halides there is no advantage of the magnesium–anthracene method over that involving highly activated metal with a catalytic amount of anthracene or Mg(anthracene)(THF)$_3$ as a promoter (ca. 2 mol % of Mg(anthracene)(THF)$_3$ relative to magnesium metal) [4,18,33]. The generation of allyl Grignards using magnesium–anthracene is possible in THF, toluene and diethyl ether, even at −78°C [4,33,55]. Propargyl chloride [HC≡CCH$_2$Cl] fails to reacts with activated magnesium in THF, but reacts with Mg(anthracene)(THF)$_3$ affording allenylmagnesium chloride [CH$_2$=C=CHMgCl] [4,33]. At −78°C an intense blue colour of the solution persists until the addition of another drop of the halide which suggests that at this temperature the radical anion complex of magnesium is formed. Allenylmagnesium chloride is also formed using a catalytic amount of Mg(anthracene)(THF)$_3$, and the reaction takes place *via* the reaction of the halide with the magnesium–anthracene complex rather than with the metal itself.

Tris(trimethylsilyl)methyl chloride is the only non-benzylic or allylic halide to afford a significant amount of the Grignard reagent. Here addition to the anthracene is sterically unfavourable [44]. The Grignard reagent is not accessible using activated magnesium. Bis(trimethylsilyl)methyl chloride, in contrast, readily gives the Grignard reagent using

bulk metal, and using magnesium–anthracene results in addition, Scheme 8.5, as well as the formation of ill-defined products.

8.4.2 Di- and Tri-Grignard Reagents

Poly-Grignard reagents are accessible in high yield on treating benzylic halides with magnesium–anthracene complexes [44,35]. Examples are shown in Figure 8.2 and are best prepared from the chloride and at room temperature, the reaction of 1,2-bis(chloro)methylbenzene excepted. In this case the reaction is optimized at −10°C, resulting in >90% of the target di-Grignard reagent. At 0°C this drops to 87%, and to 80% at room temperature. The competing reaction is partial Wurtz—coupling followed by the formation of the di-Grignard reagent of the coupled compound, equation (8.6).

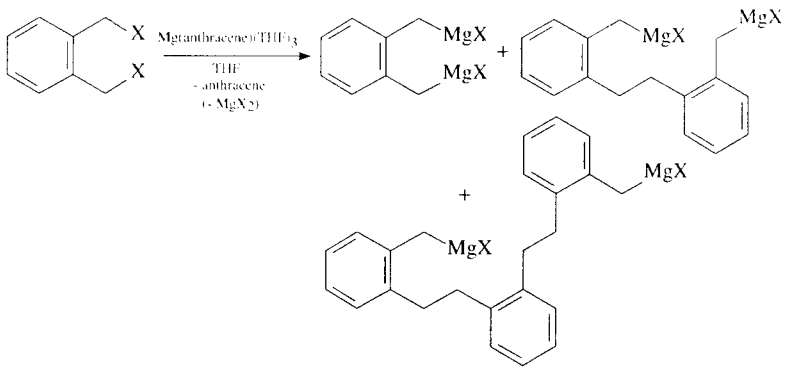

(8.6)

The di-Grignard reagent in Figure 8.2(h) is accessible using elemental magnesium but requiring the use of THF as the solvent and target concentrations of ca. 0.1 M concentrations. Attempts to prepare the corresponding di-bromide however, result in intra-molecular cyclization, Scheme 8.7 [46]. The same di-bromide with Mg(anthracene)(THF)$_3$ gives 60–65% of the di-Grignard reagent. 1,8-Bis(chloromethyl)naphthalene gives little or no di-Grignard reagent even using highly activated magnesium [57], but using Mg(anthracene)(THF)$_3$ in THF the di-Grignard, Figure 8.2(g), is formed in high yield [44].

At room temperature the di-bromide gives only 17% of the target di-Grignard, and 66% of the analogous coupled di-Grignard, and 6% of the next highest coupled product. The extent of coupling is not significantly reduced on lowering the temperature. In the classical reaction the bromide results in formation of polymeric $(C_8H_8)_n$ [46]. Reaction of 1,4-bis(chloromethyl)benzene with Mg(anthracene)(THF)$_3$ at 20°C gives a 1 : 1 mixture of the target di-Grignard reagent and the di-Grignard reagent of the coupled compound, whereas at −10°C the same di-Grignard is formed in >90% yield. There is no inherent problem in forming the 1,3-isomeric di-Grignard reagent, as is the case for the axially asymmetric biphenyls analogues, Figure 8.2(h,i) [9,56], and the tri-Grignard of 1,3,5-tris(chloro- or bromo)methylbenzene, Figure 8.2(j).

o- and *p*-Chloromethyl(methoxymethyl)benzenes rapidly afford the 'di-Grignard' reagents in >95% yield, arising from insertion of magnesium into both the O–CH$_2$ and Cl–C bonds [35]. The *m*-isomer gives only the mono-Grignard reagent derived from insertion into the Cl–C bond, and attempts to form the analogous mono-Grignard reagent for the *o*- and *p*-isomers give mixtures of the di-Grignard reagent and unchanged methoxy/chloro compound. Using elemental magnesium the *o*- and *p*-isomers give polymeric $(C_8H_8)_n$, arising from polymerization of quinodimethanes, whereas the *m*-isomer which is unable to form a

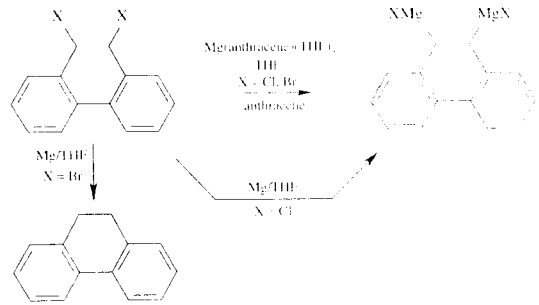

SCHEME 8.7

quinodimethane gives the mono-Grignard reagent. The corresponding dimethoxy compounds all react slowly with Mg(anthracene)(THF)$_3$ to give some di-Grignard reagent (*o*- and *p*-) or some mono-Grignard reagent [35]. Formation of the 'di-Grignards' of *o*- and *p*-chloromethyl(methoxymethyl) benzenes is *via* insertion into the C–Cl bond as the primary process (involving electron transfer processes) and this activates the methoxy group at the *o*- or *p*-methylene group. It is possible that the quinodimethanes are formed for the *o*- and *p*-isomers but are rapidly reduced by electron transfer from the magnesium anthracene complex or a radical anion of anthracene. In general the insertion of Mg into O–C bonds usually requires rather forcing conditions, e.g. Rieke's magnesium reacts slowly with dibenzyl ether [19,58].

8.4.3 Mechanism

Magnesium–anthracene complexes undergo electron transfer reactions in forming Grignard reagents of benzylic halides [4,24,44,45], electron transfer reactions being the accepted mechanism of formation of Grignard reagents using bulk magnesium [59], and also a mechanism of reaction of organomagnesium reagents with organic halides. This is based on: (i) the detection of radicals, most likely of anthracene, during formation of the Grignard reagents; (ii) reaction of 9-chloromethylanthracene with two equivalents of Mg(anthracene)(THF)$_3$ yields solutions containing the Grignard reagent, Figure 8.2(a), and the radical anion of anthracene, (iii) $[Mg_2Cl_3(THF)_6]^+[anthracene]^\bullet$ is also effective in generating Grignard reagents of benzylic halides, and thus both magnesium anthracene complexes and the radical anions of anthracene can contribute to Grignard reagent formation. The cage species $[Mg^{2+}, (anthracene)^{\bullet-}, RX^{\bullet-}]$ can collapse to RMgX, whereas reactions involving (anthracene)$^{\bullet-}$ would yield initially $RX^{\bullet-}$ and/or R$^\bullet$. These can then encounter another radical anion of anthracene to form RMgX. Scheme 8.8 depicts the likely sequence of electron transfer reactions affording Grignard reagents, and also addition products, starting with Mg(anthracene)(THF)$_3$.

Radical anion anthracene species present during Grignard reagent formation may arise from the reaction of Mg(anthracene)(THF)$_3$ with preformed anthracene and MgX$_2$, Scheme 8.1; a shift in the Schlenk equilibrium, $2RMgX \rightleftharpoons MgX_2 + MgR_2$, is a likely source of MgX$_2$. The ability of magnesium anthracene complexes to act as a single electron donor relates to the ease with which the anthracene dianion moiety can be transformed to radical anion species such as $[Mg(THF)_6]^{2+}[anthracene]^{\bullet-}_2$ and $[Mg_2Cl_3(THF)_6]^+[anthracene]^{\bullet-}$ [4, 15,33].

Benzylic bromides tend to give more Wurtz—coupling compared to the corresponding chlorides, which is consistent with Br$^-$ being a better leaving group than Cl$^-$, affording R$^\bullet$ from $RX^{\bullet-}$, Scheme 8.8. It is also consistent with bond energy

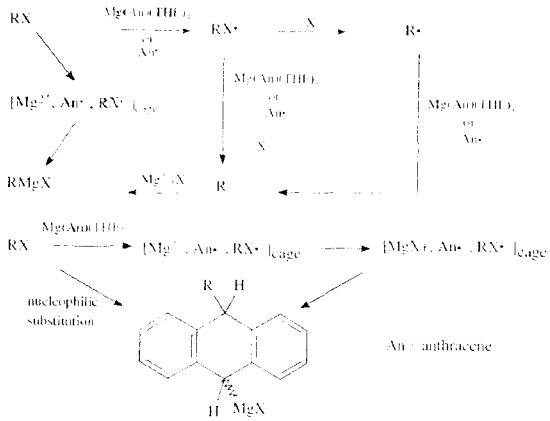

SCHEME 8.8

differences; C–Cl is greater than C–Br and thus loss of Br^- is more favoured both kinetically and thermodynamically.

Magnesium–anthracene complexes are formed by equilibration involving metal and anthracene in THF. In their reactions in THF it is unlikely that small particles of magnesium are the active species in forming Grignard reagents since such particles would yield Grignard reagents with aryl and alkyl halides and this is not the case. As a test example, the di-Grignard of 1,8-bis(chloromethyl)naphthalene, Figure 8.2(g), is formed in 20% yield with highly activated magnesium formed by extensive sonication of magnesium in THF with a catalytic amount of anthracene. Wurtz coupling being the favoured reaction. In contrast the di-Grignard is formed in >95% yield using magnesium anthracene complexes [44]. Thus a stoichiometric amount of a magnesium anthracene is highly effective in forming the Grignard reagent, but not so using a catalytic amount of anthracene. In many cases the latter may suffice but it is important to realize the distinction between the two approaches. Magnesium fluoranthene radical anion species react with benzyl chloride giving the Wurtz—coupled product [44], and magnesium–naphthalene radical anion species cleave epoxides *via* electron transfer processes [56].

Where addition to anthracene prevails, Scheme 8.5, two reaction pathways are plausible, namely concerted nucleophilic substitution and formation of the diradical cage $[Mg^{2+}, (anthracene)^{\bullet-}, RX^{\bullet-}]$, Scheme 8.8. In the absence of any detectable radical intermediates, this cage must collapse instead of releasing $RX^{\bullet-}$ and/or R•. This is conceivable considering the low stability of such radicals relative to those based on allylic, benzylic, and tris(trimethylsilyl)methyl moieties. Moreover, the absence of Grignard reagent or coupled products rules out formation of $RX^{\bullet-}$ and/or R•. Reactions of magnesium–anthracene complexes with alkyl halides in THF in the presence of $FeCl_2$ fail to give any Grignard reagent or Wurtz—coupled product. In this context it is noteworthy that transition metal halides can favour electron transfer processes over nucleophilic substitution [60,61].

8.5 REACTIONS OF OTHER ORGANIC HALIDES

Benzylic, and allylic Grignard reagents, are formed using organic chlorides and bromides, although the organic chlorides are more reliable. Reactions involving other types of organic halides either:

(i) give exclusively the Wurtz—coupled product, e.g. benzyl iodide; (ii) fail to react, e.g. chlorobenzene and 1,2-difluorobenzene; or (iii) give predominantly addition product(s), Scheme 8.5. The latter occurs for bromobenzene (along with proton abstraction from THF), vinyl bromide, and various alkyl halides [33,44,55,62]. With primary and secondary alkyl halides in THF the major products are the dialkyl substituted di-hydroanthracenes (9,10- and 1,4-isomers) and with *tert*-butyl halides the major products are the mono-alkyl substituted dihydroanthracenes (9- and 2-isomers of the substituted anthracenes), Scheme 8.5 [4,24,33,55]. In toluene, however, the major product for primary and secondary alkyls is the Grignard reagent, the yield increasing with temperature, e.g. *n*-butyl chloride at 0°C gives 44% of the Grignard, 52% anthracene, and 27% substituted anthracenes, *cf.* respectively 62, 57 and 28% at room temperature, 79, 82 and 10% at 50–80°C [33]. A competing reaction now is the decomposition of the magnesium–anthracene complex to anthracene and activated magnesium, which then reacts with the organic halide.

The reaction of Mg(anthracene)$(THF)_3$ with MeI is exceptional; during the reaction methane and ethane are formed, and $MgI_2(THF)_6$ precipitates from solution which contains some dimethylmagnesium [33]. Protolysis gives mainly 9,10- and 1,4-dihydroanthracenes. The reaction follows the electron transfer pathway, with the primary process being generation of $MeI^{\bullet-}$, which is analogous to the reaction of alkyl halides with sodium naphthalene [63]. This arises from the lower reduction potential of alkyl iodides compared to chlorides and bromides resulting in dimerization of methyl radical forming the ethane [33]. Another unusual result is the extended reaction time for *tert*-butyl bromide with Mg(anthracene)$(THF)_3$, which on protolysis of the reaction mixture gives 10-*tert*-butyl-9,10-dihydro-9,9-bis(4-hydroxybutyl)-anthracene which is a product arising from cleavage of THF [33].

Where addition to anthracene prevails, the solutions become red or dark brown rather than green (Section 8.4.3) throughout the reaction which suggests that the mechanism here does not involve electron transfer as the primary process, rather it is nucleophilic substitution. This is one of the common reaction pathways for organic halides with organomagnesium reagents in general, the other being electron transfer. The addition is not *via* attack of preformed Grignard reagent on anthracene, equation (8.5). Reaction of *o*-$BrC_6H_4CH_2Br$ with Mg(anthracene)$(THF)_3$ gives a complex mixture containing the mono-Grignard reagent derived from oxidative addition of magnesium to the benzylic–bromine bond and ca. 25% of the addition product of the aryl bromide of this Grignard reagent, equation (8.7) [44]. Another report claimed the reaction gives the di-Grignard reagent of *o*-$BrC_6H_4CH_2Br$ [64]. Bromo-, (bromoethyl)- and (bromopropyl)polystyrene are reported to give the corresponding Grignard reagents when treated with Mg(anthracene)$(THF)_3$ [47], but this has been disputed [44].

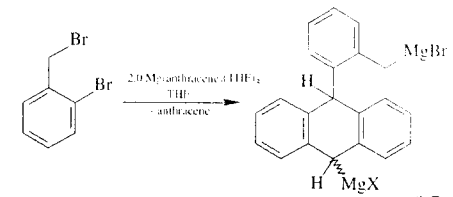

(8.7)

Reactions of bromo- and iodo-benzene with Mg(anthracene)$(THF)_3$ in THF give benzene, arising from abstraction of a hydrogen atom from the solvent. The resulting 2-tetrahydrofuran radical combines with the radical anion of anthracene to give, after protolysis, a substituted di-hydroanthracene, Scheme 8.9 [33,55]. Chlorobenzene reacts sluggishly with Mg(anthracene)$(THF)_3$, and at 60°C in toluene or refluxing diethyl ether gives the Grignard reagent in 85–90% yield, and as for such conditions with primary and secondary alkyl halides leading to formation of Grignard reagents, the active species is finely divided magnesium [33].

α,α-Dichlorocyclopropanes with Mg(anthracene)$(THF)_3$ in THF at low temperature give mainly the addition/hydrogen atom abstraction products, Scheme 8.10 [45]. In toluene a highly selective reduction to the chlorocyclopropane occurs *via* electron transfer/hydrogen atom abstraction,

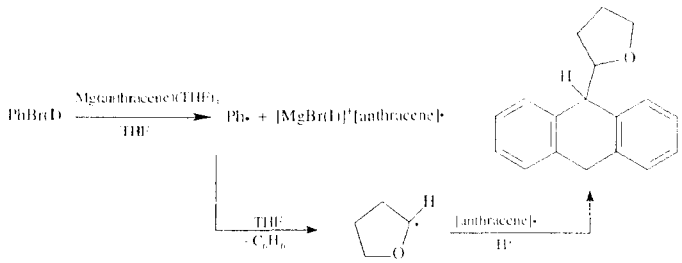

SCHEME 8.9

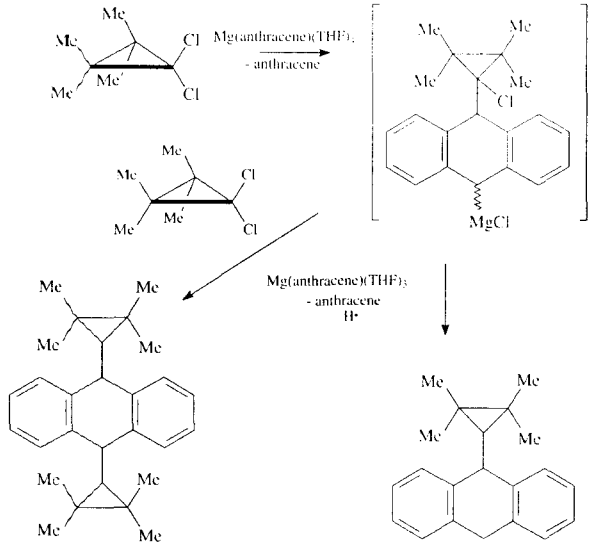

SCHEME 8.10

Scheme 8.9. Overall, the reaction products, which also include carbene species, depend on the substrate and on the reaction conditions. 7,7-Dichloronorcarane gives mainly the addition products, analogous to those in Scheme 8.10, whereas the dibromo-compound gives products derived from electron transfer/hydrogen radical atom abstraction [45].

α,α-Dichlorocyclobutanones are reduced in modest to good yields by Mg(anthracene)$(THF)_3$ in THF to the corresponding α-chlorocyclobutanones, equation (8.8) [45]. Similarly 2-haloketones are converted to halo-free compounds, albeit at low temperature, equation (8.9) [45]. Both reactions proceed *via* electron transfer/solvent hydrogen atom abstraction pathways.

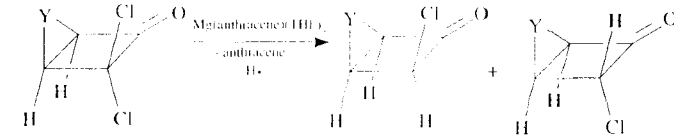

(8.8)

endo- exo-

Y = $-(CH_2)_8-$, 56:44 (77%); Y = $-CH(CH_2)_2CH-$, 98:2 (72%)

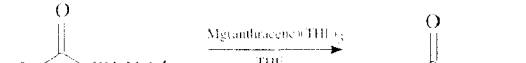

(8.9)

e.g. X = Cl, R = R′ = Me, 45%; X = Br, R = Bu^t, R′ = H, 28%

8.6 SUPPORTED MAGNESIUM ANTHRACENE COMPLEXES

8.6.1 Synthesis

Both silica and polymer supported magnesium anthracene complexes have been developed and shown to deliver magnesium to benzylic halides affording the corresponding Grignard reagents. This overcomes the practical inconvenience of having Grignard reagent solutions loaded with anthracene when using Mg(anthracene)$(THF)_3$ and related compounds as the source of magnesium [25,26,30]. Preparation of the polymer supported material is summarized in Scheme 8.11. The starting material is microporous chloromethylated polystyrene (crosslinked by 1% divinylbenzene) at a low loading, 1.20–1.34 mmol g^{-1} Cl, and high loading, 4.11–4.15 mmol g^{-1} Cl. This is a benzylic halide and is readily converted to the corresponding Grignard reagent on treating with Mg(anthracene)$(THF)_3$ in THF, >95% and >75%, respectively for the two loadings [26,65]. The reactions are characterized by the appearance of deep green solutions containing paramagnetic species, as observed during the reactions of molecular benzylic halides, and are consistent with electron transfer processes. The presence of residual radicals in the reactions involving stoichiometric quantities of the two reactants suggests that increased cross-linking of the polymers occurs during Grignard reagent formation through intramacromolecular Wurtz coupling. The extent of Wurtz coupling is minimal for the lower loading whereas for the higher loading the amount of Mg(anthracene)$(THF)_3$ consumed is significantly less than calculated, as expected with a higher probability of intra-macromolecular encounter of a preformed Grignard centre with a chloromethyl group. The ability to prepare supported Grignard reagents stems from magnesium–anthracene being a THF soluble source of the magnesium which is mobilized in the polymer.

Lithiomethylated polystyrene can be prepared from the same chloromethylated polystyrene on treating it with LiSn(n-butyl)$_3$ and then MeLi to effect cleavage of the arylCH_2-Sn bonds [66]. This can then be converted to the corresponding supported potassium complex *via* metal–metal exchange involving potassium *tert*-pentanoxide [66]. In principle the lithiomethylated polymer offers scope for forming Grignard reagents by treating it with magnesium halides. This approach has been successfully employed for the formation of the Grignard reagent of lithiopolystyrene (from bromopolystyrene) [67]. The polymer supported Grignard reagents in Scheme 8.11 yield anthracene functionalized polymers on treatment with 9-(chlorodimethylsilyl)anthracene. Scheme 8.11. These react with Mg(anthracene)$(THF)_3$

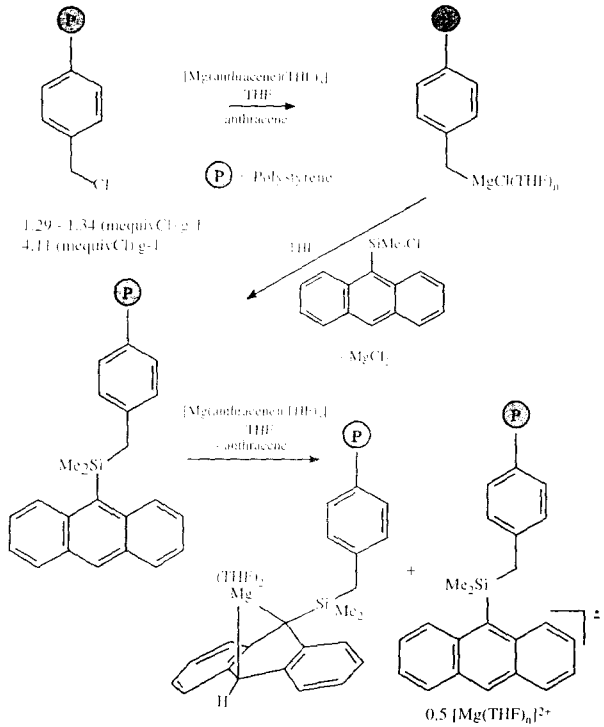

SCHEME 8.11

yielding deep green paramagnetic material containing both dianion, and radical anions of the substituted anthracenes. The metathetical exchange of magnesium relates to the ability of silicon to stabilize charge by polarization [33], and that silylated anthracenes are more readily reduced than anthracene. The polymer supported Grignard reagents in Scheme 8.11 have been used to prepare polymer supported silylanthracenes, and their corresponding radical anion complexes of lithium and sodium. This involves the use of solutions of metal radical anion naphthalenes to effect the cation and electron transfer [68].

The presence of radical centres in the polymer most likely arises from two anthracene units being in close proximity to a single magnesium cation, such as $[Mg(THF)_6]^{2+}$. This may occur either as a result of space limitations within the polymer matrix, or electrostatic constraints in building up two negative charges per anthracene within a confined volume, *viz* communication effects between anthracene units. Silica supported magnesium anthracene, Scheme 8.12, which is similarly prepared and based on a 9-dimethylsilyl substituted anthracene gives exclusively anthracene dianion sites [30]. Here the functional groups are exposed directly to the solvent and any space limitations for uptake of magnesium would be minimal as would charge limitations associated with anthracene groups spread out on a surface.

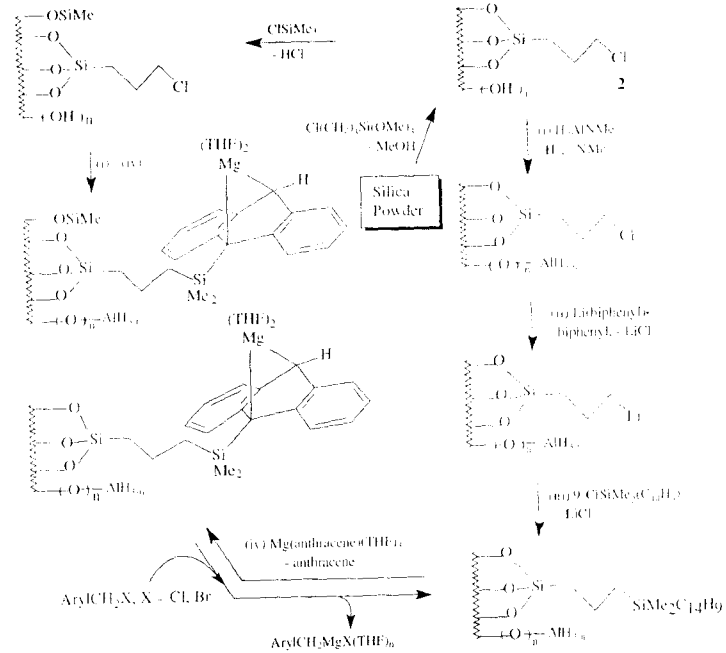

SCHEME 8.12

The relative ratios of the radical anion and dianion centres in polymer supported magnesium–anthracene is 1:1. This is based on the uptake of magnesium when reacted with Mg(anthracene)$(THF)_3$ and the reactivity of the polymer towards benzylic halides (quantity of material converted to the Grignard reagent), further supported by the paramagnetic character of the material. The model compound 9-(benzyldimethylsilyl)anthracene when treated with magnesium or Mg(anthracene)$(THF)_3$ gives exclusively the compound based on the dianion, {Mg[9-(benzyldimethylsilyl) anthracene]}$(THF)_2$.

The polymer supported magnesium–anthracene suffers from relatively low loading of the active sites and this lead to the development of the silica supported analogues, Scheme 8.12 [30]. This approach uses hydroxyl depleted silica surfaces derived from treating chloropropylsilyl (or chloropropylsilyl/trimethylsilyl) functionalized silica with H_3AlNMe_3 then successively $Li^+(biphenyl)^-$, 9-(chlorodimethylsilyl)anthracene and Mg(anthracene)$(THF)_3$. In the absence of the H_3AlNMe_3 treatment, a several-fold excess of $Li^+(biphenyl)^-$ is required to generate the supported lithium reagent, and similarly a several-fold excess of Mg(anthracene)$(THF)_3$ in required to form the supported magnesium–anthracene complex.

8.6.2 Grignard Reagents

The polymer supported magnesium–anthracene complexes also give Grignard reagents from a wide range of benzylic halides, including Grignard reagents in Figure 8.2, as well as Grignard reagents

of allylic halides, including $MeCH{=}CHCH_2MgCl$, and $PhCH{=}CHCH_2MgCl$ [25,26]. Typical target concentrations of the Grignard reagents are 0.1 M and yields are high, and for the benzylic halides they are comparable to those obtained using $Mg(anthracene)(THF)_3$ and related complexes. In a typical experiment the organic halide is added slowly as a THF solution to a THF slurry of the polymer. This results in dissipation of the deep green colour and formation of the corresponding anthracene-free Grignard reagent in *ca.* 90% yield. Unlike reactions involving $Mg(anthracene)(THF)_3$ there is no visible evidence for the formation of radical species during Grignard reagent formation, although this does not preclude a radical pathway. Alternatively, passing a THF solution of the halide through a column packed with the polymer, results in elution of a solution of pure Grignard reagent.

The dianion and radical anion sites in the polymer are both effective in reducing the organic halide. This is in accordance with the ability of the radical anion complex $[Mg(\mu\text{-}Cl)(THF)_6]^+$ [anthracene]$^{\bullet-}$ to covert benzylic halides to Grignard reagents in high yield [44]. In addition, the dianion sites are likely to form radical anion sites in undergoing single electron transfer reactions with organic halides.

The ability of supported magnesium–anthracene to form Grignard reagents of allylic halides in high yield is noteworthy. Reaction of $Mg(anthracene)(THF)_3$ with allylic halides yields 50–70% of the target Grignard reagent, the competing reactions being addition to anthracene, Scheme 8.8. For the polymer versions, Scheme 8.11, however, there is minimal addition which relates to the polymer matrix delivering sequential electrons to the halide as opposed to intimate contact of a dianion site required to form the addition product, Scheme 8.8. Other important aspects of the use of the polymers over magnesium–anthracene complexes include: (i) reduced reaction times; e.g. Grignard reagent in Figure 8.2(a) requires in excess of 36 hours using $Mg(anthracene)(THF)_3$ [44], compared to 12 hours for the polymers, and (ii) reduction in Wurtz—coupled products, e.g. 1,2-bis(chloromethyl)benzene gives 10% coupled di-Grignard reagent using $Mg(anthracene)(THF)_3$, equation (8.6), compared to <5% coupled di-Grignard and 95% of the di-Grignard using the polymer, Figure 8.2(f). Silica supported magnesium–anthracenes also give Grignard reagents of benzylic halides in THF in excellent yield [30].

8.6.3 Polymer and Silica Recycling

The uptake of magnesium by the spent polymer in forming the Grignard reagents diminishes by 6–8% for successive cycles, but the yield of derived Grignard reagent based on the amount of $Mg(anthracene)(THF)_3$ consumed in forming the Grignard reagent is unchanged. This 'poisoning' of the active sites within the polymer matrix is through formation of 9,10-dihydroanthracene moieties, established from ^{29}Si CP MAS NMR spectroscopy, and a comparison with a polymer supported dihydroanthracene. The dihydroanthracene sites may arise from proton abstraction by the dianion and/or radical anion centres from the solvent during washings to remove anthracene and excess $Mg(anthracene)(THF)_3$. Reaction with trace amounts of water in the solvent would give similar results. The cleavage of the anthracene functional groups from the support, and addition of preformed Grignard across the C(9)/C(10) positions of the supported anthracene, equation (8.5), have been excluded as possible causes of the diminished uptake of magnesium from $Mg(anthracene)(THF)_3$.

Silica supported magnesium–anthracene can be readily recycled with less than 1% reduction in the uptake of magnesium [30]. When considered with the higher loading, this material clearly has advantages over the polymer supported magnesium–anthracene, and over the use of magnesium–anthracene complexes in general [4,25].

8.7 FUTURE PROSPECTS

Grignard reagents of benzylic, and allylic halides, are accessible in high yield using magnesium–anthracene complexes, and polymer and silica supported analogues, many of them being inaccessible using classical techniques involving bulk metal, or even using highly activated metal. This can be regarded as a missing link in preparing Grignard reagents, and there now exists technology for preparing all classes of Grignard reagents, using these complexes or supported materials, magnesium powder, turnings or the various forms of activated mag

from using $Mg(anthracene)(THF)_3$ as a promoter/catalyst depending on the nature of the organic halide. The silica supported magnesium–anthracene can be readily recycled and can be used in a column. This offers new directions in the application of Grignard reagents, and also the application of the materials as potent reducing reagents without the resulting solutions being loaded with anthracene, the presence of which can be objectionable in many applications.

REFERENCES

1. B.J. Wakefield, *Organomagnesium Methods in Organic Synthesis*, Academic Press, London, **1995**; W.E. Lindsell, Magnesium, Calcium, Strontium, and Barium, Comprehensive, *Organometallic Chemistry II*, Vol. 1, (E.W. Abel, F.G.A. Stone, G. Wilkinson, and C.E. Housecroft ed.), Pergamon, Oxford, **1995**, Chap. 3
2. C.L. Raston, and G. Salem, Preparation and Use of Grignard and Group II Organometallics in Organic Synthesis, *The Chemistry of the Metal–Carbon Bond*, Vol. 4, (F.R. Hartley, ed.), John Wiley & Sons, New York, **1987**, Chap. 2.
3. *Handbook of Grignard Reagents*, G.S. Silverman, and P.E. Rakita, Marcel Dekker Inc., New York, **1996**.
4. B. Bogdanovic, *Acc. Chem. Res.*, **1988**, *21*, 261.
5. H.E. Ramsden, U.S. Patent 3 354 190, 1967; *Chem. Abstr.* **1968**, *68*, 114744.
6. C.L. Raston, and G. Salem, *J. Chem. Soc., Chem. Commun.*, **1984**, 1702.
7. B. Bogdanovic, S. Liao, M. Schwickardi, P. Sikorsky, and B. Spliethoff, *Angew. Chem., Int. Ed. Engl.*, **1980**, 19, 818; B. Bogdanovic, Eur. Patent 3564, **1982**; *Chem. Abstr.* **1979**, *91*, 159787; U. S. Patent 45541533, 1985.
8. U.M. Dzhemilev, A.G. Ibragimov, and G.A. Tolstikov, *J. Organomet. Chem.*, **1991**, *406*, 1.
9. T. Alonso, S. Harvey, P.C. Junk, C.L. Raston, B.W. Skelton, and A.H. White, *Organometallics*, **1987**, *6*, 2110.
10. B. Bogdanovic, S. Liao, R. Mynott, K. Schlichte, and U. Westeppe, *Chem. Ber.*, **1984**, *117*, 1378.
11. B. Bogdanovic, S. Liao, R. Mynott, K. Schlichte, and U. Westeppe, Magnesium–Anthracene. 3THF, *Organometallic Syntheses*, Vol. 4, (R.B. King and J.J. Eisch, ed.), Elsevier Science Publishers B.V., Netherlands, **1988**, pp 410.
12. X. Yaping, and B. Meizhi, *Hauxue Shiji*, **1994**, *16*, 49.
13. P.K. Freeman, and L.L. Hutchinson, *J. Org. Chem.*,
14. K. Mashima, Y. Matsuo, H. Fukamoto, K. Tani, H. Yasuda, and A. Nakamura, *J. Organomet. Chem.*, **1997**, *545*, 549.
15. B. Bogdanovic, N. Janke, C. Kruger, R. Maynott, K. Schlichte, and U. Westeppe, *Angew. Chem., Int. Ed. Engl.*, **1985**, *24*, 960.
16. H. Bonnemann, B. Bogdanovic, R. Brinkmann, B. Spliethoff, and D.-W. He, *J. Organomet. Chem.*, **1993**, *451*, 23.
17. E. Bartmann, B. Bogdanovic, N. Janke, S. Liao, K. Schlichte, B. Spliethoff, J. Treber, U. Westeppe, and U. Wilczok, *Chem. Ber.*, **1990**, *123*, 1517.
18. W. Oppolzer, and P. Schneider, *Tetrahedron Lett.*, **1984**, *25*, 3305.
19. T.P. Burns, and R.D. Rieke, *J. Org. Chem.*, **1987**, *52*, 3674.
20. B. Bogdanovic, Ger. Offen. DE 3340492, 1985; *Chem. Abstr.* **1985**, *103*, 196226; U.S. Patent 4659373, **1987**.
21. B. Bogdanovic, N. Janke, H.-G. Kinzelmann, and U. Westeppe, *Chem. Ber.*, **1988**, *121*, 33.
22. W. Brooks, C.L. Raston, R.E. Sue, F.J. Lincoln, and J.J. McGinnity, *Organometallics*, **1991**, *7*, 2098.
23. H. Lehmkuhl, A. Shakoor, K. Mehler, C. Kruger, K. Angermund, and Y.-H. Tsay, *Chem. Ber.*, **1985**, *118*, 4239.
24. B. Bogdanovic, N. Janke, H.-G. Kingelmann, K. Seevogel, and J. Treber, *Chem. Ber.*, **1990**, *123*, 1529.
25. S. Harvey, and C.L. Raston, *J. Chem. Soc., Chem. Commun.*, **1988**, 652.
26. T.R. van den Ancker, S. Harvey, and C.L. Raston, *J. Organomet. Chem.*, **1995**, *502*, 35.
27. R. Benn, B. Bogdanovic, M. Bruning, H. Grondey, W. Hermann, H.-G. Kinzelmann, and K. Seevogel, *Chem. Ber.*, **1993**, *126*, 225.
28. P.C. Junk, C.L. Raston, B.W. Skelton, and A.H. White, *J. Chem. Soc., Chem. Commun.*, **1987**, 1162.
29. G.E. Jacobsen, and C.L. Raston, *J. Organomet. Chem.*, **1990**, *395*, C1.
30. T.R. van den Ancker, and C.L. Raston, *Organometallics*, **1995**, *14*, 584.
31. P.V.R. Schleyer, T. Clarke, A.J. Kos, G.W. Spitznagel, C. Rhode, K.N. Houk, N.G. Rondan, and D.J. Arad, *J. Am. Chem. Soc.*, **1984**, *106*, 6467.

32. L.M. Engelhardt, S. Harvey, C.L. Raston, and A.H. White, *J. Organomet. Chem.*, **1988**, *341*, 39.
33. B. Bogdanovic, N. Janke, H.-G. Kinzelmann, *Chem. Ber.*, **1990**, *123*, 1507.
34. B. Bogdanovic, N. Janke, C. Kruger, K. Schlichte, and J. Treber, *Angew. Chem., Int. Ed. Engl.*, **1987**, *26*, 1025.
35. M.J. Gallagher, S. Harvey, C.L. Raston, and R.E. Sue, *J. Chem. Soc., Chem. Commun.*, **1988**, 289.
36. E. Bartmann, *Angew. Chem., Int. Ed. Engl.*, **1986**, *25*, 653.
37. J. Scholz, K.-H. Theile, *J. Organomet. Chem.*, **1986**, *314*, 7.
38. H. Appler, L.W. Gross, B. Mayer, and W.P. Neumann, *J. Organomet. Chem.*, **1985**, *281*, 9.
39. M. Harendeza, K. Leßmann, and W. P. Neumann, *Synlett*, **1993**, 283.
40. H. Lehmkuhl, K. Mehler, R. Benn, A. Rufinska, G. Schroth, and C. Kruger, *Chem. Ber.*, **1984**, *117*, 389.
41. H. Lehmkuhl, A. Shakoor, K. Mehler, C. Kruger, and Y.-H. Tsay, *Chem. Ber., Z. Naturforsch.*, **1985**, *40b*, 1504.
42. H. Lehmkuhl, K. Mehler, A. Shakoor, C. Kruger, Y.-H. Tsay, R. Benn, A. Rufinska, and G. Schroth, *Chem. Ber.*, **1985**, *118*, 4248.
43. J.D. Protasiewicz, P. Bianconi, I.D. Williams, S. Liu, C.P. Rao, and S.J. Lippard, *Inorg. Chem.*, **1992**, *31*, 4134.
44. S. Harvey, P.C. Junk, C.L. Raston, and G. Salem, *J. Org. Chem.*, **1987**, *53*, 3134.
45. B. Bogdanovic, K. Schlichte, and U. Westeppe, *Chem. Ber.*, **1988**, *121*, 27.
46. M.F. Lappert, T.R. Martin, C.L. Raston, B.W. Skelton, and A.H. White, *J. Chem. Soc., Dalton Trans.*, **1982**, 1959; W.-P. Leung, C.L. Raston, B.W. Skelton, and A.H. White, *J. Chem. Soc., Dalton Trans.*, **1984**, 1801; B. Jousseaume, J.G. Duboudin, and M. Petraud, *J. Organomet. Chem.*, **1982**, *238*, 171; L.M. Engelhardt, W.-P. Leung, C.L. Raston, P. Twiss, and A.H. White, *J. Chem. Soc., Dalton Trans.*, **1984**, 321.
47. Y. Kai, N. Kanehisa, K. Miki, N. Kasai, K. Mashima, H. Yasuda, and A. Nakanmura, *Chem. Letters*, **1982**, 1277.
48. M.G. Gardiner, C.L. Raston, F.G.N. Cloke, and P.B. Hitchcock, *Organometallics*, **1995**, *14*, 1339.
49. B.J. Wakefield, *Comprehensive Organometallic Chemistry*, Vol. 7, (G. Wilkinson, F.G.A. Stone, E.W. Abel eds.), Pergamon Press, Oxford, **1982**, Chap. 44, p 10.
50. G. Serettas, *J. Chem. Soc., Chem. Commun.*, **1972**, 752; J.L. Wardell, *Chemistry of the Metal–Carbon Bond* (F.G. Hartley, ed.), Wiley, New York, **1987**, Chap. 1, p 8.
51. M.F. Lappert, C.L. Raston, L.M. Engelhardt and A.H. White, *J. Chem. Soc., Chem. Commun.*, **1985**, 521.
52. T.M. Nicoletti, C.L. Raston, and M.V. Sargent, *J. Chem. Soc., Chem. Commun.*, **1988**, 1491.
53. T.M. Nicoletti, C.L. Raston, and M.V. Sargent, *J. Chem. Soc., Perkin Trans.*, **1990**, 133.
54. A.I. Meyers, R. Gabel, and E.D. Mihelich, *J. Org. Chem.*, **1978**, *43*, 1372.
55. N. Janke, Dissertation, University of Bochum, **1986**.
56. L.M. Engelhardt, R.I. Papasergio, C.L. Raston, G. Salem, and A.H. White, *J. Chem. Soc., Dalton Trans.*, **1986**, 789.
57. L.M. Engelhardt, R.I. Papasergio, C.L. Raston, and A.H. White, *J. Chem. Soc., Dalton Trans.*, **1984**, 311.
58. E. Bartmann, *J. Organomet. Chem.*, **1987**, *332*, 19.
59. E.C. Ashby, and J. Oswald *J. Org. Chem.*, *1988*, *53*, 6066; H. M. Walborsky, *Acc. Chem. Res.*, **1990**, *23*, 286, and references therein
60. M. Takagi, M. Nojima and S. Kusabayashi, *J. Am. Chem. Soc.*, **1982**, *104*, 1636; K. Muraoka, M. Nojima, and S. Kusabayashi, *J. Chem. Soc., Perkin Trans.*, **1986**, 761.
61. R.G. Lawler, and P. Livant, *J. Am. Chem. Soc.*, **1976**, *98*, 3710.
62. W. Kong, and S. Liao, Youji Hauxue, **1986**, *3*, 207; *Chem. Abstr.* **1987**, *106*, 102346.
63. J.F. Garst, J.T. Barbas, and F.E. Barton, *J. Am. Chem. Soc.*, **1968**, *90*, 7159; G.D. Sargent and J.A. Lux, *J. Am. Chem. Soc.*, **1968**, *90*, 7160; S. Bank and J.F. Bank, *Tetrahedron Lett.*, **1969**, 4533.
64. H.J.R. De Boer, O.S. Akkerman, and F. Bickelhaupt, *J. Organomet. Chem.*, **1978**, *321*, 291.
65. S. Itsuno, G.D. Darling, H.D.H. Stover, and J.M.J. Frechet, *J. Org. Chem.*, **1987**, *52*, 4645.
66. B. Brix and T. Clarke, *J. Org. Chem.*, **1988**, *53*, 3366.
67. A. McKillop and D. Bromley *Tetrahedron Lett.*, **1969**, 1623.
68. T.R. van den Ancker, G.R. Hanson, Fu-Chin Lee, and C.L. Raston, *J. Chem. Soc., Chem. Commun.*, **1997**, 125.

9

Structures of Organomagnesium Compounds as Revealed by X-ray Diffraction Studies

F. Bickelhaupt
Vrije Universiteit, Amsterdam, The Netherlands

9.1 INTRODUCTION

Organomagnesium compounds have been known since the previous century. However, they were curiosities rather than useful and important reagents until nearly 100 years ago when Victor Grignard made the seminal discovery that they could be obtained in a simple and efficient way by the reaction of an organic halide with magnesium in an ethereal solvent [1]. Immediately, the synthetic potential of these reagents was recognized which led to an ever increasing number of investigations on their preparation and application [2,3].

In contrast, the elucidation of the structure of organomagnesium reagents in solution or in the solid state lagged behind considerably; this was due to several reasons. In the first place, the high reactivity and air sensitivity of organomagnesium compounds makes the preparation of pure compounds a difficult task. Secondly, organomagnesium compounds are kinetically unstable in the sense that in solution, they often rapidly exchange substituents and coordinated Lewis bases, so that in particular the organomagnesium halides or Grignard reagents RMgX may not possess one simple well-defined structure, but often occur as mixtures of disproportionation products $R_2Mg/MgBr_2$ (the so-called Schlenk equilibrium), as aggregates (dimers, oligomers), and so on [2,3]. Finally, reliable spectroscopic methods and modern techniques for structure determination became available rather late and were applied in this area only from the beginning of the 1960s. Since then, our knowledge on the structure of organomagnesium compounds has been rapidly increasing, in particular due to the application of single crystal X-ray diffraction studies, and the structural and bonding aspects of these compounds are now fairly well categorized and understood; nevertheless, novel structures keep being reported regularly.

The literature search of X-ray crystal diffraction data was conducted by means of the Cambridge Structural Database (1997) and Beilstein Crossfire

Grignard Reagents: New Developments Edited by Herman G. Richey, Jr. © 2000 John Wiley & Sons Ltd

(mid 1998). Only very few diffraction data are available in the gas phase or in solution; they were incorporated where appropriate. Some of the data have been reviewed previously [4–6]. For this reason, the emphasis will be on recent developments, but most representative older data have been included. The material is presented in the order of increasing coordination numbers of magnesium from 2 to 6 (Sections 9.2–9.5), special classes such as difunctional, polyhapto and heteronuclear compounds are treated in Sections 9.6–9.9.

9.2 MAGNESIUM WITH COORDINATION NUMBER 2

In line with its position in the Periodic Table, magnesium is divalent and should therefore, in the most simple case, form stable compounds with two groups attached to it. In fact, this dicoordinate state is very rare in (organo)magnesium chemistry for the simple reason that in the resulting compounds, magnesium has only four electrons in its valence shell, which seriously violates the octet rule. Normally, organomagnesium compounds escape from such bonding situations by addition of Lewis bases or by aggregation via three-center/two-electron bonds or agostic interactions.

There are three conditions which alone or in combination lead to stabilization of the rare dicoordinate state of magnesium: 1) steric hindrance due to large substituents which prevent aggregation; 2) higher electron supply by substituents which are formally monovalent but *de facto* donate more than two electrons; 3) isolation of the molecules in the gas phase.

Only three compounds, **1.1**–**1.3**, belong to this category (Scheme 9.1, Table 9.1). Dineopentylmagnesium (**1.1**) owes its dicoordinate state to both condition 1 and 3: it is monomeric because of steric hindrance due to the bulky neopentyl groups, but also because its structure was determined in the *gas phase* by electron diffraction [7]. That steric bulk alone is not sufficient in this case follows from the observation that even in the gas phase, **1.1** is in equilibrium with its dimer [8]; in solution, it aggregates to form a trimer [9]. The structures of **1.2** [10] and **1.3** [11] were determined in the crystalline state. Obviously, the extreme bulkiness of their substituents, tris(trimethylsilyl)methyl and supermesityl (= 2, 4, 6-tri-(*tert*-butyl)phenyl), respectively, prevents any kind of association even in the solid state; it is remarkable that **1.3** is obtained from THF solution without coordinated solvent molecules!

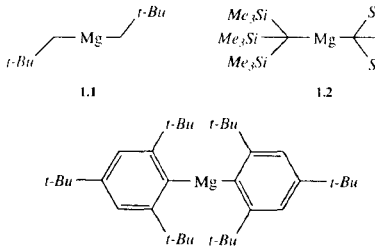

SCHEME 9.1

While in both **1.1** and **1.2**, the bonding at magnesium is strictly linear (C–Mg–C: 180°), **1.3** shows a slight deviation from linearity (C–Mg–C: 158.4°) which has been ascribed to weak interactions between the metal and C–H groups of the ortho *tert*-butyl groups [11]. It should be pointed out that linearity around divalent magnesium may be the consequence of *sp*-hybridization at the central atom, but the same geometry is expected if electrostatic or steric repulsion between the two large carbanionoid ligands is operative. In all cases, the magnesium–carbon bond is rather short, in the order of 2.12 Å, whereas in the commonly encountered tetracoordinate state, the Mg–C(sp^3) bond length is 2.15–2.17 Å (see Section 9.4).

Table 9.1. Dicoordinate magnesium: bond lengths (Å; 2 decimals) and bond angles (°; no decimals) of organomagnesium compounds R_2Mg

Cpd.		Mg–C	C–Mg–C	Remarks	Ref.
1.1	Np_2Mg	2.13	180	gas phase	[7]
1.2	$[(Me_3Si)_3C]_2Mg$	2.12	180		[10]
1.3	$(2,4,6\text{-}t\text{-}Bu_3C_6H_2)_2Mg$	2.12	158		[11]

Though organomagnesium compounds containing certain monovalent organic substituents such as cyclopentadienyl may formally be considered to be dicoordinate as they occur in discrete units such as Cp_2Mg, their delocalized anions are in fact bonded in a polyhapto fashion. Therefore, in addition to being sterically hindered (condition 1), these compounds also fulfill condition 2. They are treated in Section 9.7.

9.3 MAGNESIUM WITH COORDINATION NUMBER 3

Like dicoordination, tricoordination is rarely encountered for magnesium for similar reasons: the magnesium atom has only a sextet; bulky substituents are required to prevent association. Indeed, only five representatives of this class have been reported: **2.1**–**2.5**.

Compound **2.1** [12] may be considered to be a borderline case. Note that the Mg–C bond in the tricoordinate **2.1** (2.11 Å) is slightly shorter than in the dicoordinate **1.2** (2.12 Å); this illustrates the importance of steric effects as **2.1** carries two slightly smaller substituents (bis(trimethylsilyl) methyl versus tris(trimethylsilyl)methyl in **1.2**). Furthermore, these smaller substituents allow a close approach of the metal to one of the methyl groups of a neighboring trimethylsilyl group in an agostic fashion (Mg···C: 2.535 Å). The tricoordinate core is close to planar (Σ C–Mg–C 351.2°).

The magnesiate anions **2.2** ([13], counterion $[NpMg(2.2.1\text{-cryptand})]^+$) and **2.3** ([14], counterion $\{Li(THF)_{0.6}(Et_2O)_{0.4}\}^+$) are practically planar (Σ C–Mg–C: 360° and 358°, respectively). Surprisingly, the three Mg–C bonds in **2.3** have slightly different lengths; their average value (2.20 Å) is slightly shorter than that in **2.2** (2.22 Å), which may reflect the difference in hybridization of their carbon atoms (sp^2 versus sp^3). These values are slightly larger than those of tetracoordinate magnesium compounds (2.13–2.17 Å, slightly depending on the hybridization of carbon; see Table 9.3); apparently, bond shortening due to lower coordination is overcompensated by steric hindrance and negative charge.

A special case is **2.4** [15] which is dimeric with two bis(trimethylsilyl)amide groups in the bridging position, yet has a tricoordinate magnesium atom.

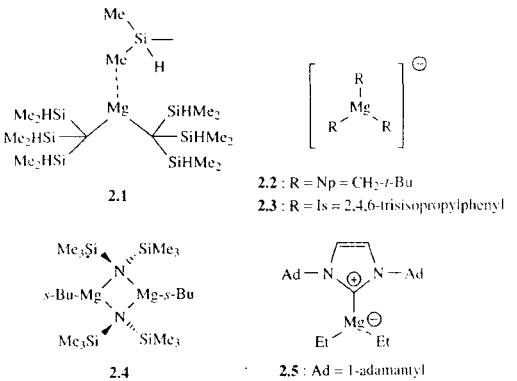

SCHEME 9.2

Table 9.2. Tricoordinate magnesium: bond lengths (Å; 2 decimals) and bond angles (°; no decimals) of organomagnesium compounds

Cpd.		Mg–C	Σ C–Mg–C	Remarks	Ref.
2.1	$[(Me_3Si)_2CH]_2Mg_2(\mu\text{-}Me\text{-}Si_2)$	2.10	351		[12]
		2.12			
		2.54		Mg-μ-Me	
2.2	Np_3Mg	2.22	360		[13]
2.3	Is_3Mg	2.15	358		[14]
		2.21			
		2.25			
	(Is = isityl = (2, 4, 6-*i*-$Pr_3C_6H_2$))				
2.4	[*s*-BuMgN($SiMe_3$)$_2$]$_2$	2.08		Mg-N 2.12 Å	[15]
				N-Mg-N 93°	
2.5	Et_2MgIm	n.a	n.a	disordered	[16]
	(Im = (1, 3-di-(1-adamantyl)imidazol-2-ylidene)				

Undoubtedly, both the bulkiness of the amido group and the high donor capacity of the amido nitrogen cooperate in stabilizing the low coordination of magnesium. It is also unusual that such a bulky group occupies a bridging position. Furthermore, the *sec*-butyl group is unique in being terminal at a tricoordinate magnesium and for that reason, the Mg–C bond is exceptionally short (2.08 Å), especially if one considers that an sp^3 carbon atom is involved; normally a Mg–C(sp^3) bond is at least 2.15 Å (*cf.* **3.5**: 2.15 Å or **3.11**: 2.18 Å, Table 9.3), the closest value being 2.10 Å for the Mg–CH_3 bond of **39** (Scheme 9.14) in which magnesium is similarly amido-bridged, but tetracoordinate. No reliable data were obtained for **2.5** due to disorder, but a monomeric structure (Scheme 9.2) could be established [16].

9.4 SIMPLE ORGANOMAGNESIUM WITH COORDINATION NUMBER 4

9.4.1 Mononuclear Compounds

The majority of organomagnesium structures is monomeric with magnesium in a distorted tetrahedral environment of four ligands as shown in structure **3** (Scheme 9.3). Presumably, the same structure is also prevailing in not too concentrated solutions of strongly basic solvents [2,3]. Two of the ligands, R and X, are organic groups and/or monovalent substituents such as alkoxy, dialkylamino or halogen, bonded to magnesium by a (strongly polar!) covalent bond, whereas the other two ligands, L, are Lewis bases such as ethers and tertiary amines with a dative bond to magnesium; L_2 may represent a bidentate ligand such as TMEDA.

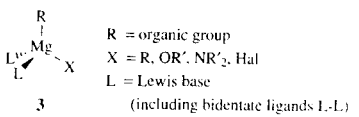

3

R = organic group
X = R, OR', NR'$_2$, Hal
L = Lewis base
(including bidentate ligands L-L)

SCHEME 9.3

Roughly speaking, all structures of type **3** display similar distorted tetrahedra with, as general features, an R–Mg–X angle which is larger than tetrahedral while L–Mg–L is smaller. The finer details vary, as one might expect, depending on the properties of the substituent: more electronegative groups enhance the *p*-character of the magnesium orbital (Bent's rule)

Table 9.3. Tetracoordinate magnesium: average bond lengths (Å; 2 decimals) and bond angles (°; no decimals) of monomeric organomagnesium compounds $RMgXL_n$

Cpd.	R	X	L_n	Mg–C	Mg–X	Mg–L	C–Mg–X	L–Mg–L	Ref.
3.1	Me	Me	TMEDA	2.17	2.17	2.24	130	82	[17]
3.2	Me	Me	(quinuclidine)$_2$	2.19	2.19	2.24	129	108	[18]
3.3	Me	NR_2	$(THF)_2$	2.16	2.07	2.05	129	95	[19]
	(NR_2 = *t*-Bu, *n*-Bu-dihydrotriazine)								
3.4	Et	Et	TMEDA	2.16	2.16	2.24	128	83	[20]
3.5	Et	Br	$(Et_2O)_2$	2.15	2.48	2.04	125	101	[21]
3.6	Et	Br	(−)-sparteine	2.24	2.48	2.15	115	84	[22]
3.7	Et	Br	(−)-α-isosparteine	2.22	2.51	2.18	112	84	[23]
3.8	Et	Br	(+)-6-Bz-sparteine	2.34	2.51	2.16	111	83	[24]
3.9	Et	NR_2	$(THF)_2$	2.14	2.09	2.07	125	89	[25]
	(NR_2 = 1, 3, 6, 8-tetra-*t*-Bu-carbazolyl)								
3.10	R	R	$(dioxane)_2$	2.16	2.16	2.04	124	100	[26]
	(R = *o*-carboranyl-CH_2)								
3.11	*s*-Bu	*s*-Bu	TMEDA	2.18	2.18	2.25	134	81	[27]
3.12	*t*-Bu	Cl	(−)-sparteine	2.19	2.33	2.17	115	84	[28]
3.13	R	R	TMEDA	2.18	2.18	2.20	113	84	[29]
	(R = 2, 4-dimethyl-2,4-pentadienyl)								
3.13	PhMeCH	PhMeCH	$(Et_2O)_2$	2.20	2.20	2.06	122	115	[30]
3.14	Ph_3C	Br	$(Et_2O)_2$	2.25	2.46	2.03	116	102	[31]
3.15	Ph	Ph	$(THF)_2$	2.13	2.13	2.03	122	94	[32]
3.16	*p*-Tol	*p*-Tol	$(THF)_2$	2.13	2.13	2.04	124	97	[32]
3.17	Ph	Ph	TMEDA	2.17	2.17	2.20	119	83	[33]
3.18	Ph	Br	$(THF)_2$	n.a.	n.a.	n.a.	n.a.	n.a.	[34]
3.19	Ph	Br	$(Et_2O)_2$	n.a.	2.44	2.03	n.a.	n.a.	[35]
3.20	Mes	Mes	$(THF)_2$	2.18	2.17	2.07	119	88	[14]
	(Mes = 2,4,6-$Me_3C_6H_2$)								
3.21	Is	Is	$(THF)_2$	2.18	2.18	2.11	123	87	[14]
	(Is = 2,4,6-*i*-$Pr_3C_6H_2$)								
3.22	viph	viph	$(THF)_2$	2.14	2.14	2.04	n.a.	91	[36]
	(viph = 2-vinylphenyl)								
3.23	Cb	Cb	$(dioxane)_2$	2.16	2.16	2.04	124	100	[37]
	(Cb = 2-Me-*o*-carboranyl)								

which leads to smaller bond angles and bond lengthening, while bulky substituents enlarge bond lengths and angles. For bidentate ligands, their geometric or conformational restrictions may lead to deviating results.

Thus, under comparable conditions, Mg–C(sp^3) bonds (**3.1, 3.2, 3.5, 3.10**: 2.15–2.17 Å) are slightly longer than Mg–C(sp^2) bonds (**3.15, 3.16, 3.22**: 2.13–2.14 Å). Larger substituents increase the Mg–C bond length (**3.15, 3.16** < **3.20** < **3.21**:

2.13 → 2.18 Å); the influence on the bond angles is smaller and less straightforward. Amine bases L tend to elongate the Mg–C bond in comparison with ethers (*e.g.* **3.17** (2.17 Å) versus **3.15** (2.13 Å)), in particular if the amine is bulky (**3.2** (2.19 Å) versus **3.1** (2.17 Å)); this effect is particularly large for certain bidentate amines from the sparteine group where it goes along with a reduction of the R–Mg–X angle (*cf.* **3.6–3.8, 3.12**); both changes indicate increased *p*-character in the R–Mg and the Mg–X bond. The elongated bonds of benzylic type organic ligands (**3.13**: 2.20 Å, **3.14**: 2.25 Å versus **3.5**: 2.15 Å) may be understood as a result of loosening of the interaction between the metal and the stabilized carbanion.

Concerning the bond distances between magnesium and the coordinated Lewis bases, the Mg–O bonds are usually shorter than the Mg–N bonds. Besides the larger radius of nitrogen, the stronger steric hindrance around the (tricoordinate) nitrogen compared to the (dicoordinate) oxygen will be responsible. However, it should be pointed out again that not all of these trends are fully consistent or easy to rationalize because a variety of factors may be involved.

The bond angles R–Mg–X are normally in the range of 115–130°. Qualitatively, this may be described as a consequence of coordination of the Lewis bases to the initially linear R–Mg–X (*cf.* **1**) which leads to a certain degree of bending. In **3**, the ideal tetrahedral geometry is never fully accomplished; there is a clear 'memory effect' which, however, is less pronounced than in the organozinc analogues which deviate less from linearity on coordination. The angles L–Mg–L vary from 80 to 100° and show a more erratic behaviour; they strongly depend on the size and on restrictions imposed by the Lewis base, in particular when L_2 is a bidentate ligand.

9.4.2 Dimeric Compounds

In concentrated solution and/or weakly basic solvents, organomagnesium compounds have a certain tendency towards association [2,3]. A considerable number of such dimeric, oligomeric and a few polymeric compounds have been characterized by X-ray crystal structures. It is remarkable that in most of these structures, the tetracoordination of magnesium is retained. The simple dimeric representatives are described in this Section (Table 9.4, Scheme 9.4). Quite a few dimeric structures are also encountered in compounds with intramolecular or polycoordination which are separately treated in Sections 9.6–9.8. Oligomeric structures are frequently found in combination of magnesium with other metals; they are described in Section 6.9. Polymers will be presented in Section 4.3.

The six known simple dimeric compounds RL(μ-X_2)MgLR (**4.1–4.6**) all have the general structure shown in Scheme 9.4 with tetracoordinate

Table 9.4. Tetracoordinate magnesium: average bond lengths (Å; 2 decimals) and bond angles (°; no decimals) of dimeric organomagnesium compounds RLMg[μ-X]$_2$MgRL

Cpd.	R	L	X	Mg–R	Mg–L	Mg–X	R–Mg–L	X–Mg–X	Ref.
4.1	Et	*i*-Pr_2O	Br	2.09	2.02	2.58	121	93	[38]
4.2	Et	NEt_3	Br	2.18	2.15	2.56	116	n.a.	[39]
4.3	Et	Im'	Et	2.13	2.28	2.26, 2.34	110	n.a.	[16]
	(Im' = 1,3-dimesitylimidazol-2-ylidene)								
4.4	*p*-Tol	THF	*p*-Tol	2.13	2.02	2.24, 2.31	107	78	[32]
4.5	An	*n*-Bu_2O	Br	2.13	2.02	2.57	113	89	[40]
		(An = 9-anthracenyl)							
4.6	*t*-Bu	THF	NH-*t*-Bu	2.19	2.08	2.10	110	90	[41]

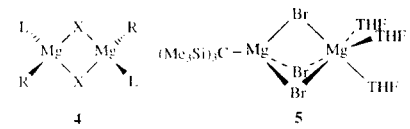

4 **5**

SCHEME 9.4

magnesium and electron deficient three-centre/two-electron bonds between magnesium and two ligands X. Not surprisingly, halogens and amides are good bridging groups, but in **4.3** and **4.4**, an organic residue is in the bridging position.

One of the driving forces for such dimerizations (and further oligomerizations, *vide infra*) is the overall reduction of strain around the central metal atom. This is illustrated for **4.1** [38] where the bridging bonds are slightly longer than those in comparable monomeric species (*cf.* Mg–Br: 2.58 Å in **4.1** and 2.48 Å in **3.5**); furthermore, the bulkiness in the vicinity of the metal is reduced when EtMgBr(*i*-$Pr_2O)_2$ is transformed, by removal of two molecules of diisopropyl ether, to Et(*i*-Pr_2O)Mg(μ-Br_2)Mg(*i*-Pr_2O)Et (= **4.1**). Dimer **4.2**, the triethylamine analogue of **4.1**, shows similar features, but a longer Mg–C bond, presumably due to the bulky triethylamine ligand.

The situation is somewhat different in **4.3** where two ethyl groups are involved in unsymmetrical bridging (2.26, 2.34 Å); the longer Mg–C bond is involved in an additional agostic interaction: Mg···H 2.16 Å. As is often the case, the terminal Mg–Et bond is rather short (2.13 Å). The Mg–C bond to the terminal 1,3-dimesitylimidazol-2-ylidene substituent (Im') is quite large (2.28 Å) if one considers that its carbon atom is sp^2-hybridized. Possibly steric factors are responsible; note that in the case of **2.5** with the even larger 1,3-diadamantylimidazol-2-ylidene group (Im), association as in **4.3** is *completely* prevented.

While, in general, the structure of **4.4** parallels that of the other representatives of **4**, several peculiarities should be pointed out. In the first place, the crystals investigated showed **4.4** to be present together with its monomer **3.16** in a 1:2 ratio. Secondly, the two bridging groups *X* = *p*-Tol are not arranged in a symmetrical fashion as they show a shorter (2.24 Å) and a longer bond (2.31 Å). In addition, the bridging *p*-Tol groups are slightly twisted from a perpendicular position relative to the Mg_2C_2 plane (76° instead of 90°), and the short bond is less bent away from the aryl plane than the longer one (dihedral angles: 28° and 46°, respectively), the latter indicator being in line with more s-character in the shorter bond. Both effects bring one of the two ortho-carbon atoms of each ring into close contact with magnesium (2.98 Å) suggesting some η^2 (or agostic?) interaction. The terminal bonds to *p*-Tol and THF (2.13 and 2.02 Å, respectively) are normal (*cf.* **3.16**).

The structure of the Grignard reagent **4.5** [40] largely corresponds to those of **4.1–4.4**. In this case, it is obviously the bulky 9-anthracenyl group which prevents addition of a second solvent molecule and thus leads to dimerization. Compound **4.6** [41] is particular in having a bridging amido group; its structural features follow the general pattern. The rather long Mg–C bond (2.19 Å) may be due to the bulky *tert*-butyl group and to the amido bridge.

A specific case is **5** (Scheme 9.4) which contains a solvent-free tetracoordinate magnesium bonded to the bulky tris(trimethylsilyl)methyl group (Mg–C: 2.16 Å) while its tetracoordination is completed by three μ-bridging bromides (Mg–Br: 2.56–2.58 Å); they in turn are μ-bonded to an 'inorganic' magnesium which is hexacoordinated by the three bromides and three THF molecules [42].

9.4.3 Polymeric Compounds

Solvent-free organomagnesium compounds are usually obtained as amorphous or microcrystalline polymeric materials. For this reason, X-ray diffraction studies depend either on the application of powder diffraction techniques [43,44] or on special and/or fortuitous methods of crystallization [32,45]. The structures **6.1–6.4** thus determined all follow essentially the same pattern: a polymeric chain formed from mutually perpendicular four-membered rings Mg_2R_2 connected via spiro magnesium atoms as shown in Scheme 9.5.

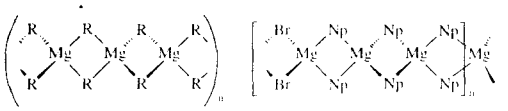

6.1: R = Me
6.2: R = Et
6.3: R = Ph

6.4

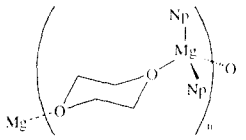

7

SCHEME 9.5

Table 9.5. Tetracoordinate magnesium: bond lengths (Å) and bond angles (°) of solvent free organomagnesium compounds

Cpd.	Mg–C		C–Mg–C int.	C–Mg–C ext.	Mg–C–Mg int.	Ref.
6.1	$(Me_2Mg)_n$	2.24	105	n.a.	75	[43]
6.2	$(Et_2Mg)_n$	2.26	108	n.a.	72	[44]
6.3	$(Ph_2Mg)_n$	2.26	102	113	78	[32]

The data for **6.1–6.3** are collected in Table 9.5. They are completely analogous: the magnesium atoms form a straight line; the four-membered Mg_2R_2 rings have typical bridging Mg–C bond lengths of 2.24–2.26 Å and internal angles C–Mg–C of 102–108° and Mg–C–Mg of 72–78°.

Compound **6.4** [45] consists of one neopentylmagnesium bromide unit and one dineopentylmagnesium unit (NpMgBr·Np_2Mg) which are arranged to form repeating units of three four-membered rings, *i.e.* one Mg_2Br_2 ring and three Mg_2Np_2 rings (Scheme 9.5). It is less symmetrical: the magnesium atoms lie on two parallel straight lines which are 1.10 Å apart, and the six independent Mg bonds vary from 2.20–2.42 Å, whereas the two Mg–Br bonds are nearly identical (2.808 and 2.818 Å), which is rather long compared to other dimeric compounds (*cf.* bridging Mg–**Br**: 2.58 Å in **4.1**).

The dioxane complex NpMgBr·dioxane (**7** [46], Scheme 9.5) also consists of parallel linear chains. However, they are of a completely different type as the arrangement around magnesium strongly resembles that in compounds **3**, the difference being that in **7**, the two ether functions are combined in one dioxane molecule. The geometric parameters of **7** are rather normal for type **3** structures with slightly shorter Mg–C (2.13 Å) and longer Mg–O bonds (2.13 Å).

9.5 SIMPLE ORGANOMAGNESIUM WITH COORDINATION NUMBER 5 AND 6

While in inorganic magnesium compounds, the coordination number 6 is the most prevalent [5], higher coordination numbers such as 5 and 6 are rare in organomagnesium chemistry as the relatively large organic substituents and Lewis bases like ethers and tertiary amines cause too much steric crowding around the central metal atom. Four (relatively) simple pentacoordinated (**8–11**, Scheme 9.6) and three hexacoordinated representatives (**12.1–12.3**) have been reported (Scheme 9.7). Other cases of penta- or hexacoordinated magnesium involve coordination to intramolecular or polydentate Lewis bases and will be treated in Section 9.8.

9.5.1 Organomagnesium Compounds with Coordination Number 5

Compound **8** [47] with the composition MeMgBr·$(THF)_3$ is the simplest of the pentacoordinate series. Presumably, the small methyl group and the strong Lewis base THF create conditions permitting pentacoordination. The long Mg–C bond (2.41 Å) might be ascribed to the apical position in a trigonal bipyramid; however, the apical Mg–Br bond (2.43 Å) is not exceptional.

In agreement with the carbenoid character of the Grignard reagent **9** [48], the Mg–C bond (2.19 Å) is also longer than normal Mg–C(sp^2) bonds (Table 9.3: about 2.13 Å), although part of the elongation may be due to the pentacoordination; the C(sp^2)–Br bond (2.01 Å) is longer than normal (1.90 Å) too, as are two of the three Mg–O bonds to the THF ligands (2.04, 2.11, 2.13 Å). The Mg–Br bond (2.52 Å) is about normal.

Increasing complexity is observed for **10** and **11**. Similar to the tetracoordinated dimers **4**, the two allyl Grignard units of **10** [49] are connected by two unsymmetrically μ-bridging chlorides (Mg–Cl: 2.40, 2.69 Å). The allyl group is η^1-bonded to magnesium by a long σ-bond (Mg–C: 2.18 Å). Pentacoordination is completed by one chelating TMEDA at each magnesium and may be responsible for the slight Mg–C bond elongation, together with an 'allyl effect' similar to the benzylic effect observed in **3.13** and **3.14**. Compound **11** [50] is a tetramer [EtMgCl·$MgCl_2$]$_2$ with two terminal pentacoordinated Grignard units EtMgCl attached via three bridging chlorides to a core of two hexacoordinate 'inorganic'

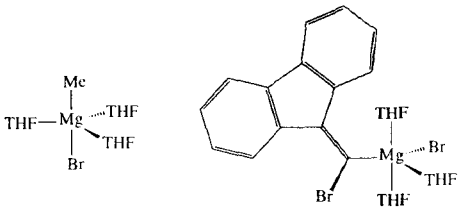

8 **9**

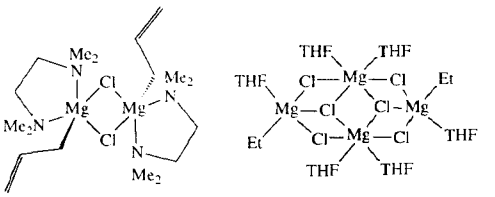

10 **11**

SCHEME 9.6

magnesiums; in this regard, it resembles **5**. The bonds are slightly on the long side (Mg–C: 2.19 Å, MgO: 2.04–2.14 Å, Mg–Cl: 2.40–2.79 Å).

9.5.2 Organomagnesium Compounds with Coordination Number 6

The three simple compounds with hexacoordinate magnesium are all of the type $(RC{\equiv}C)_2MgL_4$; apparently, the small size of the dicoordinate acetylenic *sp*-carbon atom is essential in achieving this high and rare coordination number. The crystal structure of **12.1** has not been fully resolved, but two types of crystals have been distinguished to which the *trans*-structure **12.1a** and the *cis*-structure **12.1b** (Scheme 9.7) have been tentatively assigned [51]. The structures of **12.2** [52] and **12.3** [53] confirm the trans arrangement of the two acetylenic substituents and reveal normal octahedral angles C–Mg–C of 175–180° and C–Mg–O(or N) of 90°; only the N-Mg-N angles of the TMEDA units of **12.2** (80° instead of 90°) show a stronger deviation. The bonds are longer than usual, in particular the Mg–C(*sp*) bond (2.18–2.20 Å), which must be due to hexacoordination.

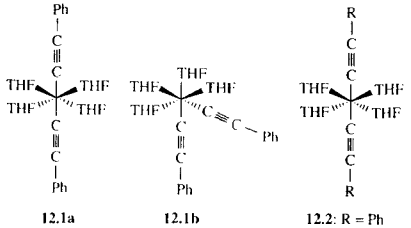

SCHEME 9.7

9.6 DIFUNCTIONAL ORGANOMAGNESIUM COMPOUNDS

From a structural point of view, the treatment of difunctional organomagnesium compounds as a separate class is somewhat arbitrary as many of them reveal structural motifs already encountered in Section 9.4. On the other hand, they are not only distinguished from other organomagnesiums by the special property of having two organometallic functions attached to the same carbon skeleton, but also by specific features such as metallaheterocycles or unique clusters.

9.6.1 Simple Difunctional Organomagnesium Compounds

The most simple difunctional organomagnesium compounds are those carrying two metals bonded to the same carbon atom such as the methylene di-Grignard reagent $CH_2(MgBr)_2$ [54]. A crystal structure of its bis(trimethylsilyl) derivative **13** (Scheme 9.8) is remarkable for several reasons [55]. In the first place, **13** is a monomer with normal tetracoordination around magnesium, whereas otherwise, sterically overloaded organomagnesium compounds tend to relieve their crowded situation by expulsion of Lewis base and aggregation as discussed in Section 9.4.2. Secondly, in spite of extreme congestion around the central carbon atom, all its bonds (Mg–C: 2.10, 2.14 Å; Si–C: 1.81, 1.85 Å) are slightly shorter than expected; this has been ascribed to the accumulation of negative charge at this carbon from its four electropositive substituents, which results in increased electrostatic attraction of the four metal(oid)s surrounding it (presumably in

Table 9.6. Hexacoordinate magnesium: bond lengths (Å) and bond angles (°) of organomagnesium compounds $(RC{\equiv}C)_2MgL_4$

Cpd.	R	L	Mg–C	C–Mg–C	Ref.
12.1	Ph	THF	n.a.	n.a.	[51]
12.2	Ph	TMEDA	2.18, 2.20	180	[52]
12.3	*t*-Bu	TMEDA	2.18	180	[53]

combination with negative hyperconjugation). The angles at carbon are close to tetrahedral (Mg–C–Mg: 112°, Si–C–Mg: 113°), and the other bond angles are quite normal.

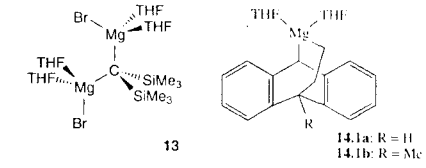

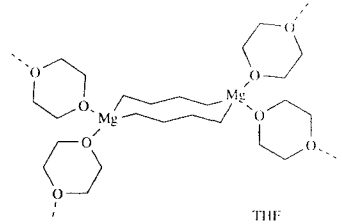

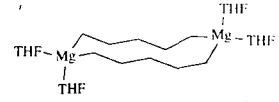

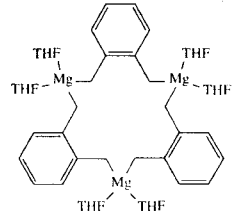

SCHEME 9.8

When the two organomagnesium functions are four or more carbon atoms apart, the resulting diorganomagnesiums behave as if they have two more or less independent functionalities [54]. This is also true with regard to their structures as illustrated by the magnesacycles **14** (Scheme 9.8, Table 9.7). Even though they are monomeric (**14.1**), dimeric (**14.2**, **14.3**) or trimeric (**14.4**), the coordination geometry around magnesium is essentially that of simple compounds of type **3**; slightly deviating are the short Mg–C bonds of **14.1** (2.11 Å) and **14.2** (2.11, 2.12 Å) and the rather large C–Mg–C angle (142°) of **14.3**. The ring size is apparently dictated by strain due the large C–Mg–C angle which cannot be incorporated into a five- or six-membered ring. It depends on the number of carbon atoms between the magnesiums: 6 carbons in **14.1** allow a strain-free monocyclic structure, while in **14.2**, **14.3** and **14.4** with 4, 5, and 4 carbons, respectively, oligomeric structures are required.

An intermediate range of distances between the two magnesiums is represented by **15.1–15.3**, where 2, 2 and 3 carbon atoms, respectively, separate the two magnesium functions; they have a completely different type of structure (Scheme 9.9). Clearly, the angle strain in a monomeric structure with a three- or four-membered ring would be excessive. Instead, a tetrameric cluster is found in all three cases; the molecular structure of **15.3** is shown as an example in Figure 9.1. Association measurements in THF show that this tetrameric state is also persistent in solution [60].

The structure of **15** may be described as consisting of a (slightly distorted) tetrahedron of magnesium atoms, each of which carries one THF ligand. On top of each face of the tetrahedron, a divalent carbanionoid organic fragment is σ-bonded to one magnesium and μ^2-bridging between the

Table 9.7. Difunctional organomagnesium compounds: average bond lengths (Å; 2 decimals) and bond angles (°; no decimals)

Cpd.	Mg–C	Mg–O	C–Mg–C	O–Mg–O	Ref.
14.1	n.a., 2.11	n.a.	n.a.	n.a.	[56]
14.2	2.11, 2.12	2.07, 2.08	128	90	[57]
14.3	2.13, 2.15	2.09, 2.11 •	142	91	[58]
14.4	2.15, 2.16, 2.17	2.07, 2.06, 2.08	127, 130	94	[59]

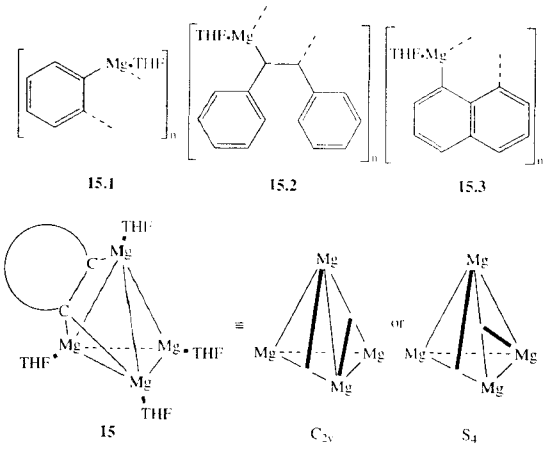

SCHEME 9.9

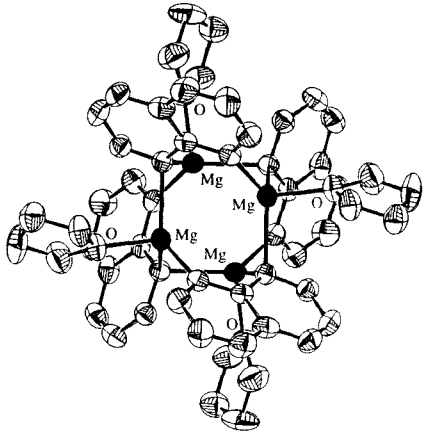

Fig. 9.1. ORTEP drawing of the molecular structure of tetrameric 1,8-naphthalinediylmagnesium (15.3).

other two. Thus, each magnesium exhibits the commonly encountered tetracoordination, and the bonding parameters are not unusual either (Mg–C(σ): 2.14–2.18 Å; Mg–C(μ): 2.26–2.29 Å; Mg–O: 2.03–2.06 Å); of course, the angles within the core are smaller than normal (C–Mg–C: 101–120°; Mg–C–Mg: 76–90°). As schematically indicated in Scheme 9.9, the planes of the organic groups, which are arranged perpendicular to the tetrahedral Mg_3 faces, may have two relative orientations; one, leading to (approximate) C_{2v} symmetry, is realized in **15.1**, the other one of (approximate) S_4 symmetry in **15.2** and **15.3**. It has been pointed out that two factors are largely responsible for this type of cluster formation [60]. Firstly, the juxtaposition of two bulky tetracoordinate magnesiums at the organic group in close vicinity would create considerable steric hindrance; this is reduced by removal of one Lewis base per magnesium and aggregate formation (*cf.* the discussion in Section 9.4.2). Secondly, the specific organization as tetrahedral tetramers is facilitated by the short distance between the two carbanionoid centers in one organic ligand: it allows a perfect fit of this ligand on top of a tetrahedral face and thus a $[Mg^{2+}R^{2-}]_4$ cluster, in analogy to the tetrahedral $[Li^{+}R^{-}]_4$ arrangement which is well-known in organolithium chemistry [61,62].

9.6.2 Organomagnesium Compounds Derived from Dienes or Diynes

The three structures described here form a heterogeneous group (Scheme 9.10): two (formal) 1,4-adducts of magnesium to a 1,3-diene (**16**) and the Lewis acid/base type interaction of magnesium with two alkyne functions (**17**).

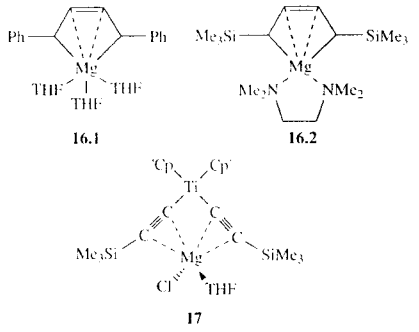

SCHEME 9.10

Superficially, both **16.1** [63] and **16.2** [64] contain allylic type Mg–C bonds in five-membered rings. Compound **16.1** has a pentacoordinate, distorted trigonal bipyramidal magnesium ($Mg–C_{ax}$: 2.32 Å, $Mg–C_{eq}$: 2.26 Å; Mg–O: 2.06, 2.12, 2.18 Å), but additional weak interaction with the 'inner' carbons of the 2-buten-1,4-ylene ligand is indicated by a rather short distance (Mg···C: 2.52, 2.56 Å) which leads to folding of the five-membered ring (Mg is 1.72 Å above the C_4 plane) and suggests heptacoordination of magnesium. In contrast, **16.2** has a rather normal tetracoordinate magnesium, but the other features are similar (Mg–C: 2.19, 2.20 Å; Mg···C: 2.38, 2.40, formal hexacoordination; Mg–N: 2.17, 2.19 Å; Mg 1.56 Å above the C_4 plane).

In **17**, a formal $ClMg(THF)^+$ cation is coordinated in a tweezer-like fashion by the two acetylenic bonds (Mg–C: 2.27, 2.28, 2.28, 2.46 Å) of a $[Cp'_2Ti(CCSiMe_3)_2]^-$ anion and thus hexacoordinate [65]. An analogous, but more complicated tweezer coordination was observed for the tetrameric compound $[Et(PhC{\equiv}C)_3Mg_2{\cdot}TMEDA]_2{\cdot}C_6H_6$ [66].

9.6.3 Anthracenemagnesium Derivatives

Altogether, there are five crystal structures known of the magnesium adducts **18** to the 9,10-position of anthracene and its derivatives. The structure of **18.3** has been obtained from two independent investigations, one in the pure crystal [68], the other in a 1:1 ratio with **18.4** [69]; both structures of **18.3** are essentially identical, as are the magnesium-dihydroanthracene partial structures of all four compounds.

The structures can be subdivided into two groups: **18.1** and **18.2** with pentacoordinate magnesium and **18.3** and **18.4** with tetracoordinate magnesium. Imposed by the dihydroanthracene ligand are the unusually acute C–Mg–C angles of 71–78° which may help to create sufficient space for pentacoordination; presumably, the two large trimethylsilyl groups in **18.3** and **18.4** overcompensate this effect. Expectedly, the benzylic type Mg–C bonds are

Table 9.8. Anthracenemagnesium compounds: average bond lengths (Å; 2 decimals) and bond angles (°; no decimals)

Cpd.	Mg–C	Mg–L	C–Mg–C	foldings[a]	Ref.
18.1	2.25–2.33	2.03–2.09	71, 72	29	[31]
18.2	2.31, 2.32	n.a.	73	41	[67]
18.3	2.23	2.00–2.02	78	45	[68]
18.4	2.22	2.23, 2.26	78	41	[69]

[a] Folding angle of the anthracene skeleton along C9-C10.

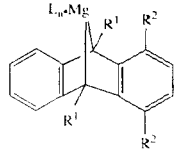

18.1: $R^1 = R^2 = H$; $L_n = THF_3$
18.2: $R^1 = H, R^2 = Me$; $L_n = THF_3$
18.3: $R^1 = SiMe_3, R^2 = H$; $L_n = THF_2$
18.4: $R^1 = SiMe_3, R^2 = H$; $L_n = TMEDA$

SCHEME 9.11

relatively long (*cf.* **3.13**, **3.14**) and tend to be longer in the pentacoordinated compounds (2.25–2.33 Å in **18.1** and **18.2** versus 2.22, 2.23 Å in **18.3** and **18.4**).

9.7 ORGANOMAGNESIUM COMPOUNDS WITH POLYHAPTO CARBON LIGANDS

9.7.1 Cyclopentadienyl Derivatives and Related Compounds

As mentioned at the end of Section 9.2, in compounds such as magnesocene (**19.1**), one sometimes concentrates on the metal–centroid interaction and consequently treats the cyclopentadienyl group as a *simple* ligand and considers these compounds to be dicoordinate; however, in view of the η^5-coordination of magnesium to the Cp ring, it is more appropriate to classify cyclopentadienyl derivatives **19** as decahapto (Scheme 9.12, Table 9.9). However, in some cases such as **19.8** and **19.13** or the indenyl (**20**, **21**) and 9-fluorenyl (**22**) derivatives, η^3- or η^1-coordination of the five-membered ring occurs, mainly for steric reasons.

Normally, the Mg–C distances are 2.30–2.43 Å and the Mg-centroid distances (Mg–D) are in the range of 2.00–2.20 Å; again, steric hindrance and/or strongly coordinating ligands at magnesium may lead to larger values. In symmetrical compounds such as **19.1**, **19.2** and **19.3**, the two five-membered rings may occur in an eclipsed or a staggered conformation. Although the data in the gas phase are not sufficiently accurate to exclude a staggered conformation, both **19.1** (= **19.1a**) and **19.2** are probably in the eclipsed conformation, while in the crystal, **19.1** is staggered (= **19.1b**). In **19.3**, the rings are nearly eclipsed which brings two bulky trimethylsilyl groups in opposition; this causes slight bending of the otherwise linear angle

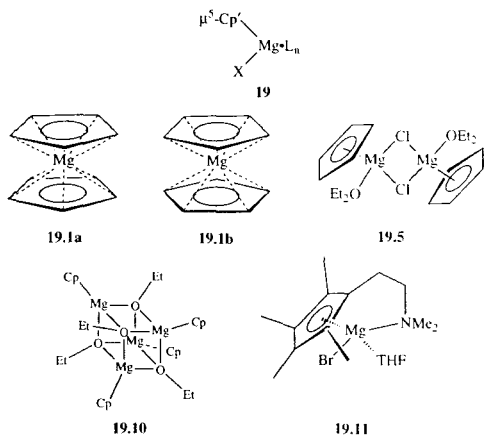

SCHEME 9.12

Table 9.9. (Substituted) cyclopentadienylmagnesium compounds $Cp'MgX{\cdot}L_n$: average bond lengths (Å; 2 decimals) and bond angles (°; no decimals)

Cpd.	Cp′	X	L_n	Hapticity of Cp	Mg–C(Cp)	Mg–D[a]	Method	Remarks	Ref.
19.1a	Cp	Cp	– –	η^5	2.34	2.01	ED	eclipsed?	[70]
19.1b	Cp	Cp	—	η^5	2.30	1.98	X-ray	staggered	[71]
19.2	C_5Me_5	C_5Me_5	—	η^5	2.34	2.01	ED	eclipsed?	[72]
19.3	Cp″[b]	Cp″	—	η^5	n.a.	2.03	X-ray	D–Mg–D = 172°	[73]
19.4	Cp″	Br	TMEDA	η^5	n.a.	2.16	X-ray	Mg–Br 2.52	
								Mg-N 2.23, 2.27	[73]
19.5	Cp	Cl	Et_2O	η^5	2.39	n.a.	X-ray	dimer	[74]
19.6	C_5Me_5	Cl	Et_2O	η^5	2.41	n.a.	X-ray	dimer	[74]
19.7	Cp	Br	TEEDA	η^5	2.55	2.21	X-ray	Mg–Br 2.6	[75]
		(TEEDA = $Et_2NCH_2CH_2NEt_2$)						Mg–N 2.17, 2.35	
19.8	Cp	Me	TMEDA	η^3	2.48 (av.)	—	X-ray	Mg–Me 2.13	[66]
								Mg–N 2.26, 2.29	
19.9	Cp	Np	—	η^5	2.33	n.a.	ED	Mg–Np 2.12	[76]
19.10	Cp	OEt	—	η^5	n.a.	2.10	X-ray	tetramer	[77]
19.11	Cp‴[c]	Br	..NMe_2/THF	η^5	2.26–2.48	n.a.	X-ray		[80]
19.12	CpCp‴[c]	μ-Br	μ-Br	η^5	2.36–2.43	n.a.	X-ray	dimer	[80]
19.13	Cp		THF/*t*-$BuNMe_2$	η^5	2.46	n.a.	X-ray		[41]
		Cp		η^1, η^2	2.37, 2.67				

[a] D = centroid of five-membered ring. [b] Cp″ = 1, 2, 4 – $(SiMe_3)_3C_5H_2$. [c] Cp‴ = $C_5Me_4CH_2CH_2NMe_2$.

at magnesium (172°). In **19.8**, steric hindrance allows not more than η^3-coordination of the Cp ligand, while in **19.13**, the coordination of two ligands to Cp_2Mg (THF and the bulky *t*-$BuNMe_2$) leads to η^5-coordination for one Cp ring only (Mg–C 2.46 Å), while the other adopts an orientation intermediate between η^1 (Mg–C 2.37 Å) and η^2 (Mg–C 2.67 Å). Compounds **19.5** (Scheme 9.12), **19.6** and **19.12** have dimeric structures similar to those of type **4** (Scheme 9.4); **19.11** shows intramolecular coordination as discussed in more detail in Section 9.8.1.

In the compounds with benzoannelated cyclopentadiene derivates, there is a clear tendency towards lower hapticity due to overcrowding. Thus, bisindenylmagnesium (Ind_2Mg, **20**; [79]) has a complicated polymeric structure (not shown) with two different magnesium environments and terminal and bridging Ind groups; Mg1 is η^5-bonded to one Ind (2.31–2.54 Å) and η^1 to two others (2.26, 2.32 Å), while Mg2 is η^5-bonded to one Ind (2.26–2.60 Å) and η^2 to the other two (2.33–2.46 Å).

Similar to the situation in **19.8**, the hapticity to the organic residue is reduced when polydentate amine ligands are involved. This tendency increases in the series Me(η^3-Ind)Mg·TMEDA (**21**), Me(η^1-fluorenyl)Mg·TMEDA (**22**) and **23** which forms an ion triplet: [PMDTA·Mg(μ^2-Me)Mg·PMDTA]$^{2+}$ (PMDTA = $Me_2NCH_2CH_2N(Me)CH_2CH_2NMe_2$) with two pentacoordinate magnesiums and two separate fluorenide anions [66] (structures not shown).

9.7.2 Carborane Derivatives

Three recently reported carborane structures fall into this category: *closo*-1-Mg(TMEDA)-2,3-$(SiMe_3)_2$-2,3-$C_2B_4H_4$) (**24**) [80], {*commo*-1,1′-Mg[2,3-$(SiMe_3)_2$-2,3-$C_2B_4H_4$]$_2$}$^{-2}$ (**25**) [81] and $(THF)_2Mg((SiMe_3)_4C_4B_8H_8)$ (**26**) [81]. The half-sandwich **24** has the magnesium coordinated to the five-membered C_2B_3 ring of the carborane in an η^5-fashion (Mg-centroid: 2.12, 2.14 Å; Mg–C: 2.60–2.65 Å). The full-sandwich **25** has an analogous arrangement (Mg-centroid: 2.02 Å; Mg–C: 2.45, 2.46 Å). In **26**, magnesium is coordinated to one of the open faces of the carborane, in particular to two carbons (Mg–C: 2.32, 2.33 Å) and two borons; the two bonds to THF (Mg–O: 2.03 Å) are normal.

9.8 ORGANOMAGNESIUM COMPOUNDS WITH INTRAMOLECULAR AND/OR POLYCOORDINATION

For practical reasons, this chapter is divided into sections describing compounds with relatively simple intramolecular coordination involving few intramolecular Lewis bases (9.8.1) and those in which polydentate ligands, mostly polyethers, are involved with (9.8.2) or without intramolecular coordination (9.8.3).

9.8.1 Intramolecular Coordination

Intramolecular coordination can occur when in the basic structure $RXMgL_n$ (*cf.* **3**, Scheme 9.3), there is a covalent connection between R and/or X and L, where L may be a mono- or polydentate ligand. Several structural motifs are encountered in this group, starting from simple monomers of type **3** via dimeric structures of type **4** to more complicated arrangements. Compounds with a covalent connection between R and L are presented in Scheme 9.13, those with a connection between X and L in Scheme 9.14.

The most simple form of intramolecular coordination involves alkoxy or alkylamino side arms as already encountered in **19.11** and **19.12** (Scheme 9.12, Table 9.9) and **27** [82] (Scheme 9.13). For **27** (Mg–C: 2.14 Å, Mg–O: 2.07 Å; C–Mg–C: 140°, O–Mg–O: 96°), the structural parameters are essentially the same as for type **3** compounds in general, and slight deviations can be understood from restrictions imposed by the chelating ligand; the same is true for other structures to be described, and therefore only essential data will be presented. Thus, **28** is a dimer of type **4** (Mg–η^1C: 2.13 Å, Mg–μ^2C: 2.29 Å, C–Mg–C: 106°, Mg–C–Mg: 74°, η^1C–Mg–μ^2C: 115°) [83]. With the same chelating ligand, **29** has a tetranuclear structure involving chloride bridging (Mg–C: 2.15 Å) [84].

Mononuclear structures prevail as illustrated by **27**, **30** (Mg–C: 2.23 Å) [85], **31** (Mg–C: 2.22 Å) [86], **32** (Mg–C: 2.24 Å) [87], **34** (Mg–C: 2.22 Å) [89] and **37** (2.16 Å) [91]; this is probably due to the fact that space-saving aggregation is not necessary because intramolecular coordination reduces crowding around the central metal when non-bonding interactions between two separate ligands are replaced by bonds. Dinuclear structures are present in **28**, **33** (Mg–C: 2.16 Å) [88] and **35** (Mg–C: 2.16 Å) [91].

Some remarkable aspects will be pointed out. In **30**, **31** and **36** [90], the chelate ring is four-membered which normally leads to considerable ring strain. Furthermore, while the normal tetracoordinate state is predominating, there are exceptions. Compound **29** shows pentacoordination of its 'organometallic' magnesium; in **37** [91], magnesium is pentacoordinate, too, as there is sufficient space to coordinate an additional 'external' THF. Compounds **32**, **34** and **35** are hexacoordinate. While one may be tempted to ascribe the rather long Mg–C bond (2.22 Å) in **34** to hexacoordination, that of the completely analogous **35** is much shorter (2.16 Å); possibly, the smaller, harder and more strongly coordinating oxygens of **35** pull the metal into closer vicinity. Other factors responsible for bond lengthening may be benzylic type carbon atoms or non-ideal positioning of the Lewis base due to conformational restrictions; *e.g.* the P–Mg–P angles in **34** (149°) and the O–Mg–O angles in **35** (146°)

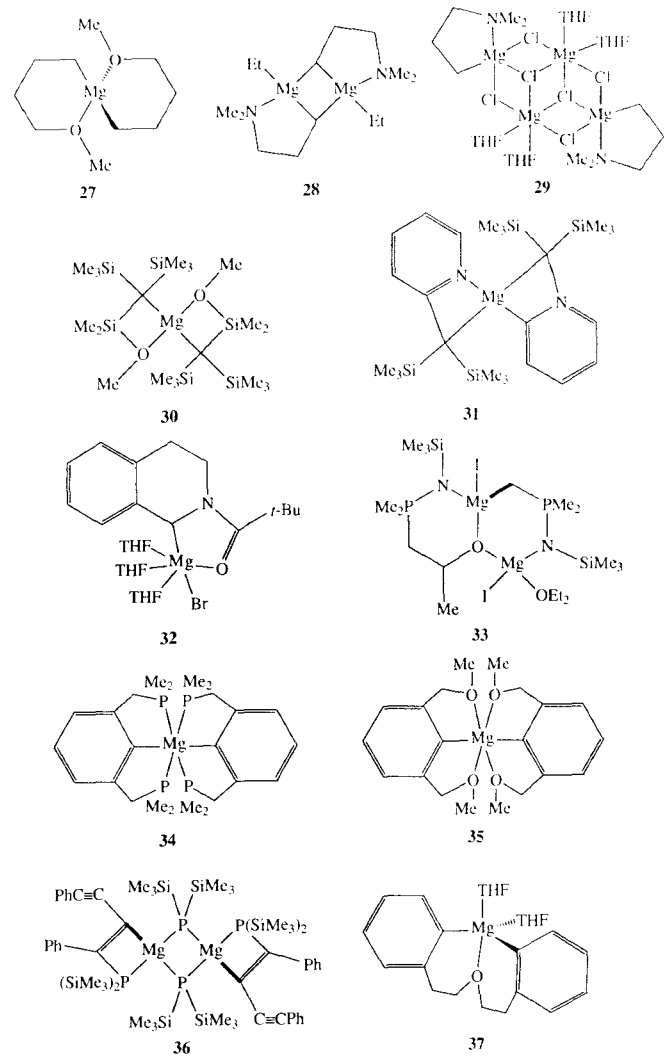

SCHEME 9.13

strongly deviate from the ideal octahedral value of 180°.

Intramolecular coordination arising from attachment of the Lewis base **L** to the bridging atom X is found in **38**, **39** and **40** (Scheme 9.14). The seemingly simple di(*o*-anisyl)magnesium (**38**) [91] has a surprisingly complex structure: it consists of dimers with both penta- and tetracoordinate magnesium (Mg1 and Mg2, respectively). Mg1 has a certain degree of cationic character because it shares one of its aryl 'anions' with Mg2 which in turn obtains partial ate characteristics. The μ^2-bridging anisyl group is also involved in four-membered ring chelation to Mg1. The bonding parameters are about normal.

In both **39** and **40**, the bridging X in a dimer of type **4** is an amido nitrogen. Compound **39** [93] has two independent molecules in the unit cell with practically identical structures (Mg–C: 2.10 Å, Mg–N(amido): 2.10 Å, Mg–N(amino): 2.20 Å; four-membered ring: MgN–Mg: 88°, NMg–N: 92°). The structure of **40** [94] (Mg–C: 2.14 Å, Mg–N(amido): 2.14 Å, Mg–N(amino): 2.20 Å; four-membered ring: Mg–N–Mg: 88°, N–Mg–N: 92°) is very similar, too.

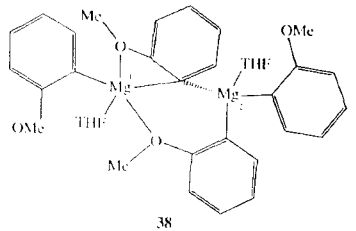

38

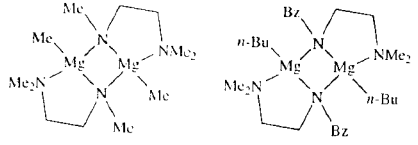

39 40

SCHEME 9.14

9.8.2 Intramolecular Polycoordination

Starting from the basic structure of phenylmagnesium bromide (**3.19**), magnesium undergoes an increasing degree of intramolecular coordination in the series **41.1**–**41.4** (Scheme 9.15) by extension

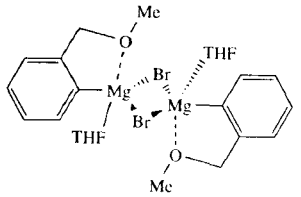

41.1

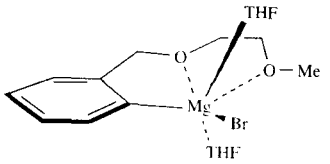

41.2

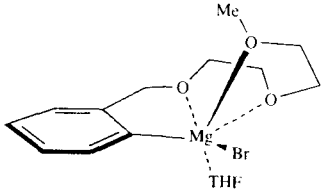

41.3

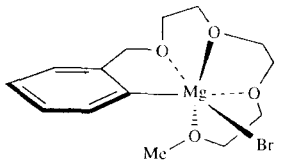

41.4

SCHEME 9.15

of an *ortho*-attached (oligo)glycol ether side arm [95]. While the parent **3.19** is tetracoordinate, the space-saving effect of intramolecular coordination allows pentacoordination in the dimer **41.1**, and hexacoordination in **41.2**, **41.3** and **41.4** which is completed by attachment of a decreasing number of THF molecules where required: two, one and none, respectively; as a result, **41.4** is a Grignard reagent with the normally highest coordination number of 6, but without any external ether ligand. The Mg–C bond lengths are normal (2.11, 2.16, 2.15, 2.15 Å, respectively) as are the Mg–Br bonds (Table 9.10); the Mg–O bonds are rather long due to the high coordination number and to conformational effects as shown for **41.4** where the Mg–O bond decreases from O1 to O4 (2.33, 2.20, 2.19, 2.15 Å, respectively), presumably because the 'remote' oxygens have more freedom to occupy ideal positions.

The organomagnesiums **42**–**44** with internally coordinating crown ethers posses structural parameters (Table 9.10, Scheme 9.16) which generally are similar to those of the configurationally less restricted **41**. Certain trends or deviations are not fully understood; to some extent, packing effects in the crystal may be involved, and if so, it is possible that the structures in solution exhibit more normal values. For example, both **42.1** and **43.1** are Grignard reagents, but their Mg–C bonds differ remarkably (2.10 and 2.18 Å, respectively), while on the other hand, the corresponding diarylmagnesium compounds **42.2** and **43.2**, respectively, have the same bond length towards the crown ether aryl group with a normal value (2.13 Å; *cf.* **3.15**, **3.16**). Furthermore, whereas **42.1** and **42.2** have the same R–Mg–X angle (128°), that of the analogous pair **43.1** (111°) and **43.2** (139°) is different; similarly, and possibly related to the previous observation, in **43.1**, it is O^1 which is uncoordinated while in **43.2**, it is O^4. The coordination number is pseudo-4 in the two crown[4] species **42** (O^1 and O^4 are only weakly coordinating at 2.33 and 2.49 Å, respectively) and 6 in **43** and **44**.

9.8.3 Intermolecular Polycoordination

As is the case for intramolecular coordinated compounds described in Section 9.8.2, polycoordination of organomagnesium compounds with *external* polyethers or polyamines often leads to interesting structures. In particular, crown ether derivatives may give rise to rotaxane formation by threading through the cavity of the polyether ring, or to ionic species by efficient solvation of the cationic part, thereby creating a variety of magnesiate species as a 'by-product'.

A special case involving polyamino ligands is that of the negatively charged tridentate tris(pyrazolyl)hydroborato ligand which forms the η^3-complexes **45.1**–**45.3** with alkylmagnesium cations [101]; magnesium assumes the common (distorted)

Table 9.10. Intramolecularly polycoordinate magnesium: average bond lengths (Å; 2 decimals) and bond angles (°; no decimals) in $RMgX{\cdot}L_n$

Cpd.	R	X	L_n	Mg–R	Mg–X	Mg–O	R–Mg–X	Ref.
41.1	*o*-C_6H_4	Br	CH_2OMe	2.11	2.51	2.10, 2.04	96	[95]
41.2	*o*-C_6H_4	Br	$CH_2OCH_2CH_2OMe$	2.16	2.57	2.15–2.19	111	[95]
41.3	*o*-C_6H_4	Br	$CH_2(OCH_2CH_2)_2OMe$	2.15	2.59	2.15–2.22	111	[95]
41.4	*o*-C_6H_4	Br	$CH_2(OCH_2CH_2)_3OMe$	2.15	2.57	2.15–2.33	107	[95]
42.1	1,3-xylylene	Br	$(OCH_2CH_2)_3O$	2.10	2.52	2.12–2.49	128	[96]
42.2	1,3-xylylene	Ph	$(OCH_2CH_2)_3O$	2.13	2.15	2.18–2.62	128	[97]
43.1	1,3-xylylene	Br	$(OCH_2CH_2)_4O$	2.18	2.60	2.13–2.33	111	[98]
43.2	1,3-xylylene	p-*t*-BuC_6H_4	$(OCH_2CH_2)_4O$	2.13	2.15	2.15–2.71	139	[99]
44	1,3-phenylene	Br	$(OCH_2CH_2)_4O$	2.19	2.66	2.08–2.32	107	[100]

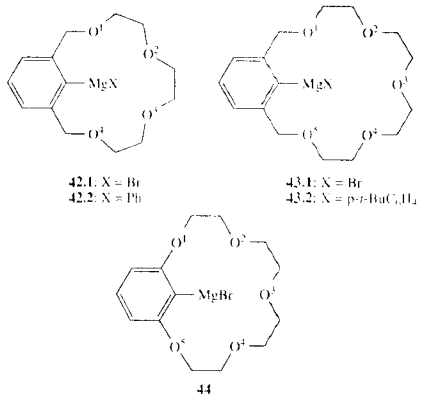

42.1: X = Br
42.2: X = Ph

43.1: X = Br
43.2: X = p-*t*-BuC$_6$H$_4$

44

SCHEME 9.16

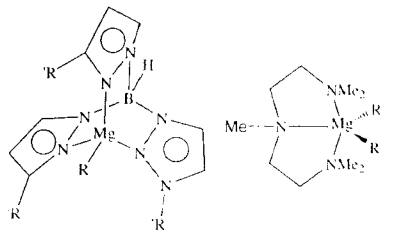

45.1: R = Me, R' = *t*-Bu
45.2: R = *i*-Pr , R' = *t*-Bu
45.3: R = CH_2SiMe_3, R' = Me

46.1: R = Me
46.2: R = Et

SCHEME 9.17

tetrahedral configuration (Scheme 9.17). Whereas **45.1** and **45.2** have a symmetrical orientation of the R–Mg bond relative to the ligand, the orientation in **45.3** is distorted due to steric hindrance between R and the methyl groups; similar interaction with the *t*-butyl groups leads to distortion of the isopropyl group in **45.2**. Another open polyamino ligand is PMDTA; besides **23**, two other pentacoordinate complexes are known: **46.1** and **46.2** [20]. The structural data are as expected (Table 9.11).

Three rotaxane complexes have been obtained by the interaction of diorganylmagnesium with crown ethers: **47** [102]), **48.1** [103] and **48.2** [104] (Scheme 9.18).

Compound **47** has a rather symmetrical structure with the linear Et–Mg–Et unit (Mg–C: 2.10 Å) oriented perpendicular to the average plane of six oxygens which are weakly bonded to magnesium due to the unusually high coordination number of 8 (Mg–O: 2.77–2.79 Å). The complexes **48.1** and **48.2** are isostructural. Magnesium is distorted hexacoordinate with slightly elongated bonds (Mg–C: 2.19 Å; Mg–O1-4: 2.20–2.55°, O^5 is not coordinating). The two aryl groups are bent away from the coordinating oxygens towards the crown ether benzene ring (C–Mg–C: 164°, 167°, respectively). Interestingly, the 30-crown-8 ligand with its larger cavity does not bind diarylmagnesiums in a rotaxane like fashion. Rather, in **49** [103], two bis(p-*t*-butylphenyl)magnesiums are externally coordinated in a pentahapto fashion; the same binding mode is also found for the open glyme ethers in **50.1** and **50.2** [103]. The coordination geometries of **49** and **50** are similar and normal; *e.g.* the Mg–C bonds are 2.19, 2.15–2.16 and 2.14–2.17 Å, respectively, and the

Table 9.11. Polycoordinate magnesium with amino ligands (Scheme 9.17): average bond lengths (Å; 2 decimals) and bond angles (°; no decimals)

Cpd.	R	Mg–C	Mg–N	R–Mg–(N/C)	Ref.
45.1	Me	2.12	2.13–2.14	(N):125	[101]
45.2	*i*-Pr	2.18	2.16–2.17	(N):124–125	[101]
45.3	CH_2SiMe_3	2.10	2.16–2.17	(N):118–134	[101]
46.1	Me	2.17, 2.19	2.33–2.41	(C):114	[20]
46.2	Et	2.17, 2.22	2.36–2.37	(C):116	[20]

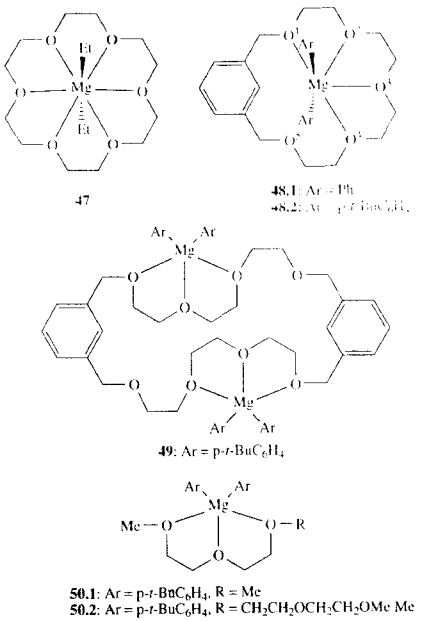

47

48.1: Ar = Ph
48.2: Ar = p-*t*-BuC$_6$H$_4$

49: Ar = p-*t*-BuC$_6$H$_4$

50.1: Ar = p-*t*-BuC$_6$H$_4$, R = Me
50.2: Ar = p-*t*-BuC$_6$H$_4$, R = $CH_2CH_2OCH_2CH_2OMe$ Me

SCHEME 9.18

three coordinating oxygens are approximately in one plane magnesium. It should be pointed out that in **50.2**, two more oxygens are available for coordination compared to **50.1**, but apparently, there is insufficient space around magnesium and/or the additional oxygens cannot reach a strain-free location. In the tetranuclear **51** [105], related motifs can be recognized at the two terminally bound diphenylmagnesium units (Mg–C: 2.15, 2.16 Å); the two central phenylmagnesium units (Mg–C: 2.13 Å) are connected by two μ^2-bridging phenoxide oxygens (Mg–O: 2.00, 2.04 Å) and are pentacoordinate (Scheme 9.19).

Another interesting feature of polydentate ligands is their tendency to fully cleave the polar magnesium carbon bond with formation of solvated cations and magnesate counterions. In this regard, there is a remarkable difference between 15-crown-5 and 18-crown-6: while the latter

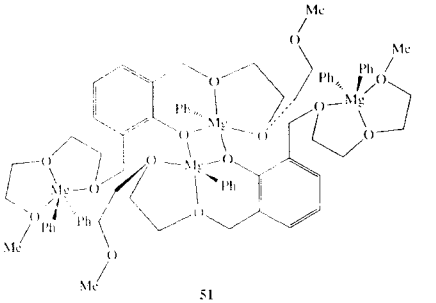

51

SCHEME 9.19

forms the rotaxane **47** with diethylmagnesium, the former apparently gives a tighter fit to magnesium allowing heterolytic cleavage of dimethylmagnesium to give **52** [106] which consists of a $[MeMg \cdot 15\text{-crown-5}]^+$ cation (Mg–C: 2.14 Å) and, weakly associated to it via one of the methyl groups (Mg–C: 3.28 Å), a polymeric chain of $[Mg_2Me_5^-]_n$ units (Mg–C (μ-Me to Mg^+ and Me(terminal)): 2.17 Å; in the chain: 2.25–2.40 Å) (Scheme 9.20).

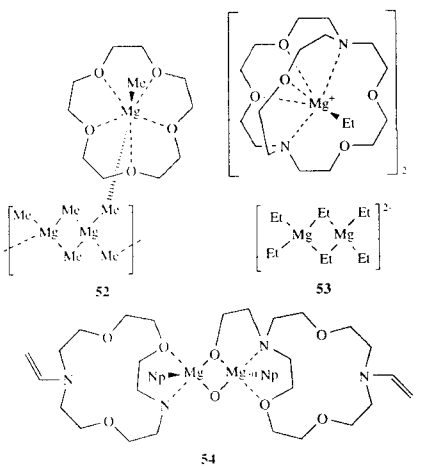

52

53

54

SCHEME 9.20

Another ligand effecting heterolytic dissociation is 2,2,1-cryptand. With diethylmagnesium, it forms **53** [13] consisting of an unsymmetrically hexacoordinate $EtMg^+$ cation, which is stabilized by bonding to 3 oxygens and 2 nitrogens, and the dinuclear anion $[Et_6Mg_2]^{2-}$ (which corresponds to the neutral compounds of type **4**); they show normal parameters (Mg–C(η^1): 2.21, 2.24 Å; Mg–C(μ^2): 2.36 Å). The analogous cation [NpMg(2,2,1-cryptand)]$^+$ is the counterion of the previously mentioned tricoordinate anion $[MgNp_3]^-$ (**2.2**, Scheme 9.2) [13]. In contrast, the ring cleavage product **54**, obtained from the neopentyl analogue of **53** by heating, is a relatively normal dimer, but with pentacoordinate magnesium (Mg–C: 2.18 Å) and bridging alkoxide oxygens (Mg–O(μ^2): 1.98 Å) [107].

Two examples are known where a polyazacycloalkane ligand stabilizes cationic organomagnesium species (Scheme 9.21). The structure of **55** [108] is quite complicated involving six magnesiums in two dinuclear $[Mg_2Me_3{\cdot}(9N3)_2]^+$ cations (9N3 = 1,4,7-trimethyl-1,4,7-triazacyclononane) and the dinuclear $[Me_6Mg_2]^{2-}$ anion (which is analogous to $[Et_6Mg_2]^{2-}$ in **53**). In **56** [109], the larger azaligand stabilizes the mononuclear cation [MeMg • (14N4)]$^+$(14N4 = 1,4,8,11-tetramethyl-1,4,8,11-tetraazacyclotetradecane) with $[CdMe_3]^-$ as the counteranion.

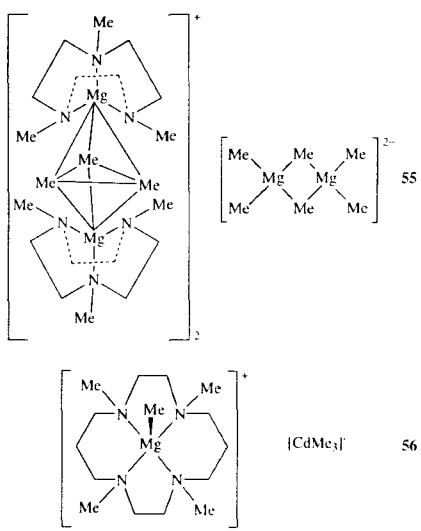

55

$[CdMe_3]^-$ **56**

SCHEME 9.21

Finally, it should be mentioned that polycoordination not only leads to interesting structures as discussed in this Section, but also to unusual and strongly enhanced reactivity; several reviews describe the interesting chemistry associated with such special high coordination states [54,105,110,111].

9.9 HETEROMETALLIC ORGANOMAGNESIUM COMPLEXES

9.9.1 Heterometallic Organomagnesium Complexes with Alkali Metals

Formally, complex **2.3** ($[Li(THF)_{0.6}(EtO)_{0.4}]^+$ $[MgIs_3]^-$) belongs to this class; it has been treated in Section 9.2. Two other simple ate type complexes are **57** [112] between a Grignard reagent and lithium bromide with the structural motif of **4**, and **58** between diphenylmagnesium and two phenylsodiums [53] (Scheme 9.22). Their structural parameters are not unusual (*e.g.* **57** Mg–C(terminal): 2.19 Å; **58** Mg–C(μ): 2.29 Å). Like **57** and **58**, **59** (Mg–C: 2.23–2.29 Å) [113] and **60** (Mg–C[μ-Li]: 2.18 - 2.19 Å); Mg–C [μ–Mg]: 2.29–2.32 Å) [114] may be regarded as ate complexes with increasing fragments derived from the polymeric chain of $(MgR_2)_n$ (**6**); again, they show the expected bond lengths. Compound **61** [115] resembles **59** in being a tetrabenzylmagnesate complex, but the attachment of the two lithium cations is different: one is bridging like in **59**, the other one is separate and solvated by two TMEDA; the MgC bonds (2.22–2.32 Å), though benzylic, are only are slightly longer than those in **59**.

While in **57–61**, magnesium is in the normal tetracoordinate state, the sterically less demanding alkynyl substituents in **62–63** allow higher coordination numbers, as was already pointed out for

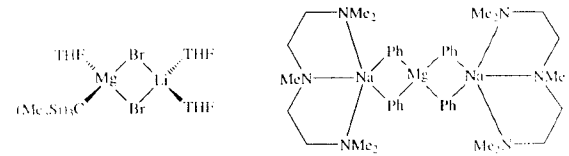

57 58

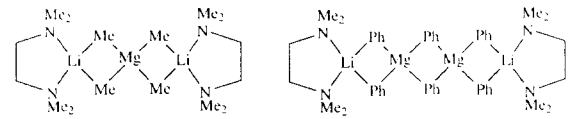

59 60

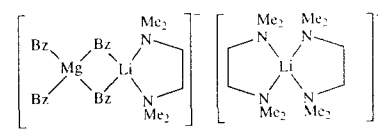

61

SCHEME 9.22

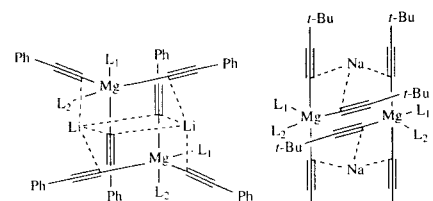

62: L_1L_2 = TMEDA **63.1**: L_1L_2 = TMEDA **63.2**: L_1L_2 = PMDTA

SCHEME 9.23

12. In **62** [115], magnesium is in the center of a distorted trigonal bipyramid with two equatorial (2.18 Å) bonds and one axial (2.31 Å) bond to the alkynyl groups; lithium is coordinated to one nitrogen and three times to the π-clouds. The structures of **63** [53] show a different arrangement of the ligands, but the connectivities and structural parameters are essentially analogous; in **63.2**, one terminal amino group of PMDTA is not coordinated.

9.9.2 Heterometallic Organomagnesium Complexes with Aluminum

Some of the compounds in this category have rather simple μ-bridged structures similar to those of **58–61**. Thus, **64** (Mg–C: 2.19–2.22 Å) has two $AlMe_2$ units attached to an ate-like $MgMe_4$ core [116] (Scheme 9.24). Compounds **65** [117] and **66** [119] have a Mg_2R_2 four-membered ring core to which two four-membered spiro rings are attached. In the case of **65**, these external rings consist of a NSiN unit (with an aluminum containing four-membered ring SiNAlN annelated to it; Mg–C: 2.20 Å); in **66**, it is formed by a NAlN unit (Mg–C: 2.16–2.30 Å). The related compounds **67** ($[R_2N MgMe]_2[MgNR_2(R_2NAlMe_3)]_2$; R = $SiMe_3$)[120] and **68** ($[Me_2Al[\mu$-$N(i-Pr_2)]_2MgMe]_4$) [118] have a more complicated structure (not shown), the novel feature of which is the nearly linear bridging of two magnesiums by a methyl group (**67**: Mg–C–Mg: 2.16, 2.43 Å, 179°; **68:** Mg–C–Mg: 2.15, 2.49 Å, 168°).

Like **18**, the two representatives of **69** are formally derived from the 9,10-dianion of

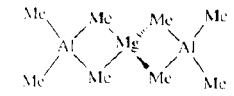

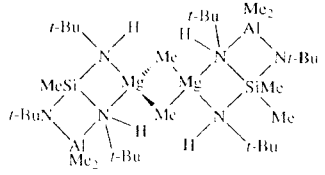

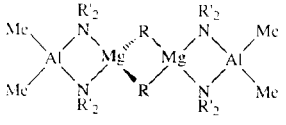

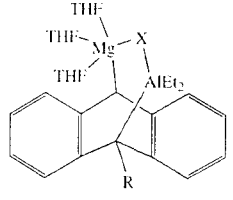

66.1: R = Me, R' = Et
66.2: R = *i*-Pr, R' = C≡CC$_6$H5
66.3: R = *i*-Pr, R' = C≡CC$_6$H$_4$-*p*-CH3
66.4: R = *i*-Pr, R' = C≡C-*p*-*t*-Bu
66.5: R = *i*-Pr, R' = C≡CSiMe$_3$
66.6: R = Et, R' = C≡CC$_6$H$_5$

69.1: X = H
69.2: R = OEt

SCHEME 9.24

9,10-dihydroanthracene, but in **69**, the two metals are different—magnesium and aluminum—, and they are connected by a μ^2-bridging anion which is a hydride in the case of **69.1** [121] and an ethoxide for **69.2** [122] (Scheme 9.24). For **69.1**, relevant parameters are Mg–C: 2.20, Mg–H: 1.96, Al–C : 1.98, Al–H: 1.62 Å; C–Mg–H: 101°; the magnesium is in a trigonal bipyramid with H and one THF in apical positions (O–Mg–H: 160°). The structure of **69.2** has not been fully resolved, but sufficiently so to allow determination of gross features.

9.9.3 Heterometallic Organomagnesium Complexes with Transition Metals

Scheme 9.25 shows the eight known compounds in which (parts of) organomagnesium compounds are connected to transition metal fragments; they reveal a great variety of structures. Compound **70** may be viewed either as an internally bridged diorganylmagnesium Mg[CH(SiMe$_3$)(ZrCp$_2$Br)]$_2$ or as an adduct of MgBr$_2$ to two carbene complexes Cp$_2$Zr = CHSiMe$_3$ [123]. The latter interpretation is supported by the short Zr–CH$_2$ bonds (2.15, 2.16 Å) although the two Mg–C bonds (2.19 Å; C–Mg–C: 133°) are only slightly longer than 2.15 Å (Table 9.3); however, the accumulation of three metal(oid)s at one carbon may cause constriction of the Mg–C bond as in **13**.

Compound **71** [124] is a tetramer composed of two Grignard reagents CyMgBr (cyclohexyl) and two 'inorganic' Grignard reagents Cp$_2$HMoMgBr; all magnesiums are tetracoordinate (Mg–Mo: 2.24, 2.85 Å; other data on the geometry around Mg have not been given) [124]. In both **72** and **73**, magnesium is pentacoordinated to a Group 8 metal fragment. This includes a bond to the metal and a weakly μ-bridging methyl group between magnesium and nickel

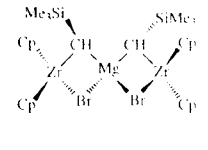

70

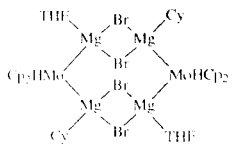

71

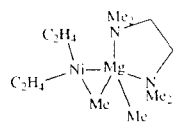

72

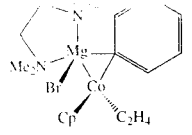

73

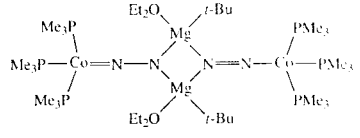

74

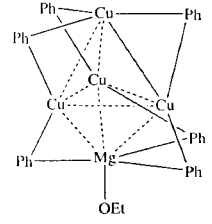

75

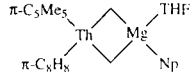

76

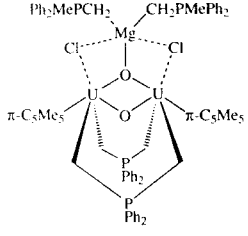

77

SCHEME 9.25

in **72** (Mg–C(μ): 2.29 Å, Mg–C(terminal): 2.15 Å, Ni–C: 2.03 Å) [125], while in **73**, the bridging group is phenyl (Mg–C: 2.57 Å, Co–C: 1.98 Å) [126]. In **74**, magnesium is tetrahedral and bridging between two dinitrogen units coordinated by tris(trimethylphosphino) cobalt; the Mg–C bond has not been reported [127]. A seldom encountered case of heptacoordination may be discerned in the copper cluster complex **75**, although the interaction with three of the coppers is weak (Mg–Cu: 2.75 Å); the three bridging phenyls have normal distances (Mg–C: 2.35 Å) [128].

Finally, of the two actinide complexes **76** [129] and **77** [130], **76** has the simple structural motif of **4** and a normal geometry around magnesium

(details not reported), whereas **77** consists of a complicated cluster of two uraniums and one pentacoordinate magnesium with a (slightly elongated) bond to the ylidic CH_2 group of two phosphoranemethylenes (Mg–C: 2.23 Å).

9.10 CONCLUSIONS

There is no doubt that the preferred coordination number of divalent magnesium is 6, as illustrated by the numerous examples from inorganic chemistry [5]. The $[Mg(H_2O)_6]^{2+}$ cation is a good illustration, but it also reveals the conditions which have to be fullfilled to attain this optimal situation: a high charge on magnesium and a small size of the ligands. Both conditions are seldom met in organomagnesium compounds such as $RMgHal{\cdot}L_n$ or $R_2Mg{\cdot}L_n$; while the charge at magnesium is high, it is certainly less than +2, and both the organic groups R and the coordinated ligands L (ethers, tertiary amines) are rather bulky. For the majority of organomagnesium compounds, a compromise is found involving tetracoordinated magnesium which may be realized in a variety of monomeric, dimeric or polymeric structures such as $RMgHal{\cdot}L_2$ (**3**), $L{\cdot}RMg(\mu\text{-Hal})_2MgR{\cdot}L$ (**4**) or $[(\mu\text{-R})_2Mg(\mu\text{-R})_2Mg]_n$ (**6**), respectively, and others. In these cases, a formal octet around magnesium is achieved, where necessary via electron deficient three-center/two-electron bonds.

However, other coordination states may be encountered depending on the interplay between electron demand and steric hindrance. Thus, the rare and highly electron deficient coordination numbers 2 (in **1**) and 3 (in **2**) are enforced by the extreme steric hindrance due to very bulky organic groups, while 'space saving' ligands such as chelating or polycoordinating ethers and amines allow the higher coordination numbers 5 and 6 to be attained.

There are many indications to support the statement that in most cases, the structures encountered in the crystal are also those occurring in solution [2,3], and for this reason, the X-ray crystal structures are indispensible for understanding the solution chemistry of Grignard reagents as illustrated by the following example. Based on the crystal structures of **35** and **37** (Scheme 9.13), the strongly divergent thermodynamic parameters

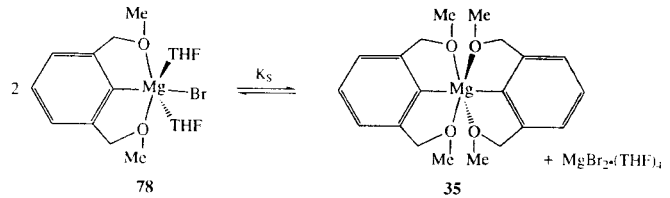

SCHEME 9.26

of the Schlenk equilibria **78** ⇌ **35** and **79** ⇌ **80** involving two seemingly highly analogous Grignard reagents could be rationalized on the basis of the coordination numbers shown in Scheme 9.26, in particular by the different number of coordinated THF molecules [91].

In a similar fashion, the interaction of organomagnesium reagents with substrates will depend on the coordination state which, in turn, determines the relative ease with which the approach of the substrate towards the coordination sphere of the reagent and/or single electron transfer reactions takes place.

REFERENCES

1. V. Grignard, *C. R. Acad. Sci. Paris*, **1900**, *130*, 1322.
2. W.E. Lindsell in *Comprehensive Organometallic Chemistry*, G. Wilkinson, F.G.A. Stone, E.W. Abel eds., Pergamon, Oxford, **1982**, Vol. *1*, p. 155–252.
3. W.E. Lindsell in *Comprehensive Organometallic Chemistry II*, E.W. Abel, F.G.A. Stone, G. Wilkinson eds., Pergamon/Elsevier, Oxford, **1995**, Vol. *1*, p. 57–127.
4. P.R. Markies, O.S. Akkerman, F. Bickelhaupt, W.J.J. Smeets, A.L. Spek, *Adv. Organomet. Chem.* **1991**, *32*, 147–226.
5. (a) C.E. Holloway, M. Melnik, *Coord. Chem. Rev.* **1994**, *135/136*, 287–301. (b) C.E. Holloway, M. Melnik, *J. Organomet. Chem.* **1994**, *465*, 1–63.
6. H.L. Uhm in *Handbook of Grignard Reagents*, G.S. Silverman, P.E. Rakita eds., Marcel Dekker, New York, **1996**, p. 117–144.
7. E.C. Ashby, L. Fernholt, A. Haaland, R. Seip, R.C. Smith, *Acta Chem. Scand.* **1980**, *A 34*, 213–217.
8. O.S. Akkerman, G. Schat, E.A.I.M. Evers, F. Bickelhaupt, *Recl. Trav. Chim. Pays-Bas*, **1983**, *102*, 109–113.
9. R.A. Anderson, G. Wilkinson, *J. Chem. Soc. Dalton Trans.* **1977**, 809–811.
10. (a) S.S. Al-Juaid, C. Eaborn, P.B. Hitchcock, C.A. McGeary, J.D. Smith, *J. Chem. Soc., Chem. Commun.* **1989**, 273–274. (b) S.S. Al-Juaid, C. Eaborn, P.B. Hitchcock, K. Kundu, C.A. McGeary, J.D. Smith, *J. Organomet. Chem.* **1994**, *480*, 199–203.
11. R.J. Wehmschulte, P.P. Power, *Organometallics*, **1995**, *14*, 3264–3267.
12. P.B. Hitchcock, J.A.K. Howard, M.F. Lappert, W.P. Leung, S.A. Mason, *J. Chem. Soc., Chem. Commun.* **1990**, 847–849.
13. E.P. Squiller, R.R. Whittle, H.G. Richey, Jr., *J. Am. Chem. Chem.* **1985**, *107*, 432–435.
14. K.M. Waggoner, P.P. Power, *Organometallics*, **1992**, *11*, 3209–3214.
15. L.M. Engelhardt, B.S. Jolly, P.C. Junk, C.L. Raston, B.W. Skelton, A.H. White, *Aust. J. Chem.* **1986**, *39*, 1337–1345.
16. A.J. Arduengo III, H.V.R. Dias, F. Davidson, R.L. Harlow, *J. Organomet. Chem.* **1993**, *462*, 13–18.
17. T. Greiser, J. Kopf, D. Thoennes, E. Weiss, *J. Organomet. Chem.* **1980**, *191*, 1–6.
18. J. Toney, G.D. Stucky, *J. Organomet. Chem.* **1970**, *22*, 241–249.
19. D.R. Armstrong, K.W. Henderson, M. MacGregor, R.E. Mulvey, M.J. Ross, W. Clegg, P.A. O'Neil, *J. Organomet. Chem.* **1995**, *486*, 79–83.
20. H. Viebrock, E. Weiss, *J. Organomet. Chem.* **1994**, *464*, 121–126.
21. (a) L.J. Guggenberger, R.E. Rundle, *J. Am. Chem. Soc.* **1964**, *86*, 5344–5345. (b) L.J. Guggenberger, R.E. Rundle, *J. Am. Chem. Soc.* **1968**, *90*, 5375–5378.
22. H. Kageyama, K. Miki, N. Tanaka, N. Kasai, Y. Okamoto, H. Yuki, *Bull. Chem. Soc. Jpn.* **1983**, *56*, 1319–1321.
23. H. Kageyama, K. Miki, Y. Kai, N. Kasai, Y. Okamoto, H. Yuki, *Acta Crystallogr. Sect. B* **1982**, *38*, 2264–2266.
24. H. Kageyama, K. Miki, Y. Kai, N. Kasai, Y. Okamoto, H. Yuki, *Bull. Chem. Soc. Jpn.* **1984**, *57*, 1189–1196.
25. N. Kuhn, M. Schulten, R. Boese, D. Bläser, *J. Organomet. Chem.* **1991**, *421*, 1–8.
26. W. Clegg, D.A. Brown, S.J. Bryan, K. Wade, *J. Organomet. Chem.* **1987**, *325*, 39–46.
27. N.D.R. Barnett, W. Clegg, R.E. Mulvey, P.A. O'Neil, D. Reed, *J. Organomet. Chem.* **1996**, *510*, 297–300.
28. H. Kageyama, K. Miki, Y. Kai, N. Kasai, Y. Okamoto, H. Yuki, *Bull. Chem. Soc. Jpn.* **1983**, *56*, 2411.
29. H. Yasuda, M. Yamauchi, A. Nakamura, T. Sei, Y. Kai, N. Yasuoka, N. Kasai, *Bull. Chem. Soc. Jpn.* **1980**, *53*, 1089–1100.
30. U. Nagel, H.G. Nedden, *Chem. Ber./Recueil*, **1997**, *130*, 535–542.
31. L.M. Engelhardt, S. Harvey, C.L. Raston, A.H. White, *J. Organomet. Chem.* **1988**, *341*, 39–51.
32. P.R. Markies, G. Schat, O.S. Akkerman, F. Bickelhaupt, W.J.J. Smeets, P. van der Sluis, A.L. Spek, *J. Organomet. Chem.* **1990**, *393*, 315–331.
33. D. Thoennes, E. Weiss, *Chem. Ber.* **1978**, *111*, 3381–3384.
34. F.A. Schröder, *Chem. Ber.* **1969**, *102*, 2035–2043.
35. G. Stucky, R.E. Rundle, *J. Am. Chem. Soc.* **1964**, *86*, 4825–4830.

36. H. Eriksson, M. Örtendahl, M. Håkansson, *Organometallics* **1996**, *15*, 4823–4831.
37. W. Clegg, D.A. Brown, S.J. Bryan, K. Wade, *J. Organomet. Chem.* **1987**, *325*, 39–46.
38. A.L. Spek, P. Voorbergen, G. Schat, C. Blomberg, F. Bickelhaupt, *J. Organomet. Chem.* **1974**, *77*, 147–151.
39. J. Toney, G.D. Stucky, *J. Chem. Soc., Chem. Commun.* **1967**, 1168–1169.
40. H. Bock, K. Ziemer, C. Näther, *J. Organomet. Chem.* **1996**, *511*, 29–35.
41. M.M. Olmstead, W.J. Grigsby, D.R. Chacon, T. Hascale, P.P. Power, *Inorg. Chim. Acta* **1996**, *251*, 273–284.
42. S.S. Al-Juaid, C. Eaborn, P.B. Hitchcock, A.J. Jaggar, J.D. Smith, *J. Organomet. Chem.* **1994**, *469*, 129–133.
43. E. Weiss, *J. Organomet. Chem.* **1964**, *2*, 314–321.
44. E. Weiss, *J. Organomet. Chem.* **1965**, *4*, 101–108.
45. P.R. Markies, G. Schat, O.S. Akkerman, F. Bickelhaupt, W.J.J. Smeets, A.J.M. Duisenberg, A.L. Spek, *J. Organomet. Chem.* **1989**, *375*, 11–20.
46. M. Parvez, A.D. Pajerski, H.G. Richey, *Acta Cryst. C*, **1988**, *44*, 1212–1215.
47. M. Vallino, *J. Organomet. Chem.* **1969**, *20*, 1–10.
48. G. Boche, K. Harms, M. Marsch, A. Müller, *J. Chem. Soc., Chem. Commun.* **1994**, 1393–1394.
49. M. Marsch, K. Harms, W. Massa, G. Boche, *Angew. Chem.* **1987**, *99*, 706–707; *Angew. Chem. Int. Ed. Engl.* **1987**, *26*, 696.
50. J. Toney and G.D. Stucky, *J. Organomet. Chem.* **1971**, *28*, 5–20.
51. M. Perucaud, J. Ducom, M. Vallino, *C. R. Acad. Sci. Paris C* **1967**, *264*, 571–574.
52. B. Schubert, U. Behrens, E. Weiss, *Chem. Ber.* **1981**, *114*, 2640–2643.
53. M. Geissler, J. Kopf, E. Weiss, *Chem. Ber.* **1989**, *122*, 1395–1402.
54. F. Bickelhaupt, *J. Organomet. Chem.* **1994**, *475*, 1–14, and references cited.
55. M. Hogenbirk, G. Schat, O.S. Akkerman, F. Bickelhaupt, W.J.J. Smeets, A.L. Spek, *J. Am. Chem. Soc.* **1992**, *114*, 7302–7303.
56. B. Bogdanovic, N. Janke, C. Krüger, K. Schlichte, J. Treber, *Angew. Chem.* **1987**, *99*, 1046–1047; *Angew. Chem. Int. Ed. Engl.* **1987**, *26*, 1025.
57. M. Vallino, *Thesis*, Université de Paris VI, 1972.
58. A.L. Spek, G. Schat, H.C. Holtkamp, C. Blomberg, F. Bickelhaupt, *J. Organomet. Chem.* **1977**, *131*, 331–340.
59. M.F. Lappert, T.R. Martin, C.L. Raston, B.W. Skelton, A.H. White, *J. Chem. Soc. Dalton Trans.* **1982**, 1959–1964.
60. M.A.G.M. Tinga, G. Schat, O.S. Akkerman, F. Bickelhaupt, E. Horn, H. Kooijman, W.J.J. Smeets, A.L. Spek, *J. Am. Chem. Soc.* **1993**, *115*, 2808–2817.
61. W.N. Setzer, P.v.R. Schleyer, *Adv. Organomet. Chem.* **1985**, *24*, 353–451.
62. C. Schade, P.v.R. Schleyer, *Adv. Organomet. Chem.* **1987**, *26*, 169–279.
63. Y. Kai, N. Kanehisa, K. Miki, N. Kasai, K. Mashima, H. Yasuda, A. Nakamura, *Chem. Letters* **1982**, 1277–1280.
64. M.G. Gardiner, C.L. Raston, F.G.N. Cloke, P.B. Hitchcock, *Organometallics*, **1995**, *14*, 1339–1353.
65. S.I. Troyanov, V. Varga, K. Mach, *Organometallics*, **1993**, *12*, 2820–2824.
66. H. Viebrock, D. Abeln, E. Weiss, *Z. Naturforsch.* **1994**, *49b*, 89–99.
67. B. Bogdanovic, N. Janke, C. Krüger, R. Mynott, K. Schlichte, U. Westeppe, *Angew. Chem.* **1985**, *97*, 972–974; *Angew. Chem. Int. Ed. Engl.* **1987**, *24*, 960.
68. H. Lehmkuhl, A. Shakoor, K. Mehler, C. Krüger, K. Angermund, Y. Tsay, *Chem. Ber.* **1985**, *118*, 4239–4247.
69. T. Alonso, S. Harvey, P.C. Junk, C.L. Raston, B.W. Skelton, A.H. White, *Organometallics*, **1987**, *6*, 2110–2116.
70. A. Haaland, J. Lusztyk, J. Brunvoll, K.B. Starowieyski, *J. Organomet. Chem.* **1975**, *85*, 279–285.
71. W. Bünder, E. Weiss, *J. Organomet. Chem.* **1975**, *92*, 1–6.
72. R.A. Andersen, R. Blom, J.M. Boncella, C.J. Burns, H.V. Volden, *Acta Chem. Scand.* **1987**, *A 41*, 24–35.
73. C.P. Morley, P. Jutzi, C. Krüger, J.M. Wallis, *Organometallics*, **1987**, *6*, 1084–1090.
74. C. Dohmeier, D. Loos, C. Robl, H. Schnöckel, D. Fenske, *J. Organomet. Chem.* **1993**, *448*, 5–8.
75. C. Johnson, J. Toney, G.D. Stucky, *J. Organomet. Chem.* **1972**, *40*, C11–C13.
76. R.A. Andersen, R. Blom, A. Haaland, B.E.R. Schilling, H.V. Volden, *Acta Chem. Scand.* **1985**, *A 39*, 563–569.
77. H. Lehmkuhl, K. Mehler, R. Benn, A. Rufinska, C. Krüger, *Chem. Ber.* **1986**, *119*, 1054–1069.
78. P. Jutzi, J. Kleimeier, T. Redeker, H.-G. Stammler, B. Neumann, *J. Organomet. Chem.* **1995**, *498*, 85–89.
79. J.L. Atwood, K.D. Smith, *J. Am. Chem. Soc.* **1974**, *96*, 994–998.
80. N.S. Hosmane, D. Zhu, J.E. McDonald, H. Zhang, J.A. Maguire, T.G. Gray, S.C. Helfert, *J. Am. Chem. Soc.* **1995**, *117*, 12362–12363.
81. N.S. Hosmane, H. Zhang, Y. Wang, K. Lu, C.J. Thomas, M.B. Ezhova, S.C. Helfert, J.A. Maguire, T.G. Gray, F. Baumann, W. Kaim, *Organometallics*, **1996**, *15*, 2425–2427.
82. K. Angermund, B. Bogdanovic, G. Koppetsch, C. Krüger, R. Mynott, M. Schwickardi, Y. Tsay, Z. *Naturforsch.* **1986**, *41b*, 455–466.
83. B. Bogdanovic, G. Koppetsch, C. Krüger, R. Mynott, Z. *Naturforsch.* **1986**, *41b*, 617–628.
84. U. Casellato, F. Ossola, *Organometallics*, **1994**, *13*, 4105–4108.
85. C. Eaborn, P.B. Hitchcock, A. Kowalewska, Z. Lu, J.D. Smith, W.A. Stanczyk, *J. Organomet. Chem.* **1996**, *521*, 113–120.
86. M.J. Henderson, R.I. Papasergio, C.L. Raston, A.H. White, M.F. Lappert, *J. Chem. Soc., Chem. Commun.* **1986**, 672–674.
87. D. Seebach, J. Hansen, P. Seiler, J.M. Gromek, *J. Organomet. Chem.* **1985**, *285*, 1–13.
88. A. Müller, M. Krieger, B. Neumüller, K. Dehnicke, J. Magull, *Z. anorg. allg. Chem.* **1997**, *623*, 1081–1087.
89. A. Pape, M. Lutz, G. Müller, *Angew. Chem.* **1994**, *106*, 2375–2377; *Angew. Chem. Int. Ed. Engl.* **1994**, *33*, 2281–2284.
90. M. Westerhausen, M.H. Digeser, H. Nöth, T. Seifert, A. Pfitzner, *J. Am. Chem. Soc.* **1998**, *120*, 6722–6725.
91. P.R. Markies, R.M. Altink, A. Villena, O.S. Akkerman, F. Bickelhaupt, W.J.J. Smeets, A.L. Spek, *J. Organomet. Chem.* **1991**, *402*, 289–312.
92. P.R. Markies, G. Schat, A. Villena, O.S. Akkerman, F. Bickelhaupt, W.J.J. Smeets, A.L. Spek, *J. Organomet. Chem.* **1991**, *411*, 291–302.
93. V.R. Magnuson, G.D. Stucky, *Inorg. Chem.* **1969**, *8*, 1427–1433.
94. K.H. Henderson, R.E. Mulvey, W. Clegg, P.A. O'Neil, *J. Organomet. Chem.* **1992**, *439*, 237–250.
95. P.R. Markies, G. Schat, S. Griffioen, A. Villena, O.S. Akkerman, F. Bickelhaupt, W.J.J. Smeets, A.L. Spek, *Organometallics*, **1991**, *10*, 1531–1546.
96. P.R. Markies, O.S. Akkerman, F. Bickelhaupt, W.J.J. Smeets, A.L. Spek., *J. Am. Chem. Soc.* **1988**, *110*, 4284–4292.
97. P.R. Markies, T. Nomoto, O.S. Akkerman, F. Bickelhaupt, W.J.J. Smeets, A.L. Spek, *Angew. Chem.* **1988**, *100*, 1143–1144; *Angew. Chem. Int. Ed. Engl.* **1988**, *27*, 1084–1086.
98. P.R. Markies, A. Villena, O.S. Akkerman, F. Bickelhaupt, W.J.J. Smeets, A.L. Spek, *J. Organomet. Chem.* **1993**, *463*, 7–21.
99. (a) P.R. Markies, T. Nomoto, G. Schat, O.S. Akkerman, F. Bickelhaupt, W.J.J. Smeets, A.L. Spek, *Organometallics*, **1991**, *10*, 3826–3837. (b) P.R. Markies, T. Nomoto, G. Schat, O.S. Akkerman, F. Bickelhaupt, W.J.J. Smeets, A.L. Spek, *Organometallics*, **1992**, *11*, 1428.
100. I.D. Kostas, G.J.M. Gruter, O.S. Akkerman, F. Bickelhaupt, H. Kooijman, W.J.J. Smeets, A.L. Spek, *Organometallics*, **1996**, *15*, 4450–4458.
101. R. Han, G. Parkin, *Organometallics*, **1991**, *10*, 1010–1020.
102. A.J. Pajerski, G.L. Bergstresser, M. Parvez, H.G. Richey, *J. Am. Chem. Soc.* **1988**, *110*, 4844–4845.
103. P.R. Markies, T. Nomoto, O.S. Akkerman, F. Bickelhaupt, W.J.J. Smeets, A.L. Spek, *J. Am. Chem. Soc.* **1988**, *110*, 4845–4846.
104. P.R. Markies, O.S. Akkerman, F. Bickelhaupt, W.J.J. Smeets, A.L. Spek, *Organometallics*, **1994**, *13*, 2616–2627.
105. (a) G.J.M. Gruter, *Thesis*, Vrije Universiteit, Amsterdam, 1994. (b) F. Bickelhaupt, *Acta Chem. Scand.* **1992**, *46*, 409–417.
106. A.J. Pajerski, M. Parvez, H.G. Richey, Jr., *J. Am. Chem. Chem.* **1988**, *110*, 2660–2662.
107. E.P. Squiller, R.R. Whittle, H.G. Richey, Jr., *Organometallics*, **1985**, *4*, 1154–1157.
108. H. Viebrock, U. Behrens, E. Weiss, *Angew. Chem.* **1994**, *106*, 1364–1365; *Angew. Chem. Int. Ed. Engl.* **1994**, *33*, 1257–1259.
109. H. Tang, M. Parvez, H.G. Richey, Jr., *Organometallics*, **1996**, *15*, 5281–5283.
110. E. Weiss, *Angew. Chem.* **1993**, *105*, 1565–1587.
111. G.J.M. Gruter, G.P.M. van Klink, O.S. Akkerman, F. Bickelhaupt, *Chem. Revs.* **1995**, *95*, 2405–2456.
112. N.H. Buttrus, C. Eaborn, M.N.A. E-Kheli, P.B. Hitchcock, J.D. Smith, K. Tavakkoli, *J. Chem. Soc., Dalton Trans.* **1988**, 381–391.
113. T. Greiser, J. Kopf, D. Thoennes, E. Weiss, *Chem. Ber.* **1981**, *114*, 209–213.
114. D. Thoennes, E. Weiss, *Chem. Ber.* **1978**, *111*, 3726–3731.
115. B. Schubert, E. Weiss, *Chem. Ber.* **1984**, *117*, 366–375.
116. J.L. Atwood, G.D. Stucky, *J. Am. Chem. Chem.* **1969**, *91*, 2538–2543.
117. M. Veith, A. Spaniol, J. Pöhlmann, F. Gross, V. Huch, *Chem. Ber.* **1993**, *126*, 2625–2635.
118. T.Y. Her, C.C. Chang, L.K. Liu, *Inorg. Chem.* **1992**, *31*, 2291–2294.
119. C.C. Chang, B. Srinivas, M.L. Wu, W.H. Chiang, M.Y. Ching, C.S. Hsiung, *Organometallics*, **1995**, *14*, 5150–5159.
120. T.Y. Her, C.C. Chang, G.H. Lee, S.M. Peng, Y. Wang, *Inorg. Chem.* **1994**, *33*, 99–104.
121. H. Lehmkuhl, K. Mehler, R. Benn, A. Rufinska, G. Schroth, C. Krüger, *Chem. Ber.* **1984**, *117*, 389–403.

122. H. Lehmkuhl, K. Mehler, A. Shakoor, C. Krüger, Y.H. Tsay, R. Benn, A. Rufinska, G. Schroth, *Chem. Ber.* **1985**, *118*, 4248–4258.
123. M. Hogenbirk, *Thesis*, Vrije Universiteit, Amsterdam, 1993.
124. (a) M.H.L. Green, G.A. Moser, I. Packer, F. Petit, R.A. Forder, K. Prout, *J. Chem. Soc., Chem. Commun.* **1974**, 839. (b) K. Prout, R.A. Forder, *Acta Cryst.* **1975**, *31*, 852.
125. W. Kaschube, K.R. Pörschke, K. Angermund, C. Krüger, G. Wilke, *Chem. Ber.* **1988**, *121*, 1921–1929.
126. K. Jonas, G. Koepe, C. Krüger, *Angew. Chem.* **1986**, *98*, 901–902; *Angew. Chem. Int. Ed. Engl.* **1986**, *25*, 923.
127. H.F. Klein, H. König, S. Koppert, K. Ellrich, J. Riede, *Organometallics*, **1987**, *6*, 1341–1345.
128. S.I. Khan, P.G. Edwards, H.S.H. Yuan, R. Bau, *J. Am. Chem. Soc.* **1985**, *107*, 1682–1684.
129. T.M. Gilbert, R.R. Rayan, A.P. Sattelberger, *Organometallics*, **1989**, *8*, 857–859.
130. R.E. Cramer, M.A. Bruck, J.W. Gilje, *Organometallics*, **1988**, *7*, 1465–1469.

10

X-ray Absorption Spectroscopy and Large Angle X-ray Scattering of Grignard Compounds

T.S. Ertel and H. Bertagnolli
Universität Stuttgart, Stuttgart, Germany

10.1 INTRODUCTION

When an X-ray beam falls on atoms two processes may occur. The beam may be scattered or the beam may be absorbed with an ejection of electrons from an atom. In the case of a crystalline material the scattering of X-rays is used to determine the structure of the solid phase and the chemist applies this method to the proof of the structure of new compounds very often. But even when a regular crystalline arrangement does not exist, as in liquids or amorphous solids, scattering patterns are produced. Like in the crystalline solid phase the scattering of X-rays on disordered systems can be used to determine the probability of distribution of atoms in the environment of any reference atom, or in other words the frequency with which interatomic distances occur.

The second process, namely the absorption of X-rays, can also be used to obtain information about the local order around a certain element, since the fine structure of the X-ray absorption coefficient on the high-energy site is related to the arrangement of the atoms in the immediate neighbourhood of the absorber atom. As the chemist is usually not familiar with the methods of X-ray scattering on non-crystalline systems and X-ray absorption spectroscopy, the fundamentals, i.e. the theoretical and experimental background as well as the data analysis, are outlined. A comparison of EXAFS and LAXS shows the strengths and weaknesses of both methods with respect to each other.

In order to give the reader an extensive overview of the current state of research concerning the structure of Grignard compounds in solution, some methods of physical chemistry are described. In contrast to EXAFS and LAXS, these methods do not provide direct structural information, i.e. for example intra- and interatomic distances. In this context it is interesting to remember the different relations between physical data and structure. From the determination of energy levels with spectroscopic techniques, for example IR and NMR

Grignard Reagents: New Developments Edited by Herman G. Richey, Jr © 2000 John Wiley & Sons Ltd

spectroscopy, one deduces the structure of the unknown compound. When performing EXAFS and LAXS investigations, however, the structural parameters are determined directly. A detailed description of the EXAFS and LAXS studies of Grignard compounds together with a summary of the obtained results is finally found in the last two main sections.

10.2 EXAFS

10.2.1 Theoretical Background

A monochromatic X-ray beam of energy E is attenuated by the passage through a material of thickness d according to equation 10.1 [1].

$$I(E) = I_0(E)e^{-\mu(E)d} \qquad (10.1)$$

$I_0(E)$ and $I(E)$ are the intensity of the incident and transmitted beams, respectively. $\mu(E)$ is the linear absorption coefficient and decreases with increasing E of the incident X-rays until a threshold energy is reached at which the energy is sufficient to remove an electron from an inner shell. At this threshold, $\mu(E)$ increases abruptly. Beyond this point, $\mu(E)$ resumes its steady decrease. This picture of the absorptions coefficient is only valid for isolated atoms. When other atoms are in the neighborhood of the absorbing atom, $\mu(E)$ shows small oscillations up to about 1000 eV above the absorption edge (Figure 10.1).

This fine structure has been known for a long time—H. Fricke [2] and G. Hertz [3] discovered it in 1920—but the effect could not be explained satisfactorily by theory at the time. R. de L. Kronig [4,5] already had the correct fundamental ideas in the 1930s, but the interpretation remained confusing until the 1970s when D.E. Sayers, E.A. Stern and F.W. Lytle [6,7] formulated a theory that has remained generally accepted until today. This theory will be briefly outlined below.

The probability for absorption of an X-ray photon by an electron of an inner shell is dependent on the initial and final states of the excited electron. The initial state is that of the core electron, while the final state is more difficult to describe. The absorption of X-ray radiation generates an electron

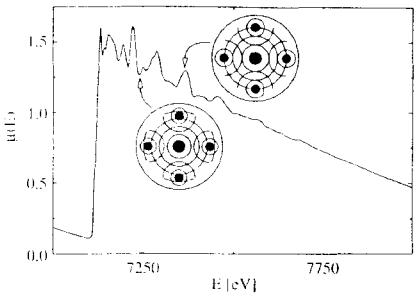

Fig. 10.1. Sample graph of the absorption coefficient $\mu(E)$ illustrating the fine structure and the corresponding constructive and destructive interference of the original and backscattered waves.

in the potentials of the neighboring atoms. In order to solve the Schrödinger equation, the following picture is used. The generated photoelectron is considered as a spherical wave originating from the absorbing atom. This wave is then backscattered by the neighboring atoms. The final state is therefore the superposition of the original and backscattered waves (Figure 10.1) The resulting constructive or destructive interference leads to the oscillations in the absorption coefficient.

This qualitative description indicates that the oscillations in the absorption coefficient $\mu(E)$ are dependent on the distance r_j, the number of neighboring atoms N_j, and the type of backscattering atom j. The backscattering ability of atom j is characterized by the backscattering amplitude F_j, and the effect of atom j on the phase of the backscattered wave is determined by the phase shift φ_{ij}. In addition, the finite lifetime of the photoelectron λ_j, must be taken into account as well as the fact that the backscattering atoms are distributed around a mean distance due to thermal vibrations and static disorder. A good approximation for this distribution is a Gaussian function with a mean-square deviation of σ_j^2. In analogy to X-ray and neutron diffraction, the quantity σ_j^2 is called the Debye–Waller factor.

According to the above considerations, precise measurements of the energy dependence of the X-ray absorption coefficient make it possible

to determine the local environment around the element which absorbs the X-rays. Methods which are based on this principle are classified as X-ray absorption spectroscopy (XAFS) or X-ray absorption fine structure spectroscopy. The energy range close to the absorption edge is called XANES (X-ray absorption near edge structure), while the range about 30–1000 eV from the edge is called EXAFS (extended X-ray absorption fine structure). XANES yields information about the spatial arrangement of backscatterers. The corresponding theory has not yet been completely developed and, therefore, mostly only qualitative comparisons are employed. In contrast, the theory for EXAFS has evolved to such an extent that reliable conclusions about local structures are possible. Since the positions of the K- and L-edges are dependent on the element in question, the appropriate choice of incident X-ray energies makes it possible to excite one specific element and, hence, to probe its environment. This method is therefore element specific, independent of the physical state of the sample, and can be employed even for low concentrations of absorbing atoms.

In order to determine the relationship between the quantities characterizing the local environment around the absorbing atom and the X-ray absorption coefficient $\mu(E)$, it is necessary to correct and normalize the modulation of $\mu(E)$ for the background absorptions $\mu_0(E)$ (equation 10.2) [8].

$$\chi(E) = \frac{\mu(E) - \mu_0(E)}{\mu_0(E)} \qquad (10.2)$$

The next step is to convert the function $\chi(E)$ in the function $\chi(k)$, where k is the magnitude of the photoelectron wave vector. k can be calculated according to equation (10.3) from the energy of the incident X-ray photon and the position of the absorption edge E_0.

$$k = \sqrt{\left(\frac{8\pi^2 m_e}{h^2}\right)(E - E_0)} \qquad (10.3)$$

The mass of the electron is denoted by m_e; h stands for Planck's constant. Equation (10.4) relates the resulting EXAFS function $\chi(k)$ to the quantities that characterize the environment of the absorbing atom [6,7].

$$\chi(k) = \sum_j \left(\frac{N_j}{kr_j^2}\right) F_j(k) e^{-2\sigma_j^2 k^2} \times e^{\frac{-2r_j}{\lambda_j(k)}} \sin(2kr_j + \varphi_{ij}(k)) \qquad (10.4)$$

The EXAFS function in k space contains all necessary information; however, it is not easy to interpret. Fourier transformation of $\chi(k)$ yields a radial distribution function $F(r)$, which has maxima at $R_j = r_j - \alpha_j$ and therefore indicates the distribution of the backscatterers (Equation 10.5).

$$F(r) = \frac{1}{\sqrt{2\pi}} \int_{k_{min}}^{k_{max}} \chi(k) \cdot k^n w(k) e^{2ikr} dk \qquad (10.5)$$

Generally, only the magnitude of $F(r)$ is plotted, called either the modulo function of the Fourier transformed EXAFS function or simply the structure function $|F(r)|$. In the course of the data interpretation it must be taken into account that all maxima are shifted to lower distances—typical shifts are between 0.2 and 0.3 Å. As the functions are only transformed in the interval $k_{min} - k_{max}$, non-real peaks can appear in the transformed functions. These peaks can be strongly dampened by the use of a window function $w(k)$, which defines the interval to be transformed as well as the weighting of all points. A typical example for $w(k)$ is a step function. While this type of function has the highest resolution, it is not always possible to avoid truncation effects. The use of a Gaussian step function lets the sides of the window slope gently downward at the edge and truncation effects are rarely observed.

The multiplication of the EXAFS function by $k^n (n = 1 - 3)$ is performed to compensate the decrease of $\chi(k)$ with increasing k. This decrease is caused by the functional form of the backscattering amplitude $F_j(k)$ and the factor $\exp(-2\sigma_j^2 k^2)$. B.K. Teo and P.A. Lee [9] proposed $n = 1$ for backscatterers with atomic number $Z > 57$, $n = 2$ for elements with $36 < Z < 57$, and $n = 3$ for $Z < 36$. Weighting with k^3 requires very high data quality, as for high k values the signal-to-noise ratio is especially unfavorable. This weighting

scheme has the advantage, however, that the EXAFS oscillations are equally weighted over the entire k region. Moreover, the use of different weighting schemes makes it possible to distinguish heavy elements from light ones.

10.2.2 Measurement Fundamentals

EXAFS measurements require an X-ray source which provides a continuous spectrum. The most suitable source is synchrotron radiation, but the bremsstrahlung of conventional X-ray sources can be employed as well [10,11]. In this case, the intensity is approximately lower by a factor of 10^6. This can partly be compensated for by the use of focusing X-ray optics and rotating anodes. The experimental effort and financial outlay are enormous, however, and the quality of the obtained spectra is much lower than those obtained with synchrotron radiation. This situation might change once it is possible to better focus X-rays; preliminary experiments in this area have been performed [12].

Which elements are suitable for an EXAFS study is determined by the spectral region of the X-ray source. If a typical range 4–26 keV for synchrotron radiation is assumed, K-edge measurements can be used for elements from $Z = 20$ (Ca) to 47 (Ag), while the L_{III} edge can be used theoretically for elements from $Z = 51$ (Sb) to 92 (U). Due to the overlap with L_{II} spectra, elements 51 (Sb) to 59 (Pr) are only partially suitable for measurements using the L_{III} edge. Starting with Nd there is an energy range of 514 eV between the L_{III} and L_{II} absorption edges and an EXAFS function with a k range of 10 Å^{-1} can be obtained. This leaves a gap between Ag and Nd, which contains important elements such as Sn, Sb, and I. These elements might become accessible for K-edge measurements if it were possible to extend the spectral range of synchrotron radiation to 50 keV. For elements lighter than calcium it is necessary to employ soft X-rays and high-vacuum techniques. This strongly limits the study of liquid samples.

As can be deduced from equation (10.1) the quantity to be measured by X-ray absorption spectroscopy is the X-ray absorption coefficient $\mu(E)$. The most common technique involves the direct measurement of $\mu(E)$. In order to obtain monochromatic X-rays, a continuous spectrum is employed. According to Bragg's law (equation 10.6) [13],

$$n\lambda = 2d \sin \vartheta \qquad (10.6)$$

(λ = wavelength; d = interplanar spacing of the crystal; 2ϑ = scattering angle, n = order of diffraction ($n = 1, 2, 3, \ldots$)) a double crystal monochromator, with the second crystal slightly detuned with respect to the first one, selects a beam of wavelength λ, while simultaneously suppressing beams with wavelengths $\lambda/2$, $\lambda/3$, etc. The absorption coefficient is found according to equation (10.1) by measuring the intensity of the X-rays before and after the sample. The energy of the incident radiation is adjusted by a stepwise change of the incident angle of the monochromator. The experimental setup is schematically shown in Figure 10.2a. The sample to be measured, a reference compound, which in many cases is used for calibration purposes, and the ionization chambers for the intensity measurements are arranged in a line. The sample is located between the first and second ionization chambers, and the reference compound is located between the second and third chambers. Typical measurement times are 20–60 minutes when synchrotron radiation is used. Rapid rotation of the monochromator can reduce these times to a few seconds [14]; however, the experimental effort is increased dramatically. The acronym for this measuring technique is QEXAFS (Q = quick). The continuous X-ray spectrum can also be used directly. It is dispersed spatially by Bragg reflection on a crystal and, after passage through the sample, can be measured with an array detector [15,16]. This measurement principle is depicted in Figure 10.2c and is called DEXAFS (D = dispersive).

Since the absorption of X-rays generates an electron vacancy, it is possible to use all subsequent decay processes to determine the absorption coefficient (Figure 10.3). An electron from an outer shell can fill the vacancy, accompanied

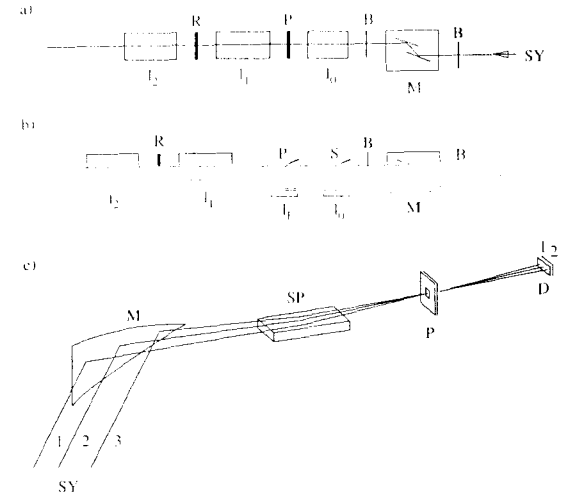

Fig. 10.2. Experimental set-up for transmission: (a) fluorescence; (b) energy-dispersive; (c) EXAFS measurements (SY = synchrotron radiation, 1, 2, 3 = beam paths, M = monochromator, I_0, I_1, I_2 ionization chambers, D = detector (diode array), S = scattering sample, P = sample, R = reference sample, B = slit, F = filter, SP = mirror).

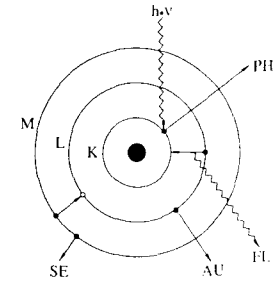

Fig. 10.3. Subsequent decay processes after creation of a hole in the electron shell by absorption of X-rays $h\nu$ (PH = photoelectron, AU = Auger electron, SE = secondary electron, FL = fluorescence radiation).

by the emission of fluorescence radiation (FL) or Auger electrons (AU). These two emissions are competing processes. The fluorescence yield increases with increasing atomic number and this process has the advantage that the background radiation can be removed by using suitable filters, which increases the sensitivity of the method. A typical setup for fluorescence measurements is shown in Figure 10.2b. In general, the emitted fluorescence is measured at a right angle to the incident beam; the sample is therefore rotated by 45°.

The detection of Auger electrons yields the same structural information as a transmission EXAFS experiment or the fluorescence method described above. Auger measurements are advantageous in situations in which the fluorescence method fails due to low quantum yields—in the case of K-edge measurements for elements with $Z < 30$, and $Z < 80$ for L-edge experiments. Due to the small mean free wavelength of the emitted electrons (ca. 100 Å), the Auger method is especially suited for the study of surfaces (SEXAFS, S = surface). It is also possible, in principle, to directly detect the photoelectrons generated. This is difficult,

however, because their spatial distribution changes with the energy of the incident X-ray beam. This effect can be effectively circumvented by detecting all electrons produced by cascading processes. This includes the Auger and photoelectrons as well as secondary electrons created by inelastic scattering of photoelectrons and fluorescence radiation.

10.2.3 Data Analysis

While the measurement of the X-ray absorption coefficient appears to be simple in principle, this is definitely not the case for the data analysis—shown schematically in Figure 10.4. Extensive discussions of the analysis can be found in references [8,17].

The most critical aspects should be outlined here. As can be deduced from equation (10.2), the modulation of the X-ray absorption coefficient is normalized to the background absorption $\mu_0(E)$. There is no exact theoretical expression for $\mu_0(E)$, which must therefore be determined empirically. A number of procedures for this purpose are discussed in the literature, for instance the approximation by a polynominal or a spline function [8]. Even though there are criteria for the choice of background, the determination of $\mu_0(E)$ is a critical aspect. The EXAFS oscillations can be dampened too much if $\mu_0(E)$ matches the experimental data too closely. The exact position of E_0—not to be confused with its absolute value—is also not known because E_0 depends on the chemical environment of the absorbing atom. E_0 is necessary (equation 10.3) for the conversion of the energy E to the magnitude of the wave vector k.

After a successful conversion of the raw data in the final $\chi(k)$ function, the last step of data analysis consists of the determination of the structural parameters r_j, N_j and σ_j. To do this, one tries by variation of these parameters according to equation (10.4), to describe the experimental $\chi(k)$ function optimally with a minimal basis set, i.e. preferably few backscatterers. Frequently, the experimental EXAFS function is, however, first dismantled by means of the Fourier filtering

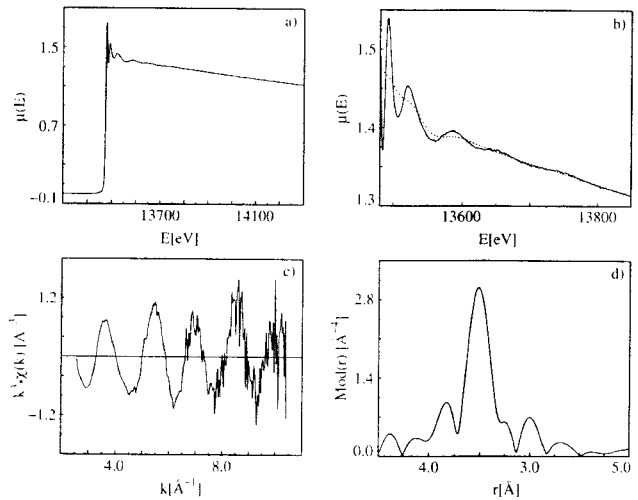

Fig. 10.4. a) Absorption spectrum $\mu(E)$ after edge correction and removal of pre-edge absorption. b) Absorption spectrum $\mu(E)$ (solid line) and background $\mu_0(E)$ (dotted line). c) k^3 weighted EXAFS function. d) Modulo function Mod(r) of the Fourier transformed $k^3\chi(k)$ function for methylmagnesium bromide in diethyl ether.

technique, where selected peaks in the structure function $|F(r)|$ are backtransformed from r-into k-space. These Fourier filtered functions are then separately fitted. For the final determination of the structural parameters, the complete set is fitted to the experimental $\chi(k)$ function in a last step again. As it becomes obvious from equation (10.4) it must of course be presupposed, that the backscattering amplitude F_j and phase φ_{ij} as well as the lifetime of the photoelectron λ_j reflect the realities of the examined system precisely. Therefore, the quality of these functions is also one of the most critical aspects in the data determination.

The theoretical calculation of backscattering amplitudes and phases was a problem for a long time and was one of the main reasons why EXAFS spectroscopy did not find wide application. The first extensive calculation of backscattering amplitudes and phases stem from B.K. Teo and P.A. Lee [9] and was based on an electron-atom scattering theory from P.A. Lee and G. Beni [18]. In this theory, the spherical wave originating from the absorbing atom was approximated by a planar wave. This approximation is valid as long as the effective atom size is small compared to the interatomic distance. In the meantime, a number of powerful program packages are available for the calculations, which use spherical waves [19]. A commonly used program is EXCURV90 and its later versions, which was developed by the Science and Engineering Research Council (SERC), Daresbury Laboratory, Warrington, UK. This program uses a formalism by S.J. Gurman *et al.* [20] to calculate the theoretical backscattering amplitudes and phases, as well as the quantity λ_j which characterizes the lifetime of the photoelectron. This formalism is based upon an electron scattering theory by P.A. Lee and J.B. Pendry [21]. Moreover, this program is also capable of including multiple scattering effects [22]. In 1986, J.J. Rehr *et al.* began the development of the program FEFF, which to date allows the most accurate theoretical calculations of mean free wavelengths λ_j and amplitude and phase functions for any given pair of absorbing and backscattering atoms [23,24].

At this point it must be noted that the backscattering amplitudes of neighbouring elements in the periodic table are only slightly different. This makes an unambiguous distinction of neighbouring elements nearly impossible. In general, however, there is sufficient additional information about the sample to enable identification of the elements involved, provided the theoretical calculated backscattering parameters do correctly model the actual backscattering behaviour. Very different chemical environments can lead to deviations. In such cases, it is necessary to employ model compounds. It is always preferable to use backscattering amplitudes and phases that were obtained from model compounds. In these cases, one measures the EXAFS spectrum of a compound with a precisely known structure. The coordination number N_j and the distance to the absorbing atom r_j are known, and the Debye–Waller factor can be estimated from X-ray data, vibrational frequencies, and different temperature measurements. The backscattering amplitudes and phases can then be determined from the experimental spectrum. However, not all compounds with known structures are suitable as model compounds, even if they are chemically similar to the system under study. To be suitable, the system must posses a well-defined coordination sphere, that is, the contribution of each term must be clearly separable from all others (equation 10.4). Model compounds of this kind are very difficult to find and in many cases, the use of calculated backscattering parameters is required.

10.3 LAXS

10.3.1 Theoretical Background

A parallel beam of monochromatic radiation hits a disordered system, for example a liquid or a glass. The incident wave of the wave length λ is characterized by the wavevector $\boldsymbol{k}_0$ [25,26]. Its magnitude is:

$$|\boldsymbol{k}_0| = \frac{2\pi}{\lambda} \qquad (10.7)$$

The scattered wave is characterized by the wavevector $\boldsymbol{k}_1$. As the scattering of X-rays is elastic within the resolution of the commonly used detectors, the relation holds:

$$|\boldsymbol{k}_0| = |\boldsymbol{k}_1| \qquad (10.8)$$

but the direction of the X-rays is changed. That means a change of the wavevector of the incident beam, which can be calculated from the scattering angle 2ϑ:

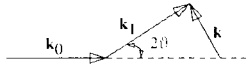

The magnitude of this change is:

$$k = |\boldsymbol{k}_0| 2 \sin\vartheta = \frac{4\pi}{\lambda} \sin\vartheta \qquad (10.9)$$

The intensity of X-rays that are scattered by a disordered system, consisting of N molecules, is given by:

$$I(k) = \frac{1}{N} \left\langle \sum_{p=1}^{N} \sum_{q=1}^{N} \sum_{i=1}^{m} \sum_{j=1}^{m} f_i(k) f_j(k) e^{i\boldsymbol{k}(\boldsymbol{r}_{pi} - \boldsymbol{r}_{qj})} \right\rangle \qquad (10.10)$$

The intensity is normalized to one molecule or for a mixture to one stoichiometric unit. The summation p and q runs over all molecules and the summation i and j over all atoms of the molecule or stoichiometric unit. The quantity $f_i(k)$ characterizes the scattering power of the atom i of the molecule p which is located at $\boldsymbol{r}_{pi}$.

If one assumes a spherical electronic distribution around the nucleus, the atomic scattering factor $f_i(k)$ of the atom i is a function only of the atom type and the change of the wavevector k. At $k = 0$ the value of the scattering factor is equal to the total number of electrons of the atom. As k increases, however, the scattering factor decreases. Equation (10.10) can be split into two terms: the self-scattering or atomic scattering and the distinct part.

$$I_{self}(k) = \sum_{i=1}^{m} f_i^2(k) \qquad (10.11)$$

$$I_{dis}(k) = \frac{1}{N} \left\langle \sum_{p=1}^{N} \sum_{q=1}^{N} \sum_{i=1}^{m} \sum_{j=1}^{m} \times f_i(k) f_j(k) e^{i\boldsymbol{k}(\boldsymbol{r}_{pi} - \boldsymbol{r}_{qj})} \right\rangle \quad pi \neq qi \qquad (10.12)$$

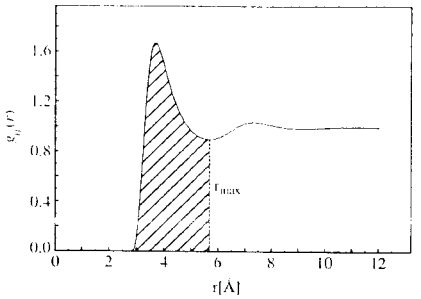

Fig. 10.5. Atom pair correlation function, as it can be determined by X-ray scattering. The hatched area gives the coordination number with respect to a reference atom within a shell of radius r_{max} (equation 10.22).

where in equation (10.12) $pi = qj$ means that the scattered intensity by the atom itself is excluded. Since the summation over all atoms of the system cannot be performed explicitly, the atom pair correlation functions $g_{ij}(r)$ are introduced (Figure 10.5). $g_{ij}(r)$ is the fundamental function in the description of the structure of disordered systems. It gives the probability of finding an atom j at distance r from an atom of type i. This function can be used to determine the most probable distances of an atom i to neighbouring atoms j and the coordination number N_j, which is calculated according to:

$$N_j = \rho \int_0^{r_{max}} g_{ij}(r) 4\pi r^2 \mathrm{d}r \qquad (10.13)$$

where ρ is the number density of the molecules or stoichiometric units. Equation (10.12) can be simplified with this definition of $g_{ij}(r)$ to:

$$I_{dis}(k) = \rho \sum_{i=1}^{m} \sum_{j=1}^{m} f_i(k) f_j(k) \times \int_0^{\infty} g_{ij}(r) e^{ikr} 4\pi r^2 \mathrm{d}r \qquad (10.14)$$

Since no preferred orientation between k and r exists, the exponential expression can be averaged over all orientations of k with respect to r. Then

equation (10.14) reduces to:

$$I_{dis}(k) = \rho \sum_{i=1}^{m} \sum_{j=1}^{m} f_i(k) f_j(k) \times \int_0^{\infty} g_{ij}(r) \frac{\sin(kr)}{kr} 4\pi r^2 dr \qquad (10.15)$$

Equations (10.11) and (10.15) are introduced into equation (10.10):

$$I(k) = I_{self}(k) + \rho \sum_{i=1}^{m} \sum_{j=1}^{m} f_i(k) f_j(k) \times \int_0^{\infty} g_{ij}(r) \frac{\sin(kr)}{kr} 4\pi r^2 dr \qquad (10.16)$$

As $g_{ij}(r)$ approaches the value 1 for large distances r, the integral of equation (10.16) diverges. This problem can be overcome by introducing the identity $[g_{ij}(r) - 1] + 1$ and integration by parts:

$$I(k) = I_{self}(k) + \rho \sum_{i=1}^{m} \sum_{j=1}^{m} f_i(k) f_j(k) \times \int_0^{\infty} \frac{\sin(kr)}{kr} 4\pi r^2 \mathrm{d}r + \rho \sum_{i=1}^{m} \sum_{j=1}^{m} f_i(k) f_j(k) \times \int_0^{\infty} [g_{ij}(r) - 1] \frac{\sin(kr)}{kr} 4\pi r^2 \mathrm{d}r \qquad (10.17)$$

The first term of the right-hand side of equation (10.17) contributes to the scattered intensity only at very small angles and can be neglected in a large angle X-ray scattering experiment, because the small angle range is experimentally not accessible. Then equation (10.17) is reduced to:

$$I(k) - I_{self}(k) = I_{dis}(k) = \rho \sum_{i=1}^{m} \sum_{j=1}^{m} f_i(k) f_j(k) \times \int_0^{\infty} [g_{ij}(r) - 1] \frac{\sin(kr)}{kr} 4\pi r^2 \mathrm{d}r \qquad (10.18)$$

The quantity of interest is not the scattered intensity, but the atom pair correlation functions, which provide information about the structure of liquids. These functions can be obtained from the distinct part by Fourier transformation. But first it is convenient to eliminate the k dependence of the atomic form factor $f_i(k)$ by dividing the distinct part by an averaged form factor

$$\bar{f}(k) = \frac{\sum_{i=1}^{m} f_i(k)}{\sum_{i=1}^{m} Z_i} \qquad (10.19)$$

where Z_i is the electron number of the atom i. It follows from equation (10.18) in a good approximation:

$$D(r) \equiv \rho \sum_{i=1}^{m} \sum_{j=1}^{m} Z_i Z_j [g_{ij}(r) - 1] 4\pi r^2 = \frac{2r}{\pi} \int_0^{\infty} \frac{k I_{dis}(k)}{\bar{f}^2(k)} \mathrm{d}k \qquad (10.20)$$

Often, the integrand in equation (10.20) is called the reduced intensity function:

$$k I_{red}(k) = \frac{k I_{dis}(k)}{\bar{f}^2(k)} \qquad (10.21)$$

and the total atom pair correlation function is introduced which is defined as:

$$G(r) \equiv \frac{\sum_{i=1}^{m} \sum_{j=1}^{m} Z_i Z_j g_{ij}(r)}{\left(\sum_{i=1}^{m} Z_i \right)^2} = 1 + \frac{1}{2\pi^2 r \rho \left(\sum_{i=1}^{m} Z_i \right)^2} \int_0^{\infty} k I_{red}(k) \mathrm{d}k \qquad (10.22)$$

As it can be seen from this equation, the sum of all atom pair correlation functions, weighted with electron numbers of the corresponding atomic pair, can be determined by measuring the scattered intensity of X-rays. In case of molecular liquids, this sum, however, includes intra- and intermolecular contributions. The scattered intensity of an isolated molecule or a stoichiometric unit can be

calculated according to:

$$I_{dis,intra}(k) = \sum_{\substack{i,j \\ i \neq j}}^{m} f_i(k) f_j(k) \frac{\sin(kr_{ij})}{kr_{ij}} e^{-\frac{1}{2}\sigma_{ij}^2 k^2} \quad (10.23)$$

where r_{ij} is the intramolecular distance between the atoms i and j and the Debye–Waller factor σ_{ij} takes into account the intramolecular vibrations.

Of course, equation (10.23) can also be applied to larger aggregates like dimers, but in this case the calculated intensity must be normalized to one molecule or stoichiometric unit. Often, the short-range order of liquids is determined in the following way. A model of the local order is assumed and its scattered intensity is calculated and compared with the experimentally determined intensity. When the agreement between theory and experiment is good, many authors conclude that the supposed model gives a correct description of the local order, but they fail to bear in mind that a completely different model of the local order can reproduce the experimental data in a similar good way. One possibility of avoiding this misinterpretation is to reduce the number of parameters to a minimum and to include all available information about the system to be studied.

10.3.2 Measurement Fundamentals and Techniques

There are two experimental arrangements in order to determine the scattering intensities of a liquid [25,26]. In the first case the X-ray source is fixed and the detector, measuring the scattering intensity as a function of the scattering angle 2ϑ, is moved. In the second case, the X-ray source and the detector are moved symmetrically in opposite directions around the horizontal axis through the sample by the angle ϑ. The advantage of this type of diffractometer, called a ϑ–ϑ diffractometer, is that the container with the liquid can be left in the same horizontal position during the measurements. Often, it is mentioned in the literature as a further advantage that the free surface of the liquid can be used without any cover. But when the liquid has a high vapour pressure or reacts with the atmosphere as do Grignard solutions, this method cannot be applied.

X-ray tubes emit a continuous spectrum and a characteristic line spectrum. In order to suppress the bremsstrahlung, metal foils that filter the primary beam are applied. Of course, crystal monochromators are also used, but they reduce the intensity significantly and when the crystal is placed as analyzer in the scattered beam immediately before the detector, the problem arises that the incoherently scattered radiation, whose wavelength shift increases with increasing scattering angle, is not reflected completely by the crystal and therefore the theoretical calculated incoherent scattering cannot be used in the data evaluation.

In order to evaluate the scattering intensity of a liquid, two independent measurements are required, namely the scattering of the container filled with liquid and the scattering of the empty container. Usually the liquids are kept in quartz or glass capillaries. However, in this case one has to bear in mind that the difference between the scattering of the empty container and the container filled with liquid is rather small and therefore large counting times are required in order to reduce experimental errors. When the absorption of X-rays by the sample is high, cylindrical containers cannot be used. Therefore, some groups use flat containers, where the liquid is covered by a thin foil, for example of capton or beryllium, which can be coated with a polymer in order to protect the metal against chemical corrosion. But when this arrangement is used, the X-ray scattering intensities must be measured in reflection mode instead of the transmission mode, and in order to focus the scattered radiation, a Bragg–Brentano focussing technique must be applied, which means that the sample is rotated about the angle ϑ when the detector is moved to the scattering angle 2ϑ.

10.3.3 Data Analysis

After the corrections of the individual measurements for absorption and polarization the corrected intensity of the empty container is subtracted from the corrected intensity of the container, filled with liquid [25]. This subtraction may be the crucial step in the data analysis, because absolute experimental errors were added. Up to this step the data are given in arbitrary units like counts per second.

An absolute scale is established by normalization of the experimental data to the sum of atom, incoherent and multiple scattering at large scattering angles or by the use of the method of J. Krogh-Moe [27] and N. Norman [28]. The atom and incoherent scattering is calculated from values tabulated for the elements [29].

The calculation of the multiple scattering is easy when one assumes that the liquid scatters isotropically, but must be performed by computer simulation when one assumes an angle dependent scattering of the liquid. In the cases where the absorption of the X-rays by the sample is low, the multiple scattering can be neglected. After normalization of the experimental data to an absolute scale, the atom incoherent and multiple scattering is subtracted. The result is a distinct term (equation 10.18) which can be Fourier transformed according to equation (10.20).

10.4 COMPARISON OF EXAFS AND LAXS TECHNIQUES

The best way to see the differences between the EXAFS spectroscopy and the X-ray scattering is to compare the expression for the EXAFS function and the distinct part. But first we have to introduce the atom pair correlation function into equation (10.4). Equation (10.4) is a good approximation for liquids with a high degree of local order. If the degree of disorder is large, $\chi(k)$ must be represented by the more general equation:

$$\chi(k) = \rho \sum_j F_j \int_0^\infty g_{ij}(r) \times \frac{e^{\frac{-2r}{\lambda_j}}}{kr^2} \sin[2kr + \varphi_{ij}(k)]\mathrm{d}r \quad (10.24)$$

and this expression must be compared with the expression for the distinct term:

$$I_{dis}(k) = \rho \sum_i \sum_j f_i(k) f_j(k) \times \int_0^\infty g_{ij}(r) \frac{4\pi r}{k} \sin(kr)\mathrm{d}r \quad (10.25)$$

As it can be deduced from these expressions, the most striking difference between the methods is that the EXAFS spectroscopy probes the local environment around a specific element, whereas the X-ray scattering gives the sum of all atom pair correlation functions, weighted with the product of the electron numbers of the corresponding atom pairs. That means explicitly that for a system consisting of m different elements, the $m/2(m+1)$ atom pair correlation function contributes to the X-ray scattering, but only m atom pair correlation functions contribute to the EXAFS function. Owing to the reduction of the number of atom pair correlation functions, the EXAFS spectroscopy can be applied to more complex systems than the X-ray scattering. Additionally, EXAFS spectroscopy is the only method applicable to samples with low concentration.

But there are further differences between the methods, which can be seen by comparison of the integrands in equations (10.24) and (10.25). The atom pair correlation function in equation (10.24) is multiplied by $\exp(-2r/\lambda_j)$, which takes into account the effect of the finite lifetime of the photoelectron and the hole generated by the absorption of the X-rays. Owing to the mean free path term $\exp(-2r/\lambda_j)$, the pair correlation functions are asymmetrical and damped with increasing distance. This effect can clearly be seen in the Fourier transform of the EXAFS function.

Slowly-varying tails of the pair correlation function contribute to EXAFS data only at low k values. Sharp peaks in the pair correlation function, however, give rise to dominant features in the EXAFS signal which persist to high k values. As the data are Fourier transformed only in a finite range and the low k data of the EXAFS signal must be omitted in the Fourier transform, the broad tail in the atom pair correlation function is often lost in the analysis of the EXAFS data. A

further aspect that must be considered is that large disorder in a system can lead to a drastic reduction of the EXAFS amplitude and hence to a lowering of the coordination number, and that X-ray scattering is sensitive to the absolute displacement of atoms from their equilibrium position, whereas the EXAFS spectroscopy is sensitive only to the relative distance between atoms.

Both methods provide pair correlation functions, but with different emphasis. X-ray diffraction is sensitive to the smooth behaviour of the pair correlation function; EXAFS spectroscopy is more sensitive to sharp features of the pair correlation function. Hence, the combination of both methods can give more complete and certain information, provided that the systems are not too complex.

10.5 PHYSICAL CHEMISTRY OF GRIGNARD COMPOUNDS

10.5.1 Introduction

In the year 1900 Victor Grignard (1871–1935) showed that magnesium reacts with alkyl halides in water-free ether at room temperature to form ether soluble compounds [30]. The application of these reagents for the synthesis of carboxylic acids, alcohols and hydrocarbons formed the basis of his thesis at the university of Lyon in the year 1901. For the continuing studies concerning the synthetic utility of these reagents, he received the Nobel prize for chemistry in the year 1912. At the present stage, the scope of applications is enormously large and the extraordinary versatility of the magnesium organic compounds is hard to assess. They are probably the most popular organometallic substrates as they are easy to obtain and can be used in a wide variety of syntheses. Besides the discovery of new preparative methods and the expansion of the synthetic applications of this class of compounds, the description of their structure in solution has always been an object of intensive research.

Therefore, the first 30 years after their discovery are characterized by controversial discussions [31–40], particularly because only a restricted set of instruments of physical chemistry was available at that time. A. Bayer and V. Villinger [31] published in 1902, and V. Grignard [32] in 1903, the following structure formulas.

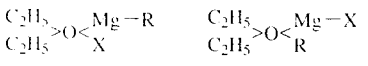

These were discarded very soon, however, and are now only of historic interest. Finally, the investigations of W. Schlenk and W. Schlenk led a crucial step further. They determined that the halogen of certain Grignard compounds can be completely removed as MgX_2 by precipitation with dioxane [40]. Due to this information and new association data [39], they postulated the equilibrium:

$$2RMgX \rightleftharpoons R_2Mg + MgX_2$$

This so-called 'Schlenk-equilibrium' is still used to describe these compounds in solution. More exact insights were only possible with the emergence of more efficient methods of physical chemistry in the sixties. So, only very few papers have been published on this topic between 1930 and 1960 after the fundamental publication of W. Schlenk and W. Schlenk. Afterwards, a marked increase is found [41–46]. Interestingly, measured in terms of the general increase of chemical publications in the nineties, the number of papers concerned with structures of Grignard compounds has again diminished. At the present stage it seems to be clear that solutions of Grignard compounds can contain a variety of chemical species which are related to each other by labile equilibria and their positions depend in a sensitive manner on at least five factors: the steric and electronic properties of the alkyl and aryl residue; the nature of the halogen atom (size, electron donor properties, ...); the nature of the solvent (Et_2O, THF, ...); the concentration and the temperature.

The appearance of certain species can also result from low levels of H_2O or O_2 impurities. Without consideration of solvation, a schematic drawing of the equilibria in solution as it is shown

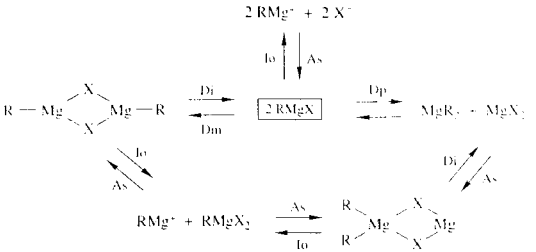

Fig. 10.6. Schematic drawing of the equilibria in solution between the possibly existing species of Grignard compounds without consideration of the solvation (Io = Ionization, As = Association, Di = Dissociation, Dp = Disproportionation, Dm = Dimerization).

in Figure 10.6 can be derived. The 'monomer' (solvated) RMgX can disproportionate according to Schlenk equilibrium [40] to MgR_2 and MgX_2 or dimerize to $RMgX_2MgR$. The monomer as well as the dimer can dissociate, and the alternative dimer R_2MgX_2Mg can be formed by recombination. Only the halogen atoms X normally play a significant role in bridging of the species in Grignard solutions (although in the absence of X, organic groups do sometimes bridge).

Hints concerning the species and the related equilibria can be obtained through a variety of methods, for example molecular weight studies, radioisotope exchange with use of ^{28}Mg, conductivity measurements, IR and NMR spectroscopy as well as theoretical calculations. In some cases the equilibrium position can be changed by partial crystallization or the addition of complexing reagents like dioxane and NEt_3. An overview of the applied methods and their results is given in the following sections.

10.5.2 Crystallography

Although crystal structure analyses cannot provide direct information about Grignard compounds in solution, they do provide ideas of which species possibly exist in solutions. In particular the EXAFS and LAXS investigations presented in Section 10.6 can only be verified with crystal structures. Chapter 9 by F. Bickelhaupt presents a more comprehensive discussion of X-ray crystallography of organomagnesium compounds. With this goal in mind, some specific studies are now described. Both ethyl- [47] as well as phenylmagnesium bromide [48] crystallize from diethyl ether solutions as monomer dietherates. The structures of both compounds are quite similar. Magnesium is located in the centre of an irregular tetrahedron and is surrounded by bromine, one ethyl or phenyl group and two solvent molecules. The Mg–Br, Mg–C, Mg–O distances as well as the Br–Mg–C, Br–Mg–O, O–Mg–C bond angles of both compounds are given in Table 10.1. Remarkable is the long Mg–Br distance indicating a weak chemical interaction between the magnesium and the bromine atom. The relatively short Mg–O distance, however, indicates a strong bonding of the solvent molecules. Both compounds have no tendency to associate. The shortest intermolecular Mg–Br, Mg–Mg and Br–Br distances in ethylmagnesium bromide dietherate are 5.81, 6.76, 5.39 Å, respectively. As expected the bulky Ph_3CMgBr molecule crystallizes from diethyl ether as a monomer dietherate [49].

In 1974 A.L. Spek *et al.* published the crystal structure of $[EtMgBr(i\text{-}Pr_2O)]_2$ [50]. The study is very revealing with respect to the above described structure of $EtMgBr(Et_2O)_2$. Normally one would expect a monomer dietherate as well. To our best knowledge this is the only paper about alkyl or arylmagnesium bromides where the existence of a

Table 10.1. Selected crystal structure data of Grignard compounds

Compound	Distances [Å][a]	Bond Angles [°][b]	Literature
$EtMgBr(Et_2O)_2$	2.48|2.15|2.04	125|103|112	[47]
$PhMgBr(Et_2O)_2$	2.44|2.20|2.04	—|103|110	[48]
$Ph_3CMgBr(Et_2O)_2$	2.47|2.25|2.03	116|104|114	[49]
$[EtMgBr(i\text{-}Pr_2O)]_2$	2.58|2.09|2.01	117|102|121	[50]
$MeMgBr(THF)_3$	2.53|2.41|2.13	126|—|—	[52]
$[EtMg_2Cl_3(THF)_3]_2$	2.41|2.19|2.14[c]	—	[54]
	2.51|—|2.08	—	
$[EtMgBr(NEt_3)]_2$	2.57|2.18|2.15	117|105|116	[55]
EtMgBr-sparteine[d]	2.50|2.27|2.16	113|—|—	[56]
t-BuMgCl-(−)sparteine	2.33|2.19|2.17	114|—|—	[56]
$[\eta^1$-AllylMgCl(TMEDA)$]_2$	2.40|2.18|2.25	125|—|—	[57]
	2.69|—|—	—	
$[C_5H_5MgCl(Et_2O)]_2$	2.43|2.40|2.05[e]	—	[58]
$[C_5Me_5MgCl(Et_2O)]_2$	2.44|2.41|2.08[e]	—	[58]
$[C_5H_5MgCl(THF)]_2$	2.42|2.38|2.02[e]	123|95|121[f]	[59]

[a] Distances in the order Mg−X, Mg−C(Alkyl,Aryl) and Mg−O(Solvent) or Mg−N, respectively. In the case of minor differences in the distances, only the average value is given.
[b] Bond angles in the order X−Mg−C, X−Mg−O or X−Mg−N and O−Mg−C or N−Mg−C, respectively. In the case of great differences in the bond angles, no values are given.
[c] Distances for the five-fold (first row) and six-fold (second row) coordinated magnesium.
[d] Average values for (−)-sparteine, (+)-6-benzylsparteine and (−)-α-isosparteine.
[e] Mg−C is the average value of the η^5-bounded cyclopentadienyl ligand.
[f] Cl−Mg−C and O−Mg−C is referred to the centre of the η^5-bounded cyclopentadienyl ligand.

Table 10.2. Bond angles of the halogen bridged dimeric units of associated Grignard compounds based on crystal structure data

Compound	Mg−X−Mg[°]	X−Mg−X[°]	Literature
$[EtMgBr(i-Pr_2O)]_2$	87	93	[50]
$[EtMg_2Cl_3(THF)_3]_2$	90–99[a]	83–89	[54]
	96	84	
$[EtMgBr(NEt_3)]_2$	90	90	[55]
$[\eta^1$ − AllylMgCl(TMEDA)$]_2$	95	84	[57]
$[C_5H_5MgCl(Et_2O)]_2$	90	90	[58]
$[C_5Me_5MgCl(Et_2O)]_2$	92	89	[58]
$[C_5H_5MgCl(THF)]_2$	90	90	[59]

[a] Bond angles for the five fold (first row) and six fold (second row) coordinated magnesium. In case of the five fold coordinated magnesium, the range of appearing bond angles is given.

dimer complex could be proven. The bond angles of the bridging Mg−Br−Mg and Br−Mg−Br units are shown in Table 10.2.

With less bulky ethers like THF, higher coordination numbers can appear as for $MeMgBr(THF)_3$, where the magnesium is pentacoordinated and located in the centre of a trigonal bipyramid[1] [52].

[1] Comment: The crystal structure of unsolvated dimethylmagnesium is completely different and consists of alkyl bridged polymer chains similar to those of dimethylberyllium [51].

$PhMgBr(THF)_2$ possesses a structure analogous to $PhMgBr(EtO_2)_2$ [53]. According to these results it seems that the organic residue rather than the solvent may have the deciding influence on the formation of higher coordination. It should be noted, however, that the paper [53] is not very reliable. A determination of the positions of the carbon ring atoms failed and there are only the cell parameters and the space group P $2_1/c$ beside some questionable coordinates of the atoms Br, Mg, O(THF) and C_1(PH) given. If one considers the etherates only of Grignard compounds the structure of $[EtMg_2Cl_3(THF)_3]_2$ is quite remarkable (Figure 10.7) [54]. There are trigonal bipyramidal pentacoordinated as well as octahedral hexacoordinated magnesium units in the complex. Four chlorine atoms are connected to two magnesium atoms and the other chlorines act as tricoordinated bridges.

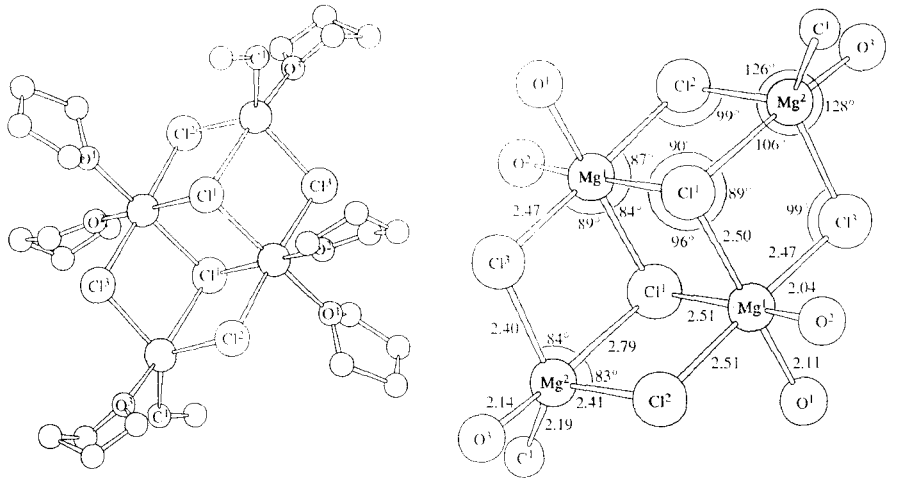

Fig. 10.7. Molecular structure of $[EtMg_2Cl_3(THF)_3]_2$ illustrating selected bond distances and angles [55].

Some crystal structures of Grignard reagents, where the ether is replaced by an amino compound, could be determined. For example, $[EtMgBr(NEt_3)]_2$ forms a dimer complex with bromine bridgings analogously to $[EtMgBr(iPr_2O)]_2$ [55]. The reaction of EtMgBr and t-BuMgCl with the chelating amino compounds (−)-sparteine, (+)-6-benzylsparteine, (−)-α-isosparteine leads to monomer complexes where the magnesium atom is tetrahedrally coordinated [56]. $[\eta^1$-AllylMgCl(TMEDA)$]_2$ (TMEDA = *N*,*N*,*N*′,*N*′-tetramethylethylendiamine) on the other hand is a dimer [57]. The uncommon fact of this compound is that two strongly different Mg−Cl distances of 2.40 and 2.69 Å are found.

In recent times also cylopentadienyl Grignard compounds were characterized crystallographically. Both $[C_5H_5MgCl(Et_2O)]_2$ and $[C_5Me_5MgCl(Et_2O)]_2$ [58] as well as $[C_5H_5MgCl(THF)]_2$ [59] can be interpreted as tetrahedral dimers. With a N,N-dimethylaminoethyl substituted cyclopentadienyl system a monomer complex $(Me_2NCH_2CH_2)C_5H_4MgBr(THF)$ with intramolecular coordinated nitrogen is formed [60]. Intramolecular coordination can also be used to generate Grignard compounds in higher coordination states (penta- and hexacoordinated) [61]. The crystal structures of some interesting compounds were determined in that paper.

10.5.3 Molecular Weight Studies

Former measurements (ebullioscopy) of the molecular weight of Grignard reagents in solution point out that a description of the compounds that exist in solution with the formula RMgX is insufficient. The investigations rather indicated that the complexes are strongly associated [37,39]. The quantitative statements of these early works.

however, are not reliable because the influence of impurities like H_2O or O_2 was not taken into account. Subsequent molecular weight studies (ebullioscopy, vapour pressure osmometry) that used a variety of apparatus generally confirmed the earlier results [62–66].

Results obtained from quite reliable measurements (ebullioscopy, vapour pressure osmometry) are given in [67,68] and can be summarized as follows. At low concentrations, up to 0.05 M, organomagnesium bromides and iodides in diethyl ether and THF are monomeric. In diethyl ether the degree of association increases with increasing concentration and many clues hint at the existence of dimers or oligomers. However, in THF monomer species are present even at higher concentrations. Alkylmagnesium chlorides in diethyl ether are dimeric up to concentrations of only 0.04 M but in THF are monomeric. The degree of association of the investigated organomagnesium halogenides varies from 1 to 4. All these studies, however, give no direct information about the degree of solvation of the Grignard compounds and furthermore cannot provide a distinction between the possible structures of the monomer and dimer species in solution [55].

10.5.4 Tracer Studies

Based upon the molecular weight studies it was obvious that solutions of Grignard compounds contain dimer species. In order to determine whether the equilibrium

$$R_2Mg + MgX_2 \rightleftharpoons 2RMgX$$

plays an important role for the description of the species existing in solution or must rather be formulated as follows,

$$R_2Mg + MgX_2 \rightleftharpoons R_2Mg \cdot MgX_2$$

radioisotope exchange experiments with labeled $^{28}MgBr_2$ and dialkylmagnesium compounds in diethyl ether and THF were performed. The first measurements showed that no exchange of ^{28}Mg takes place and the dimer must be formulated as $R_2Mg \cdot MgX_2$ [69]. Experiments performed later [70], however, could not reproduce those results; statistical exchange was found, indicating that the processes in solution are described by the classical Schlenk equilibrium.

10.5.5 Conductivity Measurements

There are many investigations concerning the electrolytic nature of Grignard reagents in solution. The fact that Grignard compounds in diethyl ether are conductive was confirmed by many teams [35, 36, 38]. Since the measured conductivity is low the concentration of the ionic species cannot be very high [71–73], particularly because a high ion mobility in a medium of such low viscosity is expected. Based upon this fact, the amount of ionic species is so small as to hardly merit consideration in the description of Grignard compounds.

10.5.6 Infrared Spectroscopy

In former IR spectroscopic investigations absorption bands at 780 and 900 cm^{-1} were assigned to the Mg–Br streching frequency [72]. Later the assignment was shown to be incorrect. In fact these absorptions are caused by coordinated diethyl ether. The band at 900 cm^{-1} is assigned to the asymmetrical C–O–C streching frequency [74, 75]. In pure diethyl ether the C–O–C streching frequency is 932 cm^{-1}. When diethyl ether is coordinated to Et_2Mg and $MgBr_2$ the value decreases to 926 cm^{-1} and 900 cm^{-1}, respectively. EtMgBr in diethyl ether shows absorption bands at 920 and 900 cm^{-1}. These bands were interpreted as evidence for the existence of dimers of the type R_2MgX_2Mg with coordinated diethyl ether.

The IR spectrum of phenylmagnesium iodide in diethyl ether is completely different from that of diphenylmagnesium and it is assumed that besides a small amount of Ph_2MgI_2Mg, mainly PhMgI exists in solution [76]. The other recorded IR spectra of alkylmagnesium halogenides and dialkylmagnesium compounds could in general not be interpreted and give no information on which any structural proposals might be based [77–79]. From the investigations of THF solutions the conclusion can be

drawn that alkylmagnesium bromides and chlorides can be described by an equilibrium between RMgX and R_2Mg/MgX_2 [76].

$MeMgBr(Et_2O)_2$ [80], allylmagnesium bromide and chloride were examined in the solid state [78,79]. RAMAN spectroscopical investigations of Grignard compounds in solution are unknown. Unfortunately, vibration frequencies still cannot be assigned satisfactorily by comparison with the few *ab initio* quantum chemistry calculations that have been reported [81–84].

10.5.7 NMR Spectroscopy

Normally the NMR spectra of Grignard compounds allow no differentiation between RMgX and R_2Mg in solution because the alkyl and aryl groups exchange so fast that only average absorptions are seen. For C_6F_5MgX (X = Cl, Br, I) and $(C_6F_5)_2Mg$ however, differentiation is possible at room temperature [85,86]. For the normal alkyl and aryl compounds, low temperatures are necessary. The exchange of Me_2Mg in THF can sufficiently be slowed down at −70°C [87]. In the presence of hexamethylphosphoramide (HMPA) as a complexing reagent a differentiation between $Me_2Mg \cdot HMPA$ and $MeMgX \cdot HMPA$ is possible at 25°C [88].

There is only one systematic ^{25}Mg NMR investigation [89]. In this study EtMgBr in THF was measured. Surprisingly, at 37°C three different signals could be detected. The first two very well pronounced signals could be assigned unambiguously to the species EtMgBr and $MgBr_2$. The third signal resulting from Et_2Mg is partially superimposed by the EtMgBr signal.

Methyl, ethyl and n-propylmagnesium halogenides in diethyl ether were investigated by ^1H NMR spectroscopy. Since the spectra of these compounds are very similar to the spectra of the corresponding dialkylmagnesium compounds, it is concluded that the species R_2MgX_2Mg is dominantly present. THF solutions were investigated with the same result [85,86,90].

In arylmagnesium reagents, two signals of R_2Mg and RMgX at −60°C were detected [85,86,90]. Additionally, the ratio $[RMgX]/[R_2Mg]$ was calculated from the spectra for the different compounds and extrapolated to 25°C. It was found that the equilibrium between RMgX and R_2Mg/MgX_2 is strongly dependent on the aryl group and the solvent used. The stronger the coordination of the solvent to magnesium, the larger the amount of R_2Mg and MgX_2.

According to ^{13}C NMR spectroscopic studies; concentrated etheral solutions of Grignard reagents can be described best in the form of $R_2Mg + MgX_2$ [91]. The ^{13}C chemical shift of the aliphatic compounds is directly correlated to that of the corresponding hydrocarbons. In connection with the determination of the coupling constants $^1J(^{13}C\text{-}^{13}C)$ and $^2J(^{13}C\text{-}^1H)$ in allylmetal complexes allylmagnesium bromide was investigated [92–94]. In a current study about the structure and dynamics of allylmagnesium Grignards it was shown that the compounds are not delocalized but instead are η^1 bonded [95]. An extensive study of a broad range of organomagnesium chlorides and bromides is found in [96]. The results of these investigations, however, allow no conclusions concerning the possible structures existing in solution.

Also ^{19}F NMR was used for the elucidation of the structures of a broad range of fluoroaryl Grignard compounds. Seemingly, an unambiguous differentiation between RMgX and MgX_2 species was possible [97]. Besides the ratio $[RMgX]/[R_2Mg]$, exchange rates of the organic residues were also determined.

10.5.8 Theoretical Studies

Most of the ab initio studies of Grignard compounds are certainly quite interesting from the theoretical point of view. With respect to the description of their structures in solution these studies, however, are of little value [81–84, 98–101]. An exception is the 1994 published investigation of Axten *et al.* in which *ab initio* molecular orbital calculations were performed on the Grignard compound CH_3MgCl [102]. To our knowledge it is also the only study in which the association as well as solvation of the compound is considered.

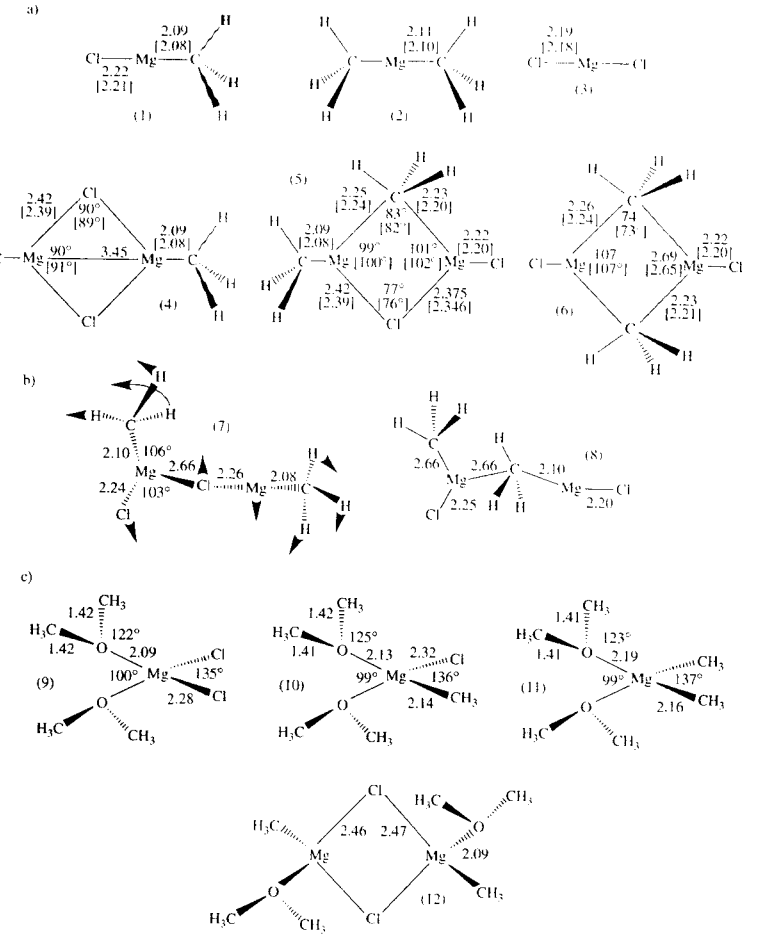

Fig. 10.8. Optimized geometries of the structures (1)–(12). Optimized parameters are at the HF/6 – 31G*//HF/6 – 31G* level, and, if available, the MP2/6 – 31G*//MP2/6 – 31G* optimized parameters are given in brackets. Arrows on transition states show the eigenvector associated with the imaginary frequency [102].

In Figure 10.8a the optimized geometries of the different possible structures (transition states included, Figure 10.8b) of unsolvated CH_3MgCl are shown. As can be seen from the energy diagram (Figure 10.9), the dimers are much more stable than the corresponding monomers and as expected $MeMgCl_2MgMe$ is the most stable compound amongst the dimers. If one takes a look at the geometry of the halogen bridging, it is remarkable that the bond angle of approximately 90°

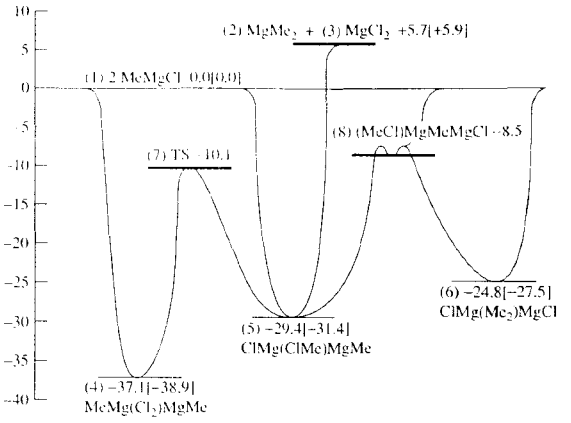

Fig. 10.9. Energies (kcal/mol) of the various reaction channels for CH_3MgCl. Unbracketed values are at the MP4SDTQ/6 – 31G*//HF/6 – 31G* level, and bracketed values are at the MP2/6 – 31G*//MP2/6 – 31G* level [102].

reflects precisely the reality found in crystalline compounds. The structures of the solvated species are shown in Figure 10.8c. Here it can be noted that the calculated Mg–O distances describe the strong interaction of the solvent with magnesium atom very well. Up to now semiempirical and density functional theoretical calculations were not able to do this.

The process of dimerization in the presence of the solvent dimethyl ether, where two strong Mg–O bonds have to be broken, shows a thermoneutral energy balance. Including thermal and entropic contributions, ΔG° is still found to be slightly negative for the formation of $[MeMgCl(Me_2O)]_2$, which concurs with the general experimental observation that dimers predominate in ether solutions of alkylmagnesium chlorides. However, the relatively small negative value of ΔG° suggests that the position of the equilibrium could easily be shifted to favour the presence of monomers by altering the halide and/or the alkyl group as well as the specific solvent.

Finally we want to point out an UV spectroscopic study [103]. RMgX with R = Ph, $PhCH_2$, $PhCMe_2$, Ph_2CH, Ph_3C, $PhCH=CHCH_2$ and X = Cl, Br in diethyl ether were investigated. The UV spectra show that the compounds possess a noticeable ionic character and that a negative partial charge is distributed over the organic residue R.

10.6 EXAFS AND LAXS OF GRIGNARD COMPOUNDS

10.6.1 Introduction

Despite numerous investigations of Grignard compounds, almost no information exists about intra- and interatomic distances of these reagents in solution. This is not necessarily remarkable, since the methods of physical chemistry discussed in the previous section are of course not able to provide such information. But X-ray absorption spectroscopy (EXAFS) and large angle X-ray scattering (LAXS) can.

In 1987 I. Persson *et al.* published the results of their EXAFS and LAXS investigations of magnesium bromide and iodide in diethyl ether and THF [104]. It was the purpose to get information about the possible structures of these two compounds in solution. MgX_2 species

play an important role in the Schlenk equilibrium of Grignard compounds. A LAXS study of organomagnesium iodides [105] and a combined EXAFS/LAXS study of organomagnesium bromides [106] followed. Finally, two EXAFS spectroscopic investigations by H. Bertagnolli and T.S. Ertel appeared in 1993 and 1995 [107,108]. Unfortunately, these are the only publications about the topic 'Grignard compounds in solution' using these methods. The reason probably is that both techniques are relatively complicated. EXAFS additionally has the disadvantage that synchrotron radiation is necessary to run the experiment.

10.6.2 EXAFS Studies

Although it seems at first glance that the whole spectrum of possible organomagnesium halogenides can be examined by means of the EXAFS technique, this is not the case. A listing of the absorption edges of the different atoms (Mg K-edge 1305 eV; Cl K-edge 2822 eV; Br-K edge 13474 eV; I K-edge 33169 eV; I L_{III} edge 4557 eV) shows that, in principle, only bromine is suitable. Iodine cannot be used as an absorber, because the K-edge lies energetically too high and measurements at the L_{III} edge are not meaningful due to the overlap with the L_{II} spectrum. Mg and Cl K-edges still remain. Due to low energy only measurements with soft X-ray under high-vacuum conditions are possible. As one can imagine, the handling of reactive liquid Grignard compounds in high vacuum is experimentally quite difficult, but is, in principle, possible.

In the following, the three EXAFS spectroscopical investigations will be described. It is possible to proceed chronologically, because the structural picture has become more complete with each publication. If meaningful, the results are described in reference to the different physical chemical studies as well as to the LAXS investigations. It furthermore appeared important to us that the experimental data and the resulting interpretation are not introduced without any comment. A critical evaluation should enable the reader to better assess the results.

I. Persson *et al.* have studied the alkylmagnesium bromides MeMgBr, EtMgBr and PhMgBr in diethyl ether at the Br K-edge in the concentration range from 0.1 to 1.0 M (Table 10.3). The X-ray absorption spectra were collected at Stanford Synchrotron Radiation Laboratory, SSRL, and at Daresbury Synchrotron Radiation Source, SRS under dedicated conditions (3–3.3 GeV, 40 mA, wiggler field at 16.5–18 kG). All the solutions as well as the model compounds (Br_2, CBr_4, $KBrO_3$, $MgBr_2$, NaBr) were measured several times in transmission mode with nitrogen-filled ion chambers. In order to optimize the sensitivity of the detection at SRS the first and the last two ion chambers were filled with 19.6 kPa Ar + 81.7 kPa He and 15.5 kPa Xe + 85.8 kPa He, respectively. The spectra shown in the publication represent an average of 2–3 scans. Energy calibration was done with a KBr film.

Data analysis was performed with the computer program XFPAKG, which was developed by R.A. Scott and co-workers at Stanford University.

Table 10.3. Complete listing of all EXAFS spectroscopically investigated Grignard compounds

Compound	Solvent	Molarity	Temperature	Literature
MeMgBr	Et_2O	0.6	RT	[106]
EtMgBr	Et_2O	0.1,1.0	RT	
PhMgBr	Et_2O	0.5,1.0	RT	
MeMgBr	Et_2O	3.1	RT	[107]
EtMgBr	Et_2O	3.0	RT	
PhMgBr	Et_2O	3.0	RT	
ViMgBr	THF	1.6	RT	
MeMgBr	n-Bu_2O	1.5	−85°C,RT	[108]
EtMgBr	n-Bu_2O	1.5	−85°C,RT	

Starting from averaged spectra, the critical background correction was done by subtracting a cubic spline, followed by normalization according to equation (10.2). The spline points were chosen empirically to minimize the residual low-frequency background without reducing the observed amplitude of the EXAFS. Fourier transforms of the data were calculated by numerical integration with k^3 weighted EXAFS functions with a k window of either 3.0–12.7 or 3.0–14.5 $Å^{-1}$, broadened by a Gaussian of width 0.1 $Å^{-1}$.

The final curve-fitting procedure was done with amplitude and phase functions extracted from the above mentioned model compounds. Fourier filtering was used to isolate the shell of interest in the model. A six-parameter function was then fitted to the extracted data. This parameterized function was used as a reference when fitting the EXAFS of Grignard compounds. When fitting the spectra the number and distance of the backscatterer were adjusted as variable parameters. Unfortunately, $MgBr_2$, the obvious model for the Mg backscattering could not be used. Due to its very high tendency to absorb water, the collected data were not reproducible. Since all magnesium bromide compounds are very hygroscopic, no suitable magnesium-containing model compound could be found, and solid NaBr was used instead.

The Fourier transforms of all Grignard compounds show one major peak that corresponds to the expected Br–Mg distance. Fourier filtering was used to isolate this peak. The subsequent curve-fitting leads to the results given in Table 10.4. A wider filter was also applied to see if there was any contribution from other backscatterers and if such a second shell could be fitted. This was, however, not the case. For phenylmagnesium bromide the fits gave an average Br–Mg distance of 2.55 Å, which is in very close agreement with the result of 2.56 Å obtained from the LAXS measurement. So it seems that the parameters extracted from NaBr give reliable results, when used for fitting Mg backscattering.

Analysing the EXAFS functions of the different solutions, one can say that the experimental spectra are of good quality. The Fourier transform of the 1.0 M PhMgBr solution (Figure 10.10) shows that the background correction was not

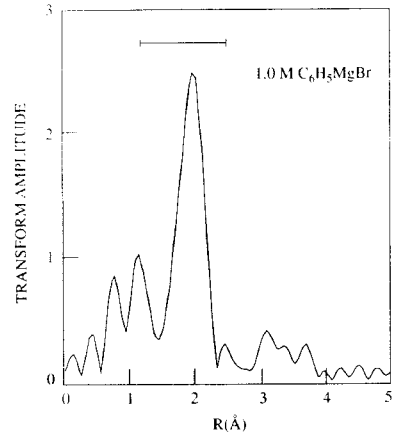

Fig. 10.10. Fourier transform of k^3 weighted EXAFS data of 1.0 M phenylmagnesium bromide in diethyl ether, k range 3.0–14.5 $Å^{-1}$. The horizontal bar indicates the width of the window used when back-transforming the data. R is related to the true distance R' by the phase shift α according to $R' = R + \alpha$ [106].

Table 10.4. EXAFS curve-fitting results of organomagnesium bromides in diethyl ether [106]

Compound	Molarity	Br–Mg distance [Å] $k = 3.0 - 12.7$ $Å^{-1}$	$k = 3.0 - 14.5$ $Å^{-1}$
MeMgBr	0.6	2.53	2.56
EtMgBr	0.1	2.54	2.58
	1.0	2.54	
PhMgBr	0.5	2.55	2.56
	1.0	2.54	2.54

performed optimally, which can be seen from the two relatively high artificial maxima at 0.9 and 1.2 Å. Although the determined Br–Mg distance of PhMgBr of the EXAFS and LAXS experiment agree very well, the method of evaluation with NaBr as the model system remains questionable, especially as it was not possible to determine the coordination number for the Mg backscatterer. [illegible] critical, the fact that the Debye–Waller factor of the model was not varied, is. From a chemical consideration it is clear that a Debye–Waller factor for crystalline NaBr cannot be transferred without any change to Grignard compounds with their dynamic equilibria and static disorder. This, however, has been done by the authors.

A further discrepancy results from the fact that in the LAXS data of PhMgBr a Br–Br distance of 3.62 Å was found, which was not detectable in the EXAFS measurements. Here the general question, of course, arises, whether a 0.5 or 1.0 molar solution (EXAFS) is comparable with a 2.0 molar one (LAXS). What one can presuppose in any case (see Section 10.5) is that, in the investigated concentration range, associated species with halogen bridging are present, explaining the detection of a Br–Br distance with LAXS. For the absence of such an absorber backscatterer pair, I. Persson *et al.* give the following explanation.

The LAXS technique is more sensitive to long and more diffuse distances than the EXAFS technique. The information about the distance r from another atom enters the theoretical intensity function of LAXS as a factor $(\sin kr)/kr$ and in the EXAFS equation as $(\sin 2kr)\exp(-2r/\lambda)/r^2$ (equations 10.5 and 10.4). An X-ray scattering experiment covers the k region 0–16 $Å^{-1}$, while EXAFS covers the region $6 \leq 2k \leq 30\ Å^{-1}$. Thus, there is better resolution when detecting the nearest-neighbour environment in the EXAFS technique but it suffers from the lack of low k data, i.e. information about long-range order is lost. The signal from shells beyond the first falls off more quickly in EXAFS than in LAXS.

In principle, these considerations are right and certainly play a role in the present case. In our opinion, however, they cannot adequately explain the absence of the Br–Br distance in the data. There are several EXAFS spectroscopic publications of metal organic complexes in solution, where it was possible to detect backscatterer at even greater distances without any problem. An explanation for the fact that no second coordination shell was found, could be the fast exchange rate of the alkyl- or aryl residue of the solvent molecules [illegible] nated to the magnesium atom. High exchange rates in solution often result indirectly in high Debye-Waller factors, making it impossible to detect the corresponding backscatterers, despite favourable distances for EXAFS spectroscopy. A way to avoid this problem is by the use of more concentrated solutions. In this case the existing species can occur in such concentrations that the corresponding backscatterers, despite the high Debye–Waller factors, are EXAFS spectroscopically detectable.

If one takes a closer look at Figure 10.10 it seems that there are some small contributions of backscatterers in the distance range between 3.0 and 4.0 Å. Of course, one cannot conclude the relevance of such contributions from the structure function. They are, however, clearly higher than the noise level, which can be estimated from the average value of the peak height between 4.0 and 5.0 Å.

Let us come now to the structural interpretation of the data. As one can see by comparison with the distance values of Table 10.3, the EXAFS spectroscopically determined Mg–Br distance lies in the expected range. Although the values of crystal structure analyses and EXAFS measurements cannot be compared directly, it is noticeable, that the Mg–Br distances for EtMgBr and PhMgBr are 0.06 and 0.11 Å greater in solution than in the crystal. Further coordination shells were not found. This makes any statement about the structure impossible. Therefore, the interpretation of I. Persson *et al.* is only based upon LAXS measurements, which will be described extensively in the next section. Including the LAXS results of organomagnesium iodides [105] it can be anticipated that RMgX solutions in diethyl ether with R = Me, Et, Ph and X = Br, I in the investigated

concentration range from 0.1 to 2.7 M can apparently be fully described by the following equation:

$$2RMgX(Et_2O)_4 \rightleftharpoons R(Et_2O)_3MgX_2Mg(Et_2O)_3R + 2Et_2O$$

The monomer and dimer complexes should have an octahedral geometry and MgX_2 does not seem

As one can deduce from the explanations given above, statements concerning the structure of Grignard compounds in solution are only possible if, not only one, but also higher coordination shells can be detected. This has succeeded in the investigation of H. Bertagnolli and T. S. Ertel. They performed EXAFS measurements on methyl-, ethyl- and phenylmagnesium bromides in diethyl ether and vinylmagnesium bromide (ViMgBr) in THF with concentrations of 3.12, 3.04, 2.96 and 1.56 M. In contrast to the study mentioned above, they investigated more highly concentrated solutions, thereby increasing the probability of detecting a second or even higher shell.

The EXAFS experiment was carried out at the Br K-edge at the beam line RÖMO II at the Hamburger Synchrotronstrahlungslabor (HASYLAB) at DESY, Hamburg, at 20°C, with a Si(311) crystal monochromator under ambient conditions (5.4 GeV, beam current 50 mA). Data were collected in transmission mode with ion chambers. The first ion chamber, monitoring I_0, with a length of 15 cm was continuously flushed with a mixture of 7% argon and 93% nitrogen. The second and third ion chambers, recording I_1 and I_2, respectively, with a length of 30 cm were flushed with 100% argon. Energy calibration was monitored with a 30 µm thick anhydrous $MgBr_2$ sample as reference. All measurements were performed under an inert gas atmosphere. A sample cell suitable for measuring air and moisture sensitive compounds was used.

Data analysis was performed with a program package, specially designed for the evaluation of liquid or amorphous systems [109]. The background removal was done by use of a modified smoothing spline algorithm, and subsequent normalization with the determined spline. The k ranges of the k^3 weighted EXAFS functions of MeMgBr, EtMgBr, PhMgBr and ViMgBr were 2.6–10.5, 2.6–10.0, 2.5–11.4 and 2.5–10.0 $Å^{-1}$, respectively. The corresponding Fourier filtering ranges including the first and second coordination shell were 1.6–3.3, 1.5–3.4, 1.6–3.4, and 1.5–3.4 Å. In order to determine the coordination number N more accurately, the $\chi(k)$ functions were deconvoluted with the monochromator resolution [illegible] the effect is very small and in principle not really relevant.

The curve-fitting procedure was done with different theoretical (McKale, FEFF, EXCURV90) as well as model amplitude and phase functions. The Fourier transforms of all Grignard compounds show a well pronounced first coordination shell. It was found that in agreement with the results of I. Persson *et al.* this peak contains the contribution of a single magnesium backscatterer. Furthermore, the Fourier transforms show a small second maximum. The question of whether this peak is an artifact, i.e. a side lobe of the first coordination shell or a real contribution of other backscatterers, was checked intensively by different methods. The result was that it is a real peak. Only in the case of ViMgBr in THF did only a single oxygen backscatterer contribute to this second coordination shell. For all the other compounds, the description with a single oxygen backscatterer was insufficient and an oxygen–bromine pair yielded the best results. With theoretical amplitude and phase functions by McKale as well as those calculated by the program FEFF the improvement reached with a third backscatterer was not significant. The results obtained with EXCURV90 provide additional evidence that the second maximum of the Fourier transform is a real peak and also here an oxygen–bromine pair yielded the best fit. EXCURV90, however, provides the possibility of calculating the significance of further shells when iterations are carried out after adding a new shell (Joyner statistic test [110]). Contrary to the result above (McKale, FEFF) there is a 99% probability for the existence of a further oxygen backscatterer contributing to the second maximum.

All fits of the experimental data with theoretical amplitude and phase functions yield values

Table 10.5. Summary of the absorber backscatterer distances r [Å] for the Grignard compounds obtained with amplitude and phase functions calculated by McKale, FEFF and EXCURV90 [107]

Backscatterer	McKale	FEFF	EXCURV90[a]	
Methylmagnesium bromide in diethyl ether				
Mg	2.48	2.48	2.45	2.45
Br	3.49	3.49	3.49	3.49
O	3.66	3.66	3.67	3.66
O	—	—	—	3.39
Ethylmagnesium bromide in diethyl ether				
Mg	2.48	2.48	2.45	2.45
Br	3.47	3.47	3.46	3.48
O	3.69	3.69	3.64	3.68
O	—	—	—	3.42
Phenylmagnesium bromide in diethyl ether				
Mg	2.46	2.46	2.44	2.44
Br	3.47	3.47	3.43	3.44
O	3.68	3.70	3.63	3.64
O	—	—	—	3.37
Vinylmagnesium bromide in tetrahydrofuran				
Mg	2.52	2.53	2.50	—
O	3.38	3.38	3.35	—

[a] Results of the three and four shell fits, respectively.

of the coordination numbers, which are unexpectedly low, even for the first coordination shell. The authors suggest, that this is caused by the shortcomings of the theoretical amplitude and phase functions that were used. Like I. Persson *et al.* therefore, they used model amplitude and phase functions of NaBr for the determination of the number of magnesium atoms in the first shell of bromine. The coordination numbers of MeMgBr, EtMgBr, PhMgBr and ViMgBr are 1.60, 1.62, 1.33 and 0.97, respectively. The distances changed to 2.56, 2.56, 2.55 and 2.61 Å. A summary of the distances obtained with the different theoretical amplitude and phase functions (McKale, FEFF, EXCURV90) is found in Table 10.5. Other structural parameters—for example coordination numbers N or Debye–Waller factors σ—are not given, because their values are not considered in the interpretation of the data.

Based upon the determined distances and the coordination numbers obtained with the model amplitude and phase functions, a relatively complex structural model for the Grignard compounds was developed by the authors. We will now describe these considerations and in the end comment on the results critically. As can be understood from Figure 10.11, the fact that the Mg coordination numbers are higher than 1 is an indication of an association of the compounds MeMgBr, EtMgBr and PhMgBr in diethyl ether. The existence of a Br–Br pair, as it is deduced from the simulation of the second shell, confirms the association, too. A Br–Br distance of about the deduced value could also be the result of an equilibrium between $MgBr_2$, MgR_2 and RMgBr. But, the coordination number for Br with respect to Mg, however, would strictly be 1 in this case. According to the Br–Mg coordination number the percentage of dimers in the ethereal solutions is 60%, 62% and 33%, respectively. The Br–Mg coordination number of 0.97 for the solution of vinylmagnesium bromide in THF confirms the existence of monomers. And, no Br–Br absorber–backscatterer pair was found by

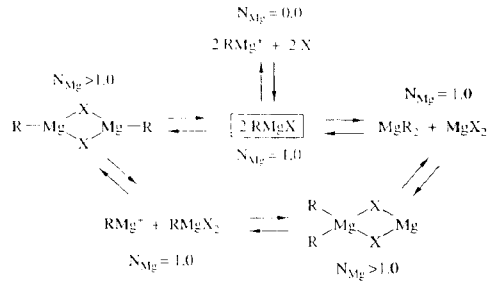

Fig. 10.11. Schematic drawing of the equilibria in solution with respect to the theoretically observed Mg coordination number.

analyzing the EXAFS data. Summarizing these results, the Grignard compounds in diethyl ether are mixtures of monomers and dimers. In THF, however, only monomers are formed.

The structure of the monomeric species is deduced from the obtained Br–Mg and Br–O distances. With the distances obtained from the three shell fits for the backscatterers Mg, Br, O and Br–Mg–O bond angles of 120.0°, 109.48° and 90.0°, the Mg–O distances were calculated for a trigonal planar, tetrahedral and octahedral coordination geometry. The average Mg–O distance in crystalline Grignard compounds is 2.1 ± 0.1 Å (Table 10.1). Assuming that there is no considerable change of this distance in solution, the calculated Mg–O distances must be about 2.1 ± 0.3 Å. For the compounds methyl-, ethyl- and phenylmagnesium bromide in diethyl ether values of Mg–O distances in the mentioned range were reproduced for a Br–Mg–O bond angle of 109.48°. A bond angle of 90° is the only reasonable one for vinylmagnesium bromide in THF (Table 10.6). The conclusion was that the monomeric species in diethyl ether and ViMgBr in THF are most likely to have tetrahedral or octahedral structure, respectively.

From the experimentally determined values of Br–Mg and Br–Br distances, a Br–Mg–Br bond angle of 90 ± 1° was deduced (Table 10.6). Since the compounds in diethyl ether are most likely

Table 10.6. The derived Br–Mg–Br bond angles and Mg–O distances, deduced from the obtained Br–Mg, Br–Br and Br–O distances [107]

Compound		(Br–Mg–Br[°]	Mg–O [Å] 120.0°	Mg–O [Å] 109.48°	Mg–O [Å] 90.0°
MeMgBr	Three shell fits	90	1.76	2.03	2.73
	Four shell fit[a]	91	1.77	2.03	2.73
			1.43	1.67	2.35
EtMgBr	Three shell fits	89	1.75	2.02	2.71
	Four shell fit	90	1.78	2.05	2.75
			1.44	1.70	2.38
PhMgBr	Three shell fits	89	1.76	2.03	2.72
	Four shell fit	90	1.74	2.01	2.70
			1.41	1.66	2.33
ViMgBr	Two shell fits	—	1.31	1.55	2.24

[a] As the consequence of the two different detected Br–O distances (Table 10.5) the Mg–O distances for a trigonal planar, tetrahedral and octahedral coordination geometry were calculated. In the second row the values for the shorter Br–O distance are given.

to have a tetrahedral monomer geometry, the monomer sub-units could form distorted tetrahedral dimers. However, the authors surprisingly exclude such a model and say that a more probable structure model with a Br–Mg–Br bond angle of 90 ± 1 is provided by the formation of octahedral dimers. Assuming such an octahedral dimer, an additional and shorter Br–O distance than the one they found with the three shell fits should have been detected. Indeed, when they performed iterations with EXCURV90, a further and definitely shorter Br–O distance with a 99% probability for its existence was determined. With the results for the Br–Mg and the short Br–O distances, the calculation of Mg–O distances for Br–Mg–O bond angles of 120°, 109.48° and 90.0° was repeated. Only a bond angle of 90.0° provides a reasonable Mg–O distance (Table 10.6). The calculated Mg–O distance gives a strong indication for the proposed octahedral dimers, but does not exclude the existence of octahedral monomers. Based upon the relatively high average deduced Mg–O distance for the octahedral geometry of 2.35 Å, the authors conclude that an octahedral monomer is not formed in solution. The distance has to be assigned only to the dimer. As an explanation for the high value, they argue that this is a consequence of the steric demands in the complex.

Summarizing the results, the Grignard compounds methyl-, ethyl- and phenylmagnesium bromide can be described by an equilibrium of tetrahedral monomers and octahedral dimers. The percentage of dimer species is 60%, 62% and 33%. For methyl- and ethylmagnesium bromide the equilibrium is on the side of the dimer and for phenylmagnesium bromide on the side of the monomer species for steric reasons. The structure of vinylmagnesium bromide in THF can be described best as an octahedral monomer.

Some critical comments concerning the interpretation of the data should now be made. First what can be said about the degrees of dimerization? It is known that the determination of coordination numbers by means of EXAFS spectroscopy is generally very difficult and can have an error of about 30%. It follows that the tendency determined for the degree of dimerization certainly is right. When the absolute values are considered one has to bear in mind the possible experimental error. Although the authors emphasize this explicitly, it should be remembered that on the basis of the EXAFS data no statements can be made about the possible appearance of higher associates such as oligomers or about the position of the organic residue. Therefore, a distinction between dimers of the types R_2MgBr_2Mg and $RMgBr_2MgR$ (with supporting molecules of solvation) is not possible.

As noted before, the authors exclude the existence of distorted tetrahedral dimers. Based upon the four shell fits, they conclude that the dominant structures are octahedral dimers. Although the Joyner statistic test gives a 99% probability for the existence of a further Br–O distance, it remains unclear why a proof failed with the amplitude and phase functions of McKale and FEFF. Furthermore, it is noteworthy that the deduced Mg–O distance in the tetrahedral monomer on average is 2.03 Å compared with 2.35 Å for the octahedral dimer. An explanation on the basis of the higher steric demands in the octahedral dimer seems plausible. It is surprising, however, that such high solvent distances are not observed in crystal structure data. If one assumes that the Joyner statistic test has failed in the present case another interpretation of the data is required. An octahedral geometry can no longer be assumed, although all other conclusions remain correct.

In view of the problem addressed above, a recent EXAFS study of Grignard compounds in solution gives very interesting information. MeMgBr and EtMgBr in n-Bu_2O (1.5 M) were investigated at room temperature and −85°C at the magnesium and bromine K-edges. It is remarkable that the, experimentally very difficult, measurements at the Mg K-edge were performed here for the first time. Measurement at both absorption edges has, moreover, the big advantage that complementary structure information can be received.

The bromine K EXAFS spectra were recorded in transmission geometry at beamline RÖMO II at the HASYLAB in Hamburg with a Si(311) double crystal monochromator. Data were collected with ion chambers. The first ion chamber, monitoring

I_0, with a length of 15 cm was flushed with nitrogen. The second ion chamber, monitoring I_1, with a length of 30 cm was flushed with argon. A sample cell suitable for measuring air and moisture sensitive compounds was used. To cool the cell down to −85 °C, cold nitrogen vapour was used and the temperature of the sample was controlled with a thermocouple. Absorption spectra were measured in the photon energy range from 13350 to 14250 eV. Data were recorded equidistant in k space, with $\Delta k = 1/15$ Å^{-1}. Sampling time at each data point was increased from 1 s at the beginning to 6 s at the end of a spectrum and four to ten spectra were summed up for each Grignard compound and temperature.

Magnesium K fluorescence EXAFS spectra were recorded with the HE-PGM-2 plane grating monochromator with a resolution of 5–10 eV at the electron storage ring BESSY in Berlin. The experiments were performed at the BESSY fluorescence chamber that is especially designed for fluorescence EXAFS experiments with soft X-rays. The intensity of the incoming synchrotron radiation was monitored by the total electron yield of a gold grid of 80% transmission. To study the fluorescence radiation, emitted by the sample, a high purity germanium detector with a resolution of approximately 100 eV at the magnesium K edge and a multi-channel analyser were used. The sample was mounted on the cold finger of a rotatable sample manipulator which can be cooled with liquid nitrogen. Fluorescence spectra were measured in the photon energy range from 1260 to 1560 eV and data were recorded equidistant in energy with $\Delta E = 2$ eV. Because photon flux at the magnesium K edge is relatively low at BESSY, a large number of spectra was accumulated for each Grignard compound and temperature, so that the sampling time at each data point was approximately 6 minutes. As all window materials strongly absorb soft X-rays, the vacuum of the BESSY fluorescence chamber is directly connected to the vacuum of the electron storage ring, without any windows. Therefore, the liquid sample had to be stored in a UHV tight cell, appropriate for temperature dependent fluorescence measurements in the soft X-ray region. A schematic drawing of the cell is shown in Figure 10.12. The main component is the 5 µm thick beryllium window, which is coated with a chemical-resistant polymer film of 1 µm thickness. Temperatures of the liquid sample below room temperature can be adjusted by cooling the cell with a cold finger and simultaneously heating the cell with the heater.

For the bromine transmission measurements $\mu(E)$ was calculated in the usual manner. In the case of the magnesium fluorescence measurements, the linear absorption coefficient is calculated with the relation $\mu(E) = I_F(E)/I_0(E)$, where I_F stands for the detected intensity of fluorescence radiation and I_0 for the normalized current, which is proportional to the primary radiation intensity. Self absorption is neglected, because the amount is too small. Figures 10.13a and 10.13b show the bromine and magnesium X-ray absorption spectra of the 1.5 M solutions of MeMgBr and EtMgBr in n-Bu_2O at RT and −85 °C, respectively.

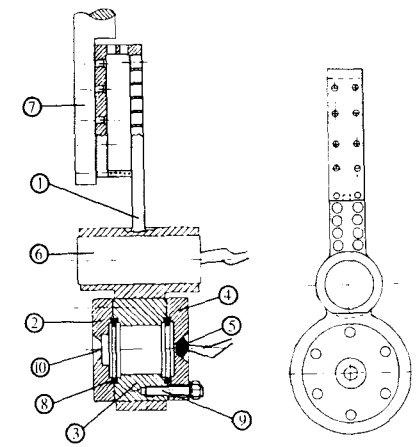

Fig. 10.12. Cell for temperature dependent fluorescence EXAFS measurements of liquids with soft X-rays. The cell consists of holder (1), window flange (2), double-sided flange (3) containing the liquid sample, blind flange (4), thermocouple (5), cartridge heater (6), copper gaskets (8), screw bolts (9) and polymer coated beryllium window (10). During the experiment, the cell is mounted on the cold finger (7) of a sample manipulator [108].

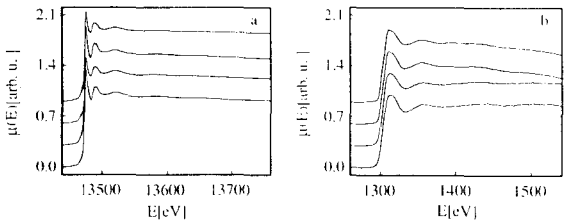

Fig. 10.13. Normalized X-ray absorption spectra at the bromine (a) and magnesium K-edge (b) of 1.5 M solutions of the Grignard compounds in n-Bu_2O. The spectra correspond to MeMgBr at RT, MeMgBr at −85°C, EtMgBr at RT and EtMgBr at −85°C (from top to bottom) [108].

The data analysis was performed according to reference [109]. To determine the smooth part of the background subtracted spectrum, a modified smoothing spline algorithm was used. The EXAFS $\chi(k)$ functions were multiplied with k^3 and Fourier filtered in the ranges 1.40–3.50 Å for the bromine EXAFS spectra and 1.00–3.40 Å for the magnesium EXAFS spectra.

Curve-fitting in k space was performed with the program EXCURV90 and with theoretical amplitude and phase functions calculated with the program FEFF. The experimental $k^3\chi(k)$ functions, their Fourier transforms and fits to the experimental data are shown in Figures 10.14 and 10.15. According to Figures 10.14 and 10.15, the Fourier transforms of the $k^3\chi(k)$ functions of bromine and magnesium show a main peak at small distances and additional smaller structures at larger distances. In the case of the magnesium central atom, least-square refinements of the main peak with carbon atoms of bonded alkyl groups, oxygen atoms of coordinated solvent molecules and with a combination of carbon and oxygen atoms, were performed. With both programs EXCURV90 and FEFF, a single coordination shell of oxygen atoms at a distance of approximately 2.02 Å resulted in a significantly better fit than a single coordination shell of carbon atoms at a distance of approximately 2.10 Å. Fits with both oxygen and carbon backscatterers were only successful with EXCURV90. With this program, two coordination shells of oxygen and carbon atoms at a distance of approximately 2.00 and 2.15 to 2.36 Å, respectively, gave a significantly better fit than a single coordination shell of oxygen atoms. The structures at larger distances can be described by two coordination shells of bromine and magnesium atoms. In the case of the bromine central atom, the main peak and the structures at larger distances can be described with three coordination shells of magnesium, bromine and oxygen or carbon atoms. As carbon atoms were difficult to detect by magnesium K-edge measurements, the authors stated that the light backscatterer detected by bromine K-edge measurements was most probably oxygen.

As before, in the former EXAFS investigation, only the interatomic distances were used to analyze the possible geometries of the monomers and the dimers of MeMgBr and EtMgBr in n-Bu_2O. The obtained values are summarized in Table 10.7 and fulfill the following consistency criteria. First, the analysis of the magnesium and the bromine EXAFS functions resulted in the same value for the Mg–Br distance, to a very good approximation. Secondly, the distances increase with temperature, as is expected owing to the anharmonicity of the atomic interaction potentials. With the experimentally determined distances, the O–Mg–Br, Br–Mg–Br and Mg–Br–Mg angles of the Grignard compounds can be calculated. These angles are 109°, 87° and 85°, respectively.

From the calculated O–Mg–Br angle it follows that the geometry of monomers is tetrahedral. As the Br–Mg–Br and Mg–Br–Mg angles are approximately 90°, association to dimers distorts the tetrahedral geometry of the

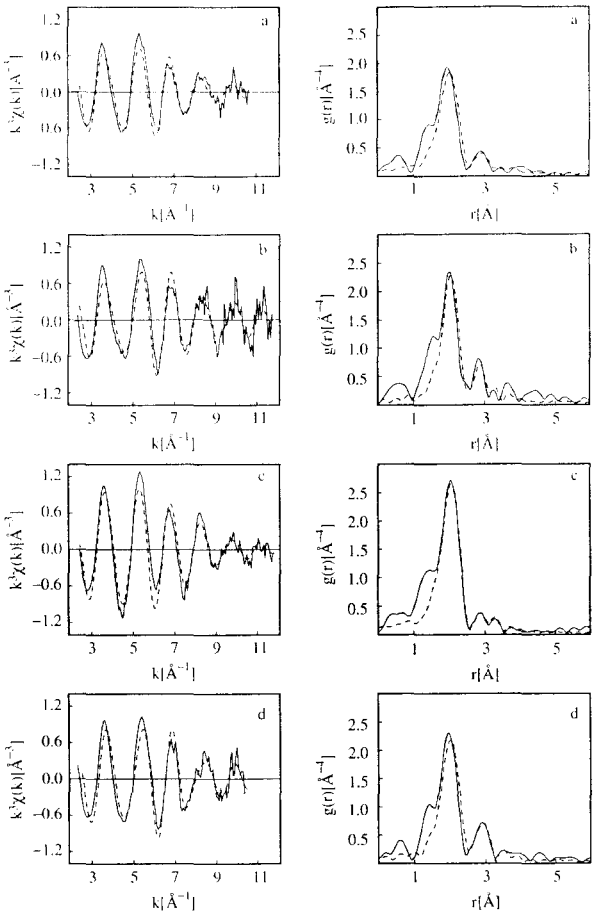

Fig. 10.14. Experimental (solid curve) and calculated (dashed curve) EXAFS functions above the magnesium K-edge of 1.5 M solutions of Grignard compounds in n-Bu_2O and the corresponding Fourier transforms. The figures correspond to MeMgBr at RT (a), MeMgBr at −85°C (b), EtMgBr at RT (c) and EtMgBr at −85°C (d) [108].

monomers and the obvious hypothesis has to be considered that the magnesium atoms of the dimers may become octahedrally coordinated. With the experimentally determined Mg–O and Mg–Br distances, the Br–O distance of hypothetical octahedral dimers can be calculated as being approximately 3.4 Å. According to the following considerations, oxygen atoms of hypothetical octahedral dimers should be detectable by bromine EXAFS spectroscopy. Based upon the detection

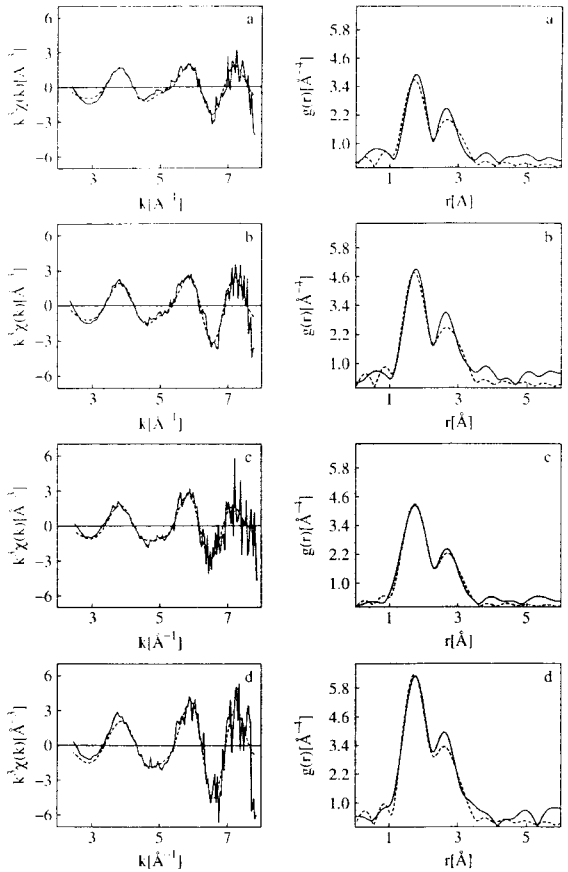

Fig. 10.15. Experimental (solid curve) and calculated (dashed curve) EXAFS functions above the bromine K-edge of 1.5 M solutions of Grignard compounds in n-Bu_2O and the corresponding Fourier transforms. The figures correspond to MeMgBr at RT (a), MeMgBr at −85°C (b), EtMgBr at RT (c) and EtMgBr at −85°C (d) [108].

of magnesium and bromine backscatterers, there will be a considerable amount of dimer species existing in solution. Additionally, in the case of the existence of an octahedral dimer, depending on the position of the carbon atoms of the bonded alkyl groups, four to five oxygen atoms would be placed at a distance of 3.4 Å from the bromine atoms and should be detectable by bromine EXAFS spectroscopy. As oxygen atoms at a distance of 3.4 Å from the bromine atoms were not detected, neither at RT nor at −85°C, octahedral geometry is very unlikely for the dimers of MeMgBr and EtMgBr in n-Bu_2O. The derived distances and angles suggest tetrahedral monomers

Table 10.7. Summary of the absorber backscatterer distances r [Å] for the Grignard compounds MeMgBr and EtMgBr in n-Bu_2O obtained with amplitude and phase functions calculated by FEFF and EXCURV90 [108]

Backscatterer	MeMgBr, RT	MeMgBr, −85 C	EtMgBr, RT	EtMgBr, −85 C
Absorber Br				
Mg	2.49	2.48	2.50	2.47
Br	3.46	3.42	3.41	3.43
O	3.71	3.67	3.67	3.64
Absorber Mg				
O	2.00	2.01	2.01	2.00
C	2.15	2.17	2.36	2.34
Br	2.47	2.48	2.51	2.47
Mg	3.34	3.33	3.36	3.31

and distorted tetrahedral structures for dimers as given in Figure 10.16.

Although the results of this investigation supply a very consistent picture of the Grignard compounds and some questions previously not clarified could unambiguously be answered, one point still remains open. In none of the described studies could a carbon backscatterer be identified convincingly. That this failed for the bromine absorption edge is understandable. First of all one knows from crystal structure analyses that the solvent molecules are more strongly bounded to the magnesium atom than are the organic residues. Furthermore it is known from NMR

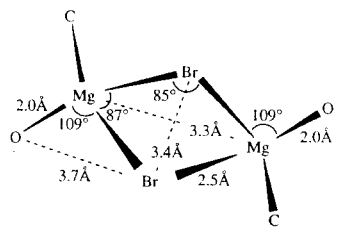

Fig. 10.16. Proposed geometry of dimers of MeMgBr and EtMgBr in n-Bu_2O at RT and −85°C. Only two of the four possible oxygen coordination sites are actually occupied by oxygen atoms of n-Bu_2O solvent molecules. For carbon atoms of coordinated alkyl groups, angles cannot be calculated from the EXAFS spectroscopically determined structural parameters [108].

data that the alkyl or aryl groups exchange extremely fast. Only at temperatures below about −60°C is the exchange slow enough to permit distinguishing between the different species using NMR spectroscopy. From the magnesium absorption edge, however, one would have expected that a carbon backscatterer could be detected at least at −85°C. This succeeded indeed with EXCURV90 but not with the amplitude and phase functions of FEFF. A possible explanation could be that the theoretical functions of the oxygen and carbon backscatterers only differ negligibly. Both backscatterers are in a distance range that impedes a separation of both contributions. Since the direct environment at the magnesium atom is dominated by the solvent molecules, it is possible by fitting with solely an oxygen backscatterer that the contribution of the carbon backscatterer can be is included as well. An unambiguous complete explanation for this phenomena remains to be established.

10.6.3 LAXS Studies

We found only two studies of Grignard compounds in solution in which the large angle X-ray scattering technique was applied [105,106]. In the first paper methyl-, ethyl- and phenylmagnesium iodides, dissolved in diethyl ether, were investigated with the composition, expressed in terms of stoichiometric units, $CH_3MgI \cdot 6.79Et_2O$, $CH_3MgI \cdot 3.41Et_2O$, $C_2H_5MgI \cdot 10.33Et_2O$, $C_2H_5MgI \cdot 2.31$

Et_2O, $C_6H_5MgI \cdot 10.33Et_2O$, $C_6H_5MgI \cdot 5.67Et_2O$, which corresponds to a concentration range 0.9–2.7 M. The solutions were kept in a cylindrical, thin-walled glass vessel, which was half-filled. A large ϑ–ϑ diffractometer was used to measure the scattered intensities and the monochromator was positioned before the scintillation counter. Therefore, the incoherent scattering is not completely recorded at large scattering angles. The scattered intensities were collected in the range $4 \leq \vartheta \leq 55°$, which corresponds to $1.23 \leq k \leq 14.48\ Å^{-1}$ for Mo-K_α radiation ($\lambda = 0.7107\ Å$), with a step size of about 0.1°. The counting time for each sample point was never less than 20 minutes. That means a duration of one week for one scan. This is a typical time, when liquids are studied with X-rays, and requires very stable experimental conditions. The data were evaluated, as described in Section 10.3.3.

In Figure 10.17 the distinct part, weighted with k and normalized to the averaged form factor, is given together with theoretical calculations. In Figure 10.18 the Fourier transforms of the functions, given in Figure 10.17, are depicted. These functions are the sum of all pair correlations functions, weighted by the product of the electron number of the corresponding atom pairs. In order to see how the individual atom pair correlation functions contribute to this sum, the total atom pair correlation function $G(r)$

$$G(r) = \frac{\sum_{i=1}^{m}\sum_{j=1}^{m} Z_i Z_j g_{ij}(r)}{\left(\sum_{i=1}^{m} Z_i\right)^2} \qquad (10.26)$$

is calculated for the solution $CH_3MgI \cdot 6.79\ Et_2O$ explicitly with the abbreviation Et for 6.79 Et_2O and Me for CH_3:

$$\begin{aligned} G(r) = {} & 0.0006 g_{\mathrm{MeMe}}(r) + 0.0016 g_{\mathrm{MeMg}}(r) \\ & + 0.0073 g_{\mathrm{MeI}}(r) \\ & 0.0400 g_{\mathrm{MeEt}}(r) + 0.0011 g_{\mathrm{MgMg}}(r) \\ & + 0.0099 g_{\mathrm{MgI}}(r) \\ & 0.0530 g_{\mathrm{MgEt}}(r) + 0.0220 g_{\mathrm{II}}(r) \\ & + 0.2344 g_{\mathrm{IEt}}(r) \\ & 0.6307 g_{\mathrm{EtEt}}(r) \end{aligned}$$

The problem that arises when solutions are studied by X-rays, can be seen very clearly from this formula. Although the concentration of the Grignard compound is rather large and iodine is a strong scatterer, the contribution of the pair correlation function of interest, namely $g_{\mathrm{MgI}}(r)$, $g_{\mathrm{II}}(r)$ and $g_{\mathrm{MeI}}(r)$ totally is less than eight percent. Of course, one is tempted to measure the solvent without the solute and to extract the contribution of the Grignard compound from the difference of the measurements of the solution and the pure solvent. But one has to bear in mind that the solute may change the structure of the solvent, and in view of the rather small number of solvent molecules—the ratio is 7:1—it is very likely that the structure of the solvation shell is different from the microscopic structure of the pure solvent. Therefore, this procedure cannot be applied.

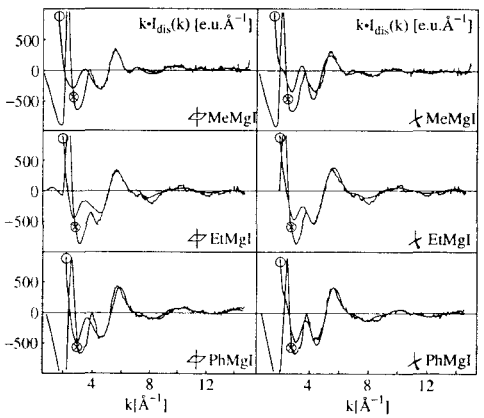

Fig. 10.17. Reduced intensities $kI_{red}(k)$ for the 1.0 M organomagnesium iodides in diethyl ether [105]. Experimental and functions calculated from the final structural models are marked with ⊗ and ⊙, respectively. The models with octahedrally and tetrahedrally coordinated magnesium are shown to the left and right, respectively.

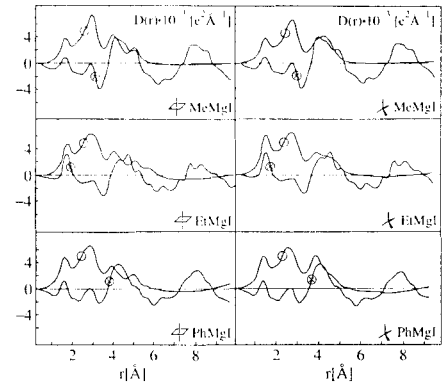

Fig. 10.18. Differential electronic radial distribution function $D(r)$ for the 1.0 M organomagnesium iodides in diethyl ether [105]. Experimental and functions calculated from the final structural models are marked with ⊗ and ⊙, respectively. The models with octahedrally and tetrahedrally coordinated magnesium are shown to the left and right, respectively.

In view of the small weight of the pair correlation functions of interest and taking into account the experimental errors it seems to be impossible to extract information about the structure of the Grignard compounds from the experimentally determined function. Nevertheless, the authors of the two papers [105, 106] deduced the structures of the Grignard compound in solution. The way in which they do it is demonstrated for the system $CH_3MgI \cdot 6.79\ Et_2O$. The weighted sum of atom pair correlation functions exhibits a pronounced peak at 2.8 Å. This peak is assigned to a Mg–I distance. Then the peak area is determined. With the assumption that solely Mg–I pairs contribute to the peak at 2.8 Å, the number of iodine atoms, coordinated at the magnesium atom, is calculated as 1.46. As this number is larger than 1, it is concluded that monomers and dimers exist. This conclusion is correct, as far as the assumption is valid that there are no other atom pairs which contribute to the peak in the range in which the coordination number was determined.

At this point, the question about the structure of the dimers arises. The authors tested a tetrahedral and octahedral geometry and calculated the corresponding I–I and I–C distances from the experimentally determined Mg–I distance and a Mg–C distance, which is taken from other data, preferably from crystal structure data. As the coordination number is known from the peak area and the values of the Debye–Waller factors of these distances were set, the contribution of the distances I–I and I–C (methyl) to the distinct part can be calculated according to equation (10.20).

But at this stage, the question about the structure of the monomer remains unanswered. The authors admit that it is impossible from the present data to distinguish between tetrahedral and octahedral geometry and assume in the first step of the data interpretation that both monomeric and dimeric Grignard species, where magnesium is octahedrally or tetrahedrally coordinated, exist. With these assumptions three parameters are sufficient to calculate the contributions of the Mg–I, I–I and I–C distances to the distinct part of the scattered intensity. The three parameters are the I–I distance, its Debye–Waller factor and the coordination number. Their values were determined by curve-fitting to the experimental data. All the other parameters, as for example the geometry of the diethyl ether molecule, were taken from other studies.

The results of the least-squares refinements are shown in Figures 10.17 and 10.18. The

models with octahedrally coordinated magnesium are shown to the left, and the corresponding models with tetrahedrally coordinated magnesium are shown to the right. As can be seen from the comparison of both models, it is hard to favour one model. Nevertheless, the authors conclude that a model involving both monomeric and dimeric species [illegible] dimeric, gives the best fit to the experimental data and determines the degree of dimerization from the number of I–I distances. For phenylmagnesium iodide, however, no distinction between tetrahedrally and octahedrally coordinated magnesium could be made, because a similarly good fit was obtained for both models. The authors are convinced that dimers exist in diethyl ether solutions, since they succeeded in fitting the number of I–I distances for two different concentrations with only one dimerization constant, which, however, is rather small. But they admit also that the refinement of the data was very difficult and they are unable to exclude the dimeric structure R_2MgX_2Mg.

In the second paper the same authors studied phenylmagnesium bromide in diethyl ether with the composition $C_6H_5MgBr \cdot 4.80\ Et_2O$. Also here the total atom pair correlation function is calculated explicitly in order to see the individual weight of the atom pair correlation function of interest

$$G(r) = 0.0020g_{PhPh}(r) + 0.0120g_{PhMg}(r) + 0.0340g_{PhBr}(r) 0.0197g_{PhEt}(r) + 0.0020g_{MgMg}(r) + 0.0100g_{MgBr}(r) 0.0580g_{MgEt}(r) + 0.0150g_{BrBr}(r) + 0.1685g_{BrEt}(r) 0.4835g_{EtEt}(r)$$

with the abbreviation Ph for the phenyl group and Et for 4.80 Et_2O. As can be seen from this equation, the contribution of the Mg–Br and Br–Br pair correlation function is 1 and 2 percent, respectively.

The measurements were performed in the same manner as those with the organomagnesium iodides. The reduced intensity and the total atom pair correlation functions are shown in Figures 10.19. The interpretation of the total atom pair correlation function followed the outline given in the previous section. The peak at 2.55 Å was assigned to a Mg–Br distance and the shoulder at 3.6 Å to a Br–Br distance. From the area of this shoulder—the limits of the integration are not given—the number of

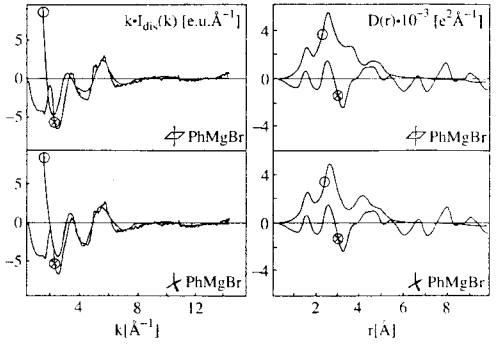

Fig. 10.19. Reduced intensities $kI_{exp}(k)$ and differential electronic radial distribution function $D(r)$ for 2.0 M phenylmagnesium bromide in diethyl ether [106]. Experimental and functions calculated from the final structural models are marked with ⊗ and ⊙, respectively. The models with octahedrally and tetrahedrally coordinated magnesium are shown in the upper and lower part, respectively.

Br–Br distances was determined as 0.25, which corresponds to the presence of 50 percent of the dimeric species. Least-squares refinements of the Mg–Br and Br–Br distances were performed with an octahedral and tetrahedral coordination around the magnesium atom. The other distances were calculated from the refined distances or taken from [illegible] Figure 19. According to the opinion of the authors, an octahedral model fits the experimental data significantly better than a tetrahedral model and it is concluded that phenylmagnesium bromide, dissolved in diethyl ether, forms both dimeric and monomeric complexes with magnesium octahedrally coordinated in both cases. In view of the low weight which the atom pair correlation functions $g_{MgBr}(r)$ and $g_{BrBr}(r)$ contribute to the total atom pair correlation, however, the question arises whether the interpretation of the data is unambigous.

Both studies show very clearly the problems when solutions are studied with X-rays. The main problem is that an X-ray experiment provides the sum of all atom pair correlation functions, weighted with the mole fraction and the electron number of the corresponding atom pairs. If the concentration of the solute is not very high, the contribution of the atom pairs, from which the local structure can be deduced, to the total atom pair correlation function is too small for an unambiguous assignment of certain peaks to definite atom pairs and for a reliable determination of the coordination number. Nevertheless, the X-ray studies of liquids or solutions have their merits, when they are combined with other experimental methods and are compared with theoretical calculations.

10.7 CONCLUDING REMARK: CURRENT STRUCTURAL PICTURE

Which conclusion can be drawn from the results of the EXAFS and LAXS investigations? First, one can say that real structural information, i.e. intra- and intermolecular distances in solution, can be determined by these methods. On the basis of the data it was even possible to deduce detailed structural models. The experimental data and the resulting interpretation were assessed critically. This seemed important to us in order to get, within this chapter, a general interpretation of all investigations.

The determined degrees of dimerization as well as the Br–Br and Mg–Mg distances are an unambiguous proof that MeMgX, EtMgX and PhMgX (X=Br, I) in the solvents Et_2O or n-Bu_2O are associated to a certain degree. The degree of dimerization decreases from MeMgX and EtMgX to PhMgX. Given the error limits, a differentiation between the degrees of dimerization of MeMgX and EtMgX probably is not permissible. As expected the tendency to form dimer species is lower for the organomagnesium iodides than for the bromides. ViMgBr is not associated in THF as is confirmed by molecular weight studies. Comparing the absolute values, the determined degrees of dimerization show some discrepancies. This is not remarkable, since the derived values are based on coordination numbers, and neither the EXAFS or the LAXS methods are optimally suited for accurate determination of coordination numbers.

The systems in Et_2O or Bu_2O can be best described as an equilibrium between RMgX and R_2MgX_2Mg or $RMgX_2MgR$ with coordinated solvent molecules. Unfortunately, on the basis of the data, differentiation between those dimers is not possible. The other postulated species ($2RMg^+ + 2X^-$; $MgR_2 + MgX_2$; $RMg^+ + RMgX_2^-$) seem to play a minor role in the description of the investigated compounds (Figure 10.6). Statements about the geometry of the monomers and dimers are contradictory. I. Persson *et al.* propose only octrahedral models for both species. In the publication [107] however, an equilibrium between tetrahedral monomers and octahedral dimers is postulated. The newest EXAFS spectroscopical investigation, on the other hand, can unambiguously exclude octahedral monomers and dimers.

After detailed consideration, in our opinion an equilibrium between tetrahedral monomers and distorted tetrahedral dimers exists in solution.

From the determination in the older investigations of halogen bridging with Br–Mg–Br and Mg–Br–Mg bond angles of approximately 90°, the authors were led mistakenly to conclude the existence of octahedral dimers. Surprisingly, the authors have not studied crystal structure analyses sufficiently, with respect to this problem. Although crystal structures are not necessarily comparable to structures in solution, they do present a striking picture (Table 10.2). In dimers, a tetrahedral geometry is clearly preferred and the bond angles of the halogen bridging in all cases are approximately 90°.

Since systematic investigations of Grignard compounds in THF with EXAFS and LAXS still are lacking, generalization of the results for ViMgBr is certainly not allowable. It possesses an octahedral coordination geometry in contrast to the other systems. This result confirms the long held assumption that the solvent has a strong influence not only on the degree of association but also on the type of structure that is formed.

REFERENCES

1. C. Gerthsen, H. Kneser, H. Vogel, *Physik*, Springer Verlag, Berlin, 15th edition, **1986**.
2. H. Fricke, *Phys. Rev. 16*, 202, **1920**.
3. G. Hertz, *Z. Phys. 3*, 19, **1920**.
4. R. de L. Kronig, *Z. Phys. 70*, 317, **1931**.
5. R. de L. Kronig, *Z. Phys. 75*, 468, **1932**.
6. D.E. Sayers, E.A. Stern, F.W. Lytle, *Phys. Rev. Lett. 27*, 1204, **1971**.
7. F.W. Lytle, D.E. Sayers, E.A. Stern, *Phys. Rev. B 11*, 4825, **1975**.
8. B.K. Teo, *EXAFS: Basic Principles and Data Analysis*, Springer Verlag, Berlin, **1986**.
9. B.K. Teo, P.A. Lee, *J. Am. Chem. Soc. 101*, 2815, **1979**.
10. W. Thulke, R. Haensel, P. Rabe, *Rev. Sci. Instrum. 54*, 277, **1983**.
11. K. Tohji, Y. Udagawa, T. Kawasaki, K. Masuda, *Rev. Sci. Instrum. 54*, 1482, **1983**.
12. I. Amato, *Science 252*, 208, **1991**.
13. G.H. Stout, L.H. Jensen, *X-Ray Structure Determination*, John Wiley & Sons, New York, **1989**.
14. R. Frahm, *Physica B 158*, 342, **1989**.
15. M. Hagelstein, S. Cunis, R. Frahm, W. Niemann, P. Rabe, *Physica B 158*, 324, **1989**.
16. A. Fontaine, E. Dartyge, J.P. Itie', A. Fuchs, A. Polain, H. Tolentino, G. Tourillon, *Top. Curr. Chem. 151*, 179, **1989**.
17. D.C. Koningsberger, R. Prins, *X-Ray-Absorption: Principles, Applications, Techniques of EXAFS, SEXAFS and XANES*, John Wiley & Sons, New York, **1988**.
18. P.A. Lee, G. Beni, *Phys. Rev. B 15*, 2862, **1977**.
19. A.G. McKale, B.W. Veal, A.P. Paulikas, S.K. Chan, G.S. Knapp, *J. Am. Chem. Soc. 110*, 3763, **1988**.
20. S.J. Gurman, N. Binsted, I. Ross, *J. Phys. C 17*, 143 **1984**.
21. P.A. Lee, J.B. Pendry, *Phys. Rev. B 11*, 2795, **1975**.
22. S.J. Gurman, N. Binsted, I. Ross, *J. Phys. C 19*, 1845, **1986**.
23. J.J. Rehr, R.C. Albers, C.R. Natoli, E.A. Stern, *Phys. Rev. B 34*, 4350, **1986**.
24. J.J. Rehr, J. Mustre de Leon, S.I. Zabinsky, R.C. Albers, *J. Am. Chem. Soc. 113*, 5135, **1991**.
25. H.P. Klug, L.E. Alexander, *X-Ray Diffraction Procedures*, John Wiley & Sons, New York, **1954**.
26. R.W. James, *The Optical Principles of the Diffraction of X-Rays*, G. Bell & Sons, London, **1967**.
27. J. Krogh-Moe, *Acta Crystallogr. 9*, 951, **1956**.
28. N. Norman, *Acta Crystallogr. 10*, 370, **1957**.
29. D. Reidel, *International Table for X-Ray Crystallography*, Publishing Company, Dordrecht, Boston, London, Vol. III, **1983**.
30. V. Grignard, *Compt. Rend. 130*, 1322, **1900**.
31. A. Baeyer, V. Villinger, *Chem. Ber. 35*, 1201, **1902**.
32. V. Grignard, *Compt. Rend. 136*, 1260, **1903**.
33. T. Zrevitinov, *Chem. Ber. 41*, 2244, **1908**.
34. P. Jolibois, *Compt. Rend. 155*, 353, **1912**.
35. J.M. Nelson, W.V. Evans, *J. Am. Chem. Soc. 39*, 82, **1917**.
36. F. Kondrycw, *Chem. Ber. 58*, 459, **1925**.
37. A.P. Terentjew, *Z. Anorg. Allg. Chem. 156*, 73, **1926**.
38. L.W. Gaddum, H.E. French, *J. Am. Chem. Soc. 49*, 1295, **1927**.
39. J. Meisendheimer, W. Schlichenmaier, *Chem. Ber. 61*, 720, **1928**.
40. W. Schlenk, W. Schlenk, *Chem. Ber. 62*, 920, **1929**.
41. B.J. Wakefield, *Organomet. Chem. Rev. 1*, 131, **1966**.
42. E.C. Ashby, *Quart. Rev. 21*, 259, **1967**.
43. E.C. Ashby, *Bull. Soc. Chem. France*, 2133, **1972**.
44. E.C. Ashby, *Pure Appl. Chem. 52*, 545, **1980**.
45. M. Lasperas, A. Perez-Rubalcaba, M.L. Quiroga-Feijoo, *Tetrahedron, 36*, 3403, **1980**.
46. H. Yamataka, Y. Kawafuji, K. Nagareda, N. Miyano, T. Hanafusa, *J. Org. Chem. 54*, 4706, **1989**.

47. L.J. Guggenberger, R.E. Rundle, *J. Am. Chem. Soc. 90*, 5375, **1968**.
48. G.D. Stucky, R.E. Rundle, *J. Am. Chem. Soc. 86*, 4825, **1964**.
49. L.M. Engelhardt, S. Harvey, C.L. Raston, A.H. White, *J. Organomet. Chem. 341*, 39, **1988**.
50. A.L. Spek, P. Voorbergen, G. Schat, C. Blomberg, F. Bickelhaupt, *J. Organomet. Chem. 77*, 147, **1974**.
51. E. Weiss, *J. Organomet. Chem. 2*, 314, **1964**.
52. M. Vallino, *J. Organomet. Chem. 20*, 1, **1969**.
53. F.A. Schröder, *Chem. Ber. 102*, 2035, **1969**.
54. J. Toney, G.D. Stucky, *J. Organomet. Chem. 28*, 5, **1971**.
55. J. Toney, G.D. Stucky, *Chem. Comm.* 1168, **1967**.
56. H. Kageyama, K. Miki, Y. Kai, N. Kasai, Y. Okamoto, H. Yuki, *Bull. Chem. Soc. Jpn. 57*, 1189, **1984**.
57. M. Marsch, K. Harms, W. Massa, G. Boche, *Angew. Chem. 99*, 706, **1987**.
58. C. Dohmeier, D. Loos, C. Robl, H. Schnöckel, D. Fenske, *J. Organomet. Chem. 448*, 5, **1993**.
59. R.E. Cramer, P.N. Richmann, J.W. Gilje, *J. Organomet. Chem. 408*, 131, **1991**.
60. P. Jutzi, J. Kleimeier, T. Redeker, H. Stammler, B. Neumann, *J. Organomet. Chem. 498*, 85, **1995**.
61. P.R. Markies, G. Schat, S. Griffioen, A. Villena, O.S. Akkerman, F. Bickelhaupt, W.J. J. Smeets, A.L. Spek, *Organometallics 10*, 1531, **1991**.
62. W. Slough, A.R. Ubbelohde, *J. Chem. Soc.*, 108, **1955**.
63. S. Hayes, *Bull. Soc. Chim. France*, 1404, **1963**.
64. A.D. Vreugdenhil, C. Blomberg, *Rec. Trav. Chim. 82*, 453, **1963**.
65. A.D. Vreugdenhil, C. Blomberg, *Rec. Trav. Chim. 82*, 461, **1963**.
66. A.D. Vreugdenhil, C. Blomberg, *Rec. Trav. Chim. 84*, 39, **1965**.
67. E.C. Ashby, W.E. Becker, *J. Am. Chem. Soc. 85*, 118, **1963**.
68. E.C. Ashby, M.B. Smith, *J. Am. Chem. Soc. 86*, 4363, **1964**.
69. R.E. Dessy, G.S. Handler, J.H. Wotiz, C.A. Hallingsworth, *J. Am. Chem. Soc. 79*, 3476, **1957**.
70. R.E. Dessy, S.E.I. Green, R.M. Salinger, *Tetrahedron Lett. 21*, 1396, **1964**.
71. W.V. Evans, F.H. Lee, *J. Am. Chem. Soc. 55*, 1474, **1933**.
72. W. Zeil, *Z. Electrochem. 56*, 789, **1952**.
73. R.E. Dessy, R.M. Jones, *J. Org. Chem. 24*, 1685, **1959**.
74. R. Hamelin, S. Hayes, *Compt. Rend. 252*, 1616, **1961**.
75. A. Kirrmann, R. Hamelin, S. Hayes, *Bull. Soc. Chim. France*, 1395, **1963**.
76. R.M. Salinger, H.S. Mosher, *J. Am. Chem. Soc. 86*, 1782, **1964**.
77. C. Sourisseau, J. Guillermet, B. Pasquier, *C.R. Acad. Sci., Ser. B 278*, 239, **1974**.
78. C. Sourisseau, J. Guillermet, B. Pasquier, *Chem. Phys. Lett. 26*, 564, **1974**.
79. C. Sourisseau, B. Pasquier, J. Hervieu, *Spectrochim. Acta, Part A. 31A*, 287, **1975**.
80. J. Kress, A. Novak, *Proc. Int. Conf. Coord. Chem. Univ. Colloq., Dublin 16*, 2, **1974**.
81. S. Sakai, K.D. Jordan, *J. Am. Chem. Soc. 104*, 4019, **1982**.
82. A.V. Nemukhin, I.A. Topol, F. Weinhold, *Inorg. Chem. 34*, 2980, **1995**.
83. A.V. Nemukhin, V.N. Solov'ev, G.B. Sergeev, I.A. Topol, *Mendeleev. Commun.*, 5, **1996**.
84. V.N. Solov'ev, G.B. Sergeev, A.V. Nemukhin, S.K. Burt, I.A. Topol, *J. Phys. Chem. A 101*, 8625, **1997**.
85. D.F. Evans, G.V. Fazakerley, *Chem. Comm.* 1974, **1968**.
86. D.F. Evans, G.V. Fazakerley, *J. Chem. Soc.* 184, **1971**.
87. G.E. Parris, E.C. Ashby, *J. Am. Chem. Soc. 93*, 1206, **1971**.
88. J. Ducom, *Bull. Soc. Chim. Fr.* 3518, **1971**.
89. R. Benn, H. Lehmkuhl, K. Mehler, A. Rufinska, *Angew. Chem. Int. Ed. Engl. 23*, 534, **1984**.
90. P.E. M. Allen, S. Hagias, S.F. Lincoln, C. Mair, E.H. Williams, *Ber. Bunsenges. Phys. Chem. 86*, 515, **1982**.
91. D. Leibfritz, B.O. Wagner, J.D. Roberts, *Liebigs Ann. Chem. 763*, 173, **1972**.
92. M. Schlosser, M. Staehle, *Angew. Chem. 92*, 497, **1980**.
93. M. Schlosser, M. Staehle, *Angew. Chem. 94*, 142, **1982**.
94. R. Benn, A. Rufinska, *J. Organomet. Chem. 239*, C19, **1982**.
95. E.A. Hill, W.A. Boyd, H. Desai, A. Darki, L. Bivens, *J. Organomet. Chem. 514*, 1, **1996**.
96. R.R. Muslukhov, L.M. Khalilov, A.A. Ibragimov, U.M. Dzhemilev, A.A. Panasenko, *Metalloorg. Khim. 1*, 680, **1988**.
97. D.F. Evans, M.S. Khan, *J. Chem. Soc. A 10*, 1643, **1967**.
98. C.P. Baskin, C.F. Bender, R.R. Lucchese, C.W. Bauschlicher, H.F. Schaefer, *J. Mol. Struct. 32*, 125, **1976**.
99. M.A. Ratner, J.W. Moskowitz, S. Topiol, *J. Am. Chem. Soc. 100*, 2329, **1978**.
100. P.G. Jasien, C.E. Dykstra, *J. Am. Chem. Soc. 105*, 2089, **1983**.
101. S.R. Davis, *J. Am. Chem. Soc. 113*, 4145, **1991**.
102. J. Axten, J. Troy, P. Jiang, M. Trachtman, C.W. Bock, *Struct. Chem. 5*, 99, **1994**.

103. H.F. Ebel, B.O. Wagner, *Chem. Ber. 104*, 307, **1971**.
104. A. Ericson, I. Persson, *J. Organomet. Chem. 326*, 151, **1987**.
105. A. Wellmar, I. Persson, *J. Organomet. Chem. 415*, 155, **1991**.
106. A. Wellmar, A. Hallberg, I. Persson, *J. Organomet. Chem. 415*, 167, **1991**.
107. T.S. Ertel, H. Bertagnolli, *Polyhedron 12*, 2175, **1993**.
108. I. Abraham, W. Hörner, T.S. Ertel, H. Bertagnolli, *Polyhedron 15*, 3993, **1996**.
109. T.S. Ertel, H. Bertagnolli, S. Hückmann, U. Kolb, D. Peter, *Appl. Spectrosc. 46*, 690, **1992**.
110. R.W. Joyner, K.J. Martin, P. Meehan, *J. Phys. C: Solid State Phys. 20*, 4005, **1987**.

11

Di- and Polyfunctional Organomagnesium Compounds

F. Bickelhaupt
Vrije Universiteit, Amsterdam, The Netherlands

11.1 INTRODUCTION

Di-Grignard reagents HalMg-Z-MgHal (**1**) are of special interest for several reasons. Like the normal monofunctional Grignard reagents RMgHal, they may serve in organic synthesis for the formation of carbon–carbon bonds by reaction of a nucleophilic carbon atom with an electrophile—with the obvious difference that this process will occur twice and thus lead, depending on the electrophile, to a bifunctional or a cyclic product, e.g. to **2** or **3**, respectively (Scheme 11.1). In this regard, they complement the carbon–carbon bond formation via S_N2 reactions of the dihalides **4** leading to **5** or **6**, where the reacting carbons are electrophilic. It is of interest to point out that the most simple way to prepare **1** is the 'direct reaction' of **4** with magnesium which may thus be regarded as an Umpolung of the carbon atoms involved.

Of even greater practical interest has proven to be the application of **1** as synthons for the preparation of other difunctional organometallic compounds, both acyclic (**7**) or cyclic (**8**) (Scheme 11.2). Because magnesium is more electropositive than all other metals except the alkali and higher alkaline earth metals, this approach is bound to be

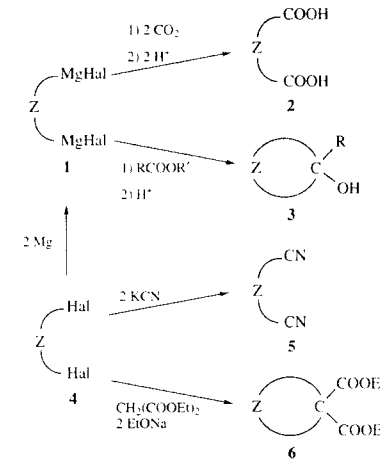

SCHEME 11.1

Grignard Reagents: New Developments Edited by Herman G. Richey, Jr. © 2000 John Wiley & Sons Ltd.

successful and has often been used, in particular for the preparation of a great number of otherwise not, or not easily, accessible transition metal containing rings.

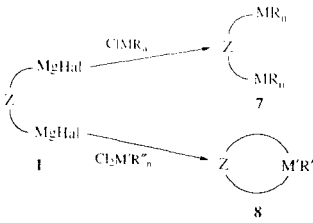

SCHEME 11.2

A completely different reason for being interested in difunctional organomagnesiums is that they often show unusual structures and bonding situations. As an example, the Schlenk equilibrium, well-known for the monofunctional Grignard reagents (Scheme 11.3, eq. (a)) may in the case of 1 lead to a cyclic diorganylmagnesium reagent **9** (Scheme 11.3, eq. (b)).

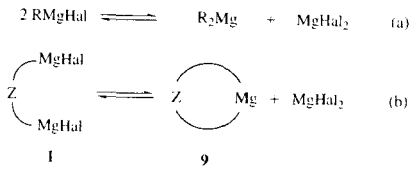

SCHEME 11.3

Finally, depending on the nature of the organic residue, the preparation of difunctional or cyclic organomagnesium compounds may pose a considerable synthetic challenge; this is particularly true for the 'short' di-Grignard reagents in which only three or less carbon atoms separate the two functionalities. Although these synthetic aspects will be treated in detail in the appropriate sections, it may be useful to present a short survey of the three major strategies which are available.

As already mentioned in the context of Scheme 1, the most simple route—where applicable—is the classical 'direct synthesis' of **1** from the corresponding organic dihalide **4** (Scheme 4, pathway (a)). Like for normal monofunctional Grignard reagents, the traditional magnesium turnings are applied, but in special cases, more activated forms of the metal may be necessary. An alternative approach, which is more tedious but gives pure cyclic compounds **9** in high yield, is the treatment of the corresponding mercury compound **10** with magnesium (Scheme 4, pathway (b)); **10**, in turn, may be prepared from **4** either directly with sodium amalgam (pathway (b')) or via **1** by reaction with a mercuric dihalide (pathway (a)/(b'')), the latter detour permitting the overall conversion of **4** via **1** and **10** to pure **9** because the stable intermediate **10** is easy to purify.

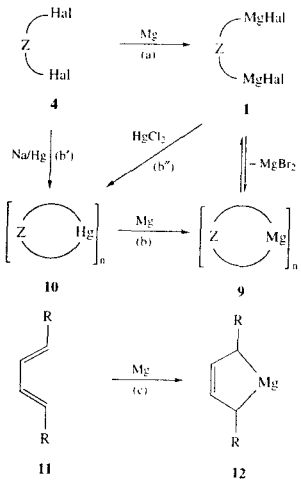

SCHEME 11.4

A less general method is the reaction of unsaturated compounds such as certain alkenes, dienes or aromatics with activated magnesium; this is illustrated for the conversion of a substituted butadiene **11** to the magnesacyclopentene **12** (Scheme 11.4, pathway (c)).

In view of this diversity of interesting aspects, it is not surprising that the chemistry of di- and polyfunctional organomagnesium compounds has received considerable attention. Only a few years after the discovery of the Grignard reaction in 1900 [1], the conversion of 1,9-dibromononane [2] and of 1,5-dibromopentane [3,4] to the corresponding di-Grignard reagents was achieved (Scheme 11.4, pathway (a): Hal = Br, Z = $(CH_2)_9$ and $(CH_2)_5$, respectively), and the synthesis and application of such reagents kept growing ever since. A number of reviews has appeared describing the older [5–7] and more recent [8–13] developments in this field, and for that reason, the emphasis will be on recent achievements and on the present state of our insight and knowledge.

In this chapter, the rather large class of difunctional organomagnesium compounds is arranged in the order of increasing length of the carbon chain connecting the two organometallic functions, which may consist of 1,2,3, or 4 and more carbon atoms (Sections 11.2 to 11.5). The few known polyfunctional reagents will be treated in Section 11.6.

11.2 1,1-DI-ORGANOMAGNESIUM REAGENTS

11.2.1 Synthesis and Structure

The most simple di-Grignard reagent is methylenedimagnesium dibromide (**13a**). It was first prepared as early as 1926 by Emschwiller by direct synthesis from dibromomethane and magnesium [14], but the yield was low and the product quite impure. Better results were obtained with 1% magnesium amalgam, either in benzene/diethyl ether in a ratio 1 : 1 [15,16] or, preferentially, in diisopropyl ether [17] (Scheme 11.5). The latter minimizes the formation of the, often rather obnoxious, reduction product methylmagnesium bromide which moreover is soluble in diisopropyl ether and therefore easily removed by decantation; the insoluble **13a** is thus obtained in yields of up to 80%, and for synthetic applications, it may be dissolved in the benzene/ether mixture. Finally, it should be mentioned that **13a** was also formed in 40% yield in the reaction of diiodomethane with lithium 4,4'-di-(*tert*-butyl)biphenyl in THF in the presence of magnesium bromide at −100° [18] (*cf.* also Section 11.3).

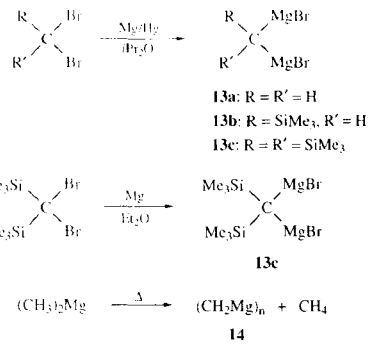

SCHEME 11.5

Unfortunately, this approach does not work for substituted 1,1-dibromides with the notable exception of the trimethylsilyl substituent: the mono- and disubstituted derivatives **13b** [19] and **13c** [20], respectively, were prepared in comparable yields. In the case of **13c**, it is not necessary to use the tedious amalgam procedure as the reaction proceeds in the normal way with magnesium in diethyl ether (Scheme 11.5); pure crystalline **13c** can be isolated in 35% yield on concentrating and cooling the reaction mixture [20].

Little is known about the structure of 1,1-di-Grignard reagents. It is remarkable that **13a** dissolves in the benzene/ether mixture but is nearly insoluble in pure diethyl ether. Extraction of the product obtained in benzene/diethyl ether with pure diethyl ether removes magnesium bromide to give residues which have the approximate composition of $CH_2(MgBr_2/MgBr_2$, while THF removes more $MgBr_2$ leading to the composition $CH_2Mg/MgBr_2$ (**13a'**) [16b]; in view of their low solubility, these white powders must have polymeric structures as is probably also the case for the white, insoluble methylenemagnesium (**14**) which

was obtained by Ziegler *et al.* by pyrolysis of dimethylmagnesium [21] (Scheme 11.5).

The only 1,1-di-Grignard reagent which has been characterized by an X-ray crystal structure determination is **13c** [22]. Amazingly, it has the straightforward composition of monomeric $(Me_3Si)_2C(MgBr{\cdot}THF_2)_2$ involving tetracoordinate magnesium and shows two remarkable features which help to explain the low reactivity of the compound (see Section 11.2.2): the nucleophilic central carbon atom is completely shielded by the four bulky groups surrounding it and hardly 'visible' from outside; however, in spite of the steric congestion, all four bonds to this carbon atom are relatively short, which was ascribed to bond strengthening due to the accumulation of negative charge at carbon and to negative hyperconjugation [22] (see Chapter 9.6.1).

11.2.2 Applications

The relatively low reactivity of **13** compared to normal Grignard reagents is a characteristic and general feature. As indicated above, this is probably caused by both steric and electronic factors, and the reactivity decreases with increasing substitution by silicon. This lack of reactivity sometimes limits the achievement of certain synthetic goals; the only electrophile which always reacts instantaneously is water (or D_2O)!

The most important application in organic synthesis is a Wittig-type olefination of carbonyl compounds as illustrated for the preparation of **15** and **16** in Scheme 11.6. With **13b**, carbonyl compounds with α-hydrogens are mainly enolized instead of forming **15b**. The diminished nucleophilicity is still more pronounced for **13c**: while it does react with benzaldehyde to give 70% of **16**, the reaction with benzophenone is extremely sluggish and, after 23 days, yields only 7% of **17**, the rest being unreacted **13c** as shown by deuterolysis to furnish **18** [23]. A few other examples of olefinations of steroids and sugar derivatives have also been reported [15,24,25].

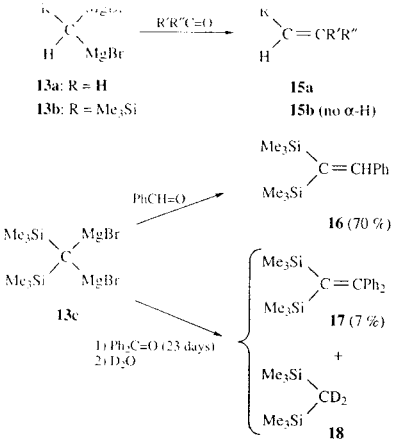

SCHEME 11.6

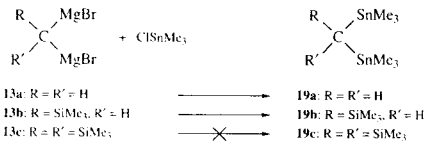

SCHEME 11.7

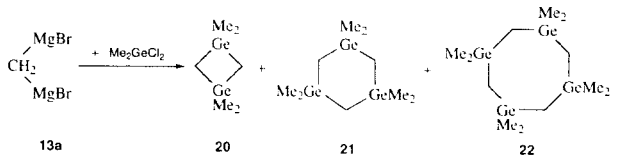

SCHEME 11.8

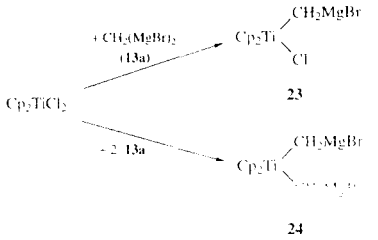

SCHEME 11.9

More numerous are the applications in organometallic synthesis. This is especially true for **13a**; for **13b**, and even more so for **13c**, the reactivity is often insufficient to yield the desired products such as **19** [16,17,20] (Scheme 11.7).

Particularly successful was the synthesis of a number of four-membered metallacycles starting from **13a**. With Me_2GeCl_2, the 1,3-digermacyclobutane **20** was obtained, together with its trimeric (**21**) and tetrameric (**22**) homologs [16b,c] (Scheme 11.8); yields are higher when the reagents contain less $MgBr_2$ such as **13a'** (*vide supra*).

Reaction of Cp_2TiCl_2 with one or two molar equivalents of **13a** gives the useful reagents **23** or **24**, respectively (Scheme 11.9).

Compound **23** [26] is an analogue of the well known Tebbe reagent **30** (Scheme 11.10) [27] and shows analogous transformations with alkenes and alkynes to furnish titanacyclobutanes **25** and titanacyclobutenes **26**, respectively; with trimethylphosphine and THF, MgBrCl is extruded to give the titanocene-carbene complex **27** and its dimer **28**, respectively; on evaporation of the solvent benzene/ether from **23** and addition of the apolar toluene, **29** dissolves and, according to its composition and spectral properties, has a structure strongly analogous to that of **30**. Finally, with benzophenone, **23** undergoes a Wittig-type carbonyl olefination reaction yielding 1,1-diphenylethene.

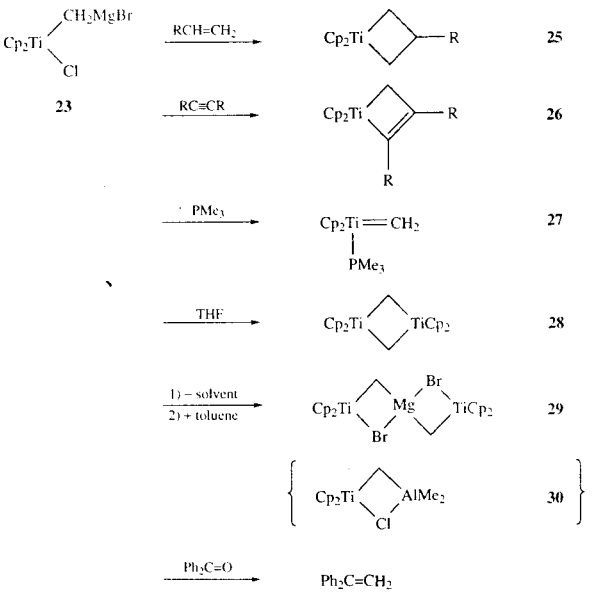

SCHEME 11.10

Compound **24** is formally a 1,3-di-Grignard reagent (see Section 11.4.2) and has proven useful for the preparation of a number of 1,3-dimetallacyclobutanes **31** of Groups 4 and 14 [17a] (Scheme 11.11). Reaction of **24** with silicon tetrachloride gave the spiro compound **32** [28].

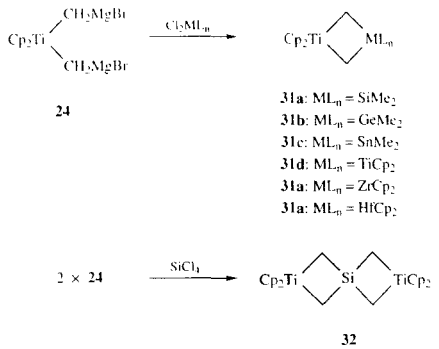

SCHEME 11.11

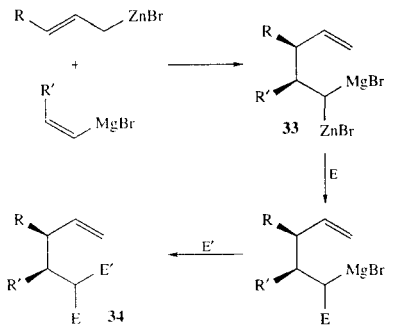

SCHEME 11.12

Finally, although formally beyond the scope of this review, it should be pointed out that Knochel *et al.* [29] have developed the chemistry of the related mixed 1,1-dimetallic compounds **33** which are obtained by addition of allylzinc reagents to alkenylmagnesium halides and are of synthetic interest because the presence of two different metals at the same carbon atom allows step-wise substitution by two different electrophiles yielding **34** as shown in Scheme 11.12.

11.3 1,2-DI-ORGANOMAGNESIUM REAGENTS

11.3.1 Synthesis and Structure

Amongst the di-Grignard reagents, the vicinal or 1,2-disubstituted ones are the most difficult to prepare, and only a limited number of compounds is known. As Grignard himself found out [30] only one year after the discovery of his famous 'direct synthesis' [1], the reason is that after the first halogen has reacted, β-elimination of magnesium dihalide occurs quite rapidly before the second halogen gets a chance to react; this is illustrated for 1,2-dibromoethane in Scheme 11.13: presumably, **35** is formed as an intermediate, but **36** is not obtained and ethene is the only product observed.

β-Elimination can be retarded if ring strain is introduced in the elimination product. This factor is responsible for a limited success which has been obtained by 'direct synthesis' in two cases (Scheme 11.13). Firstly, both the cis- and the trans-isomer of **37** have been converted to *cis*-**40** in 15% yield; apparently, the high ring strain in cyclopropene (**39**) sufficiently counteracts its formation, slowing it down sufficiently to give the alternative reaction of intermediate **38** with a second magnesium a chance [31]. Secondly, in aromatic compounds, β-elimination is somewhat retarded because the product of, elimination is a highly energetic aryne. Thus, 1,2-dibromobenzene reacts with magnesium in THF (via **41**) to give 20–40% of the di-Grignard reagent **43** (besides the main product benzyne (**42**)) [10]; however, this approach is not of practical importance because the corresponding diorganylmagnesium **44** can be obtained by another route in good yield and purity (see Scheme 11.15).

The parent 1,2-di-Grignard reagent **36** has been obtained in 10% yield from the reaction of

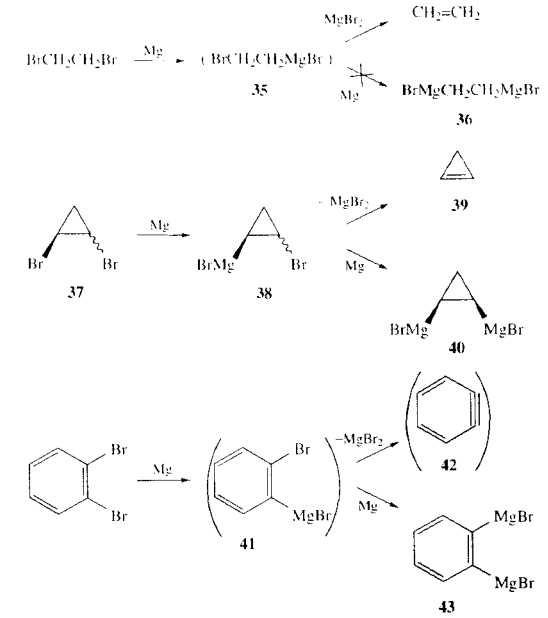

SCHEME 11.13

diiodomethane and lithium 4,4′-di-(*tert*-butyl)biphenyl in the presence of magnesium bromide in THF at 100° [18]; again, this approach is not attractive from a preparative point of view as **36** is formed in a mixture containing also the mono-, tri- and tetramethylene analogues **13a**, **45** and **46**, respectively, as indicated by their conversion to the corresponding tin compounds (Scheme 11.14).

As mentioned above, **44** (Scheme 11.15) was prepared in 68% isolated yield from its mercury analogue **47** by stirring with magnesium in THF (*cf.* route (b) in Scheme 11.4) [32]. It has been

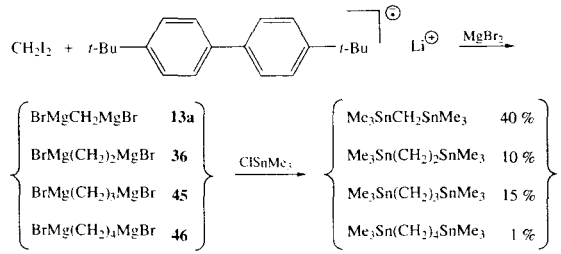

SCHEME 11.14

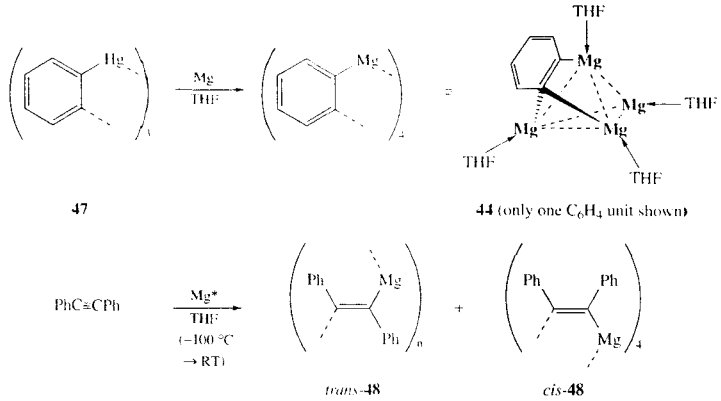

SCHEME 11.15

successfully applied in organometallic synthesis (see Section 11.3.2), but it is also of interest because of its tetrameric structure ($[C_6H_4Mg]_4$) both in solution and in the crystal (see also Chapter 9.6.4); such tetrahedral arrangements are rare in organomagnesium chemistry, but they are quite normal for the structures of organolithium compounds $(RLi)_4$. This structural analogy is probably due to analogous electrostatic and spatial interactions in compounds of type $R^{2-}M^{2+}$ on the one hand, and R^-Li^+ on the other [32].

By a different approach, *i.e.* sublimation of magnesium vapour into a frozen solution of diphenylacetylene in THF at 196°C followed by slow warming to room temperature, (cf. route (c), Scheme 11.4), **48** was obtained as a mixture of the *cis*- and *trans*-isomers (Scheme 11.15). By decantation from the reaction mixture and cooling, bright yellow crystals of *cis*-**48** were isolated and shown by X-ray crystallography to have a tetrameric structure analogous to that of **44**; only the orientation of the four 'ortho-phenylene dianions' on top of the four Mg_3 triangles relative to each other differ in such a way that **44** has approximate C_{2v} symmetry while that of *cis*-**48** is S_4 [32].

Finally, it should be pointed out that **49**, the double magnesium bromide salt of acetylene, is also a 1,2-di-Grignard reagent, even though it is not often ranked as such. It can be prepared from acetylene and RMgBr (Scheme 11.16); its structure is unknown [5,7,12].

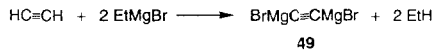

SCHEME 11.16

11.3.2 Applications

Because of the difficult accessibility of the 1,2-organomagnesium compounds, only few applications are known other than trivial derivatization reactions, e.g. with D_2O or $ClSnMe_3$. The exception is **44**, which has proven attractive as starting material for 9,10-dihydroanthracenes of Groups 13 (**50**–**52**) and 14 (**53**) (Scheme 11.17) [33] and for 9,10-dimetallatriptycenes of Groups 14 and 15 (**54**) (Scheme 11.18) [33a,34,35].

The reaction of **44** with methyl dihalides of Group 13 are straightforward, but the products **50** appear in some cases to consist of more than one (oligomeric?) species and have only been characterized by their spectroscopic properties [33a], whereas **51** [33a] and **52** [33b] have been identified by X-ray crystal structures.

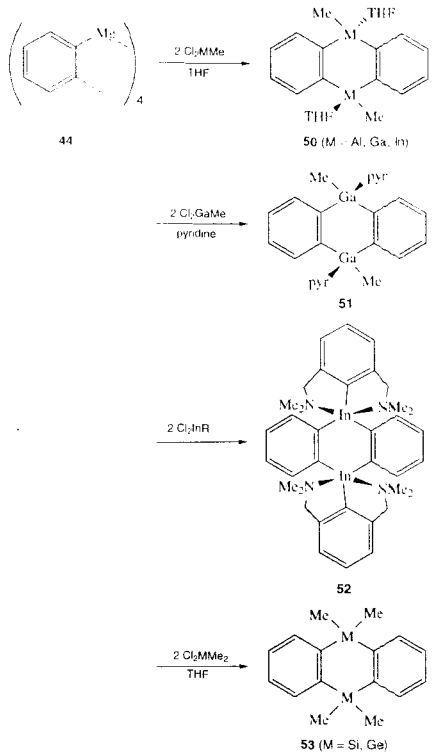

SCHEME 11.17

The reaction of **44** with trihalides of Group 14 (Cl_3MR; M = Si, Ge, Sn) or 15 (*M* = *P*, As, Sb) may be performed in a one step [34a] or in a two-step procedure [33a,34b,c,35] as shown in Scheme 11.18. Probably in both modes of addition, and favoured by the close vicinity of the four magnesiums in the tetrameric cluster of **44**, the reaction proceeds first by substitution of all three chlorines of one molar equivalent of Cl_3MR to furnish an intermediate tri-Grignard reagent **55** (which will be briefly discussed in Section 11.6); next, **54** is formed by reaction of **55** with the second equivalent of the trihalide. The two-step process is attractive because it allows the introduction of a different metal *M'* and/or a different substituent *R'* in the second step. In the present context, it would go too far to discuss all aspects of this interesting reaction. The yields vary between 0% and 85%, depending on the combination of *M* and *R*: apparently for steric reasons, the yield of **54** tends to be higher when *M* is large (Ge, Sn) and *R* is small (H, Me), but in all cases **55** is formed even if **54** is not.

Compound **49** (Scheme 11.16) has been used to prepare silicon-bridged acetylenes **56** (Scheme 11.19) [36], amongst which are the six-membered ring derivatives **56a** (n = 4, R = Me or Et; 52–55% yield) [36b]; in this case, only very little of the dimeric species was obtained (≤ 1%).

11.4 1,3-DI-ORGANOMAGNESIUM REAGENTS

11.4.1 Synthesis and Structure

In the 'direct reaction' with magnesium, aliphatic 1,3-dihalides such as **57** have a high tendency to eliminate magnesium dihalide at the intermediate stage of **58** [30] (Scheme 11.20), which is analogous to the behaviour of 1,2-dihalides (see Scheme 11.13). In fact, the reaction of **57** (or analogous 1,3-dibromoalkanes) with magnesium (or zinc) is one of the best methods to prepare three-membered rings such as cyclopropane (**59a**) and its 2,2-dimethyl derivative **59b**, etc. However, when the reaction is performed under special conditions, with triply sublimed magnesium and by very slow addition of the organic dihalide, preferably in a sealed high-vaccuum system, the 1,3-di-Grignard reagents **60a** (30% isolated yield [37]) and **60b** (15% [38]) can be obtained in moderate yields, which nevertheless are useful as the starting materials are cheap and the purification is easy. While **60b** contains no detrimental (organometallic) impurities and can be used directly as formed, **60a** is purified by addition of THF which precipitates the (polymeric ?) 1,3-trimethylenemagnesium (**61**); for preparative applications, magnesium bromide in diethyl ether is added to reconstitute **60a** and to dissolve it.

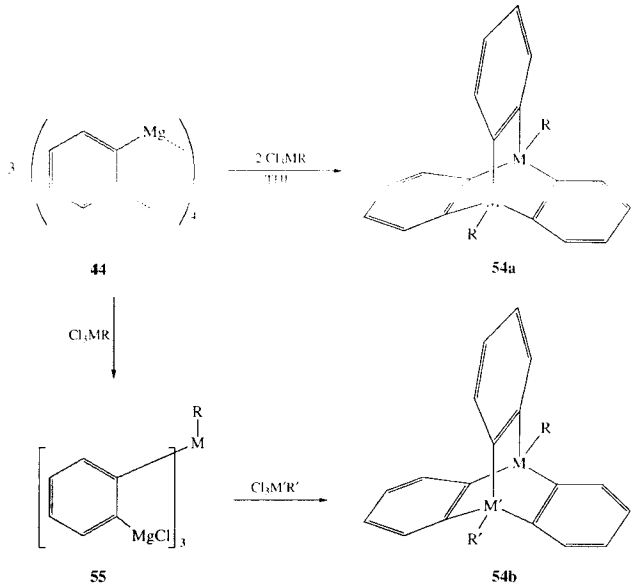

44 **54a** **55** **54b**

SCHEME 11.18

An earlier synthesis of **60a** by a multi-step route starting from allene gave an impure product in low yield [39].

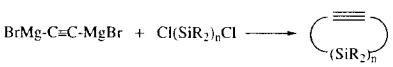

49 **56**

SCHEME 11.19

Other 1,3-di-Grignard reagents are rare. In the aliphatic series, **63a, b** are the only other representatives (Scheme 11.21). The expectation that the yields of **63** in the 'direct reaction' from **62** would be substantially higher because of higher strain in the bicyclic elimination products **64** was not fulfilled; the yields were 7% (**63a**) and < 45% (**63b**) [40].

The situation is completely different for 1,3-dimagnesium compounds containing both an aryl- and a benzyl-type of attachment such as **65** [40] and **66** [42] (Scheme 11.22). Apparently, in this case, the 1,3-elimination at the stage of the intermediate mono-Grignard reagent (leading in this case to a highly strained cycloproparene) is too unfavourable, and therefore the yields are high (**65**: 90%; **66**: 85%) when proper reaction conditions are obeyed.

Similarly, 1,3-elimination is no problem in the 'direct reaction' of fully aromatic dihalides which usually give di-Grignard reagents in good yields. Thus, **67** [43] and **68** (90% yield) [32] were obtained from the corresponding dibromides (Scheme 11.23). The diiodo analogue of **68** can also be prepared from 1,8-diiodonaphthalene in 2-methyl-THF; these di-Grignard reagents have a high tendency to cleave off magnesium dihalide

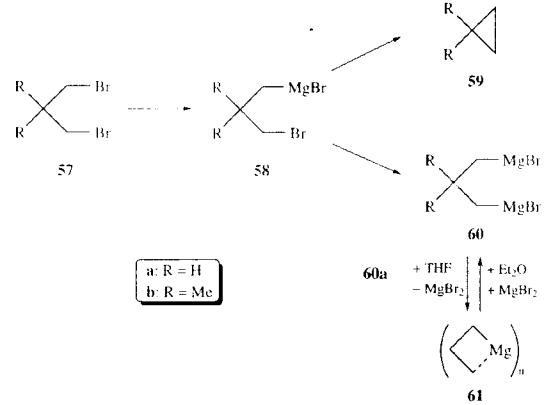

SCHEME 11.20

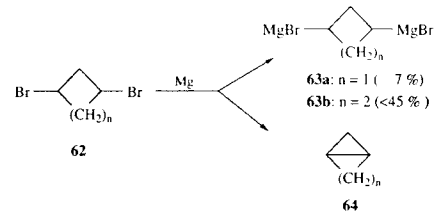

SCHEME 11.21

with formation of the tetrameric diorganylmagnesium **69**.

Little is known about the structures of 1,3-dimagnesium compounds. The only X-ray crystal structure is that of **69**. It consists of a tetrameric cluster of S_4 symmetry analogous to that of *cis*-**48** (Scheme 11.15), and the tetrameric arrangement persists in THF solution, too [32] (see Chapter 9.6.1). Compounds **61** and **65** apparently have an oligomeric or polymeric structure as their solubility in THF is low [41]. The structure of **66** shows an interesting phenomenon [42] (Scheme 11.22). According to UV and NMR spectroscopic data, it exists in an equilibrium between two forms **66a** and **66b**; the former is yellow and thus possibly (nearly) ionic, whereas the latter is colourless. Probably, the degree of association is 3 for **66a** and 2 for **66b**, but unfortunately, these values could not be determined with high accuracy because in THF, **66** slowly decomposes to give 2-methylnaphthaline.

11.4.2 Applications

1,3-Diorganomagnesium compounds have, apart from simple derivatization reactions with ketones or carbon dioxide, not often been used in organic synthesis. An exception is **60a** which (in the crude reaction mixture) on slow exposure to gaseous carbon dioxide (3 h at room temperature) gave 33% of cyclobutanone (**70**); this constitutes the most efficient preparation of this compound [44] (Scheme 11.24).

Again, more important are the applications in the synthesis of (mostly) four-membered ring compounds containing a main group or transition metal in the ring [8–13,45]. Examples using **60** are presented in Scheme 11.25. Several aspects deserve further comment. In the first place, it appears that germanium is particularly inclined to form four-membered rings. Secondly, while the yields for tin are lower (in the case of **73a**, the

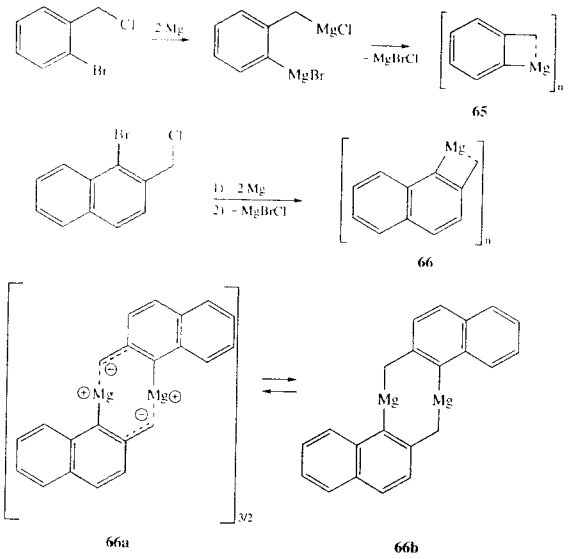

SCHEME 11.22

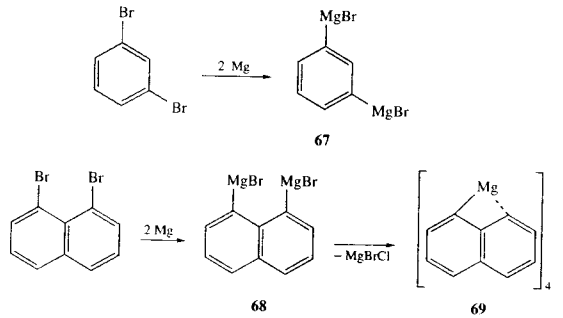

SCHEME 11.23

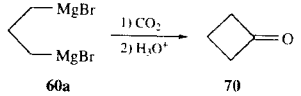

SCHEME 11.24

major part of the products are the corresponding dimer, trimer and tetramer (formed in a combined yield of 70%), this approach nevertheless is valuable because so far, it is the only one which has furnished stannacyclobutanes. Another example is the reaction of **60b** with silicon or germanium

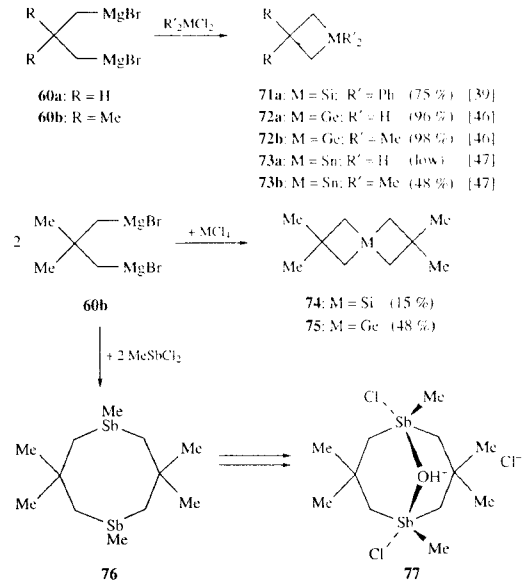

SCHEME 11.25

tetrachloride which gave the spiro compounds **74** (15%) and **75** (48%), respectively [48]. For antimony, the tendency to form a four-membered ring is even smaller; thus, **60b** with $MeSbCl_2$ gave **76** which was characterized as **77** by an X-ray structure [49].

Similarly, a number of metallacyclobutanes (**78**–**85**) of transition metals were obtained from **60b** (Scheme 11.26). In this context, the synthesis of **31** and **32** from the formal 2-titana-1,3-di-Grignard reagent **24** (Scheme 11.11) should also be mentioned.

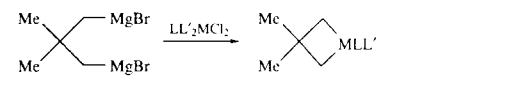

SCHEME 11.26

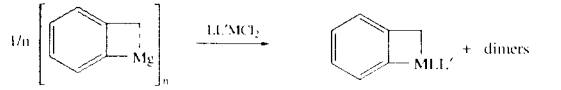

65

86: M = Si; L = L′ = Me (58 %) [54]
87: M = Ge; L = L′ = Me (56 %) [54]
88: M = Sn; L = L′ = Me (0 %) [54]
89: M = Ti; L = L′ = Cp (93 %) [41a]
90: M = Re; L = Cp*, L′ = O (60 %) [52]
91: M = Pt; LL′ = COD (51 %) [55]

SCHEME 11.27

From **65**, the 1,2-dihydro-1-metallacyclobutanes **86–91** were obtained with the exception of **88**; in this case only a dimeric species was formed (Scheme 11.27).

Finally, **69** served as starting material for a number of four-membered 1,8-naphthalenediyl metallacycles of Group 14 elements: **92**, **93** (with some of the corresponding dimeric eight-membered ring product); instead of **94**, the dimer was obtained exclusively) [56]. The analogous transition metal derivatives **95–99** were obtained in a similar fashion [57] (Scheme 11.28).

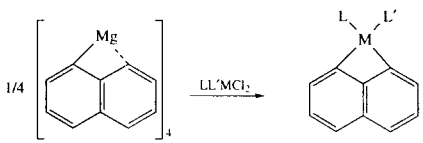

69

92: M = Si; L = L′ = Me
93: M = Ge; L = L′ = Me
94: M = Sn L = L′ = Me; 0 %]
95: M = Ti; L = L′ = Cp
96: M = Zr; L = L′ = Cp*
97: M = Pt; L = L′ = PEt_3
98: M = Rh; L = Cp*, L′ = PPh_3
99: M = Ir; L = Cp*, L′ = PPh_3

SCHEME 11.28

11.5 1,4- AND LARGER α, ω-DI-ORGANOMAGNESIUM REAGENTS

As already indicated in the previous sections, organic dihalides in general, and organic dibromides in particular, react smoothly with metallic magnesium in the 'direct synthesis' when there are four or more carbon atoms between the two halide functions (Scheme 11.4, pathway (a)); occasionally, other pathways of Scheme 11.4 have proven useful, too. It is therefore not surprising that from the early days of Grignard chemistry [2–4], a great number and variety of such divalent organomagnesium species have been prepared and applied in synthesis. In general, it is safe to say that in the absence of obvious structural incompatibilities, these di-Grignard reagents can be prepared in the same fashion as their mono-Grignard analogues.

For that reason, and as this area is too vast for a comprehensive treatment in the present context, the interested reader is referred to previous reviews covering the field [5–13]. In order to illustrate the potential of these interesting compounds, a few representative examples and facts will be discussed here.

11.5.1 Synthesis and Structure

The most simple di-Grignard reagents are the oligomethylene derivatives **1′** (Scheme 4: **1**, Z = $(CH_2)_n$). They are obtained by 'direct synthesis' from the corresponding dihalides **4′** [2–13] (*cf.* Scheme 11.4, pathway (a)). Their cyclic diorganylmagnesium analogues **9′** may be obtained either from **1′** by precipitation of magnesium dibromide with 1,4-dioxane or, highly pure, from **4′** via the mercury analogues **10′** (Scheme 11.4, pathway (b)). It may sometimes be advantageous to perform the transformation of **1′** to **10′** via the α, ω-oligomethylenebis(mercuric halides) **100** as

the latter are usually crystalline and more stable, and therefore easy to purify; subsequently, **100** is converted to **10′** by reduction *e.g.* with tin dichloride in alkaline solution [58–60] (Scheme 11.29); alternatively, **100** may be converted to pure **1′** by treatment with magnesium metal.

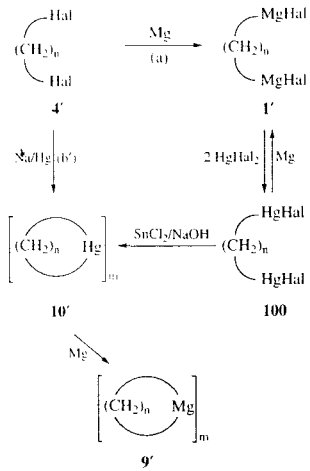

SCHEME 11.29

An arbitrary selection of other di-Grignard reagents **101–105** is given in Scheme 11.30. While **101–104** ([61]–[64], respectively) were obtained more or less by the classical direct approach, **105** [65a,b] and other benzylic Grignard reagents [65c–e] require the use of the magnesium-anthracene adduct (*vide infra*) which, in a way, may be considered as a 'soluble' and activated form of magnesium, in order to obtain satisfactory results.

Different and more specific preparations are shown in Scheme 11.31. Compounds **106** [66] and **107** [67a] illustrate the formation of a di-Grignard species by transmetallation from alkali metalorganic analogues; **107** has also been obtained by direct ortho-metallation with $Mg(TMP)_2$ (*bis*(2,2,6,6-tetramethylpiperidino)magnesium), as has **108** [67b].

A considerable number of cyclic diorganylmagnesium compounds have been prepared by addition of normal or activated magnesium to conjugated unsaturated systems such as 1,3-dienes, cyclooctatetraene, or anthracene. Thus, the addition of Rieke magnesium (obtained by reduction of magnesium dichloride with potassium or with lithium naphthalenide) to acyclic or cyclic 1,3-dienes gives rise to five-membered magnesacycles of type **12** (Scheme 11.4, pathway (c)); this is illustrated for **109–112** in Scheme 11.32, but many other substituted dienes have been used in this and similar transformations [68–70].

Cyclooctatetraene, too, gives an adduct **113** with various forms of activated magnesium; presumably, **113** is a (contact) ion pair, but in its reactions, it behaves like a 1,4-adduct analogous to **12** [71,72] (Scheme 11.33).

Similarly, a number of methods have been developed to prepare the magnesium adducts **114** of anthracene and many of its 9,10-substituted derivatives [12,13,72a,73,74] (Scheme 11.33). Depending on the substituents, **114** may be in equilibrium with its components. The unsubsubstituted parent adduct slowly decomposes to magnesium and anthracene at room temperature and faster on heating; the magnesium thus obtained or **114** itself are often used as a source of 'active magnesium' (*cf.* the synthesis of **105**). Finally, the preparation of **115** by cyclomagnesiation catalyzed by zirconocene should be mentioned [75].

The structures of the compounds described in this section have also received considerable attention. Most crystal structures pertain to the halogen-free, metallocyclic derivatives; they are described in Chapter 9. In general, due to the large C–Mg–C angle of about 120–140°, the magnesacycles are at least dimeric as exemplified by **116a** [76,77] and **116b** [77], while **117** is a trimer [78] (Scheme 34).

On the other hand, cyclic compounds with allylic or benzylic type bonds such as those shown in Schemes 11.32 and 11.33 tend to be monomeric, at least in the solid state. This is illustrated by **118** [79], **119** [80], and **120** [81–84] (Scheme 11.35).

In solution, the situation may be different. Thus, while **116a** remains purely dimeric in THF [85], **116b** shows a monomer/dimer equilibrium which

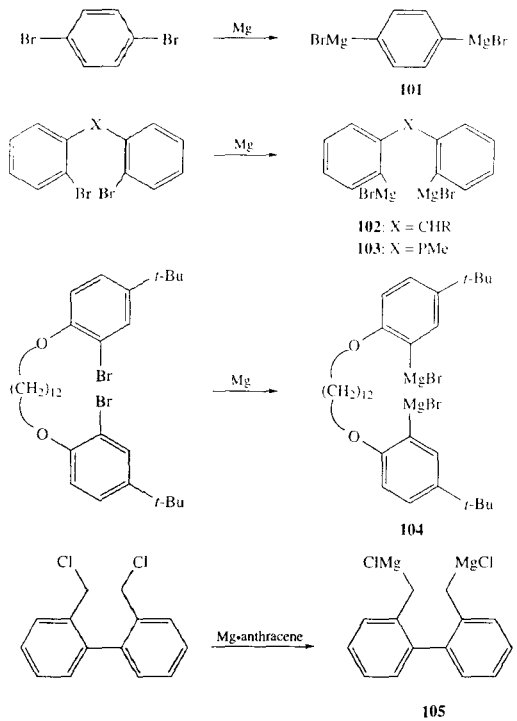

SCHEME 11.30

is strongly shifted towards the dimer ($\Delta H = -8$ kcal mole^{-1}, $\Delta S = -15$ cal mole^{-1} K^{-1}) [60a] (Scheme 11.36). An interplay of ring and torsional strain makes the other representatives of **9′** dimeric, while **121** and **122** reveal an increasing trend to become a monomer; finally, intramolecular coordination removes steric interactions and allows **123–125** to be purely monomeric [86].

11.5.2 Applications

The number of investigations concerning the applications of large di-Grignard reagents is even larger than that dealing with their synthesis and structure. As briefly indicated in the Introduction (Section 11.1), in principle, the same type of reactions as of monovalent Grignard reagents is feasible [5–13], and this potential has been exploited early on [2–4] both for the synthesis of organic derivatives [87], but in particular for the preparation of cyclic organometallic compounds. Thus, the first metallacycles of mercury [58], silicon [88], tin [89], phosphorus, arsenic, antimony, and bismuth [90] were prepared from di-Grignard reagents corresponding to type **9′** in the second decade of this century. At present, this method has become routine, and again, a few representative examples must suffice to illustrate the broad range of possibilities.

The reaction of *e.g.* $BrMg(CH_2)_4MgBr$ with simple electrophiles such as ketones or CO_2 has

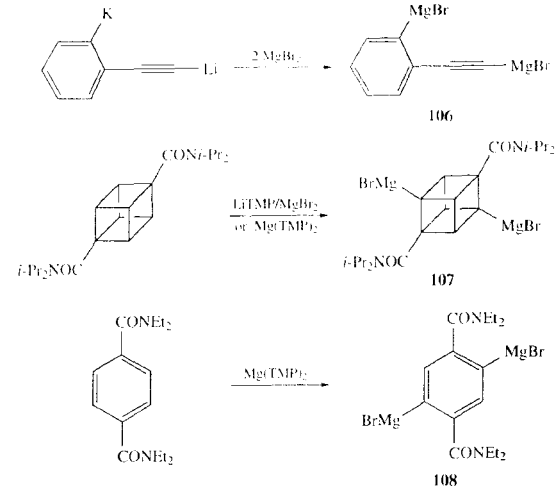

SCHEME 11.31

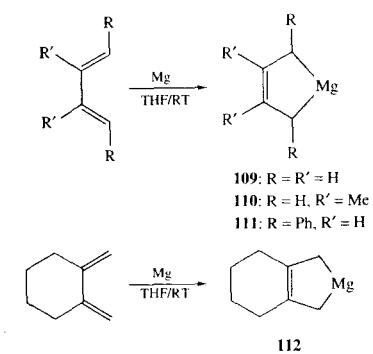

SCHEME 11.32

long been known to give the corresponding difunctional products [87], but the reaction may take a complicated course as is the case for diisopropyl ketone where the expected diol **126** was obtained in 12% yield only [91] (Scheme 11.37). Of greater practical value is the reaction with esters or carboxylic acid anhydrides which leads

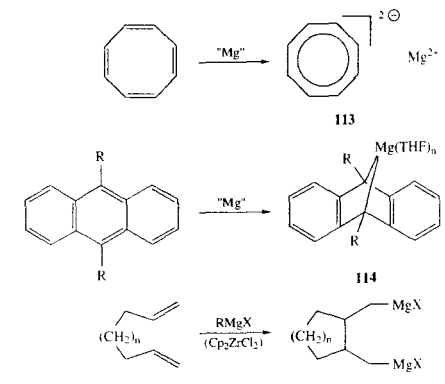

SCHEME 11.33

in usually good yields to cyclic diols **127** or lactone **128**, respectively; both the di-Grignard reagent and the substrate may carry a variety of substituents [92]. Other examples are the preparation of the labelled ketone **129** [93] and, very

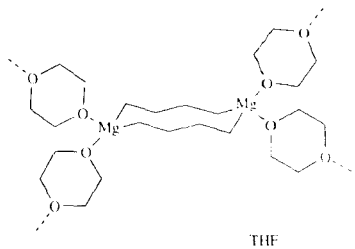

116a

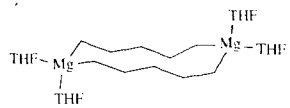

116b

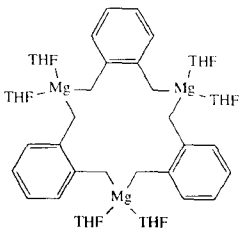

117

SCHEME 11.34

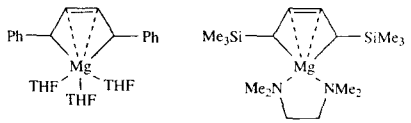

118 119

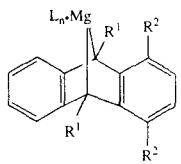

120a: $R^1 = R^2 = H$; $L_n = THF_3$
120b: $R^1 = H$, $R^2 = Me$; $L_n = THF_3$
120c: $R^1 = SiMe_3$, $R^2 = H$; $L_n = THF_2$
120d: $R^1 = SiMe_3$, $R^2 = H$; $L_n = TMEDA$

SCHEME 11.35

recently, the synthesis of the diketones **130** from the corresponding benzimidazolium salts **131** [94].

Degree of association of magnesacycles

	n	m
9'	4	2
	5	1–2
	6	2
	9	2

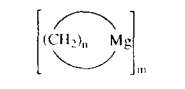

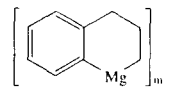

121

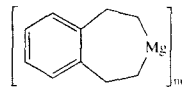

122

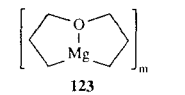

123

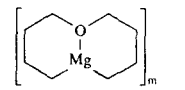

124

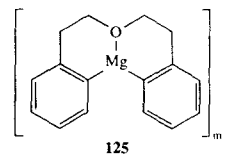

125

SCHEME 11.36

The diene adducts **109–112** (Scheme 11.32) and their analogues have found several interesting applications. Their two carbon–magnesium bonds react in a step-wise fashion with mono- or divalent electrophiles; depending on the electrophiles, different regioselectivities, *i.e.* 1,2- or 1,4-addition products, were observed [70]. Illustrative examples are **131–133** and the spiroannulation products **134** and **135** (Scheme 11.38).

Two examples involving transition metal catalysis in the preparation of bicyclic systems are **136** [95] and **137** [96] (Scheme 11.39).

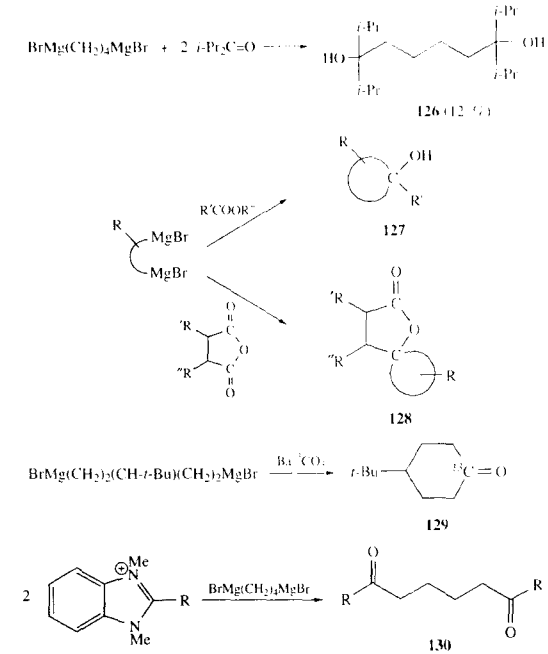

SCHEME 11.37

Ample use has also been made of di-Grignard reagents in organometallic synthesis. In addition to some older examples already cited [87–90], the following examples are selected to highlight the great diversity of applications, ranging from the simple, but useful **138** [78] and **140** [97] (Scheme 11.40) as acyclic compounds to **139** [98] (Scheme 11.40) and **141** [62,99,100], **142** [101], and **143** [101] as metallacyclic systems (Scheme 11.41).

Finally, **144** is an exotic example involving a completely different application of a cyclic diorganylmagnesium compound; it was derived from the di-Grignard reagent **104** (Scheme 11.30) by removal of magnesium dibromide with dioxane and used for the formation of the unique metallacyclic catenane **145** (which is in equilibrium with its side-on coordinated analogue) [64] (Scheme 11.42).

11.6 TRI- AND POLYORGANOMAGNESIUM REAGENTS

Organic molecules containing more than one carbon–magnesium bond seem to be scarce, although sometimes they may occur as intermediates which are either not recognized or not characterized. An example discussed in the context of Section 11.3.2 is **55** (Scheme 11.18) which is a useful intermediate in the synthesis of 9,10-dimetallatrypticenes. The structure of **55a** is not known, but magnesium dichloride can be precipitated to give a solution with the composition of **146** [33a]; however, this structure remains speculative (Scheme 11.43).

A tri-Grignard reagent may have been involved in the conversion of **147** to **148** (*cf.* Scheme 11.31), but a step-wise functionalization is likely [102]

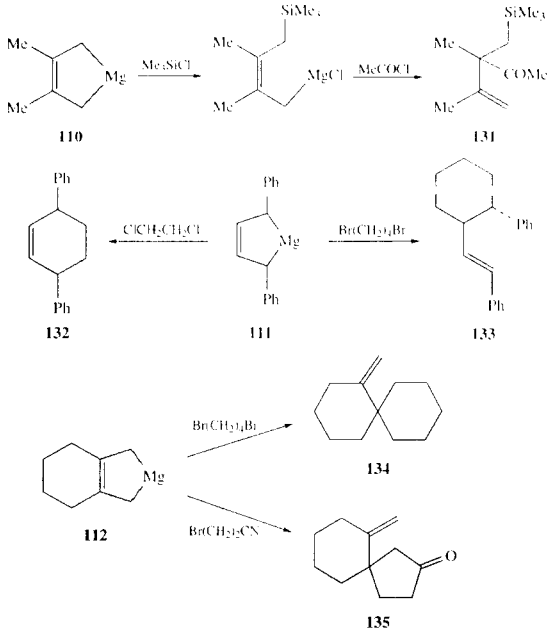

SCHEME 11.38

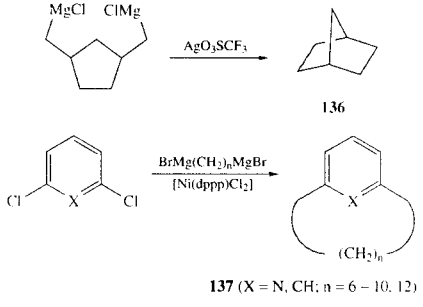

SCHEME 11.39

(Scheme 11.44). Two tri-Grignard reagents have been reported involving magnesium bonded to saturated carbon, *i.e.* **149** [103], and **151** [65c]; **149** has been used to prepare the 1-silaadamantane **150**.

While the direct reaction of 1,3,5-tribromobenzene with magnesium does not give satisfactory results [35], it can be converted to the aromatic tri-Grignard reagent **152** by treating it with lithium (di-tert-butyl)biphenyl (LiDBB) to form the trilithio reagent **153** and reacting the latter with magnesium dibromide [104] (Scheme 11.45).

Well defined higher metallated organomagnesium compounds are not known with two remarkable exceptions: the dimeric pentamagnesiated ruthenocene **154** and the decamagnesiated ruthenocene **155**, both obtained from the corresponding mercury compounds by treatment with methylmagnesium chloride [105] (Scheme 11.46).

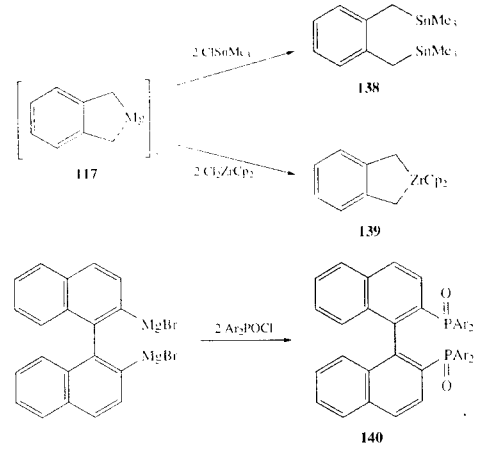

SCHEME 11.40

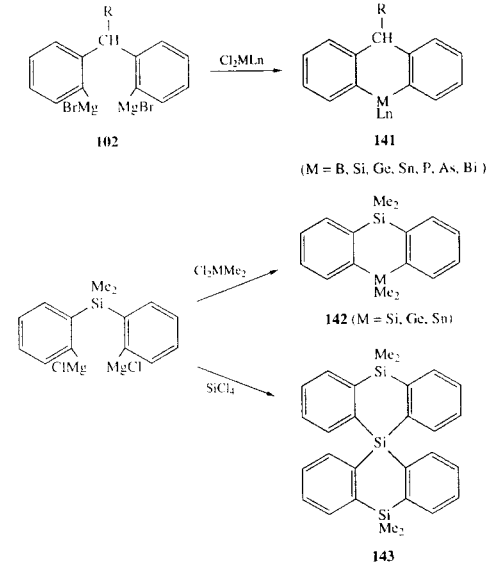

SCHEME 11.41

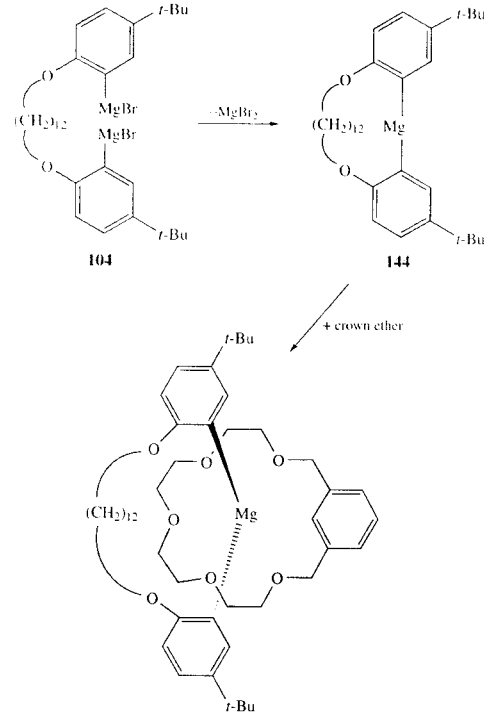

104 144 145

SCHEME 11.42

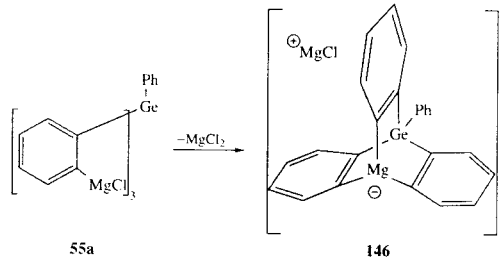

55a 146

SCHEME 11.43

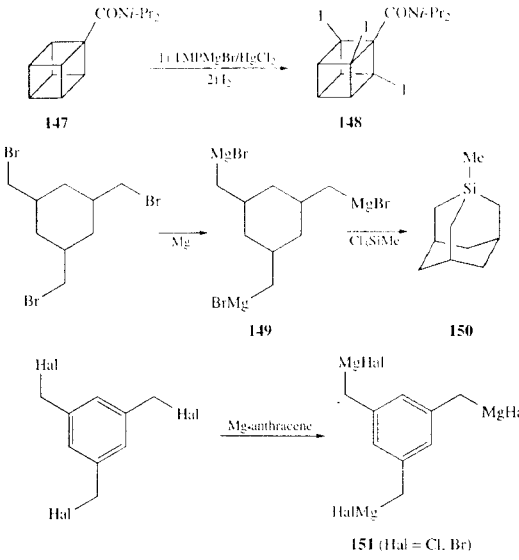

147 148 149 150 151 (Hal = Cl, Br)

SCHEME 11.44

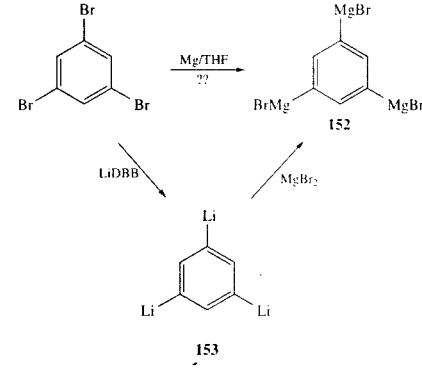

152 153

SCHEME 11.45

11.7 CONCLUSION

Even though the present review had to concentrate on a selection from the vast literature on the topic of di- and polymetallated organomagnesium compounds with an emphasis on newer developments, it may have become obvious that their chemistry is rich and rewarding. In principle, the same potential is present as in the chemistry of monofunctional Grignard reagents and challenging applications are feasible; however, occasionally two types of problems may arise.

Firstly, several of the higher metallated compounds are inherently less stable than their monovalent counterparts, presumably because the accumulation of negative charge from the highly polar carbon–magnesium bond imparts instability to the molecule, so that the compound has to be handled at low temperature and/or converted as fast as possible. Secondly, even if the stability is sufficient, derailments often occur during the preparation, and it may be tricky to find the proper pathways and conditions. However, the increasing number of such compounds testifies to the skill and perseverance of chemists and does make us optimistic for the future.

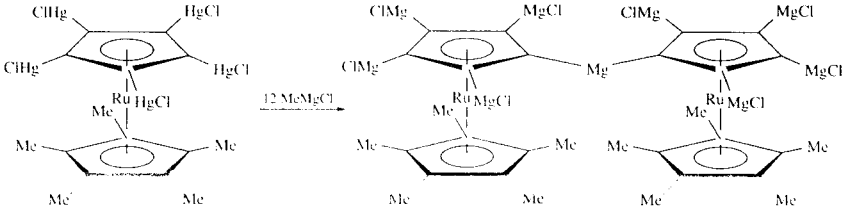

154

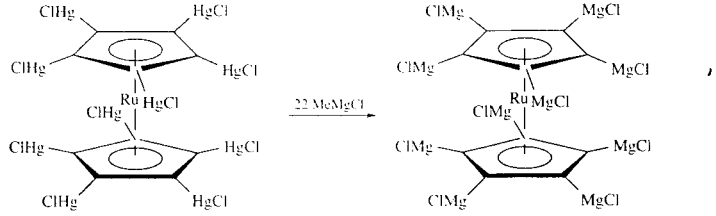

155

SCHEME 11.46

REFERENCES

1. V. Grignard, *C. R. Acad. Sci. Paris* **1900**, *130*, 1322.
2. E.E. Blaise, Houillon, *Bull. Soc. Chim. Paris, Ser. 3* **1904**, *31*, 960.
3. V. Grignard, G. Vignon *C. R. Acad. Sci. Paris* **1907**, *144*, 1358.
4. J. von Braun, *Ber. Dtsch. Chem. Ges.* **1907**, *40*, 4065.
5. M.S. Kharasch, O. Reinmuth, *Grignard Reactions of Nonmetallic Substances*, Prentice-Hall, New York, **1954**.
6. *Houben-Weyl, Methoden der Organischen Chemie*, 4th edition, E. Müller ed., Thieme, Stuttgart, Vol. *13/1-8*, **1970–1978**.
7. W.E. Lindsell in *Comprehensive Organometallic Chemistry*, G. Wilkinson, F.G.A. Stone, E.W. Abel eds., Pergamon, Oxford, **1982**, Vol. *1*, p. 155–252.
8. F. Bickelhaupt, *Angew. Chem.* **1987**, *99*, 1020–1035.
9. F. Bickelhaupt in *Organometallics in Organic Synthesis*, H. Werner, G. Erker eds. Springer, Berlin, Vol. 2, **1989**, p. 145–160.
10. F. Bickelhaupt, *Pure & Appl. Chem.* **1990**, *62*, 699–706.
11. F. Bickelhaupt, *J. Organomet. Chem.* **1994**, *475*, 1–14.
12. W.E. Lindsell in *Comprehensive Organometallic Chemistry II*, E.W. Abel, F.G.A. Stone, G. Wilkinson eds., Pergamon/Elsevier, Oxford, **1995**, Vol. *1*, p. 57–127.
13. K.C. Cannon, G.R. Crow in *Handbook of Grignard Reagents*, G.S. Silverman, P.E. Rakita eds., Marcel Dekker, New York, **1996**, p. 497–526.
14. G. Emschwiller, *C. R. Acad. Sci. Paris* **1926**, *183*, 665.
15. F. Bertini, P. Grasselli, G. Zubiani, G. Cainelli, *Tetrahedron* **1970**, *26*, 1281, and ref. cited.
16. (a) J.W. Bruin, G. Schat, O.S. Akkerman, F. Bickelhaupt, *Tetrahedron Lett.* **1983**, *24*, 3935–3936. (b) J.W. Bruin, G. Schat, O.S. Akkerman, F. Bickelhaupt, *J. Organomet. Chem.* **1985**, *288*, 13–25. (c) A. Haaland, S. Samdal, T.G. Strand, M.A. Tafipolsky, H.V. Volden, B.J.J. van de Heisteeg, O.S. Akkerman, F. Bickelhaupt, *J. Organomet. Chem.* **1997**, *537*, 217–221.
17. (a) B.J.J. van de Heisteeg, G. Schat, O.S. Akkerman, F. Bickelhaupt, *J. Organomet. Chem.* **1986**, *308*, 1–10. (b) B.J.J. van de Heisteeg, G. Schat, O.S. Akkerman, F. Bickelhaupt in *Organometallic Syntheses*, R.B. King, J.J. Eisch eds., Elsevier, Amsterdam, **1988**, Vol. *4*, 389–391.
18. N.J.R. van Eikema Hommes, F. Bickelhaupt, G.W. Klumpp, *Recl. Trav. Chim. Pays Bas.* **1988**, *107*, 393–394.

19. B.J.J. van de Heisteeg, G. Schat, M.A.G.M. Tinga, O.S. Akkerman, F. Bickelhaupt, *Tetrahedron Lett.* **1986**, *27*, 6123–6124.
20. M. Hogenbirk, N.J.R. van Eikema Hommes, G. Schat, O.S. Akkerman, F. Bickelhaupt, G.W. Klumpp, *Tetrahedron Lett.* **1989**, *30*, 6195–6198.
21. K. Ziegler, K. Nagel, M. Patheiger, *Z. Anorg. Allg. Chem.* **1955**, *282*, 345.
22. M. Hogenbirk, G. Schat, O.S. Akkerman, F. Bickelhaupt, W.J.J. Smeets, A.L. Spek, *J. Am. Chem. Soc.* **1992**, *114*, 7302–7303.
23. M. Hogenbirk, *Thesis*, Vrije Universiteit, Amsterdam, **1993**.
24. S. Miyano, Y. Miyazaki, N. Takeda, H. Hashimoto, *Nippon Kagaku Kaishi* **1972**, 1760.; *Chem. Abstr.* **1972**, *77*, 151556.
25. J. Yoshimura, K. Sako, H. Wakai, M. Funabashi, *Bull. Chem. Soc. Japan* **1976**, *49*, 1169.
26. B.J.J. van de Heisteeg, G. Schat, O.S. Akkerman, F. Bickelhaupt, *Tetrahedron Lett.* **1987**, *28*, 6493–6496.
27. F.N. Tebbe, G.W. Parshall, G.S. Reddy, *J. Am. Chem. Soc.* **1978**, *100*, 3611–36B.
28. B.J.J. van de Heisteeg, G. Schat, O.S. Akkerman, F. Bickelhaupt, *Organometallics* **1986**, *5*, 1749–1750.
29. P. Knochel in *Handbook of Grignard Reagents*, G.S. Silverman, P.E. Rakita eds., Marcel Dekker, New York, **1996**, p. 633–643.
30. V. Grignard, Tissier, *C. R. Acad. Sci.* **1901**, *132*, 835–837.
31. J.W.F.L. Seetz, O.S. Akkerman, F. Bickelhaupt, *Tetrahedron Lett.* **1981**, *22*, 4857–4860.
32. M.A.G.M. Tinga, G. Schat, O.S. Akkerman, F. Bickelhaupt, E. Horn, H. Kooijman, W.J.J. Smeets, A.L. Spek, *J. Am. Chem. Soc.* **1993**, *115*, 2808–2817.
33. (a) M.A. Dam, *Thesis*, Vrije Universiteit, Amsterdam, 1996. (b) M.A. Dam, T. Nijbakker, B.C. de Pater, F.J.J. de Kanter, O.S. Akkerman, F. Bickelhaupt, *Organometallics*, **1997**, *16*, 511–512.
34. (a) M.A. Dam, O.S. Akkerman, F.J.J. de Kanter, F. Bickelhaupt, N. Veldman, A.L. Spek, *Chem. Eur. J.* **1996**, *2*, 1139–1142. (b) M.A. Dam, F.J.J. de Kanter, F. Bickelhaupt, W.J.J. Smeets, A.L. Spek, J. Fornies-Camer, C. Cardin, *J. Organomet. Chem.* **1998**, *550*, 347–353. (c) M.A. Dam, W.J. Hoogervorst, F.J.J. de Kanter, F. Bickelhaupt, A.L. Spek, *Organometallics*, **1998**, *17*, 1762–1768.
35. N. Rot, *Thesis*, Vrije Universiteit, Amsterdam, **1998**.
36. (a) W. Ando, N. Nakayama, Y. Kabe, T. Shimizu, *Tetrahedron Lett.* **1990**, *31*, 3597–3598. (b) W. Ando, F. Hojo, S. Sekigawa, N. Nakayama, T. Shimizu, *Organometallics* **1992**, *11*, 1009–1011. (c) F. Hojo, S. Sekigawa, N. Nakayama, T. Shimizu, W. Ando, *Organometallics* **1993**, *12*, 803–810.
37. J.W.F.L. Seetz, F.A. Hartog, H.P.Böhm, C. Blomberg, O.S. Akkerman, F. Bickelhaupt, *Tetrahedron Lett.* **1982**, *23*, 1497–1500.
38. (a) J.W.F.L. Seetz, G. Schat, O.S. Akkerman, F. Bickelhaupt, *Angew. Chem.* **1983**, *95*, 242–243; *Angew. Chem. Int. Ed. Engl.* **1983**, *22*, 248–249. (b) J.W.F.L. Seetz, B.J.J. van de Heisteeg, H.J.R. de Boer, G. Schat, O.S. Akkerman, F. Bickelhaupt, in *Organometallic Syntheses*, R.B. King, J.J. Eisch eds., Elsevier, Amsterdam, **1988**, Vol. *4*, 392–394.
39. L.C. Costa, G.M. Whitesides, *J. Am. Chem. Soc.* **1977**, *99*, 2390–2391.
40. J.W.F.L. Seetz, H. Ent, R. Boer Rookhuizen, O.S. Akkerman, F. Bickelhaupt, *Recl. Trav. Chim. Pays-Bas* **1988**, *107*, 160–162.
41. (a) H.J.R. de Boer, O.S. Akkerman, F. Bickelhaupt, G. Erker, P. Czisch, R. Mynott, J.M. Wallis, C. Krüger, *Angew. Chem.* **1986**, *98*, 641–643; *Angew. Chem. Int. Ed. Engl.* **1986**, *25*, 639. (b) H.J.R. de Boer, O.S. Akkerman, F. Bickelhaupt in *Organometallic Syntheses*, R.B. King, J.J. Eisch eds., Elsevier, Amsterdam, **1988**, Vol. *4*, 396–398.
42. M. Schreuder Goedheijt, *Thesis*, Vrije Universiteit, Amsterdam, **1996**.
43. J. Salkind, P. Roganina, *J. Russ. Phys. Chem. Ges.* **1927**, *59*, 1013–1018; *Chem. Zentralbl.* **1928 I**, 2939.
44. J.W.F.L. Seetz, R. Tol, O.S. Akkerman, F. Bickelhaupt, *Synthesis* **1983**, 721.
45. J.W.F.L. Seetz, B.J.J. van de Heisteeg, G. Schat, O.S. Akkerman, F. Bickelhaupt, *J. Mol. Cat.* **1985**, *28*, 71–83.
46. J.W.F.L. Seetz, B.J.J. van de Heisteeg, G. Schat, O.S. Akkerman, F. Bickelhaupt, *J. Organomet. Chem.* **1984**, *277*, 319–322.
47. J.W.F.L. Seetz, G. Schat, O.S. Akkerman, F. Bickelhaupt, *J. Am. Chem. Soc.* **1983**, *105*, 3336–3337.
48. B.J.J. van de Heisteeg, M.A.G.M. Tinga, Y. van den Winkel, O.S. Akkerman, F. Bickelhaupt, *J. Organomet. Chem.* **1986**, *316*, 51–55.
49. M.A.G.M. Tinga, M.K. Groeneveld, O.S. Akkerman, F. Bickelhaupt, *Recl. Trav. Chim. Pays-Bas* **1991**, *110*, 290–293.
50. J.W.F.L. Seetz, B.J.J. van de Heisteeg, G. Schat, O.S. Akkerman, F. Bickelhaupt, *J. Organomet. Chem.* **1984**, *274*, 173–181.
51. H.J.R.de Boer, B.J.J. van de Heisteeg, G. Schat, O.S. Akkerman, F. Bickelhaupt, *J. Organomet. Chem.* **1988**, *346*, 197–200.
52. H.J.R. de Boer, B.J.J. van de Heisteeg, M. Flöel, W.A. Herrmann, O.S. Akkerman, F. Bickelhaupt, *Angew. Chem.* **1987**, *99*, 88–89; *Angew. Chem. Int. Ed. Engl.* **1987**, *26*, 73.
53. H.J.R. de Boer, O.S. Akkerman, F. Bickelhaupt, *J. Organomet. Chem.* **1987**, *336*, 447–452.
54. H.J.R. de Boer, O.S. Akkerman, F. Bickelhaupt, *J. Organomet. Chem.* **1987**, *321*, 291–306.

55. H.J.R. de Boer, G. Schat, O.S. Akkerman, F. Bickelhaupt, M. de Wit, A.L. Spek, *Organometallics* **1989**, *8*, 1288–1291.
56. M.A.G.M. Tinga, G.J.H. Buisman, G. Schat, O.S. Akkerman, F. Bickelhaupt, W.W.J. Smeets, A.L. Spek, *J. Organomet. Chem.* **1994**, *484*, 137–145.
57. M.A.G.M. Tinga, G. Schat, O.S. Akkerman, F. Bickelhaupt, W.W.J. Smeets, A.L. Spek, *Chem. Ber.* **1994**, *127*, 1851–1856.
58. S. Hilpert, G. Grüttner, *Ber. Dtsch. Chem. Ges.* **1914**, *47*, 177–185.
59. S. Sawatzky, G. Wright, *Can. J. Chem.* **1958**, *36*, 1555.
60. (a) H. Holtkamp, C. Blomberg, F. Bickelhaupt, *J. Organomet. Chem.* **1969**, *19*, 279–285. (b) F. Bickelhaupt, O.S. Akkerman in *Organometallic Syntheses*, R.B. King, J.J. Eisch eds., Elsevier, Amsterdam, **1986**, Vol. *3*, 403–406.
61. J. Houben, *Ber. Dtsch. Chem. Ges.* **1905**, *38*, 3796–3804.
62. (a) F. Bickelhaupt, C. Jongsma, P. de Koe, R. Lourens, N.R. Mast, G.L. van Mourik, H. Vermeer, R.J.M. Weustink, *Tetrahedron* **1976**, *32*, 1921–1930. (b) F. Bickelhaupt, R. van Veen in *Organometallic Syntheses*, R.B. King, J.J. Eisch eds., Elsevier, Amsterdam, **1986**, Vol. *3*, 450–452.
63. K. Jurkschat, H.P. Abicht, *Z. Chem.* **1985**, *25*, 338.
64. G.J.M. Gruter, F.J.J. de Kanter, P.R. Markies, T. Nomoto, O.S. Akkerman, F. Bickelhaupt, *J. Am. Chem. Soc.* **1993**, *115*, 12179–12180.
65. (a) C.L. Raston, G. Salem, *J. Chem. Soc., Chem. Commun.* **1984**, 1702–1703. (b) L.M. Engelhardt, W.P. Leung, C.L. Raston, P. Twiss, A.H. White, *J. Chem. Soc. Dalton Trans.* **1984**, 331–340. (c) S. Harvey, P.C. Junk, C.L. Raston, G. Salem, *J. Org. Chem.* **1988**, *53*, 3134–3140. (d) B. Bogdanovic, N. Janke, H.G. Kinzelmann, *Chem. Ber.* **1990**, *123*, 1507–1515. (e) B. Bogdanovic, N.Janke, H.G. Kinzelmann, K. Seevogel, J. Treber, *Chem. Ber.* **1990**, *123*, 1529–1537.
66. H. Hommes, H.D. Verkruisse, L. Brandsma, *Tetrahedron Lett.* **1981**, *22*, 2495–2596.
67. (a) P.E. Eaton, *Angew. Chem.* **1992**, *104*, 1447–1462; *Angew. Chem. Int. Ed. Engl.* **1992**, *31*, 1421. (b) P.E. Eaton, C.H. Lee, Y. Xiong, *J. Am. Chem. Soc.* **1989**, *111*, 8016–8018.
68. G. Erker, C. Krüger, G. Müller, *Adv. Organomet. Chem.* **1985**, *24*, 1–39.
69. H. Yasuda, K. Tasumi, A. Nakamura, *Acc. Chem. Res.* **1985**, *18*, 120–126.
70. (a) R.D. Rieke, H. Xiong, *J. Org. Chem.* **1991**, *56*, 3109–3118. (b) R.D. Rieke, H. Xiong, *J. Org. Chem.* **1992**, *57*, 6560–6565. (c) H. Xiong, R.D. Rieke, *J. Am. Chem. Soc.* **1992**, *114*, 4415–4417. (d) H. Xiong, R.D. Rieke, *J. Org. Chem.* **1992**, *57*, 7007–7008. (e) R.D. Rieke, M.S. Sell in *Handbook of Grignard Reagents*, G.S. Silverman, P.E. Rakita eds., Marcel Dekker, New York, **1996**, p. 527–538. (f) R.D. Rieke, M.S. Sell in *Handbook of Grignard Reagents*, G.S.Silverman, P.E. Rakita eds., Marcel Dekker, New York, **1996**, p. 539–555.
71. U. Dzhemilev, A.G. Ibragimov, E.V. Gribanova, L.M. Khalilov, *Bull. Acad. Sci. USSR, Div. Chem. Sci. (Engl. Transl.)* **1988**, *37*, 347.
72. (a) T. Alonso, S. Harvey, P.C. Junk, C.L. Raston, B.W. Skelton, A.H. White, *Organometallics* **1987**, *6*, 2110–2116. (b) W.M. Brooks, C.L. Raston, R.E. Sue, F.J. Lincoln, J.J. McGinnity, *Organometallics* **1991**, *10*, 2098–2100.
73. (a) B. Bogdanovic, S.T. Liao, R. Mynott, K. Schlichte, U. Westeppe, *Chem. Ber.* **1984**, *117*, 1378–1392. (b) B. Bogdanovic, S.T. Liao, R. Mynott, U. Westeppe in *Organometallic Syntheses*, R.B. King, J.J. Eisch eds., Elsevier, Amsterdam, **1988**, Vol. *4*, 410–413. (c) B. Bogdanovic, K. Schlichte, U. Westeppe, *Chem. Ber.* **1988**, *121*, 27–32.
74. P.K. Freeman, L.L. Hutchinson, *J. Org. Chem.* **1983**, *48*, 879–881.
75. (a) K.S. Knight, R.M. Waymouth, *J. Am. Chem. Soc.* **1991**, *113*, 6268–6270. (b) U. Wischmeyer, K.S. Knight, R.M. Waymouth, *Tetrahedron Lett.* **1992**, *33*, 7735–7738.
76. M. Vallino, *Thesis*, Université de Paris VI, 1972.
77. A.L. Spek, G. Schat, H.C. Holtkamp, C. Blomberg, F. Bickelhaupt, *J. Organomet. Chem.* **1977**, *131*, 331–340.
78. M.F. Lappert, T.R. Martin, C.L. Raston, B.W. Skelton, A.H. White, *J. Chem. Soc. Dalton Trans.* **1982**, 1959–1964.
79. Y. Kai, N. Kanehisa, K. Miki, N. Kasai, K. Mashima, H. Yasuda, A. Nakamura, *Chem. Letters* **1982**, 1277–1280.
80. M.G. Gardiner, C.L. Raston, F.G.N. Cloke, P.B. Hitchcock, *Organometallics* **1995**, *14*, 1339–1353.
81. H. Viebrock, D. Abeln, E. Weiss, *Z. Naturforsch.* **1994**, *49b*, 89–99.
82. B. Bogdanovic, N Janke, C. Krüger, R. Mynott, K. Schlichte, U. Westeppe, *Angew. Chem.* **1985**, *97*, 972–974; *Angew. Chem. Int. Ed. Engl.* **1987**, *24*, 960.
83. H. Lehmkuhl, A. Shakoor, K. Mehler, C. Krüger, K. Angermund, Y. Tsay, *Chem. Ber.* **1985**, *118*, 4239–4247.
84. T. Alonso, S. Harvey, P.C. Junk, C.L. Raston, B.W. Skelton, A.H. White, *Organometallics* **1987**, *6*, 2110–2116.
85. H. Holtkamp, C. Blomberg, F. Bickelhaupt, *J. Organomet. Chem.* **1982**, *240*, 1–8.
86. F. Bickelhaupt, *Pure Appl. Chem.* **1986**, *58*, 537–542.

87. J. von Braun, W. Sobecki, *Ber. Dtsch. Chem. Ges.* **1911**, *44*, 1918–1931.
88. A. Bygdén, *Ber. Dtsch. Chem. Ges.* **1915**, *48*, 1236–1242.
89. G. Grüttner, E. Krause, M. Wiernik, *Ber. Dtsch. Chem. Ges.* **1917**, *50*, 1549–1558.
90. (a) G. Grüttner, M. Wiernik, *Ber. Dtsch. Chem. Ges.* **1915**, *48*, 1473–1486. (b) G. Grüttner, E. Krause, *Ber. Dtsch. Chem. Ges.* **1916**, *49*, 437–444.
91. B. Denise, J. Ducom, J.F. Fauvarque, *Bull. Soc. Chim. France* **1972**, 990–1000.
92. P. Cannone, R. Boulanger, B. Chantegrel, *Tetrahedron* **1987**, *43*, 663–668, and references cited.
93. J.C. Facelli, A.M. Orendt, A.J. Beller, M.S. Solum, G. Depke, K.D. Malsch, J.W. Downing, P.S. Murthy, D.M. Grant, J. Michl, *J. Am. Chem. Soc.* **1985**, *107*, 6749–6754.
94. J.L. Jiang, Z. Shi, *Synthetic Commun.* **1998**, *28*, 4137–4142.
95. G.M. Whitesides and E.D. Gutowski, *J. Org. Chem.* **1976**, *41*, 2882–2885.
96. K. Tamao, S. Kodama, T. Nakatsuka, Y. Kiso, M. Kumada, *J. Am. Chem. Soc.* **1975**, *97*, 4405–4406.
97. (a) G.S. Bristow, M.F. Lappert, T.R. Martin, J.L. Atwood, W.F. Hunter, *J. Chem. Soc. Dalton Trans.* **1984**, 399–413. (b) J. Karl, G. Erker, R. Fröhlich, F. Zippel, F. Bickelhaupt, M. Schreuder Goedheijt, O.S. Akkerman, P. Binger, J. Stannek, *Angew. Chem.* **1997**, *109*, 2914–2917; *Angew. Chem. Int. Ed. Engl.* **1997**, *36*, 2771–2774.
98. (a) H. Takaya, K. Mashima, K. Koyano, M. Yagi, H. Kumobayashi, T. Taketomi, S. Akutagawa, *J. Org. Chem.* **1986**, *51*, 629–635. (b) K. Mashima, K. Kusano, N. Sato, Y. Matsumura, H. Nozaki, H. Kumobayashi, N. Sayo, Y. Hori, T. Ishizaki, S. Akutagawa, H. Takaya, *J. Org. Chem.* **1994**, *59*, 3064–3076.
99. H. Suzuki, T. Murafuji, N. Azuma, *J. Chem. Soc. Perkin Trans.* **1992**, 1593–1600.
100. P. Jutzi, *Chem. Ber.* **1971**, *104*, 1455–1467.
101. (a) W.Z. McCarthy, J.Y. Corey, E.R. Corey, *Organometallics* **1984**, *3*, 255–263. (b) J.Y. Corey, W.Z. McCarthy, *J. Organomet. Chem.* **1984**, *271*, 319–326.
102. P.E. Eaton, Y. Xiong, J.P. Zhou, *J. Org. Chem.* **1992**, *57*, 4277–4281.
103. P. Boudjouk, R. Sooriyakumaran, C.A. Kapfer, *J. Organomet. Chem.* **1985**, *281*, C21–C23.
104. N. Rot, F. Bickelhaupt, *Organometallics* **1997**, *23*, 5027–5031.
105. C.H. Winter, K.N. Seneviratne, A. Brettschneider-Hurley, *Comments Inorg. Chem.* **1996**, *19*, 1–23.

12

Unusual Organomagnesium Compounds

V.V. Smirnov, L.A. Tjurina and I.P. Beletskaya
Moscow State University, Russia

12.1 INTRODUCTION

The Grignard reagent, RMgX, is one of the most used synthetic reagents. We know, of course, that a solution of the Grignard reagent that we write as RMgX really contains an equilibrium mixture of RMgX, R_2Mg, and MgX_2, further complicated by association together of these species and by coordination to the magnesium atoms of solvents (such as ethers) that have oxygen or nitrogen atoms. In spite of these structural complications, a Grignard reagent solution has a Mg to R ratio of 1. In recent, years, however, there has been evidence for species in which the Mg to R ratio is much greater than 1. These include species, generally relatively unstable and difficult to characterize, that apparently have compositions $R(Mg)_nX$ and $R(Mg)_nH$ where n is greater than 1. These polymagnesium species are the subject of this chapter, which will describe the synthetic procedures that have led to them, the evidence currently available for their compositions, and some information about their chemical reactivities.

12.2 CLUSTER GRIGNARD REAGENTS

12.2.1 Metal Vapour Cryosynthesis

The study of several organometallic reactions involving co-condensation of a metal vapour and an organic ligand began in the 1960's and 1970's. When metal vapours are co-deposited at 77 K with an excess of an organic compound, unexpected reactions often take place. With this method, it has been feasible to synthesize organometallic compounds (such as dibenzenechromium) which are difficult or (such as lanthanide derivatives of unsaturated hydrocarbons) even impossible to prepare by other methods [1,2].

The cryochemical technique has been used to prepare organomagnesium compounds. Skell and Girard were the first to report [3] an investigation of the low-temperature co-condensation of magnesium and an organic halide. Magnesium vapour co-condensates were obtained with propyl chloride and propyl bromide at 77 K. The products

Grignard Reagents: New Developments Edited by Herman G. Richey, Jr. © 2000 John Wiley & Sons Ltd

of these reactions using metal vapour synthesis (MVS) gave propane on hydrolysis, just as does hydrolysis of a solution of a Grignard reagent prepared in a conventional way from magnesium and the same alkyl halides in solution. The authors concluded that the Grignard reagent is formed in MVS as in solution. MVS offers the important advantage of furnishing a Grignard reagent unsolvated by a coordinating solvent. Yields of organomagnesium compounds in such MVS reactions, however, never have been 100% based on magnesium, but instead are very much less [1,3]. Investigators have attempted to explain this by the low reactivity of the alkyl halide.

Further investigation, however, has led to stunning results. Organic halides that do not react with magnesium in solution do react in the cryosynthesis procedure. Reactions have been carried out for magnesium with chlorobenzene [4], fluorobenzene [5], and carbon tetrachloride [6].

What is the mechanism of these unusual reactions? Co-condensates formed at 77 K have been examined by ESR spectroscopy at that temperature [4,7]. The formation from alkyl and aryl halides of the corresponding free radicals was detected by observing their spectra. Dimerization products, R–R, that would form by coupling of these radicals also were observed. Particularly when R is aryl, the ESR spectra also show singlet signals with g-factors close to 2 which may be due to Mg^{+} $RX^{\cdot-}$ ion–radical pairs. In fact, in the reactions of PhF, only a singlet of an ion radical pair was observed. The authors proposed that ion–radical pairs are responsible for the formation of organomagnesium compounds. An interesting feature in the reaction scheme suggested by the authors [7] is magnesium cluster incorporation into ion–radical pairs, $RX^{\cdot-}$ Mg_n^{+} where $n > 1$. It was assumed that the fate of such species is decomposition to the Grignard reagent and magnesium.

Under MVS conditions with which even PhF reacts with magnesium, Grignard reagent yields are low. The reaction scheme [7] includes the possible role of clusters in MVS reactions, but does not explain the low Grignard reagent yields.

The next, very important observations were due to Klabunde and co-workers [8,9], who showed that magnesium clusters can be important in MVS reactions with C–X bonds.

12.2.2 The Role of Clusters in the Low-Temperature Cryosynthesis of Organomagnesium Compounds

In surveying many reactions of magnesium with alkyl and aryl halides, it was noted that high matrix concentrations of magnesium sometimes are necessary for RMgX formation to occur under cryochemical conditions. This observation led to the study of Mg, Mg_2, Mg_3, Ca, Ca_2, Ca_n (small clusters) with alkyl halides under matrix isolation conditions [8,9]. The results were intriguing. When magnesium or calcium vapours were co-deposited with alkyl halides and argon at 12 K, only dimers and clusters of the metals were consumed. Single atoms did not react. It was proposed that RMg_2X, RMg_3X, RCa_2X, and RCa_nX were formed initially, and only upon heating in the presence of excess organic halide were RMgX and RCaX formed. Support for this assumption was provided by theoretical calculations by Jasien and Dykstra [10]. This result is not unexpected, since it is known that magnesium atoms do not react with organic chlorides in the gas phase at either low or high temperatures [11]. The higher reactivity of clusters than of atoms may be connected with lower ionization potentials or with participation of bonding by more than one magnesium.

Similar results were obtained by Ault [12], who also obtained IR spectra of co-condensates of magnesium with methyl bromide and iodide in an argon matrix. Large changes of stretching modes of C–H bonds and bending modes of the methyl group were detected. No absorptions were identified, however, which could be attributed to C–Mg bonds.

It should be noted that the temperature required for the reaction of magnesium and an organic halide is about 100–150 K [1,3]. Consequently, it was impossible to observe Grignard reagent formation when the co-condensation was carried out at 12 K. But it was essential that aggregation [8] of magnesium into clusters preceded the Grignard reagent formation at higher temperature.

The possibility of the stabilization of organopolymagnesium derivatives has been discussed on the basis of the results of quantum chemical calculations of structures, energies, and vibration spectra of RMg_nX species [10,13,14]. It was shown that introduction of a second magnesium atom into an RMgX molecule always is energetically favourable. The stabilization energy, however, is not great—from 4 to 8 kcal/mol, depending on the choice of calculation method but practically independent of the particular R and X. The introduction of each additional magnesium atom is less advantageous. In fact, beginning with n of approximately 4, the addition of more magnesium atoms becomes endothermic. According to these calculations, therefore, cluster Grignard reagents may be stable at low temperatures but their stability should decrease rapidly with increasing cluster nuclearity.

This conclusion about low cluster stability for high values of n, however, cannot be considered well established. First, the calculations referred to do not take into account the formation of bridged cluster structures. The stabilization energy of the bridge dimer **1**, for example, is calculated to be 62 kcal/mol [15]. This value is considerably higher than the formation energy of a classical Grignard reagent from magnesium atoms and methyl chloride or methyl bromide (from 28 to 54 kcal/mol depending on the choice of calculation method) [16]. Therefore, the possibility of forming different species in the organic halide—magnesium systems and their stabilities are determined mainly by the stability of bridge bonds. To reach a realistic conclusion, it is necessary to calculate the stabilities of bridged dimers of cluster structures and to compare the results with those obtained for classical systems. A second reason for uncertainty about the conclusion is the *a priori* assumption in the calculations of linear structures for the metal nuclei in clusters having $n \geq 3$. For the hydrogen analogs, HMg_nH, it will be shown below that beginning with $n = 4$, a more compact (e.g., rhombic or tetrahedral) arrangement of Mg_n is more stable than a linear one. Therefore, taking into account both bridge association and non-linear structures, stability may well increase with increasing nuclearity. Consequently, the results of the calculations are not necessarily inconsistent with the proposal that cluster Grignard reagents are formed and have some stability.

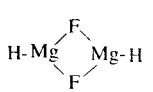

1

The hypothesis that cluster structures are formed provides an explanation of the comparatively low hydrocarbon yields (usually 50–75%) often observed on hydrolysis of co-condensates from organic halides and magnesium [1,3]. It should be noted that the yields do not correlate with organic halide reactivity. The nature of the organic halide seems to be unimportant. All organic halides react with magnesium under cryosynthesis conditions, and the yields of organometallic derivatives from alkyl bromides and fluorobenzene are similar, not more than 75%. The low yields cannot be explained only by side reactions, but can be understood if we assume the formation of cluster Grignard reagents. Hydrolysis of a dimagnesium compound, for example, must proceed as shown in equation (12.1), so the yield of hydrocarbon (based on Mg) cannot exceed 50%.

$$RMg_2X + 3H_2O \longrightarrow RH + Mg(OH)X + Mg(OH)_2 + H_2 \qquad (12.1)$$

12.2.3 Cluster Grignard Reagents—Characterization

What has been learned relating to the cluster Grignard reagent concept?

In all experiments, magnesium vapour has been co-deposited with an excess of an organic halide RX (R = alkyl, allyl, or aryl; X = F, Cl, Br, or I) at 77 K. Aryl halides that are normally unreactive in classical Grignard reagent preparations react under these conditions. Several cluster Grignard reagents RMg_nX, $n = 2$–4, have been isolated

as colourless microcrystalline solids. Quantitative analysis of hydrolysis (deuterolysis) products and combustion elemental analyses have led to empirical formulas for these novel organopolymagnesium halides. Controlled thermal decompositions have shown relative stabilities to be $PhMg_4F$ > $PhMg_3Cl$ > (alkyl)Mg_nX. The nuclearity of the RMg_nX species depends on the particular RX. Correlations with R–X bond strengths suggest that Mg_4, Mg_3, and Mg_2 react with stronger bonds (such as C–F and C–Cl) whereas Mg atoms do not. Thus the formation of cluster Grignard reagents seems to depend on the high reactivity of Mg clusters.

In the experiments, magnesium vapour was co-condensed with organic halides onto a surface cooled to about 77 K. RX/Mg ratios were in the range 100–1000. The matrices formed at 77 K were dark brown but became colourless liquids when warmed to ambient temperature after the deposition had ended. These solutions were filtered to exclude the possibility of the presence of aggregated Mg. The excess RX was then evaporated, leaving colourless microcrystals of RMg_nX compounds. Elemental analyses indicate the compositions to be RMg_nX in which n = 1 for R = allyl, n = 2 for R = alkyl, and, depending on the halide, n = 2–4 for R = aryl. Thus n = 2 for bromobenzene and iodobenzene, and n = 4 for fluorobenzene.

The nuclearity of these organomagnesium cluster compounds has also been determined by quantitative analysis of hydrolysis products (Table 12.1) [17,18].

$$RMg_nX + (2n-1)H_2O \longrightarrow RH + Mg(OH)X + (n-1)Mg(OH)_2 + (n-1)H_2 \quad (12.2)$$

Equation (12.2) indicates two ways to determine the formula of RMg_nX: (1) Mg/RH must equal n and (2) H_2/RH must equal n−1. The nuclearities of magnesium determined for the products of cryosynthesis from various aryl halides are presented in Table 12.1 along with comparison data for products obtained from some alkyl chlorides. The data in Table 12.1 indicate that the nuclearities obtained by elemental analyses and in two ways from the compositions of hydrolysis products are rather similar.

Practically the only alternative to cluster formation to explain the results is that cryosynthesis might result in a magnesium colloid solution. In fact, stable colloid magnesium solutions can readily be obtained using cryosynthesis techniques. Co-condensation of magnesium with tertiary amines results in the formation of colloids in which the size of the metallic particles is 10^1–10^2 nm [19]. Several pieces of evidence, however, indicate that the systems derived from magnesium and organic halides are true solutions. First, when the excess organic halide is evaporated, colourless or light yellow microcrystals result. These dissolve completely in the organic halide. Further, the solutions do not possess the turbidity spectrum due to light scattering that is characteristic of colloid systems.

Table 12.1. The nuclearity n of RMg_nX obtained in three ways for preparations from different organic halides

RX	n = [Mg]/[RH]	n = ([H_2]/[RH]) + 1	n from elemental analysis†	Energy of C–X bond, Kcal/mol
PhF	3.4–4.0	3.0–3.8	3.9	117
PhCl	3.0–3.5	2.8–3.2	3.2	94.2
PhBr	2.0–2.2	1.6–2.0	—	71.3
PhI	2.0–2.1	1.6–2.0	2.0	63.6
n-$C_8H_{17}Cl$	1.5–2.5	1.5–2.2	2.0	80.4
C_3H_5Cl*	1.0–1.1	0	—	59.8
PhBr*	1.0	0	—	71.3

*The Grignard reagent was prepared in solution by the classical method.
†Average of different experiments.

The solutions are stable to shaking, centrifugation, and addition of inert organic solvents, whereas magnesium colloid solutions are known to decompose on addition of alkanes. Finally, comparison of the benzene and hydrogen yields obtained on hydrolysis as well as the empirical formulas of the solids indicate that all of the magnesium is in organometallic compounds. Unfortunately, attempted X-ray diffraction analyses of the materials have so far failed, primarily because good single crystals have not been obtained. This may be because the products of co-condensation are mixtures of RMg_nX compounds having different nuclearities.

The data in Table 12.1 show a rough trend of cluster nuclearity with C–X bond strength of the organic halide. Magnesium aggregation is the main process competing with formation of organometallic compounds. Magnesium vapour is mainly monomeric Mg; magnesium aggregates form after condensation in amounts depending on time and temperature. Reactions with active halides, such as allyl chloride, proceed so quickly upon condensation that measurable amounts of aggregates are not formed. Reaction of iodobenzene or bromobenzene requires at least magnesium dimers. Compounds with stronger C–X bonds (chlorobenzene and especially fluorobenzene) seem to react mainly with magnesium trimers or tetramers. In effect, clusters are selected by the reactivity of the halide—the size of the reacting cluster is related to the bond strength of the organic halide.

Phenylpolymagnesium chlorides and fluorides can be isolated as solids and kept in vacuum for many days. Degradation in the presence of excess PhCl (equation 12.3) becomes more noticeable with increasing temperature.

$$PhMg_3Cl + 2PhCl \longrightarrow 3PhMgCl \quad (12.3)$$

Effective reaction rate constants for decomposition are given in Table 12.2. The temperature dependence corresponds to an activation energy of 16.7 kcal/mol, which must be an average for the various RMg_nX species present in the solution. This value is close to the dissociation energy (23.4 kcal/mol) [20] calculated for a Mg–Mg bond in a singly ionized magnesium

Table 12.2. Rate constants for decomposition of $PhMg_3Cl$ to PhMgCl at different temperatures

T, K	328	350	368	388
10^5 k, s^{-1}	0.36	1.85	10.0	17.5

dimer. This dimer might be a good model for the cluster [illegible] (RMg_2X). Therefore, it is reasonable to assume that RMg_nX decomposition includes a stage of homolytic magnesium–magnesium bond cleavage.

Alkyl polymagnesium halides are much less stable than their aryl counterparts. Solutions of alkylpolymagnesium halides decompose slowly at room temperature with the formation of magnesium metal powder. The decomposition, considerably accelerated by heating, is very rapid at 370 K.

The differences in the behaviour of aryl and alkyl polymagnesium derivatives are one of the enigmas in the chemistry of polymagnesium compounds. For the simplest structure with a linear arrangement of atoms, R–Mg–Mg–X, it is difficult to define reasons for the considerably greater stability when R is aryl rather than alkyl. One possible explanation is that the stabilizing role of aromatic nuclei is due to intermolecular rather than intramolecular interactions. In organopolymagnesium halides, for example, complex formation is possible between an aromatic ring and a coordinatively unsaturated magnesium atom in a different molecule. (In Section 12.3.2.4 we will consider effects of aromatic rings on the stabilities and yields of hydride products in cryochemical reactions of magnesium with 1-alkenes.)

Thus it appears that cluster Grignard reagents derived from halobenzenes possess appreciable kinetic stability due to considerable energy barriers to their decomposition.

12.2.4 Cluster Grignard Reagents—Reactions with Organic Halides

Experimental studies of polymagnesium derivatives have been restricted by difficulties in obtaining them in significant amounts. Besides

Table 12.3. Product compositions for reactions in THF of allyl halides with $PhMg_nX$ and with conventional phenyl Grignard reagents (PhMgX). $[PhMg_nX]_0 = 0.08$ M, $[C_3H_5X']_0 = 0.6$ M, T = 293 K, reaction time = 1 h

Reagents			Product composition, %				
	X′	n	PhC_3H_5	PhX′	Ph_2	PhH	$(C_3H_5)_2$
PhMgI	Br	1.0	15–17	1–2	0	0	0
PhMgBr	Br	1.0	16–19	<1	0	0	0
[illegible]	[illegible]	[illegible]	[illegible]	[illegible]	[illegible]	[illegible]	0
$PhMg_nI$	Br	2.1	68–70	10–12	4–6	8–10	6–8
$PhMg_nBr$	Br	2.1	74–76	0	2–5	12–15	6–8
$PhMg_nCl$	Br	3.0	28–30	56–58	1–2	4–6	6–8
$PhMg_nCl$	Br	3.2	30–33	57–60	1–2	5–7	8–10
$PhMg_nCl$	Br	3.5	10–12	68–70	<1	10–12	12–15
$PhMg_nF$	Br	4.1	7–9	74–76	<1	12–15	10–12
$PhMg_nF$	Cl	3.8	3–5	33–36	<1	3–5	5–8

hydrolysis and thermal decomposition, only their reaction with another organic halide has been investigated. Reaction with an organic halide to give a coupling product (equation 12.4) is a classical and important reaction of an ordinary Grignard reagent.

$$RMgX + R'X' \longrightarrow RR' + MgXX' \qquad (12.4)$$

These reactions are speeded by the presence of certain transition metal compounds, which act as catalysts.

Cluster Grignard reagents react with allyl halides to give the product mixtures summarized in Table 12.3. Phenylpolymagnesium halides react with allyl bromide differently depending on their nuclearity. The cross-coupling reaction product, allylbenzene, is formed from reactions of phenyldimagnesium iodides and bromides ($PhMg_2X$) as well from reactions of classical Grignard reagents (PhMgX). However, phenylpolymagnesium fluorides with n = 3–4 do not significantly undergo the cross-coupling reaction. Exchange of phenyl and allyl groups (halogen–metal exchange), however, an exchange which is not important in reactions of classical Grignard reagents, is significant with the phenylpolymagnesium fluorides and chlorides.

Phenylpolymagnesium halides show greater reactivity than do classical Grignard reagents. In the reaction with allyl bromide, conversion of PhMgBr is less than 20% in an hour. Under the same conditions, conversion of $PhMg_2Br$ is 90–100%. Alkyl halides are considerably less reactive than allyl bromide, reacting hardly at all with classical Grignard reagents. Octyl chloride reacts readily with $PhMg_2Br$ however, with conversion of 90% in an hour. Rates of organomagnesium cluster reactions with allyl bromide and alkyl chlorides are similar; the particular halide in R′Y apparently has little influence.

Kinetic data for the reaction of $PhMg_2Br$ and $PhMg_2I$ are described by the second-order equation $d[PhR']/dt = k[PhMg_2X][R'Br]$; k is 9.6×10^{-4} L M^{-1} s^{-1} for $PhMg_2Br$ and 9.1×10^{-4} L M^{-1} s^{-1} for $PhMg_2I$. The cross-coupling reaction of Grignard reagents with organic halides is described by a similar kinetic equation. Kinetic and activation parameters of reactions of organic halides with phenylpolymagnesium halides and with phenyl Grignard reagents are presented in Table 12.4. The rate constants of cross-coupling reactions of allyl bromide with PhMgBr and PhMgI are 1.3×10^{-4} and 1.1×10^{-4} L M^{-1} s^{-1}, respectively, nearly an order of magnitude less than rates of reactions of the corresponding $PhMg_2X$ species. It is interesting to note that the pseudo first-order rate constants for the reactions of $PhMg_2Br$ with allyl bromide and octyl chloride are very similar, 6.7×10^{-4} and 6.9×10^{-4} s^{-1}, respectively. The general

Table 12.4. Rate constants for reactions of $PhMg_nX$ with R′X′ at 298 K. k[R′X′] is a pseudo first-order rate constant determined in the presence of a large excess of R′X′ ($[R'X']_0 = 0.7$ M)

$PhMg_nX$	R′X′	Solvent	Main product	10^4 k, L M^{-1} s^{-1}	10^4 k[R′X′], s^{-1}	Activation energy, Kcal/mol
PhMgI	C_3H_5Br	THF	PhR′	1.1	0.77	—
PhMgBr	C_3H_5Br	THF	PhR′	1.3	0.92	—
PhMgCl	C_3H_5Br	THF	PhR′	—	0.7–0.9	—
$PhMg_2I$	C_3H_5Br	THF	PhR′	9.1	6.4	0.5
$PhMg_2Br$	C_3H_5Br	THF	PhR′	9.6	6.7	2.9
$PhMg_2Br$	$C_8H_{17}Cl$	C_6H_{14}	PhX′	—	5.3	—
$PhMg_2Br$	$C_8H_{17}Cl$	CH_2Cl_2	PhX′	—	2.1	—
$PhMg_2Br$	$C_8H_{17}Cl$	PhBr	PhX′	—	6.9	0.5
$PhMg_3Cl$	C_3H_5Br	THF	PhX′	—	6.8	—
$PhMg_4F$	C_8H_5Br	THF	PhX′	—	8.0	—
$PhMg_4F$	C_3H_5Cl	THF	PhX′	—	2.5	—

Table 12.5. Rate constants for exchange of organic groups between $PhMg_2Br$ and octyl chloride at different temperatures

T, K	250	257	263	280	293
10^4 k, s^{-1}	6.24	6.50	6.67	6.89	6.95

experience that reactions of Grignard reagents with allyl bromide are faster than with octyl chloride does not seem to extend to reactions of their polymagnesium analogs, suggesting different mechanisms for the reactions of ordinary and cluster Grignard reagents.

Exchange of organic groups between $PhMg_nX$ and organic halides also is pseudo first-order in $PhMg_nX$. The pseudo first-order rate constant for exchange between $PhMg_3Cl$ and allyl bromide is 4.5×10^{-4} s^{-1}. The rate of reaction of $PhMg_2Br$ with octyl chloride changes little with temperature (Table 12.5), the activation energy being only 0.5 kcal/mol.

12.3 CLUSTER MAGNESIUM HYDRIDES

12.3.1 Theory

The insertion of magnesium clusters into C–F bonds raises the question whether magnesium clusters could react with other strong bonds, C–H for example. The observation of insertion into C–H bonds obviously would be of great interest. Particularly for non-transition metals, only a limited number of examples are known of interactions of metals with C–H bonds. The synthesis of hydride Grignard reagent analogs (RMg_nH) is much more difficult than of Grignard reagents. We would expect the same for the corresponding magnesium hydride clusters. Besides the low stability of magnesium clusters, the Mg–H bond is weak. Magnesium hydride, for example, has never been obtained by the direct interaction of the elements (equation 12.5) in the gaseous state; the equilibrium favours Mg and H_2 in the available temperature range.

$$Mg + H_2 \rightleftharpoons MgH_2 \qquad (12.5)$$

Magnesium hydride can be obtained only in the solid state and with much difficulty; photochemical activation is needed for its formation [21]. Solid magnesium hydride is stabilized by hydrogen bridges. Recently methods have been developed for preparation of XMgH compounds in the form of complexes in solution [22,23]. The preparations rely on the tendency of magnesium to increase its coordination number. The species that are formed either are bridged, **2** or **3**, or complexed with the solvent (S), **4**. The energy gain resulting

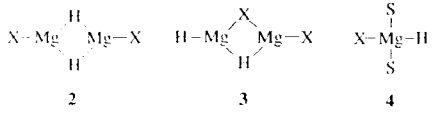

2 3 4

from bridging is greater than 30 kcal/mol, a value exceeding the endothermicity of the reaction in equation (12.5). In analogy to the reactions with hydrogen, direct insertion of magnesium into C–H bonds (equation 12.6) is also endothermic for R = alkyl, aryl, or 1-alkenyl.

$$Mg + RH \rightleftharpoons RMgH \qquad (12.6)$$

Hydride derivatives can be prepared only due to formation of bridge structures or to association with molecules of the medium, THF, for example.

Ab initio calculations carried out by the authors on the MP2(full)/G-31G* level indicate that cluster hydride (RMg_nH) formation and cluster Grignard (RMg_nX) formation are energetically more advantageous than formation of the corresponding monomagnesium ($n = 1$) species. The calculated energies of processes resulting in linear cluster hydride derivatives are given below:

$$HMgH + Mg \longrightarrow HMgMgH + 3.7 \text{ kcal/mol}$$

$$HMgMgH + Mg \longrightarrow HMgMgMgH + 3.0 \text{ kcal/mol}$$

$$HMgMgMgH + Mg \longrightarrow HMgMgMgMgH + 2.95 \text{ kcal/mol}$$

At first glance, the tendency noted by Dykstra [10] for RMg_nX—decreasing stability with increasing cluster nuclearity—seems to be reproduced for HMg_nH derivatives (good models for RMg_nH derivatives, which should exhibit the same trends). For both the hydride and halide derivatives, however, this decrease in stability with increasing nuclearity is an artifact of the calculation. The stability of linear structures indeed decreases with increasing nuclearity. But linear structures appear to be most stable only for $n \leq 3$. The situation changes for $n = 4$, for which a rhombic

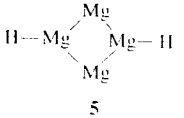

5

structure (**5**) is the most stable. Compared to HMgMgMgH and Mg, the stabilization energy is about 8 kcal/mol. The energies of structures having distorted Mg_4 tetrahedral nuclei also are less than of linear structures. The energy of insertion of Mg into $HMg_{3(lin)}H$ to form $HMg_{4(tetr)}H$ (where lin indicates a linear and tetr a tetrahedral structure) is −14.8 kcal/mol. The most stable isomer of Mg_5H_2 is a trigonal bipyramid (tribip). Its stabilization compared with $Mg_4H_{2(lin)} + Mg$ is 21.1 kcal/mol. The energies of Mg insertion into methyl derivatives are as follows:

$$CH_3Mg_2H + Mg \longrightarrow CH_3Mg_{3(lin)}H + 3.0 \text{ kcal/mol}$$

$$CH_3Mg_{3(lin)}H + Mg \longrightarrow CH_3Mg_{4(tetr)}H + 14.3 \text{ kcal/mol}$$

$$CH_3Mg_{4(tetr)}H + Mg \longrightarrow CH_3Mg_{5(tribip)}H + 22.0 \text{ kcal/mol}$$

Thus the theory predicts increasing stability with increasing nuclearity beginning with a threshold value of 4 for n.

In general, the conclusions made for clusters containing only magnesium and hydrogen are true also for RMg_nH, where R is methyl, another alkyl group, or phenyl. The stabilization energy for $n = 2$ ranges from 3.6 kcal/mol for R = methyl to 4.8 kcal/mol for R = phenyl, and the stability of linear molecules also decreases with increasing nuclearity. However, for $n = 4$ this effect is compensated for by the energy gained in forming a compact structure.

It should be noted that the alternative reaction in equation (12.7) cannot compete.

$$2RH + Mg(Mg_n) \longrightarrow RMgR(RMg_nR) + H_2 \qquad (12.7)$$

The endothermicity of this reaction is calculated to be 10–15 kcal/mol greater than calculated for the insertion of Mg or Mg_n into C–H bonds.

In summary, the following predictions can be made about organomagnesium cluster hydride formation:

1. Formation is possible in principle; mononuclear organic hydrides (RMgH) have been obtained, and the stabilities of cluster derivatives (RMg_nH) should be greater.
2. The possibility of cluster hydride formation depends on the nuclearity. Compounds with Mg_2 cores are rather unstable. Compounds with many magnesium nuclei are unlikely to be formed in significant amounts because of the low probability of formation in the low-temperature condensates of Mg_n where n is large. Consequently, we most expect to find clusters with n = 4–6.
3. Some additional stabilizing factor is necessary for the formation of measurable quantities of hydride clusters. It could be the formation of complexes with molecules in the matrix formed on condensation at low temperature. Alkanes cannot coordinate to magnesium, and therefore should not aid hydride cluster formation. The presence of molecules such as alkenes or aromatics that can form π-complexes with magnesium, however, could exert a favourable influence on the cluster hydride yield. In solutions, there are possibilities for stabilization by association of magnesium with solvent molecules.
4. Cluster organomagnesium hydrides should have high liabilities and reactivities. Consequently, these compounds can be expected to have unusual reactions.

In the following section, we will examine how experimental data for co-condensations of magnesium with several types of hydrocarbons correlate with these theoretical predictions.

12.3.2 Magnesium–Hydrocarbon Cryosyntheses

The first magnesium co-condensation with an alkane was carried out by Klabunde and coworkers [24]. As would be expected, no indication of the formation of organomagnesium products was detected. Chemical reactions were observed, however, with hydrocarbons activated by conjugation with a π system or by some other interaction. Reaction of magnesium with the activated hydrocarbons proceeds through the stages usual for cryosynthesis. Dark (usually dark brown) co-condensates are formed at 77 K but become colourless on heating, results pointing to formation of organomagnesium derivatives. At even higher temperatures, partial or complete decomposition is observed. As described in the following sections, however, marked differences in behaviour are observed for different types of hydrocarbons.

12.3.2.1 Alkylbenzenes

Co-condensation of magnesium vapour with toluene at 77 K leads to formation of a dark brown film which becomes light brown after heating to 110 K. Analysis of the reaction mixture after heating to room temperature shows the formation of methane, benzene, and isomers of xylene, their combined yield being a few percent per magnesium. Deuterolysis of the co-condensates by condensing D_2O on their films at 77 K followed by fast heating to room temperature results in formation of small amounts of toluene deuterated in the methyl group but not in the aromatic ring. The yields of the deuterolysis products ($PhCH_2D$ and $PhCHD_2$) depend on the deuterolysis temperature. At 77 K their combined yield is about 2.5% per Mg and at 100 K it is the same or lower. If the samples are heated to 130 K (which is higher than the temperature of colour disappearance) before deuterolysis, however, the yield of deuterotoluenes decreases to 1%. No deuterotoluenes are formed when deuterolysis is at 180 K. Heating to room temperature gives gray samples with properties characteristic of ultra-fine magnesium particles; on treatment with D_2O, no deuterotoluenes are found but H_2 emission is observed.

The deuterolysis data are in accord with the following sequence of conversions:

1. Formation during co-condensation of magnesium atom or cluster complexes with toluene and of small amounts of hydride compounds.

2. Formation on heating of organomagnesium compounds of unknown (possibly sandwich) structures that give no deuterotoluene on deuterolysis.
3. Decomposition of the major part of the organomagnesium derivatives on heating and melting the samples. At this stage, regeneration of the initial hydrocarbon takes place. Secondary reactions form small quantities of methane and alkylbenzenes. Measurable quantities of deuterotoluene are obtained only if the unstable hydrides are treated with D_2O at low temperatures.

The proposed hydride formation is confirmed by the results of interaction with carbon tetrachloride. Reaction with CCl_4 (equation 12.8) is a generally accepted test for metal–hydrogen (M–H) bonds [25].

$$RMH + CCl_4 \longrightarrow RMCl + CHCl_3 \qquad (12.8)$$

Data on the yields of chloroform following CCl_4 treatment and also the yields of deuterotoluenes after deuterolysis are presented in Table 12.6 for different initial ratios of the reactants (toluene and magnesium) and temperatures at which the sample is hydrolyzed. The correlation of the deuterotoluene and chloroform yields, leads us to conclude that both products are formed from the same initial substance which has an Mg–H bond.

In general, co-condensation reactions of magnesium with ethyl-, propyl-, butyl-, and *tert*-butylbenzenes proceed in the same way. The yields of hydrides at 80–110 K are about 2.0–2.5% and decrease quickly on raising the temperature. Benzene, various alkylbenzenes, polyalkylbenzenes, and C_1–C_4 alkanes are detected after heating the samples, but with combined yields of only 1–2.5%. The maximum yield of $CHCl_3$ in the reactions with CCl_4 is 3.1% per Mg for samples maintained at 77 K or heated to 110 K.

The data suggest the formation of compounds, stable at 77–130 K, having Mg–H bonds. Increasing the temperature leads to their conversion to other compounds that decompose to C_1–C_4 alkanes and polyalkylbenzenes. The yields and stabilities of the hydride magnesium adducts formed from alkylbenzenes are low, however, and the data therefore are not particularly satisfying evidence for magnesium insertion into C–H bonds. Fortunately, more definitive data have been obtained using more active hydrocarbons.

12.3.2.2 Cyclopentadiene

The general pattern of conversion is the same as with alkylbenzenes, co-condensates becoming colourless at about 90 K. Important information about the nature of the products has been obtained by means of infrared spectroscopy. At 90–100 K, a broad band, not belonging to cyclopentadiene or cyclopentadiene dimers [26], appears at 1300 cm^{-1}. On heating to 148 K, the co-condensates become colourless and the intensity of this infrared absorption increases; on further heating to 180 K, the absorption gradually

Table 12.6. The yields per Mg of deuterium containing products from deuterolysis and $CHCl_3$ from CCl_4 treatment at different temperatures of Mg-toluene co-condensates prepared with different reactant ratios

T, K	$PhCH_3$/Mg	$[PhCH_2D + PhCD_2H]$/Mg	$CHCl_3$/Mg
80	56	0.018	0.021
80	112	0.023	0.028
80	150	0.025	0.031
81	145*	0.0	0
100	55	0.019	0.024
100	158	0.025	0.030
150	56	0.001	0.003
298	52	0	0
298	168	0	0.0003

* Reagents are not co-condensed; alternating layers of Mg and $PhCH_3$ are deposited.

disappears. This infrared absorption is in the region characteristic of Mg–H–Mg bridge bonds [27].

Hydride formation is also confirmed by reactions with CCl_4 similar to those described for magnesium-alkylbenzene products. Data for $CHCl_3$ formation are presented in Table 12.7. The yield of $CHCl_3$ per Mg is considerably greater than observed for alkylbenzenes. The temperature range in which the 1300 cm^{-1} absorption is seen coincides with that in which significant amounts of $CHCl_3$ are formed. It is significant that the infrared absorption disappears, independent of the temperature, after condensation of CCl_4 on the samples. Simultaneously, the C–H stretching absorptions of $CHCl_3$ in the 3050 cm^{-1} region appear. Although the magnesium-cyclopentadiene adducts are decomposed by heating to room temperature, it is clear that they are more stable than the magnesium-alkylbenzene adducts. A further increase in stability and in yields of organomagnesium derivatives is observed when the hydrocarbon is phenylacetylene.

12.3.2.3 Phenylacetylene

The ≡C–H bond of phenylacetylene differs significantly from those in the hydrocarbons described above: its energy of homolytic cleavage and acidity are both higher. In spite of these differences, the behaviour of magnesium–phenylacetylene systems at low temperature is similar to those described for the alkylbenzene and cyclopentadiene systems. The main difference is that higher hydride bond yields are estimated on the basis of the $CHCl_3$ yields in reactions with CCl_4; the yields of $CHCl_3$ (Table 12.8) reach 80–90% per Mg after CCl_4 condensation on magnesium-phenylacetylene films at low temperature. The yields of a deuterium-containing product (PhC≡CD), however, are lower, 2.0–2.9% per Mg at 80–240 K. Similar discrepancies between yields of deuterated products and $CHCl_3$ are found in reactions with other hydrocarbons and will be explained in Section 12.3.2.5. That there is no decrease in $CHCl_3$ yield at 240 K indicates that the adducts obtained from phenylacetylene are considerably more stable than those from the hydrocarbons discussed previously. Even at room temperature, the reactions of co-condensates with CCl_4 give $CHCl_3$ yields of 10–20% per magnesium. Thus the formation of compounds which seem to have hydride nature is also characteristic of phenylacetylene.

Data from infrared spectroscopy also support the conclusion that hydride compounds are formed in the co-condensates. For phenylacetylene at 80 K, as for cyclopentadiene, a strong absorption, absent in the spectrum of the reactant hydrocarbon, is observed (at 1380 cm^{-1}). Its intensity increases upon heating the sample to 200 K, just as for cyclopentadiene. At 240 K, a new absorption

Table 12.7. The yields of $CHCl_3$ per Mg in reactions of CCl_4 at different temperatures with Mg-cyclopentadiene (CPD) co-condensates prepared with different reactant ratios

T, K	CPD/Mg	$CHCl_3$/Mg
80	23	0.20
80	56	0.25
80	115	0.28
150	58	0.35
150	86	0.46
150	115	0.53
150	110*	0.001
180	120	0.65
180	115*	0.001
298	85	0.10

*Reagents are not co-condensed; alternating layers of Mg and cyclopentadiene are deposited.

Table 12.8. The yields of $CHCl_3$ per Mg in reactions of CCl_4 at different temperatures with Mg-phenylacetylene co-condensates prepared with different reactant ratios

T, K	PhC≡CH/Mg	$CHCl_3$/Mg
80	54	0.8
80	50*	0
80	108	0.9
80	156	0.9
200	156	0.9
200	150*	0.001
240	153	0.9
240	112	0.9
298	159	0.2
298	53	0.1

*Reagents are not co-condensed; alternating layers of Mg and phenylacetylene are deposited.

appears at 1230 cm^{-1} and the intensity of the 1380 cm^{-1} absorption decreases. Note that even at 240 K the co-condensates react with CCl_4 to give almost quantitative yields of $CHCl_3$ per Mg. Therefore the changes in infrared spectra reasonably reflect the conversion of one hydride product to a comparable amount of another that has somewhat different Mg–H bonds. It should be noted that in the magnesium–phenylacetylene system, another type of reaction is possible: displacement of the relatively acidic ≡CH hydrogen with the formation of a magnesium acetylide. $(PhC{\equiv}C)_2Mg$, however, is not expected to have strong absorptions in the 1200–1400 cm^{-1} region [28].

Unfortunately, a more detailed investigation of this system failed because of polymerization of phenylacetylene in the solid state at 210–220 K in the presence of organomagnesium adducts. Upon heating to room temperature, a sample becomes a red-brown polymer which contains solid magnesium. In reactions in which cryochemically produced organomagnesium derivatives are used as catalysts for further reactions of the hydrocarbon (additional acetylene is added on top of the first: PhC≡CH/Mg 50–1000, 240–298 K), about 300–400 moles of phenylacetylene are polymerized per mole of magnesium. Such behaviour is not unique to phenylacetylene; as described below, ordinary alkenes undergo catalytic conversions in their co-condensates with magnesium.

12.3.2.4 1-Alkenes

1-Alkenes react with magnesium in co-condensates to form a wide range of products. Reaction at low temperatures seem generally to be characteristic of a variety of alkenes, but studies with 1-hexene will be described since these have been the most detailed.

In general, the appearance and behaviour of co-condensates formed from magnesium and 1-hexene are similar to those formed from the other types of hydrocarbons described in the preceding sections. The principal difference is that the 1-hexene co-condensates never become completely colourless. As in other hydrocarbon systems, characteristic absorptions appear in infrared spectra (at 1260 and 1310 cm^{-1}) and disappear at temperatures above about 150 K. Deuterolysis of the co-condensates at 80–100 K leads to monodeuterated hexenes. As in all cases already discussed, condensation of CCl_4 on the cold (77 K) samples leads to the disappearance of the characteristic infrared absorptions and to formation of $CHCl_3$ in yields depending on the ratio of the 1-hexene and magnesium reactants and the temperature to which the co-condensate has been exposed (Table 12.9). The $CHCl_3$ yields, probably a good indicator of Mg–H quantities, are lower than for the cyclopentadiene and phenylacetylene systems.

The behaviour of triple co-condensates of benzene, 1-hexene, and magnesium is different, however. Neither infrared spectra nor deuterolysis of co-condensates of benzene and magnesium indicate any sign of reaction. Addition of benzene to the 1-hexene–magnesium system, however, considerably changes its properties. A number of new infrared absorptions, absent in the system without benzene, are detected in the 1200–1400 cm^{-1} region. At the same time the yield of $CHCl_3$ in reactions at 300 K of the co-condensate with CCl_4 increases to 90% per Mg. The effect of benzene very possibly is to stabilize the magnesium clusters, for example by forming π complexes.

For both 1-hexene–Mg and 1-hexene–benzene–Mg systems, the infrared absorptions attributed to Mg–H bonds disappear after samples formed at

Table 12.9. The yields of $CHCl_3$ per Mg in reactions of CCl_4 at different temperatures with Mg-1-hexene co-condensates prepared with different reactant ratios

T, K	C_6H_{12}/Mg	$CHCl_3$/Mg
80	20	0.1
80	50	0.16
80	100	0.15
80	100*	0
298	20	0.01
298	50	0.03
298	200	0.05

*Reagents are not co-condensed; alternating layers of Mg and 1-hexene are deposited.

77 K are heated to room temperature. CCl_4 treatment of samples heated to room temperature does not lead to formation of $CHCl_3$ or of any other products. Evidently the active organomagnesium compounds, formed at low temperature during or immediately after condensation, decompose during heating. The composition of the reaction mixture after cryosynthesis differs greatly from the reactants. Principally 2-hexene and 3-hexene formed by double bond migration, but also several other hydrocarbons, are present. Also present are polymeric products, insoluble in organic solvents and resembling soot. The combined 2-hexene and 3-hexene yield is about seven times that of the magnesium content in the samples. Isomerization, therefore, is a catalytic process. The catalysts must be unstable organomagnesium compounds. Isomerization is not observed if the alkene is condensed onto a precondensed magnesium film nor in samples that are prepared by deposition of alternating layers of magnesium and alkene. Therefore we can reject an alternative hypothesis that isomerization is due to highly dispersed magnesium.

Surprisingly, formation of some hexane was observed; the yields (in reactions without hydrolysis) were 1–15% per magnesium. Thus there is autohydrogenation of hexene giving hexane and condensation products. Autohydrogenation was not observed on highly dispersed magnesium and hence must be the consequence of metastable organomagnesium derivatives. Participation of labile organomagnesium derivatives with Mg–H bonds is quite possible.

The infrared spectra, formation of $CHCl_3$ in reactions with CCl_4, and formation of deuterated products on deuterolysis lead us to assume the presence of Mg–H bonds in magnesium-hexene adducts. However, low stability results in decomposition of these species on heating to room temperature.

Fortunately, magnesium interaction with a polycyclic hydrocarbon gives more stable adducts.

12.3.2.5 Anthracene

Anthracene is particularly interesting because, in contrast to the hydrocarbons described above, it

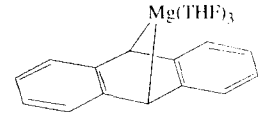

6

reacts with magnesium in solution, forming anthracenylmagnesium (**6**) [29,30]. Magnesium co-condensation with anthracene at low temperature also leads to the formation of stable adducts, but they are not similar to **6**.

Reagent co-deposition at 77 K gives dark films that become colourless on heating to 100 K [31]. A peculiarity of the reactions with anthracene is the appearance of an intense green colour at temperatures immediately below that at which the sample completely loses colour. This may point to the formation of ion-radical adduct pairs. Indeed, in the ESR spectrum there is an intense singlet with a g-factor of about 2.0 that appears at the temperature of green colour formation and disappears with decolourization. This absorption probably is due to the ion–radical pair Mg_n^{+} $RH^{\cdot-}$.

Simultaneously with decolourization, a broad absorption at 1260 cm^{-1} appears in infrared spectra; as for similar absorptions observed in reactions of other hydrocarbons, this can be attributed to Mg–H bonds. At the same time, C–Mg stretching modes appear in the 500–560 cm^{-1} region. All of these absorptions disappear on treating the co-condensates with H_2O (D_2O) or CCl_4.

Deuterolysis of the magnesium–anthracene adduct at 100–130 K gives 9-deuteroanthracene and 9,10-dideuteroanthracene. Deuterolysis at room temperature leads to the formation of these compounds and 9,10-dideuterdihydroanthracene. The formation of two types of deuterolysis product can be related to two types of interaction taking place in the magnesium–anthracene system. The precursor of the dideuterodihydroanthracene is probably **6**. Formation of deuterosubstituted anthracene must result from magnesium insertion into C–H bonds.

Reactions of the magnesium–anthracene adducts at room temperature with CCl_4 give somewhat

higher yields (Table 12.10) of $CHCl_3$ than did reactions of the hydrocarbons described in previous sections. It should be noted again that while co-condensation leads to Mg–H bond formation, there is no significant product formation if alternating layers of the reactants are condensed.

The stability of the cryosynthesis products permitted carrying out elemental analyses to determine their composition. Since the presence of even small amounts of unreacted magnesium could distort the results, special efforts were made to achieve complete magnesium conversion. In a series of experiments, a 20-fold excess of the organic component was shown to be necessary for complete conversion of the magnesium. In the experiments aimed at determining empirical formulas, a 500-fold excess was used to guarantee the absence of even micro amounts of magnesium. Unreacted anthracene was removed by continuous pumping until there was a constant vacuum above the film. The elemental analyses gave formulas $C_{14}H_{10}Mg_n$; the value of n lies in the range 2–8, a particular value depending on the cryosynthesis conditions (reagent ratio, rate of co-condensation, apparatus geometry, etc.). Since the deuterolysis results show that magnesium is bonded only to the 9 and 10 carbons of anthracene, the formulas that are obtained can be considered evidence for the adducts being clusters. At low temperatures, magnesium exists mainly in hydride compounds, RMg_nH or HMg_nRMg_nH. At ambient temperature, there are other forms, namely cluster analogs of **6** or perhaps a sandwich adduct, forms which possibly may interconvert.

Table 12.10. The yields of $CHCl_3$ per Mg in reactions of CCl_4 at different temperatures with Mg-anthracene co-condensates prepared with different reactant ratios

T, K	Anthracene/Mg	$CHCl_3$/Mg
100	5	0.3
100	50	0.4
298	10	0.2
298	50	0.4
298	50*	0.002

*Reagents are not co-condensed; alternating layers of Mg and anthracene are deposited.

As is the case for phenylacetylene–magnesium adducts, the yields of magnesium–anthracene adducts estimated from hydrolysis data are much lower than estimated from reactions with CCl_4 (Table 12.11). To investigate this discrepancy, the reaction of magnesium–anthracene adducts with CCl_4 was studied in solution at 298 K. The $CHCl_3$ yield, which at low temperature had been 40% of the amount of magnesium, increased with time and reached 35 moles per mole of magnesium. At room temperature catalytic hydrogenolysis of CCl_4 is taking place. Besides chloroform, chloro-substituted anthracenes are formed. So anthracene, which is in large excess, serves as a hydrogen source for hydrogenolysis of CCl_4. In $PhCD_3$ solution in the absence of excess anthracene, $CDCl_3$ is formed.

The cluster magnesium–anthracene adduct is extraordinarily active. Reactions are observed upon attempts to dissolve it even in such comparatively inert solvents as THF, CH_2Cl_2, toluene, or benzene. In these solvents, autohydrogenolysis takes places with the formation of dihydroanthracene and condensation products. The use as the solvent of CH_2Cl_2 leads to polymers containing chlorine and use of THF leads to products of ring cleavage of the THF.

Many of the reactions mentioned are catalytic, the total yields of products exceeding 100% per magnesium. Dihydroanthracene formation proceeds with catalytic yields (Table 12.12) in the presence of excess anthracene. It is apparent that the hydrogen source for hydrogenation can be not only anthracene but also the solvent. When the solvent is $PhCD_3$, deuterodihydroanthracene has been detected; also obtained are $PhCD_2H$ and

Table 12.11. The maximum yields per Mg of deuterium containing products from deuterolysis and $CHCl_3$ from CCl_4 treatment of co-condensates obtained from Mg and various hydrocarbons

RH–Mg	RD yield, % per Mg	$CHCl_3$ yield, % per Mg
$PhCH_3$–Mg	2.5	3.1
Phenylacetylene–Mg	2.5	90
Anthracene–Mg	2.9	40

Table 12.12. The yields of 9,10-dihydroanthracene per Mg in reactions at 300 K of solutions in benzene or toluene of Mg-anthracene co-condensates prepared with different reactant ratios

RH/Mg	Solvent	Yield of dihydroanthracene, mol/mol Mg
2.1	Benzene	8.2
3.5	Toluene	3.1
5.8	Toluene	4.6
12	Toluene	5.3

$PhCDH_2$ in amounts very much greater than the amount of magnesium.

Throughout the studies of Mg–RX systems, one can infer the insertion of magnesium into C–H bonds with cluster formation. The predictions from theory in Section 12.3.1 have been confirmed experimentally by studies of reactions of magnesium with C–H bonds of different polarities and strengths. For hydride adduct formation, additional stabilizing factors are necessary. In proceeding from alkanes to alkylbenzenes, the tendency of the metal to interact with C–H bonds becomes evident. The products with alkylbenzenes, however, are stable only at low temperature. With the condensed aromatic anthracene and the possibility of increased stabilizing interactions, a magnesium-hydrocarbon adduct stable at ambient temperature was observed. Its reactivity and lability lead to unusual properties, as was predicted in Section 12.3.1 for such cluster organomagnesium hydride species.

12.3.3 Catalytic Properties of Magnesium–Hydrocarbon Adducts

We have found unusual catalytic properties of the anthracene–magnesium adduct in various reactions that involve C–H and C–C bonds—isomerization of alkenes, autohydrogenolysis, and D–H exchange. Control experiments showed that these reactions cannot be observed in the presence of dispersed magnesium, classical Grignard reagents, or magnesium halides. At 120–298 K in the presence of magnesium-hydrocarbon adducts as catalysts, the catalytic reactions proceed with various degrees of effectiveness. For example, 2-alkenes and 3-alkenes are always detected in the products of magnesium-1-alkene cryosynthesis after heating the co-condensates to 298 K. The combined yields of 2-alkene and 3-alkene are 7–15 moles per mole of Mg. The isomerization mainly takes place during heating from 77 to 298 K. Even at 298 K, however, 1–3 moles of 2-alkene and 3-alkene are formed per mole of Mg. It may be that much of the catalytically active species is destroyed by a melting process, but even at room temperature some quantity of catalyst remains or has been transformed into a more stable but less catalytically active form.

Another route for isomerization of 1-alkenes by magnesium–hydrocarbon adducts is initiated by addition of 1-alkenes to the Mg-anthracene adduct at low or room temperature. The combined yield of 2-octene, 3-octene, and 4-octene formed from 1-octene ranges from 2.1 to 4.5 moles per mole of Mg.

Autohydrogenolysis of unsaturated hydrocarbons is another catalytic process taking place on magnesium cluster adducts. Cryosyntheses in the 1-alkene–magnesium systems lead not only to isomerization of the 1-alkene but also to its reduction to the corresponding alkane. The yield of alkane is 25–35% per Mg. Alkane forms only at low temperatures; its yield does not increase at room temperature. A higher yield of alkane, 50–85% per Mg, can be obtained in the presence of the magnesium–anthracene adduct. The most effective reduction is observed in the magnesium–anthracene system—the yield of dihydroanthracene can reach 3 moles per mole of Mg. Experiments to detect the hydrogen source in these reductions lead to observation of catalytic H–D exchange. Indeed, in $PhCD_3$, the magnesium–anthracene adduct gives not only dihydroanthracene and monodeutero- and dideutero-dihydroanthracenes, but also $PhCD_2H$, $PhCH_2D$, and even $PhCH_3$. After 24 hours, the combined yields of the last three products are 20–180 moles per mole of Mg.

The catalytic properties in the various reactions appear to be due to reversible magnesium cluster

insertion into C–H and C–Cl bonds. Cluster organomagnesium hydride derivatives must possess unique properties. We hope that deeper and broader investigations of these adducts will lead to new catalysts and modes of catalysis.

12.4 CONCLUSION

[illegible] vapour and organic halides or suitable hydrocarbons can synthesize new materials with interesting properties. The available evidence indicates these materials to have compositions RMg_nCl and RMg_nH. Most of the evidence so far has been indirect, e.g., inference from products of hydrolysis or from reactions with CCl_4, although there are some elemental analyses for the halides and some infrared spectral data for the hydrides. Further characterization of these materials is a high priority. Obtaining suitable crystals that would permit X-ray crystal structure determinations would be highly desirable. For the present, however, it is evident that interesting new materials have been formed. In particular, the magnesium hydride materials possess interesting catalytic properties. Clearly this area deserves further study.

Note added at proof. In a recent study, magnesium atoms generated by laser ablation were reacted with methyl halides (X = F, C Br, and I) diluted with argon followed by trapping at 10 K in an argon matrix [32]. Analysis by infrared spectroscopy showed the presence in each case of monomeric CH_3MgX and some secondary reaction products. The reactions are thought to be of excited (^3P) magnesium atoms. The absence of polymagnesium species is in accord with the discussion of the role of magnesium aggregates in the formation of such species. That monomeric CH_3MgX species are present is an indication of the difficulty of aggregation processes under matrix isolation conditions.

REFERENCES

1. M. Moskovits and G.A. Ozin, Eds. *Cryochemistry*; John Wiley and Sons, New York, **1976**.
2. K.J. Klabunde, *Chemistry of Free Atoms and Particles*; Academic Press, New York, **1980**.
3. P.S. Skell and J.E. Girard, *J. Am. Chem Soc., 94*, 5518, **1972**.
4. G.B. Sergeev, V.V. Smirnov, and V.V. Zagorsky *J. Organomet. Chem., 201*, 9, **1980**.
5. G.B. Sergeev, V.V. Smirnov, and F.Z. Badaev, *J. Organomet. Chem., 224*, C29 **1982**.
6. G.B. Sergeev, V.V. Smirnov, V.V. Zagorsky, and A.M. Kosolapov, *Dokl. Akad. Nauk SSSR, 256*, 1169, **1981**.
7. G.B. Sergeev, V.V. Zagorsky, and F.Z. Badaev, *J. Organomet. Chem., 243*, 123, **1983**.
8. Y. Imizu and K.J. Klabunde, *Inorg. Chem., 23*, 3602, **1984**.
9. K.J. Klabunde and A. Whetten, *J. Am. Chem. Soc., 108*, 6529, **1986**.
10. P.G. Jasien and C.E. Dykstra, *J. Am. Chem. Soc., 107*, 1891, **1985**.
11. N. Shafizadeh, J. Rostas, G. Taieb, B. Bourguignon, and M. Prisant, *Chem. Phys., 142*, 111, **1990**.
12. B.S. Ault, *J. Am. Chem. Soc. 102*, 3480, **1980**.
13. A.V. Nemukhin, I.A. Topol, and F. Weinhold, *Inorg. Chem., 34*, 2980, **1995**.
14. V.N. Solov'ev, G.B. Sergeev, A.V. Nemukhin, S.K. Burt, and I.A. Topol, *J. Phys. Chem A, 101*, 8625, **1997**.
15. A.V. Nemukhin, V.N. Solov'ev, G.B. Sergeev, and I.A. Topol, *Mendeleev Commun., 5*, **1996**.
16. S.R. Davis, *J. Am. Chem. Soc., 113*, 4145, **1991**.
17. S.V. Kombarova, L.A. Tyurina, and V.V. Smirnov, *Metalloorg. Khim., 5*, 1038 **1992**.
18. V.V. Smirnov and L.A. Tyurina, *Usp. Khim.*, 63, 1 **1994**; *Russ. Chem. Rev. (Engl. Transl.), 63*, 55, **1994**.
19. S.E. Kondakov and V.V. Smirnov, *Bull. Soc. Chim. Belg., 103*, 131, **1994**.
20. P.L. Po and R.F. Porter, *J. Phys. Chem., 81*, 2233, **1977**.
21. J.G. McCaffrey, J.M. Parnis, G.A. Ozin, and W.H. Breckenridge, *J. Phys. Chem., 89*, 4945, **1985**.
22. E.C. Ashby and A.B. Goel, *Inorg. Chem., 16*, 2941, **1977**.
23. B. Bogdanović and M. Schwickardi, *Z. Naturforsch. B: Chem. Sci., 39*, 1001, **1984**.
24. K.J. Klabunde, H.F. Efner, L. Satek, and W. Donley, *J. Organomet. Chem., 71*, 309, **1974**.
25. W.J. Evans, K.M. Coleson, and S.C. Engerer, *Inorg. Chem., 20*, 4320, **1981**.
26. W.T. Ford, *J. Organomet. Chem., 32*, 27, **1971**.
27. E.C. Ashby and A.B. Goel, *J. Org. Chem., 42*, 3480, **1977**.
28. M.A. Coles and F.A. Hart, *J. Organomet. Chem., 32*, 279, **1971**.
29. B.Bogdanović, S.-T.Liao, R.Mynott, K.Schlichte, and U.Westeppe, *Chem. Ber., 117*, 1378, **1984**.
30. B. Bogdanović, *Acc. Chem. Res., 21*, 261, **1988**.
31. G.B. Barkovskii, L.A. Tyurina and V.V. Smirnov, *Vestn Mosk. Univ., Ser. 2: Khim., 32*, 464, **1991**.
32. W.D. Bare and L. Andrews, *J. Am. Chem. Soc., 120*, 7293, **1998**.

Index

Acetaldehyde, phenylmagnesium bromide addition to 140
Acetals 53
Acetone 2
  phenylmagnesium bromide addition to 140
Acetylenes, hydromagnesiation 82–4
Acid derivatives 18
Activated ethers 53
Acyl chlorides 70
Adamantyl bromide 229–30
Addition-elimination mechanism 58–9
Addition process 16
Advocin 176
Aldehydes
  addition of configurationally stable Grignard agents to 145–6
  α-aminoorganometallic addition to 143
  benzylic Grignard agents addition to 148–53
  diastereoselectivity in addition of configurationally labile, nonracemic, chiral α-aminoorganometallics to 149–51
  phenylmagnesium bromide addition to 141
  stereoselective additions to 139–64
Aliphatic ketones 17–18
Alkali metals, heterometallic organomagnesium complexes with 320–1
Alkaloid synthesis 153–62
Alkenes 58, 406–7
  catalytic enantioselective alkylation 125–6
    with alkylmagnesium halides 114–19
  heteroatom-directed addition to 108
  hydromagnesiation 67–79, 75–6
  Ni-catalyzed stereoselective alkylation of 126–34
  stereoselective addition to 107–37
Alkoxy 53
Alkyl bromides 248
Alkyl exchanges 43
Alkyl Grignard reagents 39–42
Alkyl halides 59, 206–13
  saturated 39–42
  simple 29
Alkyl iodides 248
Alkyl radicals 248
Alkylaluminums 125–6
Alkylbenzenes 403–4
Alkylmagnesium bromides 10
Alkylmagnesium chlorides, (EBTHI)Zr-catalyzed enantioselective carbomagnesation of unsaturated heterocycles with longer chain 118
Alkylmagnesium halides 107
  catalytic enantioselective alkylation of alkenes with 114–19
Alkynes
  Cp_2TiCl_2-catalyzed, hydromagnesiation 97–102
  hydromagnesiation 82–93, 97
Allyl chloride 49
Allyl halides 60, 400
Allylic acetals, Ni-catalyzed asymmetric addition to 134
Allylic alcohols 127
  Zr-catalyzed diastereoselective carbomagnesation of 109–14
  Zr-catalyzed diastereoselective ethylmagnesation of 109–11
Allylic ethers 55, 127
  Ni-catalyzed asymmetric addition to 132–4
  Ni-catalyzed diastereoselective addition to 126–32
  Ni-catalyzed directed addition to 126–31
  Ni-catalyzed reactions of 130
  Zr-catalyzed diastereoselective carbomagnesation of 109–14
  Zr-catalyzed diastereoselective ethylmagnesation of 109–11
Allylic Grignard reagents 42
Allylic halides 31, 43–5, 225–6, 284
Allylmagnesium bromide 15
endo-2-Allylnorbornane 45
Aluminum, heterometallic organomagnesium complexes with 321–2
β-Amino alcohols 144
Aminomagnesium monohydrides 72
α-Aminonitriles 56
α-Aminoorganometallic addition to aldehyde 143

Anion-radical intermediates in reductions of organic halides 238–47
Anthracene 407–9
Anthracenemagnesium derivatives 311–12
Aromatic aldehydes, diastereoselective addition of tetrahydroisoquinoline Grignard reagents to 153
Arrhenius activation energy 13
Aryl halides 222
Arylmagnesium halides 107
Arylmethyl compounds 46–8
Association between RMgX and carbonyl compounds 6–7
Association equilibria 5–7
Atomic-force microscopy (AFM) 254–5
Azobenzene 22–3

Benzaldehyde 145
  diastereoselectivity
    in addition of configurationally labile, racemic, chiral α-aminoorganometallics to 148
    in addition of configurationally stable chiral α-amino Grignard reagents to 146
  diethylzinc addition to 142
Benzophenone 2
  reactions
    new investigation 16–17
    with Grignard reagents 7–17
Benzotriazoles, I-substituted 56
Benzyl ethers 55
Benzyl halides 60
Benzylic Grignard reagents 42
  addition to aldehydes 148–53
  configurational lability of 146–8
Benzylic halides 31, 43–5, 225–6, 284, 289, 293, 295
Benzylmagnesium chloride 180
Benzylmagnesium compounds 68
Bicuculline 162
  synthesis 161
Bicyclic allylic ethers, Ni-catalyzed addition to 131–2
Bicyclic homoallylic alcohols, Zr-catalyzed diastereoselective carbomagnesation of 114
Bicyclic homoallylic ethers, Zr-catalyzed diastereoselective carbomagnesation of 114
Boronolide, synthesis 94
1-Bromo-1-methyl-2,2-diphenylcyclopropane 221, 250
β-Bromostyrene 58
Butyllithium 94–5
Butylmagnesium chloride 20
t-Butylmagnesium chloride 2, 9, 13, 15

^{13}C-KIEs 15
^{14}C-KIEs 14
Camphor-oxazoline chiral auxiliary 158
Carbanion intermediates in Grignard reactions 235
Carbenoid intermediates 48
Carbocations 50
Carbomagnesiation 96
Carbon, nucleophilic displacements at 27–64
Carbonyl compounds 6–7, 70, 73
  α,β-unsaturated 19–20
  association with RMgX 6–7
  reductive dimerization 21
  Wittig-type olefination 370
Carborane derivatives 314
Carboxylate esters 52–3
Catalytic enantioselective alkylation of alkenes 125–6
C–C bond 1–2, 28, 53, 59, 65, 127, 132, 135
C–H bond 46
Chain mechanisms in Grignard reactions 235
Chaulmoograic acid 70
Chemically Induced Dynamic Nuclear Polarization. *See* CIDNP Chiral Grignard reagents 139–64
Chiral stationary phase HPLC 156
Chirality effect 130
2-Chloro-3-iodopropene 49
CIDNP 38, 41, 43, 48, 60, 195, 201, 261
  polarization 40, 47, 57, 59
  signals 16
Cinnamic esters 23
Cluster Grignard reagents
  characterization 397–9
  metal vapour cryosynthesis 395–6
  reactions with organic halides 399–401
Cluster magnesium hydrides, theory 401–3
Clusters, role in low-temperature cryosynthesis of organomagnesium compounds 396–7
C–Mg bond 1–2, 5, 27
  dissociation energies 3
C–N double bonds 102
C–O bond 127
Configuration 143–5
Configurational lability of benzylic Grignard agents 146–8
Configurationally stable Grignard agents, addition to aldehydes 145–6
Conjugated dienes, hydromagnesiation 79–82
Contact trajectory 198
Corlumine 162
  synthesis 156, 161
Corrosion reactions 188
Corytensine 162
  synthesis 161
Coupling reactions with organic halides 29–30
Cp_2TiCl_2-catalyzed hydromagnesiation of alkynes 97–102
CpBr 251

CpD 250–1
CpH 250–1
Cross-coupling reactions, mechanisms 30–46
Crotyl *o*-anisyl ether 55
Crotyl chloride 45
Cyclic allylic ethers
  addition to (EBTHI)Zr-alkene complex 124
  Zr-catalyzed kinetic resolution of 123–4
Cyclooctatetraene (COD) 131
Cyclopentadiene 404–5
Cyclopropyl bromide 214–15, 217, 221
Cyclopropyl halides 213–22

Danofloxacin 176
Darvon 180
DCPD trapping 251
DCPH(D) trapping 250–1
Debye–Waller factor 330, 350
Decumbensine 158, 162
Desoxyasperdiol, synthesis 95
Deuterium substitution 15–16
Dialkylacetylenes 83, 85
  hydromagnesiation 84
Dialkylmagnesiums 70–1
Diastereoselectivity in addition of configurationally labile, nonracemic, chiral α aminoorganometallics to aldehydes 149–51
Diastereoselectivity in addition of configurationally labile, racemic, chiral α-aminoorganometallics to benzaldehyde 148
Diastereoselectivity in addition of configurationally stable chiral α-amino Grignard reagents to benzaldehyde 146
Diastereoselectivity in addition of tetrahydroisoquinoline Grignard reagents to aromatic aldehydes 153
Dibenzoyl-(+)-tartaric acid 180
1,2-Dibromoethane 174–5
α,α-Dichlorocyclobutanones 292
2,3-Dichloropropene 49
α,α-Dideuteriopentylmagnesium bromide 16
Dienes, organomagnesium compounds derived from 211
1,3-Dienes, 4-substituted 67
Diethyl ether (DEE) 6, 9, 10, 24, 167, 180, 185, 229, 250–1, 263, 349, 362
Diethylzinc addition to benzaldehyde 142
Diffusion effects 228
Diffusion-reaction equations 197
Diffusion trajectory 198
Di-Grignard reagents 288–9, 367–85
9,10-Dihydroanthracene 409
Dihydrofurans, zirconocene-catalyzed kinetic resolution of 122
1,2-Dimethoxyethane (DME) 229
Dimethoxyisoquinolyloxazoline 159
Dimethyl ether 46
β-Dimethylamino-α-methyl-propiophenone 180
2,5-Dimethylfuran (2,5-DMF) 110
Dineopentylmagnesium 300
Di-organomagnesium forms 165
1,1-Di-organomagnesium reagents
  applications 370–2
  synthesis and structure 369–70
1,2-Di-organomagnesium reagents, applications 374–5
1,3-Di-organomagnesium reagents, applications 377–80
1,2-Di-organomagnesium reagents, synthesis and structure 372–4
1,3-Di-organomagnesium reagents, synthesis and structure 375–7
1,4-(and larger) α,ω-di-organomagnesium reagents
  applications 382–5
  synthesis and structure 380–2
Dioxane (DXN) 229
Diphenylacetylene, hydromagnesiation 67
1,2-Diphenylethane 67
Diynes, organomagnesium compounds derived from 211
Droloxifene 175
Duality 2

EBTHI 115
EBTHI metallocenes 135
(EBTHI)Zr-alkene complex
  cyclic allylic ethers addition to 124
  interaction with heterocyclic alkene substrates 120
(EBTHI)Zr-catalyzed enantioselective carbomagnesation of unsaturated heterocycles with longer chain alkylmagnesium chlorides 118
(EBTHI)Zr-catalyzed enantioselective ethylmagnesation of unsaturated heterocycles 115
(EBTHI)Zr-catalyzed kinetic resolution of unsaturated pyrans 120
$(EBTHI)ZrCl_2$ 120
Egenine 162
  synthesis 161
Electrochemical corrosion 188
Electrode potentials 40
Electron transfer 9, 19, 22, 35, 40, 187
  see also ET
Enantiopure α-hydroxybenzylisoquinolines 162
Epi-α-decumbensine 158, 162
Epiophiocarpine 154
Epoxides (oxiranes) 54–5
EPR spectroscopy 16, 38
Equipment
  configuration 166–7
  drying 172
  flow diagram 166

ET radical mechanism 7
ET reactions 10–11, 13
  substrates other than benzophenone 20–3
Ethyl propionate 70
Ethylene, hydromagnesiation 69
Ethylene oxide 54
Ethylenebistetrahydroindenyl. *See* EBTHI
EtMgBr 132
EXAFS 331
  comparison with LAXS 330–[illegible]
  current structural picture 362–3
  data analysis 334–5
  Grignard reagents 347–59
  measurement fundamentals and techniques 332–4
  theoretical background 330–2
Exotherm control 168–70
Extended X-ray absorption fine structure. *See* EXAFS

Farnesol, synthesis 94
Fick's First Law 196
First-order decay 201
Franck–Condon Principle 34
Freckled magnesium 264–6
Free radicals 38
Furfuryl aldehyde 176

Geminate reaction 220
Grignard additions, stereoselectivity in 139–41
Grignard chemistry 165
  industrial 175–81
Grignard radicals 248–9
Grignard reactions 185
  activation 189
  apparatus for studies 192
  carbanion intermediates in 235
  chain mechanisms in 235
  hypotheses 190
  induction period 189
  inhibition 189
  initiation 171–5, 189
  inorganic part of mechanism 186–9, 253–66
    activation 257–9
    entrainment 259
    initiation 255–7
    Mg(I) intermediates 260–2
    two liquid phases 263–4
  organic part of mechanism 186, 191–253
    A model 253, 289
    AB dynamics 195–7
    AB kinetics 198–202
    D model 189, 203–6, 247–53
    experimental techniques 191–3
    infinite-dilution D model 202–3
    models 195–7
    pathway R 193–5
    radical intermediates 193–5
    rate constants 195–7
    rate law 193
    rates 195–7
    retention of configuration 247–8
    Walborsky mechanism 250
    ZB dynamics 195–7
    ZB kinetics 198–202
  overview 186–9
  Rieke-magnesium 257
  [illegible] 220
Grignard reagents
  absorber backscatterer distances 352
  alkyl 39–42
  allylic 42
  as base 176–8
  benzylic 42, 146–53
  chiral 139–64
  cluster 395–9
  conductivity measurements 344
  crystallography 341–3
  detecting initiation of reaction 175
  di-Grignard reagents 288–9, 367–85
  EXAFS 347–59
  formation
    from magnesium anthracene complexes 284–90
    from supported magnesium-anthracene complexes 295–6
    process controls and interlocks 168–71
  formation mechanisms 185–275, 289–90
  future prospects 296–7
  halogen in 227–9
  industrial applications and strategy 165–83
  infrared spectroscopy 344–5
  LAXS 359–63
  miscellaneous industrial applications 181
  molecular weight studies 343–4
  mono-, special features 286–8
  NMR spectroscopy 345
  overview 1
  physical chemistry 340–7
  poly- 288–9
  preparation 1
  properties 3–7
  reactivity 171
  saturated 39–42
  small portion 174
  theoretical studies 345–7
  tracer studies 344
  see also specific reagents

Halide concentration 226–7
Halobenzenes 45
α-Halocycloalkanones 49
α-Haloethers 32, 45–6
Halogen in Grignard reactions 227–9
Halogen-atom transfer 187

α-Haloketones 49–50
1-Halo-1-methyl-2,2-diphenylcyclopropanes 218, 221, 228
α-Halothioethers 32
Hammett rho values 14–15
Hammett sigma values 9
Heat of formation 3
Heating/cooling fluids 171
Heteroatom-directed addition to alkenes 108
[illegible]
5-Hexenyl bromide 212
5-Hexenyl halides 212
HMPA 131
Hoffmann eliminations 56–7
Homoallylic alcohols
  Zr-catalyzed diastereoselective carbomagnesation 109–14
  Zr-catalyzed diastereoselective ethylmagnesation 112–14
Homoallylic ethers
  Zr-catalyzed diastereoselective carbomagnesation 109–14
  Zr-catalyzed diastereoselective ethylmagnesation 112–14
β-Hydrastine 154
β-Hydrogen reduction 18–19
Hydromagnesiation 65–105
  acetylenes 66, 82–4
    titanium-catalyzed 93
  1-alkenes 75–6
  alkenes 67–79
  alkynes 82–93, 97
    Cp_2TiCl_2-catalyzed 97–102
  conjugated dienes 79–82
  dialkylacetylenes 84
  diphenylacetylene 67
  ethylene 69
  in selective synthesis of natural products 93–7
  magnesium hydride 69
  Ni-catalyzed 78
  olefins 66, 71, 74
    titanium-catalyzed 93
  propargyl alcohols 88–9
  silylacetylenes 101
  silyl(other than trimethylsilyl) alcohols 92
  stannylpropargyl alcohols 92
  styrene 69, 76–77
  1-(trimethylsilyl)-1-alkyne 68, 101
  (trimethylsilyl)alkynes 86–7
  (trimethylsilyl)propargyl alcohols 90
  3-(trimethylsilyl)-2-propyn-1-ol 87
  unsaturated bonds 102
Hydrotitanation, silylacetylene 67
Hydroxy 53
Hydroxybenzyl isoquinoline alkaloids 151
  synthesis of 155
Hydroxybenzyl isoquinolines 153, 161

Industrial applications 165–83
  engineering considerations 166–71
  safety considerations 166–71
Infrared spectroscopy, Grignard reagents 344–5
Iodine addition 174
Iron-catalyzed Grignard exchange 79
Iron salts 40
Isoquinoline alkaloids, synthesis 153

β-Ketoesters 176
  synthesis 179
Kharasch reaction 20–1
Kinetic isotope effects (KIEs) 14–16

Large angle X-ray scattering. *See* LAXS
Lasioderma serricorne F 96
LAXS 329–30, 335–9
  comparison with EXAFS 339–40
  current structural picture 362–3
  data analysis 338–9
  Grignard reagents 359–63
  measurement fundamentals and techniques 338
  theoretical background 335–8
Leaving groups 30, 33, 50–7
Lewis acid/base type interaction 311
Lewis acidity 33
Lewis basicity 33, 112, 114
Linear free energy correlations 8–11
Lithiated tetrahydroisoquinolines 151

Magnesiated tetrahydroisoquinolyl oxazoline 152
Magnesium
  coordination number 2 300–1
  coordination number 3 301–2
  coordination number 4 302–6
    dimeric compounds 304–5
    mononuclear compounds 302–4
    polymeric compounds 305–6
  coordination number 5 307–8
  coordination number 6 306–8
  forms of 172–3
  safe handling of 171
Magnesium anthracene 277–98, 293
  formation and properties 278–81
  formation of Grignard reagents 284–90
    mechanism 289–90
  molecular projection 282
  reactions 281–4
  supported complexes 293–6
Magnesium-anthracene adduct 409
Magnesium-anthracene co-condensates 409
Magnesium-anthracene complexes 284–90
Magnesium bromide 154

Magnesium bromide etherate 191
Magnesium clusters, slurries of 230–5
Magnesium coordination number 353
Magnesium enolates 176
Magnesium hydride 66, 72
  hydromagnesiation 69
  see also Cluster magnesium hydrides
Magnesium-hydrocarbon adducts, catalytic properties 409–10
Magnesium-hydrocarbon cryosyntheses 403
Magnesium(I) intermediates 187
Magnesium K fluorescence EXAFS spectra 355
Magnesium malonate 178–9
Magnesium surface area 226
Maltol/ethyl maltol 178
Marcus theory 34–5
MeMgBr 129–30, 132
Mercury addition 174
Metal catalysis 20–1
Metal-halogen exchange 43
Metal hydrides 65
Metal vapour cryosynthesis 395–6
Metallic corrosion 259–60
2-Methoxyethanol 174
N-Methyl (bis)-methylenedioxy compounds 159
Methyl esterification 96
Methyl iodide 174–5
Methylenecyclohexane 68
Methylenedioxyisoquinolyloxazoline 159
Methylmagnesium bromide 2
Methylmagnesium chloride 178
Mg_Z 185–6, 188, 195, 204–5, 226, 264–5
Mg_Z-solution interface 262–3
Mono-alkyl oxiranes 55
Mono-Grignard reagents, special features 286–8

Naproxen 178
Ni-catalyzed asymmetric addition
  to allylic acetals 134
  to allylic ethers 132–4
Ni-catalyzed diastereoselective addition to allylic ethers 126–32
Ni-catalyzed directed addition to allylic ethers 126–31
Ni-catalyzed hydromagnesiation 78
  of conjugated dienes 81
  see also Hydromagnesiation
Ni-catalyzed reactions of allylic ethers 130
Ni-catalyzed stereoselective addition to bicyclic allylic ethers 131–2
Ni-catalyzed stereoselective alkylation of alkenes 126–34
Nitroxyl radical 38
NMR spectroscopy, Grignard compounds 345
Non-contact trajectory 198
Norbornylmagnesium bond 45
Noyes theory 196, 267
Nucleophilic displacements at carbon 27–64
Nucleophilic substitutions 56

^{18}O KIE 15
Occam's razor 190–1, 247
Olefins, hydromagnesiation 71, 74
Ophiocarpine 154
Organic halides 174–5, 290–2
  anion-radical intermediates in reductions of 238–47
  coupling reactions with 29–30
  reactions with cluster Grignard reagents 399–401
  reactive 30
  reduction potentials of 36
Organomagnesium bromides 349
Organomagnesium complexes
  heterometallic complexes
    with alkali metals 320–1
    with aluminum 321–2
    with transition metals 322–4
Organomagnesium compounds
  carborane derivatives 314
  cyclopentadienyl derivatives and related compounds 312–13
  derived from dienes or diynes 311
  difunctional 308–12, 367–85
  intramolecular polycoordination 314–20
  mechanistic features of reactions 1–26
  polyfunctional 385–6
  polyhapto carbon ligands 312–14
  polymagnesium species 395–410
  role of clusters in low-temperature cryosynthesis 396–7
  simple difunctional 308–10
  X-ray diffraction studies 299–328
Organomagnesium halide 165
Orthoesters 53
Oxazolines 152
  chiral auxiliary 158
Oxidation potentials 4–5, 10
Oxide layer 189
Oxy-anions 51–6
Oxygen, ET reactions 21–2
Oxygen-magnesium bond 4

Pauson–Khand cyclization reaction 121
1,3-Pentadiene 67
Pentylmagnesium bromide 58
Peroxides, ET reactions 21–2
Phenylacetylene 405–6
(Phenyldimethylsilyl)propargyl alcohols 89
Phenyliminophenylindole 12

Phenylmagnesium bromide 349, 362
  addition to acetaldehyde 140
  addition to acetone 140
  addition to aldehyde 141
Phenyl(methyl)acetylene 83
Phenylpolymagnesium halides 400
PhMgBr 129–30
Phosphate esters 51–2
Phthalide isoquinoline alkaloid synthesis 160
Phthalide isoquinolines 158
Pictet–Spengler cyclization 154
PMDETA 280
Polar concerted reaction mechanisms 17–19
Poly-Grignard reagents 288–9
Polyhalogen compounds 48
Polyisoprenepolyols 74
Polymer recycling 296
Polyorganomagnesium reagents 385–6
Process hazards analysis (PHA) 167–8
Process safety interlocks 170
Propane 46
Propargyl alcohols 95
  hydromagnesiation 88–9
Propoxyphene 180–1

Quinolone 176

Radiation boundary condition 197
Radical coupling/disproportionation 248
Radical mechanism and early evidence 7–8
Radical probes 11–13
Reactivity of Grignard reagents 171
Reactivity series 8–11
Recurrence theorem 199
Reduction potentials of organic halides 36
Reductive dimerization of carbonyl compounds 21
Rieke-magnesium 289
  Grignard reactions 257

Safe handling of magnesium 171
Safety interlocks 170
Saturated Grignard reagents 39–42
Schlenk equilibrium 5, 33, 340, 368
Secondary isotope effects 16
Seebach–Prelog definition of relative topicity 144
Self association 5–6
Sex pheromone 96
Silica recycling 296
Silylacetylenes
  hydromagnesiation 101
  hydrotitanation 67
Silylalcohols (other than trimethylsilyl), hydromagnesiation 92
1-Silyl-1-alkynes 83
Silylpropargyl alcohols 89
Single electron transfer (SET) mechanism 34–43, 45–7, 49, 50, 58, 60, 142, 145, 159
Slurries of magnesium clusters 230–5
Smoluchowski-Collins-Kimball (SCK) decay 201
Smoluchowski-Collins-Kimball (SCK) theory 196, 267
S_N1 mechanism 2–3, 30, 33–4, 39, 43, 45
S_N2 mechanism 2–3, 28, 30–3, 38–9, 43, 45, 55, 59–60
Solvent effects 24
  in Grignard reactions 229
Solvents, choice of 167
Solvolysis reactions 39
$S_{RN}1$ 59
Standard electrode potentials 38
Standard oxidation potentials 37
Standard potentials 35
Stannylpropargyl alcohols, hydromagnesiation 92
Stereoselective additions
  to aldehydes 139–64
  to alkenes 107–37
Stereoselectivity in Grignard additions 139–41
  cis-stilbene 67
  trans-stilbene 67
Styrene, hydromagnesiation 69, 76–7
Sulfate esters 51
Sulfonate esters 51
Sulfones 58
Sulfoxides 57–8
Surface initiators 174
Surface spectroscopy 255

Tamoxifen 175
TEMPO 251
Terminology 143–5
Tetrahydrofuran. *See* THF
Tetrahydroisoquinoline 153, 156
Tetramethylcyclopropyl bromide 216
Tetra-substituted Olefin–Droloxifene 177
Thermochemistry 3–4
THF 5–9, 11, 17, 24, 42, 67, 112, 131, 146–7, 167, 185, 212, 219, 229, 250, 277, 353–4, 372, 400
Thioethers 56
α-Thioethers 45–6
Titanium-catalyzed Grignard exchange reaction 74
Titanium-catalyzed hydromagnesiation of olefins and acetylenes 93
Titanium/magnesium transmetallation 67
Titanocene dichloride 68
TMEDA 280, 302, 308
Topicity 143–5
Transition metal catalysts 72
Transition states 141–3
(Tribenzylsilyl)ethylene 76

Tri-Grignard reagents 288–9, 385–6
1-(trimethylsilyl)-1-alkyne 67
  hydromagnesiation 68, 101
(Trimethylsilyl)alkynes, hydromagnesiation 86–7
(Trimethylsilyl)propargyl alcohols, hydromagnesiation 90
3-(Trimethylsilyl)-2-propyn-1-ol, hydromagnesiation 87
Triorganomagnesium reagents 385–6
[illegible]
Trityl ethers 55

Unsaturated heterocycles, Zr-catalyzed kinetic resolution 119–22
α,β-Unsaturated ketones 19
Unsaturated pyrans, (EBTHI)Zr-catalyzed kinetic resolution 120

Valine-derived oxazoline auxiliary 159
Veltol and Veltol Plus 176
Vent sizing (DIERS) calculations 168
Vicinal dihalides 48
Vinyl halides 222–5
Vinylstannanes 92
Vitride 173–4

Walborsky mechanism 189–91, 250
Waste disposal 181
Water effects 171–2
Wittig rearrangement 12
Wittig-type olefination of carbonyl compounds 370
Wurtz coupling 291, 293

X-ray absorption near edge structure (XANES) 331
X-ray absorption spectroscopy (XAFS) 329–35
X-ray crystal structure 157–8
X-ray diffraction studies, organomagnesium compounds 299–328

Zirconocene–alkene complex, alkene insertion 117
Zirconocene-catalyzed enantioselective alkylation reactions 114–26
Zirconocene-catalyzed kinetic resolution
  of 2-substituted medium-ring heterocycles 121
  of dihydrofurans 122
Zoapatanol, synthesis 96
Zr-catalyzed diastereoselective carbomagnesation
  of allylic alcohols and ethers 109–14
  of bicyclic homoallylic alcohols and ethers 114
  of homoallylic alcohols and ethers 109–14
Zr-catalyzed diastereoselective ethylmagnesation
  of allylic alcohols and ethers 109–11
  of homoallylic alcohols and ethers 112–14
Zr-catalyzed kinetic resolution
  of cyclic allylic ethers 123–4
  of unsaturated heterocycles 119–22
Zr-catalyzed resolution technology 121

Index compiled by Geoffrey Jones, Information Index

Grignard Reagents

New Developments

Edited by
Herman G. Richey, Jr.
The Pennsylvania State University, USA

Publishing 100 years after Grignard proposed his simple procedure for preparing solutions of organomagnesium compounds, leading experts present authoritative perspectives on the current status of 12 areas that have developed significantly in recent years. Contents include:

- New Reactions of Grignard Reagents
- Stereoselective Reactions of Organomagnesium Compounds
- Mechanistic Features of Organomagnesium Compounds
- Industrial Applications and Strategy
- Unusual Organomagnesium Compounds
- Structures of Organomagnesium Solids and Solutions

At the close of its first century, these chapters demonstrate the significant developments that are still taking place using Grignard Reagents and related organomagnesium compounds.

Grignard Reagents: New Developments will prove of great interest to academic and industrial chemists active in organometallic chemistry of main group metals, organic syntheses, reaction mechanisms and structural organic chemistry.

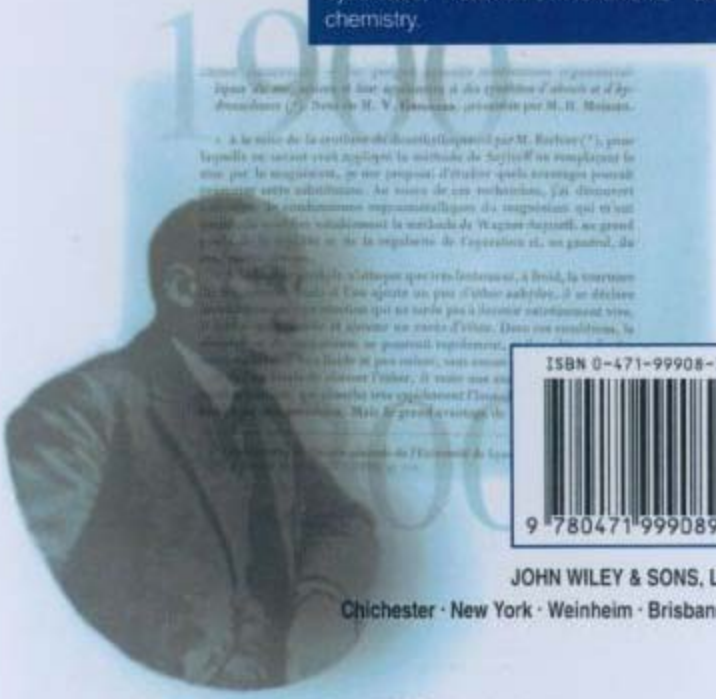

ISBN 0-471-99908-3

JOHN WILEY & SONS, LTD
Chichester · New York · Weinheim · Brisbane · Singapore · Toronto